frontiers | Research Topics

Advanced molecular targets in the diagnosis and treatment of gastrointestinal cancers, volume II

Edited by
Zsolt Kovács, Cornelia Braicu and Simona Gurzu

Published in
Frontiers in Oncology

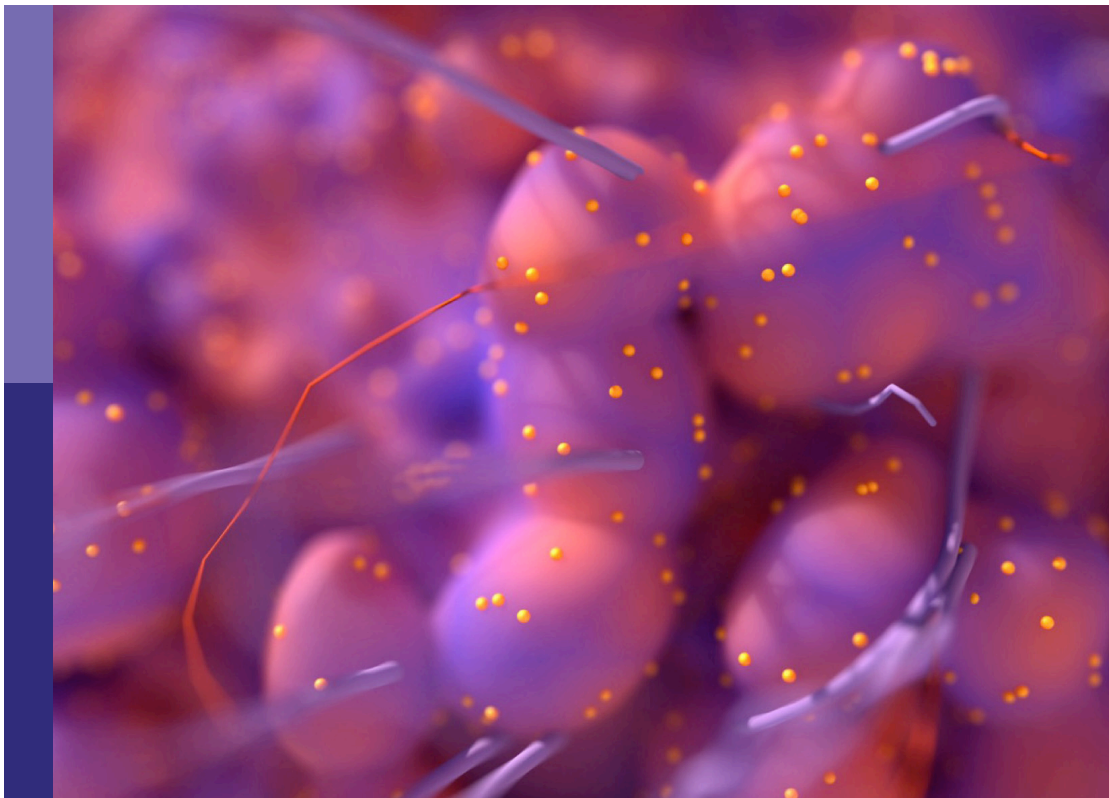

ISSN 1664-8714
ISBN 978-2-8325-5679-5
DOI 10.3389/978-2-8325-5679-5

About Frontiers

Frontiers is more than just an open access publisher of scholarly articles: it is a pioneering approach to the world of academia, radically improving the way scholarly research is managed. The grand vision of Frontiers is a world where all people have an equal opportunity to seek, share and generate knowledge. Frontiers provides immediate and permanent online open access to all its publications, but this alone is not enough to realize our grand goals.

Frontiers journal series

The Frontiers journal series is a multi-tier and interdisciplinary set of open-access, online journals, promising a paradigm shift from the current review, selection and dissemination processes in academic publishing. All Frontiers journals are driven by researchers for researchers; therefore, they constitute a service to the scholarly community. At the same time, the *Frontiers journal series* operates on a revolutionary invention, the tiered publishing system, initially addressing specific communities of scholars, and gradually climbing up to broader public understanding, thus serving the interests of the lay society, too.

Dedication to quality

Each Frontiers article is a landmark of the highest quality, thanks to genuinely collaborative interactions between authors and review editors, who include some of the world's best academicians. Research must be certified by peers before entering a stream of knowledge that may eventually reach the public - and shape society; therefore, Frontiers only applies the most rigorous and unbiased reviews. Frontiers revolutionizes research publishing by freely delivering the most outstanding research, evaluated with no bias from both the academic and social point of view. By applying the most advanced information technologies, Frontiers is catapulting scholarly publishing into a new generation.

What are Frontiers Research Topics?

Frontiers Research Topics are very popular trademarks of the *Frontiers journals series*: they are collections of at least ten articles, all centered on a particular subject. With their unique mix of varied contributions from Original Research to Review Articles, Frontiers Research Topics unify the most influential researchers, the latest key findings and historical advances in a hot research area.

Find out more on how to host your own Frontiers Research Topic or contribute to one as an author by contacting the Frontiers editorial office: frontiersin.org/about/contact

Advanced molecular targets in the diagnosis and treatment of gastrointestinal cancers, volume II

Topic editors

Zsolt Kovács — George Emil Palade University of Medicine, Pharmacy, Sciences and Technology of Târgu Mureş, Romania

Cornelia Braicu — University of Medicine and Pharmacy Iuliu Hatieganu, Romania

Simona Gurzu — George Emil Palade University of Medicine, Pharmacy, Sciences and Technology of Târgu Mureş, Romania

Citation

Kovács, Z., Braicu, C., Gurzu, S., eds. (2024). *Advanced molecular targets in the diagnosis and treatment of gastrointestinal cancers, volume II*.

Lausanne: Frontiers Media SA. doi: 10.3389/978-2-8325-5679-5

Table of contents

frontiers | Frontiers in Oncology

TYPE Editorial
PUBLISHED 03 December 2024
DOI 10.3389/fonc.2024.1528137

OPEN ACCESS

EDITED AND REVIEWED BY
Liang Qiao,
The University of Sydney, Australia

*CORRESPONDENCE
Zsolt Kovacs
zsolt.kovacs@umfst.ro

RECEIVED 14 November 2024
ACCEPTED 20 November 2024
PUBLISHED 03 December 2024

CITATION
Kovacs Z, Braicu C and Gurzu S (2024) Editorial: Advanced molecular targets in the diagnosis and treatment of gastrointestinal cancers, volume II.
Front. Oncol. 14:1528137.
doi: 10.3389/fonc.2024.1528137

Editorial: Advanced molecular targets in the diagnosis and treatment of gastrointestinal cancers, volume II

Zsolt Kovacs[1,2]*, Cornelia Braicu[3] and Simona Gurzu[2,4,5]

[1]Department of Biochemistry, Environmental Chemistry, "George Email Palade" University of Medicine, Pharmacy, Science and Technology of Targu Mures, Targu Mures, Romania, [2]Centre of Research in Oncology and Translational Medicine, Centre of Research in Oncology and Translational Medicine (CCOMT), Targu Mures, Romania, [3]Centre of Research for Functional Genomics, Biomedicine and Translational Medicine, University of Medicine and Pharmacy Iuliu Hatieganu, Cluj Napoca, Romania, [4]Department of Pathology, "George Email Palade" University of Medicine, Pharmacy, Science and Technology of Targu Mures, Targu Mures, Romania, [5]Department of Medicine, Romania Academy of Science, Bucharest, Romania

KEYWORDS

gastrointestinal cancer (GI cancer), targeted therapy, personalized treatment, precision medicine, molecular oncology

Editorial on the Research Topic
Advanced molecular targets in the diagnosis and treatment of gastrointestinal cancers, volume II

In our Research Topic entitled "*Advanced Molecular Targets in the Diagnosis and Treatment of Gastrointestinal Cancers, volume II*", we managed to publish 15 articles, original researches, case studies and reviews of the literature. This editorial synthesizes advances across 15 studies, highlighting innovative diagnostic and therapeutic strategies in gastrointestinal oncology. Case studies emphasize targeted approaches for rare cancers, such as SMARCA4-deficient tumors and metastatic hepatocellular carcinoma, underscoring precision medicine's role. Some of the original researches unveils promising biomarkers like cuproptosis and angiogenesis markers in colorectal cancer, methylation subtypes predicting immunotherapy response, and novel imaging techniques distinguishing gastric tumors. Studies on socioeconomic factors reveals organized screening's role in reducing gastric cancer disparities. A systematic review of guanylate cyclase-C signaling suggests new colorectal cancer therapies. Together, these research papers advance precision oncology and health equity in gastrointestinal cancers (Figure 1).

Liang et al. reviews the efficacy and safety of zolbetuximab, a monoclonal antibody targeting Claudin 18.2, for first-line treatment of advanced gastric and gastro-esophageal junction (G/GEJ) adenocarcinoma. A meta-analysis of three randomized controlled trials involving 1,402 patients found that zolbetuximab combined with chemotherapy significantly improved overall survival and progression-free survival compared to chemotherapy alone, especially in patients with high Claudin 18.2 expression. Although associated with more grade 3+ adverse events, primarily nausea and vomiting, these side effects were generally manageable. This combination therapy offers a promising new treatment option for CLDN18.2-positive G/GEJ adenocarcinoma.

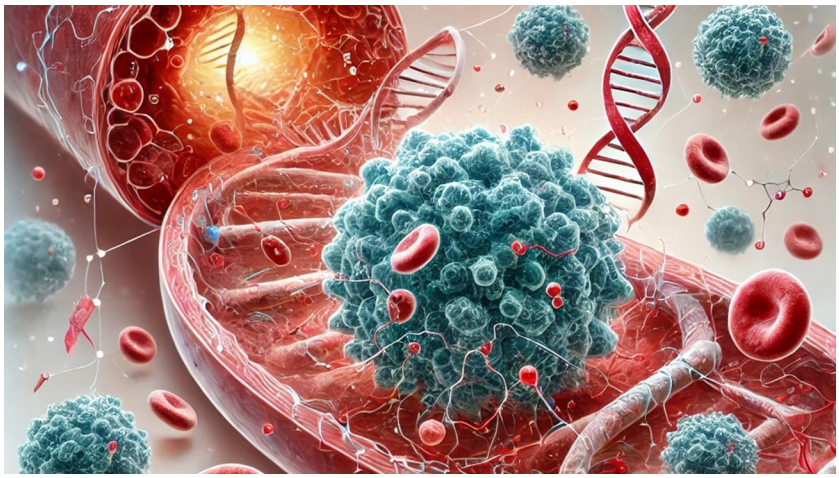

FIGURE 1
Graphical representation of the Research Topic.

Piroozkhah et al. systematically reviews the guanylate cyclase-C (GC-C) signaling pathway's role in colorectal cancer (CRC) as a potential target for diagnosis, prognosis, and therapy. The GC-C receptor, activated by endogenous peptides guanylin and uroguanylin, regulates intestinal fluid homeostasis and may influence CRC development. Disruption of GC-C signaling is linked to tumorigenesis and reduced cell differentiation. Targeting GC-C through novel treatments, such as vaccines and chimeric antigen receptors, shows promise in preclinical trials. The study underscores GC-C as a significant therapeutic and diagnostic marker, proposing it as a viable target for future CRC treatments.

Zhou et al. reports two cases of gastrointestinal neuroendocrine carcinoma (GI NEC) with SMARCA4 deficiency, a rare genetic alteration associated with aggressive cancer behavior. Both cases, one in the duodenal papilla and the other in the stomach, presented as poorly differentiated tumors with high proliferation indexes. Despite receiving chemotherapy and anti-PD-1 immunotherapy, the outcomes were poor: one patient died within nine months, while the other showed no disease evidence for ten months post-surgery. SMARCA4 deficiency, marked by loss of BRG1 expression, emerges as a potential prognostic and therapeutic biomarker, warranting further investigation.

Li et al. in their study investigates colorectal cancer (CRC) recurrence prediction through a model based on cuproptosis and angiogenesis markers. Using long non-coding RNAs (lncRNAs) related to copper-induced cell death (cuproptosis) and angiogenesis, researchers developed a Cox regression model to identify high-risk CRC patients for recurrence post-surgery. Results showed strong prediction accuracy, validated across different datasets. Additionally, the study highlights a negative correlation between cuproptosis and angiogenesis, supported by differential immune cell compositions in high- and low-risk groups. This model potentially aids in personalized therapy, identifying patients likely to benefit from more intensive treatment strategies.

The corrigendum by Du et al. addresses a funding statement error in a previous article on cardiac tamponade, a rare complication following gastric cardia cancer resection combined with neoadjuvant chemotherapy and immunotherapy. The corrected funding source is "Key Projects of Medical Science Research of Hebei Province (20230795)" rather than "(2023079)." This amendment does not affect the scientific conclusions or findings discussed in the original publication.

Lin et al. presents two cases of SMARCA4-deficient gastric carcinoma, a rare and aggressive cancer variant marked by the loss of SMARCA4 expression. Both cases exhibited poor differentiation with distinct histological characteristics, including rhabdoid cells, and showed poor response to conventional therapies. A review of 29 reported cases emphasizes high mortality rates and poor prognosis, with a median survival of eight months. The study categorizes SMARCA4-deficient gastric carcinomas into three subtypes based on histological features and immunophenotype, advocating for precise diagnosis and potentially exploring targeted therapies like EZH2 inhibitors for these challenging cases.

Chen et al. by their study investigates the prognostic value of preoperative plasma fibrinogen (PF) and C-reactive protein/albumin (CRP/Alb) ratio in pancreatic carcinoma patients. Analyzing 250 patients, it finds that higher PF and CRP/Alb levels correlate with poor overall survival (OS) and advanced clinical stages. Particularly, in patients with pancreatic ductal adenocarcinoma (PDAC), combining high PF and CRP/Alb levels serves as a stronger predictor of OS compared to each marker alone. The findings suggest that the PF and CRP/Alb ratio could help identify high-risk patients who might benefit from more aggressive treatment strategies.

Wojakowska et al. explores proteomic and metabolomic markers in rectal cancer to predict patient response to preoperative radiotherapy (neo-RT). By analyzing tissue samples, researchers identified proteins and metabolites associated with good and poor responses to treatment. Key differences were found in energy metabolism, amino acid degradation, and immune-related pathways. Proteins like CEACAM5 and metabolic shifts, such as elevated glycolysis in poor responders, were highlighted. The

findings suggest that multi-omic panels can serve as biomarkers to predict and monitor radiotherapy efficacy, potentially guiding personalized treatment strategies for rectal cancer patients.

One of the researches made by Cao et al. studies a randomized controlled trial protocol for using the Yiqi Wenyang Jiedu prescription (YWJP), a traditional Chinese medicine (TCM) formula, to prevent recurrence and metastasis in gastric cancer (GC) patients post-surgery. Involving 212 patients who completed adjuvant chemotherapy, the trial will assess the effectiveness of YWJP in enhancing disease-free survival (DFS) compared to a placebo. Secondary outcomes include overall survival, recurrence rates, quality of life, and adverse reactions. This study aims to provide robust evidence for YWJP's role in GC management, potentially aiding in the development of integrative postoperative therapies.

Xu et al. identifies DNA methylation-driven subtypes of colon cancer to predict immunotherapy responsiveness. Using multi-omics data, researchers identified a specific cluster (Cluster 1) with distinct immune characteristics, such as high tumor mutational burden (TMB), CD8+ T-cell infiltration, and immune checkpoint expression, suggesting better outcomes with immunotherapy. The study also highlights three methylation markers—PCDH20, APCDD1, and COCH—as effective indicators for this immunotherapy-beneficial subtype. Validation showed these markers' strong predictive capability, supporting their use in expanding immunotherapy eligibility beyond microsatellite instability status. The findings provide a promising approach for precision immunotherapy in colon cancer.

Liu et al. in their case report describes a rare malignant glomus tumor of the esophagus with metastases to the lungs and liver in a 49-year-old patient. The treatment combined Anlotinib, a multi-target anti-angiogenic agent, with Tislelizumab, an immunotherapy drug, based on genetic testing. This personalized approach achieved significant clinical improvement, including tumor size reduction and improved quality of life. However, the disease ultimately progressed, leading to the patient's death due to gastrointestinal bleeding. This case underscores the potential of precision medicine, especially the role of next-generation sequencing, in treating rare malignancies with targeted therapies.

Zhao et al. in their retrospective study developed a diagnostic model to differentiate gastric schwannomas from gastrointestinal stromal tumors (GISTs) using computed tomography (CT) imaging features. A nomogram was constructed based on factors such as growth pattern, absence of necrosis, presence of tumor-associated lymph nodes, and contrast differences across CT phases. The model, validated in multiple centers, demonstrated high diagnostic accuracy with an area under the curve (AUC) of 0.937 in the training set and 0.921 in the validation set. This non-invasive tool supports accurate preoperative identification, helping inform surgical decisions and improve patient.

Esmaeili et al. identifies the role of RNA modification, specifically N6-methyladenosine (m6A), in the progression of chronic inflammation-induced colorectal cancer (CRC) via the JAK-STAT3 and STAT5 signaling pathways. m6A modification impacts RNA stability, splicing, and translation, influencing gene expression linked to cancer cell proliferation and metastasis. Dysregulation of m6A and STAT pathways is shown to promote CRC by altering inflammatory responses, immune regulation, and epithelial integrity. The study emphasizes m6A's potential as a therapeutic target, proposing that targeting m6A and JAK-STAT interactions could offer new avenues for CRC treatment.

The last case report by Cui et al. discusses a patient with advanced hepatocellular carcinoma (HCC) and extrahepatic metastasis achieving complete remission through a combination of sintilimab (an immune checkpoint inhibitor) and sorafenib (an anti-angiogenic agent), followed by liver resection. After six cycles of the combination therapy, significant tumor reduction and metastasis resolution were observed, enabling surgical resection. Post-surgery, the patient has remained disease-free for over two years. This case suggests that combining immunotherapy and targeted therapy could downstage advanced HCC to allow curative resection, potentially leading to prolonged survival even in metastatic cases.

Luu et al. analyzes socioeconomic inequalities in gastric cancer (GC) screening in Korea, using data from the Korean National Cancer Screening Survey (2009–2022). Organized GC screening rates increased significantly, from 38.2% in 2009 to 70.8% in 2022, while opportunistic screening rates declined. Socioeconomic disparities were minimal in organized screenings, indicating equitable access across different income and education levels. However, substantial inequalities persisted in opportunistic screenings, with higher rates among wealthier and more educated individuals. The findings emphasize the role of organized screening programs in reducing inequalities and improving cancer screening accessibility across socioeconomic groups.

Our Research Topic highlights significant strides in precision oncology. Through innovative biomarkers, genetic profiling, and targeted therapies, these studies illustrate how molecular insights are reshaping diagnosis, treatment, and screening strategies, particularly for challenging cases like rare SMARCA4-deficient cancers and advanced-stage hepatocellular carcinoma. Research on socioeconomic disparities in gastric cancer screening also reveals the importance of equitable healthcare access, aligning molecular advancements with public health goals. Collectively, this Research Topic reinforces the critical role of molecular targets in transforming gastrointestinal cancer care toward personalized and accessible approaches by publishing 15 extremely valuable articles.

Author contributions

ZK: Conceptualization, Data curation, Writing – original draft. CB: Supervision, Writing – review & editing. SG: Supervision, Writing – review & editing.

Conflict of interest

The authors declare that the research was conducted in the absence of any commercial or financial relationships that could be construed as a potential conflict of interest.

The author(s) declared that they were an editorial board member of Frontiers, at the time of submission. This had no impact on the peer review process and the final decision.

Generative AI statement

We acknowledge AI for the preparation of Figure 1.

Publisher's note

frontiers | Frontiers in Oncology

TYPE Original Research
PUBLISHED 09 October 2023
DOI 10.3389/fonc.2023.1258347

OPEN ACCESS

EDITED BY
Zsolt Kovács,
George Emil Palade University of Medicine, Pharmacy, Sciences and Technology of Târgu Mureş, Romania

REVIEWED BY
Juan Du,
Nanjing Drum Tower Hospital, China
Zahra Hosseini-khah,
Mazandaran University of Medical Sciences, Iran
Ziv Radisavljevic,
Harvard Medical School, United States

*CORRESPONDENCE
Cantu Fang
3568076269@qq.com

†These authors share first authorship

RECEIVED 13 July 2023
ACCEPTED 15 September 2023
PUBLISHED 09 October 2023

CITATION
Liang Z, Liu L, Li W, Lai H, Li L, Wu J, Zhang H and Fang C (2023) Efficacy and safety of zolbetuximab for first-line treatment of advanced Claudin 18. 2-positive gastric or gastro-esophageal junction adenocarcinoma: a systematic review and meta-analysis of randomized controlled trials.
Front. Oncol. 13:1258347.
doi: 10.3389/fonc.2023.1258347

Efficacy and safety of zolbetuximab for first-line treatment of advanced Claudin 18. 2-positive gastric or gastro-esophageal junction adenocarcinoma: a systematic review and meta-analysis of randomized controlled trials

Zhanpeng Liang†, Liwen Liu†, Wenxia Li, Huiqin Lai, Luzhen Li, Jiaming Wu, Huatang Zhang and Cantu Fang*

Department of Oncology, Zhongshan Hospital of Traditional Chinese Medicine Affiliated to Guangzhou University of Traditional Chinese Medicine, Zhongshan, China

Objective: Zolbetuximab is a "first-in-class" chimeric lgG1 monoclonal antibody targeting Claudin18.2 (CLDN 18.2). In recent years, several important trials have been published showing that zolbetuximab is associated with improved prognosis in patients with advanced gastric or gastro-esophageal junction (G/GEJ) adenocarcinoma. This promises great change to the current treatment landscape. Therefore, we conducted a systematic review and meta-analysis to evaluate the efficacy and safety of zolbetuximab for first-line treatment of advanced CLDN 18. 2-positive G/GEJ adenocarcinoma.

Methods: The following databases were searched for relevant studies: PubMed, EMBASE, and Cochrane library (updated 10 June 2023). All randomized trials comparing zolbetuximab plus chemotherapy versus first-line chemotherapy alone for first-line treatment of advanced CLDN 18. 2-positive G/GEJ adenocarcinoma were eligible for inclusion. Data were analyzed using Review Manager 5.4.1 (Cochrane collaboration software). Primary outcomes and measures included overall survival (OS), progression-free survival (PFS), objective response rate (ORR), and adverse events (AEs).

Results: This systematic review and meta-analysis included three randomized controlled studies involving 1,402 patients (699 receiving zolbetuximab plus chemotherapy and 703 receiving chemotherapy alone). Compared with chemotherapy alone, zolbetuximab plus chemotherapy significantly improved OS (HR = 0.73; 95% CI: 0.68–0.84) and PFS (HR = 0.64; 95% CI: 0.50–0.82), but did not result in a higher ORR (RR = 0.92; 95% CI: 0.82–1.03). Further analysis of CLDN 18.2 expression showed a more significant benefit for OS (HR = 0.69; 95% CI: 0.55–0.87; p = 0.002) and PFS (HR = 0.61; 95% CI: 0.44–0.84; p = 0.003) from zolbetuximab in patients with high expression, while there was significant

benefit in patients with lower expression. In terms of AEs, zolbetuximab plus chemotherapy was associated with higher risk of grade 3 and higher AEs, but increased risk of nausea and vomiting were more common.

Conclusion: This systematic review and meta-analysis revealed that the effect of zolbetuximab plus chemotherapy was superior to that of chemotherapy alone for first-line treatment of advanced CLDN 18.2-positive G/GEJ adenocarcinoma. Thus, zolbetuximab plus chemotherapy represents a new first-line treatment for these patients. Zolbetuximab plus chemotherapy was associated with higher risk of grade 3 and higher AEs, but was generally manageable.

Systematic Review Registration: https://www.crd.york.ac.uk/prospero, identifier (CRD42023437126).

KEYWORDS

zolbetuximab, Claudin18.2, gastric or gastro-oesophageal junction adenocarcinoma, targeted therapy, meta-analysis

1 Introduction

Gastric and gastro-esophageal junction (G/GEJ) adenocarcinoma is an aggressive form of malignant tumor, and its occurrence has been increasing year-over-year. This not only threatens human health, but also exerts immense financial costs on society. Surgery is a common and effective treatment for resectable G/GEJ adenocarcinoma, but most patients have early local recurrence or distant metastasis after surgery. Advanced metastatic G/GEJ adenocarcinoma is a refractory tumor with poor prognosis, and a median overall survival of 9–14 months (1–5). At present, the first-line standard treatment is guided by three types of molecular characteristics: HER2-positive, HER2-negative, and dMMR/MSI-H. Anti-HER2-targeted therapy and immunotherapy have greatly improved the survival of HER2-positive and PD-L1 highly expressed gastric cancer patients (4, 5). However, it is difficult for HER2-negative patients with low PD-L1 expression to benefit from anti-HER2-targeted therapy and immunotherapy, resulting in its treatment being limited to chemotherapy, which is not an effective way to control the disease (6, 7). Changes in claudin at tight junctions are associated with tight adhesion impairment and epithelial cells' polarity. These structural abnormalities can lead to increased cell proliferation, epithelial–mesenchymal transformation, invasion, and metastasis (8–10). Despite significant advances in systemic treatment in recent years, the unmet need remains significant. As tumor therapy gradually transitions towards the macromolecular era, target selection for Claudin 18.2 (CLDN 18.2) has become the focus of new drug research and development. Studies have shown that gastric cancers with positive CLDN 18.2 expression (defined as more than 40% of tumor cells with IHC staining intensity ≥2+) account for approximately 49%–85% of gastric cancers (11–13), while gastric cancers with high CLDN 18.2 expression account for approximately 24%–36% of gastric cancers (14, 15). On account of its specificity and high expression in patients with gastric cancer, CLDN 18.2 has become an emerging target for developing new gastric cancer drugs, providing a new direction for targeted gastric cancer therapy. Zolbetuximab is a "first-in-class" chimeric lgG1 monoclonal antibody targeting CLDN 18.2 (16, 17), which is currently being developed for first-line treatment with HER2-negative CLDN 18.2 strongly positive locally advanced unresectable or metastatic G/GEJ adenocarcinoma. Recently, several important trials have been published, showing that first-line treatment with zolbetuximab plus chemotherapy can improve prognosis in patients with advanced G/GEJ adenocarcinoma (18–20). Therefore, we conducted a systematic review and meta-analysis to evaluate the efficacy and safety of zolbetuximab plus chemotherapy for first-line treatment of advanced CLDN 18. 2-positive G/GEJ adenocarcinoma.

Abbreviations: G/GEJ, gastric or gastro-esophageal junction; CLDN 18.2, Claudin18.2; OS, overall survival, PFS, progression-free survival; ORR, objective response rate; AEs, adverse events; RR, risk ratio; HR, hazard ratio.

2 Methods

This study was registered in the PROSPERO database (CRD42023437126) and was conducted according to the preferred reporting project for systematic review and meta-analysis (PRISMA) statement (21). The purpose of this study was to compare the efficacy and safety of zolbetuximab plus chemotherapy and chemotherapy alone for first-line treatment of advanced CLDN 18. 2-positive G/GEJ adenocarcinoma.

2.1 Eligibility criteria

The studies were screened independently by two authors. The inclusion criteria for selecting studies in this meta-analysis were as

follows: (1) patients with advanced CLDN 18.2-positive G/GEJ adenocarcinoma diagnosed cytologically or pathologically; (2) patients older than 18 years; (3) prospective phase II or III, randomized clinical trials evaluating the efficacy and safety of zolbetuximab; and (4) studies reporting at least one of the following outcomes: overall survival (OS), progression-free survival (PFS), objective response rate (ORR), and adverse events (AEs). CLDN 18.2 positivity was defined as moderate (2+) or strong CLDN18.2 staining (3+) in ≥40% of tumor cells. CLDN 18.2 high expression was defined as moderate (2+) or strong CLDN18.2 staining (3+) in ≥70% of tumor cells.

Exclusion criteria were as follows: (1) patients with early G/GEJ adenocarcinoma; (2) non-randomized controlled studies, basic studies, retrospective studies, case reports, duplicate publications, and studies for which no relevant data could be extracted; and (3) randomized controlled trials (RCTs) that were based on overlapping patients.

2.2 Search strategy

RCTs evaluating the efficacy and safety of zolbetuximab for first-line treatment of advanced CLDN 18. 2-positive G/GEJ adenocarcinoma were identified by a computerized search of PubMed, Embase, and Cochrane Library, using the following search terms: gastric cancer, gastro-esophageal adenocarcinoma, zolbetuximab, claudin 18.2, and IMAB362. The relevant bibliography of candidate articles was manually searched to identify additional studies. The proceedings of the American Society of Clinical Oncology (ASCO) and the European Society of Medical Oncology (ESMO)/European Cancer Congress (ECC) annual meetings were searched for abstract reports of relevant studies. If there was any overlapping data, the most complete and updated report was selected for inclusion in this meta-analysis. Additionally, the references from all eligible studies were manually reviewed to identify any other relevant studies.

2.3 Study selection and data extraction

Two experienced investigators independently screened the records for eligibility. Differences were resolved by consulting a third investigator. Titles and abstracts were browsed to complete an initial selection, followed by a full review of potentially eligible articles and the selection of eligible articles based on pre-established criteria.

Extracted data included baseline characteristics, sample size and interventions used, number of assessable patients, PFS, OS, ORR, grade 3, and higher AEs. Two investigators independently extracted relevant data and resolved any differences by consulting a third investigator. When multiple articles contained overlapping patient series, we prioritized the extraction of outcome data from the primary articles with the largest sample size for early outcomes and the articles with the longest follow-up duration for the late outcomes.

2.4 Outcome

The results of this review include OS, PFS, ORR, and AEs. OS is defined as the time from randomization to death. PFS is defined as the time from randomization to death or disease progression, whichever occurs first. ORR reflects the proportion of patients with complete response and partial response. AEs, graded according to National Cancer Institute Common Terminology Criteria for Adverse Events version 4.03, included all grades of AEs and grade 3 or higher AEs.

2.5 Risk of bias

Two investigators independently assessed the quality of the included trials using the Cochrane Collaboration tools with respect to randomized sequence generation, assignment concealment, blinding, incomplete outcome data, and selective outcome reporting (22). Any differences in quality assessment were resolved by consulting a third investigator.

2.6 Statistical analysis

Data were analyzed using Review Manager 5.4.1 (Cochrane Collaboration Software). These measures were either extracted directly from the articles or calculated. ORR and AEs were reported as risk ratio (RR) with corresponding 95% confidence intervals (95% CI). PFS and OS were reported as hazard ratio (HR) and had 95% CI. $p < 0.05$ was considered statistically significant. For effectiveness or side effects, HR or RR > 1 favored chemotherapy alone (control), while HR or RR < 1 favored zolbetuximab plus chemotherapy (experimental). Heterogeneity was tested with an I^2 statistic. Unless heterogeneity was high, in which case a random-effects model was used, a fixed-effects model is used for data synthesis (23, 24). Funnel plots and an Egger test were adopted to investigate the potential for publication bias (25). Subgroup analysis was conducted for age, sex, region, previous gastric cancer surgery, Lauren classification, tumor location, and number of metastatic sites.

3 Results

3.1 Study identification and quality assessment

A total of 255 articles were retrieved from PubMed, EMBASE, and the Cochrane Library. One additional article was retrieved from ASCO. Duplicates were excluded in 61 cases, and 180 cases were excluded by reading the title and abstract. Fifteen articles were read in full. Three RCTs (18–20), involving 1,402 patients, were included. A PRISMA flow chart describing study identification and selection is shown in Figure 1. Since all studies included were randomized, selection and loss bias were minimized. In one trial (18), blinding was not applied, which could have resulted in some bias.

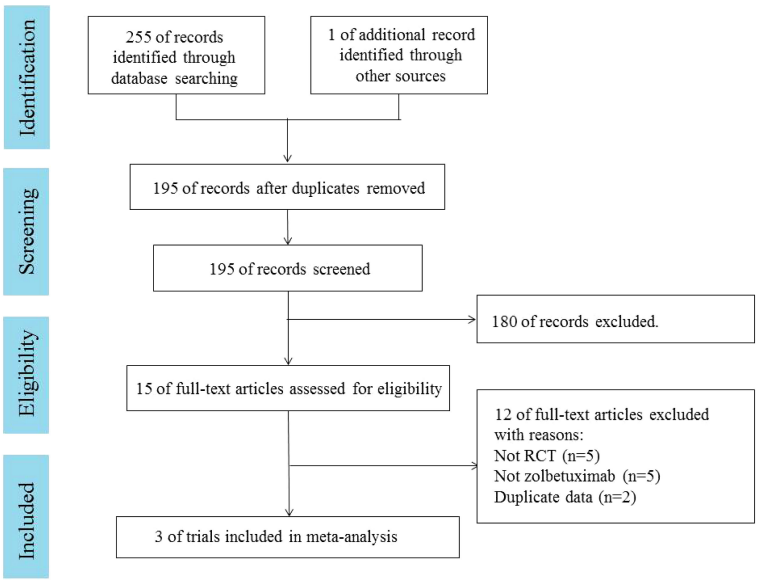

FIGURE 1
PRISMA flow diagram. RCT, randomized controlled trial.

3.2 Study and patient characteristics

FAST (18) was an open-label, randomized controlled, phase II clinical trial that enrolled 252 eligible patients between July 2012 and June 2014. SPOTLIGHT (19) is a multicenter, randomized, double-blind, phase III trial that enrolled 565 eligible patients between June 2018 and April 2022. GLOW (20) is also a multicenter, randomized, double-blind, phase III trial that enrolled 507 eligible patients between November 2018 and February 2022.

All three trials evaluated the prognostic effect of zolbetuximab plus chemotherapy as a first-line treatment for HER2-negative, CLDN 18.2-positive, locally advanced, unresectable or metastatic G/GEJ adenocarcinoma. However, the chemotherapy regimens differed among the three trials. The EOX regimen (epirubicin, oxaliplatin, and capecitabine) was used in FAST (18). In SPOTLIGHT (19), patients received chemotherapy with the mFOLFOX6 regimen (modified folinic acid [or levofolinate], fluorouracil, and oxaliplatin regimen). Patients were treated with chemotherapy with the CAPOX regimen (oxaliplatin and capecitabine) in GLOW (20).

FAST (18) evaluated two different doses of zolbetuximab. One was administered at a loading dose of 800 mg/m^2 in Cycle 1 followed by 600 mg/m^2 in subsequent cycles, which was the same as that used in SPOTLIGHT (19) and GLOW (20). The other was administered at 1,000 mg/m^2 per cycle. All three trials included patients with strong CLDN 18.2 positivity, with similar, but non-identical, definitions. The FAST (18) study enrolled advanced G/GEJ adenocarcinoma patients with moderate-to-strong CLDN18.2 expression in ≥40% tumor cells. SPOTLIGHT (19) and GLOW (20) enrolled advanced G/GEJ adenocarcinoma patients with moderate-to-strong CLDN 18.2 expression in ≥75% tumor cells. The baseline characteristics of the patients included in the study are detailed in Table 1.

3.3.1 Overall survival

Results for OS came from three studies (18–20) involving a total of 1,402 patients. The results showed that zolbetuximab plus chemotherapy further increased OS and reduced the risk of death by 27% (HR = 0.73; 95% CI: 0.68–0.84; $p < 0.00001$) (Figure 2). Additionally, low heterogeneity was found among the trials (χ^2 = 3.35; df = 3 [$p = 0.34$]; $I^2 = 11\%$). No significant benefit was found in the high-dose study, but the results still favored zolbetuximab plus chemotherapy after excluding the high-dose study (HR = 0.72; 95% CI: 0.62–0.83; $p < 0.00001$) (eFigure 1). Further analysis of CLDN 18.2 expression revealed that zolbetuximab plus chemotherapy was associated with significant OS benefit in patients with high expression, reducing the risk of death by 31% (HR = 0.69; 95% CI: 0.55–0.87; $p = 0.002$), but no significant benefit was found in patients with lower expression (eFigure 2).

3.3.2 Progression-free survival

Results for PFS were extracted from three studies (18–20), which included a total of 1,400 patients. Zolbetuximab plus chemotherapy was associated with higher PFS (HR = 0.68; 95% CI: 0.60–0.78; $p <$ 0.00001), and it reduced the risk of disease progression by 32%. Moderate heterogeneity was found among the trials ($\chi^2 = 5.24$; df = 3 [$p = 0.16$]; $I^2 = 43\%$) (Figure 3). Significant benefit was found in the high-dose study, and the results still favored zolbetuximab plus chemotherapy after excluding the high-dose study (HR = 0.64; 95% CI: 0.50–0.82; $p = 0.0005$) (eFigure 3). Further analysis of CLDN 18.2 expression showed that zolbetuximab plus chemotherapy was associated with a significant PFS benefit in patients with high expression, reducing the risk of death by 39% (HR = 0.61; 95% CI:

10.3389/fonc.2023.1258347

TABLE 1 Characteristics of included studies and patients.

	FAST			SPOTLIGHT		GLOW	
	Zolbetuximab (800/600 mg/m²)	Zolbetuximab (1,000 mg/m²)	Control	Zolbetuximab	Control	Zolbetuximab	Control
Key eligibility criteria	Moderate-to-strong CLDN18.2 expression in ≥40% tumor cells			Moderate-to-strong CLDN18.2 expression in ≥75% tumor cells		Moderate-to-strong CLDN18.2 expression in ≥75% tumor cells	
Schedule	Zolbetuximab (loading dose, 800 mg/m² then 600 mg/m² Q3W) + EOX	Zolbetuximab (1,000 mg/m² Q3W) + EOX	EOX	Zolbetuximab (loading dose, 800 mg/m² then 600 mg/m² Q3W) + mFOLFOX6	Placebo + mFOLFOX6	Zolbetuximab (loading dose, 800 mg/m² then 600 mg/m² Q3W) + CAPOX	Placebo + CAPOX
Patients randomized	77	85	84	283	282	254	253
Sex							
Male	47 (61%)	57 (67%)	56 (67%)	176 (62%)	175 (62%)	159 (63%)	156 (62%)
Female	30 (39%)	28 (33%)	28 (33%)	107 (38%)	107 (38%)	95 (37%)	97 (38%)
Median age (range)	59 (22–77)	60 (28–77)	57 (24–73)	62 (NA)	60 (NA)	61 (22–82)	59 (21–83)
Region	NA	NA	NA				
Asia				88 (31%)	89 (32%)	157 (62%)	158 (63%)
Non-Asia				195 (69%)	193 (68%)	97 (38%)	95 (37%)
Tumor site							
Stomach	62 (81%)	77 (91%)	68 (81%)	219 (77%)	210 (74%)	219 (86%)	209 (83%)
GEJ	15 (19%)	8 (9%)	16 (19%)	64 (23%)	72 (26%)	35 (14%)	44 (17%)
ECOG							
0	23 (30%)	27 (32%)	25 (30%)	125 (44%)	115 (41%)	108 (43%)	108 (43%)
1	54 (70%)	58 (68%)	59 (70%)	153 (54%)	163 (58%)	145 (57%)	142 (57%)
2	0	0	0	1 (<1%)	0	0	0
Missing	0	0	0	4 (1%)	4 (1%)	1 (<1%)	1 (<1%)
Lauren classification							
Diffuse	35 (45%)	39 (46%)	38 (45%)	82 (29%)	117 (41%)	87 (34%)	100 (40%)
Intestinal	26 (34%)	23 (27%)	27 (32%)	70 (25%)	66 (23%)	36 (14%)	41 (16%)
Mixed/ Unknown/ Other	16 (21%)	23 (17%)	19 (23%)	130 (46%)	95 (35%)	130 (51%)	112 (44%)
Missing	0	0	0	1 (<1%)	4 (1%)	1 (<1%)	0
Organs with metastases	NA	NA	NA				
0–2				219 (77%)	219 (78%)	189 (74%)	188 (74%)
3				64 (23%)	63 (22%)	65 (26%)	65 (26%)
Previous gastrectomy							
Yes	21 (27%)	24 (28%)	23 (27%)	84 (30%)	82 (29%)	179 (70%)	178 (70%)
No	56 (73%)	81 (72%)	61 (73%)	199 (70%)	200 (71%)	75 (30%)	75 (30%)

EOX, epirubicin, oxaliplatin, and capecitabine; mFOLFOX6, folinic acid (or levofolinate optionally in Japan), fluorouracil, and oxaliplatin; CAPOX, capecitabine and oxaliplatin; NA, not available; ECOG, performance status score; GEJ, gastro-esophageal junction.

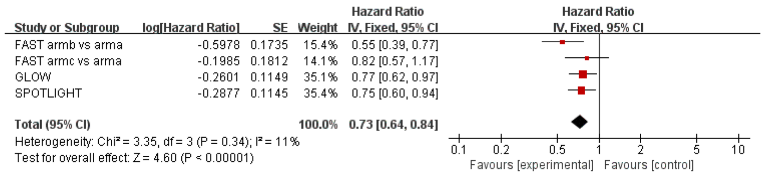

FIGURE 2
Assessment of overall survival. The diamond indicates best estimate of the true (pooled) outcome (with width indicating 95% CI); HR, hazard ratio; experimental stands for zolbetuximab plus chemotherapy; control stands for chemotherapy alone. Since there is low heterogeneity, a fixed-effects model is used.

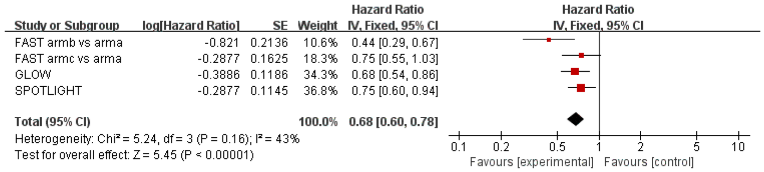

FIGURE 3
Assessment of progression-free survival. The diamond indicates best estimate of the true (pooled) outcome (with width indicating 95% CI); HR, hazard ratio; experimental stands for zolbetuximab plus chemotherapy; control stands for chemotherapy alone. Since there is moderate heterogeneity, a fixed-effects model is used.

0.44–0.84; $p = 0.003$), but no significant benefit was found in patients with lower expression (eFigure 4).

3.3.3 Objective response rate

ORR results were extracted from three studies (18–20) involving a total of 1,231 patients. Zolbetuximab plus chemotherapy did not result in a higher ORR (RR = 0.92; 95% CI: 0.82–1.03; $p = 0.016$) (Figure 4). Moderate heterogeneity was found among the trials ($\chi^2 = 3.15$; df = 2 [$p = 0.21$]; $I^2 = 37\%$).

3.3.4 Adverse events

Data on AEs were extracted from three studies (18–20) involving 1,394 patients. In terms of AEs of all grades, there was no statistical difference between zolbetuximab plus chemotherapy and chemotherapy alone due to the higher incidence of AEs (Table 2). In all of grade AEs by preferred terms, zolbetuximab plus chemotherapy was associated with a higher incidence of nausea, vomiting, neutropenia, decreased appetite, and peripheral edema. On the other hand, zolbetuximab plus chemotherapy resulted in a higher risk of grade 3 and higher AEs, including nausea, vomiting, neutropenia, decreased appetite, and weight loss. Further analysis showed that zolbetuximab plus chemotherapy significantly increased nausea and vomiting in patients who did not undergo gastrectomy compared with chemotherapy alone. In patients who had undergone gastrectomy, zolbetuximab plus chemotherapy increased vomiting, but not nausea (eFigures 5, 6). However, owing to the small amount of data included, the data on AEs were not yet mature.

3.4 Subgroup analysis of patients with CLDN 18.2 high expression

Overall, we found differences in subgroup analysis of age, region, number of metastatic sites, primary sites, and Lauren classification. However, no differences were observed in subgroup analyses of sex or previous gastrectomy. In the ≤65 years old, Asian, 0–2 metastatic sites, stomach, diffuse, and intestinal subgroups, zolbetuximab significantly improved OS and PFS. However, in the > 65 years old, non-Asian, ≥3 metastatic sites, GEJ, and mixed or other subgroups, zolbetuximab did not lead to higher OS or PFS (Table 3 and eFigures 7, 8).

3.5 Sensitivity analyses and publication bias

Sensitivity analysis via study-by-study removal showed that no study affected the overall effect of the efficacy and safety endpoints, meaning that all of the results were stable. Qualitative assessment was performed by assessing various measures for each individual study using the Cochrane Risk of Bias Tool. Overall, these trials were considered to have low risk of bias. The main source of bias was the lack of blinding in one study (18). Funnel plot asymmetry is not obvious to any efficacy endpoints (eFigures 9–11). Egger regression test results showed that OS ($p = 0.579$), PFS ($p = 0.233$), and ORR ($p = 0.243$) had a low potential for publication bias.

4 Discussion

In unresectable G/GEJ adenocarcinoma, first-line treatment consists of chemotherapy plus either immunotherapy for HER2-negative CPS-PDL1-positive (≥5) tumors (5) or trastuzumab for HER2-positive disease (4). However, the prognosis for HER2-negative and CPS-PDL1 positive (<5) advanced gastric cancer patients treated mainly by chemotherapy is still not optimistic. This indicates an urgent need for new and more efficient therapies for advanced gastric cancer indications in the clinic. CLDN 18.2 is a

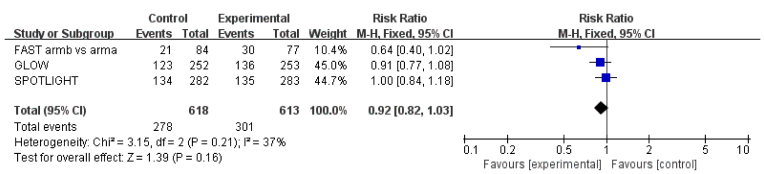

FIGURE 4
Assessment of objective response rate. The diamond indicates best estimate of the true (pooled) outcome (with width indicating 95% CI); RR, risk ratio; experimental stands for zolbetuximab plus chemotherapy; control stands for chemotherapy alone. Since there is moderate heterogeneity, a fixed-effects model is used.

TABLE 2 Results of adverse events.

Toxicity	All grade AEs (risk ratio)	No. of trials	Grade 3+ AEs (risk ratio)	No. of trials
Any adverse event	1.00 [0.98 1.01]	4	1.08 [1.02, 1.15]	3
Gastrointestinal disorders				
Nausea	1.23 [1.09, 1.39]	4	2.59 [1.70, 3.94]	3
Vomiting	1.66 [1.32, 2.10]	4	3.02 [2.00, 4.56]	3
Diarrhea	0.79 [0.55, 1.14]	4	1.01 [0.61, 1.65]	3
Hematologic disorders				
Anemia	1.07 [0.91, 1.26]	4	1.01 [0.72, 1.41]	3
Neutropenia	1.22 [1.04, 1.43]	4	1.39 [1.09, 1.76]	3
Thrombocytopenia	0.91 [0.62, 1.33]	4	0.80 [0.37, 1.73]	3
Metabolism and nutrition disorder				
Weight loss	1.20 [0.87, 1.65]	4	2.62 [1.04, 6.62]	3
Increased ALT	0.73 [0.49, 1.09]	4	0.41 [0.16, 1.03]	3
Increased AST	0.91 [0.73, 1.13]	4	0.81 [0.38, 1.70]	3
Increased GGT	1.47 [0.73, 2.98]	2	Not estimable	2
Nervous system disorders				
Paresthesia	1.04 [0.76, 1.43]	3	Not estimable	
Headache	0.81 [0.59, 1.12]	3	0.74 [0.14, 3.81]	2
General disorders				
Fatigue	1.00 [0.76, 1.30]	4	1.13 [0.67, 1.89]	3
Asthenia	1.08 [0.88, 1.34]	4	1.07 [0.67, 1.71]	3
Other disorders				
Decreased appetite	1.23 [1.01, 1.48]	4	2.17 [1.20, 3.93]	3
Upper abdominal pain	0.68 [0.27, 1.72]	3	1.93 [0.08, 45.83]	2
Abdominal pain	0.83 [0.68, 1.02]	4	1.18 [0.55, 2.52]	3
Alopecia	1.34 [0.91, 1.99]	2	Not estimable	
Pyrexia	0.92 [0.59, 1.43]	4	1.66 [0.22, 12.53]	2
Peripheral edema	2.14 [1.52, 3.01]	4	4.98 [0.24, 103.31]	2
Palmar–plantar syndrome	0.93 [0.54, 1.62]	3	Not estimable	

ALT, alanine aminotransferase; AST, aspartate aminotransferase; GGT, gamma-glutamyl transferase.

membrane protein involved in maintaining intercellular adhesion and connection. It has two subtypes: Claudin 18.1 and CLDN 18.2. The former is mainly expressed in normal lung cells, while the latter is only expressed in the differentiated epithelial cells of gastric mucosa (26). Jovov et al. (27) recently described how CLDN18.2 is activated during the metaplastic transition from the stratified squamous cell epithelium of the esophagus to the specialized columnar epithelium. This occurs in the context of gastro-esophageal reflux and predisposes subjects to distal esophageal adenocarcinoma, suggesting that ectopic activation of CLDN 18.2 may be an early event of esophageal adenocarcinoma. Moreover, various Claudins in human cancers have a wide range of expression patterns. CLDN3, 4, and 7 are highly expressed in most normal epithelial cells and their corresponding tumors (28). In contrast to CLDN 18.2, these claudins are widely expressed in healthy tissues. Therefore, therapy targeting of these claudins inevitably leads to significant toxicity. In contrast, other studies have shown that CLDN 18.2 is absent in the stem cell region of gastric cancer, but its exclusive expression in differentiated gastric cells, combined with transient gastrointestinal toxicity, is a common and manageable adverse event (13), making this molecule an effective drug target for G/GEJ adenocarcinoma. Zolbetuximab is highly selective against CLDN 18.2, both *in vivo* and *in vitro*. It binds to cancer-specific targets expressed primarily in tumor cells, and mediates tumor cell death through antibody-dependent cell-mediated cytotoxicity (ADCC) and complement-dependent cytotoxicity (CDC) (29).

10.3389/fonc.2023.1258347

TABLE 3 Results of subgroup analysis.

Subgroup	Overall survival (HR)	No. of trials	*p*-value	Progression-free survival (HR)	No. of trials	*p*-value
Age						
≤65	0.70 [0.58, 0.85]	2	0.0003	0.68 [0.54, 0.86]	2	0.001
>65	0.84 [0.64, 1.10]	2	0.20	0.79 [0.60, 1.05]	2	0.11
Sex						
Male	0.77 [0.63, 0.93]	2	0.008	0.73 [0.60, 0.89]	2	0.002
Female	0.73 [0.56, 0.95]	2	0.02	0.71 [0.54, 0.92]	2	0.01
Region						
Asia	0.66 [0.53, 0.83]	2	0.0004	0.58 [0.45, 0.73]	2	<0.00001
Non-Asia	0.84 [0.67, 1.03]	2	0.10	0.88 [0.71, 1.09]	2	0.23
Number of metastatic sites						
0–2	0.74 [0.61, 0.89]	2	0.001	0.71 [0.59, 0.86]	2	0.0003
≥3	0.78 [0.58, 1.05]	2	0.10	0.76 [0.56, 1.02]	2	0.07
Primary site						
Stomach	0.67 [0.57, 0.78]	3	<0.00001	0.61 [0.50, 0.75]	3	<0.00001
GEJ	0.90 [0.57, 1.44]	3	0.67	0.99 [0.57, 1.72]	3	0.97
Lauren classification						
Diffuse	0.61 [0.40, 0.94]	3	0.02	0.57 [0.36, 0.89]	3	0.01
Intestinal	0.64 [0.47, 0.87]	3	0.005	0.60 [0.44, 0.83]	3	0.002
Mixed or other	0.74 [0.41, 1.33]	3	0.31	0.79 [0.55, 1.15]	3	0.22
Previous gastrectomy						
No	0.50 [0.35, 0.73]	3	0.0003	0.56 [0.38, 0.83]	3	0.004
Yes	0.82 [0.69, 0.98]	3	0.003	0.74 [0.61, 0.89]	3	0.001

HR, Hazard ratio; GEJ, Gastro-esophageal junction.

Recent clinical trials have shown that zolbetuximab is associated with significant improvement in the prognosis of patients with advanced G/GEJ cancer. This verifies the druggability of the CLDN 18.2 target (18–20). Therefore, we performed a meta-analysis to evaluate the efficacy and safety of zolbetuximab in advanced CLDN 18. 2-positive G/GEJ adenocarcinoma. The pooled results showed that zolbetuximab plus chemotherapy for first-line treatment significantly improved PFS and OS in patients with advanced unresectable G/GEJ adenocarcinoma compared to chemotherapy alone.

A phase I study in Japan evaluating zolbetuximab monotherapy in previously treated Japanese patients with CLDN 18.2-positive locally advanced G/GEJ adenocarcinoma showed that 11 of 17 patients achieved stable disease (30). MONO, a phase II study, showed that zolbetuximab monotherapy in recurrent/refractory CLDN 18.2-positive gastric cancer had an ORR of 9% and a clinical benefit rate of 23% (31). The finding that the single drug zolbetuximab has certain anti-tumor activities is not novel. Preclinical studies found that chemotherapy agents upregulated CLDN 18.2 expression and enhance zolbetuximab-induced ADCC (17, 29). These results suggest that zolbetuximab combined with chemotherapy may have superior efficacy. Additionally, the ILUSTRO trial showed that zolbetuximab plus mFOLFOX6 for first-line treatment showed positive results (32). These data support further development of zolbetuximab as a first-line treatment. FAST is the first RCT to evaluate the efficacy of zolbetuximab, compared to zolbetuximab plus EOX and EOX alone. OS and PFS showed significant improvement in the combined treatment group, indicating that zolbetuximab may be an effective supplement to chemotherapy (18). Stratified analysis of CLDN 18.2 expression intensity showed that patients with high CLDN 18.2 expression benefited more from zolbetuximab, but patients with lower CLDN 18.2 expression did not benefit. Therefore, two phase III trials, SPOTLIGHT and GLOW, only included patients with advanced G/GEJ cancer with high CLDN 18.2 expression (19, 20). Our meta-analysis also stratified CLDN 18.2 expression intensity, and the results were consistent with those of the FAST trial. However, since only one study reported survival data in patients with lower CLDN 18.2 expression, further clinical trials are needed to explore CLDN 18.2 expression's effect on zolbetuximab efficacy. On the other hand, FAST evaluated two different doses of zolbetuximab. Interestingly, high doses of zolbetuximab did not improve survival in CLDN 18.2-

positive patients with advanced gastric cancer (18). Our meta-analysis showed that the pooled results were still favorable for zolbetuximab after excluding studies with high doses of zolbetuximab, possibly because high doses of zolbetuximab led to higher discontinuation rates and reduced treatment duration, thus curbing its efficacy. The included studies used different chemotherapy regimens, but they were all approved for first-line treatment of gastric cancer, and their benefits in first-line gastric cancer treatment were similar. In addition, baseline characteristics were balanced in both groups of patients enrolled in the trial. Notably, zolbetuximab plus chemotherapy reduced the risk of death similarly in the SPOTLIGHT (19) and GLOW (20) trials, and low heterogeneity was observed in the outcomes of PFS and OS in our study. Therefore, different chemotherapy regimens have little effect on the efficacy of zolbetuximab. On the other hand, chemotherapy duration does affect zolbetuximab efficacy. Since chemotherapy can boost zolbetuximab's effectiveness, the longer the chemotherapy treatment duration, the more effective zolbetuximab may be. The median exposure times for chemotherapy in the three trials included in our study were similar (18–20), and thus, the difference in this effect was small.

In the analysis of 523 cases of G/GEJ cancer tissue samples, COATI et al. (33) found that the difference in CLDN 18.2 expression was related to tumor location, Lauren classification, and Epstein–Barr virus infection. In addition, studies (14, 34) have shown that the CLDN 18.2 expression is also correlated with age, tumor stage, peritoneal metastasis, and liver metastasis. In contrast, other studies (11, 33) have shown that CLDN 18.2 expression is not associated with race, age, sex, or tumor stage. To further explore baseline characteristics' effects on zolbetuximab efficacy, we performed a subgroup analysis. In the ≤65 years old, Asian, 0–2 metastatic sites, stomach, diffuse, and intestinal subgroups, zolbetuximab plus chemotherapy significantly improved OS and PFS. However, in the > 65 years old, non-Asian, ≥3 metastatic sites, GEJ, and mixed or other subgroups, zolbetuximab did not lead to higher OS or PFS. Our meta-analysis indicated that zolbetuximab's efficacy appeared to be correlated with age, region, number of metastatic sites, primary sites, and Lauren classification. It is worth noting that the results of subgroup analysis should be interpreted with caution because the subgroup analysis data are still immature.

For AEs, owing to the numerous side effects of chemotherapy, the incidence of adverse events of all grades for chemotherapy alone and zolbetuximab plus chemotherapy were high, and there was no statistical difference between the two groups. Thus, it was difficult to evaluate zolbetuximab's safety. Therefore, we conducted a summary analysis of grade 3 and higher AEs. Zolbetuximab plus chemotherapy were found to be associated with higher risk of grade 3 and higher AEs, but mainly with an increased risk of nausea and vomiting, which can be alleviated with preventative drugs and with treatment. Patients in the combination treatment group were associated with longer drug treatment duration, leading to longer exposure to chemotherapy, which may have contributed to the increased risk of nausea and vomiting. Overall, the adverse effects of zolbetuximab were manageable. Further analysis showed that zolbetuximab plus chemotherapy significantly increased nausea and vomiting in patients who had not undergone gastrectomy compared with chemotherapy alone. In patients with previous gastrectomy, zolbetuximab plus chemotherapy increased the incidence of vomiting, but not nausea. Looking at incidence alone, in the three included trials, patients treated with zolbetuximab who had not undergone gastrectomy had a higher incidence of nausea and vomiting than patients who had previously undergone gastrectomy (18–20). Target-specific organ toxicity based on a drug-related pharmacodynamic mechanism, a higher antigen load in the stomach with the primary tumor still present, or the absence of an intact stomach as an effector organ for vomiting may be explanations for this (31). In FAST (18), no treatment-related fatal AEs occurred, and in SPOTLIGHT, five and four treatment-related fatal AEs were reported in the zolbetuximab plus chemotherapy and chemotherapy alone groups, respectively (19). In addition, treatment-related fatal AEs in the GLOW trial were reported in six and seven cases in the zolbetuximab plus chemotherapy and chemotherapy alone groups, respectively (20). Treatment-related fatal AEs were not statistically different between the two groups.

As a target that has attracted much attention from the global industry in recent years, CLDN 18.2 has been shown to be expressed in various cancer types, including gastric, pancreatic, and esophageal cancer (13). Although zolbetuximab is the first monoclonal antibody to target CLDN 18.2, a major limitation of its efficacy is that it can only be used in patients with high Claudin18.2 expression and is very limited in patients with low CLDN 18.2 expression. Osemitamab (TST001) is a monoclonal antibody with a higher affinity for CLDN 18.2 (35). ASCO recently published a prospective phase II clinical study of Osemitamab to explore the safety and efficacy of TST001 in combination with capecitabine and oxaliplatin (CAPOX) as a first-line treatment for advanced G/GEJ cancer. A total of 42 patients had measurable lesions, of which 28 (66.7%) achieved a partial response (36). Of note, G/GEJ cancer patients with low CLDN18.2 expression (≥10% of tumor cells with CLDN18.2 membrane staining intensity ≥1+) still benefitted from Osemitamab. However, this was a phase II clinical study with a small sample size, and more large RCT s are needed for further verification. In SPOTLIGHT, patients showed significant improvements in OS and PFS regardless of the PD-L1 expression level (19). The combination of anti-CLDN 18.2 drugs and anti-PD-1 drugs may also become a new therapeutic direction. An ongoing phase II study (ILUSTRO) is evaluating zolbetuximab in combination with nivolumab for first-line treatment of gastric cancer. It is expected that the results will provide a meaningful reference for clinical practice.

Our meta-analysis has some limitations. First, we only included a small number of trials. Second, in one trial, blindness was not used, which may have introduced some bias. Third, there were insufficient data to assess zolbetuximab's efficacy in patients with lower CLDN18.2 expression. Thus, the benefit of zolbetuximab was still limited to patients with high CLDN18.2 expression. Fourth, we did not have access to individual data for logistic regression to adjust the variables such as age, tumor site, previous gastrectomy, etc.

5 Conclusion

Our meta-analysis showed that zolbetuximab plus chemotherapy for first-line treatment significantly improved PFS and OS in patients with advanced CLDN 18.2-positive G/GEJ adenocarcinoma compared to using chemotherapy alone. Patients with high CLDN 18.2 expression were more likely to benefit from additional zolbetuximab. Zolbetuximab was associated with higher risk of grade 3 and higher AEs, but mainly with an increased risk of nausea and vomiting, which can be alleviated with drug prevention and treatment. Additional studies are needed to evaluate the effect of CLDN 18.2 expression and baseline characteristics on zolbetuximab's efficacy.

Data availability statement

The original contributions presented in the study are included in the article/Supplementary Material. Further inquiries can be directed to the corresponding author.

Author contributions

ZL: Conceptualization, Data curation, Formal Analysis, Investigation, Methodology, Project administration, Software, Writing – original draft. LWL: Conceptualization, Data curation, Formal Analysis, Funding acquisition, Investigation, Methodology, Software, Writing – original draft. WL: Formal Analysis, Methodology, Software, Writing – review & editing. HL: Data curation, Formal Analysis, Methodology, Software, Writing – review & editing. LZL: Resources, Supervision, Validation, Visualization, Writing – review & editing. JW: Resources, Supervision, Validation, Visualization, Writing – review & editing. HZ: Resources, Supervision, Validation, Visualization, Writing – review & editing. CF: Conceptualization, Funding acquisition, Project administration, Resources, Software, Supervision, Validation, Visualization, Writing – review & editing.

Funding

The author(s) declare that no financial support was received for the research, authorship, and/or publication of this article.

Conflict of interest

The authors declare that the research was conducted in the absence of any commercial or financial relationships that could be construed as a potential conflict of interest.

Publisher's note

Supplementary material

The Supplementary Material for this article can be found online at: https://www.frontiersin.org/articles/10.3389/fonc.2023.1258347/full#supplementary-material

References

1. Van Cutsem E, Moiseyenko VM, Tjulandin S, Majlis A, Constenla M, Boni C, et al. Phase III study of docetaxel and cisplatin plus fluorouracil compared with cisplatin and fluorouracil as first-line therapy for advanced gastric cancer: a report of the V325 Study Group. *J Clin Oncol* (2006) 24:4991–7. doi: 10.1200/JCO.2006.06.8429

2. Al-Batran SE, Hartmann JT, Probst S, Schmalenberg H, Hollerbach S, Hofheinz R, et al. Phase III trial in metastatic gastroesophageal adenocarcinoma with fluorouracil, leucovorin plus either oxaliplatin or cisplatin: a study of the Arbeitsgemeinschaft Internistische Onkologie. *J Clin Oncol* (2008) 26:1435–42. doi: 10.1200/JCO.2007.13.9378

3. Kang YK, Kang WK, Shin DB, Chen J, Xiong J, Wang J, et al. Capecitabine/cisplatin versus 5-fluorouracil/cisplatin as first-line therapy in patients with advanced gastric cancer: a randomised phase III noninferiority trial. *Ann Oncol* (2009) 20:666–73. doi: 10.1093/annonc/mdn717

4. Bang YJ, Van Cutsem E, Feyereislova A, Chung HC, Shen L, Sawaki A, et al. Trastuzumab in combination with chemotherapy versus chemotherapy alone for treatment of HER2-positive advanced gastric or gastro-oesophageal junction cancer (ToGA): a phase 3, open-label, randomised controlled trial. *Lancet* (2010) 376:687–97. doi: 10.1016/S0140-6736(10)61121-X

5. Janjigian YY, Shitara K, Moehler M, Garrido M, Salman P, Shen L, et al. First-line nivolumab plus chemotherapy versus chemotherapy alone for advanced gastric, gastro-oesophageal junction, and oesophageal adenocarcinoma (CheckMate 649): a randomised, open-label, phase 3 trial. *Lancet* (2021) 398:27–40. doi: 10.1016/S0140-6736(21)00797-2

6. Zhao JJ, Yap DWT, Chan YH, Tan BKJ, Teo CB, Syn NL, et al. Low programmed death-ligand 1-expressing subgroup outcomes of first-line immune checkpoint inhibitors in gastric or esophageal adenocarcinoma. *J Clin Oncol* (2022) 40:392–402. doi: 10.1200/JCO.21.01862

7. Xie T, Zhang Z, Zhang X, Qi C, Shen L, Peng Z. Appropriate PD-L1 cutoff value for gastric cancer immunotherapy: A systematic review and meta-analysis. *Front Oncol* (2021) 11:646355. doi: 10.3389/fonc.2021.646355

8. Turksen K. Claudins and cancer stem cells. *Stem Cell Rev Rep* (2011) 7:797–8. doi: 10.1007/s12015-011-9267-1

9. Shin K, Fogg VC, Margolis B. Tight junctions and cell polarity. *Annu Rev Cell Dev Biol* (2006) 22:207–35. doi: 10.1146/annurev.cellbio.22.010305.104219

10. Hollande F, Blanc EM, Bali JP, Whitehead RH, Pelegrin A, Baldwin GS, et al. HGF regulates tight junctions in new nontumorigenic gastric epithelial cell line. *Am J Physiol Gastrointest Liver Physiol* (2001) 280:G910–21. doi: 10.1152/ajpgi.2001.280.5.G910

11. Rohde C, Yamaguchi R, Mukhina S, Sahin U, Itoh K, Türeci Ö. Comparison of Claudin 18.2 expression in primary tumors and lymph node metastases in Japanese patients with gastric adenocarcinoma. *Jpn J Clin Oncol* (2019) 49:870–6. doi: 10.1093/jjco/hyz068

12. Qi C, Gong J, Li J, Liu D, Qin Y, Ge S, et al. Claudin18.2-specific CAR T cells in gastrointestinal cancers: phase 1 trial interim results. *Nat Med* (2022) 28:1189–98. doi: 10.1038/s41591-022-01800-8

13. Sahin U, Koslowski M, Dhaene K, Usener D, Brandenburg G, Seitz G, et al. Claudin-18 splice variant 2 is a pan-cancer target suitable for therapeutic antibody development. *Clin Cancer Res* (2008) 14:7624–34. doi: 10.1158/1078-0432.CCR-08-1547

14. Pellino A, Brignola S, Riello E, Niero M, Murgioni S, Guido M, et al. Association of CLDN18 protein expression with clinicopathological features and prognosis in advanced gastric and gastroesophageal junction adenocarcinomas. *J Pers Med* (2021) 11:1095. doi: 10.3390/jpm11111095

15. Wang Z, Yang Y, Cui Y, Wang C, Lai Z, Li Y, et al. Tumor-associated macrophages regulate gastric cancer cell invasion and metastasis through TGFβ2/NF-κB/Kindlin-2 axis. *Chin J Cancer Res* (2022) 32:72–88. doi: 10.21147/j.issn.1000-9604.2022.01.07

16. Sahin U, Schuler M, Richly H, Bauer S, Krilova A, Dechow T, et al. A phase I dose-escalation study of IMAB362 (Zolbetuximab) in patients with advanced gastric and gastro-oesophageal junction cancer. *Eur J Cancer.* (2018) 100:17–26. doi: 10.1016/j.ejca.2018.05.007

17. Türeci Ö, Mitnacht-Kraus R, Wöll S, Yamada T, Sahin U. Characterization of zolbetuximab in pancreatic cancer models. *Oncoimmunology* (2019) 8:e1523096. doi: 10.1080/2162402X.2018.1523096.-

18. Sahin U, Türeci Ö, Manikhas G, Lordick F, Rusyn A, Vynnychenko I, et al. FAST: a randomised phase II study of zolbetuximab (IMAB362) plus EOX versus EOX alone for first-line treatment of advanced CLDN18.2-positive gastric and gastro-oesophageal adenocarcinoma. *Ann Oncol* (2021) 32:609–19. doi: 10.1016/j.annonc.2021.02.005

19. Shitara K, Lordick F, Bang YJ, Enzinger P, Ilson D, Shah MA, et al. Zolbetuximab plus mFOLFOX6 in patients with CLDN18.2-positive, HER2-negative, untreated, locally advanced unresectable or metastatic gastric or gastro-oesophageal junction adenocarcinoma (SPOTLIGHT): a multicentre, randomised, double-blind, phase 3 trial. *Lancet* (2023) 401:1655–68. doi: 10.1016/S0140-6736(23)00620-7

20. Shitara K, Ajani JA, Bang Y-J, Enzinger PC, Ilson DH, Lordick F, et al. Zolbetuximab + CAPOX in 1L claudin-18.2+ (CLDN18.2+)/HER2– locally advanced (LA) or metastatic gastric or gastroesophageal junction (mG/GEJ) adenocarcinoma: Primary phase 3 results from GLOW. *J Clin Oncol* (2023) 41:405736–. doi: 10.1200/JCO.2023.41.36_suppl.405736

21. Liberati A, Altman DG, Tetzlaff J, Mulrow C, Gøtzsche PC, Ioannidis JP, et al. The PRISMA statement for reporting systematic reviews and meta-analyses of studies that evaluate healthcare interventions: explanation and elaboration. *Bmj* (2009) 339:b2700. doi: 10.1136/bmj.b2700

22. Higgins JP, Altman DG, Gøtzsche PC, Jüni P, Moher D, Oxman AD, et al. The Cochrane Collaboration's tool for assessing risk of bias in randomised trials. *Bmj* (2011) 343:d5928. doi: 10.1136/bmj.d5928

23. Higgins JP, Thompson SG, Deeks JJ, Altman DG. Measuring inconsistency in meta-analyses. *Bmj* (2003) 327:557–60. doi: 10.1136/bmj.327.7414.557

24. Higgins JP, Thompson SG. Quantifying heterogeneity in a meta-analysis. *Stat Med* (2002) 21:1539–58. doi: 10.1002/sim.1186

25. Egger M, Davey Smith G, Schneider M, Minder C. Bias in meta-analysis detected by a simple, graphical test. *Bmj* (1997) 315:629–34. doi: 10.1136/bmj.315.7109.629

26. Türeci O, Koslowski M, Helftenbein G, Castle J, Rohde C, Dhaene K, et al. Claudin-18 gene structure, regulation, and expression is evolutionary conserved in mammals. *Gene* (2011) 481:83–92. doi: 10.1016/j.gene.2011.04.007

27. Jovov B, Van Itallie CM, Shaheen NJ, Carson JL, Gambling TM, Anderson JM, et al. Claudin-18: a dominant tight junction protein in Barrett's esophagus and likely contributor to its acid resistance. *Am J Physiol Gastrointest Liver Physiol* (2007) 293:G1106–13. doi: 10.1152/ajpgi.00158.2007

28. Hewitt KJ, Agarwal R, Morin PJ. The claudin gene family: expression in normal and neoplastic tissues. *BMC Cancer.* (2006) 6:186. doi: 10.1186/1471-2407-6-186

29. Mitnacht-Kraus R, Kreuzberg M, Utsch M, Sahin U, Türeci Ö. Preclinical characterization of IMAB362 for the treatment of gastric carcinoma. *Ann Oncol* (2017) 28:v126. doi: 10.1093/annonc/mdx367.012

30. Shitara K, Kawazoe A, Hirakawa A, Nakanishi Y, Furuki S, Fukuda M, et al. Phase 1 trial of zolbetuximab in Japanese patients with CLDN18.2+ gastric or gastroesophageal junction adenocarcinoma. *Cancer Sci* (2023) 114:1606–15. doi: 10.1111/cas.15684

31. Türeci O, Sahin U, Schulze-Bergkamen H, Zvirbule Z, Lordick F, Koeberle D, et al. A multicentre, phase IIa study of zolbetuximab as a single agent in patients with recurrent or refractory advanced adenocarcinoma of the stomach or lower oesophagus: the MONO study. *Ann Oncol* (2019) 30:1487–95. doi: 10.1093/annonc/mdz199

32. Klempner SJ, Lee KW, Shitara K, Metges JP, Lonardi S, Ilson DH, et al. ILUSTRO: phase 2 multicohort trial of zolbetuximab in patients with advanced or metastatic claudin 18.2-positive gastric or gastroesophageal junction adenocarcinoma. *Clin Cancer Res* (2023). doi: 10.1158/1078-0432.CCR-23-0204

33. Coati I, Lotz G, Fanelli GN, Brignola S, Lanza C, Cappellesso R, et al. Claudin-18 expression in oesophagogastric adenocarcinomas: a tissue microarray study of 523 molecularly profiled cases. *Br J Cancer.* (2019) 121:257–63. doi: 10.1038/s41416-019-0508-4

34. Kim SR, Shin K, Park JM, Lee HH, Song KY, Lee SH, et al. Clinical significance of CLDN18.2 expression in metastatic diffuse-type gastric cancer. *J Gastric Cancer* (2020) 20:408–20. doi: 10.5230/jgc.2020.20.e33

35. Teng F, Gu Y, Chai H, Guo H, Li H, Wu X, et al. Abstract 5183: The preclinical characterization of TST001, a novel humanized anti-claudin18.2 mAb with enhanced binding affinity and anti-tumor activity. *Cancer Res* (2020) 80:5183–. doi: 10.1158/1538-7445.AM2020-5183

36. *TRANSCENTA, Osemitamab plus Capecitabine and Oxaliplatin (CAPOX) as the First-LineTreatment of Advanced G/GEJ Cancer -Updated Efficacy Data per Claudin 18.2 Expression Level from Study TranStar102/TST001-1002-Cohort C* . Available at: https://www.transcenta.com/Scientific_Publications.html (Accessed 20 June 2023).

frontiers | Frontiers in Public Health

TYPE Original Research
PUBLISHED 09 October 2023
DOI 10.3389/fpubh.2023.1256525

OPEN ACCESS

EDITED BY
Simona Gurzu,
George Emil Palade University of Medicine, Pharmacy, Sciences and Technology of Târgu Mureş, Romania

REVIEWED BY
Bibha Dhungel,
Waseda University, Japan
Seyed Aria Nejadghaderi,
Tabriz University of Medical Sciences, Iran

*CORRESPONDENCE
Kui Son Choi
✉ kschoi@ncc.re.kr

RECEIVED 11 July 2023
ACCEPTED 15 September 2023
PUBLISHED 09 October 2023

CITATION
Luu XQ, Lee K, Jun JK, Suh M and Choi KS (2023) Socioeconomic inequality in organized and opportunistic screening for gastric cancer: results from the Korean National Cancer Screening Survey 2009–2022. *Front. Public Health* 11:1256525. doi: 10.3389/fpubh.2023.1256525

Socioeconomic inequality in organized and opportunistic screening for gastric cancer: results from the Korean National Cancer Screening Survey 2009–2022

Xuan Quy Luu[1], Kyeongmin Lee[1], Jae Kwan Jun[2], Mina Suh[2] and Kui Son Choi[1]*

[1]Department of Cancer Control and Population Health, Graduate School of Cancer Science and Policy, National Cancer Center, Goyang, Republic of Korea, [2]National Cancer Control Institute, National Cancer Center, Goyang, Republic of Korea

Objectives: This study aimed to evaluate the socioeconomic inequality in gastric cancer (GC) screening in Korea. Socioeconomic inequality was assessed using both organized and opportunistic screening according to income and educational level.

Methods: GC screening data were obtained from the 2009–2022 Korean National Cancer Screening Survey. The final analysis included 47,163 cancer-free men and women. The weighted cancer screening rate was estimated using joinpoint regression. The inequality indices were measured in terms of both the absolute slope index of inequality (SII) and the relative index of inequality (RII) using the Poisson regression model.

Results: The organized screening rate for GC increased from 38.2% in 2009 to 70.8% in 2022, whereas the opportunistic screening rate decreased from 18.8 to 4.5%. Regarding educational inequality, a negative SII value was observed [−3.5, 95% confidence interval (CI), −7.63–0.83%] in organized screening, while a positive SII (9.30%; 95% CI, 6.69–11.91%) and RII (1.98%; 95% CI, 1.59–2.46) were observed in opportunistic screening. Furthermore, income inequality was not found in organized GC screening; however, overall SII and RII for opportunistic screening were 7.72% (95% CI, 5.39–10.5) and 1.61 (95% CI, 1.42–1.81), respectively.

Conclusion: Organized screening rates have grown gradually over time and account for the majority of GC screenings in South Korea. While no socioeconomic inequalities were found in organized screening, significant socioeconomic inequalities were found in opportunistic screening.

KEYWORDS

gastric cancer, Korea, socioeconomic inequality, organized screening, opportunistic screening

1. Introduction

Gastric cancer (GC) has large regional variations worldwide (1). More than 60% of the incidence of GC cases occur in Eastern Asia, with an age-standardized rate (ASR) of 22.4 cases per 100,000 (1). This figure was much lower in Western countries and regions where the ASR was about 7 per 100,000 in Southern Europe, Central America, and only 4.6 in Northern Europe (1). The differences are due to the various socio- demographic characteristics, dietary behaviors, prevalence of *Helicobacter pylori* infection, and genetic factors (2–4). Although its incidence rate has recently been decreasing, GC remains the fourth leading cause of cancer-related deaths worldwide (1). In Korea, GC has been decreasing constantly, with an annual percentage change (APC) of −4.8; however, it still ranks as the fourth most common cancer, with 26,662 new GC cases in 2020 (an ASR of 25.7 cases per 100,000) according to the Korea Central Cancer Registry (KCCR) (5). Almost two-thirds of cancer cases were prevalent in men, and people aged between 60 and 69 years had the highest GC burden (6). In addition to regional differences in GC burden, significant inequalities in GC incidence and outcomes within the country have also been reported (7–9). Using data from Korea Central Cancer Registry, a study found that the ASR of GC was lower in the metropolitan areas (6). In the US, compared to non-Hispanic White people, other ethnic groups have a higher risk of GC and GC mortality; it could be up to 1.89 times higher among non-Hispanic Asian/Pacific Islanders for GC incidence and 2.6 times higher among non-Hispanic Black people for GC mortality (8). The uneven distribution of the GC burden can be explained by not only ethnic/regional factors but also an individual's socioeconomic status (SES) and health related systems, such as accessibility to healthcare services, low health literacy, and financial difficulties (7, 10–12).

Some Asian countries have introduced GC screening programs (13–16). Organized screening programs are known to contribute not only to reducing the cancer burden but also to reducing inequality in disease burden (11, 12). However, inequality issues in cancer screening, wherein advantaged people had a higher participation rate (11, 12, 17, 18), have been reported. In Korea, the Korean National Cancer Screening Program (KNCSP) offers either an upper gastrointestinal series (UGIS) or upper endoscopy as the primary GC screening test for people aged ≥40 years biannually (19). GC screening, particularly endoscopy, has been demonstrated to have a positive impact on the survival of patients with GC and significantly decrease GC mortality (20–22). Since the introduction of GC screening in Korea, the overall GC screening rate, including organized and opportunistic screening, has steadily increased from 39.2% in 2004 to 72.8% in 2018 (23). Specifically, the participation rate of the KNCSP for GC increased significantly from 7.4% in 2002 to 62.9% in 2019 (24). As one of the main goals of the KNCSP is to eliminate socioeconomic inequality, some studies have been conducted to assess this aspect (18, 25, 26). However, these studies focused only on investigating the inequality in the overall screening rate (18, 26) or were conducted during the early phase of the KNCSP (25). Thus, an updated and comprehensive evaluation of inequalities in GC screening is required, particularly when comparing organized and opportunistic screening approaches.

Therefore, this study aims to evaluate the socioeconomic inequality in GC screening in Korea. Socioeconomic inequality was assessed in both organized screening and opportunistic screening according to income and educational level.

2. Materials and methods

2.1. Study material

This study used data from the Korean National Cancer Screening Survey (KNCSS), a national survey conducted annually since 2004, to investigate cancer screening behaviors among Korean men and women. The KNCSS was designed using a stratified multistage sampling method based on the area, age, and sex of the population. The study data were collected through face-to-face interviews that were conducted by a professional research agency. In case of any missing information, a trained staff member contacted the respondent via telephone to ensure the completeness of the records. After conducting the survey for over two decades, the study sample size has been adjusted and expanded to improve the survey quality and to reflect the change in the screening policy. During the early years of the KNCSS, the overall survey sample size was approximately 2,000 men aged 40–75 years and women aged 30–75 years, which was later increased to 4,100 in 2010 and 4,500 in 2014. The detailed sampling method for the KNCSS has been previously described (19, 23). The current study analyzed the KNCSS data from 2009 to 2022 to compare the annual trend of the screening rate according to socioeconomic factors. Since the main concern of the current study was GC screening, only individuals aged 40–75 were included according to the protocol of the KNCSP in Korea. The final dataset comprised 47,163 men and women aged 40–75 with no history of any type of cancer.

This study was approved by the Institutional Review Board of the National Cancer Center of Korea (IRB Number: NCC-2019-0233). All participants were informed of the purpose and use of the data before enrollment in the study, and the requirement for written informed consent was waived.

2.2. Measurements

According to the KNSCP protocol, both upper endoscopy and UGIS are recommended for examining and visualizing the entire upper GI tract every 2 years for men and women aged 40 years or above (23). During the upper endoscopy procedure, if any abnormal tissue (recorded as possible GC, early GC, advanced GC, or others where the physician deemed it necessary) is detected, a biopsy may also be performed for investigation. In the case of those who chose UGIS, if suspicious findings were observed, the patient was referred for follow-up procedure with upper endoscopy and biopsy for the final laboratory confirmation.

Recommendation-based GC screening was defined based on the question, "Have you ever undergone gastric cancer screening by [UGIS/upper endoscopy]?" and "When was the last screening round you had with this test method?" Individuals who underwent screening with the recommendation were defined as those who underwent screening by either UGIS or upper endoscopy within the past 2 years, according to the recommendation of GC screening in Korea. Furthermore, screening types were divided into organized and opportunistic groups using questions about the source of their

payment. Organized screening is a systematic and planned program that targets a specific population. In Korea, the government introduced the KNCSP as an organized cancer screening program, and screening costs are largely covered by the National Health Insurance System (NHIS). Opportunistic screening is sporadic and occurs when individuals seek medical care or when healthcare providers offer screening tests based on an individual's demographics, risk factors, or symptoms and generally require individuals to pay. Therefore, those who responded that the government or NHIS paid for GC screening were classified as organized screened, and those who reported that they paid for themselves were classified as opportunistic screened. The demographic characteristics included age, sex, and residential area. Socioeconomic factors included education level and household income. There were four subgroups based on the highest completed educational level: elementary school or no formal education, middle school, high school, and college/university or higher. Monthly household income contained three labels: low, middle, and high, which were divided based on the tertile distribution of the 13 original categories, ranging from approximately 1,000 USD to 10,000 USD or more. Owing to the change in the SES of the population over the study period, different cut-off points were applied for the original income categories to illustrate the income distribution of the target population. The household income was divided as follows: <2000, 2000–3,499, ≥3,500 for 2009; <2,500, 2,500–3,999, ≥4,000 from 2010 to 2012; <3,000, 3,000–4,499, ≥4,500 for 2013; <3,500, 3,500–4,499, ≥4,500 from 2014 to 2018; and < 3,500, 3,500–4,999, ≥5,000 from 2019 to 2022.

2.3. Statistical analysis

The weighted screening rate was reported by the type of screening (organized or opportunistic screening) for each survey year from 2009 to 2022. The trend in the screening rate was assessed using the joinpoint regression model. Based on the real pattern of the screening rate, the model produced the best-fit line(s), which could be either single or multiple segments. To summarize and compare the trends in screening rates, the average annual percentage change (AAPC) of GC screening rates over the past 14 years is reported.

Inequality indices are measured in both absolute and relative terms to obtain a comprehensive view of inequality. The absolute inequality was reported as the slope index of inequality (SII). The weighted sample for each year of the survey was ranked in consecutive order from the lowest education/income level to the highest education/income level. The weighted rankings accounted for the distribution of the target population in each subgroup. Subsequently, based on the cumulative proportion of the ranked socioeconomic variables and the midpoint of this socioeconomic variable, a new socioeconomic variable was generated and input into the Poisson regression model to estimate the regression coefficient (SII). A zero SII indicates no inequality; a positive SII reflects higher screening participation among advantaged people; and a negative value indicates the opposite. The relative index of inequality (RII) was estimated using the same procedure, in which RII is the ratio of the screening rate in the most privileged SES group to the least privileged SES group. A RII of one indicates no inequality. A RII value of >1 is interpreted as the fold change in the screening rate between the most privileged individuals and the least privileged individuals, and the opposite is true for an RII value of <1. The pooled SII and RII over 14 years of study were estimated using a random-effects meta-analysis model. The time trend was estimated by fitting the meta-regression model, wherein the survey year was treated as an independent variable. Further, a subgroup analysis was conducted to investigate the issue of inequality by sex and residential area.

Descriptive analyses and estimations of the SII and RII were performed using Stata version 16 (Stata Corp., College Station, TX, United States). The Joinpoint Regression Program, version 4.9.1.0 (Statistical Research and Applications Branch; National Cancer Institute, Rockville, MD, United States), was used for the trend analysis of the screening rate. Statistical significance was set at a p-value <0.05.

3. Results

Table 1 shows the weighted baseline characteristics of the KNCSS over 14 years of study. Except for the 2009 survey, most surveys included information from approximately 3,500 men and women eligible for GC screening. The unweighted baseline characteristics of the study are presented in Supplementary Table S1. The overall screening rate with the recommendation increased constantly from 57.0% in 2009 to more than 75.2% in 2022, where organized screening had a similar pattern and contributed to the majority of the GC screening rate (Figure 1). The GC screening rate rapidly increased in the period 2009–2014, with an APC of 4.81% ($p < 0.001$); however, it fluctuated in the subsequent years (Supplementary Figure S1). Supplementary Table S2 shows the overall screening rate by subgroup according to trend.

The organized screening rate for GC has nearly doubled, increasing from 38.2% in 2009 to 70.2% in 2022, with an AAPC of 4.2 ($p < 0.001$) (Table 2). The sharpest increase in organized screening rate was observed between 2009 and 2015, with an APC of 6.7% ($p < 0.001$) (Supplementary Figure S1). A statistically significant increase in organized screening rates was observed in almost all the subgroups (Table 2). The opportunistic screening rate fluctuated between 2009 and 2014 and subsequently experienced a significant decrease to only 4.5% in 2022, with an AAPC of −4.9% ($p < 0.001$) (Table 3 and Supplementary Figure S1). The steepest decrease in the opportunistic screening rate was observed among older individuals, high school graduates, those with lower levels of education, and people with low household income (Table 3).

Figure 2 illustrates the absolute and relative inequalities in terms of educational level for both organized and opportunistic GC screenings. Negative SII values were observed in eight of the 14 years of the study, while significant positive SII values were recorded only in 2019 and 2022 (Figure 2A). The pool estimate of SII for organized GC screening was −3.5% (95% CI, −7.63–0.83%). Similarly, the RII was mostly below 1, and no significant inequality was observed in the overall estimate of the index (RII 0.93; 95% CI, 0.86–1.01) (Figure 2B). In contrast, the SII for opportunistic screening remains significantly positive in almost all years of the survey except for 2009 and 2014, given the pooled SII of 9.3% (95% CI, 6.69–11.91%) for the whole period of 14 years (Figure 2C). The RII for educational inequality in opportunistic screening ranges from approximately 1 in 2014 to 7.25 in 2022. The overall RII was 1.98 (95% CI, 1.59–2.46), indicating that university graduates are about two times more likely to engage in

10.3389/fpubh.2023.1256525

TABLE 1 Baseline characteristics of the study population in the Korean National Cancer Screening Survey, 2009–2022.

	2009	2010	2011	2012	2013	2014	2015	2016	2017	2018	2019	2020	2021	2022
Total, no.	1,640	3,411	3,474	3,498	3,509	3,441	3,441	3,480	3,484	3,495	3,539	3,647	3,552	3,552
Sex, %														
Male	49.1	49.5	49.6	49.6	49.5	49.7	49.8	49.8	49.8	49.8	49.4	49.4	49.9	49.9
Female	50.9	50.5	50.4	50.4	50.5	50.3	50.2	50.2	50.2	50.2	50.6	50.6	50.1	50.1
Age group, %														
40–49	42.9	41.0	39.9	39.9	38.6	38.0	37.2	36.3	35.5	34.8	31.5	30.6	31.7	31.6
50–59	30.6	32.2	33.8	33.8	34.8	34.7	34.6	34.6	34.6	34.5	32.4	31.8	33.1	33.1
60–69	19.5	19.5	19.1	18.9	19.6	19.7	20.7	21.7	22.5	23.3	22.9	24.0	27.0	27.2
70–75	7.1	7.3	7.3	7.4	7.0	7.7	7.6	7.3	7.3	7.4	13.2	13.5	8.2	8.1
Residential area, %														
Metropolitan	46.2	44.0	44.8	44.6	44.1	44.5	45.4	43.9	44.8	44.0	43.7	45.4	43.0	43.0
Non-metropolitan	53.8	56.0	55.2	55.4	55.9	55.5	54.6	56.1	55.2	56.0	56.3	54.6	57.0	57.0
Education level, %														
Elementary or lower	18.1	9.8	9.5	11.2	6.0	6.4	5.9	4.4	5.0	4.2	4.5	4.7	3.8	3.3
Middle school graduates	13.3	13.0	12.4	10.1	8.4	9.3	9.7	7.2	11.0	9.6	11.9	10.0	7.8	7.2
High school graduates	46.7	52.4	52.9	53.4	53.9	56.2	54.8	55.6	52.9	52.0	52.3	53.7	50.2	49.6
College/ University or higher	21.9	24.8	25.1	25.3	31.7	28.0	29.7	32.7	31.0	34.3	31.3	31.7	38.2	39.9
Household income, %														
Low	28.9	32.6	32.3	27.6	25.4	36.9	37.6	37.8	38.3	35.5	34.9	36.5	30.2	25.3
Middle	45.1	36.2	36.5	44.9	34.6	26.5	27.4	30.2	31.7	25.9	37.5	32.5	32.6	28.6
High	26.0	31.2	31.2	27.5	40.0	36.6	35.0	32.0	30.0	38.5	27.7	31.0	37.1	46.1

opportunistic screening compared to those who completed elementary school or lower.

No significant income inequality in either absolute or relative terms was observed in 12 of the 14 years of the study period (Figures 3A,B). The overall SII and RII for income inequality in organized GC screening were 0.79% (95% CI, −2.38–3.96%) and 1.02 (95% CI, 0.96–1.08), respectively (Figure 3B). In contrast, the opportunistic screening showed significant income inequality with positive SII in most years, and the overall SII was 7.72% (95% CI, 5.39–10.5) (Figure 3C). The RII of income inequality ranged from 1.18 (95% CI, 0.95–1.47) in 2013 to 2.47 (95% CI, 1.28–4.79) (Figure 3D). Overall, the high-income group had 1.61 times (95% CI, 1.42–1.81) higher opportunistic screening rate compared to the low-income group (Figure 3D).

In the subgroup analysis by sex, educational inequality was more evident among men in both the absolute (men: SII of 12.3, 95% CI, 8.08–16.18; women: SII of 5.89, 95% CI, 2.85–8.93) and relative measures (men: RII of 2.22, 95% CI, 1.68–2.93; women: RII of 1.65, 95% CI, 1.27–2.14) of inequality for opportunistic screening (Supplementary Figures S2, S3). Notably, a significant increasing trend was observed in relative educational inequality for opportunistic screening in women (p for trend = 0.017). The pattern was relatively similar for income inequality between both sexes with no significant trend observed (Supplementary Figures S4, S5). For the organized screening method, no inequalities were found in the overall estimates for both education and income. By residential area type, there were no obvious differences between people living in metropolitan and nonmetropolitan areas; educational inequality was also in good agreement with the main analysis (Supplementary Figures S6, S7). There was a significant decreasing trend for income inequality in SII for opportunistic screening (p for trend = 0.033); however, no trend was observed in RII (Supplementary Figures S9C,D).

4. Discussion

This study indicated a noteworthy increase in the GC screening rate, primarily driven by higher participation in organized screening. In contrast, opportunistic screening experienced a significant decrease in the overall rate and among specific subgroups. While certain years of the study showed education and income inequalities, no socioeconomic inequality was observed in the overall estimates of

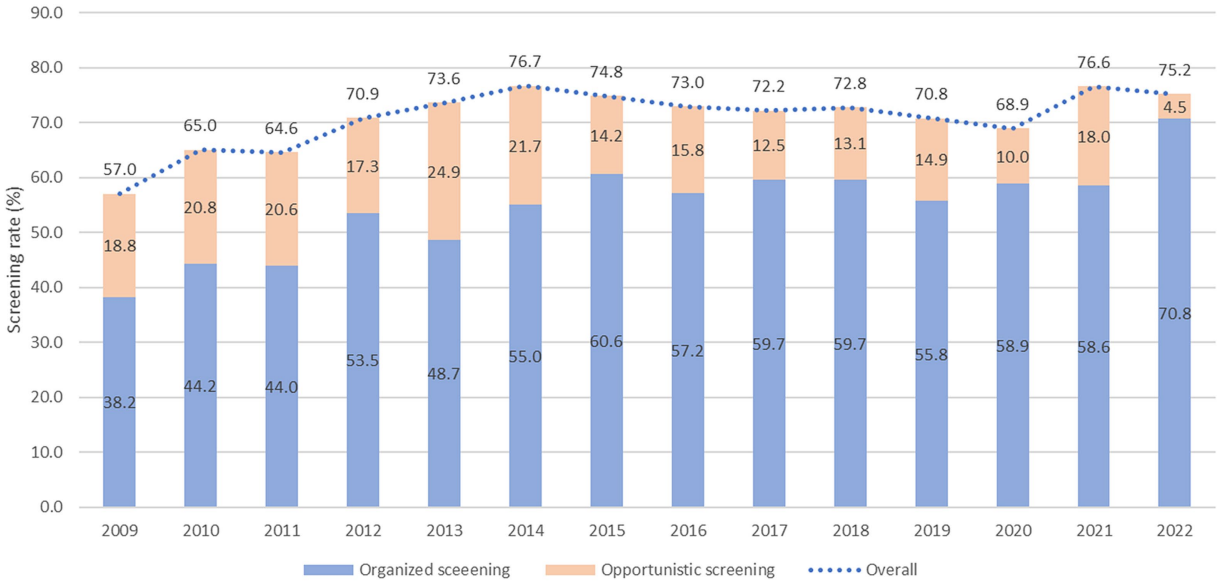

FIGURE 1
Gastric cancer screening rate by type of screening from 2009 to 2022.

both absolute and relative indices for organized GC screening. However, socioeconomic inequality was frequently observed in opportunistic screening throughout each year of the study as well as in the pooled estimates, suggesting that individuals with lower SES encounter barriers or inequalities in accessing and utilizing opportunistic screening for GC. However, these barriers or inequalities were not observed in organized screening.

Income and educational level have been well addressed as the main socioeconomic factors influencing participation in GC screening (27–29). Using data from the Korean National Health and Nutrition Examination Survey, Kwon et al. and Chang et al. reported significant differences in GC screening attendance, wherein higher educational qualifications or higher income were positively associated with GC screening (27, 29). An analysis of more than 15,000 Japanese women reported that those with a lower SES were less likely to participate in GC screening in urban areas (28). Lee et al. found socioeconomic inequality in GC screening for both education and income (18). Unfortunately, this study did not investigate the inequality by screening type. In the context of cancer screening, inequality is reportedly less serious in regions with organized screening than in countries without screening programs (30, 31). A nationwide survey in Korea reported that the educational inequality index in organized screening moved toward zero (no inequality) between 2005 and 2009, whereas inequality in opportunistic screening persisted and tended to increase (25), suggesting that organized screening programs play a positive role in reducing socioeconomic inequality during cancer screening, which is consistent with our findings.

In the current study, an organized screening program appeared to be more effective in achieving equitable utilization of GC screening across different socioeconomic groups, highlighting the importance of organized screening programs to reduce SES-related inequalities in GC screening. Organized screening, with its structured and systematic approach, may have been effective in reaching and engaging individuals of lower SES. Furthermore, alleviating the individual cost burden of GC screening by providing 100 or 90% of the screening costs in the public sector is believed to have significantly contributed to mitigating the inequality associated with the financial burden of screening. Opportunistic screening for GC primarily involves an upper endoscopic screening test, which is also included as a primary screening test in the KNCSP (13). Through the promotion and implementation of a screening invitation system, more individuals have become aware of the KNCSP. Additionally, the screening units in the KNCSP have extended their operating hours, offering services until 9 p.m. on specific days of the week and even opening on weekends. As a result, the overall participation rate in GC screening, particularly organized screening, has increased to over 70% in recent years.

Notably, the screening rate can also be influenced by external factors, such as the COVID-19 pandemic (32, 33). In 2021, when COVID-19 was serious and several social distancing policies had been implemented, the opportunistic screening rate had increased to 18% from approximately 10% in previous years. This increase can be attributed to individuals' fear of contracting COVID-19 in crowded and high-risk areas such as hospitals or general clinics. Consequently, some individuals are willing to pay for opportunistic screenings. Since socioeconomic inequality is significantly associated with opportunistic screening participation, the rise in opportunistic screening participation during the COVID-19 pandemic could potentially lead to broader inequalities.

Based on our findings, we note that a well-organized screening program is essential for reducing the inequality in cancer screening and the overall cancer burden. While both opportunistic and organized screening facilities are available for the general population, policy makers should consider adopting/revising the appropriate screening policy to maximize participation in organized screening policies. Some insights that can be taken from the implementation of GC screening in Korea include the offering of high-quality screening tests, conducting mass media campaigns for screening, a

TABLE 2 Organized screening rates for gastric cancer according to socioeconomic status in the Korean National Cancer Screening Survey 2009–2022 (%).

	2009	2010	2011	2012	2013	2014	2015	2016	2017	2018	2019	2020	2021	2022	AAPC (95% CI)
Total	38.2	44.2	44.0	53.5	48.7	55.0	60.6	57.2	59.7	59.7	55.8	58.9	58.6	70.8	4.2 (1.2–7.4)
Sex															
Male	32.6	39.2	39.5	49.7	46.4	53.8	59.0	54.7	54.8	57.2	54.6	57.4	54.7	71.0	3.6 (2.1–5.2)
Female	43.6	49.2	48.4	57.3	50.9	56.2	62.2	59.6	64.5	62.1	57.0	60.4	62.5	70.5	2.4 (1.4–3.5)
Age group															
40–49	29.4	35.9	35.4	46.3	46.3	50.5	53.0	50.9	58.4	54.2	51.6	53.1	50.8	68.5	4.0. (2.3–5.8)
50–59	43.7	50.3	49.2	58.1	50.2	56.5	63.8	59.5	59.7	62.1	58.7	61.2	60.2	71.8	2.3 (1.2–3.4)
60–69	48.4	52.0	51.3	59.1	49.9	59.4	68.4	63.6	61.1	65.4	62.1	66.0	64.0	73.4	2.4 (1.3–3.4)
70–75	39.7	43.6	47.7	57.2	51.0	59.3	61.8	58.1	61.8	56.0	47.6	54.0	64.8	66.4	3.5 (−1.1–8.4)
Residential area															
Metropolitan	37.6	45.1	45.1	48.7	50.4	60.5	64.7	59.8	60.6	63.9	56.7	58.8	59.0	72.4	3.0 (1.7–7.8)
Non-metropolitan	38.8	43.5	43.1	57.4	47.4	50.6	57.2	55.1	58.9	56.3	55.1	59.0	58.3	69.6	2.9 (1.6–4.2)
Education level															
Elementary or lower	47.8	51.4	52.8	59.4	51.5	48.7	54.1	68.4	74.3	49.5	50.3	55.8	61.2	65.4	1.8 (−0.3–3.8)
Middle school graduates	46.8	50.7	50.1	58.7	52.9	53.9	62.6	64.9	58.1	65.7	45.9	60.2	63.5	67.2	1.8 (0.3–3.4)
High school graduates	34.6	44.5	44.2	55.1	50.1	56.7	63.2	58.6	59.7	60.7	59.0	62.2	63.4	70.1	3.0 (1.8–4.2)
College or higher	32.8	37.5	37.1	45.6	44.8	53.5	56.6	51.5	57.8	57.7	55.1	53.3	51.0	72.7	4.2 (2.3–6.1)
Household income															
Low	46.0	49.8	49.8	55.9	47.1	56.4	60.7	60.9	59.8	59.0	54.4	58.5	63.1	69.3	2.1 (1.0–3.2)
Middle	35.0	40.5	40.3	53.2	48.6	58.5	60.8	55.9	59.2	59.6	54.8	57.4	57.5	70.3	5.0 (0.5–9.7)
High	35.1	42.7	42.3	51.8	49.8	51.1	60.4	53.9	60.0	60.3	59.0	61.0	55.8	71.8	3.6 (2.3–4.9)

Screening with recommendation was defined as the upper gastrointestinal series, or upper endoscopy, during the past 2 years. AAPC, Average Annual Percent Change; 95% CI, 95% confidence interval.

10.3389/fpubh.2023.1256525

TABLE 3 Opportunistic screening rates for gastric cancer according to socioeconomic status in the Korean National Cancer Screening Survey 2009–2022 (%).

	2009	2010	2011	2012	2013	2014	2015	2016	2017	2018	2019	2020	2021	2022	AAPC (95% CI)
Total	18.8	20.8	20.6	17.3	24.9	21.7	14.2	15.8	12.5	13.1	14.9	10.0	18.0	4.5	−4.9 (−8.6 to −1.1)
Sex															
Male	19.7	24.4	24.0	20.1	26.0	23.4	16.5	16.8	15.6	15.9	16.2	11.9	22.1	5.3	−4.3 (−7.8 to −0.7)
Female	17.9	17.2	17.2	14.6	23.8	20.0	12.0	14.9	9.3	10.4	13.7	8.2	14.0	3.6	−5.7 (−9.9 to −1.2)
Age group															
40–49	18.1	23.8	23.6	18.8	26.2	25.4	17.6	17.7	11.4	17.9	18.4	12.9	23.2	4.0	−3.3 (−7.4–0.9)
50–59	18.8	19.3	19.6	18.0	24.4	21.0	13.6	14.9	15.3	12.3	15.4	10.0	19.8	5.1	−4.0 (−7.8 to 0.1)
60–69	21.4	17.8	17.7	15.8	24.5	18.5	11.0	12.9	10.9	9.1	13.0	7.6	12.2	4.3	−7.2 (−10.9 to −3.4)
70–75	16.3	18.5	15.9	10.4	21.3	14.1	9.2	19.7	9.0	7.4	9.1	7.8	10.0	4.2	−7.5 (−11.9 to −2.9)
Residential area															
Metropolitan	17.4	19.9	19.3	20.7	23.9	18.1	10.3	15.7	12.6	12.5	16.3	9.5	18.2	4.8	−4.6 (−8.5 to −0.5)
Non-metropolitan	20.0	21.4	21.6	14.6	25.7	24.5	17.5	15.9	12.3	13.7	13.9	10.5	17.9	4.2	−5.3 (−9.3 to −1.1)
Education level															
Elementary or lower	15.8	14.0	12.5	10.9	23.5	21.9	9.4	11.0	7.4	2.8	5.5	5.2	10.4	0.9	−6.1 (−13.3 to 1.8)
Middle school graduates	17.5	14.4	14.1	14.1	17.0	21.0	12.0	15.2	8.9	7.5	10.3	3.8	8.3	1.5	−7.1 (−12.0 to −2.0)
High school graduates	17.9	18.8	18.7	15.9	24.3	20.6	12.8	14.2	11.0	11.8	13.2	8.4	12.5	3.3	−6.7 (−10.5 to −2.7)
College or higher	24.2	31.0	30.8	24.5	28.2	24.0	18.5	19.4	17.1	18.0	20.9	15.6	28.1	6.7	−3.9 (−7.7 to 0.1)
Household income															
Low	14.3	14.4	13.5	13.8	24.0	18.6	11.1	12.7	9.8	9.5	11.2	8.0	9.2	2.8	−6.7 (−11.3 to −1.8)
Middle	18.8	21.0	21.0	15.9	23.3	20.4	12.5	16.3	11.2	14.0	14.4	9.6	18.9	3.5	−3.6 (−7.7 to 0.8)
High	23.8	27.2	27.4	23.1	26.8	25.7	19.0	19.1	17.2	15.9	20.4	12.8	24.5	6.0	−3.9 (−8.2 to 0.6)

Screening with recommendation was defined as the upper gastrointestinal series, or upper endoscopy, during the past 2 years. AAPC, Average Annual Percent Change; 95% CI, 95% confidence interval.

10.3389/fpubh.2023.1256525

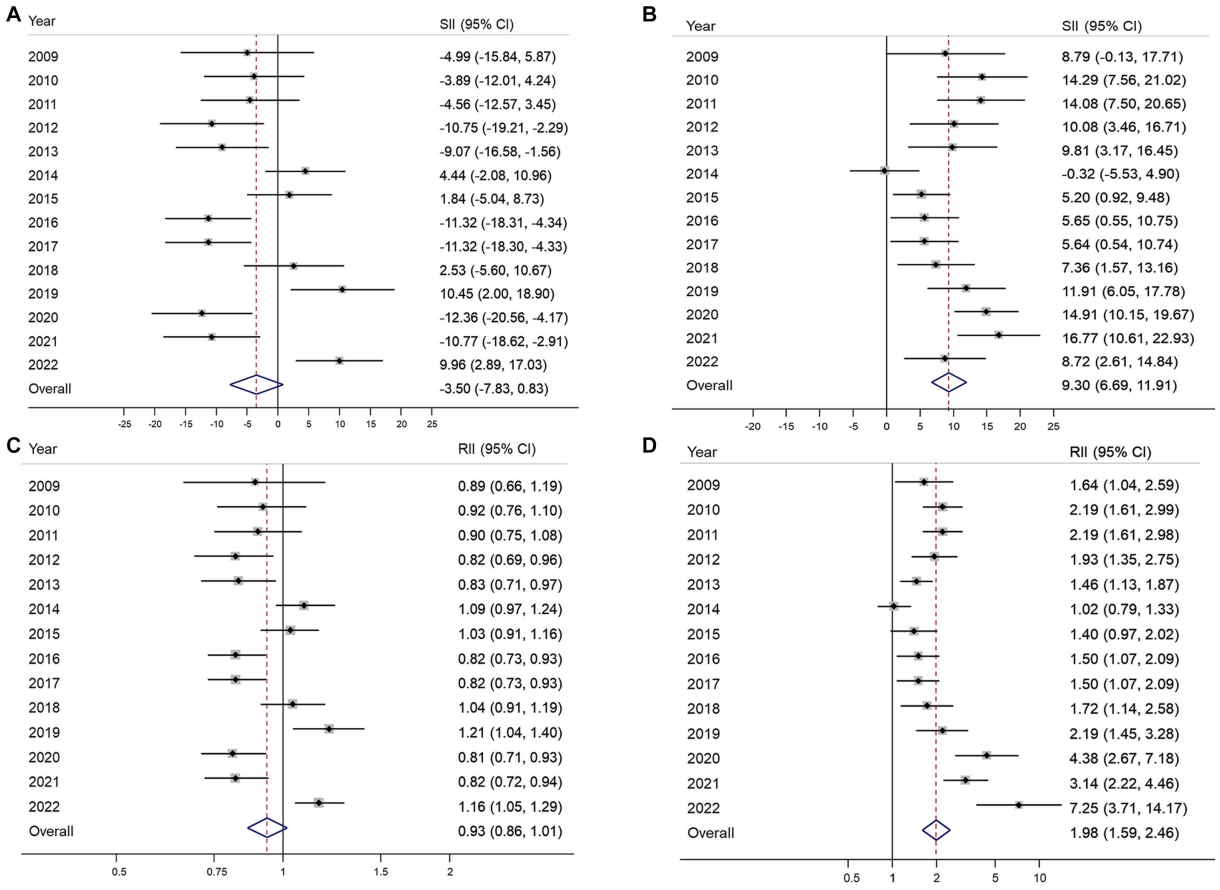

FIGURE 2
Absolute and relative educational inequalities in organized **(A,B)** and opportunistic **(C,D)** gastric cancer screening from 2009 to 2022. SII, absolute slope index of inequality; RII, relative index of inequality; 95% CI, 95% confidence interval.

comprehensive invitation/follow-up system, and individualized strategies for the lower SES groups (23, 25, 29). Similarly, for GC burden, Japan has been implementing a national cancer screening program since the 1980s. Currently, both radiographic and endoscopy tests are being recommended for GC screening in Japan. However, compared with Korea, the participation rate has remained low, and this relates to the different aspects of the guidelines and management system (34). There is a lack of regulation for quality assurance in screening programs in Japan (34). In contrast, the KNCSP's quality assurance system is governed by law, and the results of all cancer screenings are collected and linked to other national databases such as the cancer registry and death certificates for the process of continuous monitoring and evaluation of the KNCSP (16, 19, 34). Further, as the issue of inequality is subjected to change by the internal and external factors of the screening program, continuous monitoring/evaluation of the program indicators and the inequality issue will help the program to have on-time action for a good quality screening program. The GC screening program contributes significantly toward improving the survival of GC cancer patients and eventually reducing the GC mortality rate (21, 22). Thus, the equal delivery of organized screening has a positive effect on the inequality in the GC cancer burden as well, where people, especially in the low SES group, have an equal opportunity to screen and detect cancer at the early stage with a much lower cost of treatment and a higher survival or cure rate.

The current study has some limitations. First, the use of survey data might impose some recall bias on the reported information. However, we used non-clinical information such as sociodemographic characteristics, which has been reported to have good accuracy (35, 36). For the screening history, when comparing the self-reported history and clinical records, the sensitivity ranged from 96.5% in Tsuruda et al.'s study and up to 100% in the results reported by Hoffmeister et al. (35) and Tsuruda et al. (36) Therefore, the use of self-reported GC screening information, especially within the last 2 years, is highly accurate in our study. Second, the use of SII and RII requires ordinal variables; therefore, only education and income levels were used in our analysis. Future studies should also consider including the other variables in sensitivity analysis for a more comprehensive assessment. Despite these limitations, this study has several strengths. Our study offers a comprehensive and updated evaluation of the inequality in GC screening, encompassing both organized and opportunistic screenings. Additionally, as we have used data from a high-quality national survey designed to monitor screening behavior, our results are highly representative and generalizable.

In conclusion, the KNCSP has played a crucial role in increasing the rate of organized screening while simultaneously reducing the prevalence of opportunistic screening. Over the 14-year study period, no socioeconomic inequalities were observed during the organized

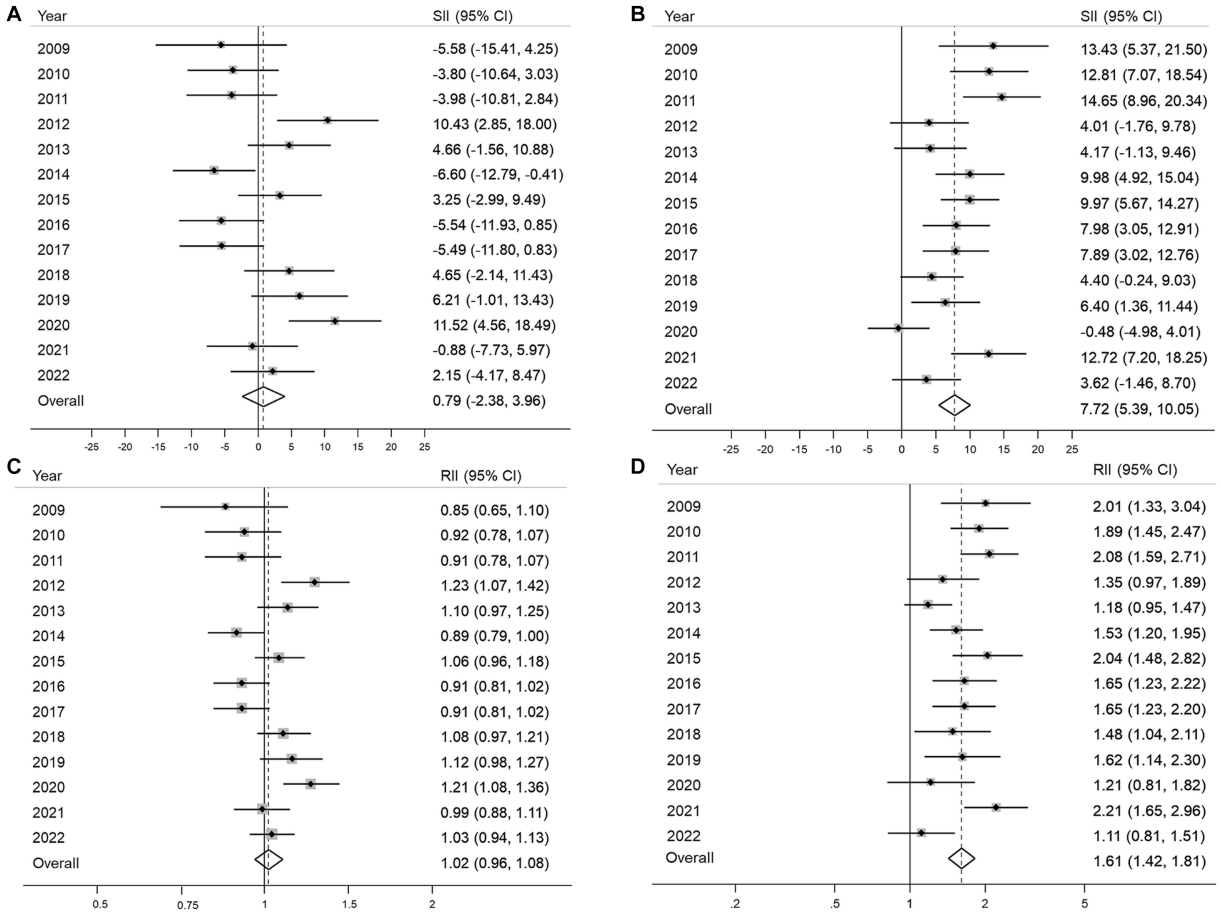

FIGURE 3
Absolute and relative income inequalities in organized **(A,B)** and opportunistic **(C,D)** gastric cancer screening from 2009 to 2022 SII, absolute slope index of inequality; RII, relative index of inequality; 95% CI, 95% confidence interval.

screening. Overall, our study sheds light on the positive impacts of the KNCSP and highlights the importance of addressing socioeconomic inequalities in accessing screening services. These findings have implications for improving cancer screening programs and promoting equitable healthcare delivery. Future studies should continue to monitor the issue of GC inequality carefully not only in the screening services but also a comprehensive evaluation of the cancer incidence and outcomes using additional factors besides income and education.

Data availability statement

The datasets supporting this study's findings are available from the corresponding author upon reasonable request.

Ethics statement

The studies involving humans were approved by Institutional Review Board of the National Cancer Center of Korea. The studies were conducted in accordance with the local legislation and institutional requirements. The ethics committee/institutional review board waived the requirement of written informed consent for participation from the participants or the participants' legal guardians/next of kin because All participants were informed of the purpose and use of the data before enrollment in the survey, and the requirement for written informed consent was waived.

Author contributions

XL: Conceptualization, Formal analysis, Investigation, Methodology, Writing – original draft. KL: Formal analysis, Writing – review & editing. JJ: Methodology, Writing – review & editing. MS: Methodology, Writing – review & editing. KC: Conceptualization, Funding acquisition, Methodology, Supervision, Writing – review & editing.

Funding

The author(s) declare financial support was received for the research, authorship, and/or publication of this article. This study was funded by a Grant-in-Aid for Cancer Research and Control from the National Cancer Center, Korea (#2210772).

Conflict of interest

The authors declare that the research was conducted in the absence of any commercial or financial relationships that could be construed as a potential conflict of interest.

Publisher's note

All claims expressed in this article are solely those of the authors and do not necessarily represent those of their affiliated organizations, or those of the publisher, the editors and the reviewers. Any product that may be evaluated in this article, or claim that may be made by its manufacturer, is not guaranteed or endorsed by the publisher.

Supplementary material

The Supplementary material for this article can be found online at: https://www.frontiersin.org/articles/10.3389/fpubh.2023.1256525/full#supplementary-material

References

1. Sung H, Ferlay J, Siegel RL, Laversanne M, Soerjomataram I, Jemal A, et al. Global cancer statistics 2020: GLOBOCAN estimates of incidence and mortality worldwide for 36 cancers in 185 countries. *CA Cancer J Clin*. (2021) 71:209–49. doi: 10.3322/caac.21660

2. Natsume H, Szczepaniak K, Yamada H, Iwashita Y, Gędek M, Šuto J, et al. Non-CpG sites preference in G:C > a:T transition of TP53 in gastric cancer of Eastern Europe (Poland, Romania and Hungary) compared to east Asian countries (China and Japan). *Genes Environ*. (2023) 45:1. doi: 10.1186/s41021-022-00257-y

3. Hooi JKY, Lai WY, Ng WK, Suen MMY, Underwood FE, Tanyingoh D, et al. Global prevalence of *Helicobacter pylori* infection: systematic review and Meta-analysis. *Gastroenterology*. (2017) 153:420–9. doi: 10.1053/j.gastro.2017.04.022

4. Ning F-L, Lyu J, Pei J-P, Gu W-J, Zhang N-N, Cao S-Y, et al. The burden and trend of gastric cancer and possible risk factors in five Asian countries from 1990 to 2019. *Sci Rep*. (2022) 12:5980. doi: 10.1038/s41598-022-10014-4

5. Kang MJ, Jung K-W, Bang SH, Choi SH, Park EH, Yun EH, et al. Cancer statistics in Korea: incidence, mortality, survival, and prevalence in 2020. *Cancer Res Treat*. (2023) 55:385–99. doi: 10.4143/crt.2023.447

6. Park SH, Kang MJ, Yun EH, Jung KW. Epidemiology of gastric cancer in Korea: trends in incidence and survival based on Korea central Cancer registry data (1999-2019). *J Gastric Cancer*. (2022) 22:160–8. doi: 10.5230/jgc.2022.22.e21

7. Uthman OA, Jadidi E, Moradi T. Socioeconomic position and incidence of gastric cancer: a systematic review and meta-analysis. *J Epidemiol Community Health*. (2013) 67:854–60. doi: 10.1136/jech-2012-201108

8. Bui A, Yang L, Soroudi C, May FP. Racial and ethnic disparities in incidence and mortality for the five most common gastrointestinal cancers in the United States. *J Natl Med Assoc*. (2022) 114:426–9. doi: 10.1016/j.jnma.2022.04.001

9. Zhang G, Zhao X, Li J, Yuan Y, Wen M, Hao X, et al. Racial disparities in stage-specific gastric cancer: analysis of results from the surveillance epidemiology and end results (SEER) program database. *J Investig Med*. (2017) 65:991–8. doi: 10.1136/jim-2017-000413

10. Magge D, Tan M. Disparities in gastric cancer: can we do better? *Ann Surg Oncol*. (2021) 28:2936–8. doi: 10.1245/s10434-020-09528-w

11. Vaccarella S, Lortet-Tieulent J, Saracci R, Conway DI, Straif K, Wild CP eds. *Reducing social inequalities in cancer: evidence and priorities for research*. Lyon: International Agency for Research on Cancer (2019).

12. Van Hal G, Zeeb H, de Koning HJ. Editorial: social inequality in cancer screening. *Front Public Health*. (2022) 10:854659. doi: 10.3389/fpubh.2022.854659

13. Choi KS, Suh M. Screening for gastric cancer: the usefulness of endoscopy. *Clin Endosc*. (2014) 47:490–6. doi: 10.5946/ce.2014.47.6.490

14. Hamashima CSystematic Review Group and Guideline Development Group for Gastric Cancer Screening Guidelines. Update version of the Japanese guidelines for gastric cancer screening. *Jpn J Clin Oncol*. (2018) 48:673–83. doi: 10.1093/jjco/hyy077

15. Leung WK, Wu M-s, Kakugawa Y, Kim JJ, Yeoh K-g, Goh KL, et al. Screening for gastric cancer in Asia: current evidence and practice. *Lancet Oncol*. (2008) 9:279–87. doi: 10.1016/S1470-2045(08)70072-X

16. Park HA, Nam SY, Lee SK, Kim SG, Shim K-N, Park SM, et al. The Korean guideline for gastric cancer screening. *J Korean Med Assoc*. (2015) 58:373–84. doi: 10.5124/jkma.2015.58.5.373

17. Florea A, Brown HE, Harris RB, Oren E. Ethnic disparities in gastric cancer presentation and screening practice in the United States: analysis of 1997–2010 surveillance, epidemiology, and end results-medicare data. *Cancer Epidemiol Biomark Prev*. (2019) 28:659–65. doi: 10.1158/1055-9965.Epi-18-0471

18. Lee E-y, Lee YY, Suh M, Choi E, Mai TTX, Cho H, et al. Socioeconomic inequalities in stomach cancer screening in Korea, 2005–2015: after the introduction of the National Cancer Screening Program. *Yonsei Med J*. (2018) 59:923–9. doi: 10.3349/ymj.2018.59.8.923

19. Suh M, Song S, Cho HN, Park B, Jun JK, Choi E, et al. Trends in participation rates for the National Cancer Screening Program in Korea, 2002-2012. *Cancer Res Treat*. (2017) 49:798–806. doi: 10.4143/crt.2016.186

20. Choi KS, Jun JK, Suh M, Park B, Noh DK, Song SH, et al. Effect of endoscopy screening on stage at gastric cancer diagnosis: results of the National Cancer Screening Programme in Korea. *Br J Cancer*. (2015) 112:608–12. doi: 10.1038/bjc.2014.608

21. Jun JK, Choi KS, Lee H-Y, Suh M, Park B, Song SH, et al. Effectiveness of the Korean National Cancer Screening Program in reducing gastric cancer mortality. *Gastroenterology*. (2017) 152:1319–1328.e7. doi: 10.1053/j.gastro.2017.01.029

22. Luu XQ, Lee K, Jun JK, Suh M, Jung KW, Choi KS. Effect of gastric cancer screening on long-term survival of gastric cancer patients: results of Korean national cancer screening program. *J Gastroenterol*. (2022) 57:464–75. doi: 10.1007/s00535-022-01878-4

23. Hong S, Lee YY, Lee J, Kim Y, Choi KS, Jun JK, et al. Trends in cancer screening rates among Korean men and women: results of the Korean National Cancer Screening Survey, 2004-2018. *Cancer Res Treat*. (2021) 53:330–8. doi: 10.4143/crt.2020.263

24. Kim Y-I, Choi IJ. Current status of the gastric cancer screening program in Korea. *J Korean Med Assoc*. (2022) 65:250–7. doi: 10.5124/jkma.2022.65.5.250

25. Lee H-Y, Park E-C, Jun JK, Hahm M-I, Jung K-W, Kim Y, et al. Trends in socioeconomic disparities in organized and opportunistic gastric Cancer screening in Korea (2005-2009). *Cancer Epidemiol Biomark Prev*. (2010) 19:1919–26. doi: 10.1158/1055-9965.Epi-09-1308

26. Kim S, Hwang J. Assessment of trends in socioeconomic inequalities in cancer screening services in Korea, 1998–2012. *Int J Equity Health*. (2016) 15:30. doi: 10.1186/s12939-016-0319-7

27. Chang Y, Cho B, Son KY, Shin DW, Shin H, Yang H-K, et al. Determinants of gastric cancer screening attendance in Korea: a multi-level analysis. *BMC Cancer*. (2015) 15:336. doi: 10.1186/s12885-015-1328-4

28. Fukuda Y, Nakamura K, Takano T. Reduced likelihood of cancer screening among women in urban areas and with low socio-economic status: a multilevel analysis in Japan. *Public Health*. (2005) 119:875–84. doi: 10.1016/j.puhe.2005.03.013

29. Kwon YM, Lim HT, Lee K, Cho BL, Park MS, Son KY, et al. Factors associated with use of gastric cancer screening services in Korea. *World J Gastroenterol*. (2009) 15:3653–9. doi: 10.3748/wjg.15.3653

30. Palencia L, Espelt A, Rodriguez-Sanz M, Puigpinos R, Pons-Vigues M, Pasarin MI, et al. Socio-economic inequalities in breast and cervical cancer screening practices in Europe: influence of the type of screening program. *Int J Epidemiol*. (2010) 39:757–65. doi: 10.1093/ije/dyq003

31. Sarfati D, Shaw C, Simmonds S. Commentary: inequalities in cancer screening programmes. *Int J Epidemiol*. (2010) 39:766–8. doi: 10.1093/ije/dyq039

32. Lee K, Suh M, Jun JK, Choi KS. Impact of the COVID-19 pandemic on gastric cancer screening in South Korea: results from the Korean National Cancer Screening Survey (2017-2021). *J Gastric Cancer*. (2022) 22:264–72. doi: 10.5230/jgc.2022.22.e36

33. Park H, Seo SH, Park JH, Yoo SH, Keam B, Shin A. The impact of COVID-19 on screening for colorectal, gastric, breast, and cervical cancer in Korea. *Epidemiol Health*. (2022) 44:e2022053. doi: 10.4178/epih.e2022053

34. Hamashima C, Kim Y, Choi KS. Comparison of guidelines and management for gastric cancer screening between Korea and Japan. *Value Health*. (2015) 18:A272. doi: 10.1016/j.jval.2015.03.1589

35. Hoffmeister M, Chang-Claude J, Brenner H. Validity of self-reported endoscopies of the large bowel and implications for estimates of colorectal cancer risk. *Am J Epidemiol*. (2007) 166:130–6. doi: 10.1093/aje/kwm062

36. Tsuruda KM, Sagstad S, Sebuødegård S, Hofvind S. Validity and reliability of self-reported health indicators among women attending organized mammographic screening. *Scand J Public Health*. (2018) 46:744–51. doi: 10.1177/1403494817749393

frontiers | Frontiers in Oncology

TYPE Systematic Review
PUBLISHED 20 October 2023
DOI 10.3389/fonc.2023.1277265

OPEN ACCESS

EDITED BY
Zsolt Kovács,
George Emil Palade University of Medicine, Pharmacy, Sciences and Technology of Târgu Mureş, Romania

REVIEWED BY
Li Zhang,
University of Minnesota Twin Cities, United States
Shinobu Ohnuma,
Tohoku University, Japan

*CORRESPONDENCE
Zahra Salehi
Zahra.salehi6463@yahoo.com

†These authors have contributed equally to this work and share first authorship

RECEIVED 14 August 2023
ACCEPTED 28 September 2023
PUBLISHED 20 October 2023

CITATION
Piroozkhah M, Aghajani A, Jalali P, Shahmoradi A, Piroozkhah M, Tadlili Y and Salehi Z (2023) Guanylate cyclase-C Signaling Axis as a theragnostic target in colorectal cancer: a systematic review of literature. *Front. Oncol.* 13:1277265. doi: 10.3389/fonc.2023.1277265

Guanylate cyclase-C Signaling Axis as a theragnostic target in colorectal cancer: a systematic review of literature

Moein Piroozkhah[1†], Ali Aghajani[1†], Pooya Jalali[1], Arvin Shahmoradi[2], Mobin Piroozkhah[1,3], Younes Tadlili[4] and Zahra Salehi[5*]

[1]Basic and Molecular Epidemiology of Gastrointestinal Disorders Research Centre, Research Institute for Gastroenterology and Liver Diseases, Shahid Beheshti University of Medical Sciences, Tehran, Iran, [2]Department of Laboratory Medicine, Faculty of Paramedical, Kurdistan University of Medical Sciences, Sanandaj, Iran, [3]School of Medicine, Tehran University of Medical Sciences, Tehran, Iran, [4]Department of Molecular Cell Biology, Microbiology Trend, Faculty of Basic Sciences, Islamic Azad University, Central Tehran Branch, Tehran, Iran, [5]Hematology-Oncology and Stem Cell Transplantation Research Center, Tehran University of Medical Sciences, Tehran, Iran

Introduction: Colorectal cancer (CRC) is a devastating disease that affects millions of people worldwide. Recent research has highlighted the crucial role of the guanylate cyclase-C (GC-C) signaling axis in CRC, from the early stages of tumorigenesis to disease progression. GC-C is activated by endogenous peptides guanylin (GU) and uroguanylin (UG), which are critical in maintaining intestinal fluid homeostasis. However, it has been found that these peptides may also contribute to the development of CRC. This systematic review focuses on the latest research on the GC-C signaling axis in CRC.

Methods: According to the aim of the study, a systematic literature search was conducted on Medline and PubMed databases. Ultimately, a total of 40 articles were gathered for the systematic review.

Results: Our systematic literature search revealed that alterations in GC-C signaling compartments in CRC tissue have demonstrated potential as diagnostic, prognostic, and therapeutic markers. This research highlights a potential treatment for CRC by targeting the GC-C signaling axis. Promising results from recent studies have explored the use of this signaling axis to develop new vaccines and chimeric antigen receptors that may be used in future clinical trials.

Conclusion: The findings presented in this review provide compelling evidence that targeting the GC-C signaling axis may be an advantageous approach for treating CRC.

KEYWORDS

Guanylate cyclase-C Signaling Axis, Guanylyl cyclase C, guanylin, uroguanylin, colorectal cancer, therapeutic target

Highlights

- 1. The progression of colorectal cancer (CRC) is attributed to GC-C, GN, and UG peptides.
- 2. In CRC, the GN and GU expression is lost due to abnormal APC-β-catenin-TCF transcriptional regulation in the early phase of tumor formation. This impairs the GC-C signaling axis and disrupts intestinal homeostasis, contributing to tumor initiation.
- 3. When the GC-C axis is blocked, there is excessive cell growth, increased crypt size, and reduced cell differentiation in the secretory lineage.
- 4. Targeting GC-C with CAR-T cells could be an innovative and practical approach to treating advanced stages of CRC or those resistant to traditional therapies.
- 5. The repurposing of GC-C signaling axis-targeted treatments developed for other diseases is a promising strategy for CRC treatment. Further research is needed to investigate their safety and efficacy.

1 Introduction

Globally, colorectal cancer (CRC) is the third most prevalent form of cancer and has the second-highest mortality rate among all cancers. The CRC mortality rate has been decreasing at a rate of around 2% each year during the last decade. Projections indicate that by the end of 2023, there will have been over 150,000 new cases and about 53,000 fatalities (1). Population-wide shifts toward better lifestyles (e.g., less consumption of red and processed meat) and increased participation in the cancer screening program have been attributed to a decline in colorectal cancer incidence (2, 3). However, this improvement has been made since the early 2000s, primarily because of increased colonoscopy screening methods and the removal of precursor lesions. The primary prevention of colorectal cancer continues to be the most efficient way of reducing the rising global burden of this disease (4–7).

Symptoms of CRC in its early stages are unspecific, which might lead to missed diagnoses or mistaken assessments. Therefore, most cases of CRC are detected in the late stages (8). Surgical resection, radiation therapy before surgery (for rectal cancer), chemotherapy after surgery (for stages III/IV and high-risk stage II colon cancer), and targeted therapy are the most common therapies for CRC (9, 10). Although development in anticancer therapy, particularly immune checkpoint inhibitors (ICIs), has revolutionized CRC treatment, only a fraction of patients respond to these treatments appropriately, and the reason for failure in other patients has not yet been known properly (7, 11). Thus, understanding the molecular mechanism in cancers is crucial for creating reliable diagnostic and prognostic biomarkers in both practice and research (12). Significant advancements in microarray and high-efficiency sequencing technologies like next-generation sequencing have accelerated the exploration and identification of the essential genetic or epigenetic modifications in carcinogenesis, tumor growth, disease recurrence, and metastasis in CRC as well as the discovery of cancer biomarkers with the potential for the development of novel diagnostic, prognostic, and therapeutic techniques (13, 14). Over the past few decades, key driver and passenger genes in CRC have been recognized (15). Auspiciously, apart from the main oncogenes leading to CRC, numerous other genes implicated in CRC development and progression are being discovered and may be exploited as new biomarkers in clinical settings to predict prognosis or therapy response in the future (16).

The transmembrane receptor GC-C is selectively expressed from duodenal to rectal intestinal epithelial cells (17). GC-C is activated by endogenous peptides GN and UG, as well as exogenous ligands such as heat-stable enterotoxins (STs), which are secreted by diarrhea-producing enterotoxigenic E. coli (ETEC) (18).

GN and UG are very close in structure and biological functions. The GC-C signal transduction controls the equilibrium of liquid and electrolyte transport and secretion in the digestive tract (19, 20). However, new findings indicate that these novel peptides have diverse physiological roles alongside those previously documented for the control of homeostasis and might contribute to the tumorigenesis of colorectal adenocarcinoma (21–25). The coincidence of the emergence and development of CRC with the presence of GC-C, GN, and UG proteins, along with their encoding genes *GUCY2C*, *GUCA2A*, and *GUCA2B*, respectively, has piqued the interest of researchers. Particularly, GUCY2C has been found to play a regulatory role in intestinal inflammation and inflammatory bowel disease pathology. Studies of intestinal inflammation in Gucy2c knockout mice have reported the impairment of the epithelial barrier, increased invasiveness of pathogenic bacteria, and alterations in the intestinal microbiota (26, 27). Overall, these data suggest that IBD susceptibility may be mediated by alterations in the intestinal microbiota caused by changes in intestinal ion transportation regulated by GC-C. As a result, we have undertaken a comprehensive review of the literature to explore the relationship between these genes and CRC. Our systematic review not only examines how these genes contribute to CRC development but also emphasizes their potential uses in diagnosing and treating the disease, illustrated as schematic abstract (Figure 1).

2 Materials and methods

2.1 Search strategy and data extraction

This study presents a systematic review focusing on the role of the Guanylate cyclase-C Signaling Axis CRC. The search for relevant articles was conducted until May 27, 2023, extensively utilizing the Medline and PubMed databases. The search algorithm incorporated key terms related to the Guanylate cyclase-C Signaling Axis, including Guanylyl cyclase C, Guanylin, uroguanylin, their associated genes, and colorectal cancer. Meta-analyses, reviews, case reports, correspondences, and personal opinions studies were excluded (Table 1).

2.2 Inclusion and exclusion criteria, population, intervention, and outcomes

During the initial screening process, duplicate articles and those published before 2018 were excluded. Additionally, only articles

10.3389/fonc.2023.1277265

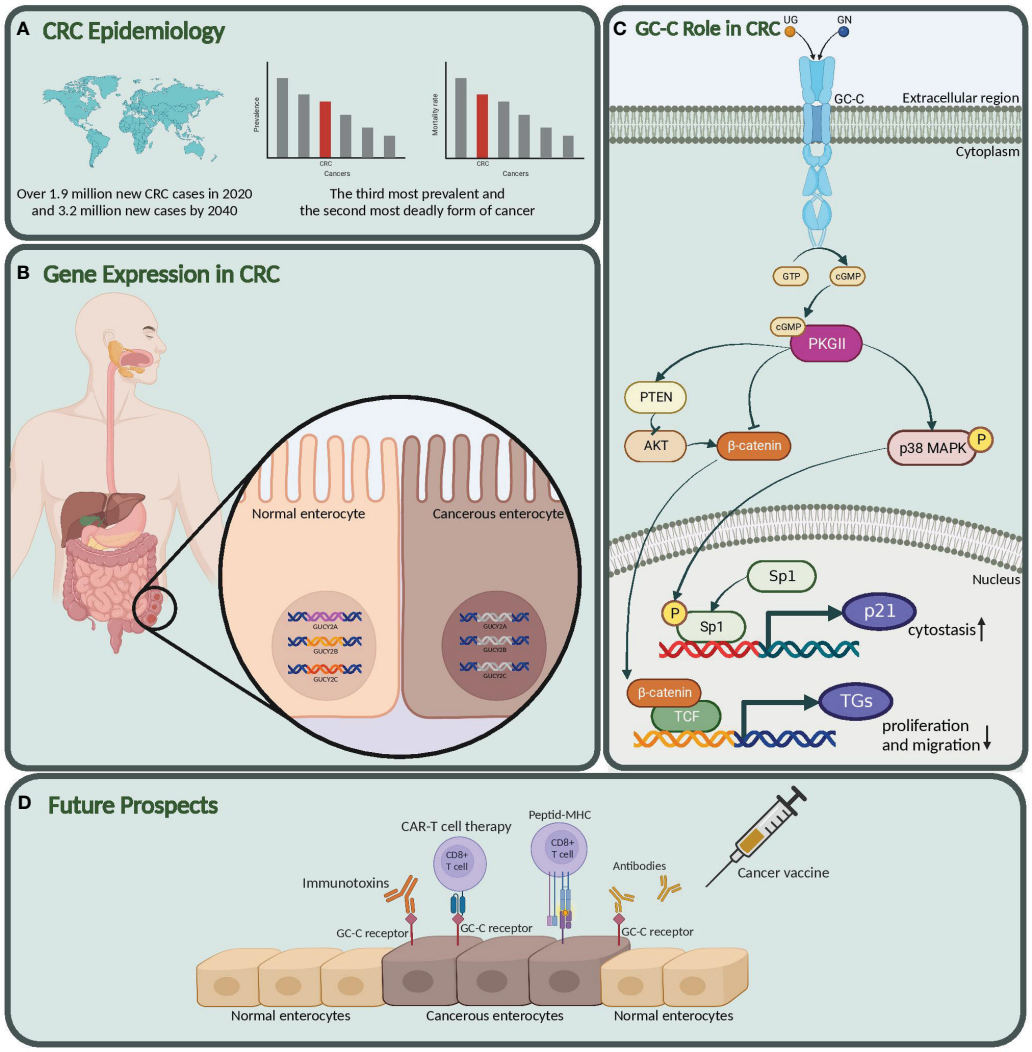

FIGURE 1
Graphical abstract. **(A)** CRC epidemiology. Global impact of colorectal cancer. **(B)** Gene expression in CRC. suppressed expression in *GUCY2C*, *GUCA2A*, and *GUCA2B* in Cancerous vs. Normal Enterocytes. **(C)** GC-C role in CRC. Here, we also explored the molecular mechanism and role of this pathway in the pathogenesis of colon cancer. **(D)** Future prospects. Our study highlights the potential of the Guanylate cyclase-c (GC-C) signaling pathway as a diagnostic biomarker, prognostic indicator, and target for new therapeutic strategies in colorectal cancer. *GUCY2C*, Guanylate Cyclase 2C; *GUCA2A*, Guanylyl cyclase-activating protein 2A; *GUCA2B*, Guanylate Cyclase Activator 2B; GC-C, Guanylate Cyclase-C; CRC, Colorectal Cancer. Created with BioRender.com.

TABLE 1 Search strategy performed in PubMed.

Query	Search Algorithm	Number of Records
#1	(((GUCA2B[Title/Abstract]) OR (GUCY2C[Title/Abstract]) OR (GUCA2A[Title/Abstract]) OR ("guanylyl cyclase C"[Title/Abstract]) OR ("Guanylate cyclase"[Title/Abstract]) OR ("Gc-c receptor"[Title/Abstract]) OR ("guanylate"[Title/Abstract]) OR ("Guanylin"[Title/Abstract]) OR ("uroguanylin"[Title/Abstract])) AND ((Colorectal [Title/Abstract]) OR (intesti*[Title/Abstract]) OR (gastro*[Title/Abstract]) OR (colon[Title/Abstract])) AND ((cancer[Title/Abstract]) OR (malignan*[Title/Abstract]) OR (carcino*[Title/Abstract]) OR (neoplasm*[Title/Abstract])))	69

written in English were included to mitigate potential language and publication biases. Two experts (MEP and AA) independently evaluated article content, demographics, research methodologies, and outcomes to identify potentially eligible studies. Inclusion criteria encompassed studies involving human, animal, *in vivo*, and *in vitro* colorectal cancer samples, focusing on applying the guanylate cyclase-c signaling axis for diagnostic, prognostic, therapeutic targeting, and survival assessment purposes. Studieswith inadequate research designs or misaligned outcomes were excluded from consideration. The search terms and methodologies applied (including database searches, screening, selection, and inclusion criteria) were consistently employed to ensure comprehensive coverage of relevant articles, adhering to the PRISMA statement of 2020 (28).

2.3 Risk of bias

Two assessors (MEP and AA) conducted independent assessments to evaluate potential bias. In cases of disagreement, a third assessor (PJ) was consulted. The evaluation of bias employed the Risk Of Bias In Non-randomized Studies - of Interventions (ROBINS-I) tool, which encompassed eight domains: bias arising from confounding; bias in participant selection; bias in classification; bias due to deviations in intended interventions; bias resulting from missing data; bias due to outcome measurement; bias in the selection of reported results; and overall bias. This rigorous approach ensured a comprehensive assessment of potential biases in the included studies (29).

3 Results

Figure 2 is a flowchart of the searching, screening, and process of the references we selected from the literature. According to the search strategy, 138 published papers were found in each database. After omitting 69 papers as duplicate articles, two separate team members screened 69 titles and abstracts. Twenty-nine articles were eliminated after the title and abstract screening (Review n=20) (Not CRC n=1) (Not Guanylate cyclase axis n=8), and the remaining 40 articles were evaluated for eligibility. All full-text original articles are obtained via open access or institutional subscription. All papers were in English, and none were excluded during the full-text screening stage. Ultimately, a total of 40 articles were gathered for the systematic review. There were 21 papers focused on *GUCY2C* (Table 2), eight papers on *GUCA2A* (Table 3), eight more papers on *GUCA2B* (Table 4), and finally, three papers that covered both *GUCA2A* and *GUCA2B*.

3.1 GUCY2C

The *GUCY2C* gene encodes the GC-C receptor, a membrane protein composed of various domains, including extracellular binding, transmembrane, juxta-membrane, kinase homology, linker, guanylyl cyclase, and C-terminal domains (Figure 3) (69, 70). GC-C is triggered by the guanylin family of peptides, which consists of endogenous peptides, including GN, UG, and lymphoguanylin, and an exogenous peptide toxin produced by enteric bacteria (71, 72).

Growing evidence suggests a close association between CRC and dysbiosis of gut microbiota. Recent studies have shed light on the specific roles of intestinal microorganisms in initiating and facilitating the development of CRC. Notably, our review demonstrates that ETEC produces a substance called ST, which binds to the GC-C receptor with high affinity. ETEC is an important cause of diarrheal disease,

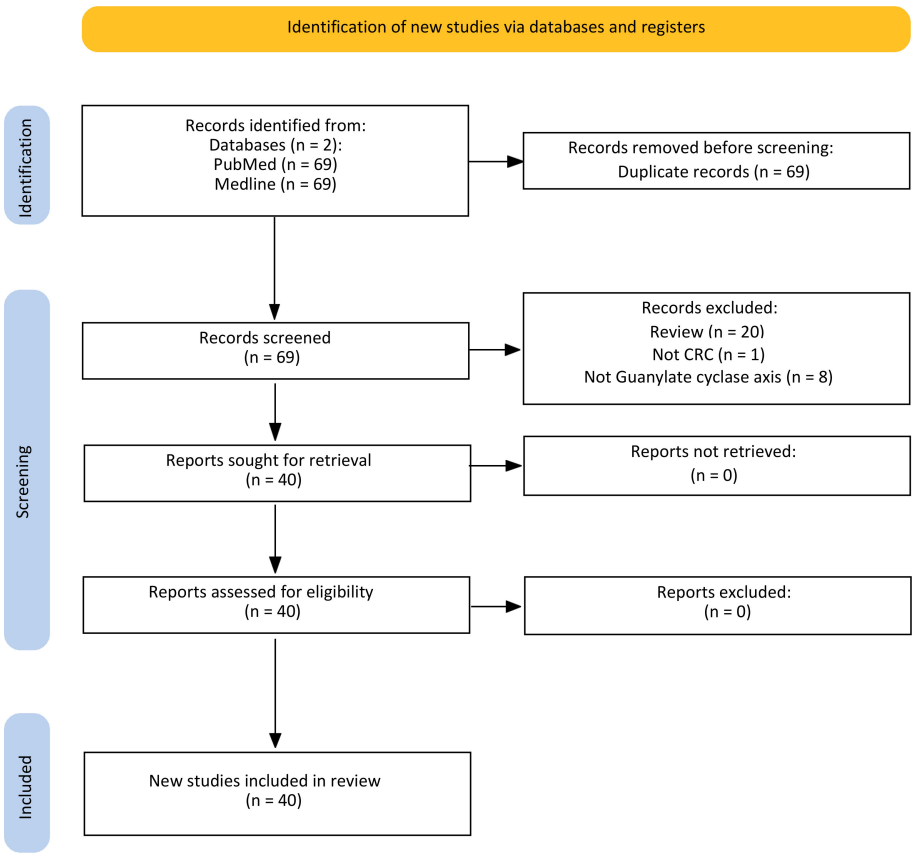

FIGURE 2
Flow chart of the literature search for Guanylate cyclase-C signaling pathway related to colorectal cancer.

TABLE 2 GUCY2C-associated studies included in the systematic review.

Aim	Methods		Result	Ref.
	Data acquisition	Statistical analysis: Algorithms, R packages, etc.		
• Proposing a new method for predicting qRT-PCR efficiency by simulating the kinetics of PCR amplification used to evaluate the expression of GUCY2C mRNA in the blood samples of patients having colorectal cancer.	• 577 human blood samples	• qRT-PCR	• Correlation between the duration until reoccurrence and the longitudinal patterns in GUCY2C. expression was clinically meaningful	(30)
• Investigation of the impact of time, temperature, and ionic strength on the efficiency of radiolabeling and the attainable specific activity of a DOTA-conjugated high-lipophilic peptide, which incorporates three disulfide cyclization bonds.	• DOTA-MLN6907 as a GCC-specific peptide • ^{68}Ga	• Reagents: Citric acid solution Sodium acetate buffers Ethanol solution •Classic and modified acetone approach • Purification and quality assessment following labeling using C-18 • Classic and alternative purification approaches • Detection of free thiol groups • Radiochemical purity and instrumentation	• The radiolabeling process achieved an efficiency exceeding 99%, with a specific activity surpassing 35 $MB_{q/nmole}$ within time frame of under 30 minutes. • The fine-tuned parameters were suitable for implementing an automated 68Ge/68Ga generator and a fluid-handling system, enabling the clinical-scale production of the [68Ga] DOTA-MLN6907 peptide targeted to the GCC receptor. • The chemical properties unique to each peptide dictate the optimal conditions for radiolabeling, ensuring effective preparation of radiopharmaceuticals.	(31)
• Vaccine: Employing the CT26 murine colorectal tumor model to investigate the capacity of non-thermal plasmas to trigger immunogenic cell death *in vivo*	• Non-thermal plasmas • Cell lines CT26.WT CT26-GUCY2C • Balb/c mice	• *In vitro* plasma treatment • *In vivo* plasma treatment • Cell viability assay • ATP release assay • Detection of calreticulin exposed on the cell surface using fluorescence-based methods. • Anti-tumor vaccination assay • Staining tissue sections with H&E and evaluation of tissue damage. •Immunofluorescence staining of tumor tissue • ELISpot analysis	• Application of plasma treatment to subcutaneous tumors resulted in the release of danger signals and the attraction of antigen-presenting cells into the tumor microenvironment. • Enhanced T cell responses directed against the colorectal cancer-specific antigen GUCY2C were noted. • This research offers initial proof that non-thermal plasma genuinely triggers immunogenic cell death, underscoring its potential for practical application in cancer immunotherapy.	(32)
• Investigation of the effectiveness of a human-specific, GUCY2C-directed scFv as a foundation for constructing chimeric antigen receptors aimed at targeting metastases expressing human GUCY2C.	• Cell lines and reagents: CT26 β-galactosidase–expressing CT26.CL25 T84 SW480 CT26.CL25.hGUCY2C Luciferase-containing T84.fLuc 293FT 293F Metastatic tumor models: BALB/c mice NSG mice	• Cell culture • Murine CAR-T Cell Generation • Human CAR-T Cell Generation • CAR Surface Detection • Characterization of mouse T-cells through analysis of phenotypic markers, assessment of activation markers, and intracellular staining of cytokines. • Detection and analysis of activation markers in human T-cells, along with intracellular staining of cytokines. • T-Cell Cytotoxicity Assays	• Murine CAR-T cells directed toward human GUCY2C exhibited antigen-driven activation of T-cells, as evidenced by increased expression of activation markers, cytokine secretion, and selective elimination of GUCY2C-positive cancer cells *in vitro*. • CAR-T cells targeting GUCY2C conferred enduring safeguarding against lung metastases originating from murine colorectal cancer cells modified to express human GUCY2C, as demonstrated in a syngeneic mouse model. • Murine CAR-T cells targeting GUCY2C effectively identified and eliminated human colorectal cancer cells naturally expressing GUCY2C, leading to prolonged survival in a human xenograft model using immunodeficient mice.	(33)

(Continued)

TABLE 2 Continued

Aim	Methods		Result	Ref.
	Data acquisition	Statistical analysis: Algorithms, R packages, etc.		
• Evaluating the impact of cGMP-elevating substances on the process of tumorigenesis within the $Apc^{Min/+}$ mouse model, a recognized model for intestinal cancer.	• Animal models of intestinal cancer male C57/BL6J-*Apc*$^{Min/+}$ mice and female C57/BL6J mice	• Histopathology • qRT-PCR	• Administering *Apc*$^{Min/+}$ mice with the receptor GCC agonist linaclotide or the PDE5 inhibitor sildenafil resulted in a noteworthy decrease in the polyp count per individual mouse. • Both PDE5 inhibitors and receptor GCC agonists demonstrate equal capability in inhibiting intestinal tumorigenesis in mice. • This study emphasizes the promising prospect of manipulating cGMP signaling as a strategy for chemopreventing colorectal cancer in human individuals with elevated risk.	(34)
• Evaluate the effects of TAK-264 in Asian patients with GI malignancies	• 12 patients aged ≥ 18 years diagnosed with GI carcinoma expressing GCC	• Patients' eligibility test: immunohistochemistry • TAK-264 intravenous infusions as a human monoclonal anti-GCC antibody conjugated to monomethyl auristatin E • Evaluations: Dose-limiting toxicities Maximum tolerated dose Pharmacokinetics	• TAK-264 exhibited an acceptable safety record with modest effectiveness against tumors, aligning with findings from research involving patients with advanced gastrointestinal cancers in Western populations. • The amount of TAK-264 in the body rose in direct proportion to the dosage administered.	(35)
• Describing TCRs that identify both the intestinal epithelial cell receptor and the GUCY2C antigen associated with colorectal cancer. • Developing a framework for investigating mechanisms of self-antigen-specific tolerance.	• Animal models: BALB/c Gucy2c$^{-/-}$ and Guc2yc$^{+/+}$ and Rag1$^{-/-}$ mice - Rag1−/− mice as the retrogenic model -	• Immunization with Ad5-GUCY2CECD • Immune responses: ELISpot or intracellular cytokine staining • GUCY2C-specific CD4 + T-cell isolation and TCR sequencing • Creating TCRs, generating retroviruses, and introducing TCRs into T-cells through transduction. • Surface markers and intracellular cytokine staining • Dual-color enzyme-linked ImmunoSpot assays • TCR avidity analysis	• Gucy2c$^{-/-}$ mice lack self-tolerance toward the GUCY2C protein, leading to the production of immune responses targeting this protein. • GUCY2C-specific T-cell responses were observed upon immunization of Gucy2c$^{-/-}$ mice carrying the TCR 4A or 5B variant. • GUCY2C-specific CD4+ T-cell responses, which were suppressed by tolerance in Gucy2c$^{+/+}$ mice, were detected in Gucy2c$^{-/-}$ mice that lacked tolerance mechanisms. • Collectively, these findings validate the effectiveness of TCR retrogenic mice generated through ex vivo TCR repertoire sequencing as a valuable model for investigating mechanisms related to GUCY2C-specific tolerance.	(36)
• Assess the potential therapeutic value of TAK-164, an advanced investigational ADC of the human anti-GCC monoclonal antibody linked to the potent DNA alkylator DGN549 through a peptide linker.	• HEK293 cell line • CB17 severe combined immunodeficient • Nude female mice	• Generation of anti-GCC antibodies and conjugation to DGN549 • Flow cytometry • *In vitro* cytotoxicity assay • Human xenograft tumor studies in mice • HEK-293 GCC cells or human primary tumors in DMEM were injected to mice • Pharmacokinetics analysis • Immunohistochemistry • ^{89}Zr-immuno PET imaging	• Imaging investigations examined the uptake and functionality of TAK-164, revealing positive associations between tumor uptake and GCC expression, which were consistent with the observed antitumor effects. • TAK-164 exhibits significant efficacy across various GCC-positive tumors, even in cases where TAK-264, a GCC-targeted auristatin ADC, has proven ineffective. • A robust correlation exists among the uptake of 89Zr-labeled TAK-164, the extent of GCC expression, and notably, the response to TAK-164 treatment in both GCC-expressing xenografts and PHTX models.	(37)

(Continued)

TABLE 2 Continued

Aim	Methods		Result	Ref.
	Data acquisition	Statistical analysis: Algorithms, R packages, etc.		
• Investigation into the implications of mutant APC-β-catenin-TCF nuclear transcriptional reprogramming on GUCY2C-cGMP signaling pathways.	• Human samples: tumors originated through the conventional pathway (Apc-β-catenin) • Animal models: Apc^{CKO} mice contain a conditional knockout allele of APC • Cells: LS174T DLD1 HT29	• Cell culture •Immunofluorescence • Immunoblots • Messenger RNA analysis • New RNA synthesis	• In both human and mouse APC-dependent tumors, the loss of guanylin hormone expression occurs at the initial stages of transformation, while the GUCY2C receptor remains unaffected. • Broadening the mechanistic framework for colorectal cancer from being solely characterized by irrevocable mutations in APC and β-catenin, to encompass the loss of guanylin hormone, whose restoration and revival of GUCY2C signaling might hold the potential to deter tumorigenesis.	(38)
• Vaccine: Assessing the capacity of a chimeric adenoviral vector (Ad5.F35), created by combining the Ad5 capsid with the Ad35 fiber, to stimulate immune reactions targeting the tumor-associated antigen GUCY2C.	• BALB/cJ mice • Adenovirus vectors: Ad5.F35-GUCY2C-S1 • Vaccine: Adenovirus (Ad-GUCY2C) • Ad5-GUCY2C-S1, Ad5.F35-GUCY2C-S1, or Ad5.F35-GFP (control)	• Western blot • Quantifying T-cell responses by ELISpot • CRC cells *in vivo* tumor studies • Antibody neutralization assay • Ad5 neutralizing immunity studies • Biodistribution and toxicology study	• Ad5.F35-GUCY2C-S1 elicits a targeted immune response against GUCY2C, fostering antitumor immunity. • Antibody responses directed specifically against GUCY2C do not exhibit observable antitumor effects. • Both Ad5 and Ad5.F35 vaccines generated similar S1-specific CD4+ T-cell responses	(39)
• The objective is to explore the presence of circulating GCC mRNA and its connection with clinicopathological features, distant organ metastasis, and long-term survival among patients with stage I–III CRC.	• Circulating GCC mRNA of 160 CRC patient at stage I–III venous blood samples	• qRT-PCR	• The study demonstrated that circulating GCC mRNA serves as a dependable indicator for predicting metastasis and as a prognostic marker in patients with early-stage CRC. This underscores its potential to offer valuable guidance for initiating clinical interventions before tumor dissemination occurs.	(40)
• The promising therapeutic potential and tumor-specific effectiveness of PF-07062119, a CD3-bispecific T-cell engager designed to target tumors expressing GUCY2C. Its role also includes addressing immune evasion mechanisms employed by these tumors.	• Balb/c mice • OASIS 3.0 database for cell lines • PBMC Collection and Isolation of Human T cells for *in vitro* and *in vivo* studies • Whole blood of healthy donors for mononuclear cell and T cell isolation	• Generation of anti-GUCY2C antibodies • Mouse lymphoma 300.19 cells over-expressing human GUCY2C • Characterization of KRAS and BRAF mutational status of Colorectal Cancer CLX and PDX models • Immunohistochemistry • Human T Cell Adoptive Transfer Established Tumor Model • LS1034 Colorectal Orthotopic Tumor Model • CT26-mGUCY2C efficacy study in human CD3ϵ transgenic mice • Pharmacokinetic Measurements of GUCY2C(M)-CD3 in LS1034 Adoptive Transfer Model	• Tumors that express GUCY2C can be specifically targeted using an anti-GUCY2C/anti-CD3ϵ bispecific antibody, which results in the preferential distribution of the drug to the tumor sites. • F-07062119 demonstrated strong T-cell mediated activity *in vitro* and significant effectiveness *in vivo* across various human colorectal cancer xenograft models, including those with KRAS and BRAF mutations. Additionally, its efficacy was confirmed in an immunocompetent mouse model with syngeneic tumors. • The activity of PF-07062119 was amplified through synergistic effects when administered in combination with anti-PD-1/PD-L-1 treatment or alongside anti-angiogenic therapy.	(41)

(Continued)

TABLE 2 Continued

Aim	Methods		Result	Ref.
	Data acquisition	Statistical analysis: Algorithms, R packages, etc.		
		• Cell Culture • GUCY2C Receptor Density Measurements • Characterization of PF-07062119 Binding to human T cells and GUCY2C expressing tumor cells • Cytotoxic T Lymphocyte Assay • IFNγ Induced *In Vitro* by PF-07062119		
• Explored the role of APC heterozygosity in mechanisms repressing hormone expression which could contribute to loss of heterozygosity	• Animal model as a monoallelic Apc loss $Apc^{min}/^{+}$ mice • Tissue specimens from two FAP patients as the human samples	• TCGA database • Immunofluorescence • Western blots • Messenger RNA analysis	• The presence of monoallelic APC loss in $Apc^{min}/^{+}$ mice did not result in any changes to hormone expression. • In patients with FAP, the loss of one allele of APC led to the expression of guanylin, whereas adenomas and cases with biallelic APC loss did not exhibit hormone expression. • Normal intestinal epithelial cells maintain uroguanylin and guanylin expression despite APC heterozygosity, but this expression is lost only after tumor initiation due to APC LOH.	(42)
• The objective is to assess the potential of PTGS2, JAG1, GUCY2C, and PGF-circulating RNA as biomarkers in metastatic CRC.	• 59 serum and blood samples of metastatic CRC patients • 35 patients received chemotherapy + antiangiogenic treatment and 24 patients received just chemotherapy. • Samples from 47 age- and sex-matched healthy controls were selected	• Digital PCR	• In terms of predicting treatment response, serum GUCY2C gene expression emerged as the most effective marker, demonstrating its utility in forecasting patient responses for both individuals receiving antiangiogenic treatment and those not undergoing such therapy. • Serum expression of GUCY2C and GUCY2C/PTGS2 demonstrated significant correlations with therapeutic response. However, none of the biomarkers showed correlations with overall survival or progression-free survival.	(43)
• The study involved the utilization of 89Zr-Df-IAB22M2C (also known as 89Zr-Df-Crefmirlimab), a human CD8-specific minibody, for the purpose of monitoring the infiltration of CD8+ T cells into tumors using positron emission tomography imaging.	• Whole blood of healthy donors for obtaining human T cells • Female NSG mice for xenograft studies	• Generation of anti-GUCY2C antibodies • PBMC collection and isolation and expansion of human T cells • LS1034 xenograft tumor model and bispecific antibody treatment • PET/CT Imaging and Tissue Assessments and analysis • CD8 Immunohistochemistry	• Substantial uptake of 89Zr-Df-IAB22M2C was seen in PF-07062119-treated tumors, significantly higher than controls, and response varied with PF-07062119 dose and treatment duration. • A moderate correlation was found between the uptake of radioactivity in tumor tissue and the density of CD8+ cells, underscoring the imaging agent's utility for non-invasive evaluation of intra-tumoral CD8+ T cells and the mechanism of action of PF-07062119.	(44)
• Investigation into the potential application of oral dolcanatide, an uroguanylin analog designed for improved stability and extended presence in the gastrointestinal tract, to activate GUCY2C and induce cGMP production in the epithelial cells of the distal rectum among healthy volunteers.	• 27 screened healthy volunteers • Eight biopsies collected from the rectum during a flexible sigmoidoscopy procedure	• Direct comparison of cGMP levels versus placebo • Cyclic GMP quantification • Messenger RNA quantification	• While dolcanatide's improved stability allows it to persist along the entire length of the small and large intestine, this alone is insufficient to effectively regulate GUCY2C throughout the colorectum and prevent tumorigenesis.	(45)

(Continued)

TABLE 2 Continued

Aim	Methods		Result	Ref.
	Data acquisition	Statistical analysis: Algorithms, R packages, etc.		
• To detect genes as signature related to CRC which can help to recognition of CRC in the early stage	• GEO database: GSE21510, GSE4107, GSE25071, GSE15781 and GSE8671	• GEO2R • STRING database	• GUCY2C was found as a suppressor gene in PPi networks of downregulated DEGs between CRC and normal samples in GSE datasets	(46)
• Vaccine: Investigating the immune response elicited by a Listeria monocytogenes (Lm) vaccine targeting the colorectal tumor antigen GUCY2C (Lm-GUCY2C).	• Lm-GUCY2C • Lm-LacZ • BALB/cJ mice • CT26 cell line for *in vivo* tumor studies	• live-attenuated double-deleted strain of Lm containing deletions in virulence factors internalin B and actA • IFNγ ELISpot Assay • MHC Class I Stability Assay • CAR Surface Detection • Tumor Studies	• Lm-GUCY2C induced strong CD8+ T-cell reactions against Lm-specific peptides, implying that the GUCY2C254-262 peptide might have a subordinate role compared to the Lm-derived peptides. • By introducing an amino acid substitution at a crucial anchoring site for H-2Kd binding, resulting in GUCY2CF255Y, the stability of the peptide complex improved significantly with H-2Kd. This modification effectively restored the immunogenicity of GUCY2C254-262 when integrated into the context of Lm vaccination.	(47)
• Vaccine: Investigating a prime-boost approach involving a chimeric adenoviral vector (Ad5.F35) engineered to overcome pre-existing immunity, followed by recombinant Lm to enhance immune response toward the gastrointestinal cancer antigen GUCY2C.	• Vaccines: Ad-GUCY2C • Adenovirus expressing mouse GUCY2C1-429 fused to the influenza HA107-119 CD4+ T-cell epitope • Lm-GUCY2C and Lm-LacZ • mouse macrophage cell line J774A.1 (ATCC) • BALB/cJ mice	• *In vitro* infections • Immunizations • Ad5-neutralizing immunity studies • IFNγ ELISpot assay • Intracellular cytokine staining • *In vivo* tumor studies • Safety studies • Blood chemistry and cytokine analyses • Western blot	• Immunization with both heterologous Ad-GUCY2C and Lm-GUCY2C enhances CD8+ T-cell responses specific to GUCY2C and boosts antitumor immune activity. • Previous exposure to Ad5 restricts the effectiveness of Ad5.F35+Lm immunization protocols, whereas prior Lm exposure does not impose such limitations. • Alterations in the qualitative characteristics of the CD8+ T-cell population after a prime-boost vaccination regimen. • Lm-GUCY2C could potentially be employed to enhance GUCY2C-specific immune responses in patients undergoing clinical trials with adenovirus-based GUCY2C vaccines, aiming to prevent or manage recurrent GI cancer.	(48)
• Investigating the process of GUCY2C ligand transcriptional suppression mediated by β-catenin/TCF signaling.	• RNA-seq gene expression data from normal mucosa n=51 and primary colon tumors n=380 from TCGA COAD/READ dataset • 4 unique conditional human colon cancer cell models of β-catenin/TCF signaling • Wild-type C57B/6(J) mice • Cell lines: DLD1, LS174T, TCF7L2, LS174T	• RNA sequencing analysis • luciferase reporters • Immunofluorescence • Immunoblots •RNA analysis and sequencing • Plasmids and Cloning • CRISPR Cell Line Generation • Lentiviral Production and Transduction • Chromatin Immunoprecipitation and sequencing • TCGA dataset analysis	• RNA sequencing analyses uncover GUCY2C hormones as among the most responsive targets of β-catenin/TCF signaling, indicative of transcriptional downregulation. • The GUCY2C hormones are situated within a distinct genomic region, featuring a novel locus control region positioned upstream of the guanylin promoter. This regulatory element plays a role in orchestrating the simultaneous suppression of both genes. • Using CRISPR epigenome editing to target this region led to the restoration of GUCY2C ligand expression, effectively overcoming the gene inactivation caused by mutant β-catenin/TCF signaling.	(49)
• Evaluating the safety and tolerability profile of TAK-164, an experimental antibody-drug conjugate targeting GCC	• 31 patients with GCC-positive, advanced gastrointestinal cancers	• Intravenous TAK-164 on day 1 of 21-day cycles via a Bayesian model	• Except cycle 1, dose-limiting toxicities evaluation in subsequent cycles dose-limiting treatment-emergent adverse events such as grade 3 pyrexia, grade 5 hepatic failure, decline in platelet and neutrophil count in patents were observed • A single patient (at a dose of 0.008 mg/kg) who exhibited elevated initial GCC expression demonstrated a preliminary but unconfirmed partial response.	(50)

(Continued)

TABLE 2 Continued

Aim	Methods		Result	Ref.
	Data acquisition	Statistical analysis: Algorithms, R packages, etc.		
			• TAK-164 exhibited a controlled and well-handled safety profile when administered at a dose of 0.064 mg/kg. • The Recommended Phase 2 Dose (RP2D) of 0.064 mg/kg was deemed inadequate to achieve clinical benefit, consequently leading to the decision of not pursuing further clinical development.	

qRT-PCR, Quantitative Real-Time Polymerase Chain Reaction; GUCY2C, Guanylate Cyclase 2C;DOTA, Dodecane Tetraacetic Acid; ScFv, Single-chain variable fragments; H&E, haematoxylin and eosin; TCR, T cell receptor; CAR, Chimeric Antigen Receptors; APC, Adenomatous Polyposis Coli; PDE, phosphodiesterase; GC-C, Guanylate Cyclase-C; TCR, T cell receptor; ELISpot, enzyme-linked immunosorbent spot; DMEM, Dulbecco's Modified Eagle Medium; PET, positron emission tomography; PHTX, Primary Human Tumor Xenograft; TCF, T Cell Factor; ADC, antibody-dug conjugate; CRC, colorectal cancer; Ad, Adenovirus; GFP, Green Fluorescent Protein; PBMC, Peripheral Blood Mononuclear Cells; CLX, cell line xenograft; PDX, patient-derived xenograft; TCGA, The Cancer Genome Atlas; FAP, Familial Adenomatous Polyposis; LOH, loss of heterozygosity; NSG, NOD-scid IL2Rγnull; GEO, Gene Expression Omnibus; STRING, Search Tool for the Retrieval of Interacting Genes/Proteins; PPi, Protein–protein interaction; DEGs, Differentially Expressed Genes; Lm, Listeria Monocytogenes; ATCC, American Type Culture Collection; MHC, Histocompatibility Complex; GI, Gastrointestinal; CRISPR, clustered regularly interspaced short palindromic repeats; RP2D, Recommended Phase II Dose.

TABLE 3 GUCY2A-associated studies included in the systematic review.

Aim	Methods		Result(s)	Ref.
	Data acquisition	Statistical analysis: Algorithms, R packages, etc.		
Exploring the potential significance of the GUCA2A-GUCY2C axis and its viability as a target in tumors originating from the SA and MSI pathways.	• TCGA database • GEO database • Human tumor tissues and histological interpretation • Mouse tissues • RNA isolation • Quantitative reverse-transcription polymerase chain reaction • Immunoblot analysis	• GraphPad Prism	• Guanylin hormone expression was omitted in TAs, SAs, and MSI tumors compared to their corresponding normal adjacent tissues. • Silence GUCA2A in pathophysiology and utilize oral hormone replacement to restore GUCY2C signaling, preventing MSI tumors.	(51)
To pinpoint a gene with notable clinical relevance for CRC diagnosis, treatment, and prognosis prediction.	• GEO database • WGCNA • RRA Analysis • Survival Analysis • qRT-PCR	• Limma package • RobustRankAggreg • WGCNA package	• GUCA2A was identified as a hubgene in CRC. • GUCA2A expression was significantly correlated with the OS of CRC patients. • qPCR analysis showed that GUCA2A expression in tumor and metastatic tissues was significantly low compared with adjacent normal tissues. • GUCA2A has a potential diagnostic value for CRC patients with 80.6% sensitivity and 83.5% AUC.	(52)
To pinpoint fundamental genes linked to CRC.	• GEO database • GEPIA database • Limma package • Enrichment analysis • qRT-PCR • STRING database	• clusterProfile package • Limma package • VennDiagram package	• GUCA2A identified as a hub gene in CRC. • Expression levels of GUCA2A were not correlated with the overall survival in CRC patients. • qRT-PCR showed that there was no significant differential expression of GUCA2A between CRC tissues and normal colorectal tissues.	(16)
To explore potential gene targets for the diagnosis and treatment of PCRC	• GEO database • TCGA database • DAVID database	• GEO2R	• GUCA2A was identified as a hub gene in PCRC. • Expression level of GUCA2A was not	(53)

(Continued)

TABLE 3 Continued

Aim	Methods		Result(s)	Ref.
	Data acquisition	Statistical analysis: Algorithms, R packages, etc.		
	• Enrichment analysis • STRING database • cBioPortal database • Xena database • GEPIA database • Kaplan-Meier plotter • comparative toxicogenomics database		correlated with the overall survival of PCRC patients.	
To extract the gene expression profile data of colon cancer from TCGA database, and explore the potential utility of the TMB in immunotherapy and individualized medication.	• TCGA database • TMB value estimation • Relationship between TMB value and overall survival • Correlation between TMB value and clinicopathological features • Relationship between TMB and differentially-expressed genes	• CRAN package • Limma package • Pheatmap package • clusterProfiler package • org.Hs.eg.db package • ggplot2 package • CIBER-SORT analysis platform • Survival package	• GUCA2A is positively correlated with CRC patients' survival	(54)
Assess gender-related distinctions in the transcriptome of both non-tumor colon epithelium and CRC	• TCGA database • RNA isolation • qPCR • feature selection • machine learning classification • Overall survival analysis	• Bioconductor package	• GUCA2A identified as a CRC prognostic biomarker in males	(55)
To identify CRC-associated genes	• GEO database • Identifcation of common DEGs in CRC and diferentially expressed miRNAs • STRING database • Identifcation of CRC–associated core genes	• Limma package	GUCA2A identified as a core gene in CRC.	(56)
Discover potential novel biomarkers for CRC and gain deeper insights into the molecular pathways contributing to CRC development.	• GEO database • Processing of lncRNA expression profiles • WGCNA and the identification of modules	• GEOquery package • Limma package • WGCNA package	• GUCA2A identified as a hub gen in CRC.	(57)
To mine the GEO datasets associated with CRC studies and identify potential targets correlated with CRC pathogenesis.	• GEO database • Screening common DEGs • Kaplan–Meier Survival Analysis of Patients with CRC	• GREIN-iLINCS	• GUCA2A was identified in a key sub-network in CRC. • Expression level of GUCA2A was not correlated with the overall survival of CRC patients.	(58)

(Continued)

TABLE 3 Continued

Aim	Methods		Result(s)	Ref.
	Data acquisition	Statistical analysis: Algorithms, R packages, etc.		
To discover key pathways and genes implicated in the onset, development, and adverse prognosis of CRC.	• GEO database • GEPIA database • UALCAN database • OncoLnc database • DAVID database • STRING database	• GEO2R	• GUCA2A identified as a hub gene in CRC. • GUCA2A demonstrated a significant association with lower survival rates.	(59)
To identify central genes linked to colorectal adenocarcinoma and subsequently assess their prognostic relevance.	• GEO database • TCGA database • WGCNA analysis • Enrichment analysis • STRING database • HPA database	• Limma package	• GUCA2A identified as a hub gene in CRC. • CLCA1, CLCA4, and GUCA2A were identified as a 3-Gene Signature in CRC • Protein levels of GUCA2A are significantly lower than normal tissues.	(60)

GUCA2A, Guanylyl cyclase-activating protein 2A; TCGA, The Cancer Genome Atlas; GEO, Gene Expression Omnibus; TA, tubular adenomas; SA, serrated adenoma; MSI, microsatellite instability; CRC, colorectal cancer; WGCNA, Weighted gene correlation network analysis; RRA, Rapid Risk Assessment; OS, overall survival; qPCR, quantitative polymerase chain reaction; AUC, Area under the Curve; PCRC, Primary colorectal cancer; GEPIA, Gene Expression Profiling Interactive Analysis; STRING, Search Tool for the Retrieval of Interacting Genes; DEGs, Differentially Expressed Genes; DAVID, database for annotation; visualization and integrated discovery; CLCA, Chloride channel accessory; HPA, The Human Protein Atlas.

TABLE 4 GUCY2B-associated studies included in the systematic review.

Aim	Methods		Result	Ref.
	Data acquisition	Statistical analysis: Algorithms, R packages, etc.		
suggesting a diagnostic method based on KRAS mutation and gene expression analysis that may be regularly used in clinics to choose the best course of action for each patient.	• Twenty-four patients who underwent surgery in the years 2013 or 2014 at the two University hospitals "Kaspela" and "St. George"	• DNA Isolation • RNA Isolation • qPCR	• GUCA2B is the gene with the most severe downregulation. • GUCA2B exhibits the most pronounced transcriptional downregulation.	(61)
In order to outline the indicators and transcriptional conditions, the goal is to recognize a colonic epithelial cell and reveal essential factors that lead to barrier dysfunction in inflammatory bowel disease.	• Isolation of epithelial cells from patients with IBD biopsies • GEO database: GSE116222 • Github • ProteomeXchange Consortium	• Isolation of epithelial cells from patient biopsies • Droplet-based single-cell RNA sequencing • Plate-based scRNAseq • RT-PCR • Proteomic analysis of BEST4/OTOP2 cell population • Animal Experiment • SEM and TEM • Organoid culture *Computational analysis: Cell Ranger • Crypt-axis score • Semisupervised clustering of public scRNA-seq data • TCGA	• GUCA2B's peptide uroguanylin activates GC-C and cyclic GMP in epithelial cells containing metallothionein genes, guarding against free radicals and transporting and storing metals. • BEST4/OTOP2 cell which expresses uroguanylin, identified. According to the research, IBD and colorectal cancer cases have lower levels of uroguanylin-producing colonic epithelial cells.	(62)

(Continued)

TABLE 4 Continued

Aim	Methods		Result	Ref.
	Data acquisition	Statistical analysis: Algorithms, R packages, etc.		
		• Cluster marker and differentially expressed gene identification • Microarray analysis • Ontology enrichment analysis • Smart-seq2 scRNA-seq data processing and analysis • Proteomics data analysis • BEST4/OTOP2 cell marker overlap • Trajectory and pseudo-time analysis • Analysis of tissue-specific • expression of GWAS loci		
Using bioinformatics, this study aims to investigate possible gene targets for the detection and therapy of PCRC	• GEO database: 1. GSE81558 dataset • GO database • KEGG database • DAVID	• GEO2R • Limma • GEOquery • Metascape • GSEA • STRING • Molecular Complex Detection • cytoHubba • cBioPortal • GEPIA • Kaplan-Meier plotter • CTD	• The expression of GUCA2B did not have any statistically significant effects on OS. • GUCA2B is a key gene among DEGs.	(53)
The current study aims to apply bioinformatics to discover the PCRC hub genes and to confirm their impact on patients' overall survival based on clinical data.	• GEO database: GSE81558, GSE41258 and GSE81558 • DAVID • KEGG database	• Pearson's correlation test • principal component analysis • GEO2R • Limma package • GEOquery • SangerBox • online Venn tool • STRING • Gene Ontology analysis • Molecular Complex Detection tool • Cytoscape • cytoHubba • cBioPortal • Coexpedia • GEPIA	• GUCA2B is a key gene among 10 hub genes. • The expression of GUCA2B did not show a statistically significant impact on overall survival	(63)

(Continued)

TABLE 4 Continued

Aim	Methods		Result	Ref.
	Data acquisition	Statistical analysis: Algorithms, R packages, etc.		
		• SPSS software • RT-qPCR assay		
This study employed an integrated analysis, combining gene expression patterns from four microarray datasets in GEO with miRNA expression profiles. The analysis aimed to identify genes associated with CRC through microarray data analysis.	• GEO database: GSE37182, GSE25070, GSE10950 and GSE113513 datasets • miRNA platform: • GSE115513 and GSE30454 • DAVID • KEGG database	• Limma package • Venn diagrams website • Gene ontology analysis • STRING website • Cytoscape program	• GUCA2B is a key gene among 10 hub genes. • GUCA2B with a score of 8 and standing in 4th rank between other hub genes and interacting with other nine hub genes suggesting their crucial role in CRC progression	(56)
Through an in-depth examination of the data in TCGA, the current work aims to acquire an understanding of the processes regulating B4GALNT2 expression and its relationship to cancer	• Oncolnc website • Gene expression data of 626 colorectal adenocarcinomas (COADREAD) from TCGA • Gene methylation data of 288 tumor samples were downloaded from TCGA • CSmiRTar website	• Kaplan–Meier survival curve • Smartapp tool • genecards.org"	• A larger molecular profile, including GUCA2B, is linked to high B4GALNT2 expression as a reliable indicator of a favorable prognosis in CRC.	(64)
Suggesting chemically altering uroguanylin, which is expressed in tumors that have metastatic CRC, to encourage its anchoring to SNs (UroGm-SNs).		• Preparation of UroGm-SNs • Physicochemical characterization • Morphological examination • Ligand density calculation • Preparation of dual-loaded SNs • Cell viability studies • Cellular internalization studies • Colony forming assays • *In vivo* effectiveness of UroGm-Etp-SNs in mice harboring SW620 xenografts.	• UroGm was effectively engineered to anchor onto the surface of nanoparticles, maintaining its therapeutic attributes without compromise.	(65)
The primary objective of the recent study was to investigate possible transcriptome biomarkers or treatment targets of CRC.	• GEO database: 2. GSE89393 dataset • preservation analysis: 3. GSE41328, GSE54986, GSE81582, GSE100179, GSE113513, and GSE137327 datasets • RNA-seq data: 4. Colon Adenocarcinoma (COAD) patients were obtained from the TCGA database • UCSC Cancer Browser • TargetScan databases • GSE180202 dataset	• edgeR package • CluePedia • WGCNA • TOM • dissimilarity TOM (dissTOM) • Module Eigengene • GEPIA • RT-qPCR • Shapiro-Wilk normality test • Venny software • STRING website	• The brown module correlated positively with CRC in WGCNA. • CRC tissues showed lower GUCA2B expression by RT-qPCR. • GUCA2B is a key gene among DEGs. • The top miRNAs associated with GUCA2B were found. • According to ROC studies, GUCA2B has a strong diagnostic performance for CRC.	(66)

(Continued)

TABLE 4 Continued

Aim	Methods		Result	Ref.
	Data acquisition	Statistical analysis: Algorithms, R packages, etc.		
To find possible targets linked to CRC pathogenesis, we mined the GEO datasets connected to CRC research.	• GEO database: 5. GSE50760 and GSE104178 datasets • KEGG database	• GREIN-iLINCS online analysis tool • EnrichR • STRING tool • miRDB • Cytohubba tool • Cytoscape software • Kaplan Meier plotter • GEPIA tool	• There was no correlation between the expression levels of GUCA2B with the overall survival of CRC patients. • GUCA2B is a key gene among DEGs.	(58)
This study investigated the association between ICIs in CRC and missense mutations in DNAH7, the gene encoding the axonemal dynein heavy chain.	• A clinical cohort (n=690) • TCGA database • GO database • KEGG database • MSIgDB database	• VarScan software • TCGAbiolinks package • GenePattern5, GISTIC2.0 • Wilcoxon rank-sum test • DESeq2 package • Gene Ontology analysis • ClusterProfiler R software package • GSEA • ESTIMATE analysis • The Mann-Whitney U test • STRING online tool • Cytoscape (V3.7.2) • Maximal Clique Centrality (MCC) algorithm • cytoHubba	• GUCA2B emerges as a prominent key gene linked to the DNAH7 mutation.	(67)
To explore the molecular signatures causing CRC as receptors and drug agents as inhibitors by using integrated statistics and bioinformatics approaches.	• GEO database: 6. GSE9348, GSE110224, GSE23878, and GSE35279 datasets.	• LIMMA package • STRING database • GEPIA • TIMER • MethSurv • Enrichr • DisGeNET • miRTarBase • DSigDB	• GUCA2B is a key gene among DEGs. • Downregulation of GUCA2B in COAD and READ. • GUCA2B gene is significantly methylated at the CpG site	(68)

qPCR, quantitative polymerase chain reaction; GUCA2B, Guanylate Cyclase Activator 2B; GEO, Gene Expression Omnibus; RT-PCR, Reverse transcription polymerase chain reaction; SEM, Scanning electron microscopy; TEM, Transmission electron microscopy; GC-C, Guanylate cyclase-C; IBD, Inflammatory bowel disease; TCGA, The Cancer Genome Atlas; KEGG, Kyoto Encyclopedia of Genes and Genomes; DAVID, database for annotation; visualization and integrated discovery; GSEA, Gene set enrichment analysis; STRING, Search Tool for the Retrieval of Interacting Genes; GEPIA, Gene Expression Profiling Interactive Analysis; CTD, The comparative toxicogenomics database; CRC, colorectal cancer; SNs, sphingomyelin nanosystems; UroGm, uroguanylin expressed in metastatic colorectal cancer tumors; WGCNA, Weighted gene correlation network analysis; TOM, Topological Overlap Matrix; DEGs, Differentially Expressed Genes; ROS, Receiver operating characteristic; READ, Rectal Adenocarcinoma.

particularly in low- and middle-income countries (73). Conversely, the incidence of CRC in developed countries is up to ten times higher than in underdeveloped countries (74). Intriguingly, an inverse epidemiological correlation exists between diarrheal diseases caused by ST-producing ETEC and colorectal cancer. This inverse correlation may be attributed to the involvement of *GUCY2C* as a tumor suppressor in CRC pathophysiology, particularly in developing countries. A recent study in mice has revealed that chronic colonization with ST-producing Escherichia coli counters the development of colorectal tumors. These findings suggest that bacterially produced ST reinstates *GUYC2C* signaling, which in turn opposes the tumor transformation (75). Additionally, more research is

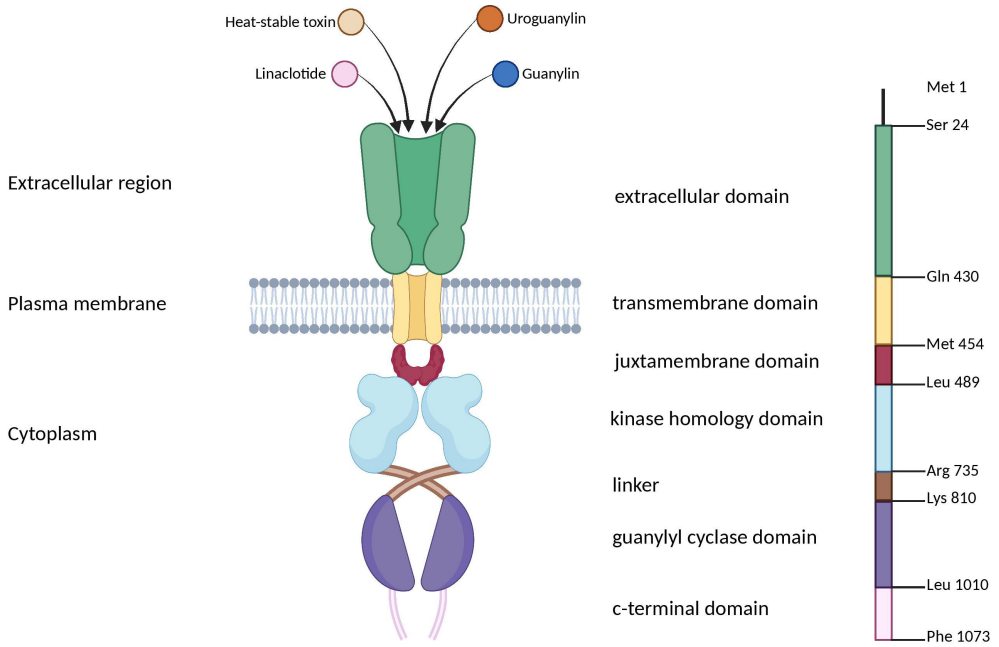

FIGURE 3
Schematic representation of domain organization of the guanylyl cyclase GC-C receptor. GC-C is predicted to be a transmembrane receptor homodimer with seven functional domains. These domains include the extracellular domain responsible for binding peptide ligands such as STs, guanylin, uroguanylin, and the FDA-approved ST analog, Linaclotide. Additionally, there is a transmembrane domain, a juxta membrane domain, a kinase-homology domain, and a linker region that may facilitate catalytic subunit dimerization and regulate its function. GC-C, Guanylate Cyclase-C; ST, heat-stable enterotoxins. Created with BioRender.com.

needed to investigate the potential of using ST as a possible prophylactic or therapeutic approach for preventing or treating CRC. These studies could pave the way for developing novel strategies for CRC prevention and treatment.

Moreover, the activation of the GC-C signaling axis is pH-dependent, meaning that different parts of the gastrointestinal (GI) tract have different regulatory effects (28, 29). The distribution of GC-C receptors throughout the GI tract is widespread, but their activation patterns depend on the location and type of activator. In the upper small intestine, GC-C receptors are more strongly activated at lower pH levels (~ pH 5.5) by UG. On the other hand, in the lower small intestine and colorectum, these receptors are activated at higher pH levels (~ pH 8.0) by GN (Figure 4) (76, 77).

Upon binding of agonist peptides to the extracellular domain of the GC-C receptor, the intracellular catalytic domain converts guanosine triphosphate into cyclic guanosine monophosphate (cGMP). This second messenger then activates cGMP-dependent protein kinases G (PKG), cyclic-nucleotide-gated (CNG) channels, and cGMP-regulated cyclic-nucleotide phosphodiesterase (78). In intestinal cells, protein kinase G II (PKGII) phosphorylates the cystic fibrosis transmembrane conductance regulator (CFTR), leading to increased efflux of chloride (Cl^-) and bicarbonate (HCO^-) ions from intestinal cells into the lumen. The resulting anion efflux causes a net osmotic increase, driving water into the GI tract and promoting fluid secretion (Figure 5A) (78, 79).

GC-C also controls the balance between proliferation and differentiation by increasing p21 expression under normal physiological circumstances (77, 80). It has been shown that GC-C mediates antitumorigenic processes in addition to p21-mediated cytostasis. One prominent instance is the GC-C signaling-mediated attenuation of β-catenin-mediated TCF transcriptional activity. PKGII-mediated signaling opposes β-catenin/TCF-mediated proliferative and promigratory phenotypes (81, 82). β-catenin/TCF signaling, in turn, suppresses the GC-C axis by inhibiting the transcription of its ligands, GN and UG. Additionally, GC-C blocks PTEN-mediated pro-tumorigenic Akt signaling (Figure 5B) (78, 83–85). As a tumor suppressor, GC-C regulates the migration and differentiation of stem cells at the base of intestinal crypts into enterocytes and other cell types (23). In fact, inhibiting the GC-C axis results in hyper-proliferation, hyperplasia of proliferating crypts, accelerated migration, diminished differentiation along the secretory lineage, and decreased apoptosis (77).

Another noteworthy aspect of GC-C is its potential as a tumor biomarker for CRC detection. While guanylyl cyclase family members are typically only expressed in normal intestinal cells, GC-C is found in approximately 95% of colorectal and some other gastrointestinal cancers, such as pancreatic tumors. In contrast, GC-C expression is rare in non-intestinal tissues and tumors. This suggests that GC-C could be a valuable and novel biomarker for identifying CRC (17, 86, 87).

In a study conducted by Jimenez-Luna et al. (43), the potential of *GUCY2C*, *PTGS2*, *JAG1*, and *PGF* circulating RNAs as biomarkers in metastatic CRC (mCRC) was investigated. The researchers collected 59 serum and blood samples from mCRC patients, divided into two groups: one receiving chemotherapy plus antiangiogenic treatment and the other receiving only

10.3389/fonc.2023.1277265

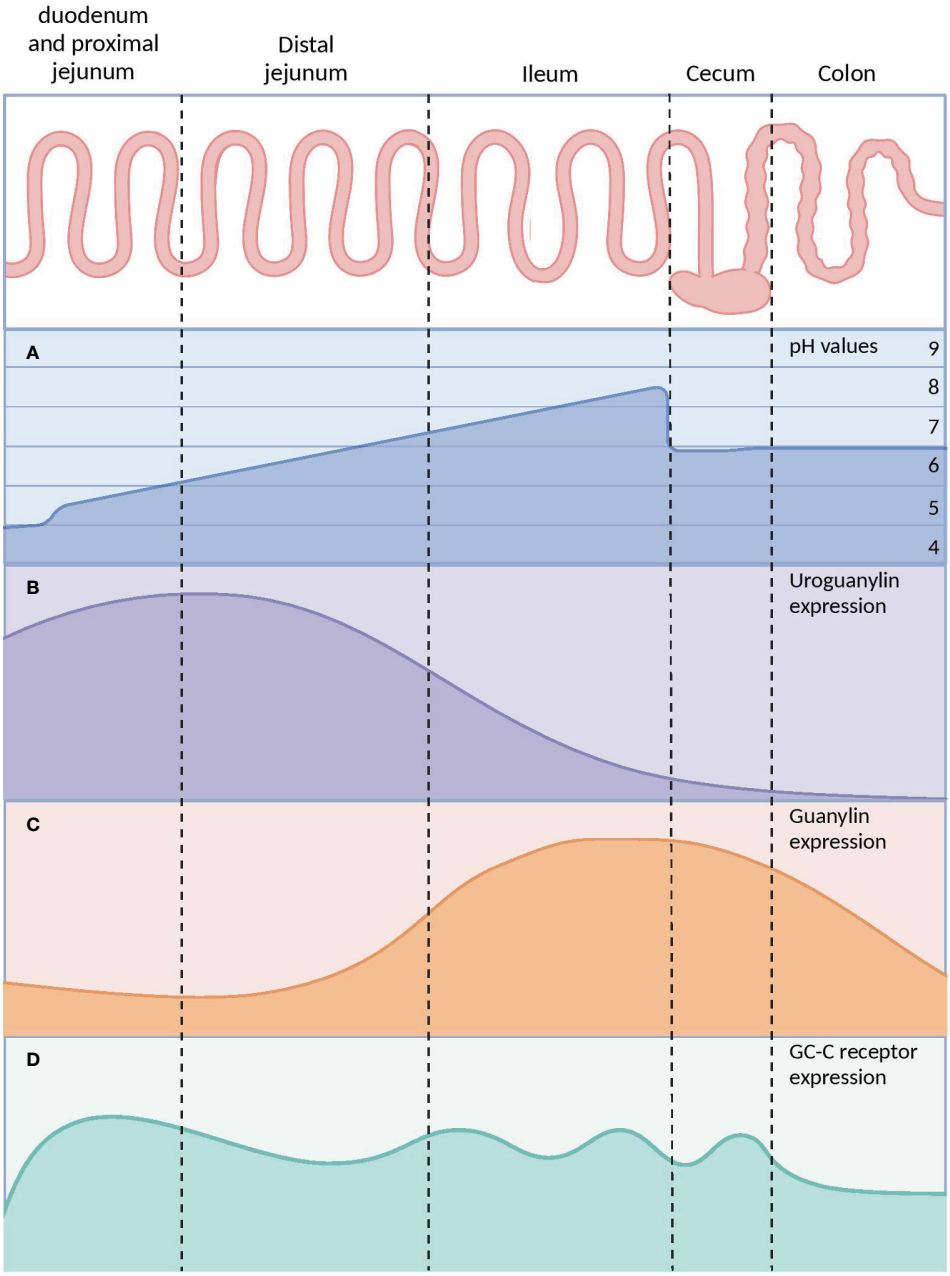

FIGURE 4
The differences in pH and GC-C signaling axis parts throughout the gastrointestinal tract. **(A)** The pH of the small intestine increases gradually while the pH of the caecum decreases due to microorganism populations. **(B)** UG expression is at its maximum in the distal jejunum and at its lowest in the colon. **(C)** GN concentrations rise along the distal small intestine, peak in the caecum, and then drop rapidly in the distal colon. **(D)** The expression of GC-C receptors is constant throughout the intestine. GC-C, Guanylate Cyclase-C; UG, Uroguanylin; GN, Guanylin. Created with BioRender.com.

chemotherapy. Additionally, 47 healthy control samples were included. The samples were then analyzed using digital polymerase chain reaction (PCR). The study revealed a significant correlation between *GUCY2C* and *GUCY2C/PTGS2* expression in the bloodstream and the response to anti-angiogenic agents. These results suggest that evaluating genes involved in the process of angiogenesis could serve as a promising non-invasive diagnostic tool for metastatic colorectal cancer and predict its response to anti-angiogenic therapy (43) (Table 2).

Blomain et al. (38) contributed significantly to understanding intestinal tumorigenesis by uncovering the crucial role of the GN hormone and GC-C receptor signaling in tumor initiation and progression. Specifically, their study revealed that the loss of GN hormone expression, but not the GC-C receptor, occurs at the earliest stages of adenomatous polyposis coli (APC)-dependent tumor transformation in both humans and mice. This loss of GN expression results from mutant APC-β-catenin-TCF transcriptional regulation, which suppresses GC-C signaling and perturbs intestinal

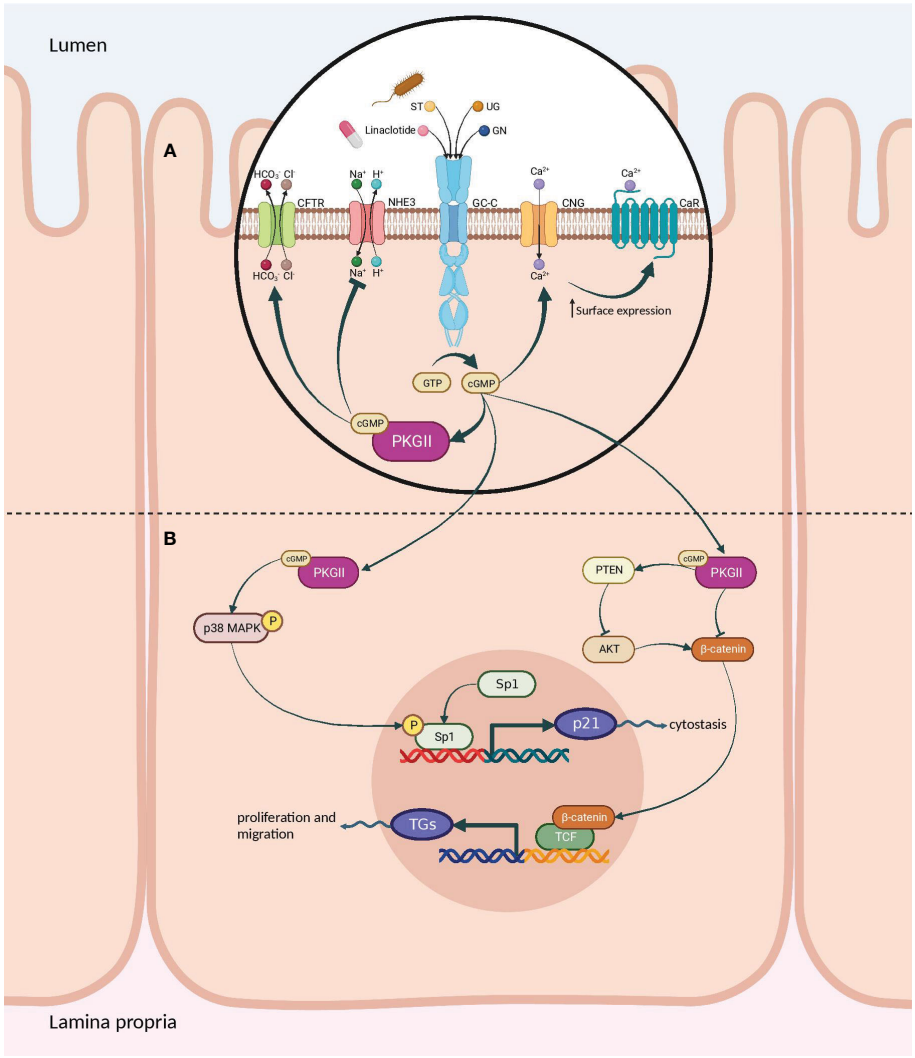

FIGURE 5
Signaling pathways of the GC-C/cGMP axis that regulate fluid-ion homeostasis and cellular proliferation in the intestine. **(A)** The binding of ligands to GC-C catalyzes the formation of cGMP from GTP. Increased intracellular cGMP levels result in the activation of cGMP-dependent PKGII. Reduced intestinal sodium absorption is caused by PKGII-mediated inhibitory phosphorylation of NHE3. PKGII phosphorylated and activated the CFTR anion channel, increasing intestinal chloride and water secretion. Increased cGMP activates CNG ion channels, promoting $Ca2^+$influx, which recruits CaR to the plasma membrane. **(B)** Cyclic GMP production activates PKGII and p38 MAPK, resulting in phosphorylation of the Sp1 transcription factor. Sp1 upregulates the expression of p21 and mediates cytostasis. PKGII-mediated signaling opposes pro-survival and pro-proliferative phenotypes mediated by the β-catenin/TCF and Akt pathways. GC-C, Guanylate Cyclase-C; PKGII, Protein kinase G II; Protein kinase; NHE3, Na^+/H^+ exchanger isoform 3; CFTR, Cystic fibrosis transmembrane conductance regulator; CNG, Cyclic nucleotide-gated; CaR, calcium-sensing G-protein coupled receptors; MAPK, Mitogen-activated protein kinases; TCF, T cell factor. Created with BioRender.com.

homeostatic mechanisms, contributing to tumor progression. The authors proposed that the replacement and reconstitution of GC-C signaling could prevent tumorigenesis by restoring the GN hormone expression (38). This finding provides a potential therapeutic target for preventing the development and progression of intestinal tumors.

Recent studies have focused on the extensive utilization of *GUCY2C* biology in experimental cancer immunotherapy, including developing vaccines, immunotoxins, and chimeric antigen receptor (CAR) T cells (88). Developing cancer vaccines that can activate the immune system to identify and destroy cancer cells holds immense potential (89). One approach that has recently piqued interest is targeting the GC-C receptor to create effective cancer vaccines. For example, the promising results in preclinical and clinical trials suggest that GC-C-based therapies could effectively treat cancer. In the study by Flickinger et al. (48), a prime-boost strategy was investigated that involved the use of a chimeric adenoviral vector (Ad5.F35) that is resistant to pre-existing immunity, followed by recombinant Listeria monocytogenes (Lm) to amplify immunity to the GI cancer antigen GUCY2C. It was found that the combination of Ad5.F35 and Lm-GUCY2C enhanced the quantity, avidity, polyfunctionality, and antitumor efficacy of GUCY2C-specific effector CD8+ T cells in mice. The results suggest that Lm-GUCY2C could be used to increase GUCY2C-specific immunity in patients who are given adenovirus-based GUCY2C vaccines that

are currently being tested in clinical trials to prevent or treat recurrent GI cancer (48).

In another study, Lin et al. (32) demonstrated the potential of non-thermal, atmospheric pressure plasma (NTP) in inducing immunogenic cell death in an animal model of CRC. The study included assessments of cell viability, anti-tumor vaccination assays, and ELISpot analysis. The findings suggest that NTP treatment can enhance T-cell responses targeting the CRC-specific antigen GC-C, potentially enhancing the immune system's ability to recognize and eliminate cancer cells. The study sheds light on the possible role of non-thermal plasma in stimulating immunogenic cell death for future clinical applications in cancer immunotherapy and vaccine manufacturing, particularly for CRC.

CAR T-cell therapy is a promising treatment method by engineering T cells to express CARs that can target cancer cells. By doing this, the immune system can selectively attack and eliminate tumors (90). A highly optimistic target for this therapy is the GC-C receptor. In an investigation, Magee et al. (33) engineered a human-specific single-chain variable fragment (scFv) directed toward GC-C to engineer CAR-T cells for the treatment of colorectal cancer metastasis. The CAR-T cells were tested in preclinical murine models and provided long-term protection against murine colorectal cancer cells expressing human *GUCY2C* lung metastases. The study also demonstrated the ability of the CAR-T cells to recognize and kill human colorectal cancer cells expressing *GUCY2C* in a xenograft model in immunodeficient mice. These findings suggest the potential of human *GUCY2C*-specific CAR-T cell therapy for the treatment of metastatic colorectal cancer expressing *GUCY2C* (33). GUCY2C-targeted CAR T cells could offer a novel and effective strategy for treating CRC, particularly those in advanced stages of cancer or refractory to conventional therapies.

3.2 GUCA2A

The Guanylate Cyclase Activator 2A (*GUCA2A*) gene encodes Guanylin (GN), which is a bioactive peptide synthesized in the intestinal mucosa and acts as an endocrine ligand for GC-C. GN serves crucial functions in maintaining intestinal fluid homeostasis and preserving gut physiology (91). The mature form of guanylin consists of 15 amino acids derived from the C-terminus of a longer pre-proguanylin peptide. This longer peptide includes a signal sequence and a proguanylin sequence span residues 1-21 and 22-115, respectively (92). Although some studies indicate that proguanylin is the primary form of the peptide that is secreted, the specific enzymatic pathway that processes proguanylin into its bioactive GN form has not been entirely understood yet (93). The GN peptide comprises four cysteine residues, enabling the assembly of two intramolecular disulfide bonds. The disulfide bonds in the peptide are essential for keeping the peptide in its proper shape, which is required for binding to the GC-C receptor (Figure 6A) (94). The GC-C receptor is additionally stimulated by the enteric bacterial ST peptides, which comprise 19 amino acids and three disulfide bonds and are homologs of GN (93, 95). The 3-disulfide structure of ST peptides significantly enhances their potency at the GC-C receptor, surpassing that of endogenous GC-C agonists (94). GN exists in two isoforms, a right-handed and a left-handed spiral form, which exhibits different biological activities and has varying affinities for binding to GC-C (95). The bioactive isomer of GN binds to the extracellular domain of GC-C, leading to the activation of the receptor's intracellular domain. The biological relevance and mechanism of the interconversion of these isomers remain unknown (95). Research efforts have aimed to identify the cellular source of guanylin, with early studies proposing that enteroendocrine cells, such as goblet cells, paneth cells, tuft cells, and enterocytes, were responsible for producing these peptides due to their proposed hormonal function. However, discrepancies between studies and techniques have made it difficult to determine a definitive source (93, 96, 97). Although the stimuli that trigger proguanylin secretion remain poorly characterized, evidence suggests a strong association with the salt consumption (98).

The loss of GN has been shown to have detrimental effects on the intestinal epithelial cells that produce GC-C, disrupting the homeostatic mechanisms necessary for organizing the crypt-villus axis. The GC-C expression remains consistent across the crypt-to-villus axis. However, the endogenous ligands GN and UG are secreted in an ascending gradient, with the highest concentration in the differentiated villus compartment and the lowest in the proliferating crypt compartment. This gradient restricts proliferation and reprograms metabolism in crypts, contributing to maintaining a healthy intestinal epithelium (99) (Figure 7). The perturbation of GN production leads to deficiencies in cellular

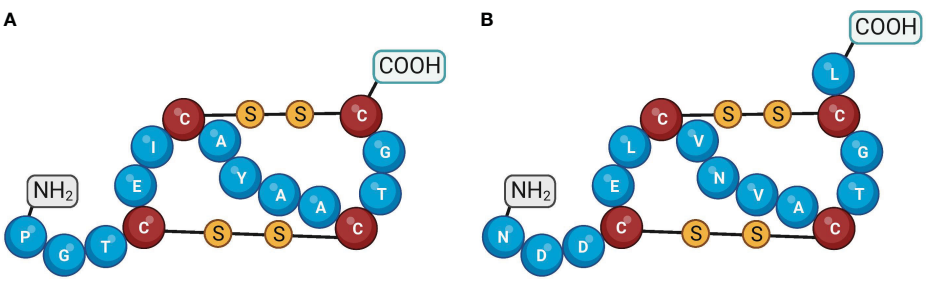

FIGURE 6
Amino acid structures of guanylin and uroguanylin. Guanylin **(A)** and uroguanylin **(B)** The cysteine residues are shown by the different colors of the amino acid and by the disulfide bonds. Created with BioRender.com.

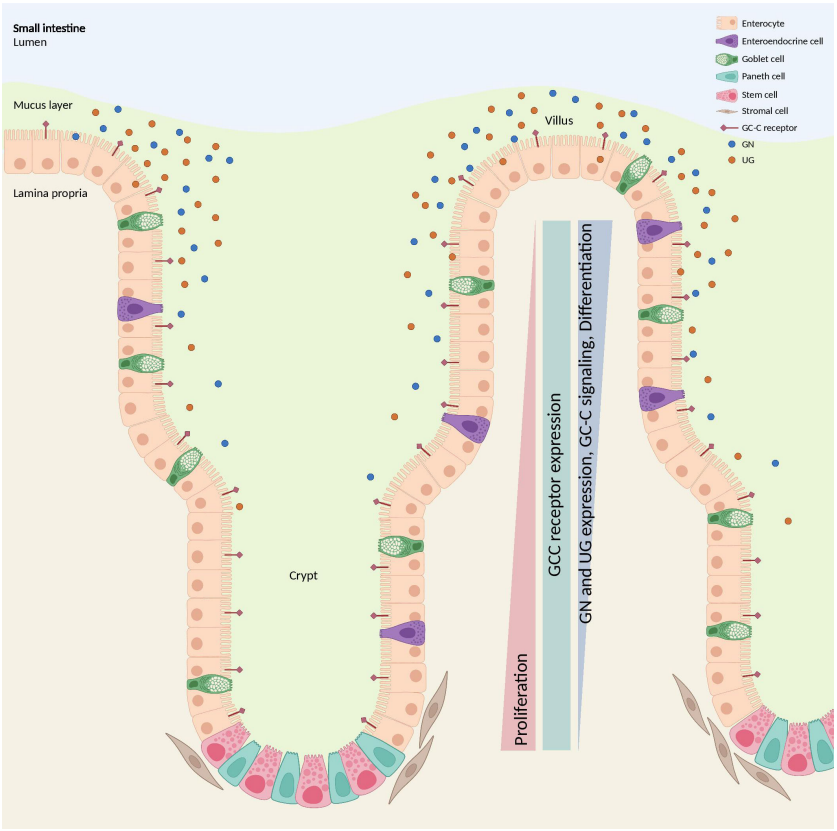

FIGURE 7
GC-C signaling regulates crypt-villus proliferation. While the GC-C receptors are expressed along the crypt-surface axes, the endogenous ligands GN and UG are produced by differentiated cells bordering the lumen and are absent in crypts. GC-C signaling opposes the proliferative gradient along that vertical axis by restricting cell growth in the crypts and promoting the maturation of differentiated cells. GC-C, guanylate cyclase c; GN, Guanylin; UG, Uroguanylin. Created with BioRender.com.

proliferation, sensing and repair of DNA damage, and metabolic programming, collectively contributing to the development of tumors (85, 100). GN stands out as a frequently absent gene product in the context of colorectal tumorigenesis and is regarded as one of the initial occurrences in the progression of intestinal tissue transformation (101, 102). In an investigation involving a cohort of patients diagnosed with stage I-III CRC, it was observed that both *GUCA2A* mRNA and peptides exhibited a loss or substantial reduction in cancerous tissues when compared to adjacent healthy tissues in more than 85% of the cases (102). Moreover, lower circulating levels of proguanylin were observed in individuals with obesity, and levels increased following Roux-en-Y gastric bypass surgery, suggesting potential links to metabolism or food intake (103). Consistent with these results, GN expression and peptide levels were reduced in mice fed a high-fat diet. Conversely, the risk of developing colon cancer due to obesity was decreased when GN was forcibly re-expressed (100).

Bashir et al. (51) found that *GUCA2A* expression was lost in both tubular and serrated adenomas compared to their corresponding normal colon tissues. The study also suggested that this loss may silence *GUCY2C*, which could lead to the development of microsatellite instability tumors (51) (Table 3). Blomain et al. (38) reported a similar finding, demonstrating that the loss of GN expression occurs early in APC-dependent tumors in both humans and mice, whereas the GC-C receptor remains intact. In 2022, Liu et al. (60) conducted an integrated bioinformatics analysis to identify hub genes associated with colorectal adenocarcinoma and assess their prognostic significance. They collected colon adenocarcinoma (COAD)/rectum adenocarcinoma (READ) data from the Cancer Genome Atlas (TCGA) database (https://www.cancer.gov/ccg/access-data). Additionally, they utilized the gene expression profile of GSE25070 from the Gene Expression Omnibus (GEO) database (https://www.ncbi.nlm.nih.gov/geo/). This data collection aimed to explore differentially expressed genes between colorectal adenocarcinoma and normal tissues. Their analysis led to the identification of a *GUCA2A-CLCA1-CLCA4* gene signature that could accurately predict the prognosis of CRC patients (60). Another study by Ming Li et al. (59) utilized three microarray datasets (GSE23878, GSE33113, and GSE41328) to investigate the relationship between gene expression and patient outcomes in CRC. They identified four differentially expressed genes (DEGs), including *GUCA2A*, *ADH1C*, *CLCA4*, and *CXCL8*, all of which were associated with significantly lower overall survival in CRC patients (59). Chen et al. (16) analyzed 437 mutation data from colon cancer samples and discovered a positive correlation between *GUCA2A* expression and patient survival. In a separate

study, Hases et al. (55) used data from TCGA database analyzed clinical samples of colorectal tumors, and matched noncancerous adjacent tissue from CRC patients to identify sex-specific biomarkers for CRC. *GUCA2A* was identified as a prognostic biomarker for CRC, specifically in males (55). Zhang et al. (52) identified *GUCA2A* as a hub gene significantly correlating with patients' overall survival (OS). Furthermore, they conducted qPCR analysis and found that *GUCA2A* is significantly downregulated in tumor and metastatic tissues when compared to adjacent normal tissues (52).

3.3 GUCA2B

The human gene encoding uroguanylin (UG) termed Guanylate Cyclase Activator 2B (*GUCA2B*), is located on chromosome 1 in humans (1p34.2), which consists of 3 exons. The expression of *GUCA2B* mRNA resembled that of *GUCA2A* expression, indicating that *GUCA2A* promoter-proximal and upstream super-enhancer elements synchronize the expression of both genes (49). UG peptide comprises 16 amino acids and, equal to GN, consists of two disulfide bonds between positions seven and 15 (Figure 6B) (93). This peptide is produced and expressed in enterochromaffin cells predominantly in the proximal part of the small intestine (76, 104). Plasma UG circulates as both propeptide (proUG) and active forms, while plasma GN circulates mainly as proGN (105). Renal tubular brush border membrane-associated enzymes convert the inactive proUG through a proteolytic process into the bioactive UG, resulting in high amounts of UG in the urine (106). Of significance, the expression of UG is invariably lost early during neoplastic transformation in the intestine (107, 108). By the oral administration of human UG, Shailubhai et al. (22) demonstrated that the number of polyps was reduced by 50% in ApcMin/+ mice (mice carrying mutations in the APC gene) as well as the progression of polyps into adenocarcinoma was decreased. In agreement with this finding, Basu et al. (80) showed that oral administration of UG prevented ApcMin/+ mice from forming adenomas, their progression to colon tumors, and the development of inflammation-induced colonic tumors in ApcMin/+ mice. As a bioinformatics research sample, Chu et al. (109) used prediction analysis of microarray (PAM), artificial neural network (ANN), classification and regression trees (CART), and C5.0 to identify gene expression profiles of CRC and normal mucosa. They pooled 16 datasets containing 88 normal mucosal tissues and 1186 CRCs and identified the top eight differential genes in CRCs, including suppressor genes *GUCA2B*, *CA7*, *IL6R SPIB*, *CWH43*, and *AQP8*; and oncogenes *TCN1* and *SPP1* (109).

Recently, Yang et al. (67) performed a comprehensive *in silico* analysis and discovered that patients with *DNAH7* missense mutations might benefit more from ICIs (Table 4). Through establishing the protein-protein interaction (PPI), they identified the top key genes associated with the *DNAH7* mutation, including *GUCA2B*, *AQP8*, *MS4A12*, and *ZG16* (67). These results may shed light on the possible role of the *GUCA2B* gene as a predictor of ICIs response in CRC patients, which requires further studies in this regard. Ebadfardzadeh et al. (56) conducted a comprehensive analysis of gene expression patterns in four microarray datasets (GSE113513, GSE10950, GSE25070, and GSE37182) available in GEO, as well as miRNA expression profiles. After analyzing the data, the researchers identified a total of 43 DEGs, including ten hub genes; *GUCA2B*, *GUCA2A*, *CLCA4*, *SLC26A3*, *KRT20*, *CLCA1*, *MAOA*, *MS4A12*, *AQP8*, and *ADH1A*. Additionally, the team identified four differentially expressed miRNAs that compromise *miR-502-3p*, *miR-552*, *miR-490-5p*, and *miR-423-5p*. Based on their bioinformatics analysis, the DEGs identified in this study could serve as significant biomarkers in the molecular mechanisms of CRC development, potentially aiding in developing novel strategies for predicting, screening, and diagnosing CRC patients (56). In another study, the GSE41258 and GSE81558 microarray datasets were analyzed by Han et al. to search for specific molecular targets for diagnosis and prognosis in CRC patients (63). A total of 53 DEGs were identified between CRC and normal colorectal tissues. The list was narrowed to ten hub genes, including *GUCA2A*, *GUCA2B*, *GCG*, *SST*, *MS4A12*, *PLP1*, *CHGA*, *PYY*, *VIP*, and *CLCA4*. However, just *CLCA4* and *MS4A12* expression levels had a statistically significant effect on CRC patients' OS (63). In the same vein, the GSE50760 and GSE104178 datasets were further mined to identify potential target genes correlated with CRC pathogenesis. There were 53 overlapped DEGs in these three datasets. The researchers utilized the String-db online tool to assess the possible interaction of the shared DEGs (110). Ultimately, they identified a significant sub-network of ten genes, including *GUCA2B*, *GUCA2A*, *GCG*, *BEST4*, *UCN3*, *SST*, *NPY*, *PYY*, *OTOP2*, and *TMEM82*. However, expression levels of *GUCA2B* and *GUCA2A* have no correlation with the OS of patients with CRC in this study either (58). Nomiri et al. (66) sought to identify a potential target for CRC therapy using Weighted Gene Co-expression Network Analysis (WGCNA) to investigate key modules, hub genes, and mRNA-miRNA regulatory networks correlated with CRC. The study found 372 genes to be considerably positively associated with CRC (r = 0.98, P-value = 9e-07) and determined 22 hub genes through survival and differential expression analyses. Among these hub genes, *GUCA2B*, *C2ORF88*, and *CCDC68* were found to play crucial roles in the overall survival rate of CRC patients. The expression analysis was consistent with RT-qPCR results, demonstrating a significant reduction in the expression of *GUCA2B* in CRC tissues. In addition, the study identified top microRNAs correlated with *GUCA2B*, and receiver operating characteristic (ROC) analyses indicated that *GUCA2B* has a high diagnostic performance for CRC (66). In 2022, Rappaport et al. (49) examined a GUCY2C ligand transcriptional silencing mechanism by β-catenin/TCF signaling. In this regard, they performed RNA sequencing analysis of conditional human colon cancer cell lines of β-catenin/TCF signaling to map the core Wnt-transcriptional program. As an important result of this investigation, a novel locus control region regulated by APC-β-catenin-TCF silences *GUCA2A* and *GUCA2B* transcription was discerned. With this discovery, they introduced a unique opportunity to reverse *GUCY2C* ligand silencing and oppose tumorigenesis in the context of mutant Wnt signaling (49). A former study by Pucci et al. (111) has established that higher *B4GALNT2* gene expression in CRC patients strongly predicts a

good prognosis for their cancer outcome. In another study, to further illustrate the biological importance of this gene in CRC, Pucci and her group obtained gene expression data of 626 COAD/READ samples from the TCGA database and divided CRC patients based on *B4GALNT2* expression into two different groups, including higher and lower expressers. Patient stratification revealed that the higher expression cohort displayed a concomitantly high level of other genes associated with a favorable prognosis, such as *GUCA2B, ZG16, ITLN1*, and *BEST2* (64).

4 Discussion and future prospects

Early detection of colorectal cancer is crucial, as it enables access to a broader range of therapeutic interventions and significantly impacts patient survival. Our review study highlights the critical involvement of the guanylate cyclase-c signaling pathway in the early stages of colon carcinogenesis. Investigating the signaling pathway expression in individuals with high-risk colon polyps or early stages of colon carcinoma may be beneficial. This could assess the GC-C axis as a diagnostic marker in a cohort study.

To our knowledge, no studies have yet measured the levels of guanylin and uroguanylin in the serum of patients with CRC. Further investigation is needed to fill this gap by examining the serum levels of these proteins in diverse patient cohorts, as well as their correlation with the cancer stage. This information could provide valuable insights into the severity of CRC and help predict disease progression.

In light of the promising advancements in immunotherapy for cancer treatment, investigating the immune roles of *GUCA2A*, *GUCA2B*, and *GUCY2C* genes could provide valuable insights into their potential as targets for immunotherapy. Specifically, *GUCY2C* has been found to play a regulatory role in intestinal inflammation and inflammatory bowel disease pathology. At the same time, *GUCA2A* has been associated with the immune signature of CRC. Therefore, further investigations into the immune-related functions of these genes could pave the way for developing more effective immunotherapies for treating CRC.

Recent studies have suggested that targeting *GUCA2A*, *GUCA2B*, and *GUCY2C* genes could be a promising approach for treating CRC. For instance, linaclotide (a GC-C receptor agonist) has been used in previous studies for the prevention of CRC (112), and is currently being evaluated in phase I (NCT01950403) and phase II (NCT03796884) clinical trials for the treatment of CRC. Further research into the use of drugs targeting the GC-C receptor or those that affect these genes could lead to developing more effective and targeted treatments for CRC patients. Many studies have examined the effects of GC-C receptor agonists in treating CRC. However, there is a shortage of drugs specifically targeting the expression of *GUCA2A* and *GUCA2B* genes related to CRC. Although research on GN and UG has mainly been done through bioinformatics, it is crucial to carry out *in vivo*, *in vitro*, and human studies on *GUCA2A* and *GUCA2B* to better comprehend how these genes contribute to CRC growth and advancement.

Finally, the future prospects for the Guanylate cyclase-C signaling pathway in oncology are hopeful, with potential applications in the diagnosis, prognosis, and treatment of CRC. Further research and clinical trials are demanded to fully realize these peptides' potential and develop novel drug delivery systems that enhance their therapeutic efficacy.

Although research studies have unveiled the significance of the GC-C signaling pathway in colorectal cancer, its practical application in clinical oncology remains constrained. To address this limitation, we propose some future directions for integrating this pathway into clinical settings. Achieving a comprehensive understanding of the GC-C signaling pathway in gastrointestinal cancer, particularly colon cancer, necessitates a comprehensive evaluation of all its constituent components (GUCY2C, GUCA2A, and GUCA2B). Recognizing the transformative impact of systems biology approaches in elucidating complex biological phenomena, we advocate for a multi-layered assessment encompassing this pathway's transcriptomics, proteomics, metabolomics, and metagenomics, employing high-resolution methods.

5 Conclusion

To sum up, this systematic review provides a comprehensive summary of the current state of knowledge on the potential role of the guanylyl cyclase-c receptor (GC-C) and its endogenous ligands, Guanylin and Uroguanylin, in the development and progression of colorectal cancer (CRC). Clinical studies have shown that GC-C expression and its activators are associated with patient outcomes, suggesting their potential as prognostic tools. The review also underscores the therapeutic potential of GC-C targeted therapies in CRC treatment. The findings suggest that combining GC-C targeted therapies with other treatment modalities could enhance their effectiveness and overcome drug resistance. Hopefully, these results will serve as a valuable resource for researchers and clinicians developing new and effective therapies for CRC patients, ultimately leading to improved patient outcomes. Further research is warranted to determine the efficacy and safety of GC-C targeted therapies, and the reviewed literature provides a foundation for future studies in this field.

Data availability statement

The original contributions presented in the study are included in the article/supplementary material. Further inquiries can be directed to the corresponding author.

Author contributions

MoeinP: Methodology, Writing – original draft, Writing – review & editing. AA: Methodology, Writing – original draft. PJ: Writing – original draft. AS: Writing – original draft. MobinP: Writing – original draft. YT: Writing – original draft. ZS: Conceptualization, Supervision, Writing – review & editing.

Funding

The author(s) declare that no financial support was received for the research, authorship, and/or publication of this article.

Acknowledgments

We would like to thank BioRender.com for providing the high-quality figures used in this manuscript. Further, the Research Institute of Gastroenterology and Liver Disease is gratefully acknowledged for their support and provision of resources throughout the duration of this research.

Conflict of interest

The authors declare that the research was conducted in the absence of any commercial or financial relationships that could be construed as a potential conflict of interest.

Publisher's note

References

1. Siegel R, Miller K, Wagle NS, Jemal A. Cancer statistic. *CA: A Cancer J Clin* (2023) 73(1):17–48. doi: 10.3322/caac.21763

2. Edwards BK, Ward E, Kohler BA, Eheman C, Zauber AG, Anderson RN, et al. Annual report to the nation on the status of cancer 1975-2006, featuring colorectal cancer trends and impact of interventions (risk factors, screening, and treatment) to reduce future rates. *Cancer* (2010) 116:544–73. doi: 10.1002/cncr.24760

3. Arnold M, Abnet C, Neale R, Vignat J, Giovannucci E, Mcglynn K, et al. Global burden of 5 major types of gastrointestinal cancer. *Gastroenterology* (2020) 159(1):335–49.e15. doi: 10.1053/j.gastro.2020.02.068

4. Siegel RL, Ward EM, Jemal A. Trends in colorectal cancer incidence rates in the United States by tumor location and stage 1992-2008. *Cancer Epidemiol Biomarkers Prev* (2012) 21:411–6. doi: 10.1158/1055-9965.EPI-11-1020

5. Schreuders EH, Ruco A, Rabeneck L, Schoen RE, Sung JJ, Young GP, et al. Colorectal cancer screening: a global overview of existing programmes. *Gut* (2015) 64:1637–49. doi: 10.1136/gutjnl-2014-309086

6. Keum N, Giovannucci E. Global burden of colorectal cancer: emerging trends, risk factors and prevention strategies. *Nat Rev Gastroenterol Hepatol* (2019) 16:713–32. doi: 10.1038/s41575-019-0189-8

7. Sung H, Ferlay J, Siegel RL, Laversanne M, Soerjomataram I, Jemal A, et al. Global cancer statistics 2020: GLOBOCAN estimates of incidence and mortality worldwide for 36 cancers in 185 countries. *CA Cancer J Clin* (2021) 71:209–49. doi: 10.3322/caac.21660

8. Kijima S, Sasaki T, Nagata K, Utano K, Lefor AT, Sugimoto H. Preoperative evaluation of colorectal cancer using CT colonography, MRI, and PET/CT. *World J Gastroenterol* (2014) 20:16964–75. doi: 10.3748/wjg.v20.i45.16964

9. Brenner H, Kloor M, Pox CP. Colorectal cancer. *Lancet* (2014) 383:1490–502. doi: 10.1016/S0140-6736(13)61649-9

10. Ohhara Y, Fukuda N, Takeuchi S, Honma R, Shimizu Y, Kinoshita I, et al. Role of targeted therapy in metastatic colorectal cancer. *World J Gastrointestinal Oncol* (2016) 8:642. doi: 10.4251/wjgo.v8.i9.642

11. Hinoue T, Weisenberger DJ, Lange CP, Shen H, Byun HM, Van Den Berg D, et al. Genome-scale analysis of aberrant DNA methylation in colorectal cancer. *Genome Res* (2012) 22:271–82. doi: 10.1101/gr.117523.110

12. Eynali S, Khoei S, Khoee S, Esmaelbeygi E. Evaluation of the cytotoxic effects of hyperthermia and 5-fluorouracil-loaded magnetic nanoparticles on human colon cancer cell line HT-29. *Int J Hyperthermia* (2017) 33:327–35. doi: 10.1080/02656736.2016.1243260

13. Nannini M, Pantaleo MA, Maleddu A, Astolfi A, Formica S, Biasco G. Gene expression profiling in colorectal cancer using microarray technologies: results and perspectives. *Cancer Treat Rev* (2009) 35:201–9. doi: 10.1016/j.ctrv.2008.10.006

14. Muzny DM, Bainbridge MN, Chang K, Dinh HH, Drummond JA, Fowler G, et al. Comprehensive molecular characterization of human colon and rectal cancer. *Nature* (2012) 487:330–7. doi: 10.1038/nature11252

15. Huang D, Sun W, Zhou Y, Li P, Chen F, Chen H, et al. Mutations of key driver genes in colorectal cancer progression and metastasis. *Cancer Metastasis Rev* (2018) 37:173–87. doi: 10.1007/s10555-017-9726-5

16. Xu H, Ma Y, Zhang J, Gu J, Jing X, Lu S, et al. Identification and verification of core genes in colorectal cancer. *BioMed Res Int* (2020) 2020:8082697. doi: 10.1155/2020/8082697

17. Blomain ES, Merlino DJ, Pattison AM, Snook AE, Waldman SA. Guanylyl cyclase C hormone axis at the intersection of obesity and colorectal cancer. *Mol Pharmacol* (2016) 90:199–204. doi: 10.1124/mol.115.103192

18. Entezari AA, Snook AE, Waldman SA. Guanylyl cyclase 2C (GUCY2C) in gastrointestinal cancers: recent innovations and therapeutic potential. *Expert Opin Ther Targets* (2021) 25:335–46. doi: 10.1080/14728222.2021.1937124

19. Forte LR. Guanylin regulatory peptides: structures, biological activities mediated by cyclic GMP and pathobiology. *Regul Pept* (1999) 81:25–39. doi: 10.1016/S0167-0115(99)00033-6

20. Li P, Lin JE, Marszlowicz GP, Valentino MA, Chang C, Schulz S, et al. GCC signaling in colorectal cancer: Is colorectal cancer a paracrine deficiency syndrome? *Drug News Perspect* (2009) 22:313–8. doi: 10.1358/dnp.2009.22.6.1395254

21. Cohen MB, Hawkins JA, Witte DP. Guanylin mRNA expression in human intestine and colorectal adenocarcinoma. *Lab Invest* (1998) 78:101–8.

22. Shailubhai K, Yu HH, Karunanandaa K, Wang JY, Eber SL, Wang Y, et al. Uroguanylin treatment suppresses polyp formation in the Apc(Min/+) mouse and induces apoptosis in human colon adenocarcinoma cells via cyclic GMP. *Cancer Res* (2000) 60:5151–7.

23. Li P, Schulz S, Bombonati A, Palazzo JP, Hyslop TM, Xu Y, et al. Guanylyl cyclase C suppresses intestinal tumorigenesis by restricting proliferation and maintaining genomic integrity. *Gastroenterology* (2007) 133:599–607. doi: 10.1053/j.gastro.2007.05.052

24. Pitari GM, Li P, Lin JE, Zuzga D, Gibbons AV, Snook AE, et al. The paracrine hormone hypothesis of colorectal cancer. *Clin Pharmacol Ther* (2007) 82:441–7. doi: 10.1038/sj.clpt.6100325

25. Waldman SA, Hyslop T, Schulz S, Barkun A, Nielsen K, Haaf J, et al. Association of GUCY2C expression in lymph nodes with time to recurrence and disease-free survival in pN0 colorectal cancer. *Jama* (2009) 301:745–52. doi: 10.1001/jama.2009.141

26. Steinbrecher KA, Harmel-Laws E, Garin-Laflam MP, Mann EA, Bezerra LD, Hogan SP, et al. Murine guanylate cyclase C regulates colonic injury and inflammation. *J Immunol* (2011) 186:7205–14. doi: 10.4049/jimmunol.1002469

27. Mann EA, Harmel-Laws E, Cohen MB, Steinbrecher KA. Guanylate cyclase C limits systemic dissemination of a murine enteric pathogen. *BMC Gastroenterol* (2013) 13:135. doi: 10.1186/1471-230X-13-135

28. Page MJ, Mckenzie JE, Bossuyt PM, Boutron I, Hoffmann TC, Mulrow CD, et al. The PRISMA 2020 statement: an updated guideline for reporting systematic reviews. *Bmj* (2021) 372:n71. doi: 10.1016/j.rec.2021.07.010

29. Sterne JA, Hernán MA, Reeves BC, Savović J, Berkman ND, Viswanathan M, et al. ROBINS-I: a tool for assessing risk of bias in non-randomised studies of interventions. *Bmj* (2016) 355:i4919. doi: 10.1136/bmj.i4919

30. Chervoneva I, Freydin B, Hyslop T, Waldman SA. Modeling qRT-PCR dynamics with application to cancer biomarker quantification. *Stat Methods Med Res* (2018) 27:2581–95. doi: 10.1177/0962280216683204

31. Ghai A, Singh B, Li M, Daniels TA, Coelho R, Orcutt K, et al. Optimizing the radiosynthesis of [(68)Ga]DOTA-MLN6907 peptide containing three disulfide cyclization bonds - a GCC specific chelate for clinical radiopharmaceuticals. *Appl Radiat Isot* (2018) 140:333–41. doi: 10.1016/j.apradiso.2018.08.006

32. Lin AG, Xiang B, Merlino DJ, Baybutt TR, Sahu J, Fridman A, et al. Non-thermal plasma induces immunogenic cell death *in vivo* in murine CT26 colorectal tumors. *Oncoimmunology* (2018) 7:e1484978. doi: 10.1080/2162402X.2018.1484978

33. Magee MS, Abraham TS, Baybutt TR, Flickinger JCJr., Ridge NA, Marszalowicz GP, et al. Human GUCY2C-targeted chimeric antigen receptor (CAR)-expressing T cells eliminate colorectal cancer metastases. *Cancer Immunol Res* (2018) 6:509–16. doi: 10.1158/2326-6066.CIR-16-0362

34. Sharman SK, Islam BN, Hou Y, Singh N, Berger FG, Sridhar S, et al. Cyclic-GMP-elevating agents suppress polyposis in apc(Min) mice by targeting the preneoplastic epithelium. *Cancer Prev Res (Phila)* (2018) 11:81–92. doi: 10.1158/1940-6207.CAPR-17-0267

35. Bang YJ, Takano T, Lin CC, Fasanmade A, Yang H, Danaee H, et al. TAK-264 (MLN0264) in previously treated asian patients with advanced gastrointestinal carcinoma expressing guanylyl cyclase C: results from an open-label, non-randomized phase 1 study. *Cancer Res Treat* (2018) 50:398–404. doi: 10.4143/crt.2017.074

36. Abraham TS, Flickinger JCJr., Waldman SA, Snook AE. TCR retrogenic mice as a model to map self-tolerance mechanisms to the cancer mucosa antigen GUCY2C. *J Immunol* (2019) 202:1301–10. doi: 10.4049/jimmunol.1801206

37. Abu-Yousif AO, Cvet D, Gallery M, Bannerman BM, Ganno ML, Smith MD, et al. Preclinical antitumor activity and biodistribution of a novel anti-GCC antibody-drug conjugate in patient-derived xenografts. *Mol Cancer Ther* (2020) 19:2079–88. doi: 10.1158/1535-7163.MCT-19-1102

38. Blomain ES, Rappaport JA, Pattison AM, Bashir B, Caparosa E, Stem J, et al. APC-β-catenin-TCF signaling silences the intestinal guanylin-GUCY2C tumor suppressor axis. *Cancer Biol Ther* (2020) 21:441–51. doi: 10.1080/15384047.2020.1721262

39. Flickinger JC Jr., Singh J, Carlson R, Leong E, Baybutt TR, Barton J, et al. Chimeric Ad5.F35 vector evades anti-adenovirus serotype 5 neutralization opposing GUCY2C-targeted antitumor immunity. *J Immunother Cancer* (2020) 8(2):e001046. doi: 10.1136/jitc-2020-001046

40. Jiang L, Feng JG, Wang G, Zhu YP, Ju HX, Li DC, et al. Circulating guanylyl cyclase C (GCC) mRNA is a reliable metastatic predictor and prognostic index of colorectal cancer. *Transl Cancer Res* (2020) 9:1843–50. doi: 10.21037/tcr.2020.02.34

41. Mathur D, Root AR, Bugaj-Gaweda B, Bisulco S, Tan X, Fang W, et al. A novel GUCY2C-CD3 T-cell engaging bispecific construct (PF-07062119) for the treatment of gastrointestinal cancers. *Clin Cancer Res* (2020) 26:2188–202. doi: 10.1158/1078-0432.CCR-19-3275

42. Pattison AM, Barton JR, Entezari AA, Zalewski A, Rappaport JA, Snook AE, et al. Silencing the intestinal GUCY2C tumor suppressor axis requires APC loss of heterozygosity. *Cancer Biol Ther* (2020) 21:799–805. doi: 10.1080/15384047.2020.1779005

43. Jimenez-Luna C, González-Flores E, Ortiz R, Martínez-González LJ, Antúnez-Rodríguez A, Expósito-Ruiz M, et al. Circulating PTGS2, JAG1, GUCY2C and PGF mRNA in peripheral blood and serum as potential biomarkers for patients with metastatic colon cancer. *J Clin Med* (2021) 10(11):2248. doi: 10.3390/jcm10112248

44. Maresca KP, Chen J, Mathur D, Giddabasappa A, Root A, Narula J, et al. Preclinical evaluation of (89)Zr-df-iab22m2c pet as an imaging biomarker for the development of the gucy2c-Cd3 bispecific Pf-07062119 as A T cell engaging therapy. *Mol Imaging Biol* (2021) 23:941–51. doi: 10.1007/s11307-021-01621-0

45. Weinberg DS, Foster NR, Della'zanna G, Mcmurray RP, Kraft WK, Pallotto A, et al. Phase I double-blind, placebo-controlled trial of dolcanatide (SP-333) 27 mg to explore colorectal bioactivity in healthy volunteers. *Cancer Biol Ther* (2021) 22:544–53. doi: 10.1080/15384047.2021.1967036

46. Asghari Alashti F, Goliaei B, Minuchehr Z. Analyzing large scale gene expression data in colorectal cancer reveals important clues; CLCA1 and SELENBP1 downregulated in CRC not in normal and not in adenoma. *Am J Cancer Res* (2022) 12:371–80.

47. Flickinger JCJr., Singh J, Yarman Y, Carlson RD, Barton JR, Waldman SA, et al. T-cell responses to immunodominant listeria epitopes limit vaccine-directed responses to the colorectal cancer antigen, guanylyl cyclase C. *Front Immunol* (2022) 13:855759. doi: 10.3389/fimmu.2022.855759

48. Flickinger JCJr., Staudt RE, Singh J, Carlson RD, Barton JR, Baybutt TR, et al. Chimeric adenoviral (Ad5.F35) and listeria vector prime-boost immunization is safe and effective for cancer immunotherapy. *NPJ Vaccines* (2022) 7:61. doi: 10.1038/s41541-022-00483-z

49. Rappaport JA, Entezari AA, Caspi A, Caksa S, Jhaveri AV, Stanek TJ, et al. A β-catenin-TCF-sensitive locus control region mediates GUCY2C ligand loss in colorectal cancer. *Cell Mol Gastroenterol Hepatol* (2022) 13:1276–96. doi: 10.1016/j.jcmgh.2021.12.014

50. Kim R, Leal AD, Parikh A, Ryan DP, Wang S, Bahamon B, et al. A phase I, first-in-human study of TAK-164, an antibody-drug conjugate, in patients with advanced gastrointestinal cancers expressing guanylyl cyclase C. *Cancer Chemother Pharmacol* (2023) 91:291–300. doi: 10.1007/s00280-023-04507-w

51. Bashir B, Merlino DJ, Rappaport JA, Gnass E, Palazzo JP, Feng Y, et al. Silencing the GUCA2A-GUCY2C tumor suppressor axis in CIN, serrated, and MSI colorectal neoplasia. *Hum Pathol* (2019) 87:103–14. doi: 10.1016/j.humpath.2018.11.032

52. Zhang H, Du Y, Wang Z, Lou R, Wu J, Feng J. Integrated analysis of oncogenic networks in colorectal cancer identifies GUCA2A as a molecular marker. *Biochem Res Int* (2019) 2019:6469420. doi: 10.1155/2019/6469420

53. Zheng ZG, Ma BQ, Xiao Y, Wang TX, Yu T, Huo YH, et al. Identification of biomarkers for the diagnosis and treatment of primary colorectal cancer based on microarray technology. *Trans Cancer Res* (2020) 9:3453. doi: 10.21037/tcr-19-2290

54. Chen J, Apizi A, Wang L, Wu G, Zhu Z, Yao H, et al. TCGA database analysis of the tumor mutation burden and its clinical significance in colon cancer. *J Gastrointestinal Oncol* (2021) 12:2244. doi: 10.21037/jgo-21-661

55. Hases L, Ibrahim A, Chen X, Liu Y, Hartman J, Williams C. The importance of sex in the discovery of colorectal cancer prognostic biomarkers. *Int J Mol Sci* (2021) 22(3):1354. doi: 10.3390/ijms22031354

56. Ebadfardzadeh J, Kazemi M, Aghazadeh A, Rezaei M, Shirvaliloo M, Sheervalilou R. Employing bioinformatics analysis to identify hub genes and microRNAs involved in colorectal cancer. *Med Oncol* (2021) 38:114. doi: 10.1007/s12032-021-01543-5

57. Chodary Khameneh S, Razi S, Shamdani S, Uzan G, Naserian S. Weighted correlation network analysis revealed novel long non-coding RNAs for colorectal cancer. *Sci Rep* (2022) 12:2990. doi: 10.1038/s41598-022-06934-w

58. Guo S, Sun Y. OTOP2, inversely modulated by miR-3148, inhibits CRC cell migration, proliferation and epithelial-mesenchymal transition: evidence from bioinformatics data mining and experimental verification. *Cancer Manag Res* (2022) 14:1371–84. doi: 10.2147/CMAR.S345299

59. Li M, Liu Z, Song J, Wang T, Wang H, Wang Y, et al. Identification of down-regulated ADH1C is associated with poor prognosis in colorectal cancer using bioinformatics analysis. *Front Mol Biosci* (2022) 9:791249. doi: 10.3389/fmolb.2022.791249

60. Liu Y, Chen L, Meng X, Ye S, Ma L. Identification of hub genes in colorectal adenocarcinoma by integrated bioinformatics. *Front Cell Dev Biol* (2022) 10:897568. doi: 10.3389/fcell.2022.897568

61. Feodorova Y, Tashkova D, Koev I, Todorov A, Kostov G, Simitchiev K, et al. Novel insights into transcriptional dysregulation in colorectal cancer. *Neoplasma* (2018) 65:415–24. doi: 10.4149/neo_2018_170707N467

62. Parikh K, Antanaviciute A, Fawkner-Corbett D, Jagielowicz M, Aulicino A, Lagerholm C, et al. Colonic epithelial cell diversity in health and inflammatory bowel disease. *Nature* (2019) 567:49–55. doi: 10.1038/s41586-019-0992-y

63. Han J, Zhang X, Liu Y, Jing L, Liu YB, Feng L. CLCA4 and MS4A12 as the significant gene biomarkers of primary colorectal cancer. *Biosci Rep* (2020) 40(8):BSR20200963. doi: 10.1042/BSR20200963

64. Pucci M, Malagolini N, Dall'olio F. Glycosyltransferase B4GALNT2 as a predictor of good prognosis in colon cancer: lessons from databases. *Int J Mol Sci* (2021) 22(9):4331. doi: 10.3390/ijms22094331

65. Bouzo BL, Lores S, Jatal R, Alijas S, Alonso MJ, Conejos-Sánchez I, et al. Sphingomyelin nanosystems loaded with uroguanylin and etoposide for treating metastatic colorectal cancer. *Sci Rep* (2021) 11:17213. doi: 10.1038/s41598-021-96578-z

66. Nomiri S, Hoshyar R, Chamani E, Rezaei Z, Salmani F, Larki P, et al. Prediction and validation of GUCA2B as the hub-gene in colorectal cancer based on co-expression network analysis: *In-silico* and *in-vivo* study. *BioMed Pharmacother* (2022) 147:112691. doi: 10.1016/j.biopha.2022.112691

67. Yang W, Shen Z, Yang T, Wu M. DNAH7 mutations benefit colorectal cancer patients receiving immune checkpoint inhibitors. *Ann Transl Med* (2022) 10:1335. doi: 10.21037/atm-22-6166

68. Horaira MA, Islam MA, Kibria MK, Alam MJ, Kabir SR, Mollah MNH. Bioinformatics screening of colorectal-cancer causing molecular signatures through gene expression profiles to discover therapeutic targets and candidate agents. *BMC Med Genomics* (2023) 16:64. doi: 10.1186/s12920-023-01488-w

69. Horst BG, Yokom AL, Rosenberg DJ, Morris KL, Hammel M, Hurley JH, et al. Allosteric activation of the nitric oxide receptor soluble guanylate cyclase mapped by cryo-electron microscopy. *Elife* (2019) 8:e50634. doi: 10.7554/eLife.50634

70. Kang Y, Liu R, Wu JX, Chen L. Structural insights into the mechanism of human soluble guanylate cyclase. *Nature* (2019) 574:206–10. doi: 10.1038/s41586-019-1584-6

71. Yarla NS, Gali H, Pathuri G, Smriti S, Farooqui M, Panneerselvam J, et al. Targeting the paracrine hormone-dependent guanylate cyclase/cGMP/phosphodiesterases signaling pathway for colorectal cancer prevention. *Semin Cancer Biol* (2019) 56:168–74. doi: 10.1016/j.semcancer.2018.08.011

72. Bose A, Visweswariah SS. The pseudokinase domain in receptor guanylyl cyclases. *Methods Enzymol* (2022) 667:535–74. doi: 10.1016/bs.mie.2022.03.046

73. Khalil I, Walker R, Porter CK, Muhib F, Chilengi R, Cravioto A, et al. Enterotoxigenic Escherichia coli (ETEC) vaccines: Priority activities to enable product development, licensure, and global access. *Vaccine* (2021) 39:4266–77. doi: 10.1016/j.vaccine.2021.04.018

74. Hossain MS, Karuniawati H, Jairoun AA, Urbi Z, Ooi J, John A, et al. Colorectal cancer: A review of carcinogenesis, global epidemiology, current challenges, risk factors, preventive and treatment strategies. *Cancers (Basel)* (2022) 14(7):1732. doi: 10.3390/cancers14071732

75. Li P, Lin JE, Snook AE, Waldman SA. ST-producing E. coli oppose carcinogen-induced colorectal tumorigenesis in mice. *Toxins (Basel)* (2017) 9(9):279. doi: 10.3390/toxins9090279

76. Rahbi H, Narayan H, Jones DJ, Ng LL. The uroguanylin system and human disease. *Clin Sci (Lond)* (2012) 123:659–68. doi: 10.1042/CS20120021

77. Waldman SA, Camilleri M. Guanylate cyclase-C as a therapeutic target in gastrointestinal disorders. *Gut* (2018) 67:1543–52. doi: 10.1136/gutjnl-2018-316029

78. Prasad H, Mathew JKK, Visweswariah SS. Receptor guanylyl cyclase C and cyclic GMP in health and disease: perspectives and therapeutic opportunities. *Front Endocrinol (Lausanne)* (2022) 13:911459. doi: 10.3389/fendo.2022.911459

79. Bose A, Banerjee S, Visweswariah SS. Mutational landscape of receptor guanylyl cyclase C: Functional analysis and disease-related mutations. *IUBMB Life* (2020) 72:1145–59. doi: 10.1002/iub.2283

80. Basu N, Saha S, Khan I, Ramachandra SG, Visweswariah SS. Intestinal cell proliferation and senescence are regulated by receptor guanylyl cyclase C and p21. *J Biol Chem* (2014) 289:581–93. doi: 10.1074/jbc.M113.511311

81. Thompson WJ, Piazza GA, Li H, Liu L, Fetter J, Zhu B, et al. Exisulind induction of apoptosis involves guanosine 3',5'-cyclic monophosphate phosphodiesterase inhibition, protein kinase G activation, and attenuated beta-catenin. *Cancer Res* (2000) 60:3338–42.

82. Li N, Lee K, Xi Y, Zhu B, Gary BD, Ramírez-Alcántara V, et al. Phosphodiesterase 10A: a novel target for selective inhibition of colon tumor cell growth and β-catenin-dependent TCF transcriptional activity. *Oncogene* (2015) 34:1499–509. doi: 10.1038/onc.2014.94

83. Deguchi A, Thompson WJ, Weinstein IB. Activation of protein kinase G is sufficient to induce apoptosis and inhibit cell migration in colon cancer cells. *Cancer Res* (2004) 64:3966–73. doi: 10.1158/0008-5472.CAN-03-3740

84. Basu N, Bhandari R, Natarajan VT, Visweswariah SS. Cross talk between receptor guanylyl cyclase C and c-src tyrosine kinase regulates colon cancer cell cytostasis. *Mol Cell Biol* (2009) 29:5277–89. doi: 10.1128/MCB.00001-09

85. Lin JE, Li P, Snook AE, Schulz S, Dasgupta A, Hyslop TM, et al. The hormone receptor GUCY2C suppresses intestinal tumor formation by inhibiting AKT signaling. *Gastroenterology* (2010) 138:241–54. doi: 10.1053/j.gastro.2009.08.064

86. Pattison AM, Merlino DJ, Blomain ES, Waldman SA. Guanylyl cyclase C signaling axis and colon cancer prevention. *World J Gastroenterol* (2016) 22:8070–7. doi: 10.3748/wjg.v22.i36.8070

87. Lisby AN, Flickinger JCJr., Bashir B, Weindorfer M, Shelukar S, Crutcher M, et al. GUCY2C as a biomarker to target precision therapies for patients with colorectal cancer. *Expert Rev Precis Med Drug Dev* (2021) 6:117–29. doi: 10.1080/23808993.2021.1876518

88. Baybutt TR, Aka AA, Snook AE. The heat-stable enterotoxin receptor, guanylyl cyclase C, as a pharmacological target in colorectal cancer immunotherapy: A bench-to-bedside current report. *Toxins (Basel)* (2017) 9(9):282. doi: 10.3390/toxins9090282

89. Morse MA, Gwin WR, Mitchell DA. Vaccine therapies for cancer: then and now. *Target Oncol* (2021) 16:121–52. doi: 10.1007/s11523-020-00788-w

90. Hong M, Clubb JD, Chen YY. Engineering CAR-T cells for next-generation cancer therapy. *Cancer Cell* (2020) 38:473–88. doi: 10.1016/j.ccell.2020.07.005

91. Caspi A, Entezari AA, Crutcher M, Snook AE, Waldman SA. Guanylyl cyclase C as a diagnostic and therapeutic target in colorectal cancer. *Personalized Med* (2022) 19:457–72. doi: 10.2217/pme-2022-0026

92. Porto WF, Franco OL, Alencar SA. Computational analyses and prediction of guanylin deleterious SNPs. *Peptides* (2015) 69:92–102. doi: 10.1016/j.peptides.2015.04.013

93. De Sauvage FJ, Keshav S, Kuang WJ, Gillett N, Henzel W, Goeddel DV. Precursor structure, expression, and tissue distribution of human guanylin. *Proc Natl Acad Sci U.S.A.* (1992) 89:9089–93. doi: 10.1073/pnas.89.19.9089

94. Camilleri M. Guanylate cyclase C agonists: emerging gastrointestinal therapies and actions. *Gastroenterology* (2015) 148:483–7. doi: 10.1053/j.gastro.2015.01.003

95. Skelton NJ, Garcia KC, Goeddel DV, Quan C, Burnier JP. Determination of the solution structure of the peptide hormone guanylin: observation of a novel form of topological stereoisomerism. *Biochemistry* (1994) 33:13581–92. doi: 10.1021/bi00250a010

96. Ikpa PT, Sleddens HF, Steinbrecher KA, Peppelenbosch MP, De Jonge HR, Smits R, et al. Guanylin and uroguanylin are produced by mouse intestinal epithelial cells of columnar and secretory lineage. *Histochem Cell Biol* (2016) 146:445–55. doi: 10.1007/s00418-016-1453-4

97. Dye FS, Larraufie P, Kay R, Darwish T, Rievaj J, Goldspink DA, et al. Characterisation of proguanylin expressing cells in the intestine - evidence for constitutive luminal secretion. *Sci Rep* (2019) 9:15574. doi: 10.1038/s41598-019-52049-0

98. Kita T, Kitamura K, Sakata J, Eto T. Marked increase of guanylin secretion in response to salt loading in the rat small intestine. *Am J Physiol* (1999) 277:G960–6. doi: 10.1152/ajpgi.1999.277.5.G960

99. Li P, Lin JE, Schulz S, Pitari GM, Waldman SA. Can colorectal cancer be prevented or treated by oral hormone replacement therapy? *Curr Mol Pharmacol* (2009) 2:285–92. doi: 10.2174/1874-470210902030285

100. Lin JE, Colon-Gonzalez F, Blomain E, Kim GW, Aing A, Stoecker B, et al. Obesity-induced colorectal cancer is driven by caloric silencing of the guanylin-GUCY2C paracrine signaling axis. *Cancer Res* (2016) 76:339–46. doi: 10.1158/0008-5472.CAN-15-1467-T

101. Notterman DA, Alon U, Sierk AJ, Levine AJ. Transcriptional gene expression profiles of colorectal adenoma, adenocarcinoma, and normal tissue examined by oligonucleotide arrays. *Cancer Res* (2001) 61:3124–30.

102. Wilson C, Lin JE, Li P, Snook AE, Gong J, Sato T, et al. The paracrine hormone for the GUCY2C tumor suppressor, guanylin, is universally lost in colorectal cancer. *Cancer Epidemiol Biomarkers Prev* (2014) 23:2328–37. doi: 10.1158/1055-9965.EPI-14-0440

103. Fernandez-Cachon ML, Pedersen SL, Rigbolt KT, Zhang C, Fabricius K, Hansen HH, et al. Guanylin and uroguanylin mRNA expression is increased following Roux-en-Y gastric bypass, but guanylins do not play a significant role in body weight regulation and glycemic control. *Peptides* (2018) 101:32–43. doi: 10.1016/j.peptides.2017.12.024

104. Qian X, Prabhakar S, Nandi A, Visweswariah SS, Goy MF. Expression of GC-C, a receptor-guanylate cyclase, and its endogenous ligands uroguanylin and guanylin along the rostrocaudal axis of the intestine. *Endocrinology* (2000) 141:3210–24. doi: 10.1210/endo.141.9.7644

105. Moss NG, Fellner RC, Qian X, Yu SJ, Li Z, Nakazato M, et al. Uroguanylin, an intestinal natriuretic peptide, is delivered to the kidney as an unprocessed propeptide. *Endocrinology* (2008) 149:4486–98. doi: 10.1210/en.2007-1725

106. Qian X, Moss NG, Fellner RC, Goy MF. Circulating prouroguanylin is processed to its active natriuretic form exclusively within the renal tubules. *Endocrinology* (2008) 149:4499–509. doi: 10.1210/en.2007-1724

107. Pitari GM, Baksh RI, Harris DM, Li P, Kazerounian S, Waldman SA. Interruption of homologous desensitization in cyclic guanosine 3',5'-monophosphate signaling restores colon cancer cytostasis by bacterial enterotoxins. *Cancer Res* (2005) 65:11129–35. doi: 10.1158/0008-5472.CAN-05-2381

108. Lin JE, Snook AE, Li P, Stoecker BA, Kim GW, Magee MS, et al. GUCY2C opposes systemic genotoxic tumorigenesis by regulating AKT-dependent intestinal barrier integrity. *PloS One* (2012) 7:e31686. doi: 10.1371/journal.pone.0031686

109. Chu CM, Yao CT, Chang YT, Chou HL, Chou YC, Chen KH, et al. Gene expression profiling of colorectal tumors and normal mucosa by microarrays meta-analysis using prediction analysis of microarray, artificial neural network, classification, and regression trees. *Dis Markers* (2014) 2014:634123. doi: 10.1155/2014/634123

110. Szklarczyk D, Franceschini A, Wyder S, Forslund K, Heller D, Huerta-Cepas J, et al. STRING v10: protein–protein interaction networks, integrated over the tree of life. *Nucleic Acids Res* (2015) 43:D447–52. doi: 10.1093/nar/gku1003

111. Pucci M, Gomes Ferreira I, Orlandani M, Malagolini N, Ferracin M, Dall'olio F. High expression of the sd(a) synthase B4GALNT2 associates with good prognosis and attenuates stemness in colon cancer. *Cells* (2020) 9(4):948. doi: 10.3390/cells9040948

112. Weinberg DS, Lin JE, Foster NR, Della'zanna G, Umar A, Seisler D, et al. Bioactivity of oral linaclotide in human colorectum for cancer chemoprevention. *Cancer Prev Res (Phila)* (2017) 10:345–54. doi: 10.1158/1940-6207.CAPR-16-0286

frontiers | Frontiers in Oncology

TYPE Case Report
PUBLISHED 28 November 2023
DOI 10.3389/fonc.2023.1290717

OPEN ACCESS

EDITED BY
Zsolt Kovács,
Sciences and Technology of Târgu Mureș, Romania

REVIEWED BY
Xiaoyan Liao,
University of Rochester Medical Center, United States
Valeria Maffeis,
Ospedale di Treviso, Italy

*CORRESPONDENCE
Weiya Wang
151422303@qq.com

RECEIVED 07 September 2023
ACCEPTED 09 November 2023
PUBLISHED 28 November 2023

CITATION
Zhou P, Fu Y and Wang W (2023) Case Report: Gastrointestinal neuroendocrine carcinoma with SMARCA4 deficiency: a clinicopathological report of two rare cases.
Front. Oncol. 13:1290717.
doi: 10.3389/fonc.2023.1290717

Case Report: Gastrointestinal neuroendocrine carcinoma with SMARCA4 deficiency: a clinicopathological report of two rare cases

Ping Zhou, Yiyun Fu and Weiya Wang*

Department of Pathology, West China Hospital, Sichuan University, Chengdu, China

Background: Gastrointestinal neuroendocrine carcinoma (GI NEC) is a rare but highly malignant neoplasm with an aggressive clinical course. SMARCA4 is one of the subunits of the SWI/SNF chromatin remodeling complex. SMARCA4 deficiency can occur rarely in subsets of NECs. Reports of the clinicopathological features of GI NECs with SMARCA4 deficiency are limited.

Methods: In this study, we retrospectively reported two rare cases of GI NEC with SMARCA4 deficiency and described the clinicopathological, radiographic and histopathological features.

Results: Case 1 was a 43-year-old male with a stage cT3NxM1, IV tumor. Case 2 was a 64-year-old female with a stage cT4aN1M0, IIIA tumor. Both tumors presented as ulcerated masses with infiltration. Pathological examination indicated a solid architecture with poorly differentiated morphology, and complete loss of SMARCA4 (BRG1) was found. Immunohistochemical staining showed positivity for Syn, CgA and CD56. The Ki-67 index was 90% and 70%, respectively. None of the cases had mismatch repair (MMR) deficiency. Case 1 received treatment with chemotherapy and anti-PD-1 immunotherapy. He did not respond to treatment, and died 9 months later. Case 2 received neoadjuvant chemotherapy before surgical treatment, and the tumor showed TRG3 in response to neoadjuvant chemotherapy, chemotherapy and anti-PD-1 immunotherapy were continued after surgical resection. There was no evidence of disease for 10 months.

Conclusions: GI NEC with SMARCA4 deficiency is a rare entity of gastric NEC. SMARCA4 may be a promising targetable and prognostic biomarker. BRG1 immunohistochemical staining could be performed for GI NECs. Further studies with a larger cohort will be needed.

KEYWORDS

SWI/SNF, SMARCA4, BRG1, gastric cancer, neuroendocrine carcinoma

Abbreviations: SWI/SNF, SWItch/Sucrose Non-Fermentable; BRG1, Brahma-related gene 1; NEC, neuroendocrine carcinoma; CT, computed tomography; CgA, chromogranin A; Syn, synaptophysin; EBER, Epstein–Barr virus-encoded small RNA; TRG, tumor regression grade.

Introduction

Gastric cancer (GC) is one of the most common malignancies globally and has poor outcomes, especially in Asia (1, 2). Neuroendocrine neoplasms are epithelial neoplasms with neuroendocrine differentiation. Gastrointestinal neuroendocrine carcinoma (GI NEC) is a rare but highly malignant neoplasm with an aggressive clinical course (3). Chemotherapy has been the mainstay of treatment in unresectable or advanced high-grade GI NEC (4). A randomized clinical trial demonstrated that both etoposide plus cisplatin (EP) and irinotecan plus cisplatin (IP) can be standard first-line chemotherapy options for advanced neuroendocrine carcinoma (NEC) (4).

Recently, switch/sucrose non-fermentable (SWI/SNF) complexes were found to be a highly preserved group of multiprotein complexes that regulate chromatin remodeling and play an important role in proliferation, differentiation and tumor suppression (5, 6). *SMARCA4*, a tumor suppressor gene and one of the subunits of the SWI/SNF chromatin remodeling complex, encodes Brahma-related gene 1 (BRG1) (6). *SMARCA4* mutations were found to be present in a diverse set of cancer types at frequencies of up to 16% in solid tumors from 131,668 cancer patients (7). SMARCA4/BRG1 deficiency has been detected in a wide variety of tumors (8–15), such as small cell carcinoma of the ovary, hypercalcemic type (SCCOHT) and thoracic SMARCA4 undifferentiated tumors.

SMARCA4 mutations have been reported in a few neuroendocrine carcinomas. Germline and somatic alterations in the *SMARCA4* gene and loss of BRG1 protein expression have been established as defining events in small cell carcinoma of the ovary, hypercalcemic type (SCCOHT) (8). SMARCA4 deficiency can be present in TTF-1-negative neuroendocrine carcinomas (16). GI NEC with SMARCA4 deficiency may represent a rare phenotype of GI NEC and has not been reported in published English literature. Herein, we report two rare cases of GI NEC with SMARCA4 deficiency and provide insight into the clinicopathological features of this highly aggressive malignant tumor.

Methods and patients

Patient collection

Data from two cases of GI NEC with SMARCA4 deficiency were reviewed between January 2020 and December 2022 from the database of the Department of Pathology, West China Hospital, Sichuan University. Clinical and radiographic features were obtained from patients' medical records and follow-up. Ethics approval was obtained from the respective ethics committees of West China Hospital, Sichuan University, China (NO.2022317).

H&E and immunohistochemical staining

H&E and immunohistochemical staining was performed on 4-μm-thick unstained sections of representative formalin-fixed paraffin-embedded blocks. Immunohistochemistry was performed with the EnVision detection system. Antigen retrieval and staining were performed using standardized automated protocols in the presence of appropriate controls. Staining for SMARCA4 (anti-BRG1 antibody, 1:200 dilution, clone EPNCIR111A; Abcam, Cambridge, MA) was performed, as well as pancytokeratin (PCK) (clone AE1/AE3, ZSGB-BIO), epithelial membrane antigen (EMA) (clone GP1.4, ZSGB-BIO), CK20 (clone EP23, ZSGB-BIO), CK7 (clone EP16, ZSGB-BIO), CK8/18 (clone 5D3, MXB), p53 (clone D0-7, ZSGB-BIO), RB (clone 13A10, CELNOVTE), synaptophysin (Syn) (clone EP158, ZSGB-BIO), chromogranin A (CgA) (clone LK2H10, ZSGB-BIO), CD56 (clone UMAB83, ZSGB-BIO), Ki67 (clone MIB-1, ZSGB-BIO), LCA (clone 2B11&PD7/26, ZSGB-BIO), MLH1 (clone ES05, ZSGB-BIO), MSH2 (clone RED2, ZSGB-BIO), MSH6 (clone EP49, ZSGB-BIO) and PMS2 (clone EP51, ZSGB-BIO). Staining results were determined by 2 independent pathologists.

In situ hybridization of Epstein–Barr virus-encoded small RNA (EBER)

We stained 4-μm-thick sections for *in situ* hybridization to examine the Epstein–Barr virus (EBV) infection status. The EBER probe was detected using the PNA ISH Detection Kit (Dako).

Results

Clinical presentation

Detailed clinical features of the two patients of GI NEC with SMARCA4 deficiency are summarized in Table 1.

Case 1

A 43-year-old male patient presented with epigastric pain with yellowness of the skin for seven months. Gastroscopy showed a 1.5-cm thickened lesion in the duodenal papillae (Figure 1A), and a biopsy was performed. A computed tomography (CT) scan of the abdomen showed a 1.5-cm thickened lesion in the duodenal papillae (Figure 1B) and multiple nodules in the liver, indicating metastases of the liver. The clinical stage was cT3NxM1, IV.

Morphological analysis of the biopsy tissue showed poorly differentiated cells forming a solid architecture of neuroendocrine morphology (Figures 1D, E). The large-sized tumor cells were epithelioid ovoid with abundant cytoplasm. Nuclei were round and pleomorphic. Necrosis was not found in the small biopsy. Lymphocyte, eosinophil, and neutrophil infiltration was observed. Immunohistochemistry (Figure 1) indicated complete loss of BRG1 in the tumor nuclei, with endothelial and inflammatory cells as internal positive controls. CgA, Syn and CD56 were positively stained. The Ki67 index was approximately 90%. The tumor was positive for epithelial markers (PCK, CK8/18 and EMA) and negative for LCA. The expression of INI1, MLH1,

10.3389/fonc.2023.1290717

TABLE 1 Clinical features of gastrointestinal NEC with SMARCA4-deficiency.

Cases	Age/ Gender	Symptoms	Tumor size	Tumor location	TNM Stage	Treatment	MTS/Survival
Case 1	43/M	Epigastric pain with yellowness of the skin for seven months	1.5 cm	Duodenal papillae	cT3NxM1, IV	Chemotherapy (etoposide plus cisplatin) and anti-PD-1 immunotherapy (serplulimab)	DOD (9 months), liver and intraperitoneal MTS, and retroperitoneal lymph node MTS.
Case 2	64/F	Epigastric pain for nine months	2.9 cm	The greater curvature of the stomach	cT4aN1M0, IIIA	Surgical resection followed by chemotherapy (etoposide plus cisplatin), and continued to be treated with chemotherapy (cisplatin) and anti-PD-1 immunotherapy (sintilimab)	NED (10 months)

M: male; F: female; y, years; TNM, tumor-node-metastasis; PD-1, programmed cell death protein 1; NED, no evidence of disease; DOD, died of disease, MTS, metastasis.

MSH2, MSH6 and PMS2 was retained. *In situ* hybridization for EBER was negative. Due to the small biopsy, there was neither abundant tumor tissue nor sufficient well-preserved nucleic acids for next-generation sequencing (NGS) after immunohistochemistry.

Based on the morphological and immunohistochemical features, the tumor was diagnosed as GI NEC with SMARCA4 deficiency. The patient received chemotherapy (etoposide plus cisplatin) and anti-programmed cell death protein 1 (anti-PD-1) immunotherapy (serplulimab) for three cycles. The CT scan of the abdomen and gastroscopy showed a 3.0-cm thickened lesion in the duodenal papillae, multiple liver metastases (Figure 1C, triangles), and intraperitoneal metastases, and enlarged and partially fused retroperitoneal lymph nodes (Figure 1C, arrows). The tumor did not respond to treatment with chemotherapy and anti-PD-1 immunotherapy, and the patient died 9 months later.

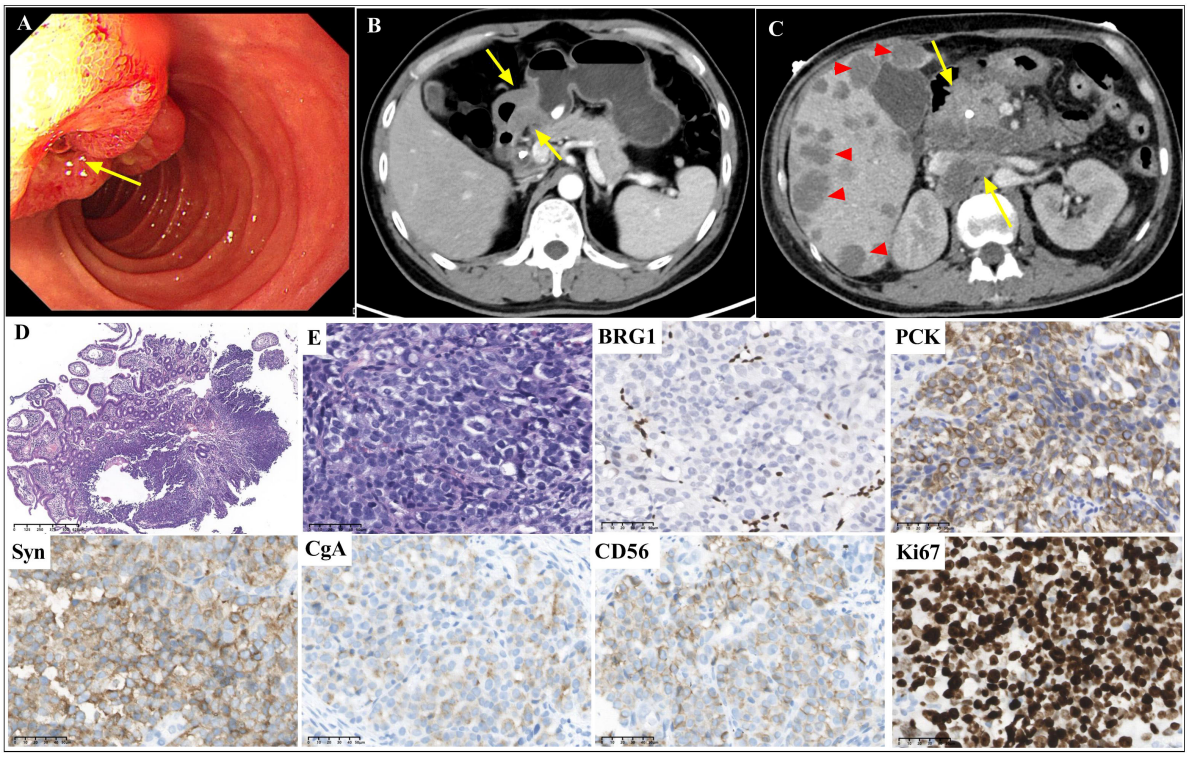

FIGURE 1
Gastroscopic, radiological, histopathological and immunohistochemical features of case 1 Gastroscopy (**A**, arrow) and abdominal CT scans (**B**, arrow) showed a thickened lesion in duodenal papilla. The abdominal CT scan showed multiple liver metastases (**C**, triangles), intraperitoneal metastases and retroperitoneal lymph node metastases (**C**, arrows) after chemotherapy. The biopsy showed a solid pattern with poorly differentiated tumor cells with inflammatory infiltration (**D**, magnification x40; and **E**, magnification x400). BRG1 was deficient. PCK, CgA, Syn and CD56 were positively stained. The Ki67 index was approximately 90% (magnification x400).

Case 2

A 64-year-old female patient presented with epigastric pain for nine months. Gastroscopy (Figure 2A) and a CT scan of the abdomen (Figure 2B) showed a 2.9-cm irregular ulcerative tumor in the greater curvature of the stomach, and a biopsy was performed. The clinical stage was cT4aN1M0, IIIA. The patient was administered neoadjuvant treatment with chemotherapy (etoposide plus cisplatin) for two cycles. Gastroscopy (Figure 2D) and a CT scan of the abdomen (Figure 2E) showed a larger irregular ulcerative tumor in the greater curvature of the stomach after neoadjuvant chemotherapy. The clinical assessment was

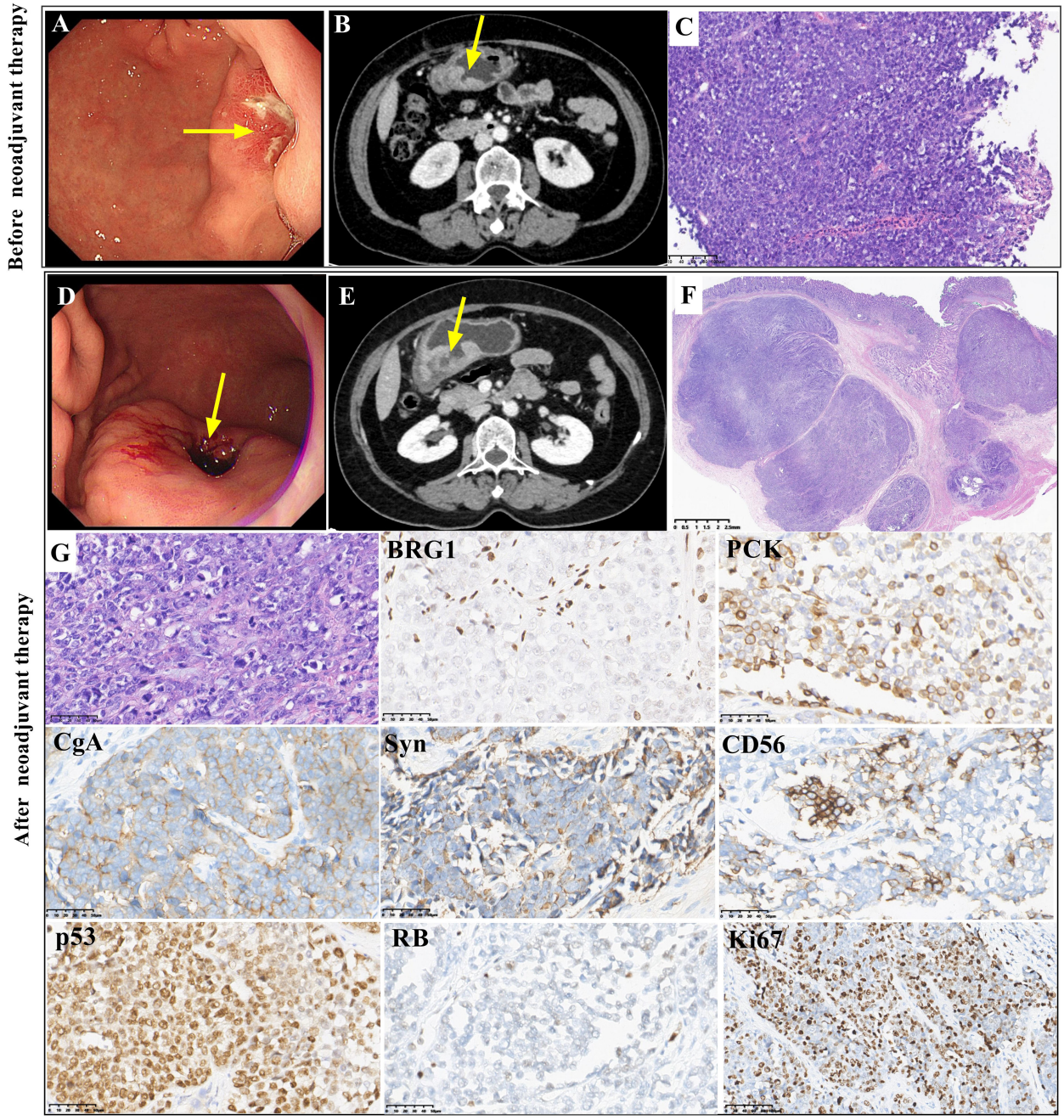

FIGURE 2
Gastroscopic, radiological, histopathological and immunohistochemical features of case 2 Gastroscopy (**A**, arrow) and abdominal CT scans (**B**, arrow) showed an irregularly thickened area in the greater curvature of the stomach before neoadjuvant treatment. The biopsy showed a solid pattern with poorly differentiated tumor cells before neoadjuvant treatment (**C**, magnification x100). Gastroscopy (**D**, arrow) and abdominal CT scans (**E**, arrow) showed a larger irregular thickened area of the greater curvature of the stomach after neoadjuvant treatment. The resected tumor showed a solid pattern with poorly differentiated tumor cells after neoadjuvant treatment, and there was no obvious response to neoadjuvant therapy (TRG3) (**F** and **G**, magnification x400). Both biopsy tissue and surgical resected tumor showed similar immunohistochemical staining. BRG1 was deficient. PCK staining was positive. CgA, Syn and CD56 were positively stained. P53 staining was positive, and RB staining was deficient. The Ki67 index was approximately 70% (magnification x400).

progressive disease (PD). Then, surgical resection was performed. On gross examination, there was an ulcerative tumor in the greater curvature of the stomach measuring 2.6 cm×2.5 cmx1.1 cm.

The biopsy tissue and resected tumor showed poorly differentiated morphology with solid architecture (Figures 2C, F, G). Round, pleomorphic nuclei with prominent nucleoli were large and irregular. Mitoses were frequent. The tumor cells in the resected specimen invaded the muscularis propria. Vascular invasion was observed. The pathological stage was yT2N2M0, IIB. Few lymphocytes and neutrophils were present. The tumor regression grade (TRG) was TRG3 (without an obvious response to neoadjuvant treatment) (Figure 2F). The immunohistochemical staining results of the resected tumor were similar to those of the biopsy. Complete loss of BRG1 was observed in the tumor nuclei, which was similar to the result for case 1 (Figure 2). Immunohistochemistry showed positivity for PCK. CgA, Syn and CD56 were positively stained. P53 immunoreactivity was positive. Complete loss of RB was found. The Ki67 index was approximately 70%. Immunohistochemical staining for CK7, CDX2, CK20, HER2 and SSTR2 showed negative results. The expression of INI1, ATRX, MLH1, MSH2, MSH6 and PMS2 was retained. *In situ* hybridization for EBER was negative. Regrettably, the patient rejected NGS detection of her sample.

Based on the morphological and immunohistochemical features, the tumor was diagnosed as GI NEC with SMARCA4 deficiency. The patient continued to be treated with chemotherapy (cisplatin) and anti-PD-1 immunotherapy (sintilimab) after surgery. There was no evidence of disease for 10 months.

Discussion

Kadoch et al. demonstrated that approximately 20% of all human cancers harbor mutations in SWI/SNF chromatin-remodeling complexes (17). *SMARCA4*, one of the subunits of the SWI/SNF chromatin remodeling complex, is a tumor suppressor (6). *SMARCA4* mutations occurred in 8% (20/258) of gastric cancers in a TCGA analysis and 10% (5/50) of gastric cancers in Takeshima's study (1, 18). Loss of SMARCA4 is associated with adverse clinical characteristics (19, 20). SMARCA4 (BRG1) deficiency occurs rarely in subsets of NECs, such as SCCOHT (8) and lung neuroendocrine carcinomas (16). The present report describes two rare patients diagnosed with GI NEC with SMARCA4 deficiency, aged 43 and 64 years, who presented with ulcerated and transmural masses with infiltration and were staged as cT3NxM1, IV in case 1 and cT4aN1M0, IIIA in case 2 at the time of diagnosis.

Inactivation of SMARCA4 is more likely to occur in gastric cancer with a solid and undifferentiated morphology, presenting in large and locally advanced tumors (21–23). Aberrant SMARCA4 protein expression was reported to be frequently observed in 49% (25/51) of solid-type poorly differentiated adenocarcinomas and nonsolid-type poorly differentiated adenocarcinomas (7.5%, 3/40) (20). However, GI NEC with SMARCA4 deficiency has not been reported in the published English literature. We reported two rare GI NECs that presented with a solid architecture and poorly differentiated morphology and showed complete loss of BRG1 expression. BRG1 immunohistochemical staining is useful for identifying SMARCA4-deficient tumors. In routine practice, screening BRG1 expression could be performed for GI NEC in pathological diagnosis.

A group of tumors with similar morphological features should be excluded before diagnosing GI NEC with SMARCA4 deficiency. The differential diagnosis includes gastric carcinoma with SMARCA4 deficiency, undifferentiated carcinomas, EBV-associated carcinoma, lymphoma, melanoma, germ cell neoplasms, and so on. GI NEC often diffusely expresses neuroendocrine markers, including chromogranin, synaptophysin and CD56, and tumor cells express epithelial markers. Gastric carcinoma with SMARCA4 deficiency can be distinguished by gland architecture of differentiation. Some undifferentiated tumors with a neuroendocrine-like phenotype may show variable positivity for synaptophysin, but neither of the cases expressed more than one neuroendocrine marker. Decreased expression of PCK was observed in 58.6% (17/29) of gastric SMARCA4-deficient undifferentiated carcinomas (21). Staining for LCA, CD138, CD38, MUM1, and anaplastic lymphoma kinase (ALK) is helpful for diagnosing lymphopoietic system tumors, including plasmablastic lymphoma and ALK-positive large B-cell lymphoma. HMB45, S100, and MART-1 can be helpful for diagnosing melanoma. A combination of antibodies, including Sal-like transcription factor 4 (SALL4), octamer-binding transcription factor 3/4 (OCT3/4) and α-fetoprotein (AFP), have been used to diagnose germ cell tumors.

Poorly differentiated neuroendocrine carcinoma of the digestive system has a dismal prognosis with limited treatment options. Systemic platinum-based treatment is the standard treatment for GI NEC. For high-grade NEC in the GI tract, multiagent chemotherapy was found to be associated with superior survival compared with single-agent chemotherapy, which was superior to no chemotherapy (3). programmed cell death receptor 1/programmed cell death ligand 1 (PD-1/PD-L1) expression is a frequent occurrence in poorly differentiated neuroendocrine carcinomas of the digestive system. Checkpoint blockade targeting the PD-1/PD-L1 pathway may have a potential role in treatment (24, 25). There are no published studies on a recommended treatment for GI NEC with SMARCA4 deficiency. Patients with SMARCA4-altered GC do not benefit from chemotherapy in stages II and III (P=0.623 and 0.678) (26). SMARCA4 alteration in GC remains a significant unfavorable prognostic factor (median survival 14 versus 26 months, p=0.002) in patients with stage III disease who receive chemotherapy (26). Two patients with tumors localized to the gastroesophageal junction received neoadjuvant chemotherapy and showed no response (TRG3), showing very adverse clinical characteristics and poor survival (19). In the present study, case 1 did not respond to chemotherapy and anti-PD-1 immunotherapy. Case 2 showed TRG3 in response to neoadjuvant chemotherapy. GI NEC with SMARCA4 deficiency may have limited benefit from chemotherapy and anti-PD-1 immunotherapy. SMARCA4 in GI NEC may be a prognostic and targetable biomarker. SMARCA4-mutated cancers have a DNA repair vulnerability that can be exploited therapeutically (27). Future treatments with agents that

target the epigenetic machinery, such as inhibitors against enhancer of zeste homolog 2 (EZH2) or histone deacetylase, may prove even more effective (28, 29), which might provide more therapeutic options.

Conclusions

We retrospectively report two rare cases of GI NEC with SMARCA4 deficiency. GI NEC with SMARCA4 deficiency may not benefit from chemotherapy and has poor outcomes. SMARCA4 may be a promising targetable and prognostic biomarker for GI NEC, requiring more exploration for validation in a larger series.

Data availability statement

The original contributions presented in the study are included in the article/supplementary material. Further inquiries can be directed to the corresponding author/s.

Ethics statement

The studies involving humans were approved by Ethics approval was obtained from the respective ethics committees of West China Hospital, Sichuan University, China (NO.2022317). The studies were conducted in accordance with the local legislation and institutional requirements. The human samples used in this study were acquired from primarily isolated as part of your previous study for which ethical approval was obtained. Written informed consent for participation was not required from the participants or the participants' legal guardians/next of kin in accordance with the national legislation and institutional requirements. Written informed consent was obtained from the individual(s) for the publication of any potentially identifiable images or data included in this article.

Author contributions

PZ: Data curation, Writing – original draft, Writing – review & editing. YF: Formal Analysis, Software, Methodology. WW: Funding acquisition, Project administration, Writing – review & editing.

Funding

The author(s) declare financial support was received for the research, authorship, and/or publication of this article. The writing of the current manuscript was supported by 1.3.5 Project for Disciplines of Excellence-Clinical Research Incubation Project, West China Hospital, Sichuan University (No. 2019HXFH034 and ZYJC21074) and Sichuan Science and Technology Program (No. 2021YJ0117). The funding body played no role in the design of the study and collection, analysis, and interpretation of data and in writing the manuscript.

Conflict of interest

The authors declare that the research was conducted in the absence of any commercial or financial relationships that could be construed as a potential conflict of interest.

Publisher's note

References

1. Bass AJ, Thorsson V, Shmulevich I, Reynolds SM, Miller M, Bernard B, et al. : Comprehensive molecular characterization of gastric adenocarcinoma. *Nature* (2014) 513(7517):202–9. doi: 10.1038/nature13480

2. Yashima K, Shabana M, Kurumi H, Kawaguchi K, Isomoto H. Gastric Cancer Screening in Japan: A Narrative Review. *J Clin Med* (2022) 11:4337. doi: 10.3390/jcm11154337

3. Alese OB, Jiang R, Shaib W, Wu C, Akce M, Behera M, et al. High-Grade Gastrointestinal Neuroendocrine Carcinoma Management and Outcomes: A National Cancer Database Study. *Oncologist* (2019) 24(7):911–20. doi: 10.1634/theoncologist.2018-0382

4. Morizane C, Machida N, Honma Y, Okusaka T, Boku N, Kato K, et al. Effectiveness of Etoposide and Cisplatin vs Irinotecan and Cisplatin Therapy for Patients With Advanced Neuroendocrine Carcinoma of the Digestive System: The TOPIC-NEC Phase 3 Randomized Clinical Trial. *JAMA Oncol* (2022) 8(10):1447–55. doi: 10.1001/jamaoncol.2022.3395

5. Schaefer IM, Hornick JL. SWI/SNF complex-deficient soft tissue neoplasms: An update. *Semin Diagn Pathol* (2021) 38(3):222–31. doi: 10.1053/j.semdp.2020.05.005

6. Halliday GM, Bock VL, Moloney FJ, Lyons JG. SWI/SNF: a chromatin-remodelling complex with a role in carcinogenesis. *Int J Biochem Cell Biol* (2009) 41(4):725–8. doi: 10.1016/j.biocel.2008.04.026

7. Fernando TM, Piskol R, Bainer R, Sokol ES, Trabucco SE, Zhang Q, et al. Functional characterization of SMARCA4 variants identified by targeted exome-sequencing of 131,668 cancer patients. *Nat Commun* (2020) 11(1):5551. doi: 10.1038/s41467-020-19402-8

8. Ramos P, Karnezis AN, Craig DW, Sekulic A, Russell ML, Hendricks WPD, et al. Small cell carcinoma of the ovary, hypercalcemic type, displays frequent inactivating germline and somatic mutations in SMARCA4. *Nat Genet* (2014) 46(5):427–9. doi: 10.1038/ng.2928

9. Ramos P, Karnezis AN, Craig DW, Sekulic A, Russell ML, Hendricks WPD, et al. Small cell carcinoma of the ovary, hypercalcemic type displays frequent inactivating germline and somatic mutations in SMARCA4. *Nat Genet* (2014) 46(5):427–29. doi: 10.1038/ng.2928

10. Nambirajan A, Jain D. Recent updates in thoracic SMARCA4-deficient undifferentiated tumor. *Semin Diagn Pathol* (2021) 38(5):83–89. doi: 10.1053/j.semdp.2021.06.001

11. Imielinski M, Berger AH, Hammerman PS, Hernandez B, Pugh TJ, Hodis E, et al. Sivachenko A et al: Mapping the hallmarks of lung adenocarcinoma with massively parallel sequencing. *Cell* (2012) 150(6):1107–20. doi: 10.1016/j.cell.2012.08.029

12. Robinson G, Parker M, Kranenburg TA, Lu C, Chen X, Ding L, et al. Zhu X et al: Novel mutations target distinct subgroups of medulloblastoma. *Nature* (2012) 488 (7409):43–8. doi: 10.1038/nature11213

13. Love C, Sun Z, Jima D, Li G, Zhang J, Miles R, et al. Srivastava G et al: The genetic landscape of mutations in Burkitt lymphoma. *Nat Genet* (2012) 44(12):1321–5. doi: 10.1038/ng.2468

14. Bai J, Mei P, Zhang C, Chen F, Li C, Pan Z, et al. BRG1 is a prognostic marker and potential therapeutic target in human breast cancer. *PloS One* (2013) 8(3):e59772. doi: 10.1371/journal.pone.0059772

15. Kolin DL, Quick CM, Dong F, Fletcher CDM, Stewart CJR, Soma A, et al. SMARCA4-deficient Uterine Sarcoma and Undifferentiated Endometrial Carcinoma Are Distinct Clinicopathologic Entities. *Am J Surg Pathol* (2020) 44(2):263–70. doi: 10.1097/PAS.0000000000001375

16. Gandhi JS, Alnoor F, Sadiq Q, Solares J, Gradowski JF. SMARCA4 (BRG1) and SMARCB1 (INI1) expression in TTF-1 negative neuroendocrine carcinomas including merkel cell carcinoma. *Pathol Res Pract* (2021) 219:153341. doi: 10.1016/j.prp.2021.153341

17. Kadoch C, Crabtree GR. Mammalian SWI/SNF chromatin remodeling complexes and cancer: Mechanistic insights gained from human genomics. *Sci Adv* (2015) 1(5):e1500447. doi: 10.1126/sciadv.1500447

18. Takeshima H, Niwa T, Takahashi T, Wakabayashi M, Yamashita S, Ando T, et al. Sugiyama T et al: Frequent involvement of chromatin remodeler alterations in gastric field cancerization. *Cancer Lett* (2015) 357(1):328–38. doi: 10.1016/j.canlet.2014.11.038

19. Gluckstein MI, Dintner S, Arndt TT, Vlasenko D, Schenkirsch G, Agaimy A, et al. Comprehensive Immunohistochemical Study of the SWI/SNF Complex Expression Status in Gastric Cancer Reveals an Adverse Prognosis of SWI/SNF Deficiency in Genomically Stable Gastric Carcinomas. *Cancers (Basel)* (2021) 13 (15):3894. doi: 10.3390/cancers13153894

20. Sasaki T, Kohashi K, Kawatoko S, Ihara E, Oki E, Nakamura M, et al. Tumor progression by epithelial-mesenchymal transition in ARID1A- and SMARCA4-aberrant solid-type poorly differentiated gastric adenocarcinoma. *Virchows Arch* (2022) 480(5):1063–75. doi: 10.1007/s00428-021-03261-9

21. Chang B, Sheng W, Wang L, Zhu X, Tan C, Ni S, et al. SWI/SNF Complex-deficient Undifferentiated Carcinoma of the Gastrointestinal Tract: Clinicopathologic Study of 30 Cases With an Emphasis on Variable Morphology, Immune Features, and the Prognostic Significance of Different SMARCA4 and SMARCA2 Subunit Deficiencies. *Am J Surg Pathol* (2022) 46(7):889–906. doi: 10.1097/PAS.0000000000001836

22. Agaimy A, Daum O, Markl B, Lichtmannegger I, Michal M, Hartmann A. SWI/SNF Complex-deficient Undifferentiated/Rhabdoid Carcinomas of the Gastrointestinal Tract: A Series of 13 Cases Highlighting Mutually Exclusive Loss of SMARCA4 and SMARCA2 and Frequent Co-inactivation of SMARCB1 and SMARCA2. *Am J Surg Pathol* (2016) 40(4):544–53. doi: 10.1097/PAS.0000000000000554

23. Horton RK, Ahadi M, Gill AJ, Said S, Chen ZE, Bakhshwin A, et al. SMARCA4/SMARCA2-deficient Carcinoma of the Esophagus and Gastroesophageal Junction. *Am J Surg Pathol* (2021) 45(3):414–20. doi: 10.1097/PAS.0000000000001599

24. Roberts JA, Gonzalez RS, Das S, Berlin J, Shi C. Expression of PD-1 and PD-L1 in poorly differentiated neuroendocrine carcinomas of the digestive system: a potential target for anti-PD-1/PD-L1 therapy. *Hum Pathol* (2017) 70:49–54. doi: 10.1016/j.humpath.2017.10.003

25. Yang MW, Fu XL, Jiang YS, Chen XJ, Tao LY, Yang JY, et al. Liu PF et al: Clinical significance of programmed death 1/programmed death ligand 1 pathway in gastric neuroendocrine carcinomas. *World J Gastroenterol* (2019) 25(14):1684–96. doi: 10.3748/wjg.v25.i14.1684

26. Huang SC, Ng KF, Yeh TS, Cheng CT, Chen MC, Chao YC, et al. The clinicopathological and molecular analysis of gastric cancer with altered SMARCA4 expression. *Histopathology* (2020) 77(2):250–61. doi: 10.1111/his.14117

27. Hays E, Nettleton E, Carter C, Morales M, Vo L, Passo M, et al. The SWI/SNF ATPase BRG1 stimulates DNA end resection and homologous recombination by reducing nucleosome density at DNA double strand breaks and by promoting the recruitment of the CtIP nuclease. *Cell Cycle* (2020) 19(22):3096–114. doi: 10.1080/15384101.2020.1831256

28. Yamagishi M, Uchimaru K. Targeting EZH2 in cancer therapy. *Curr Opin Oncol* (2017) 29(5):375–81. doi: 10.1097/CCO.0000000000000390

29. Leitner K, Tsibulak I, Wieser V, Knoll K, Reimer D, Marth C, et al. Clinical impact of EZH2 and its antagonist SMARCA4 in ovarian cancer. *Sci Rep* (2020) 10 (1):20412. doi: 10.1038/s41598-020-77532-x

frontiers | Frontiers in Oncology

TYPE Original Research
PUBLISHED 09 January 2024
DOI 10.3389/fonc.2023.1322421

OPEN ACCESS

EDITED BY
Yanqing Liu,
Columbia University, United States

REVIEWED BY
Weiping Li,
Columbia University, United States
Kai Song,
University of California, Los Angeles, United States

*CORRESPONDENCE
Yan Wang
yanwang@shutcm.edu.cn
Huirong Zhu
zhu_huirong@126.com

†These authors have contributed equally to this work

RECEIVED 26 October 2023
ACCEPTED 05 December 2023
PUBLISHED 09 January 2024

CITATION
Li H, Zhang Y, Feng Y, Hu X, Bi L, Zhu H and Wang Y (2024) Predictors based on cuproptosis closely related to angiogenesis predict colorectal cancer recurrence. *Front. Oncol.* 13:1322421. doi: 10.3389/fonc.2023.1322421

Predictors based on cuproptosis closely related to angiogenesis predict colorectal cancer recurrence

Haoran Li[1†], Yingru Zhang[1†], Yuanyuan Feng[2], Xueqing Hu[1], Ling Bi[1], Huirong Zhu[1*] and Yan Wang[1,2*]

[1]Oncology Institute, Shuguang Hospital, Shanghai University of Traditional Chinese Medicine, Shanghai, China, [2]Department of Medical Oncology, Shuguang Hospital, Shanghai University of Traditional Chinese Medicine, Shanghai, China

Up to one-third of colorectal cancer (CRC) patients experience recurrence after radical surgery, and it is still very difficult to assess and predict the risk of recurrence. Angiogenesis is the key factor of recurrence as metastasis of CRC is closely related to copper metabolism. Expression profiling by microarray from two datasets in Gene Expression Omnibus (GEO) was selected for quality control, genome annotation, normalization, etc. The identified angiogenesis-derived and cuproptosis-related Long non-coding RNAs (lncRNAs) and clinical data were screened and used as predictors to construct a Cox regression model. The stability of the model was evaluated, and a nomogram was drawn. The samples were divided into high-risk and low-risk groups according to the linear prediction of the model, and a Kaplan–Meier survival analysis was performed. In this study, a model was established to predict the postoperative recurrence of colon cancer, which exhibits a high prediction accuracy. Furthermore, the negative correlation between cuproptosis and angiogenesis was validated in colorectal cancer cell lines and the expression of lncRNAs *in vitro* was examined.

KEYWORDS

colorectal cancer, recurrence, prediction model, cuproptosis, prognosis

1 Introduction

Colorectal cancer (CRC) is the third most common cancer worldwide, accounting for nearly 10% of all cases (1). Although many react positively to treatment, including surgery, radiotherapy, and chemotherapy, up to one-third of patients experience postoperative recurrence with high mortality when the local tumor is completely controlled (2), and angiogenesis is one of the most critical factors for CRC progression.

Unrestricted invasive growth and metastasis of malignant tumors depend on angiogenesis, and tumors rarely metastasize without angiogenesis (3). When the tumor proliferates a critical amount, it starts the angiogenesis phenotype, produces strong angiogenesis activity, and enters the vascularization stage. New microvessels are the first step of tumor invasion and metastasis (4). The more tumor microvessels there are, the greater the chance of tumor cells entering the blood circulation. The wall of tumor neovascularization lacks structure integrity, in which there is only one layer of endothelial cells and lacks smooth muscle, which makes it easier to be penetrated by tumor cells than normal mature blood vessels (5). Furthermore, angiogenesis has a certain invasion ability, and tumor cells can invade along the collagen cracks attributed to vessels. Inhibition of angiogenesis can significantly suppress the growth of tumors (6). Anti-angiogenesis is a new strategy different from conventional anti-tumor therapy, and it has become a great prospect in tumor research.

In March 2022, Tsvetkov (7) proposed for the first time a copper (Cu)-dependent cell death mode, cuproptosis, which is different from other known cell death modes, such as apoptosis, necroptosis, and pyroptosis, it is a metal ion-induced regulatory cell death (8). Cu is an essential mineral for organisms and the basic element of many biological processes, including mitochondrial respiration, iron absorption, antioxidation, and detoxification. There is also some evidence that copper may play a role in the etiology, severity, and progress of cancer (9). Importantly, Cu can also promote angiogenesis, which is essential for tumor progression and metastasis (10). More and more evidence has shown that Cu can activate many angiogenic factors, such as angiopoietin (ANGPT), and vascular endothelial growth factor A (VEGFA) (11). It has been reported that Cu complexes and nanomaterials display the property of matrix metalloproteinase (MMP) inhibition (12, 13). It has been found that the Cu content in the serum and tumor tissue of cancer patients has changed significantly, which decreased in the serum of patients with CRC (14). Therefore, Cu-dependent cuproptosis may be related to the prognosis of patients.

Since the MOSAIC study (15), adjuvant chemotherapy has been a standard treatment for stage III colon cancer, which can prolong survival time and reduce the risk of recurrence. Only 20% of patients benefit from adjuvant chemotherapy, and 80% of the patients suffer unnecessary toxicity. Although clinical and pathological information is important in predicting prognosis, it is insufficient to determine which patients will benefit from adjuvant chemotherapy. Recently developed molecular markers, such as microsatellite status, BRAF, and KRAS mutations (16), which are instructional for immunotherapy and targeted therapy, are also expected to be important stratification factors for adjuvant chemotherapy. Furthermore, recent studies have emphasized the prognostic value of immune infiltration (17). Whether they are pathological, immunological, or molecular prognostic markers, these predictors can help clinicians stratify patients' prognostic risks and develop individualized therapy.

Long non-coding RNA (lncRNA), a vast and unexplored region of the human genome, is a member of the non-protein coding RNA family with a length of more than 200 nucleotides. LncRNAs regulate the translation and decay of mRNA in a base-pairing-dependent manner (18) and participate in signal transduction through interaction with protein and lipids (19, 20). LncRNAs can affect signal pathways including WNT/β-catenin, PI3K/Akt, mTOR, and TP53 (21), and participate in many stages of tumor progression, including proliferation, apoptosis, angiogenesis, and metastasis. More and more transcriptome sequencing has identified many lncRNAs with altered expression and tissue specificity in cancer, which are expected to be potential prognostic markers. At present, most prognosis scores only use single-dimensional predictors: pathological data, immunity, or molecular markers. The analysis of large-scale multicenter clinical and molecular data can help integrate these factors into a comprehensive model. In this study, we aimed to verify the predictive ability of angiogenesis-derived cuproptosis-related molecular markers for colon cancer recurrence, and established a risk prediction model for colon cancer recurrence by combining clinical data with molecular biomarkers. This model stratifies the risk after radical resection, predicts the risk of recurrence, and is promising for guiding individual therapy.

2 Materials and methods

2.1 Collection and quality control of expression profiling by microarray

First, two microarray datasets based on GPL570 (Affymetrix Human Genome U133 Plus 2.0 Array) named GSE17536 and GSE17537 were selected from Gene Expression Omnibus (GEO) (22). The two datasets were obtained from expression profiling of colon cancer tissues in two medical centers. GSE17536 contains 177 samples, and GSE17537 contains 55. In this study, the original CEL files of microarray were selected for data analysis. The 232 microarrays were uniformly tested for quality, and the quality control was completed based on the R (version: 4.2.1) package "arrayQualityMetrics" (23), which includes five aspects: array comparison, array intensity distributions, variance mean dependence, Affymetrix specific plots, and individual array quality. Then, the RMA algorithm was used to sequentially perform background correcting, normalization, and summarization (24). RMA algorithm has performed logarithmic processing on gene expression. After the probes of GPL570 were annotated as gene symbols, the gene expression matrix was extracted. In the meantime, clinical information including gender, age, stage, outcome, and disease-free survival (DFS) time was further organized.

2.2 Identification of cuproptosis-related lncRNAs

mRNAs and lncRNAs were distinguished in the gene expression matrix through the annotation file of the UCSC Genome Browser (25). The mRNAs related to cuproptosis were determined through relevant published studies. Pearson's correlation analysis was performed on cuproptosis-related mRNAs and lncRNAs using R, and the lncRNAs with linear correlation with cuproptosis-related mRNAs were identified as predictors preliminarily included in the model.

2.3 Constructing a prediction model based on the training set

GSE17536 was used as the training set for model construction and predictors screening, while GSE17537 was used as the validation set for subsequent external validation and predictive evaluation of the model. Event was selected as the outcome-related dependent variable, DFS was selected time as the time-related dependent variable, and sex, age, stage, and cuproptosis-related lncRNAs were selected as independent variables of the model. In the training set, the independent variables were tested using univariate Cox regression to evaluate whether they have a significant impact on survival to preliminarily screen the predictors. The screened predictors were used to construct a least absolute shrinkage and selection operator (LASSO)-based Cox regression model and further screened by stepwise selection to prevent the model from overfitting. The package "glmnet" (26) of R was used to construct the LASSO-based Cox regression model, which compresses the coefficients of predictors to 0 by setting the penalty coefficient λ, thus excluding the predictors that have few influences on dependent variables. LASSO regression selects λ with the smallest error in 10-fold cross-validations as the penalty coefficient. On the basis of LASSO regression, further screening was carried out by stepwise selection, which selects the best predictors by gradually deleting or adding predictors from the existing model and evaluating the prediction accuracy of the model.

2.4 Principal component analysis

Principal component analysis (PCA) is a method of inducing and combining multiple variables and distinguishing different samples with the least dimensions. PCA was carried out on the expression of all RNAs, cuproptosis-related mRNAs, cuproptosis-related lncRNAs, and the predictors to distinguish the ability of different biomarkers to predict risks. Meanwhile, scree plots were drawn to calculate the cumulative contribution rate (CCR).

2.5 Evaluation of model stability

The prediction model was constructed using the predictors screened twice and evaluated using influential point, multicollinearity, and the Schoenfeld individual test. The influential point was used to detect whether there was a sample that had a significant influence on the model fitting (that is, the sample had too much influence on the model compared with most samples), which would be eliminated. Multicollinearity refers to the significant correlation between the predictors in the model; that is, the same feature is described from two similar dimensions. This is due to inadequate screening of predictors and may result in model over-fitting. The Schoenfeld individual test was used to test whether there was a correlation between time and coefficient of the predictors, and if there was a correlation, the basic assumption of Cox regression was not established.

2.6 Internal validation and external validation

The number of predictors is greatly reduced after being screened twice, which may lead to the phenomenon of underfitting and decrease the prediction accuracy of the model. Therefore, the model was internally validated and evaluated for accuracy using the area under the curve (AUC), calibration curve, and Brier score. However, an independent dataset for external validation was selected, and the model was also evaluated using AUC, calibration curve, and Brier score. AUC and calibration curve are indicators to evaluate discrimination and calibration, respectively, and the Brier score was used to comprehensively reflect the discrimination and calibration.

2.7 Establishment of the nomogram

We drew a nomogram (27), which clearly manifested the prediction probability of the DFS of the samples. The nomogram scores the predictors according to their coefficients and variable types (classified variables or continuous variables) and outputs the survival probability according to the total score.

2.8 Risk division and survival analysis

The Risk Score (RS) was defined as the linear prediction of the model, and all samples were divided into high-risk and low-risk groups according to the RS median of the training set. Afterward, Kaplan–Meier (KM) survival analysis was carried out to explore whether there were differences in survival probability between high-risk and low-risk groups.

2.9 Enrichment analysis and immune cell infiltration

We performed Gene Set Enrichment Analysis (GSEA) on high-risk and low-risk groups identified using RS to verify the correlation between cuproptosis and angiogenesis. Subsequently, we performed Kyoto Encyclopedia of Genes and Genomes (KEGG) enrichment analysis and Gene Ontology (GO) enrichment analysis on cuproptosis-related genes to explore the signal pathway and biological function of their enrichment. CIBERSORT (28) quantified the composition of immune cells in tissues according to standardized gene expression data, and the accuracy of this method was verified by flow cytometry. CIBERSORT calculated p and root mean squared error for each sample, with a default signature matrix at 100 permutations, of which p-values <0.05 were filtered and selected for the next analysis. CIBERSORT demonstrated the difference in immune cell composition between the high-risk and low-risk groups.

2.10 Expression profile of colorectal cancer cell lines from public database

We selected all colorectal cancer cell lines in Depmap [Cancer Cell Line Encyclopedia (CCLE)] and downloaded the expression profile from Expression Public 23Q2, which was then normalized. After dividing the cell lines into two groups according to their sources, we carried out GSEA to find out the differences in angiogenesis and cuproptosis. Furthermore, we drew violin plots of cuproptosis–mRNA expression in colorectal cancer cell lines.

2.11 Cell lines and culture *in vitro*

The Caco-2 and SW620 cell lines were obtained from the cell bank of the Chinese Academy of Sciences (Shanghai, China). Caco-2 cells were cultured in high-glucose Dulbecco's modified Eagle's medium (DMEM; Gibco, Grand Island, NY, USA) supplemented with 10% fetal bovine serum (FBS; Gibco, Grand Island, NY, USA), 1% penicillin, and 1% streptomycin (Gibco, Grand Island, NY, USA) and supplemented with 5% carbon dioxide–air of a 37°C humidified incubator. SW620 cell line was cultured in Leibovitz's L-15 (Corning, Shanghai, China) medium supplemented with 10% FBS, 1% penicillin, and 1% streptomycin.

2.12 Quantitative real-time PCR

Cell/Tissue Total RNA Isolation Kit V2 was used to remove genomic DNA and isolate total RNA. NanoDrop ND-1000 was used to quantify sample RNA, and III RT SuperMix for qPCR was used to further remove gDNA and perform reverse transcription. Real-time fluorescent quantitative was performed by ABI 7500 Instrument (Applied Biosystems, Foster City, CA, USA) using the SYBR Green method, and $2^{-\Delta\Delta Ct}$ was identified as the relative RNA expression. The target primers are shown in Table 1.

TABLE 1 Primer sequence.

mRNAs/lncRNAs	Primer
MMP2	Forward: TACAGGATCATTGGCTACACACC
	Reverse: GGTCACATCGCTCCAGACT
MMP7	Forward: GAGTGAGCTACAGTGGGAACA
	Reverse: CTATGACGCGGGAGTTTAACAT
PDGFA	Forward: GCAAGACCAGGACGGTCATTT
	Reverse: GGCACTTGACACTGCTCGT
ANGPT2	Forward: ACCCCACTGTTGCTAAAGAAGA
	Reverse: CCATCCTCACGTCGCTGAATA
LINC02043	Forward: GGAGCTCTCAGATGCTGGAC
	Reverse: CTACAGGGAGGTGGAATCCG
LINC02754	Forward: TTGGCAGGCTGGTATAAACTT
	Reverse: TGTGCTTGGTGGTGGTAATG
LINC02510	Forward: TTGGAATTGCCTGCTTTGAGC
	Reverse: CTCTGTTCTGGCAGGGTGAG
DLEU1	Forward: AGTGTTTGCCTTTACGCAGTC
	Reverse: GAAGCACTGCATGGTTGCAC
GAPDH	Forward: AATCAAGTGGGGCGATGCTG
	Reverse: GGGGCAGAGATGATGACCCT

3 Results

3.1 Quality control and annotation of microarray

By analyzing the original CEL file, the grayscale (Supplementary Figure S1A) of the microarray is displayed, and a statistical analysis was performed to draw a barplot, boxplot, and MA plot (Supplementary Figures S1B–D), which shows the data distribution of the original array. Ideally, the scatter points in the plot are along the M = 0 axis. There may be problems with the microarray with a large interquartile range (IQR). After quality control, the microarrays with quality problems and without clinical data were eliminated. There were 145 samples in GSE17536 and 55 samples left in GSE17537. The probe matrix with 200 columns and 54,675 rows was normalized using the RMA algorithm, as shown in Figure 1A.

There were 54,675 probes in the GPL570. Since there were multiple probes detecting the same gene, we identified 17,202 mRNAs and 1,806 lncRNAs through the annotation file of the UCSC Genome Browser. There were 19 mRNAs (Supplementary Table S1) related to cuproptosis confirmed by relevant published studies, which were included in GeneCards—the human gene database (www.genecards.org) (29). Since the two mRNAs, *DLST* and *LIPT2*, were not annotated in GPL570, Pearson's correlation analysis was performed on 17 mRNAs and 1,806 lncRNAs using R and detected 692 lncRNAs, which had a linear correlation ($p < 0.001$) with cuproptosis-related mRNAs (Figure 1B), among which there was no lncRNA significantly related to *ATP7A*.

3.2 Seven predictors after multiple screening

After the correlation test of univariate regression, 666 lncRNAs that had no significant influence on the outcome were excluded. Only "stage" and 26 lncRNAs were used as predictors for the multivariate regression (Figure 2A). In LASSO-based Cox regression, the event was selected as the outcome-related dependent variable and DFS time as the time-related dependent variable, nearly half of the predictors were screened out with $\lambda = 0.243$, and there were 13 predictors left in the model, including "stage" and 12 lncRNAs (Figures 2B, C). Through the stepwise selection, seven predictors were finally selected, including a classified variable "stage" and six continuous variables (*LINC02754*, *LINC02043*, *LINC02510*, *DLEU1*, *RNF185-AS1*, and *LINC02067*). The correlation with cuproptosis-related mRNAs is shown in Figure 1C. PCA (Figures 2D–G) manifested that the screening process was beneficial in distinguishing high- and low-

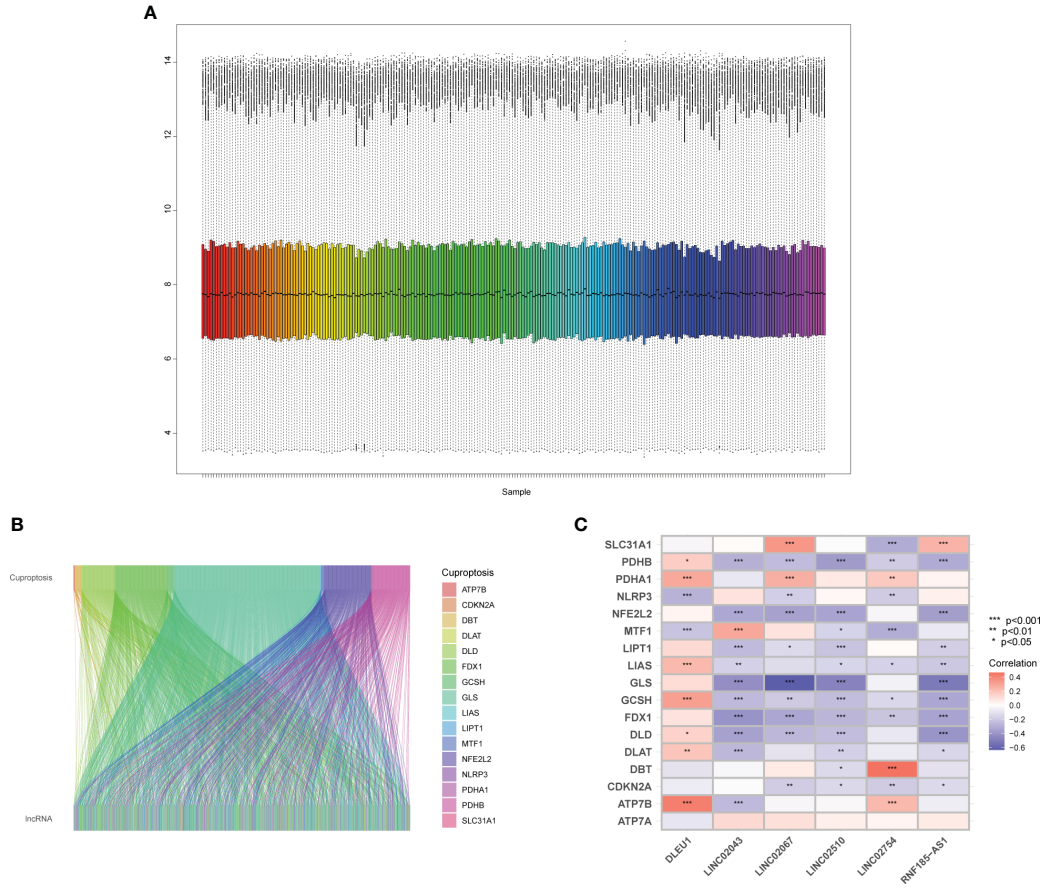

FIGURE 1
Quality control of microarray and identification of cuproptosis-related lncRNAs. **(A)** Boxplot of the expression profile of samples. **(B)** The lncRNAs have linear relationships with cuproptosis-related mRNAs. **(C)** Heatmap of cuproptosis-related mRNAs and predictors.

risk groups. Scree plots (Supplementary Figure S2) intuitively indicate that the CCR of the top 3 principal components (PCs) gradually elevated with further screening. The CCRs based on all RNAs, cuproptosis-related mRNAs, cuproptosis-related lncRNAs, and the predictors were 30.5%, 45%, 55.6%, and 64.5%, respectively, which also suggest that the discrimination between the two groups based on only three dimensions was insufficient (<80%).

3.3 Model test and stability evaluation

The test of influential point suggested that no obvious outlier was found in the residual diagram of predictors, and the residual of each predictor in the fitted model was close to 0 (Figure 3A). The multicollinearity analysis of package "rms" indicated that the variance inflation factors (VIFs) of each predictor were 1.083 (stage), 1.035 (*LINC02754*), 1.069 (*LINC02043*), 1.062 (*LINC02510*), 1.124 (*DLEU1*), 1.035 (*RNF185-AS1*), and 1.092 (*LINC02067*). When VIF < 5, it is considered that there is no multicollinearity between the predictors. In the Schoenfeld individual test (Figure 3B), $p > 0.05$ indicated that the proportional risk assumption was not rejected, and the coefficients of the seven predictors were not time-dependent.

3.4 Internal validation and external validation confirmed the high accuracy of the prediction model

First, statistical tests from the training and validation sets revealed no differences in "gender" ($p = 0.623$) and "age" ($p = 0.094$) between the two sets. After internal validation, the model performed well in the self-prediction of the training set. The AUC values of 1 year, 3 years, and 5 years in the receiver operating characteristic (ROC) curve were 0.863, 0.715, and 0.749, respectively (Figure 4A). On the basis of external validation, the AUCs of 1 year, 3 years, and 5 years in the ROC curve were 0.929, 0.941, and 0.914, respectively (Figure 4B). The longer the time span, the lower the accuracy of prediction. However, the AUC suggested that the discrimination of the model did not obviously decline within 5 years. The 5-year calibration curves of the training set and the validation set were relatively fitted to the ideal curve, with Brier scores of 0.159 and 0.096, respectively (Figures 4C, D). Meanwhile, we tested the accuracy of the model when there was only one predictor, stage, in the model. The stage itself had good discrimination (Supplementary Figures S3A, C) but a poor calibration with a Brier score >0.2 (Supplementary Figures S3B, D).

10.3389/fonc.2023.1322421

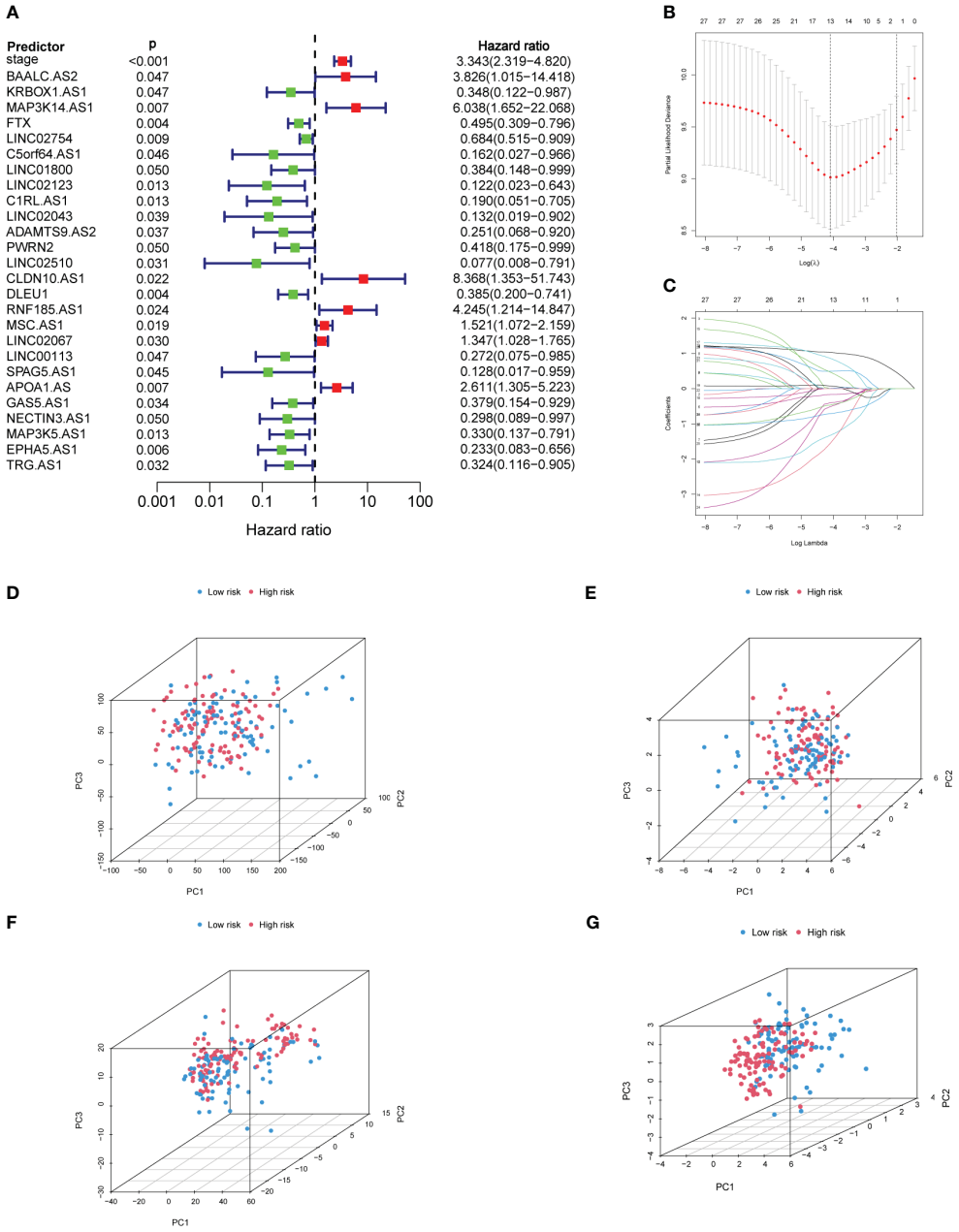

FIGURE 2
Screening of predictors and PCA. **(A)** Establishment of univariate Cox regression based on predictors. **(B)** The λ with the smallest cross-validation error in LASSO-based Cox regression was selected, and there were 13 predictors remaining in the model. **(C)** With the increase of the penalty coefficient, the predictors in the model gradually decrease. **(D)** PCA of all genes. **(E)** PCA of cuproptosis-related mRNAs. **(F)** PCA of cuproptosis-related lncRNAs. **(G)** PCA of predictors. PCA, principal component analysis; LASSO, least absolute shrinkage and selection operator. Red represents the high-risk group, and blue represents the low-risk group.

3.5 The difference in survival probability between high-risk and low-risk groups

All samples were calculated using the RS (Supplementary Tables S2, S3), which is the linear prediction based on the model, and the RS median of the training set was 0.822. The samples with an RS higher than 0.822 were classified as a high-risk group, and the rest samples were classified as a low-risk group. In addition, after sorting the validation set according to the RS (Figure 5A), it was found that the number of recurrences in the high-risk group was significantly higher than that in the low-risk group (Figure 5B). The KM survival curve (Figure 5C) indicated that the survival probability of the high-risk group was significantly lower than that of the low-risk group at the same time. The Logrank test suggested that there was a statistical difference ($p < 0.001$) in the distribution of survival time between the two groups. The nomogram intuitively revealed the predicted survival probability of samples in 1 year, 3 years, and 5 years (Figure 5D), as well as identified protective factors (*LINC02754*, *LINC02043*, *LINC02510*, and *DLEU1*) and risk factors (stage, *RNF185-AS1*, and *LINC02067*).

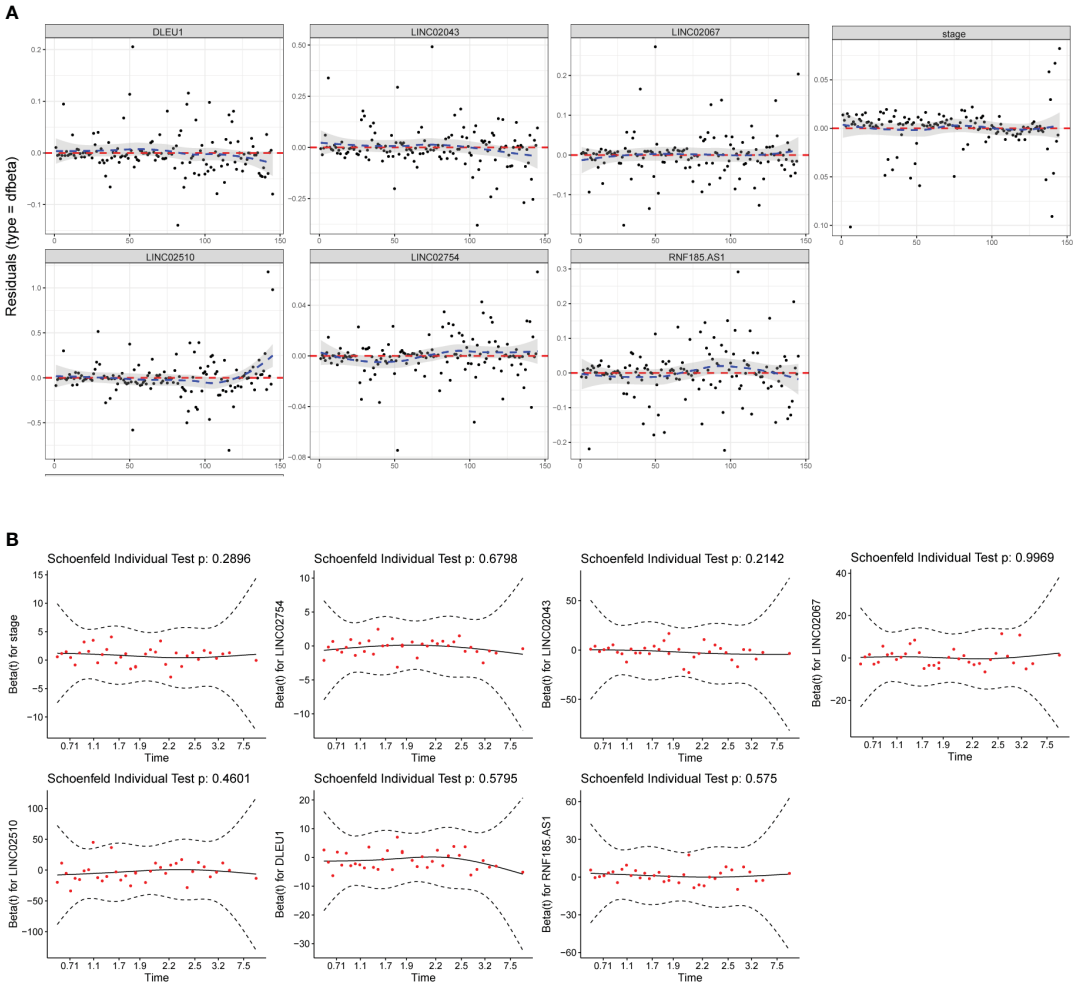

FIGURE 3
Model test and stability evaluation. **(A)** The influential point test is used to detect whether there are abnormal points with a strong influence on the model. The standardized residual for influential points is greater than 3. **(B)** The Schoenfeld individual test is to check whether predictor coefficients change over time. When $p > 0.05$, the proportional risk assumption of Cox regression is not rejected.

3.6 The differential expression of angiogenesis genes between high-risk and low-risk groups accompanied by different composition of immune cells

The CIBERSORT analysis (Figure 6A) revealed significant differences in the composition of memory B cells ($p = 0.027$) and $CD8^+$ T lymphocytes ($p = 0.01$) between the high-risk and low-risk groups. The proportion and the correlation of immune cells are also displayed in Supplementary Figure S4. Enrichment analysis (Figures 6C, D) showed that the cuproptosis-related genes refer to mitochondrial matrix processes such as acyltransferase activity, tricarboxylic acid cycle, acetyl–CoA metabolic process, acetyl–CoA biosynthetic process, pyruvate metabolism, mineral absorption, amino acid metabolism, carbon metabolism, and platinum resistance in cancer, which are not directly related to angiogenesis. However, GSEA demonstrated that the high-risk group defined by cuproptosis-related lncRNAs is significantly upregulated (enrichment score (ES) = 0.551, normalized enrichment score (NES) = 1.933, p-value <0.001) in the angiogenesis gene set (Figure 6B), suggesting the potential correlation between cuproptosis and angiogenesis.

3.7 Enrichment analysis of angiogenesis and cuproptosis in colorectal cancer cell lines and the expression of predictors *in vitro* validation

CCLE recruited 56 primary cell lines and 20 metastatic cell lines. GSEA based on normalized expression profile (Supplementary Table S4) demonstrated that, relative to primary cell lines, metastatic cell lines were downregulated (ES = −0.471, NES = −1.510, p-value = 0.019) in cuproptosis gene set and upregulated (ES = 0.332, NES = 1.727,

10.3389/fonc.2023.1322421

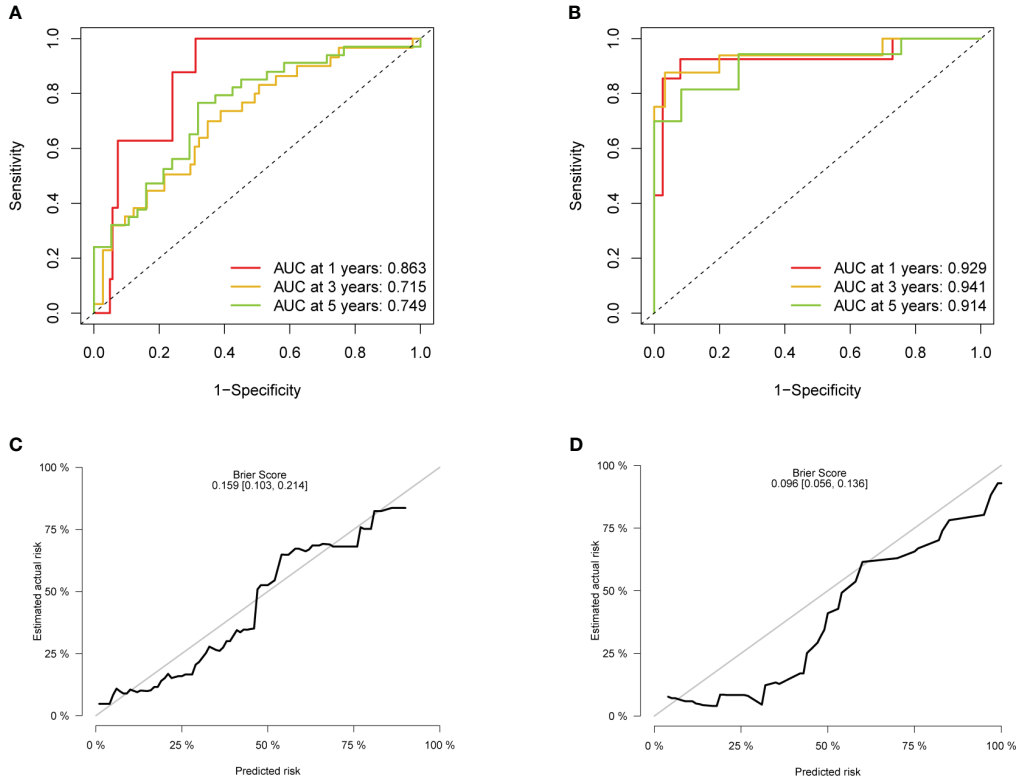

FIGURE 4
Evaluation of the accuracy. **(A)** ROC of the model in the training set. **(B)** ROC in the validation set. **(C)** Calibration plot in the training set. **(D)** Calibration plot in the validation set. ROC, receiver operating characteristic.

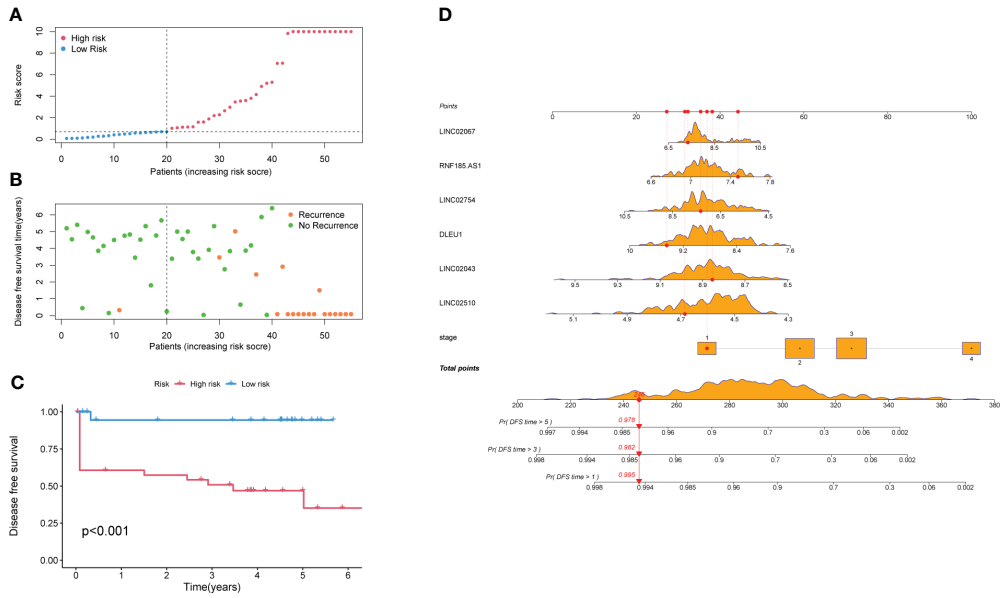

FIGURE 5
Survival analysis of high-risk and low-risk groups. **(A)** All samples are arranged by Risk Score. **(B)** Scatter plot of samples and their recurrence event. **(C)** KM survival curve. **(D)** Nomogram of the prediction model. The values of the seven predictors correspond to different scores, and the total score corresponds to the probability of DFS in 1, 3, and 5 years. The orange density plots show the distribution of training set data. The red lines represent the scores of predictors, total score, and corresponding survival probability, for the sample as an example. KM, Kaplan–Meier; DFS, disease-free survival.

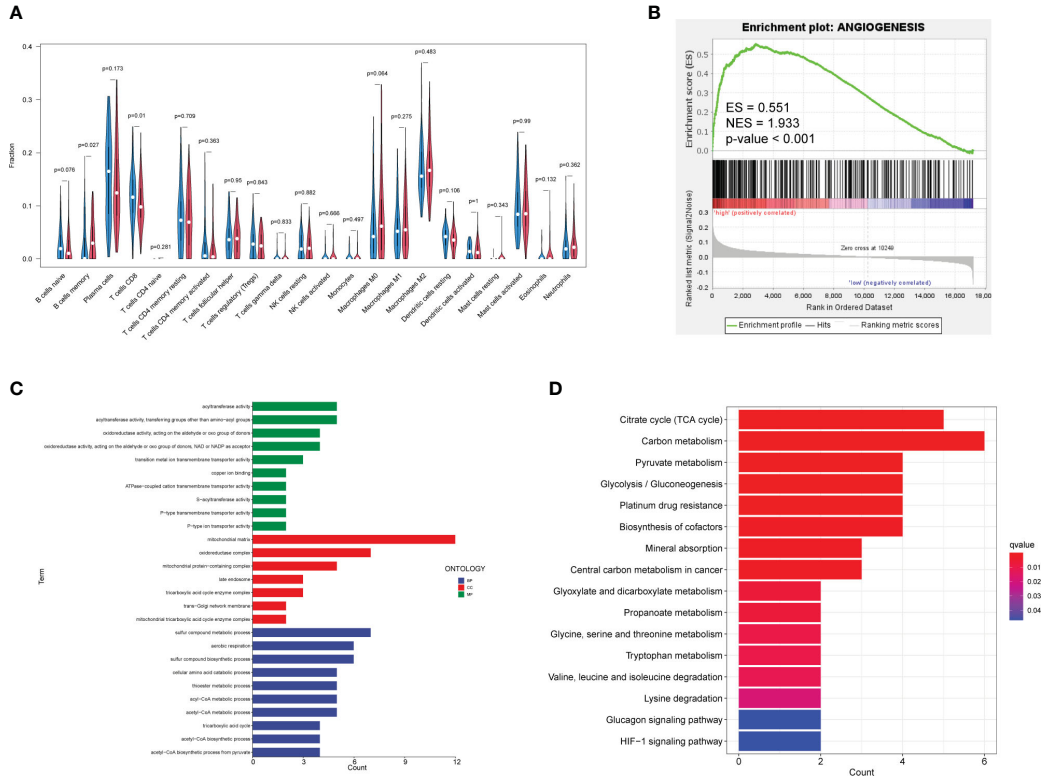

FIGURE 6
Relationship among immune infiltration, angiogenesis, and cuproptosis. **(A)** Violin plots demonstrate the difference in immune cells between high-risk and low-risk groups. Red represents the high-risk group, and blue represents the low-risk group. Nominal p-values are shown in the plot. **(B)** GSEA of two groups in the angiogenesis gene set. **(C)** GO enrichment analysis. Blue, red, and green represent the enrichment analysis of BP, MF, and CC respectively. **(D)** KEGG enrichment analysis. Red indicates significant enrichment. GO, Gene Ontology; BP, biological process; MF, molecular function; CC, cell component; KEGG, Kyoto Encyclopedia of Genes and Genomes; GSEA, Gene Set Enrichment Analysis.

p-value <0.001) in angiogenesis gene set (Figures 7A, B). Violin plots exhibit expression of cuproptosis–mRNAs in different cell lines (Supplementary Figure S5). We cultured CaCo-2, primary colon carcinoma cell, and SW620, metastatic cell, and detected the expression of angiogenesis-related mRNAs and cuproptosis-related lncRNAs in the model by qPCR. It was found that the expression of angiogenesis-related mRNAs in SW620 upregulated significantly, while the expression of protective lncRNAs decreased significantly (Figures 7C, D).

4 Discussion

The prediction of tumor recurrence risk is of great significance for guiding prognosis and clinical decision-making of adjuvant therapy. At present, there are three scoring systems based on clinical data and pathological features: Memorial Sloan Kettering Cancer Center (MSKCC) score, ACCENT score, and Numeracy. The predictors include sex, age, carcinoembryonic antigen (CEA), histopathological grade, vascular invasion or lymphatic invasion, lymph node involvement, and adjuvant therapy. However, the prediction accuracy of the scoring systems was relatively low, with a c-index of no more than 0.7 (30, 31). MSKCC score (32) is a linear regression model (c-index = 0.68), which does not take time as a dependent variable, and can only be applied to stage II and stage III. Although Numeracy is a Cox regression model, the accuracy was insufficient (c-index = 0.65) in that it only included three predictors. ACCENT score (33), as a Cox regression model, does not use molecular markers as predictors, so its accuracy was insufficient, and it was only applicable to stage III patients.

However, the prediction model using a single biomarker is also quite defective. CEA, a carcinoembryonic antigen produced by gastrointestinal epithelial tumor cells, has been used as a tumor marker for colon cancer for more than 40 years. As a blood biomarker, CEA is an inexpensive, safe, and non-invasive measure for patients with colon cancer. However, CEA may be elevated for many reasons, including malignant and benign diseases, as well as smoking. Taken together, it is not an effective predictor of early clinical recurrence with a sensitivity of 0.5–0.8.

In this study, the prediction model based on biomarkers and clinical data innovatively integrated the two dimensions. Considering the stability of the Cox model, the recommended minimum events-per-variable (EPV) is 5–15 (34). Since the number of positive events in the training set was 36, the amounts

10.3389/fonc.2023.1322421

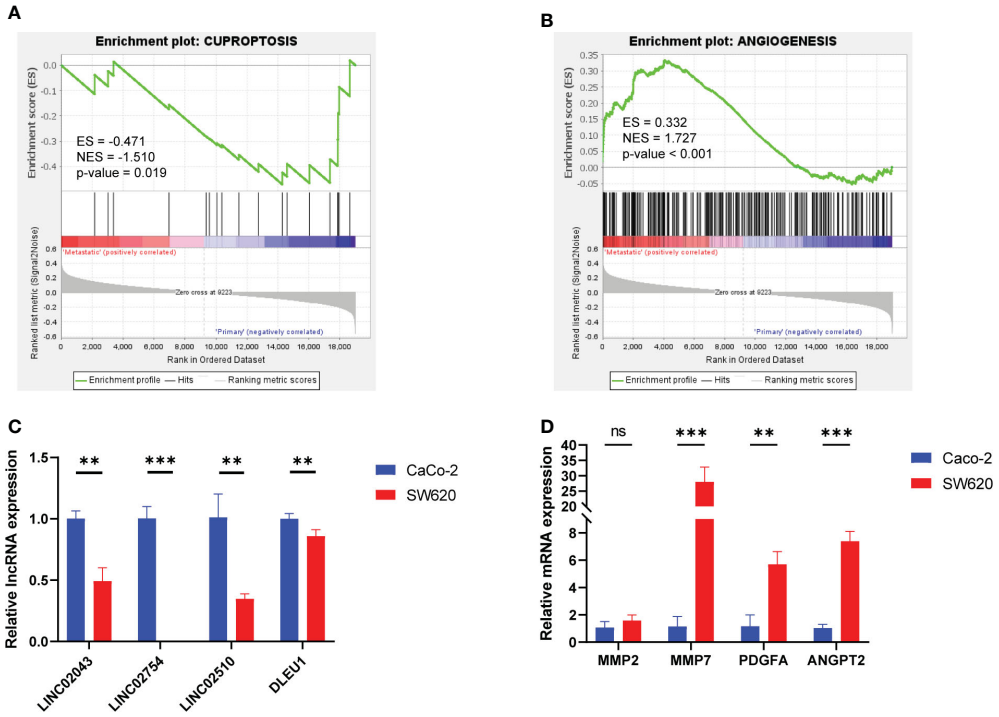

FIGURE 7
GSEA focusing on cuproptosis and angiogenesis of colorectal cancer cell lines and relative RNA expression of Caco-2 and SW620 detected by qPCR. **(A)** GSEA in the cuproptosis gene set. **(B)** GSEA in the angiogenesis gene set. **(C)** Angiogenesis–mRNA expression. **(D)** Cuproptosis–lncRNA expression. ns, $p \geq 0.05$; $^{**}p < 0.01$; $^{***}p < 0.001$. GSEA, Gene Set Enrichment Analysis.

of variables should be no more than 7.2. The pre-screening of potential variables by LASSO regression decreases the problem that the stepwise regression is less effective in the data with large variables. Compared with linear regression and logistic regression, Cox regression takes time as a dependent variable, which can predict the recurrence risk of samples at any time (35, 36). The AUC in the training set was higher than 0.7, the AUC in the validation set was higher than 0.9, and the calibration curve did not deviate from the ideal curve, which indicated a high accuracy of the model.

$CD8^+$ T cells have the ability to detect and eradicate cancer cells. As shown in Figure 6A, there was a statistical difference in the proportion of $CD8^+$ T cells between high- and low-risk groups, but the mean difference was small (approximately 1.56%). Compared with the difference between tumor and adjacent tissue, the difference in $CD8^+$ T cells between high- and low-risk groups was relatively minor. However, risk stratification based on cuproptosis-related lncRNAs suggested a potential interaction between cuproptosis and the immune microenvironment, which also presents a prospect for prognosis prediction. Since the proportion of immune cells was calculated from the expression profile in this study, we could not use the immune infiltration as a predictor in reverse. We believe that the value of immune infiltration for prognosis is the detection of the various subtypes of $CD8^+$ T cells by flow cytometry. In contrast, memory B cells were lower in the low-risk group. More and more evidence indicates that there is no inherent inhibitory effect on infiltrating B cells in tumors, and the induced regulatory B cells derived from the exposure to the tumor microenvironment, which plays an important role in inhibiting anti-tumor response and promoting tumor progress by weakening cytotoxic T lymphocytes and NK cells (37).

Relevant research indicates that *DLEU1*, as a protective predictor, is a candidate gene of tumor suppressor involved in B-cell chronic lymphocytic leukemia (38). *RNF185-AS1*, in contrast, has the effect of promoting proliferation and migration in thyroid carcinoma and liver cancer (39, 40). The effect of the two predictors in tumor progression confirmed their influence on the prediction of survival probability. As shown in Figure 5D, the higher the expression of *DLEU1*, the higher the survival probability, while the higher the expression of *RNF185-AS1*, the lower the survival probability. Similarly, although there is currently a lack of relevant research on other lncRNAs, we can speculate that *LINC02067* has the function of promoting tumor progression, while *LINC02754*, *LINC02043*, and *LINC02510* have the function of inhibiting tumor progression. This study is based on the widely recognized angiogenesis and new concepts of cuproptosis aiming to develop a more accurate prediction to evaluate the prognosis and recurrence of CRC patients.

However, microarray data derived from two different datasets must undergo unified normalization for comprehensive analysis, which increases the complexity of the study, and large-scale transcriptome sequencing studies should be carried out in the future to construct more adaptive models.

5 Conclusion

In this study, a prediction model for postoperative recurrence of CRC cancer was established, which combines clinical data and molecular markers with high prediction accuracy.

Data availability statement

The datasets presented in this study can be found in online repositories. The names of the repository/repositories and accession number(s) can be found below: https://www.ncbi.nlm.nih.gov/geo/, GSE17536 https://www.ncbi.nlm.nih.gov/geo/, GSE17537.

Author contributions

HL: Conceptualization, Data curation, Formal analysis, Investigation, Methodology, Resources, Software, Validation, Visualization, Writing – original draft. YZ: Data curation, Formal analysis, Funding acquisition, Investigation, Methodology, Resources, Software, Supervision, Validation, Writing – original draft. YF: Resources, Software, Writing – review & editing. XH: Supervision, Writing – review & editing. LB: Supervision, Writing – review & editing. HZ: Funding acquisition, Project administration, Supervision, Validation, Writing – review & editing. YW: Conceptualization, Funding acquisition, Project administration, Resources, Supervision, Validation, Writing – review & editing.

Funding

The author(s) declare financial support was received for the research, authorship, and/or publication of this article. This work was supported by the National Natural Science Foundation of China (82122075, 82074232, 82030118, 81830120), Shanghai Frontier Research Base of Disease and Syndrome Biology of Inflammatory Cancer Trans-formation (2021KJ03-12), "Shu Guang" project supported by Shanghai Municipal Education Commission and Shanghai Education Development Foundation (21SG43), Three-year Plan Project of Shanghai Traditional Chinese Medicine (ZY (2021-2023)-0208) and Shanghai Youth Talent Support Program.

Conflict of interest

The authors declare that the research was conducted in the absence of any commercial or financial relationships that could be construed as a potential conflict of interest.

Publisher's note

Supplementary material

The Supplementary Material for this article can be found online at: https://www.frontiersin.org/articles/10.3389/fonc.2023.1322421/full#supplementary-material

SUPPLEMENTARY FIGURE 1
Raw data of microarray. **(A)** The original gray scale of microarray. **(B)** MA-plot. Ideally, the scatter points in the plot are along the M = 0 axis. There may be problems with the microarray with a large IQR. IQR, interquartile range. **(C)** Histogram of signal intensity of probes. **(D)** Boxplot of the unnormalized expression profile of samples.

SUPPLEMENTARY FIGURE 2
PCA-related Scree plots demonstrate the contribution rate of principal components. **(A)** Scree plot of all genes. **(B)** Scree plot of cuproptosis-related mRNAs. **(C)** Scree plot of cuproptosis-related lncRNAs. **(D)** Scree plot of predictors. PCA, principal component analysis.

SUPPLEMENTARY FIGURE 3
Evaluation of the accuracy when there is only one predictor, stage. **(A)** ROC of the stage in the training set. **(B)** ROC in the validation set. **(C)** Calibration plot in the training set. **(D)** Calibration plot in the validation set. ROC, receiver operating characteristic.

SUPPLEMENTARY FIGURE 4
Immune infiltration by CIBERSORT. **(A)** Barplot indicates the proportion of different immune cells in each sample. **(B)** Correlation heatmap of 22 kinds of immune cells.

SUPPLEMENTARY FIGURE 5
Expression of cuproptosis-related mRNAs in colorectal cancer cell lines.

References

1. Sung H, Ferlay J, Siegel RL, Laversanne M, Soerjomataram I, Jemal A, et al. Global cancer statistics 2020: globocan estimates of incidence and mortality worldwide for 36 cancers in 185 countries. *CA Cancer J Clin* (2021) 71(3):209–49. doi: 10.3322/caac.21660

2. Hiller JG, Perry NJ, Poulogiannis G, Riedel B, Sloan EK. Perioperative events influence cancer recurrence risk after surgery. *Nat Rev Clin Oncol* (2018) 15(4):205–18. doi: 10.1038/nrclinonc.2017.194

3. Battaglin F, Puccini A, Intini R, Schirripa M, Ferro A, Bergamo F, et al. The role of tumor angiogenesis as a therapeutic target in colorectal cancer. *Expert Rev Anticancer Ther* (2018) 18(3):251–66. doi: 10.1080/14737140.2018.1428092

4. Senger DR, Davis GE. Angiogenesis. *Cold Spring Harb Perspect Biol* (2011) 3(8): a005090. doi: 10.1101/cshperspect.a005090

5. Raza A, Franklin MJ, Dudek AZ. Pericytes and vessel maturation during tumor angiogenesis and metastasis. *Am J Hematol* (2010) 85(8):593–8. doi: 10.1002/ajh.21745

6. Sakurai T, Kudo M. Signaling pathways governing tumor angiogenesis. *Oncology* (2011) 81 Suppl 1:24–9. doi: 10.1159/000333256

7. Tsvetkov P, Coy S, Petrova B, Dreishpoon M, Verma A, Abdusamad M, et al. Copper induces cell death by targeting lipoylated tca cycle proteins. *Sci (New York NY)* (2022) 375(6586):1254–61. doi: 10.1126/science.abf0529

8. Wang Y, Zhang L, Zhou F. Cuproptosis: A new form of programmed cell death. *Cell Mol Immunol* (2022) 19(8):867–8. doi: 10.1038/s41423-022-00866-1

9. Wang Z, Jin D, Zhou S, Dong N, Ji Y, An P, et al. Regulatory roles of copper metabolism and cuproptosis in human cancers. *Front Oncol* (2023) 13:1123420. doi: 10.3389/fonc.2023.1123420

10. Finney L, Vogt S, Fukai T, Glesne D. Copper and angiogenesis: unravelling a relationship key to cancer progression. *Clin Exp Pharmacol Physiol* (2009) 36(1):88–94. doi: 10.1111/j.1440-1681.2008.04969.x

11. Tisato F, Marzano C, Porchia M, Pellei M, Santini C. Copper in diseases and treatments, and copper-based anticancer strategies. *Med Res Rev* (2010) 30(4):708–49. doi: 10.1002/med.20174

12. Shi X, Chen Z, Wang Y, Guo Z, Wang X. Hypotoxic copper complexes with potent anti-metastatic and anti-angiogenic activities against cancer cells. *Dalton Trans* (2018) 47(14):5049–54. doi: 10.1039/c8dt00794b

13. Chen D, Li B, Lei T, Na D, Nie M, Yang Y, et al. Selective mediation of ovarian cancer skov3 cells death by pristine carbon quantum dots/cu(2)O composite through targeting matrix metalloproteinases, angiogenic cytokines and cytoskeleton. *J Nanobiotechnology* (2021) 19(1):68. doi: 10.1186/s12951-021-00813-8

14. Khoshdel Z, Naghibalhossaini F, Abdollahi K, Shojaei S, Moradi M, Malekzadeh M. Serum copper and zinc levels among Iranian colorectal cancer patients. *Biol Trace Elem Res* (2016) 170(2):294–9. doi: 10.1007/s12011-015-0483-4

15. André T, de Gramont A, Vernerey D, Chibaudel B, Bonnetain F, Tijeras-Raballand A, et al. Adjuvant fluorouracil, leucovorin, and oxaliplatin in stage ii to iii colon cancer: updated 10-year survival and outcomes according to braf mutation and mismatch repair status of the mosaic study. *J Clin Oncol* (2015) 33(35):4176–87. doi: 10.1200/jco.2015.63.4238

16. Taieb J, Le Malicot K, Shi Q, Penault-Llorca F, Bouché O, Tabernero J, et al. Prognostic Value of Braf and kras mutations in Msi and Mss Stage Iii Colon Cancer. *J Natl Cancer Inst* (2017) 109(5):djw272. doi: 10.1093/jnci/djw272

17. Galon J, Mlecnik B, Bindea G, Angell HK, Berger A, Lagorce C, et al. Towards the introduction of the 'Immunoscore' in the classification of Malignant tumours. *J Pathol* (2014) 232(2):199–209. doi: 10.1002/path.4287

18. Gong C, Maquat LE. Lncrnas transactivate stau1-mediated mrna decay by duplexing with 3' Utrs via alu elements. *Nature* (2011) 470(7333):284–8. doi: 10.1038/nature09701

19. Castello A, Fischer B, Frese CK, Horos R, Alleaume AM, Foehr S, et al. Comprehensive identification of rna-binding domains in human cells. *Mol Cell* (2016) 63(4):696–710. doi: 10.1016/j.molcel.2016.06.029

20. Lin A, Hu Q, Li C, Xing Z, Ma G, Wang C, et al. The Link-a Lncrna Interacts with Ptdins(3,4,5)P(3) To hyperactivate Akt and Confer Resistance to Akt inhibitors. *Nat Cell Biol* (2017) 19(3):238–51. doi: 10.1038/ncb3473

21. Galamb O, Barták BK, Kalmár A, Nagy ZB, Szigeti KA, Tulassay Z, et al. Diagnostic and prognostic potential of tissue and circulating long non-coding rnas in colorectal tumors. *World J Gastroenterol* (2019) 25(34):5026–48. doi: 10.3748/wjg.v25.i34.5026

22. Barrett T, Wilhite SE, Ledoux P, Evangelista C, Kim IF, Tomashevsky M, et al. Ncbi geo: archive for functional genomics data sets–update. *Nucleic Acids Res* (2013) 41 (Database issue):D991–5. doi: 10.1093/nar/gks1193

23. Kauffmann A, Gentleman R, Huber W. Arrayqualitymetrics–a bioconductor package for quality assessment of microarray data. *Bioinformatics* (2009) 25(3):415–6. doi: 10.1093/bioinformatics/btn647

24. Gautier L, Cope L, Bolstad BM, Irizarry RA. Affy–analysis of affymetrix genechip data at the probe level. *Bioinformatics* (2004) 20(3):307–15. doi: 10.1093/bioinformatics/btg405

25. Kent WJ, Sugnet CW, Furey TS, Roskin KM, Pringle TH, Zahler AM, et al. The human genome browser at ucsc. *Genome Res* (2002) 12(6):996–1006. doi: 10.1101/gr.229102

26. Friedman J, Hastie T, Tibshirani R. Regularization paths for generalized linear models via coordinate descent. *J Stat Softw* (2010) 33(1):1–22. doi: 10.18637/jss.v033.i01

27. Wang S, Liu Y, Yao Z, Ma L, Sun D. A Commentary on "Construction of a Nomogram to Predict Overall Survival for Patients with M1 Stage of Colorectal Cancer: A Retrospective Cohort Study" (Int J Surg 2019; Epub ahead of print). *Int J Surg* (2022) 106:106914. doi: 10.1016/j.ijsu.2022.106914

28. Newman AM, Steen CB, Liu CL, Gentles AJ, Chaudhuri AA, Scherer F, et al. Determining cell type abundance and expression from bulk tissues with digital cytometry. *Nat Biotechnol* (2019) 37(7):773–82. doi: 10.1038/s41587-019-0114-2

29. Stelzer G, Rosen N, Plaschkes I, Zimmerman S, Twik M, Fishilevich S, et al. The genecards suite: from gene data mining to disease genome sequence analyses. *Curr Protoc Bioinf* (2016) 54:1.30.1–1.3. doi: 10.1002/cpbi.5

30. Renfro LA, Grothey A, Xue Y, Saltz LB, André T, Twelves C, et al. Accent-based web calculators to predict recurrence and overall survival in stage iii colon cancer. *J Natl Cancer Inst* (2014) 106(12):dju333. doi: 10.1093/jnci/dju333

31. Weiser MR, Gönen M, Chou JF, Kattan MW, Schrag D. Predicting survival after curative colectomy for cancer: individualizing colon cancer staging. *J Clin Oncol* (2011) 29(36):4796–802. doi: 10.1200/jco.2011.36.5080

32. Mskcc launches center for molecular oncology. *Cancer Discovery* (2014) 4 (8):860–1. doi: 10.1158/2159-8290.Cd-nb2014-094

33. Jin Z, Dixon JG, Fiskum JM, Parekh HD, Sinicrope FA, Yothers G, et al. Clinicopathological and molecular characteristics of early-onset stage iii colon adenocarcinoma: an analysis of the accent database. *J Natl Cancer Inst* (2021) 113 (12):1693–704. doi: 10.1093/jnci/djab123

34. Heinze G, Dunkler D. Five myths about variable selection. *Transpl Int* (2017) 30 (1):6–10. doi: 10.1111/tri.12895

35. Feng A, He L, Chen T, Xu M. A novel cuproptosis-related lncrna nomogram to improve the prognosis prediction of gastric cancer. *Front Oncol* (2022) 12:957966. doi: 10.3389/fonc.2022.957966

36. Zhu Z, Zhao Q, Song W, Weng J, Li S, Guo T, et al. A novel cuproptosis-related molecular pattern and its tumor microenvironment characterization in colorectal cancer. *Front Immunol* (2022) 13:940774. doi: 10.3389/fimmu.2022.940774

37. Menon M, Hussell T, Ali Shuwa H. Regulatory B cells in respiratory health and diseases. *Immunol Rev* (2021) 299(1):61–73. doi: 10.1111/imr.12941

38. Liu Y, Corcoran M, Rasool O, Ivanova G, Ibbotson R, Grandér D, et al. Cloning of two candidate tumor suppressor genes within a 10 kb region on chromosome 13q14, frequently deleted in chronic lymphocytic leukemia. *Oncogene* (1997) 15(20):2463–73. doi: 10.1038/sj.onc.1201643

39. Huang C, Li K, Huang R, Zhu J, Yang J. Rnf185-as1 promotes hepatocellular carcinoma progression through targeting mir-221-5p/integrin B5 axis. *Life Sci* (2021) 267:118928. doi: 10.1016/j.lfs.2020.118928

40. Liu D, Zhang M, Song Y, Yang N. Rnf185 antisense rna 1 (Rnf185-as1) promotes proliferation, migration, and invasion in papillary thyroid carcinoma. *Anticancer Drugs* (2022) 33(6):595–606. doi: 10.1097/cad.0000000000001295

frontiers | Frontiers in Oncology

TYPE Original Research
PUBLISHED 22 January 2024
DOI 10.3389/fonc.2024.1335670

OPEN ACCESS

EDITED BY
Zsolt Kovács,
George Emil Palade University of Medicine, Pharmacy, Sciences and Technology of Târgu Mureş, Romania

REVIEWED BY
Yu-gang Huang,
Hubei University of Medicine, China
Enrico Capobianco,
Jackson Laboratory, United States

*CORRESPONDENCE
Haibo Lu
luhaibo@hrbmu.edu.cn
Yan Zhang
zhangtyo@hit.edu.cn

†These authors contributed equally to this work

RECEIVED 09 November 2023
ACCEPTED 02 January 2024
PUBLISHED 22 January 2024

CITATION
Xu B, Lian J, Pang X, Gu Y, Zhu J, Zhang Y and Lu H (2024) Identification of colon cancer subtypes based on multi-omics data—construction of methylation markers for immunotherapy.
Front. Oncol. 14:1335670.
doi: 10.3389/fonc.2024.1335670

Identification of colon cancer subtypes based on multi-omics data—construction of methylation markers for immunotherapy

Benjie Xu[1†], Jie Lian[1†], Xiangyi Pang[1], Yue Gu[2], Jiahao Zhu[1], Yan Zhang[2,3*] and Haibo Lu[1*]

[1]Department of Outpatient Chemotherapy, Harbin Medical University Cancer Hospital, Harbin, China, [2]School of Life Science and Technology, Computational Biology Research Center, Harbin Institute of Technology, Harbin, China, [3]College of Pathology, Qiqihar Medical University, Qiqihar, China

Background: Being the most widely used biomarker for immunotherapy, the microsatellite status has limitations in identifying all patients who benefit in clinical practice. It is essential to identify additional biomarkers to guide immunotherapy. Aberrant DNA methylation is consistently associated with changes in the anti-tumor immune response, which can promote tumor progression. This study aims to explore immunotherapy biomarkers for colon cancers from the perspective of DNA methylation.

Methods: The related data (RNA sequencing data and DNA methylation data) were obtained from The Cancer Genome Atlas (TCGA) and UCSC XENA database. Methylation-driven genes (MDGs) were identified through the Pearson correlation analysis. Unsupervised consensus clustering was conducted using these MDGs to identify distinct clusters of colon cancers. Subsequently, we evaluated the immune status and predicted the efficacy of immunotherapy by tumor immune dysfunction and exclusion (Tide) score. Finally, The Quantitative Differentially Methylated Regions (QDMR) software was used to identify the specific DNA methylation markers within particular clusters.

Results: A total of 282 MDGs were identified by integrating the DNA methylation and RNA-seq data. Consensus clustering using the K-means algorithm revealed that the optimal number of clusters was 4. It was revealed that the composition of the tumor immune microenvironment (TIME) in Cluster 1 was significantly different from others, and it exhibited a higher level of tumor mutation burdens (TMB) and stronger anti-tumor immune activity. Furthermore, we identified three specific hypermethylation genes that defined Cluster 1 (PCDH20, APCDD1, COCH). Receiver operating characteristic (ROC) curves demonstrated that these specific markers could effectively distinguish Cluster 1 from other clusters, with an AUC of 0.947 (95% CI 0.903-0.990). Finally, we selected clinical samples for immunohistochemical validation.

Conclusion: In conclusion, through the analysis of DNA methylation, consensus clustering of colon cancer could effectively identify the cluster that benefit from immunotherapy along with specific methylation biomarkers.

KEYWORDS

colon cancer, DNA methylation, microsatellite status, immunotherapy, specific DNA methylation markers

1 Introduction

Colon cancer, being one of the prevalent malignancies of the digestive system, exhibits the second highest mortality rates globally and ranks third in terms of incidence. This medical challenge poses a significant threat to human health (1). Systemic therapy is the primary treatment for advanced colon cancers. Unfortunately, the five-year overall survival (OS) is currently estimated at only 30% (2). Immunotherapy significantly prolonged the survival of patients with deficiency of mismatch repair (dMMR) or microsatellite instability – high (MSI -H) (3–5). However, the detection rate of dMMR or MSI-H only accounts for 5%-10% in colon cancers (6, 7). Additionally, approximately 25% of detected patients do not benefit from immunotherapy (8). It is worth noting that some patients with microsatellite stability (MSS) also experienced prolonged OS after immunotherapy (9). In a word, microsatellite status had certain limitations as a criterion for predicting the effectiveness of immunotherapy. The current research priorities are focused on identifying additional biomarkers in order to expand the accessibility of immunotherapy.

DNA methylation is a crucial epigenetic modification that plays a substantial function in regulating gene expression (10, 11). DNA methylation is the process of adding a methyl group to the 5' positions of a cytosine and guanosine (CpG) with the participation of DNA methyltransferase (DNMT). CpGs are typically abundant in the promoter region of CpG islands. Hypermethylation of promoter region always leads to the silencing of tumor suppressor gene expression (12, 13) and DNA methylation plays a regulatory role in tumor antigen presentation and the release of immune factors (14–16). To summarize, aberrant DNA methylation, especially hypermethylation of promoter regions, is frequently associated with altered anti-tumor immune responses, leading to tumor progression.

Currently, diagnostic and prognostic related methylation markers have been identified in colon cancer (17). This study is the first to identify immunotherapy biomarkers for colon cancer from the perspective of methylation. Through the identification of methylation-driven genes (MDGs), performing cluster analysis and verified by clinical samples. We identify a specific cluster of colon cancer that could be benefit from immunotherapy. Furthermore, we discovered beneficial-cluster of specific DNA methylation markers that can be used as a valuable supplement to the microsatellite status.

2 Materials and methods

2.1 Data acquisition and processing

RNA sequencing (RNA-Seq) data, somatic mutation data, clinicopathological data (including microsatellite status) of colon cancers were downloaded from The Cancer Genome Atlas (TCGA) database (https://portal.gdc.cancer.gov). DNA methylation data (Illumina Human Methylation 450) were obtained from the UCSC XENA database (https://xena.ucsc.edu/). For each probe site, methylation levels ranged from 0 (fully unmethylated) to 1 (fully methylated). Firstly, the DNA methylation data was screened, eliminating probes that exhibited missing information in over 70 percent of the samples. Secondary, probes in the sex chromosome and single nucleotide polymorphisms were also excluded. Finally, the K-nearest neighbors (KNN) algorithm was utilized to impute the missing values, implemented through the (knn) imputation procedure. Since DNA methylation in the promoter region could regulate expression of genes, we specifically analyzed the CpGs in the promoter region. The promoter was defined as the upstream 2.5 kb to downstream 0.5kb region of the transcription start site. For the expression data, we focused on analyzing the protein-encoding mRNA.

2.2 Differential analysis and identification of DNA methylation-driven genes

Between tumor and normal tissues, RNA-Seq data was analyzed using the "Deseq2" package implemented in R to detect differentially expressed genes (DEGs). The criteria for DEGs were set at a threshold of $P< 0.05$ and $|\log2FC| > 1$ (18). On the other hand, methylation data was analyzed using the limma package to identify differentially methylated genes (DMGs), with a set of $P< 0.05$ (19). The overlapped portion of the DEGs and DMGs, representing differentially expressed genes with aberrantly methylation, which were visualized using a Venn diagram.

The DNA methylation and RNA-Seq data of differentially expressed genes with aberrantly methylation were integrated for correlation analysis using the Pearson coefficient. A threshold of Pearson coefficient< -0.3 and $P< 0.05$ was set to identify MDGs for further analysis. The scatter plot of MDGs was created using ggplot2 in R (20).

2.3 Analysis of function enrichment construction of the PPI network

The"clusterProfiler", "org.Hs.eg.db", and "enrichplot" R package were used to evaluate the most significantly enriched function and pathway. The Gene Ontology (GO) and Kyoto Encyclopedia of Genes and Genomes (KEGG) analysis considered results with $P< 0.05$ and $q< 1$ as the differentially enriched (21, 22). These results were visualized using the 'ggplot2' R package.

To construct the Protein-Protein interaction network (PPI), the MDGs were uploaded to the Interactive Gene/protein Retrieval Tool Database (STRING) (https://string-db.org/). The identification of key genes and major modules in the PPI network was performed using the Cytoscape software.

2.4 Consensus clustering analysis

Consensus clustering was performed (ConsensusClusterPlus R package) to identify clusters of colon cancer with distinct molecular features (23). The K-means algorithm and Euclidean distance were employed in clustering.

$$d = \sqrt{\sum_{k=1}^{N}(x_k - y_k)^2}$$

The optimal number of clusters (k) were tested from 2 to 9 in this study. The procedure of clustering was conducted over 1000 iterations, in which 80% of the data was sampled in each iteration. The selection criteria for determining the optimal k value included the cluster's internal consistency, low coefficient of variation, and stability of the area under the cumulative distribution function (CDF) curves. The optimal number of clusters was determined using Principal component analysis (PCA) in this study. The Cumulative Density Function (ECDF) was used to calculate the area between 0.1 and 0.9 of the X-axis, the k value corresponding to the minimum ECDF area was the optimal number of clusters. Subsequently, survival analysis was used to evaluate the prognosis. The statistical significance among the clusters was evaluated using the log-rank test, with $P< 0.05$ considered significant. The performance of classification was evaluated using the receiver operating characteristic (ROC) curves.

2.5 Evaluation of the immune status among different colon cancer clusters

Unsupervised consensus clustering was performed to identify distinct clusters of colon cancers. Subsequently, we evaluated the immune status of these clusters.

The stromal score and immune score were calculated using the ESTIMATE algorithm based on expression data, which represented the presence of stromal and immune cells. The sum of stromal and immune scores was used as the estimate score to evaluate tumor purity. This evaluation was performed using the R language 'estimate' package (24). Immune checkpoint inhibitors (ICIs) could guide the immunotherapy of colon cancers. This study statistically analyzed the expression of the most common ICIs (PD-1, PD-L1, PD-L2, CTLA4, LAG3) among different clusters. Additionally, we quantified the abundance of tumor-infiltrating immune cells (TIICs) using the CIBERSORT algorithm (25). This study analyzed the immune status of clusters to determine if there was statistical difference, with $P< 0.05$ considered significant.

The Cancer-Immunity Cycle, commonly referred to as the anti-cancer immune response, consists of seven steps. These steps begin with the release of cancer cell antigens and end with the killing of cancer cells (26). The website Tracking Tumor Immunophenotype (TIP) (http://biocc.hrbmu.edu.cn/TIP) specialized in the study of the Cancer-Immunity Cycle and had calculated the immune activity scores for each step through large sample analysis (27). In the present study, we collected immune activity scores of colon cancer samples from the TIP website to analyze the differences in clusters within the Cancer-Immunity Cycle.

In addition, the somatic mutation data of colon cancers were analyzed and visualized using the R language "maftools" package (28). We specifically accessed the mutation frequencies and the level of tumor mutation burdens (TMB) from different clusters. The statistical results were depicted through the boxplots, with $P< 0.05$ considered significant.

2.6 Prediction of immunotherapy by Tide score

Immune evasion, a key factor in tumor development, significantly contributed to the failure of immunotherapy. There are two mainly mechanisms in the process of immune evasion. Firstly, tumors characterized by a substantial infiltration of cytotoxic T lymphocytes (CTLs) exhibited the induction of T cell inactivation, leading to dysfunction of immune cells. Secondly, in tumors with diminished levels of CTLs, T cell infiltration was prevented and the ability of killing tumor cells was weakened (29, 30). Based on sequencing data, the Tumor Immune Dysfunction and Exclusion (TIDE) algorithm (http://tide.dfci.harvard.edu/) could reveal the characteristics of tumor immune evasion. By utilizing CTLs observed in tumor samples, the TIDE score can be calculated to predict the efficacy of immunotherapy. Specifically, In the case of melanoma, the TIDE score demonstrates greater predictive accuracy compared to biomarkers like PD-L1 (31). Consequently, the present study employed the TIDE score to predict the efficacy of immunotherapy within distinct clusters.

2.7 Identification of specific DNA methylation markers

In our study, we utilized Quantitative Differentially Methylated Regions (QDMR) software to identify the specific DNA methylation

CpGs within particular clusters of colon cancer. QDMR was an effective tool developed based on the Shannon entropy model, which allowed for the detection of DMRs across multiple DNA methylation profiles (32). The entropy difference reflected the influence of sample S on the overall methylation difference:

$$\Delta H_{r/s} = H_{Q/}\bar{S} - H_Q$$

When region r is specifically methylated in sample S, the value of $\triangle H_{r/S}$ is greater than 0. The categorical sample-specificity $CS_{r/S}$ can be defined as:

$$CS_{r/S} = \left\{ \begin{array}{l} \Delta H_{r/S} \times \text{sign}_{r,S}, \Delta H_{r,S} > 0 \\ 0, \Delta H_{r/S} \leq 0 \end{array} \right\}$$

Therefore, $CS_{r/S}$ can be utilized to analyze identify specific DNA methylation markers in samples. $CS_{r/S}$ greater than 0 indicates specifically hypermethylated, while a value less than 0 indicates specifically hypomethylated.

2.8 Immunohistochemistry

To investigate the prediction of immunotherapy response using specific markers, our study conducted a review of colon cancer patients in our center. We retrospectively collected their follow-up and treatment records, including postoperative recurrence, immunotherapy duration and cycles, and efficacy evaluation. These records successfully helped us to screen out the validation objects. The corresponding tumor paraffin sections were analyzed by immunochemistry. After roasting the sections at 60°C for 20 minutes, they were deparaffinized with xylene and rehydrated. The antigen was then recovered from the sections by heating the EDTA buffer (100°C for 15 minutes) and the endogenous peroxidase activity was inactivated using 3% H_2O_2 (10 minutes). The sections were treated with 5% BSA and incubated at room temperature for 1 hour. They were then incubated overnight at 4°C with primary antibodies (APCDD1, 1:20, Thermo, PA535063; PCDH20, 1:25, Thermo, PA598605). After washing the sections with PBS, secondary antibodies (1:500) were added to sections and incubated at room temperature for 1 hour. Finally, color development was achieved using the DAB kit (CWBIO-CW0125), and hematoxylin solution was used for counterstaining the paraffin sections. An open-source biological image analysis platform (Fiji/ImageJ) was utilized for analyzing the sections. The evaluation of immunohistochemical was based on both the staining intensity and the percentage scores. Staining intensity was graded on a scale of 0 (absent), 1 (weak), 2 (moderate), and 3 (marked), while the percentage scores was determined by the proportion of stained cells in a chosen field: 1 (0-25%), 2 (26-50%), 3 (51-75%), and 4 (76-100%). Each tumor sample was independently scored by two observers, and the results were reported as the mean score (ranging from 0 to 14).

2.9 Statistical analysis

The statistical analyses in this study were performed by R software (4.13 version) and GraphPad Prism 8 (GraphPad Software, La Jolla, CA, USA). The correlation between the two variables was assessed by the Pearson coefficient. For continuous data, the independent Student's t-test was conducted. Additionally, the chi-square test was applied to analyze categorical data. To compare non-normally distributed variables across clusters, we utilized the Wilcoxon test. The Kruskal–Wallis test was used for multiple groups. Statistical significance was determined based on a two-tailed P-value of less than 0.05 and we also reported the hazard ratios (HRs) and 95% confidence intervals (CIs).

3 Results

3.1 DNA methylation-driven genes

The flow diagram and analytic procedure are shown in Figure 1. The data of colon cancers were downloaded from the relevant database. A total of 301 samples had both DNA methylation and RNA-seq data (282 tumor and 19 normal). For RNA-seq data, we selected mRNA (19,938 genes) for differential analysis, detecting a total of 4830 DEGs at last. The expression of DEGs between colon cancers and normal samples was showed in the heatmap (Figure 2A). In the case of DNA methylation data, we selected CpGs (164,610 sites) and corresponding genes (18,510 genes) in the promoter region for difference analysis. If multiple CpGs correspond to the same gene, the mean value of β was selected to represent the methylation level of that gene. Similarly, a total of 8547 DMGs were detected. The heatmap showed the methylation of DMGs between colon cancers and normal samples (Figure 2B). Subsequently, 2217 differentially expressed genes with aberrantly methylation were identified by overlapping DEGs and DMGs (Figure 2C, Table S1).

We conducted correlation analysis by integrating the DNA methylation and RNA-seq data of 2217 differentially expressed genes with aberrantly methylation in colon cancers. The Pearson coefficient was utilized to access the correlation. Finally, we identified 282 MDGs for further analysis based on a Pearson coefficient< -0.3 and P< 0.05 (Table S2).

3.2 Function enrichment and PPI network construction

We conducted GO and KEGG analyses on 282 MDGs to analyze their potential functions and pathways. The results of GO analysis were significantly enriched in fibroblast growth factor receptor binding, digestive system process, etc(P<0.05, Figure 2D). Additionally, KEGG pathways analysis revealed significant enrichment in virus infection (Herpes simplex virus 1, Staphylococcus aureus), intestinal immune network for IgA production, etc(P<0.05, Figure 2E).

A PPI network was conducted to illustrate the interactions and connections of 282 MDGs in colon cancers. The degree algorithm was employed to determine the significance of different genes in the PPI network, while the size and color of nodes were utilized for visualization. Among these genes, IL-10 and FGF2, as core genes, playing a crucial role in the interconnection network (Figure 2F). By employing the MCODE plugin in Cytoscape, we identified key sub-

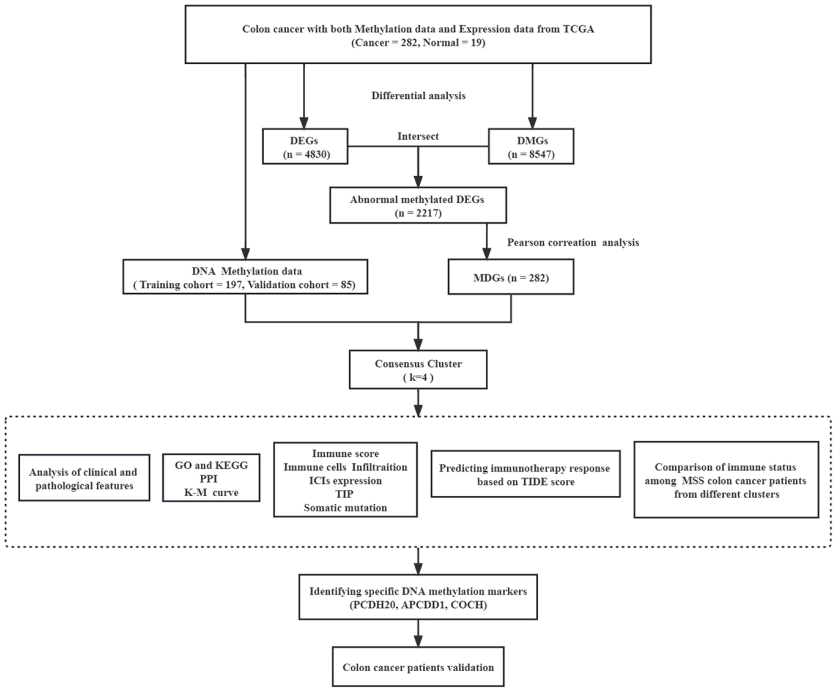

FIGURE 1
Flow diagram and analytic procedure of our study.

networks within the PPI network, which included genes such as IL-10, CD3E, MET, and others that were associated with anti-tumor immune response (Figure 2G).

Overall, our findings indicated that strong interconnections among the 282 MDGs in colon cancers, with IL-10 and FGF2 acting as core genes that are closely linked to tumor angiogenesis and anti-tumor immune response.

3.3 Consensus clustering in colon cancers

In this study, we performed consensus clustering based on the β values of the 282 MDGs to identify distinct DNA methylation molecular clusters of colon cancers. Subsequently, 282 samples were randomly divided into training (n = 197) and validation cohorts (n = 85) in a 7:3 proportion. The Chi-square test indicated that the

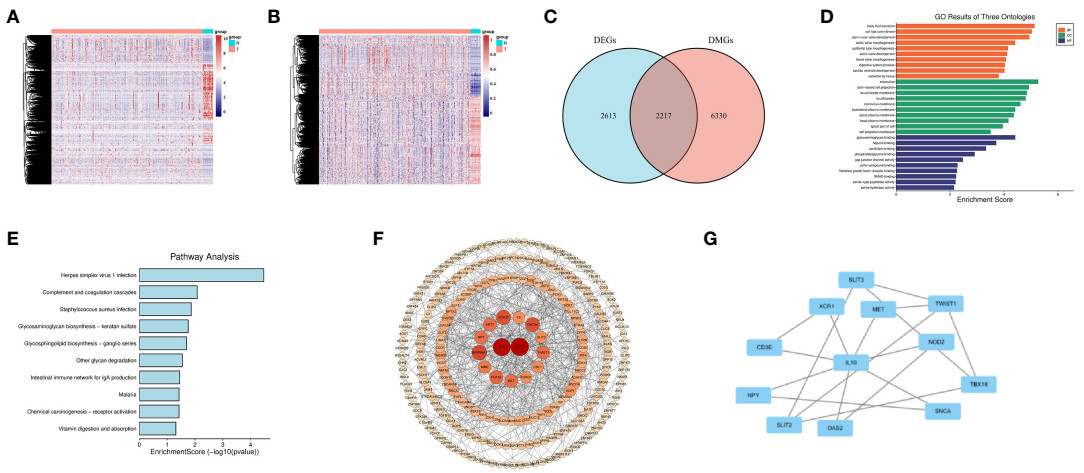

FIGURE 2
Screening for DNA Methylation-Driven Genes (MDGs). **(A)** Heatmap of Differentially Expressed Genes (DEGs) in normal samples and colon cancer samples. **(B)** Heatmap of Differentially Methylated Genes (DMGs) in normal samples and colon cancer samples. **(C)** Venn diagram for overlapping of DEGs and DMGs. **(D)** Gene Ontology (GO) enrichment results of three ontologies (including biological processes, cellular components, and molecular functions) of MDGs. **(E)** Kyoto Encyclopedia of Genes and Genomes (KEGG) enrichment analysis of MDGs. **(F, G)** Protein-Protein Interaction (PPI) network of MDGs.

clinicopathologic features of the training and validation cohorts were evenly distributed (Table S3).

The K-means algorithm was utilized for consensus clustering. According to the relative alteration observed under the CDF curve, the PCA method was finally employed to ascertain the optimal number (Figures 3A, B, Figure S1A, B). It was found that K = 4 was the optimal clustering with best stability (Figure 3C, Figure S1C). Which were termed Cluster 1 (44 patients, 22.4%), Cluster 2 (70 patients, 35.5%), Cluster 3 (52 patients, 26.4%) and Cluster 4 (31 patients, 15.7%), respectively. The K-M survival analysis revealed significant difference among the four clusters (P<0.05, Figure 3D, Figure S1D). The heatmaps displayed the significant differences among the clusters in terms of gene expression and methylation levels for 282 MDGs (Figures 3E, F). Moreover, both the training cohort and the validation cohort exhibited excellent performance in discriminating the clusters of colon cancer using the MDGs, with an AUC of 0.984 (95%CI 0.970-0.999) and 0.990 (95%CI 0.976-1.000), respectively (Figures 3G, H). The chi-square test revealed significant differences in clinicopathological characteristics among these clusters. Patients in Cluster 1 were found to be associated with age (P<0.001) and microsatellite status (P<0.001). The remaining clinicopathological characteristics showed no distribution differences among clusters (Table S4). Similar distribution was found in the validation cohort (Table S5).

3.4 Distinct immune status among colon cancer clusters

Through a series of analyses, significant differences in the immune status of different clusters were revealed. First, the composition of tumor immune microenvironment (TIME) was analyzed. Significant differences were observed in the immune score, stromal score, and tumor purity among clusters of colon cancer (P<0.001, Figures 4A, B, Figure S1E, F). Cluster 1 exhibited with a relative higher immune score and lower tumor purity, indicating a greater infiltration of immune cells. Subsequently, the expression levels of several common ICIs (PD1, PDL1, PDL2, CTLA4, LAG3) were compared among clusters. The findings illustrated that the ICIs expression in cluster 1 exhibited a significantly greater level compared to cluster 2 and 3 (P<0.001, Figure 4C, Figure S1G). Finally, the CIBERSORT algorithm was employed to visualize the infiltration abundances of TIICs in colon cancers. In cluster 1, there was a significant abundance of CD8+T cells, activated natural killer cells and M1 macrophages, which were associated with anti-tumor immune response, compared to other clusters. The abundant of immunosuppression-related Tregs cells in cluster 1 was relative lower (P<0.05, Figure 4D, Figure S2A).

The immune activity scores of colon cancers were used to evaluate the Cancer-Immunity Cycle. The results showed significant differences in the procedure of Cancer-Immunity Cycle among the clusters. The mean scores of Step1 (release of specific cancer cell antigens), Step 3 (priming and activation) and Step 7 (killing cancer cells) were significantly higher in Cluster 1, compared to Cluster 2 and 3 (P<0.01, Figure 4E). Additionally, Step 4 (trafficking of immune cells to tumors), which played a major role in the Cancer-Immunity Cycle, showed a higher abundance of CD8+ T cells, macrophages, and natural killer cells in Cluster 1 (P<0.05, Figure 4F).

These results indicated that the composition of the TIME in Cluster 1 was significantly different from others, and it exhibited a higher level of immune infiltration and stronger anti-tumor immune activity.

3.5 Somatic mutation landscape of clusters

In previous research, the critical involvement of genetic mutations in the initiation and progression of colon cancers has

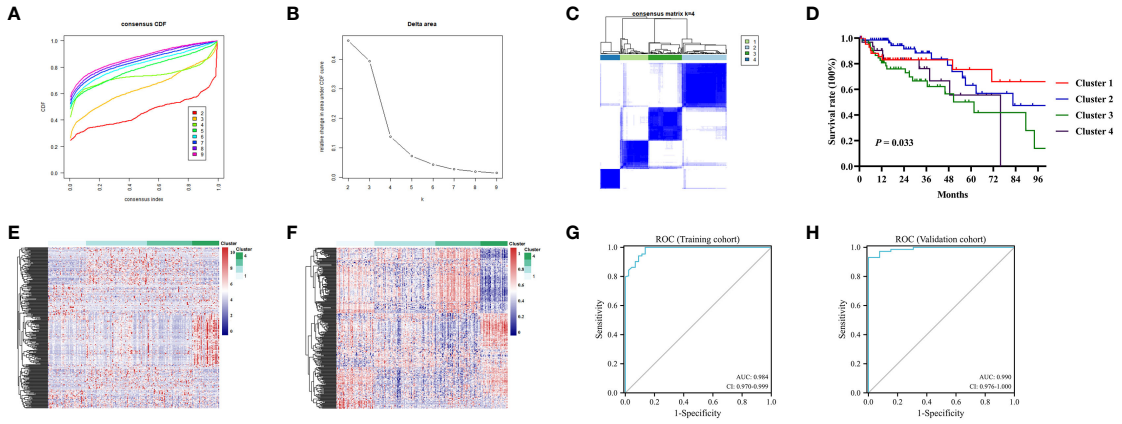

FIGURE 3
Consensus analysis for DNA methylation based on 282MDGs. **(A)** Consensus cumulative distribution function (CDF) of different clusters for colon cancer. **(B)** Delta area curve of consensus clustering. **(C)** Consensus clustering matrix for colon cancer at k = 4. **(D)** The survival curves in four DNA methylation clusters. **(E)** Heatmap of gene expression levels of 282 MDGs in the four clusters. **(F)** Heatmap of methylation levels of 282 MDGs in the four clusters. **(G)** Receiver operating characteristic (ROC)curves of the 282 MDGs in distinguishing four clusters in the train cohort. **(H)** ROC curves in the validation cohort.

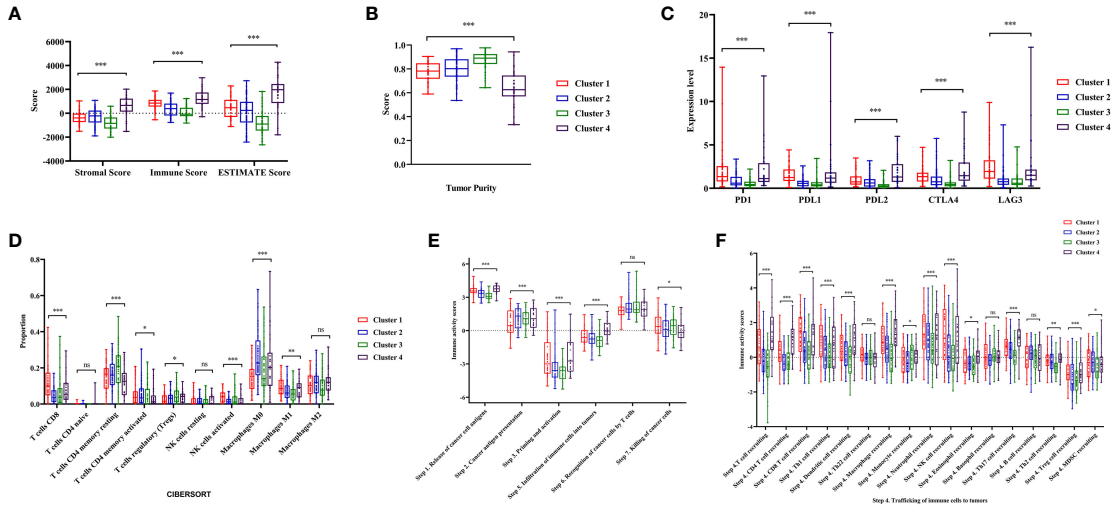

FIGURE 4
Analysis of tumor immune microenvironment and immune status during four clusters. **(A, B)** Comparisons of stromal score, immune score, ESTIMATE score and tumor purity during four clusters. **(C)**The expression level of immune checkpoints (PD1, PDL1, PDL2, CTLA4, LAG3) in the four clusters of colon cancer. **(D)** The abundance of immune cells in the four clusters of colon cancer patients evaluated by CIBERSORT algorithm. **(E, F)** Comparisons of the immune activity score from Tracking Tumor Immunophenotype (TIP) database in four clusters. 'ns' means $P > 0.05$, * means $P< 0.05$, ** means $P< 0.01$, *** means $P< 0.001$.

been investigated. Consequently, we conducted an analysis of somatic mutation information to investigate the genomic variations within distinct clusters. Among these clusters, APC, TP53, and PIK3CA were the most common gene aberrations (Figures 5A-D). This study specifically focused on the distribution of the mutation frequency of KRAS and BRAF genes across different clusters, which were important for targeted therapy in patients with colon cancer. Interestingly, the prevalence of BRAF mutations was significantly higher in Cluster 1 compared to other clusters, and a similar trend was observed for KRAS mutations in Cluster 3 ($P<0.05$, Figure 5E, Figure S2B). In addition, we also assessed the TMB, a predictive biomarker for immunotherapy. It was found that patients in Cluster 1 had a significantly higher level of TMB compared to other clusters ($P<0.001$, Figure 5F, Figure S2C). This suggested that Cluster 1 may exhibit a better response to immunotherapy (33).

3.6 Prediction of immunotherapy response among colon cancer clusters

The TIDE score was calculated to predict the efficiency of immunotherapy by analyzing the correlation between gene expression and CTLs infiltration level. In this study, the average expressions of CD8A, CD8B, GZMA, GZMB, and PRF1 genes were used to represent level of CTL in colon cancers. Based on the findings, it was observed that the Cluster 1 exhibited noticeably higher level of CTLs compared to Cluster 2 and 3 ($P<0.001$, Figure 5G, Figure S2E). Furthermore, a higher Tide score indicated a greater likelihood of immune evasion and no benefit from immunotherapy. It was found that Cluster 1 was more likely to benefit from immunotherapy as its score was significantly lower compared to Cluster 2 and 3 ($P<0.05$, Figure 5H, Figure S2F).

In this study, we compared the immune status of different clusters and found no statistical difference between Cluster 1 and Cluster 4 in the composition of TIME and the expression of ICIs. However, there were significant differences in the TMB level between Cluster 1 and Cluster 4. In addition, we used the TIDE score to predict immunotherapy responses in different clusters and found that Cluster 1 had a significantly lower score compared to Cluster 2 and 3. While, Cluster 4 exhibited a TIDE score that did not exhibit significant difference from that in Cluster 2 and 3 ($P>0.05$).

3.7 Comparison of immune status among different clusters of MSS patients

The study has confirmed that Cluster 1 was more likely to benefit from immunotherapy. It was observed that the distribution frequency of dMMR/MSI-H in Cluster 1 was significantly higher (50%) compared to other clusters ($P<0.05$, Figure 6A, Figure S2D). To investigate whether the distinct distribution of dMMR/MSI-H contributed to the varying immune status of each cluster, data from MSS patients from clusters were collected for further analysis.

It was found that the stromal, immune score and tumor purity were significantly different among clusters ($P< 0.01$, Figures 6B, C). Cluster 1 exhibited higher immune score with increased immune cell infiltration, while having relatively lower tumor purity. The expression level of ICIs in cluster 1 were significantly higher than cluster 2 and 3($P<0.05$, Figure 6D). Among the clusters, Cluster 1 showed significantly higher abundance of CD8+T cells compared to others ($P<0.001$, Figure 6E). Moreover, the abundance of immunosuppression-related Tregs cells among clusters varied statistically among clusters, with Cluster 1 showing relatively lower infiltration ($P<0.05$, Figure 6E). Although there was no significant difference in the TMB levels among clusters of colon

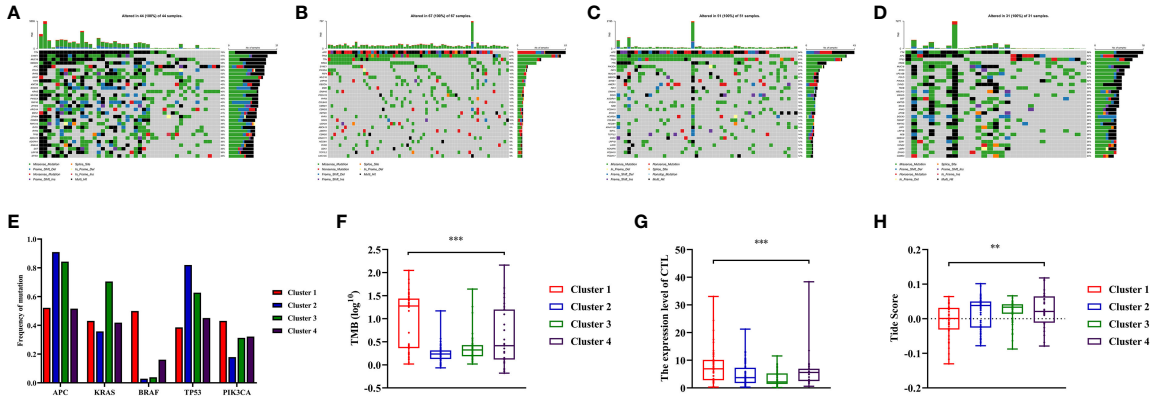

FIGURE 5
Somatic variations features during clusters of colon cancer and predicting the response to immune therapy based on Tumor Immune Dysfunction and Exclusion (TIDE) score. **(A–D)** Waterfall plots showed somatic mutation landscape and the top 10 mutated in four clusters. **(E)** Comparisons of mutation status of APC, KRAS, BRAF, TP53 and PIK3CA during different clusters of colon cancer patients. **(F)** Comparisons of Tumor Mutation Burdens (TMB) level of the four clusters. **(G)** Comparisons of cytotoxic T lymphocytes (CTL) level of the four clusters. **(H)** Comparisons of Tide score for predicting the likelihood of response to immune therapy of different clusters. ** means *P*< 0.01, *** means *P*< 0.001.

cancer (*P*=0.051, Figure 6F), the average of TMB in Cluster 1 was higher than in other clusters. Finally, the Tide score was calculated using CTL levels to predict immunotherapy response. The CTL levels of each cluster showed significant differences (*P*<0.05, Figure 6G), with cluster 1 having the highest CTL level. According to the Tide score, it was anticipated that Cluster 1 patients had a higher probability of experiencing favorable outcomes with immunotherapy, even among those with MSS status (*P*<0.05, Figure 6H).

In summary, Significant differences in the TIME of MSS patients were observed from different clusters. MSS patients in Cluster 1 exhibited a better immune status, making them more suitable for immunotherapy.

3.8 Identification specific DNA methylation markers

The QDMR software was used to identify the specific methylation genes that characterized distinct DNA methylation clusters of colon cancers. The average DNA methylation level of samples for all 282 MDGs was calculated, resulting in a

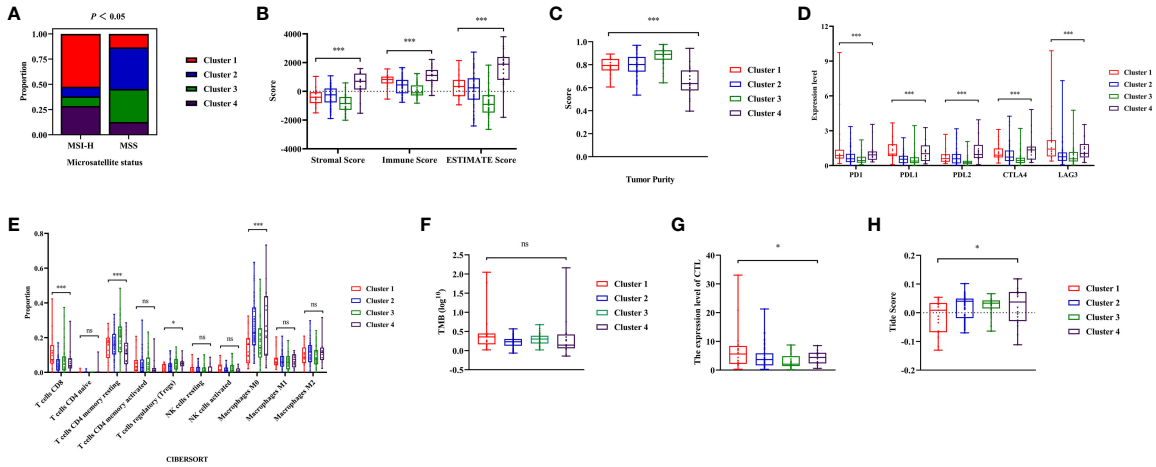

FIGURE 6
Analysis of immune status during microsatellite stability (MSS) patients from the four clusters. **(A)** The distribution frequency of microsatellite status during four clusters. **(B, C)** Comparisons of stromal score, immune score, ESTIMATE score and tumor purity during MSS patients from different clusters. **(D)** The expression level of immune checkpoints (PD1, PDL1, PDL2, CTLA4, LAG3) during MSS patients from different clusters. **(E)** Comparisons of the abundances of immune cells evaluated by CIBERSORT algorithm during MSS patients from different clusters. **(F)** Comparisons of Tumor Mutation Burdens (TMB) level of the four clusters. **(G)** Comparisons of cytotoxic T lymphocytes (CTL) level of the four clusters. **(H)** Comparisons of Tumor Immune Dysfunction and Exclusion (TIDE) score for predicting the response of immune therapy during MSS patients. 'ns' means *P*> 0.05, * means *P*< 0.05, *** means P< 0.001.

282*9dimensional matrix which was then input into QDMR. A standard deviation (SD) parameter of 0.3 was set to identify the specific markers for each cluster. Ultimately, 56 specific methylation genes were identified (Table S6). A heatmap was generated based on these specific methylation genes, clearly illustrating the differentiation among clusters (Figures 7A, E). Each cluster had its own unique set of specific methylation genes. Of particular interest were the three specific hypermethylation genes that defined Cluster 1 (PCDH20, APCDD1, COCH). Pearson correlation analysis indicated that methylation in the promoter region regulated the gene expression level of specific markers. The correlation coefficients for PCDH20, APCDD1, and COCH were -0.335 (P<0.001, Figure S3A), -0.309 (P<0.001, Figure S3B), and -0.329 (P<0.001, Figure S3C), respectively. The Cluster 1 could be clearly distinguished from the other clusters by three specific makers (Figures 7B, F). The boxplot analysis revealed significant differences in methylation levels between Cluster 1 and the remaining clusters (P<0.001, Figures 7C, G). Finally, ROC analysis showed an AUC of 0.947 (95% CI 0.903-0.990)for distinguishing Cluster 1 in the training cohort (Figure 7D) and the specific markers also had an excellent performance in the validation cohort, with an AUC of 0.912 (95% CI 0.8557-0.966) (Figure 7H). These findings indicated that the specific methylation genes (PCDH20, APCDD1, COCH) could effectively distinguish Cluster 1 from other clusters. Additionally, we aimed to investigate the relationship between these specific markers and prognosis. Patients were categorized into two groups based on the average expression and methylation levels. Survival analysis revealed that high expression of APCDD1 was associated with a better prognosis (P<0.05, Figure S4A), while the expression levels of other genes did not show statistical significance in relation to prognosis (Figure S4B, C). Interestingly, high methylation levels of APCDD1 were associated with a worse prognosis (P<0.05, Figure S4D), whereas the methylation levels of the remaining genes did not exhibit any association with prognosis (Figure S4E, F). Further subgroup analysis revealed a significant increase in the methylation level of APCDD1 in advanced-stage patients (P<0.05, Figure S5A). In contrast, the gene expression level exhibited an opposite trend (P<0.01, Figure S5B).

3.9 Immunohistochemical validation

After screening, we selected the postoperative tumor paraffin sections of 10 patients for immunohistochemical validation. Based on the efficacy evaluation results, the patients were divided into two groups: the response group (partial response (PR), n=2, stable disease (SD), n =3) and the non-response group (progressive disease (PD), n=5) (Table S7). The results revealed that the expression scores of biomarkers (PCDH20, APCDD1) were significantly downregulated in the response group compared to the non-response group (P<0.05, Figures 8A, B, D, E). The hypermethylation of the promoter region could be responsible for the decrease in gene expression levels. In the beneficial-cluster, the methylation levels of PCDH20 and APCDD1 were considerably increased in the benefit cluster, resulting in the repression of the corresponding genes. However, the results indicated that there was no significant difference in the expression of COCH between response group and non-response group (P = 0.75, Figures 8C, F).

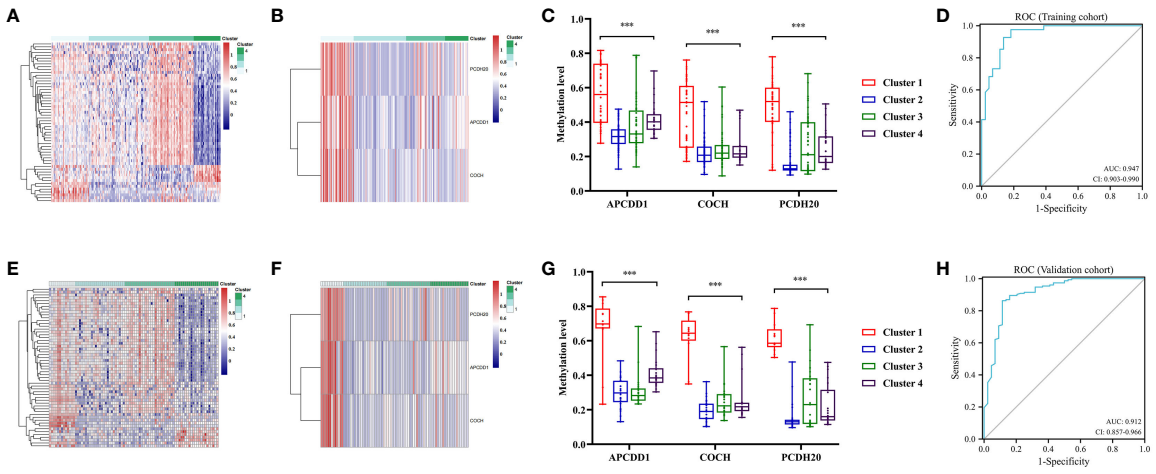

FIGURE 7
Specific methylation sites for each DNA methylation cluster. **(A)** The heatmap for the specific sites during four DNA methylation clusters in the training cohort. **(B)** The heatmap for the three specific sites (PCDH20, APCDD1, COCH) of cluster 1 during four clusters in the training cohort. **(C)** Comparisons of the methylation level for the three specific sites (PCDH20, APCDD1, COCH) during four clusters in the training cohort. **(D)** Receiver operating characteristic (ROC) curves of the three specific sites (PCDH20, APCDD1, COCH) in distinguishing the Cluster1 from other clusters in the train cohort. **(E)** The heatmap for the specific sites during four clusters in the validation cohort. **(F)** The heatmap for the three specific sites of Cluster 1 during four clusters in the validation cohort. **(G)** Comparisons of the methylation level for the three specific sites during four clusters in the validation cohort. **(H)** ROC curves of the three specific sites in distinguishing the Cluster 1 from other clusters in the validation cohort. *** means P< 0.001.

3.10 The potential association linking APCDD1 and immune status

To elucidate the underlying mechanisms between markers and immune status. we utilized bioinformatics data to investigate the association between markers and immune scores, immune cell infiltration (CD8+T cells), and immune checkpoints expression (PD-1, PD-L1). Pearson correlation analysis revealed that the methylation level of APCDD1 was positively correlated with immune score (P<0.001, 0.333) (Figures 9A-D), CD8+T cells infiltration (P<0.001, 0.383), PD-1 (P<0.001, 0.357), and PD-L1 (P<0.001, 0.383). Similarly, the methylation level of COCH exhibited a significant positive correlation with immune scores (P<0.001, 0.233), CD8+ T cells infiltration (P<0.001, 0.203), PD-1 (P<0.01, 0.183), and PD-L1 (P<0.001, 0.280) (Figures S6A-D). Additionally, the methylation level of PCDH20 showed a significant positive correlation with immune scores (P<0.01, 0.192), CD8+ T cells infiltration (P<0.001, 0.228), PD-1 (P<0.05, 0.129), and PD-L1 (P<0.01, 0.185) (Figures S6G, H). These findings indicated a significant correlation between the methylation of markers and the immune microenvironment and we chose to focus our research on APCDD1, which demonstrated the strongest correlation with the immune status.

Subsequently, APCDD1 was divided into high and low groups based on methylation level for differential analysis with a set of P< 0.05 (Figure 9E). The 2058 of DMGs were then subjected to enrichment and analysis. The results of GO analysis were significantly enriched in T cell activation, immune receptor activity (P<0.05, Figure 9F). Additionally, KEGG pathways analysis revealed significant enrichment in intestinal immune network for IgA production, (P<0.05, Figure 9G). After conducting a comprehensive Gene Set Enrichment Analysis (GSEA) (h.all.v2022.1.Hs.symbols.gmt), we observed a significant positive association between the differentially expressed genes and the Interferon-GAMMA-Response pathway(P<0.05, Figure 9H).

4 Discussion

The emergence of immunotherapy has marked the beginning of a new era in cancer therapy. However, the current situation presents a challenge with the low detection rate of microsatellite status, which is the primary standard used to guide immunotherapy. Not all patients with dMMR or MSI-H had a response to immunotherapy, a subset of MSS patients could also benefit from immunotherapy. It is essential to search for additional immunotherapy biomarkers as a supplement.

Abnormal DNA methylation modifications are closely associated with the tumor immune microenvironment. This study aimed to identify immunotherapy biomarkers for patients with colon cancer from the perspective of DNA methylation. Firstly, the most crucial step in this research is to utilize DEGs for the identification of MDGs. Our concern lies in the fact that the expression of DMGs is regulated by methylation and remains in a low expression state. Upon applying more stringent thresholds, we observed a substantial reduction in the number of DEGs. However, this reduction came at the cost of decreased sensitivity. The stricter thresholds led to the exclusion of potentially relevant MDGs that could play a crucial role in influencing the immune microenvironment. In summary, we experimented with various thresholds and selected one suitable for our study. Although it may impact sensitivity, we believe it is acceptable considering the

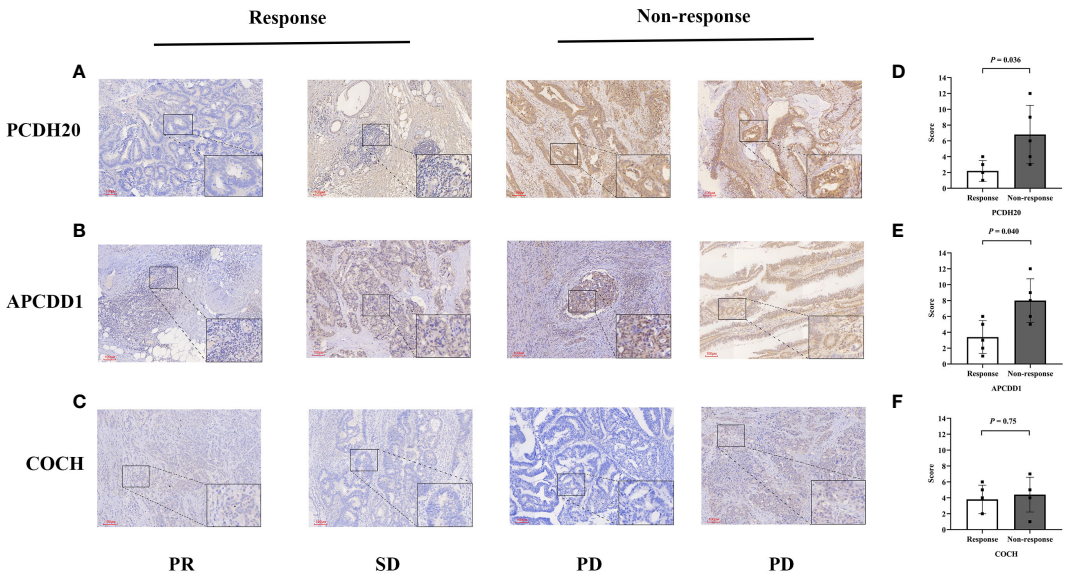

FIGURE 8
Immunohistochemical validation of colon cancers. **(A-C)** The expressions of (PCDH20, APCDD1 and COCH) in response group and non-response group. **(D, E)** Compared to non-response group, the expressions of (PCDH20 and APCDD1) were down-regulated in response group. **(F)** No significant difference of COCH expression between response group and non-response group.

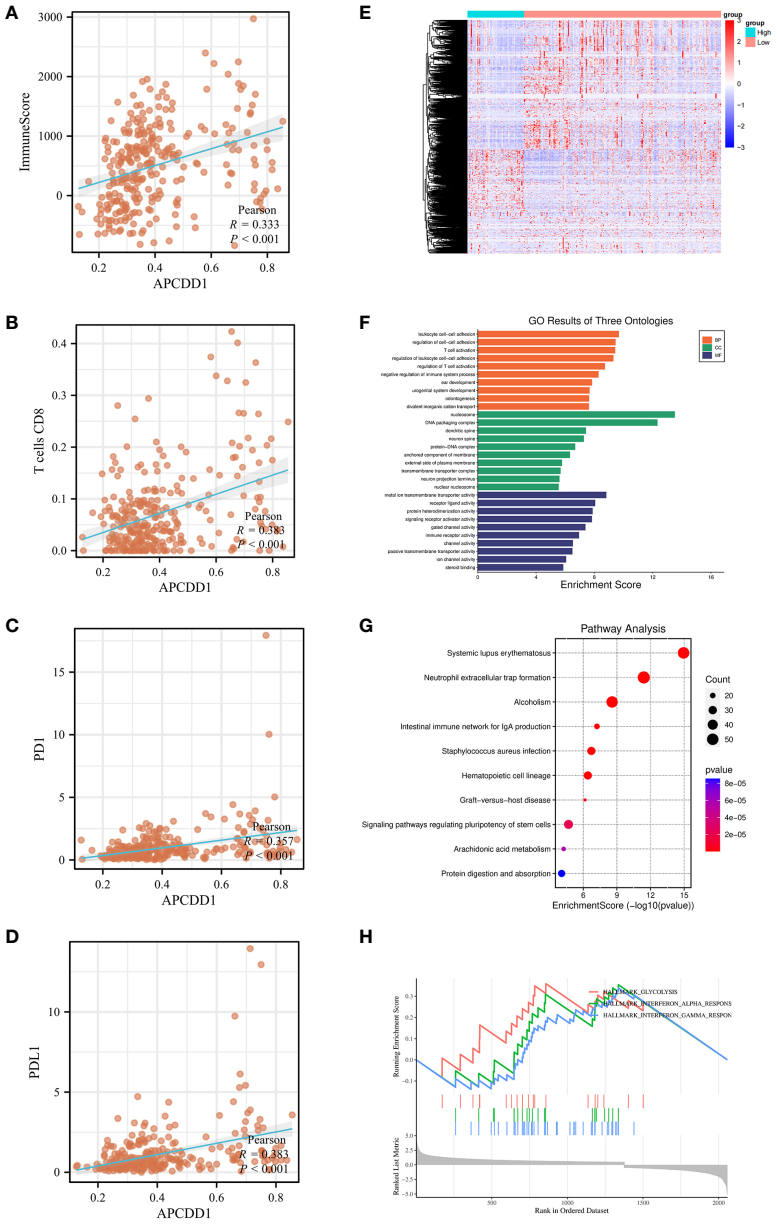

FIGURE 9
The association of APCDD1 and immune status. **(A)** The methylation level of APCDD1 and immune scores. **(B)** The methylation level of APCDD1 and CD8 T+ cells. **(C)** The methylation level of APCDD1 and PD-1 expressions. **(D)** The methylation level of APCDD1 and PD-L1 expressions. **(E)** Heatmap of Differentially Methylated Genes (DMGs) in different methylation level of APCDD1. **(F)** Gene Ontology (GO) enrichment results of three ontologies (including biological processes, cellular components, and molecular functions) of DMGs. **(G)** Kyoto Encyclopedia of Genes and Genomes **(KEGG)** enrichment analysis of DMGs. **(H)** Gene Set Enrichment Analysis (GSEA) enrichment analysis was carried out on the DMGs between high and low methylation of APCDD1.

influence of gene expression regulation by DNA methylation. Subsequently, consensus clustering was conducted to identify distinct molecular clusters of colon cancers based on the methylation data. The patients of colon cancer were then divided into four clusters, and the immune microenvironment of each cluster was further analyzed. Notably, patients in Cluster 1, characterized by stronger antitumor immunoactivity, were predicted to have a better response to immunotherapy based on the Tide score. Finally, we identified the specific methylation markers of Cluster1 (PCDH20, APCDD1, COCH), and ROC curves confirmed their excellent performance in discriminating the clusters.

There were several factors could affect the effectiveness of immunotherapy in colon cancers. The composition and quantity of infiltrating immune cells in the TIME played crucial roles in the process of tumor eradication (34). The infiltration of CD8+ T cells or CTLs had a significant positive association with antitumor immune activity (35). On the other hand, Tregs could induce the

apoptosis of cytotoxic T cells, leading to the immunosuppression (36, 37). In the present study, we statistically analyzed the infiltration abundance of immune cells from clusters. It was observed that Cluster 1 had a higher abundance of CD8+ T cells and CTL, while the infiltration of Tregs was found to be the lowest among the clusters ($P<0.05$). Other factors that affect immunotherapy include the expression of ICIs, TMB, etc. (38, 39) Compared with Cluster 2 and 3, the expression levels of ICIs were significantly higher in Cluster 1. Additionally, patients in Cluster 1 had significantly higher TMB than those in remaining clusters ($P<0.05$). The Tide scores indicated that Cluster 1 was most likely to benefit from immunotherapy. Notably, the distribution frequency of BRAF mutation (70.9%) and MSI-H (52.3%) in Cluster 1 were significantly higher than that in other clusters. There was a high overlap of 77.2% between these two groups of patients. BRAF is a serine/threonine protein kinase located downstream of RAS/RAF/MAPK pathway (40). The BRAF mutation, (primarily caused by a missense mutation at V600E) was a significant mutation in colon cancers. The relationship between BRAF mutation and MSI-H has been extensively discussed. It has been confirmed that patients with BRAF mutations have a higher rate of MSI-H. This may be due to the tumors with BRAF V600E mutation were associated with a high-level CpG island methylator phenotype (CIMP) and MLH1 promoter methylation (41, 42). However, the impact of BRAF mutation on immunotherapy response in dMMR patients has always been controversial. A recent retrospective study concluded that there were no significant differences in neoantigen tumor burden (NTB), immune score, or T cell infiltration between BRAF wild-type and mutant of colon cancer patients with MSI-H (43). This suggested that both are likely to benefit from immune checkpoint inhibitors. In conclusion, Cluster 1, which has a higher frequency of BRAF mutation and MSI-H, is more suitable for immunotherapy based on the TIME analysis.

We successfully identified specific methylation markers (PCDH20, APCDD1, COCH) of immune-beneficial cluster using the QDMR software. As a tumor suppressor gene, protocadherin 20 (PCDH20) is a member of the cadherin superfamily (44). The previous studies have shown that the expression of PCDH20 was frequently decreased or silenced in multiple cancers, primarily attributed to the methylation of the promoter region. The expression of PCDH20 was restored after the addition of DNMT inhibitors to the corresponding tumor cell lines (45, 46). In addition, it has been observed that inhibition of PCDH20 expression frequently promoted migration and invasion of tumors (47). Notably, PCDH20 plays a crucial role in maintaining the balance and structural integrity of the intestinal epithelium. A decrease in the expression level of PCDH20 can disrupt the integrity of the intestinal mucosa, which can contribute to the development of colitis and Crohn's disease (48). APCDD1 (adenomatosis polyposis down-regulated 1), a negative regulator of Wnt/β-catenin pathway, its expression was regulated by promotor methylation (49). It has been demonstrated that the methylation of WNT target genes (including APCDD1) could be serve as reliable biomarkers for predicting recurrence in colon cancers (50). As a DNA methylation marker, COCH has shown effectiveness in identifying occult lymph node metastases in non-small cell lung cancer (51). However, the effect of promoter methylation on the expression of COCH has not been extensively studied. In contrast to previous research, this study was the first to discuss the differences in methylation levels of markers (PCDH20, APCDD1, COCH) among different clusters. The methylation levels of the three specific methylation markers in Cluster 1 were found to be significantly distinct from those in the other clusters. In this study, we utilized colon cancer samples (immunohistochemistry) to validate the conclusion. However, we did not observe any significant difference in the expression of COCH between response group and non-response group. This might be attributed to the markers being associated with clustering, while the potential mechanisms related to the TIME remain unconfirmed.

DNA methylation biomarkers exhibited a better sensitivity compared to mutation-based cancer detection (52–54). Currently, DNA methylation markers are predominantly utilized as diagnostic and prognostic markers. The innovation of this study lies in exploring biomarkers of immunotherapy in colon cancers from the perspective of DNA methylation. Ultimately, specific methylation markers (PCDH20, APCDD1, and COCH) were identified as effective markers for identifying cluster that would benefit from immunotherapy in colon cancers. Our study still had some limitations. Firstly, the sample size used in the study was mainly derived from the database, we performed immunohistochemical validation of small samples to verify the research findings. However, for further validation, large sample sequencing data will be required in the future. Secondly, the potential mechanisms linking molecular markers and immune status has not been fully elucidated. Lastly, we will concentrate on assessing the markers' feasibility in clinical practice and making further enhancements and optimizations.

5 Conclusion

In conclusion, this study successfully identified a specific cluster that benefited from immunotherapy through 282 MDGs of colon cancers. Furthermore, we found beneficial-cluster of specific methylation markers (PCDH20, APCDD1, COCH) that could be used in conjunction with microsatellite status to expand the pool of colon cancer patients eligible for immunotherapy.

Data availability statement

The original contributions presented in the study are included in the article/Supplementary Materials, further inquiries can be directed to the corresponding authors.

Ethics statement

The studies involving humans were approved by Harbin Medical University Cancer Hospital ethics committee. The studies were conducted in accordance with the local legislation and

institutional requirements. The human samples used in this study were acquired from primarily isolated as part of your previous study for which ethical approval was obtained. Written informed consent for participation was not required from the participants or the participants' legal guardians/next of kin in accordance with the national legislation and institutional requirements.

Author contributions

BX: Conceptualization, Data curation, Formal Analysis, Investigation, Methodology, Resources, Software, Validation, Visualization, Writing – original draft, Writing – review & editing. JL: Data curation, Methodology, Software, Writing – review & editing. XP: Data curation, Writing – review & editing. YG: Methodology, Software, Writing – review & editing. JZ: Formal Analysis, Writing – review & editing. YZ: Conceptualization, Project administration, Resources, Supervision, Writing – review & editing. HL: Funding acquisition, Project administration, Supervision, Writing – review & editing.

Funding

The author(s) declare financial support was received for the research, authorship, and/or publication of this article. This research was supported by the National Natural Science Foundation of China (grant nos. U20A20376 and 61972116), Beijing Award Foundation (YXJL-2020-0818-0478), Wu Jieping Medical Foundation (320.6750.2020-19-20), Heilongjiang Province Postdoctoral Funding Project (LBH-Z21189), Harbin Medical University Innovative Science Research Funded Project (grant no.31041220028) and China Postdoctoral Science Foundation (grant no.2022MD713747).

Acknowledgments

The authors would like to thank all patients and staff who have participated in the TCGA and UCSC XENA database.

Conflict of interest

The authors declare that the research was conducted in the absence of any commercial or financial relationships that could be construed as a potential conflict of interest.

Publisher's note

Supplementary material

The Supplementary Material for this article can be found online at: https://www.frontiersin.org/articles/10.3389/fonc.2024.1335670/full#supplementary-material

References

1. Siegel RL, Wagle NS, Cercek A, Smith RA, Jemal A. Colorectal cancer statistics, 2023. *CA: A Cancer J Clin* (2023) 73(3):233–54. doi: 10.3322/caac.21772

2. Pang X, Xu B, Lian J, Wang R, Wang X, Shao J, et al. Real-world survival of colon cancer after radical surgery: A single-institutional retrospective analysis. *Front Oncol* (2022) 12:914076. doi: 10.3389/fonc.2022.914076

3. Le DT, Kim TW, Van Cutsem E, Geva R, Jäger D, Hara H, et al. Phase II open-label study of pembrolizumab in treatment-refractory, microsatellite instability–high/mismatch repair–deficient metastatic colorectal cancer: KEYNOTE-164. *J Clin Oncol* (2020) 38(1):11–9. doi: 10.1200/jco.19.02107

4. Overman MJ, Lonardi S, Wong KYM, Lenz H-J, Gelsomino F, Aglietta M, et al. Durable clinical benefit with nivolumab plus ipilimumab in DNA mismatch repair–deficient/microsatellite instability–high metastatic colorectal cancer. *J Clin Oncol* (2018) 36(8):773–9. doi: 10.1200/jco.2017.76.9901

5. Overman MJ, McDermott R, Leach JL, Lonardi S, Lenz H-J, Morse MA, et al. Nivolumab in patients with metastatic DNA mismatch repair-deficient or microsatellite instability-high colorectal cancer (CheckMate 142): an open-label, multicentre, phase 2 study. *Lancet Oncol* (2017) 18(9):1182–91. doi: 10.1016/s1470-2045(17)30422-9

6. Dong L, Jin X, Wang W, Ye Q, Li W, Shi S, et al. Distinct clinical phenotype and genetic testing strategy for Lynch syndrome in China based on a large colorectal cancer cohort. *Int J Cancer* (2020) 146(11):3077–86. doi: 10.1002/ijc.32914

7. Koopman M, Kortman GAM, Mekenkamp L, Ligtenberg MJL, Hoogerbrugge N, Antonini NF, et al. Deficient mismatch repair system in patients with sporadic advanced colorectal cancer. *Br J Cancer* (2009) 100(2):266–73. doi: 10.1038/sj.bjc.6604867

8. Wang R, Lian J, Wang X, Pang X, Xu B, Tang S, et al. Intrinsic resistance and efficacy of immunotherapy in microsatellite instability-high colorectal cancer: A systematic review and meta-analysis. *Biomolecules Biomed* (2023) 23(2):198–208. doi: 10.17305/bjbms.2022.8286

9. Fukuoka S, Hara H, Takahashi N, Kojima T, Kawazoe A, Asayama M, et al. Regorafenib plus nivolumab in patients with advanced gastric or colorectal cancer: an open-label, dose-escalation, and dose-expansion phase ib trial (REGONIVO, EPOC1603). *J Clin Oncol* (2020) 38(18):2053–61. doi: 10.1200/jco.19.03296

10. Kandoth C, McLellan MD, Vandin F, Ye K, Niu B, Lu C, et al. Mutational landscape and significance across 12 major cancer types. *Nature* (2013) 502(7471):333–9. doi: 10.1038/nature12634

11. Jones PA, Baylin SB. The fundamental role of epigenetic events in cancer. *Nat Rev Genet* (2002) 3(6):415–28. doi: 10.1038/nrg816

12. Sun X, Yi J, Yang J, Han Y, Qian X, Liu Y, et al. An integrated epigenomic-transcriptomic landscape of lung cancer reveals novel methylation driver genes of diagnostic and therapeutic relevance. *Theranostics* (2021) 11(11):5346–64. doi: 10.7150/thno.58385

13. Grandits AM, Nguyen CH, Schlerka A, Hackl H, Sill H, Etzler J, et al. Downregulation of MTSS1 in acute myeloid leukemia is associated with a poor prognosis, chemotherapy resistance, and disease aggressiveness. *Leukemia* (2021) 35 (10):2827–39. doi: 10.1038/s41375-021-01224-2

14. Berghoff AS, Kiesel B, Widhalm G, Wilhelm D, Rajky O, Kurscheid S, et al. Correlation of immune phenotype with IDH mutation in diffuse glioma. *Neuro-Oncology* (2017) 19(11):1460–8. doi: 10.1093/neuonc/nox054

15. Figueroa ME, Abdel-Wahab O, Lu C, Ward PS, Patel J, Shih A, et al. Leukemic IDH1 and IDH2 mutations result in a hypermethylation phenotype, disrupt TET2 function, and impair hematopoietic differentiation. *Cancer Cell* (2010) 18(6):553–67. doi: 10.1016/j.ccr.2010.11.015

16. Kohanbash G, Carrera DA, Shrivastav S, Ahn BJ, Jahan N, Mazor T, et al. Isocitrate dehydrogenase mutations suppress STAT1 and CD8+ T cell accumulation in gliomas. *J Clin Invest* (2017) 127(4):1425–37. doi: 10.1172/jci90644

17. Du C, Liu X, Li M, Zhao Y, Li J, Wen Z, et al. Analysis of 5-methylcytosine regulators and DNA methylation-driven genes in colon cancer. *Front Cell Dev Biol* (2022) 9:657092. doi: 10.3389/fcell.2021.657092

18. Love MI, Huber W, Anders S. Moderated estimation of fold change and dispersion for RNA-seq data with DESeq2. *Genome Biol* (2014) 15(12):550. doi: 10.1186/s13059-014-0550-8

19. Ritchie ME, Phipson B, Wu D, Hu Y, Law CW, Shi W, et al. limma powers differential expression analyses for RNA-sequencing and microarray studies. *Nucleic Acids Res* (2015) 43(7):e47–e. doi: 10.1093/nar/gkv007

20. Gevaert O. MethylMix: an R package for identifying DNA methylation-driven genes. *Bioinformatics* (2015) 31(11):1839–41. doi: 10.1093/bioinformatics/btv020

21. Yu G, Wang L-G, Han Y, He Q-Y. clusterProfiler: an R package for comparing biological themes among gene clusters. *OMICS: A J Integr Biol* (2012) 16(5):284–7. doi: 10.1089/omi.2011.0118

22. Luo W, Brouwer C. Pathview: an R/Bioconductor package for pathway-based data integration and visualization. *Bioinformatics* (2013) 29(14):1830–1. doi: 10.1093/bioinformatics/btt285

23. Wilkerson MD, Hayes DN. ConsensusClusterPlus: a class discovery tool with confidence assessments and item tracking. *Bioinformatics* (2010) 26(12):1572–3. doi: 10.1093/bioinformatics/btq170

24. Yoshihara K, Shahmoradgoli M, Martínez E, Vegesna R, Kim H, Torres-Garcia W, et al. Inferring tumour purity and stromal and immune cell admixture from expression data. *Nat Commun* (2013) 4(1):2612. doi: 10.1038/ncomms3612

25. Newman AM, Liu CL, Green MR, Gentles AJ, Feng W, Xu Y, et al. Robust enumeration of cell subsets from tissue expression profiles. *Nat Methods* (2015) 12 (5):453–7. doi: 10.1038/nmeth.3337

26. Chen Daniel S, Mellman I. Oncology meets immunology: the cancer-immunity cycle. *Immunity* (2013) 39(1):1–10. doi: 10.1016/j.immuni.2013.07.012

27. Xu L, Deng C, Pang B, Zhang X, Liu W, Liao G, et al. TIP: A web server for resolving tumor immunophenotype profiling. *Cancer Res* (2018) 78(23):6575–80. doi: 10.1158/0008-5472.Can-18-0689

28. Mayakonda A, Lin D-C, Assenov Y, Plass C, Koeffler HP. Maftools: efficient and comprehensive analysis of somatic variants in cancer. *Genome Res* (2018) 28(11):1747–56. doi: 10.1101/gr.239244.118

29. Gajewski TF, Schreiber H, Fu Y-X. Innate and adaptive immune cells in the tumor microenvironment. *Nat Immunol* (2013) 14(10):1014–22. doi: 10.1038/ni.2703

30. Spranger S, Gajewski TF. Tumor-intrinsic oncogene pathways mediating immune avoidance. *OncoImmunology* (2015) 5(3):e1086862. doi: 10.1080/2162402x.2015.1086862

31. Jiang P, Gu S, Pan D, Fu J, Sahu A, Hu X, et al. Signatures of T cell dysfunction and exclusion predict cancer immunotherapy response. *Nat Med* (2018) 24(10):1550–8. doi: 10.1038/s41591-018-0136-1

32. Zhang Y, Liu H, Lv J, Xiao X, Zhu J, Liu X, et al. QDMR: a quantitative method for identification of differentially methylated regions by entropy. *Nucleic Acids Res* (2011) 39(9):e58–e. doi: 10.1093/nar/gkr053

33. Samstein RM, Lee C-H, Shoushtari AN, Hellmann MD, Shen R, Janjigian YY, et al. Tumor mutational load predicts survival after immunotherapy across multiple cancer types. *Nat Genet* (2019) 51(2):202–6. doi: 10.1038/s41588-018-0312-8

34. Schmitt M, Greten FR. The inflammatory pathogenesis of colorectal cancer. *Nat Rev Immunol* (2021) 21(10):653–67. doi: 10.1038/s41577-021-00534-x

35. Reina-Campos M, Scharping NE, Goldrath AW. CD8+ T cell metabolism in infection and cancer. *Nat Rev Immunol* (2021) 21(11):718–38. doi: 10.1038/s41577-021-00537-8

36. Rooney Michael S, Shukla Sachet A, Wu Catherine J, Getz G, Hacohen N. Molecular and genetic properties of tumors associated with local immune cytolytic activity. *Cell* (2015) 160(1-2):48–61. doi: 10.1016/j.cell.2014.12.033

37. Mair F, Erickson JR, Frutoso M, Konecny AJ, Greene E, Voillet V, et al. Extricating human tumour immune alterations from tissue inflammation. *Nature* (2022) 605(7911):728–35. doi: 10.1038/s41586-022-04718-w

38. Hu F-F, Liu C-J, Liu L-L, Zhang Q, Guo A-Y. Expression profile of immune checkpoint genes and their roles in predicting immunotherapy response. *Briefings Bioinf* (2021) 22(3). doi: 10.1093/bib/bbaa176

39. McGrail DJ, Pilié PG, Rashid NU, Voorwerk L, Slagter M, Kok M, et al. Validation of cancer-type-dependent benefit from immune checkpoint blockade in TMB-H tumors identified by the FoundationOne CDx assay. *Ann Oncol* (2022) 33 (11):1204–6. doi: 10.1016/j.annonc.2022.07.009

40. Grothey A, Fakih M, Tabernero J. Management of BRAF-mutant metastatic colorectal cancer: a review of treatment options and evidence-based guidelines. *Ann Oncol* (2021) 32(8):959–67. doi: 10.1016/j.annonc.2021.03.206

41. Venderbosch S, Nagtegaal ID, Maughan TS, Smith CG, Cheadle JP, Fisher D, et al. Mismatch repair status and BRAF mutation status in metastatic colorectal cancer patients: A pooled analysis of the CAIRO, CAIRO2, COIN, and FOCUS studies. *Clin Cancer Res* (2014) 20(20):5322–30. doi: 10.1158/1078-0432.Ccr-14-0332

42. Ogino S, Nosho K, Kirkner GJ, Kawasaki T, Meyerhardt JA, Loda M, et al. CpG island methylator phenotype, microsatellite instability, BRAF mutation and clinical outcome in colon cancer. *Gut* (2008) 58(1):90–6. doi: 10.1136/gut.2008.155473

43. Salem M, Kopetz S, El-Refai S, Tabernero J, Sinicrope F, Tie J, et al. LBA SO-34 Impact of BRAF-V600E mutation on immunologic characteristics of the tumor microenvironment (TME) and associated genomic alterations in patients with microsatellite instability-high (MSI-H) or mismatch-repair–deficient (dMMR) colorectal cancer (CRC). *Ann Oncol* (2022) 33:S378. doi: 10.1016/j.annonc.2022.04.441

44. Keeler AB, Molumby MJ, Weiner JA. Protocadherins branch out: Multiple roles in dendrite development. *Cell Adhesion Migration* (2015) 9(3):214–26. doi: 10.1080/19336918.2014.1000069

45. Imoto I, Izumi H, Yokoi S, Hosoda H, Shibata T, Hosoda F, et al. Frequent silencing of the candidate tumor suppressor PCDH20 by epigenetic mechanism in non–small-cell lung cancers. *Cancer Res* (2006) 66(9):4617–26. doi: 10.1158/0008-5472.Can-05-4437

46. Lv J, Zhu P, Yang Z, Li M, Zhang X, Cheng J, et al. PCDH20 functions as a tumour-suppressor gene through antagonizing the Wnt/β-catenin signalling pathway in hepatocellular carcinoma. *J Viral Hepatitis* (2014) 22(2):201–11. doi: 10.1111/jvh.12265

47. Ning Y, Deng C, Li C, Peng W, Yan C, Ran J, et al. PCDH20 inhibits esophageal squamous cell carcinoma proliferation and migration by suppression of the mitogen-activated protein kinase 9/AKT/β-catenin pathway. *Front Oncol* (2022) 12:937716. doi: 10.3389/fonc.2022.937716

48. Huang S, Xie Z, Han J, Wang H, Yang G, Li M, et al. Protocadherin 20 maintains intestinal barrier function to protect against Crohn's disease by targeting ATF6. *Genome Biol* (2023) 24(1):159. doi: 10.1186/s13059-023-02991-0

49. Skopelitou D, Miao B, Srivastava A, Kumar A, Kuświk M, Dymerska D, et al. Whole exome sequencing identifies APCDD1 and HDAC5 genes as potentially cancer predisposing in familial colorectal cancer. *Int J Mol Sci* (2021) 22(4):1837. doi: 10.3390/ijms22041837

50. Kandimalla R, Linnekamp JF, van Hooff S, Castells A, Llor X, Andreu M, et al. Methylation of WNT target genes AXIN2 and DKK1 as robust biomarkers for recurrence prediction in stage II colon cancer. *Oncogenesis* (2017) 6(4):e308–e. doi: 10.1038/oncsis.2017.9

51. Chen Z, Xiong S, Li J, Ou L, Li C, Tao J, et al. DNA methylation markers that correlate with occult lymph node metastases of non-small cell lung cancer and a preliminary prediction model. *Trans Lung Cancer Res* (2020) 9(2):280–7. doi: 10.21037/tlcr.2020.03.13

52. Yizhak K, Aguet F, Kim J, Hess JM, Kübler K, Grimsby J, et al. RNA sequence analysis reveals macroscopic somatic clonal expansion across normal tissues. *Science* (2019) 364(6444). doi: 10.1126/science.aaw0726

53. Nassiri F, Chakravarthy A, Feng S, Shen SY, Nejad R, Zuccato JA, et al. Detection and discrimination of intracranial tumors using plasma cell-free DNA methylomes. *Nat Med* (2020) 26(7):1044–7. doi: 10.1038/s41591-020-0932-2

54. Nuzzo PV, Berchuck JE, Korthauer K, Spisak S, Nassar AH, Abou Alaiwi S, et al. Detection of renal cell carcinoma using plasma and urine cell-free DNA methylomes. *Nat Med* (2020) 26(7):1041–3. doi: 10.1038/s41591-020-0933-1

frontiers | Frontiers in Oncology

TYPE Case Report
PUBLISHED 06 February 2024
DOI 10.3389/fonc.2024.1355798

OPEN ACCESS

EDITED BY
Zsolt Kovács,
George Emil Palade University of Medicine, Pharmacy, Sciences and Technology of Târgu Mureş, Romania

REVIEWED BY
Antonella Argentiero,
National Cancer Institute Foundation (IRCCS), Italy
Abdullah Esmail,
Houston Methodist Hospital, United States

*CORRESPONDENCE
Ying Ma
m1545896474@163.com

RECEIVED 14 December 2023
ACCEPTED 16 January 2024
PUBLISHED 06 February 2024

CITATION
Cui K, Li Z, Zhong J, Shi X, Zhao L, Li H and Ma Y (2024) Achieving complete remission in metastatic hepatocellular carcinoma with sintilimab plus sorafenib therapy followed by hepatic resection: a case report.
Front. Oncol. 14:1355798.
doi: 10.3389/fonc.2024.1355798

Achieving complete remission in metastatic hepatocellular carcinoma with sintilimab plus sorafenib therapy followed by hepatic resection: a case report

Kai Cui[1], Zhongchao Li[1], Jingtao Zhong[1], Xuetao Shi[1], Lei Zhao[1], Hao Li[2] and Ying Ma[2]*

[1]Department of Hepatobiliary Surgery, Shandong Cancer Hospital Affiliated to Shandong First Medical University, Jinan, China, [2]Shandong Pharmaceutical Research Institute, Shandong First Medical University, Jinan, China

Background: The synergistic effectiveness of combining immune checkpoint inhibitors with targeted therapies has shown promise in improving the conversion rate for unresectable hepatocellular carcinoma (HCC) patients to a potentially resectable status. However, the efficacy of this approach in the context of HCC with extrahepatic metastasis remains to be conclusively determined.

Case presentation: We report a rare case of advanced HCC with extrahepatic metastasis who achieved long-term survival by a combination of systemic therapy (sintilimab and sorafenib) followed by laparoscopic hepatectomy. A 63-year-old man presented at our hospital with discomfort on the right side of his waist. An enlarged right hepatic lobe mass was subsequently revealed by CT scan. The patient's medical history, including a prior infection with hepatitis B virus, cirrhosis of the liver and an alpha-fetoprotein (AFP) level measuring 41.28 ng/ml substantiated the clinical diagnosis of HCC. On October 30th, 2019, the patient received 200 mg sintilimab intravenously (q3w) plus 200–400 mg BID sorafenib orally, along with antiviral therapy. After six cycles, his disease achieved partial response (PR). On April 26th, 2021, He underwent a laparoscopic hepatectomy. The patient achieved a sustained period of no evidence of disease for 2.5 years and with drug-free survival for 2 years after the resection. His current overall survival is estimated at approximately 4 years.

Conclusions: This case highlights the potential of combining sintilimab and sorafenib in transforming HCC with extrahepatic metastasis into a condition amenable to surgical resection, suggesting that this treatment approach, followed by surgery, may lead to complete remission.

KEYWORDS

sintilimab, sorafenib, PD-1 inhibitor, hepatocellular carcinoma, conversion therapy, extrahepatic metastasis

Background

Hepatocellular carcinoma (HCC), a predominant form of liver cancer, is the third most common cause of cancer-related mortality globally. This cancer type is especially prevalent in China, contributing to almost half of the worldwide cases and deaths (1, 2). Typically diagnosed in its advanced stages, HCC has historically been associated with a median overall survival (OS) of merely nine months for advanced-stage patients (3, 4). Recent developments in treatment, particularly the combination of immune checkpoint inhibitors (ICIs) with anti-angiogenic agents, have emerged as the frontline therapy for advanced HCC. This regime extended the median OS to 20 months (5). The increase in overall response rate (ORR) to 30–40% with this regimen is significant, potentially enabling resection by reducing tumour size or stage, which, in turn, could enhance the conversion rate for HCC treatment.

Here, we present a case of HCC with extrahepatic metastases where a complete remission was achieved through the combination of ICI with an anti-angiogenic agent, followed by a subsequent liver resection, leading to long-term survival.

Case presentation

In October 2019, a 66-year-old male presented with discomfort on the right side of his waist and was admitted to Jiaozhou Renmin Hospital, China. Initial ultrasound revealed hepatic space-occupying lesions. Subsequent contrast-enhanced computed tomography (CECT) and magnetic resonance imaging (MRI) of the abdomen conducted on 2019-10-22 confirmed multiple lesions in the inferior segment of the right liver lobe. Additionally, the CECT identified cirrhosis of the liver. Laboratory investigations revealed a positive hepatitis B virus (HBV) status with a viral load of 5.10 x 10^3 IU/mL and an alpha-fetoprotein (AFP) level of 41.56 ng/mL. No intervention was initiated.

On 2019-10-23, the patient was transferred to our hospital for detailed assessment and subsequent treatment. His medical history of hypertension or diabetes was unremarkable. Physical examination on arrival revealed a flat abdomen with mild right upper quadrant tenderness, although there was no evidence of weight loss or lymphadenopathy. The patient's Eastern Cooperative Oncology Group (ECOG) score was rated as 1. His liver function was categorised as Child–Pugh class A, with a blood alpha-fetoprotein (AFP) level of 41.28 ng/ml. A positron emission tomography-computed tomography (PET-CT) scan (Figure 1) on 2019-10-28 demonstrated an enlarged right hepatic lobe measuring 95 mm×56 mm. Multiple lymph node metastases around the pancreatic head region, posterior to the bilateral diaphragmatic crus and at T10 and T12 on the right side of the vertebral bodies were identified. Additionally, extrahepatic metastatic involvement was noted in the right erector spinae muscle and the T12 vertebral body. The diagnosis was established as Barcelona Clinic Liver Cancer (BCLC) stage C HCC (equivalent to China Liver Cancer [CNLC] stage IIIb) as shown in Figure 2.

Given his unresectable tumour, coupled with a Child–Pugh classification of A, a diagnosis of BCLC stage C and an ECOG-PS score of 1, a first-line treatment regimen was initiated for the patient, involving a combination of immunotherapy and targeted therapy. On 2019-10-30, the patient received 200 mg of sintilimab intravenously (on day one every three weeks) plus 200–400 mg BID of sorafenib orally, along with antiviral therapy (tenofovir disoproxil fumarate: 300 mg orally once a day).

After six treatment cycles, an evaluation conducted on 2020-05-21, revealed a significant therapeutic response. His disease achieved PR with a remarkable 60% reduction in the size of the target lesions, measured at 38 mm×23 mm according to RECIST criteria. Moreover, all extrahepatic metastases had been resolved, with the exception of a solitary lymph node metastasis adjacent to the T12 vertebra, measuring ~ 0.8 cm along its short axis with increased glucose metabolism (Figure 1). The patient's AFP levels had decreased substantially from 41.28 ng/ml to within the normal range (as shown in Figure 3A), while his liver function remained unimpaired. Furthermore, antiviral therapy had effectively reduced HBV-DNA levels to less than 1.0 x 10^2 IU/mL, and no adverse events (AEs) were reported during the course of the systemic treatment.

The patient continued the therapy for approximately one and a half years. A CT scan conducted on 2021-03-29, revealed a further reduction in the dimensions of liver lesions, now measuring 17 mm×28 mm. This significant response, amounting to a 70% reduction (deep response), along with the resolution of extrahepatic metastasis, prompted the consideration of surgical intervention. On 2021-04-26, a laparoscopic hepatectomy targeting segment 6 (S6) was performed under general anaesthesia. Post-operative pathological assessment confirmed HCC, with post-treatment response evident in the large necrotic area and negative resection margin. A small region of moderately differentiated HCC was encapsulated by fibrous tissue hyperplasia with hyaline degeneration and scattered inflammatory cell infiltration Figure 3B). During the post-operative period, no adverse events or complications were observed, and the patient's liver function remained within normal limits. The patient had an uneventful recovery, without the need for additional clinical intervention. A subsequent follow-up, including a PET-CT examination on 2021-04-26, revealed no clinical evidence of disease (Figure 4). Concurrently, analysis via CTCBIOPSY® unveiled a circulating tumour cell count of two per 5 mL of blood, which is considered to be at a level indicating less possibility of disease recurrence (Figure 5).

From April 2021 to October 2021, the patient sustained a combined regimen of sorafenib and sintilimab for approximately six months. At the follow-up on October 31, 2023, the patient showed no signs of disease recurrence and remained on anti-HBV therapy.

Discussion and conclusion

This report describes a case of HCC with extrahepatic metastasis, achieving complete remission with the combination of immunotherapy and anti-angiogenic therapy followed by laparoscopic hepatectomy. Although promising clinical outcomes

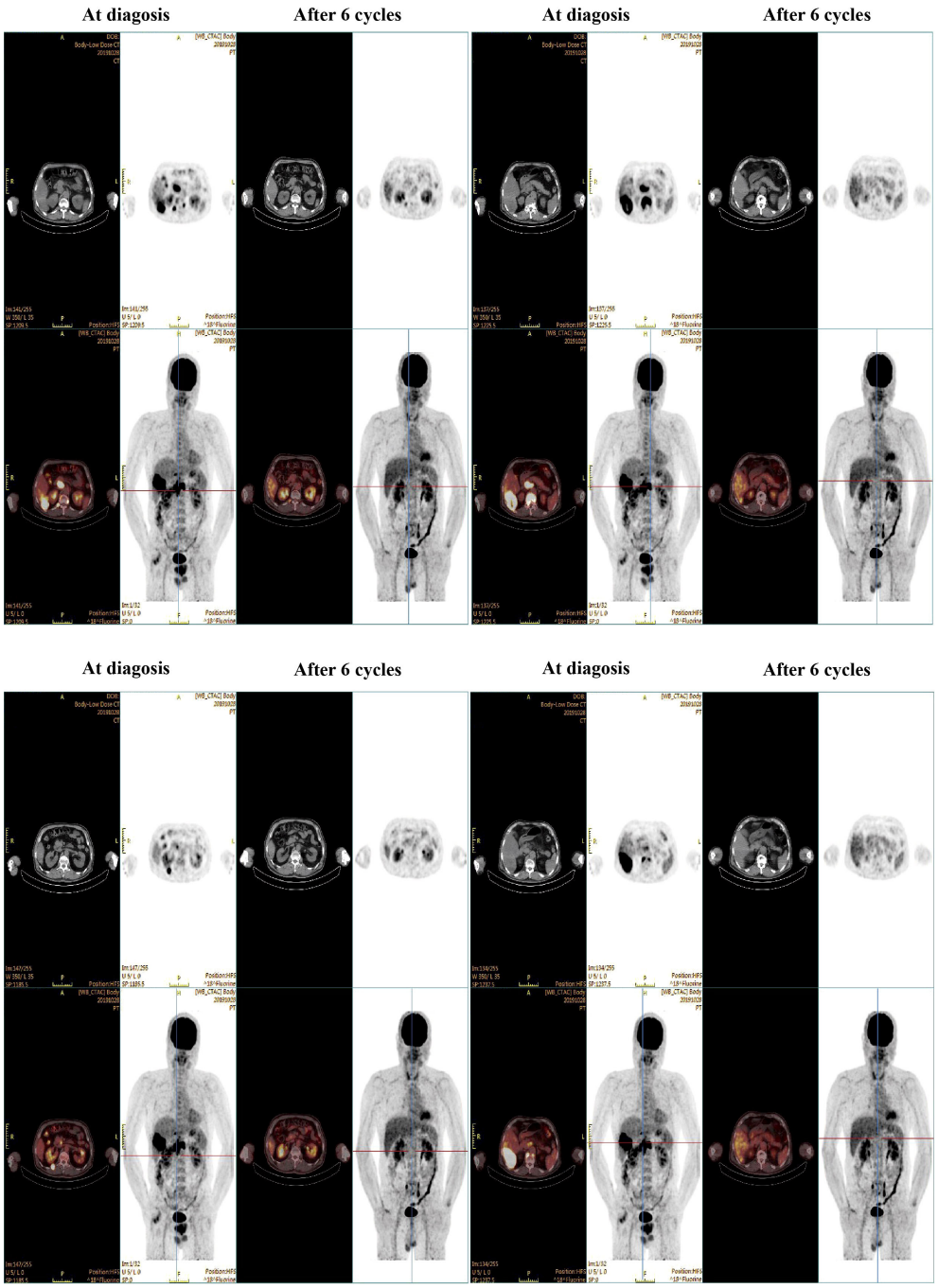

FIGURE 1
PET-CT scans at diagnosis and after 6 cycles of systemic therapy.

have been observed in advanced HCC patients without extrahepatic metastases (6–8), patients with BCLC stage C HCC typically rarely receive this treatment modality. The rationale is that widespread extrahepatic metastasis suggests extensive disease spread, making the successful resection of extra-hepatic metastases unlikely in an initial hepatectomy. In this specific case, the patient's disease was downstaged to an early phase of HCC, rendering the tumour amenable to R0 resection. Subsequent to the discontinuation of systemic therapy, the patient manifested a sustained period of disease-free and drug-free survival, spanning approximately two years. He has persevered for four years following the commencement of the treatment regimen. This case exemplifies the curative potential for this therapeutic strategy in treating advanced HCC, even in cases with extrahepatic metastasis.

Specific predictive biomarkers have been correlated with the efficacy of this treatment strategy. A deep response to the systemic therapy is of potential as one of the indicators suitable for later liver resection with curative intention. For our case, the systemic therapy led to resolved extrahepatic metastasis, with a notable response denoted by a target lesion reduction to 70%. Furthermore, the

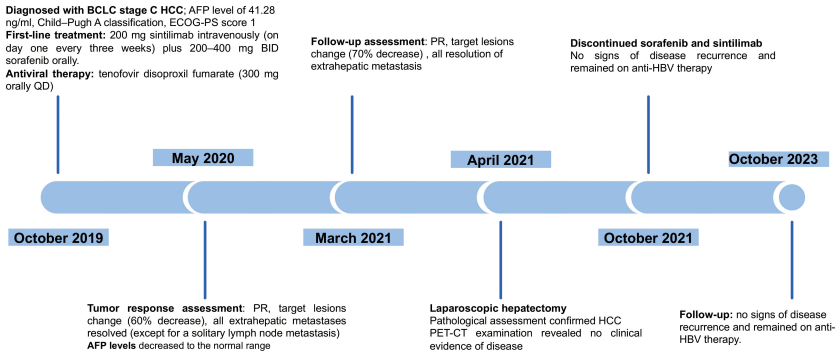

FIGURE 2
A schematic of course of disease management.

presence of pre-existing CD8 cells has been recognised as a promising biomarker for gauging the response to treatment with Lenvatinib in combination with anti-PD-1 antibodies (9). Pathological complete response (pCR) has been correlated with favourable outcomes. In our case, the patient did not achieve a pCR according to the hepatological assessments after surgery, thereby suggesting a relatively elevated likelihood of recurrence compared to patients who achieve a pCR. Consequently, a monitoring method – a CTC test – was applied in our case. It has been reported that the mOS was much shorter in the CTC-positive population with HCC, which was also associated with poorer clinical characteristics (10, 11). In our case, the patient's CTC test results were negative; according to the study by Zhou (12), this indicates a relatively low possibility of disease recurrence.

In addition, for those achieving pCR, the guidance for resection might be informed by CTC or ctDNA-driven minimal residual disease. Over-extensive resection of non-cancerous liver tissue may result in liver dysfunction, accompanied by associated conditions such as ascites, jaundice and hypoalbuminemia. Using CTC or ctDNA, liver resection might be avoided for this population. A recent study reported that among five patients who had achieved a complete remission, three had undergone an R0 resection and have remained free of disease up to the latest follow-up (13). On the other hand, a 'watch and wait' approach was chosen by the other two patients. They have sustained a disease-free condition for 7.6 and 19.7 months, respectively. In addition, a current randomised trial in China is assessing the efficacy of surgical resection following systemic treatment with atezolizumab combined with bevacizumab (14). This trial aims not only to reveal the value of hepatectomy in this treatment strategy but also to discern which patients might benefit most from sequential hepatectomy, thereby reducing unnecessary surgeries.

Further investigation for this treatment strategy in advanced HCC is warranted. First, in future studies, it is imperative to ensure a more heterogeneous participant demographic, particularly given that this treatment approach is not commonly applied to BCLC stage C HCC patients. Expanding the cohort to more comprehensively encompass individuals with advanced HCC will significantly bolster the external validity and generalisability of the research outcomes. Second, more evidence is needed to produce a consensus on the optimal timing for resection following successful conversion. According to recent data, within a median of 3.9 months following the onset of systemic therapy, 23.8% (24 out of 101 patients) underwent curative resection, resulting in an improved overall survival for these patients (15). For our case, the patient's disease achieved PR after six months of the systemic therapy. The interval to liver resection was notably longer: approximately 18 months after initiating systemic treatment. The decision to proceed with the resection earlier might have reduced the time that patients remained on systemic treatment. To

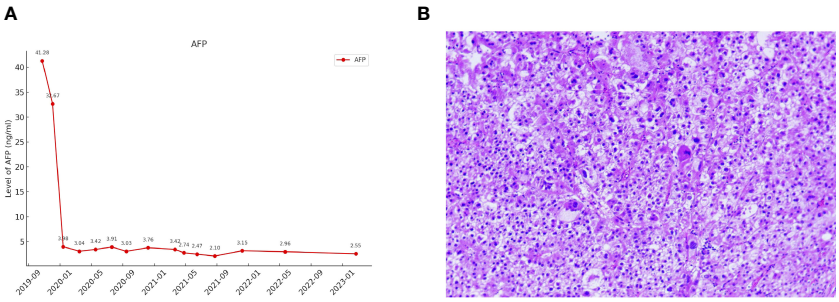

FIGURE 3
(A) The changes in AFP levels during the course of treatment. **(B)** Pathological features of the tumour lesion post-surgery (Hematoxylin and eosin stain, magnification ×200).

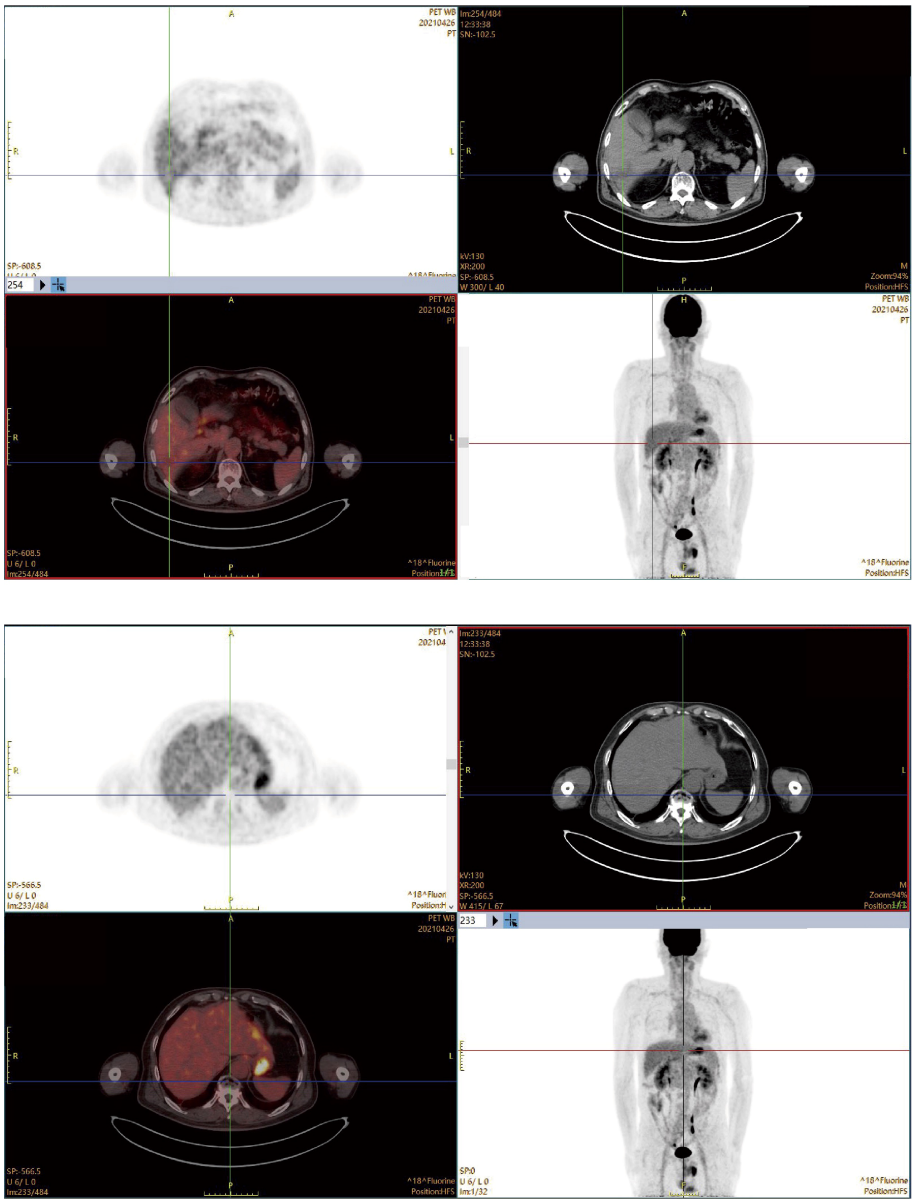

FIGURE 4
PET images showing no evidence of disease a month after the surgery.

effectively navigate the uncertainties surrounding the timing of surgical resection, it is imperative that forthcoming studies meticulously investigate the various factors that sway the clinical decision towards either an immediate or a postponed resection. Third, there is a need for focused research aimed at standardising the length of adjuvant therapy following resection. While comprehensive data are limited, insights from previous studies on adjuvant therapy suggested a postoperative adjuvant treatment duration exceeding six months. Further investigations should consider undertaking controlled trials to evaluate how varying durations of adjuvant therapy influence long-term patient outcomes. Such research could yield more definitive guidelines for clinicians in managing postoperative care. Last but not at least, not all patients may respond optimally to this primary treatment strategy. Therefore, exploring second-line treatment options will be imperative for those who experience disease progression or have suboptimal responses. It has been suggested that regorafenib and ramucirumab notably extend overall survival in comparison to placebos (16). Additionally, cabozantinib, regorafenib, ramucirumab, brivanib, axitinib and pembrolizumab demonstrated a significant enhancement in progression-free survival relative to placebos. However, given the limited efficacy of the current available second line treatments, further clinical trials are still warranted. A phase Ib/II clinical trial has recently shown promising efficacy: the confirmed ORR and disease control rate were 30% (95% CI, 14.6%-51.9%) from anti-ALK-1 monoclonal antibody plus nivolumab and BB as the second line treatment for relapsed advanced HCC patients (17).

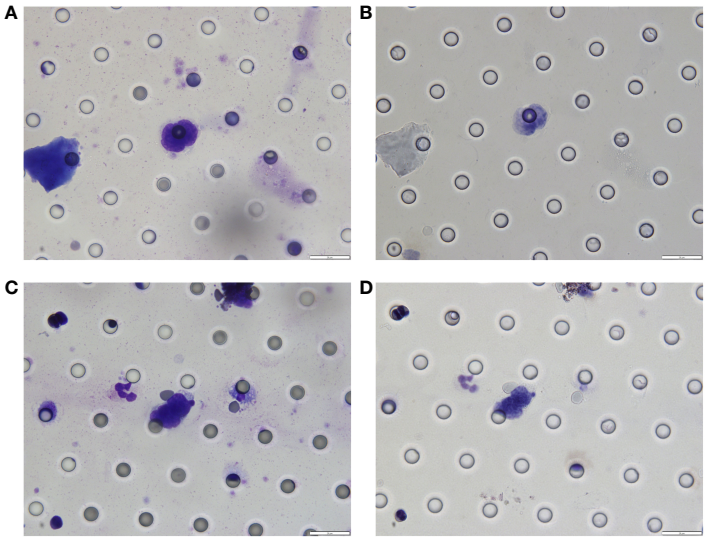

FIGURE 5
Identification of CTCs by CTCBIOPSY®.

In conclusion, this case presents a treatment strategy that successfully achieved complete remission in advanced HCC with extrahepatic metastasis, thereby extending its therapeutic efficacy to the complex cases involving extrahepatic spread.

Data availability statement

The original contributions presented in the study are included in the article/supplementary material. Further inquiries can be directed to the corresponding author.

Ethics statement

The studies involving humans were approved by Shandong cancer hospital ethics committee. The studies were conducted in accordance with the local legislation and institutional requirements. The participants provided their written informed consent to participate in this study. Written informed consent was obtained from the individual(s) for the publication of any potentially identifiable images or data included in this article.

Author contributions

KC: Data curation, Formal analysis, Funding acquisition, Writing – original draft, Writing – review & editing. ZL: Writing – original draft, Writing – review & editing. JZ: Writing – original draft, Writing – review & editing. XS: Writing – original draft, Writing – review & editing. LZ: Writing – original draft, Writing – review & editing. HL: Writing – original draft, Writing – review & editing. YM: Formal analysis, Writing – original draft, Writing – review & editing.

Funding

The author(s) declare financial support was received for the research, authorship, and/or publication of this article. The authors acknowledge financial support from the Wu Jieping Medical Foundation (Grant No. 320 .6750.2022-18-25) and Shandong province key research and development plan (2022CXGC020508) for the research, authorship, and publication of this article. The Foundation did not influence the study's design, data collection, analysis, interpretation, or the writing of the manuscript.

Acknowledgments

The authors thank the professional medical writing assistance provided for this publication by Beijing Sinuo Service.

Conflict of interest

The authors declare that the research was conducted in the absence of any commercial or financial relationships that could be construed as a potential conflict of interest.

Publisher's note

References

1. Sung H, Ferlay J, Siegel RL, Laversanne M, Soerjomataram I, Jemal A, et al. Global cancer statistics 2020: GLOBOCAN estimates of incidence and mortality worldwide for 36 cancers in 185 countries. *CA: Cancer J Clin* (2021) 71(3):209–49. doi: 10.3322/caac.21660

2. Zhang M, Jin W, Tian Y, Zhu H, Zou N, Jia Y, et al. Cancer burden variations and convergences in globalization: A comparative study on the tracheal, bronchus, and lung (TBL) and liver cancer burdens among WHO regions from 1990 to 2019. *J Epidemiol Global Health* (2023), 1–29. doi: 10.1007/s44197-023-00144-x

3. Kudo M, Finn RS, Qin S, Han KH, Ikeda K, Piscaglia F, et al. Lenvatinib versus sorafenib in first-line treatment of patients with unresectable hepatocellular carcinoma: a randomised phase 3 non-inferiority trial. *Lancet* (2018) 391(10126):1163–73. doi: 10.1016/S0140-6736(18)30207-1

4. Llovet JM, Ricci S, Mazzaferro V, Hilgard P, Gane E, Blanc JF, et al. Sorafenib in advanced hepatocellular carcinoma. *N Engl J Med* (2008) 359(4):378–90. doi: 10.1056/NEJMoa0708857

5. Lee MS, Ryoo B-Y, Hsu C-H, Numata K, Stein S, Verret W, et al. Atezolizumab with or without bevacizumab in unresectable hepatocellular carcinoma (GO30140): an open-label, multicentre, phase 1b study. *Lancet Oncol* (2020) 21(6):808–20. doi: 10.1016/S1470-2045(20)30156-X

6. Osgood C, Mulkey F, Mishra-Kalyani PS, Lemery S, Ward A, Keegan P, et al. FDA analysis of depth of response (DpR) and survival across 10 randomized controlled trials in patients with previously untreated unresectable or metastatic melanoma (UMM) by therapy type. *J Clin Oncol* (2019) 37(15_suppl):9508–. doi: 10.1200/JCO.2019.37.15_suppl.9508

7. Fucà G, Corti F, Ambrosini M, Intini R, Salati M, Fenocchio E, et al. Prognostic impact of early tumor shrinkage and depth of response in patients with microsatellite instability-high metastatic colorectal cancer receiving immune checkpoint inhibitors. *J Immunother Cancer* (2021) 9(4). doi: 10.1136/jitc-2021-002501

8. McCoach C, Blumenthal G, Zhang L, Myers A, Tang S, Sridhara R, et al. Exploratory analysis of the association of depth of response and survival in patients with metastatic non-small-cell lung cancer treated with a targeted therapy or immunotherapy. *Ann Oncol* (2017) 28(11):2707–14. doi: 10.1093/annonc/mdx414

9. Zhang W, Tong S, Hu B, Wan T, Tang H, Zhao F, et al. Lenvatinib plus anti-PD-1 antibodies as conversion therapy for patients with unresectable intermediate-advanced hepatocellular carcinoma: a single-arm, phase II trial. *J Immunotherapy Cancer* (2023) 11(9). doi: 10.1136/jitc-2023-007366

10. Yu JJ, Xiao W, Dong SL, Liang HF, Zhang ZW, Zhang BX, et al. Effect of surgical liver resection on circulating tumor cells in patients with hepatocellular carcinoma. *BMC cancer.* (2018) 18(1):835. doi: 10.1186/s12885-018-4744-4

11. Zhang Q, Rong Y, Yi K, Huang L, Chen M, Wang F. Circulating tumor cells in hepatocellular carcinoma: single-cell based analysis, preclinical models, and clinical applications. *Theranostics* (2020) 10(26):12060–71. doi: 10.7150/thno.48918

12. Zhou J, Zhang Z, Zhou H, Leng C, Hou B, Zhou C, et al. Preoperative circulating tumor cells to predict microvascular invasion and dynamical detection indicate the prognosis of hepatocellular carcinoma. *BMC cancer.* (2020) 20:1–10. doi: 10.1186/s12885-020-07488-8

13. Zhang B, Shi X, Cui K, Li Z, Li L, Liu Z, et al. Real-world practice of conversion surgery for unresectable hepatocellular carcinoma - a single center data of 26 consecutive patients. *BMC Cancer.* (2023) 23(1):465. doi: 10.1186/s12885-023-10955-7

14. Sun H-C, Shen F, Liu L, Huang Z-Y, Song T, Kuang M, et al. TALENTop: A multicenter, randomized study evaluating the efficacy and safety of hepatic resection for selected hepatocellular carcinoma with macrovascular invasion after initial atezolizumab plus bevacizumab treatment. *J Clin Oncol* (2022) 40(16_suppl): TPS4175–TPS. doi: 10.1200/JCO.2022.40.16_suppl.TPS4175

15. Zhu XD, Huang C, Shen YH, Xu B, Ge NL, Ji Y, et al. Hepatectomy after conversion therapy using tyrosine kinase inhibitors plus anti-PD-1 antibody therapy for patients with unresectable hepatocellular carcinoma. *Ann Surg Oncol* (2023) 30 (5):2782–90. doi: 10.1245/s10434-022-12530-z

16. Solimando AG, Susca N, Argentiero A, Brunetti O, Leone P, De Re V, et al. Second-line treatments for advanced hepatocellular carcinoma: A systematic review and bayesian network meta-analysis. *Clin Exp Med* (2022) 22(1):65–74. doi: 10.1007/s10238-021-00727-7

17. Hsu C, Chang Y-F, Yen C-J, Xu Y-W, Dong M, Tong Y-Z. Combination of GT90001 and nivolumab in patients with advanced hepatocellular carcinoma: a multicenter, single-arm, phase 1b/2 study. *BMC Med* (2023) 21(1):395. doi: 10.1186/s12916-023-03098-w

frontiers | Frontiers in Oncology

TYPE Case Report
PUBLISHED 06 February 2024
DOI 10.3389/fonc.2024.1297140

OPEN ACCESS

EDITED BY
Simona Gurzu,
Sciences and Technology of Târgu Mureş, Romania

REVIEWED BY
Prit Benny Malgulwar,
University of Texas MD Anderson Cancer Center, United States
Ahmad Alshomrani,
University of Nebraska Medical Center, United States

*CORRESPONDENCE
Shujing Guo
1013821977@qq.com
Yuhan Ye
406134632@qq.com
Zhengjin Liu
862501056@qq.com

RECEIVED 19 September 2023
ACCEPTED 10 January 2024
PUBLISHED 06 February 2024

CITATION
Lin Z, Li Q, He Y, Guo S, Ye Y and Liu Z (2024) Case report: Gastric carcinoma with SMARCA4 deficient: two cases report and literature review.
Front. Oncol. 14:1297140.
doi: 10.3389/fonc.2024.1297140

Case report: Gastric carcinoma with SMARCA4 deficient: two cases report and literature review

Zeyang Lin[1], Qian Li[1], Yujie He[2], Shujing Guo[1*], Yuhan Ye[1*] and Zhengjin Liu[1*]

[1]Department of Pathology, Zhongshan Hospital of Xiamen University, School of Medicine, Xiamen University, Xiamen, China, [2]Lianqian Street Community Health Service Center, First Affiliated Hospital of Xiamen University, Xiamen, China

SMARCA4-deficient gastric carcinoma has been reported sporadically since 2016. Only 29 patients have been reported; nevertheless, it is aggressive and highly malignant with poor outcomes. It has an immunohistochemical phenotype showing loss of SMARCA4 expression and can be accompanied by codeletion of other switch/sucrose non-fermentable chromatin-remodeling complex subunits. Microscopically, it displays high-grade undifferentiated histological morphology with rhabdoid cell differentiation. Rarely does the tumor contain a purely or partly adenocarcinoma component. Here, we report two cases to demonstrate these unusual morphologies analyzed using morphological and immunohistochemical techniques. In addition, there is a lack of research on the classification of these morphologies. Therefore, our report will aid the diagnosis and classification of SMARCA4-deficient gastric carcinoma.

KEYWORDS

SMARCA4, gastric carcinoma, category, therapy, case

1 Introduction

Undifferentiated gastric carcinoma is a primary tumor without specific cytological or architectural types of differentiation (1). Expression of switch/sucrose non-fermentable (SWI/SNF) chromatin-remodeling complex subunits is reportedly deficient in some cases; these subunits include SMARCA4, SMARCA2, SMARCB1, and ARID1A. SMARCA4-deficient undifferentiated carcinomas (SD-UCs) are rare and were described first in 2016 by Agaimy et al. (2) The morphological features are solid, diffuse sheets of polygonal cells with pleomorphic giant cells. These cells have vesicular nuclei and a high degree of mitosis, which are poorly cohesive. A rhabdoid cell component is common and may be the predominant pattern. Because rhabdoid cells are a diagnostic clue, the terminology undifferentiated/rhabdoid carcinoma was proposed by Chang et al. (3) A few cases of

SMARCA4-deficient undifferentiated gastric carcinoma were reported demonstrating glandular differentiation or encompassing adenocarcinoma. According to the fifth World Health Organization (WHO) classification of the digestive system, undifferentiated gastric carcinoma is a malignant epithelial tumor composed of anaplastic cells with no specific cytologic or architectural differentiation, including glandular, squamous, neuroendocrine, and sarcomatoid differentiation (1). In this context, "dedifferentiated carcinoma" was recommended for cases with adenocarcinoma components (3). There are also SMARCA4-deficient adenocarcinomas (SD-ADs), as we and Huang described (4). SMARCA4-deficient gastric carcinoma can be classified as SD-UC, where all components are undifferentiated, except the adenocarcinoma portion, according to the WHO. SMARCA4-deficient dedifferentiated carcinoma (SD-DC) is the term used for tumors with adenocarcinoma components. SD-AD is used for cases comprising purely adenocarcinoma components. These tumors are then categorized as well, moderately, or poorly differentiated based on the percentage of glandular components. Although, the latter two are not included in WHO classification.

The three subtypes have different immunophenotypes; panCK, SMARCA2, and E-cadherin are positive in adenocarcinoma areas; the opposite is true in undifferentiated areas. Attention should be paid to discriminating among the three subtypes to classify these unusual tumors.

2 Methods

Cases from Zhongshan Hospital of Xiamen University were reviewed, and the diagnosis of SD-DC and SMARCA4-deficient poorly differentiated adenocarcinoma was confirmed separately. All specimens were fixed with 3.7% neutral formaldehyde, dehydrated, paraffin-embedded, and cut into 4-μm serial sections. The sections were subjected to hematoxylin and eosin and immunohistochemical staining. The latter was performed using a two-step EnVision method. The primary antibodies included SMARCA4 (BRG1), SMARCB1 (INI-1), broad-spectrum cytokeratin (panCK), vimentin, cytokeratin (CK) 7, E-cadherin, CD34, CD56, synaptophysin (Syn), chromogranin A (CgA), spalt-like transcription factor 4 (SALL-4), Ki-67, p53, alpha-fetoprotein (AFP), and hepatocyte paraffin 1 (Hepa-1) and were purchased from Fuzhou Maixin Biotechnology Ltd. SMARCA2 (BRM) (Clone number ARC59944) was purchased from Abclonal Biotechnology, Ltd.

3 Case presentation

3.1 Case 1

A 65-year-old man presented to the Department of Gastroenterology, Zhongshan Hospital of Xiamen University, with a one-month history of indigestion after meals accompanied by pain in the right upper abdomen without any known inducement. Gastroduodenoscopy revealed a cauliflower-like mass with an ulcer in the cardia of the stomach (Figure 1A), and a biopsy was performed.

The pathological findings revealed a malignant tumor of epithelial origin. A glandular adenocarcinoma arose from the normal epithelium. High-grade intraepithelial neoplastic was present. There were features of differentiated, moderately differentiated, and poorly differentiated adenocarcinoma (Figure 1B). Cells had large round to oval nuclei and coarse chromatin. The mitosis index was 15/2 mm^2 (Figure 1C). None of the tumor expressed SMARCA4 (Figure 1D). However, panCK (Figure 1E), CK7, SALL4, E-cadherin (Figure 1F), SMARCB1, and SMARCA2 (Figure 1G) were strongly positive. Synaptophysin was weakly positive. P53 was diffusely expressed. The tumor was negative for CD34, CgA, CD56, AFP, and Hepa-1. The tumor was finally diagnosed as SMARCA4-deficient poorly differentiated adenocarcinoma.

Computed tomography revealed liver and lymphatic metastases. After careful consideration, the patient and his family chose not to undergo further treatment. Clinical follow-up was available, and the patient was still alive more than 3 months from the date of diagnosis.

3.2 Case 2

A 75-year-old man presented with persistent hematochezia and melena associated with peripheral neuropathy and abdominal pain for over a month. Gastroduodenoscopy revealed a large mass occupying 50% of the antrum. Computed tomography revealed no lymphatic metastases. He was diagnosed with a malignant gastric tumor at another hospital. He was transferred to Zhongshan Hospital of Xiamen University and underwent gastrectomy.

The pathological findings revealed an elevated solid mass measuring 6.3 cm × 5.1 cm × 1.2 cm (Figure 2A) in the antrum next to the pylorus.Microscopically, the tumor invaded the muscularis propria of the gastric wall. It abruptly transitioned from the normal epithelium (Figure 2B). Two components were differentiated. One was a poorly differentiated adenocarcinoma with gland formation (Figure 2C). The other was an undifferentiated carcinoma with diffuse sheets of polygonal and pleomorphic giant cells. Cells were discohesive. Rhabdoid cells were common; these cells had conspicuous vesicular nucleoli (Figure 2D). Both carcinomas lost expression of SMARCA4 (Figure 2E) but were positive for SMARCB1, P53, and SALL4. They were negative for CgA, CD56, and CD34. Synaptophysin was weakly positive. The poorly differentiated adenocarcinoma expressed SMARCA2 (Figure 2F), panCK (Figure 2G), and E-cadherin (Figure 2H) but lost vimentin (Figure 2I). The undifferentiated carcinoma expressed vimentin but lost E-cadherin and showed reduced expression of panCK and SMARCA2. The tumor was finally diagnosed as SD-DC (T2N0M0).

He did not receive chemotherapy, immune checkpoint inhibitors, or targeted therapy because of his poor physical condition. Follow-up was performed, and the patient was alive after over five months.

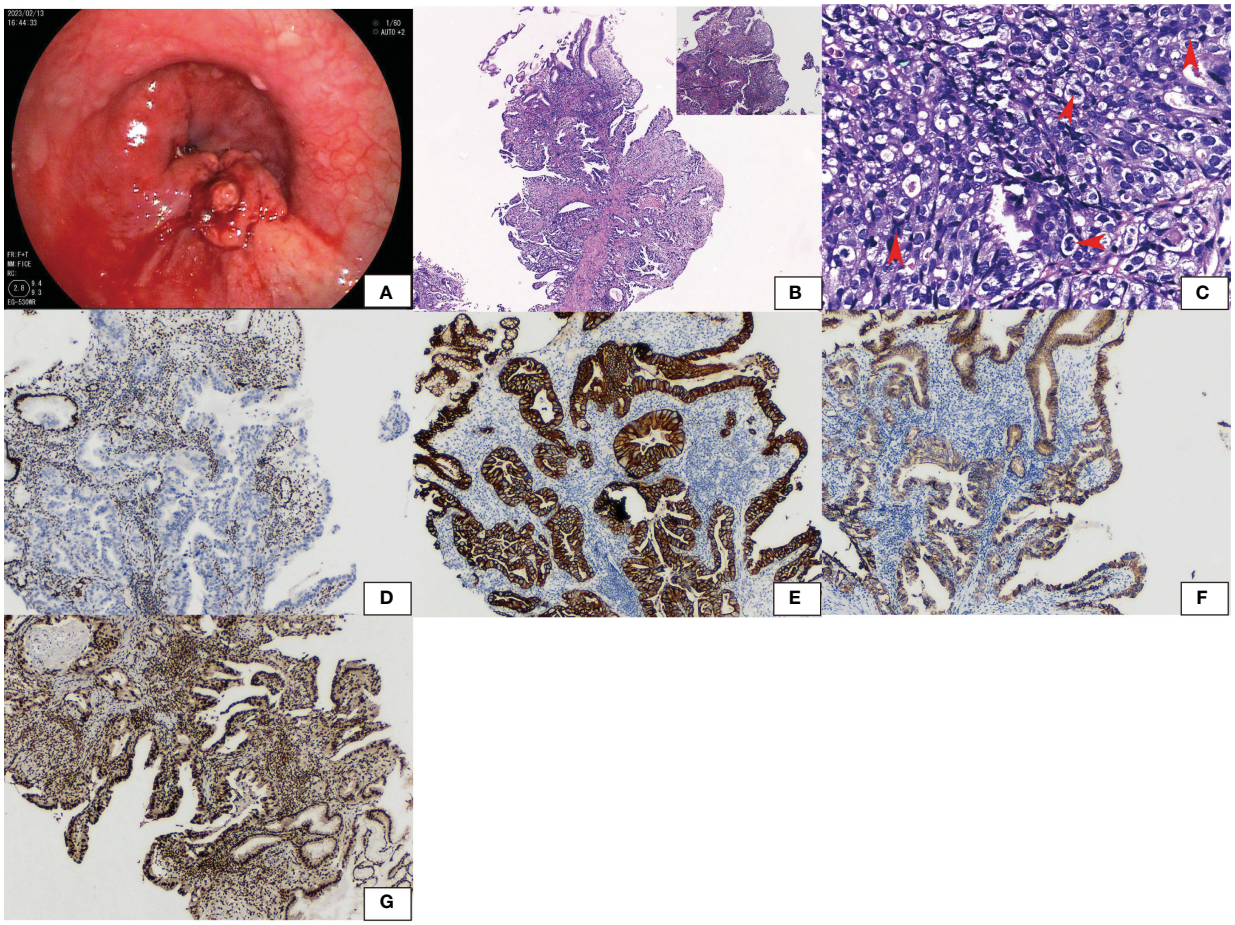

FIGURE 1
Gastroduodenoscopy showed **(A)** a cauliflower-like tumor with an ulcer in the cardia. **(B)** Hematoxylin and eosin staining showed glandular adenocarcinoma gradually transferred from the normal epithelium. High-grade intraepithelial neoplastic was seen with differentiated, moderately differentiated, and poorly differentiated adenocarcinoma. **(C)** Cells had large round to oval nuclei and coarse chromatin. The degree of mitosis was high (arrow). **(D)** Immunohistochemical staining revealed that SMARCA4 was lost in tumors while normal epithelium was retained. **(E)** PanCK, **(F)** E-cadherin, and **(G)** SMARCA2 were both positive.

3.3 Literature review

We retrieved data for "(SMARCA4) AND (gastric carcinoma)" on PubMed and found 29 reported patients described in nine studies (2–10) (Table 1), namely, 22 (76%) men and seven (24%) women aged 30–75 years (average: 62.3 years). The neoplasm sites (excluding seven patients with no description) from most to least common were the body (10/22), antrum (7/22), fundus (1/22), cardia (1/22), and angle (1/22); the remaining two involved several sites, including the cardia, fundus, and body. Tumor size ranged from 4 cm to 14 cm (average: 7.3 cm), and nine cases were not described. Metastatic lymph nodes were found in 81% (22/27), and other metastases in 30% (7/23). There were 78% (18/29) stage III or IV cases. The median overall survival was 9 months (2–190.1 months). The histomorphology varied and included diffuse sheets, nests, abortive gland lumens, and tubules of anaplastic epithelioid cell sand scattered rhabdoid multinucleated giant cells. The tumors with sheets were predominant, presenting an undifferentiated pattern in 50% (12/24). Partly glandular or mixed and dedifferentiated carcinoma occurred in 25% (6/24). Tumors with pure nests or diagnosed tubular adenocarcinoma and solid adenocarcinoma occurred in 25% (6/24) (Table 2). These tumors were classified according to histomorphology. Although they were not significantly different in clinical characteristics by existing limited data, they had different histomorphology and immunophenotypes. Interestingly, we found SMARCA2 only strongly expressed in adenocarcinoma, irrespective of subtype (Table 1). Chang (3) and Huang (4) also performed SMARCA2 staining and found it only in the adenocarcinoma areas but not in undifferentiated carcinoma.

4 Discussion

SMARCA4 is located on chromosome 19p13 and encodes the transcription activator BRG1. It is an ATP-dependent catalytic subunit of SWI/SNF chromatin-remodeling complexes that regulate chromatin structure and gene expression by supplying energy (11). The SWI/SNF chromatin-remodeling complexes usually consist of 12–15 proteins, including ATPase subunits

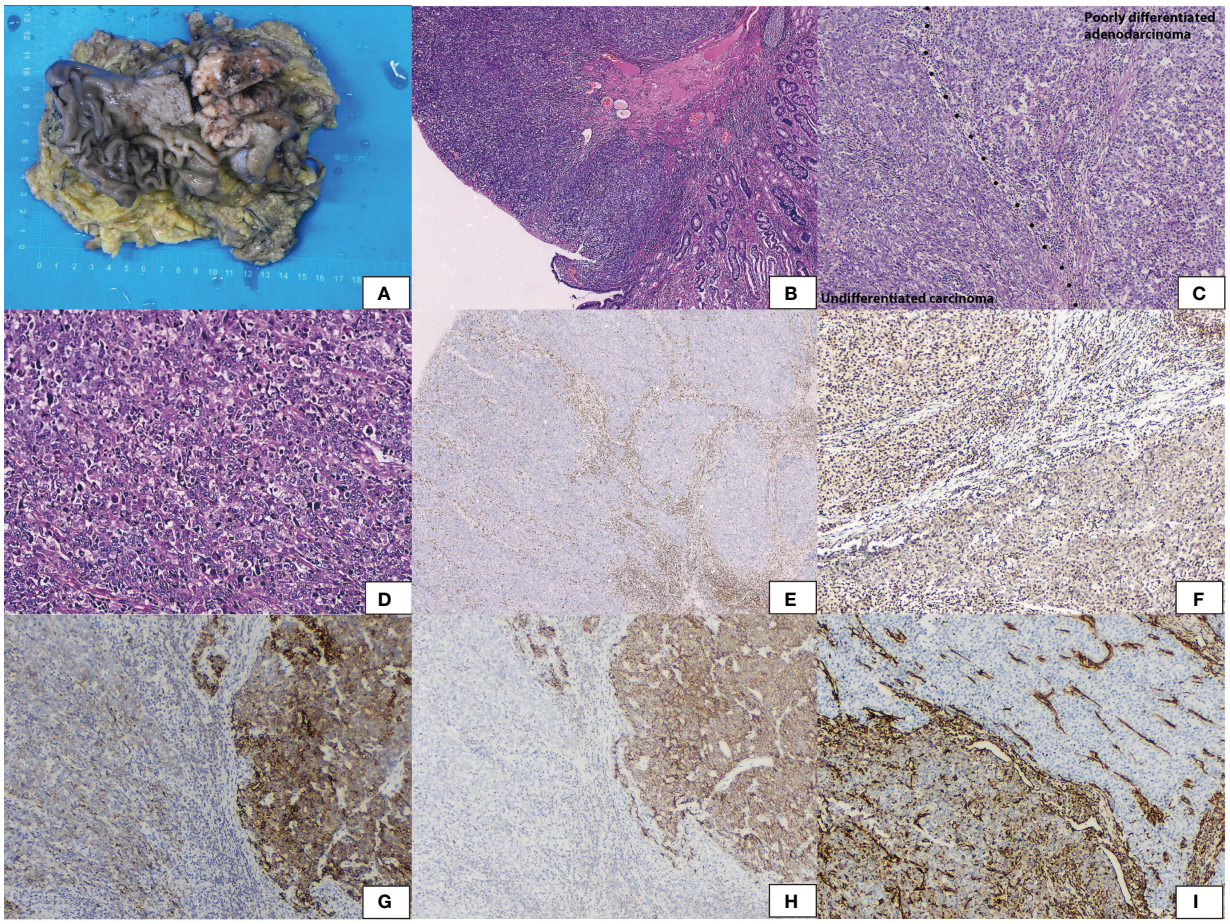

FIGURE 2
Gross appearance showed **(A)** an elevated solid mass, sized 6.3 cm × 5.1 cm × 1.2 cm in the antrum. **(B)** Hematoxylin and eosin staining showed the tumor abruptly transferred from the normal epithelium. **(C)** The tumor encompassed two components with a clear-cut surface. Poorly differentiated adenocarcinoma with gland formation and undifferentiated carcinoma with diffuse sheets without epithelial differentiation. **(D)** Undifferentiated carcinoma of polygonal cells and pleomorphic giant cells. Rhobdoid cells were common with vesicular nuclei and conspicuous nucleoli. **(E)** Immunohistochemical staining revealed both areas lost SMARCA4. **(F)** SMARCA2 was positive in poorly differentiated adenocarcinoma and was reduced in undifferentiated carcinoma. **(G)** PanCK was positive in poorly differentiated adenocarcinoma and was reduced in undifferentiated carcinoma. **(H)** E-cadherin was positive in poorly differentiated adenocarcinoma and lost in undifferentiated carcinoma. **(I)** Vimentin was positive in undifferentiated carcinoma and lost in poorly differentiated adenocarcinoma.

(SMARCA4 and SMARCA2), core subunits (SMARCB1, SMARCC1, and SMARCC2), and various regulatory subunits (ARID1A, ARID1B, and ARID2). The essential diagnostic criteria of SMARCA4-deficient undifferentiated tumor depend on the detection of SMARCA4 (BRG1) deficiency by immunohistochemistry but not a genetic diagnosis (12). Sequencing can be helpful to clarify the significance of reduced expression of SMARCA4, but it is not necessary for the diagnosis, because immunohistochemistry shows complete loss in most cases and is sufficient to document SMARCA4 deficiency. In addition, the mutation may not be detectable, depending on the limitations of the methods used. Because the second hit often copy-neutral loss heterozygosity (i.e., accompanied by duplication of the mutated allele) (13).

SMARCA4 loss is characteristic of thoracic sarcomas but, now, it represents primarily undifferentiated and dedifferentiated carcinomas rather than primary thoracic sarcomas (13). It has been sporadically identified in human carcinomas in a variety of regions, including endometrioid adenocarcinoma, non-small cell lung carcinoma, carcinoma of the sinonasal tract, and small cell carcinoma of the ovary-hypercalcemic type (14). SMARCA4-deficient carcinoma has an extremely low incidence. A literature search on SMARCA4-deficient gastric carcinoma returned 29 cases. Huang et al. screened SMARCA4 alterations using immunohistochemistry on 1,199 surgically resected gastric carcinomas and, in only six (0.5%), SMARCA4 was completely lost (4).

We reported two cases and reviewed the literature to classify these rare tumors. The clinicopathological features of our cases and reported cases were as follows (1): The tumor often occurred in middle-aged and older patients, 30–75 years old (average age: 62.3 years). Males predominated (77% [20/26]), and the clinical stages were III or IV in 78% (18/23). There was rapid progression and poor outcomes; the median overall survival was 8 months (3–190.1 months). The effect of conventional chemotherapy was poor (2). Histomorphologically, the tumors demonstrated sheets, trabecular, solid, nest, abortive gland, tubular distribution, and large epithelioid

TABLE 1 Clinical characteristics reported in SMARCA4-deficient gastric carcinoma.

No	References	Age/sex	Site	Size (cm)	TNM/metastasis	Treatment	Survival (month)	SMARCA2 expression
1	Agaimy (2)	75/M	Gastric posterior wall	8	Peritoneal and lymph node IV	Resection	NA	Reduced
2	Chang (3)	74/M	Gastric cardia fundus body	8.0	T4N3M1 IV	Resection target therapy	9	–
3		64/M	Gastric angle	NA	T4N3M1 IV	Chemotherapy	3	NA
4		57/M	Gastric antrum	NA	TxNxM1 IV	None	NA	NA
5		58/M	Gastric antrum	NA	T3N2M0 IIIA	Resection chemotherapy	14	NA
6		46/M	Gastric body	NA	TxNxM1 IV	NA	5	+
7		30/M	Gastric body	8	T3N1M0 IIB	Resection chemotherapy	3	–
8	Huang (4)	63/M	Gastric stump	7.5	T3N2M0 IIIA	NA	16.3	Heterogeneous
9		67/F	Gastric body	6.4	T4bN1M0 IIIB	NA	14.2	+
10		76/F	Gastric cardia	4.4	T4aN3bM0 IIIC	NA	4.4	–
11		46/F	Gastric antrum	4.5	T3N1M0 IIB	NA	190.1	–
12		72/M	Gastric antrum	5	T4aN2M0 IIIA	NA	23.7	+
13		62/F	Gastric body	8	T4aN1M0 IIIA	NA	26.4	–
14	Wu (5)	49/M	Gastric body	NA	IV	Resection chemotherapy PD1 immunotherapy target therapy	> 12	NA
15		66/M	Gastric body	NA	IV	Chemotherapy PD1 immunotherapy	> 10	NA
16		64/M	Gastric body antrum	NA	IV	Chemotherapy	2	NA
17		72/F	Gastric body antrum	NA	IV	NA	3	NA
18		72/M	Gastric fundus	NA	NA	NA	Miss	NA
19	Zhang (6)	55/F	Gastric antrum	4	T2N2M0 IIB	NA	11.57	–
20		57/M	Gastric body	8	T4bN0M0 IIIA	NA	8.13	–
21		71/F	Gastric antrum	14	T3N1M0 IIB	NA	5.73	–
22	Chen (7)	76/M	Gastric antrum	9	T4aN3M0 III	Resection chemotherapy	> 18	NA
23	Jin (8)	75/M	Gastric	NA	T4aN2M0 IIIA	Resection	NA	NA

(Continued)

TABLE 1 Continued

No	References	Age/sex	Site	Size (cm)	TNM/metastasis	Treatment	Survival (month)	SMARCA2 expression
24		75/M	Gastric	NA	T4aN1M0 IIIA	Resection	NA	NA
25		67/M	Gastric	NA	T4bN2M1 IV	NA	NA	NA
26		48/M	Gastric	NA	T4aN2M1 IV	NA	NA	NA
27		51/M	Gastric	NA	T3N0M0 IIA	Resection chemotherapy PD1 immunotherapy	> 7	NA
28	Wang (9)	74/M	Gastric cardia, fundus and body	8	T4aN5M0 III	Resection chemotherapy	8	–
29	Lin (10)	59/M	Gastric body	7	NA	Resection	NA	NA
30	This study	65/M	Gastric cardia	NA	NA	NA	> 3	+
31	This study	75/M	Gastric antrum	6.3	T2N0M0 IIA	Resection	> 5	Reduced

NA, not available; M, male; F, female; +, positive; –, negative.

or rhabdoid cells with low adhesion. Anaplastic cells had vesicular nuclei, prominent nucleoli, and high mitosis indexes (3). All tumors lost SMARCA4 expression; panCK was negative, and SMARCA2 was reduced or lost in the undifferentiated carcinomas. SMARCA2 was expressed in epithelial differentiation. In our cases, differentiated adenocarcinoma expressed SMARCA2, panCK, and E-cadherin but lost vimentin. The undifferentiated carcinoma expressed vimentin and but lost E-cadherin and showed reduced panCK and SMARCA2.

Considering the histomorphology and histochemistry phenotype, we propose a new category: SMARCA4-deficient gastric carcinoma, which may be divided into three subtypes (1): SD-UC, demonstrating diffuse sheets without epithelioid differentiation. Rhabdoid cells occur frequently and may be prominent. There are discohesive cells with anaplastic features. SMRCA2, E-cadherin, and epithelioid markers are negative or reduced, but vimentin is positive (2). SD-DC, demonstrating partly adenoid differentiation in SD-UC, as Chang (3) recommended. The adenocarcinoma areas express epithelioid markers, E-cadherin, and SMARCA2 but are negative for vimentin. The opposite is seen in the undifferentiated areas (3). SD-AD, encompassing purely gland, abortive glands, or nests like conventional adenocarcinoma without rhabdoid or discohesive cells. Epithelioid markers, E-cadherin, and SMARCA2 are positive.

Vimentin and E-cadherin are markers of epithelial-mesenchymal transition expressed in the undifferentiated and glandular areas, respectively, in SD-DC. In our cases, a novel observation in SD-DC was the notable loss of SMARCA2 in the transition from adenocarcinoma to undifferentiated carcinoma. In the reported literature, we also found SMARCA2 expressed in the adenocarcinoma areas in SMARCA4-deficient carcinoma. This finding suggests that SMARCA2 expression changes in the transition to SMARCA4-deficient carcinomas, as Rekhtman proposed (13).

Diagnosing this rare entity is often challenging and relies on an extensive panel of immunohistochemical stains to exclude various morphologic mimics such as neuroendocrine carcinoma, melanoma, and small cell carcinoma of the ovary-hypercalcemic type.

4.1 Large cell neuroendocrine carcinoma

Tumors are solid with nests or pseudoglandular epithelioid monoclonal and adhesive cells. It expresses epithelioid markers and at least two neuroendocrine markers. SD-UC may express synaptophysin, mainly focal or weakly positive.

4.2 Melanoma

Immunohistochemical detection of HMB45, Melan-A, and S-100 is helpful.

4.3 SMARCA4-deficient malignant rhabdoid tumors

These tumors show substantial overlap in histomorphology and immunohistochemistry. Malignant rhabdoid tumors predominantly occur in children under 3 years old.

4.4 Metastatic small cell carcinoma of the ovary-hypercalcemic type

This tumor displays unique immune features, including the expression of Wilms' tumor suppressor gene 1, EMA, vimentin, cytokeratin, and neuroendocrine markers.

TABLE 2 Morphological characteristics of reported SMARCA4-deficient gastric carcinoma.

No	Gross	Patterns	Cytology
1	Ulcerated transmural	Partly abortive gland lumens and mucinous differentiation	Anaplastic rhabdoid
2	Giant invasive ulcerated	Big nests and sheets (40%), poor cohesive pseudoglandular (45%), cords (5%), small solid nests (5%), and irregular adenoid pattern without definite lumen formation (5%)	Epithelioid tumor cells Scattered multinucleated giant cells
3	NA	Diffused sheets (> 95%) and cords (< 5%)	Epithelioid tumor cells, with focal clear cell cytoplasm (10%)
4	Ulcerated	Nests (100%)	Epithelioid tumor cells, with focal clear cell cytoplasm (20%)
5	Ulcerated	Diffuse sheets (75%) Poor cohesive nests (25%)	Epithelioid tumor cells Scattered multinucleated giant cells
6	NA	Nests (100%)	Epithelioid tumor cells
7	Endophytic	Undifferentiated component	Rhabdoid tumor cells
8	NA	Tubular adenocarcinoma	NA
9	NA	Tubular adenocarcinoma	NA
10	NA	Mixed carcinoma	NA
11	NA	Solid adenocarcinoma	NA
12	NA	Solid adenocarcinoma	NA
13	NA	Undifferentiated rhabdoid features	NA
14	NA	NA	NA
15	NA	NA	NA
16	NA	NA	NA
17	NA	NA	NA
18	NA	NA	NA
19	NA	Dedifferentiated	NA
20	NA	Dedifferentiated	Undifferentiated cell
21	NA	Undifferentiated	Undifferentiated cell
22	Ulcerative	Undifferentiated	Rhabdoid appearance
23	NA	Diffuse sheet	Anaplastic cell with rhabdoid feature
24	NA	Diffuse sheet	Anaplastic cell with rhabdoid feature
25	NA	Diffuse sheet	Anaplastic cell with rhabdoid feature
26	NA	Diffuse sheet	Anaplastic cell with rhabdoid feature
27	NA	Diffuse sheet +20% glandular	Anaplastic cell with rhabdoid feature
28	Ulcerative	Diffuse sheet	Epithelioid cell with rhabdoid feature
29	Protuberant	Sheet	Round to epithelioid undifferentiated cells
30	Protuberant	Tubular (30%) and nest (70%) with glandular differentiation	Anaplastic epithelioid cell
31	Protuberant	Nest (50%) with glandular differentiation and diffuse sheet (50%)	Anaplastic epithelioid cell and rhabdoid cell

NA, not available.

SMARCA4-deficient gastric carcinoma is aggressive and resistant to traditional chemotherapy. Based on the antagonism of SWI/SNF and polycomb repressive complex2 (PRC-2), SWI/SNF deletion leads to loss inhibition of enhancer of zeste homolog 2 (EZH2) methyltransferase, which accelerates PRC2-mediated tumorigenesis (15). Urgent, efficient therapy is required. Tazemetostat is a small molecule enhancer of the EZH2 inhibitor approved by the U.S. Food and Drug Administration in 2020 for treating INI1-negative or SMARCA4-negative tumors. Tazemetostat reduces the trimethylation of H3K27 and induces durable tumor responses. Data from a phase I clinical trial of EZH2 inhibitors showed clinical activity consisting of objective responses (complete responses and partial responses) or prolonged stable disease (6.4 to > 20 months), which exceeded 2 years in 5 (38%) of 13 patients with INI1-negative or SMARCA4-negative solid tumors (16).

In conclusion, SMARCA4-deficient gastric carcinoma should be divided into three subtypes: SD-UC, SD-DC, and SD-AD, depending on histomorphology and immunophenotype. Even though they have no significant clinical characteristics, they have different histomorphology and immunohistochemistry. We must recognize these subtypes and collect more cases to characterize SMARCA4-deficient gastric carcinoma.

Data availability statement

The original contributions presented in the study are included in the article/supplementary material. Further inquiries can be directed to the corresponding authors.

Ethics statement

The studies involving humans were approved by The Ethics Committee of the Affiliated Zhongshan Hospital, Xiamen

University. The studies were conducted in accordance with the local legislation and institutional requirements. The participants provided their written informed consent to participate in this study. Written informed consent was obtained from the individual(s) for the publication of any potentially identifiable images or data included in this article.

Author contributions

ZYL: Funding acquisition, Writing – original draft, Writing – review & editing. QL: Data curation, Conceptualization, Writing – review & editing, Validation. YH: Data curation, Conceptualization, Writing – review & editing, Investigation, Software. SG: Data curation, Investigation, Conceptualization, Writing – review & editing. YY: Conceptualization, Data curation, Writing – review & editing. ZJL: Validation, Writing – review & editing, Data curation, Supervision, Writing – original draft.

Funding

The author(s) declare financial support was received for the research, authorship, and/or publication of this article. This work was carried out under the research program Natural Science Foundation of Xiamen City, 3502Z20227104, and Natural Science Foundation of Fujian Province, 2022J011338.

Conflict of interest

The authors declare that the research was conducted in the absence of any commercial or financial relationships that could be construed as a potential conflict of interest.

Publisher's note

References

1. WHO Classification of Tumours Editorial Board. *WHO Classification of Tumours: Digestive System Tumours. 5th ed.* Lyon, France: International Agency for Research on Cancer (2019).

2. Agaimy A, Daum O, Märkl B, Lichtmannegger I, Michal M, Hartmann A. SWI/SNF complex-deficient undifferentiated/rhabdoid carcinomas of the gastrointestinal tract: A series of 13 cases highlighting mutually exclusive loss of SMARCA4 and SMARCA2 and frequent co-inactivation of SMARCB1 and SMARCA2. *Am J Surg Pathol* (2016) 40(4):544–53. doi: 10.1097/PAS.0000000000000554

3. Chang B, Sheng W, Wang L, Zhu X, Tan C, Ni S, et al. SWI/SNF complex-deficient undifferentiated carcinoma of the gastrointestinal tract: clinicopathologic study of 30 cases with an emphasis on variable morphology, immune features, and the prognostic significance of different SMARCA4 and SMARCA2 subunit deficiencies. *Am J Surg Pathol* (2022) 46(7):889–906. doi: 10.1097/PAS.0000000000001836

4. Huang SC, Ng KF, Yeh TS, Cheng CT, Chen MC, Chao YC, et al. The clinicopathological and molecular analysis of gastric cancer with altered SMARCA4 expression. *Histopathology* (2020) 77(2):250–61. doi: 10.1111/his.14117

5. Wu JY, Jiang K, Yan LJ, Yin LS, Huang XZ, Jia L, et al. Clinicopathological characteristics of gastric SMARCA4-deficient undifferentiated/rhabdoid carcinoma. *Zhonghua bing li xue za zhi = Chin J Pathol* (2023) 52(5):447–53. doi: 10.3760/cma.j.cn112151-20230206-00095

6. Zhang Z, Li Q, Sun S, Li Z, Cui ZG, Zhang M, et al. Clinicopathological and prognostic significance of SWI/SNF complex subunits in undifferentiated gastric carcinoma. *World J Surg Oncol* (2022) 20(1):1–13. doi: 10.1186/s12957-022-02847-0

7. Chen M, Yao X, Ping J, Shen H, Wei Y, Wang WL. Switch/sucrose non-fermentable complex-deficient rhabdoid carcinoma of stomach: A rare case report and literature review. *Int J Surg Pathol Published Online* (2023) 31(7):1364–74. doi: 10.1177/10668969221146204

8. Jin YP, Wang L, Wang Y, Wu DY, Zhang H, Xia QX. Gastric SWI/SNF complex deletion-associated undifferentiated carcinoma with rhabdoid phenotype: a clinicopathological and molecular analysis. *Zhonghua bing li xue za zhi = Chin J Pathol* (2022) 51(12):1229–34. doi: 10.3760/cma.j.cn112151-20220413-00282

9. Wang L, Tan C, Ni SJ, Jiang WH, Xu J, Cai X, et al. Gastric SWI/SNF-complex deficient undifferentiated/rhabdoid carcinoma: A clinicopathological study. *Chin J Pathol* (2021) 50(6):632–7. doi: 10.3760/cma.j.cn112151-20201224-00963

10. Lin JL, Wu TN, Zhang JY. An unusual case of gastric mass: SMARCA4-deficient undifferentiated gastric carcinoma. *J Gastrointest Surg* (2023) 0123456789):3–5. doi: 10.1007/s11605-023-05675-z

11. Mashtalir N, D'Avino AR, Michel BC, Luo J, Pan J, Otto JE, et al. Modular organization and assembly of SWI/SNF family chromatin remodeling complexes. *Cell* (2018) 175(5):1272–88. doi: 10.1016/j.cell.2018.09.032

12. WHO Classification of Tumours Editorial Board. *WHO Classification of Tumours: Thoracic Tumours. 5th ed.* Lyon, France: International Agency for Research on Cancer (2021).

13. Rekhtman N, Montecalvo J, Chang JC, Alex D, Ptashkin RN, Ai N, et al. SMARCA4-deficient thoracic sarcomatoid tumors represent primarily smoking-related undifferentiated carcinomas rather than primary thoracic sarcomas. *J Thorac Oncol* (2020) 15(2):231–47. doi: 10.1016/j.jtho.2019.10.023

14. Early CA, Wangsiricharoen S, Jones RM, VandenBussche CJ. Review of SMARCA4 (BRG1)-deficient carcinomas following a Malignant pleural effusion specimen confounded by reduced claudin-4 expression. *J Am Soc Cytopathol.* (2021) 10(2):197–207. doi: 10.1016/j.jasc.2020.08.002

15. Wilson BG, Wang X, Shen X, McKenna ES, Lemieux ME, Cho YJ, et al. Epigenetic antagonism between polycomb and SWI/SNF complexes during oncogenic transformation. *Cancer Cell* (2010) 18(4):316–328. doi: 10.1016/j.ccr.2010.09.006

16. Italiano A, Soria JC, Toulmonde M, Michot JM, Lucchesi C, Varga A, et al. Tazemetostat, an EZH2 inhibitor, in relapsed or refractory B-cell non-Hodgkin lymphoma and advanced solid tumours: a first-in-human, open-label, phase 1 study. *Lancet Oncol* (2018) 19(5):649–59. doi: 10.1016/S1470-2045(18)30145-1

frontiers | Frontiers in Oncology

TYPE Original Research
PUBLISHED 12 February 2024
DOI 10.3389/fonc.2024.1323961

OPEN ACCESS

EDITED BY
Zsolt Kovács,
George Emil Palade University, Romania

REVIEWED BY
Francesco P. Cammarata,
National Research Council (CNR), Italy
Michael VanSaun,
University of Kansas Medical Center, United States

*CORRESPONDENCE
Anna Wojakowska
astasz@ibch.poznan.pl

RECEIVED 18 October 2023
ACCEPTED 16 January 2024
PUBLISHED 12 February 2024

CITATION
Wojakowska A, Marczak L, Zeman M, Chekan M, Zembala-Nożyńska E, Polanski K, Strugała A, Widlak P and Pietrowska M (2024) Proteomic and metabolomic signatures of rectal tumor discriminate patients with different responses to preoperative radiotherapy. *Front. Oncol.* 14:1323961. doi: 10.3389/fonc.2024.1323961

Proteomic and metabolomic signatures of rectal tumor discriminate patients with different responses to preoperative radiotherapy

Anna Wojakowska[1]*, Lukasz Marczak[1], Marcin Zeman[2], Mykola Chekan[3], Ewa Zembala-Nożyńska[4], Krzysztof Polanski[5], Aleksander Strugała[1], Piotr Widlak[6] and Monika Pietrowska[7]

[1]Laboratory of Mass Spectrometry, Institute of Bioorganic Chemistry Polish Academy of Sciences, Poznan, Poland, [2]The Oncologic and Reconstructive Surgery Clinic, Maria Sklodowska-Curie National Research Institute of Oncology, Gliwice, Poland, [3]Department of Pathomorphology, University of Technology, Katowice, Poland, [4]Tumor Pathology Department, Maria Sklodowska-Curie National Research Institute of Oncology, Gliwice, Poland, [5]Wellcome Sanger Institute, Hinxton, Cambridge, United Kingdom, [6]2nd Department of Radiology, Medical University of Gdańsk, Gdańsk, Poland, [7]Center for Translational Research and Molecular Biology of Cancer, Maria Skłodowska-Curie National Research Institute of Oncology, Gliwice, Poland

Background: Neoadjuvant radiotherapy (neo-RT) is widely used in locally advanced rectal cancer (LARC) as a component of radical treatment. Despite the advantages of neo-RT, which typically improves outcomes in LARC patients, the lack of reliable biomarkers that predict response and monitor the efficacy of therapy, can result in the application of unnecessary aggressive therapy affecting patients' quality of life. Hence, the search for molecular biomarkers for assessing the radio responsiveness of this cancer represents a relevant issue.

Methods: Here, we combined proteomic and metabolomic approaches to identify molecular signatures, which could discriminate LARC tumors with good and poor responses to neo-RT.

Results: The integration of data on differentially accumulated proteins and metabolites made it possible to identify disrupted metabolic pathways and signaling processes connected with response to irradiation, including ketone bodies synthesis and degradation, purine metabolism, energy metabolism, degradation of fatty acid, amino acid metabolism, and focal adhesion. Moreover, we proposed multi-component panels of proteins and metabolites which could serve as a solid base to develop biomarkers for monitoring and predicting the efficacy of preoperative RT in rectal cancer patients.

Conclusion: We proved that an integrated multi-omic approach presents a valid look at the analysis of the global response to cancer treatment from the perspective of metabolomic reprogramming.

KEYWORDS

rectal cancer, radiotherapy, tissue, metabolomics, proteomics

1 Introduction

Locally advanced rectal cancer (LARC) patients with an increased risk of metastasis or local recurrence (T3-4 or N+) are eligible for neoadjuvant radiotherapy (neo-RT) before surgical resection, which generally leads to a decrease in tumor mass and improves treatment outcomes (1). However, despite the expected benefits of neo-RT, such treatment may not be effective in radioresistant tumors resulting in recurrence in some cases (2). The effectiveness of preoperative RT can be assessed by histopathological analysis of the resected tissue specimen according to tumor regression grading (TRG) system (3). TRG provides valuable prognostic information, yet the actual prediction of tumor regression remains a challenge. Rectal cancer patients are usually monitored using blood tests (e.g., CEA biomarker) and/or imaging (MR, EUS, and CT) to ensure that they remain disease-free and are treated promptly upon relapse. However, in some cases, classical clinical assessment/monitoring tools are insufficient (4). Therefore, the development of novel relevant biomarkers that could be used to predict the effectiveness of neo-RT in LARC patients is eagerly awaited (5). Moreover, there is still a lack of predictive biomarkers of sensitivity/resistance of rectal cancer to RT, which may result in the use of overly aggressive or ineffective therapy with associated negative effects on the quality of life. Therefore, an appropriate prognosis, based on specific predictors, should be the basis for selecting patient groups that require a more aggressive treatment strategy (6, 7).

An improved understanding of the cellular and molecular signaling pathways involved in disease processes, as well as the development of new therapeutic targets, may be made possible by the omics-based methods used to identify molecular risk factors and biomarkers, according to much of the evidence found (8). This could lead to the development of a more potent treatment for LARC patients. Proteomic and metabolomic approaches could be applied to prediction of the response to selected therapeutic strategies and monitoring the progression of disease (9–11). Although RT has been used extensively for a variety of tumors, little progress has been made in predicting and monitoring treatment outcomes after RT (12). There are only a few studies concerning proteomic or metabolomic profiling of tissue or serum/plasma from rectal cancer patients with various RT outcomes (13–18). The majority of these reports only cover neo-chemoradiotherapy's effects. Moreover, researchers mostly focus on a single protein or panel of a few proteins associated with known radiation effects like DNA repair, cell cycle, cell proliferation, apoptosis, altered metabolism, or immune response. There is lack of a broader, systemic studies combining proteomic and metabolomic approaches to reveal molecular processes and discriminatory molecules correlated with different patient responses to neo-RT in the LARC group. Recently our group applied a multi-omics approach to identify several differentially accumulated proteins and metabolites whose abundances detected in whole serum and serum-derived exosomes differentiated LARC patients with varying neo-RT responses. These molecules were linked to common pathways that are important for the reaction to RT, including energy metabolism, cancer-related signaling pathways, complement activation cascade, platelet functions, and the immune system (19).

In this study, we combined proteomics and metabolomics MS-based approach to identify molecules that could distinguish LARC tumors with various neo-RT responses. We proposed the panel of proteins and metabolites which could be a promising tool for the estimation of radio-responsiveness in patients with rectal cancer. Moreover, we associated differentially accumulated proteins and metabolites with molecular pathways and processes occurring in tumor tissue in response to radiation. Thus, our work provides a holistic view of the rectal cancer tissue response to irradiation from the perspective of metabolic reprogramming.

2 Materials and methods

2.1 Clinical samples

Tissue samples were taken from 24 LARC patients diagnosed with adenocarcinoma and treated at Maria Skłodowska-Curie National Research Institute of Oncology, Gliwice Branch. All patients were given neo-RT in a total dose of 39-54Gy. Tissue samples were collected between 2012 and 2014, directly during a standard surgical treatment; resected tissue samples were immediately frozen and kept at -80°C until analysis performed in 2020. The histology of three tissue slices (from the edges and center of the studied tissue sample) was assessed by an experienced pathologist for the percentage of tumor cells in each case. TRG assessed routinely in resected tumors reflected the area of residual tumor cells compared to the fibrotic area: TRG0 - complete response/no residual tumor, TRG1 - 10% of residual tumor, TRG2 - 10-50% of residual tumor, and TRG3 - >50% of residual tumor. Depending on the response to the treatment and the presence of tumor cells, collected samples were classified into two groups: good responders (GR) – 12 patients with RT-sensitive tumors (TRG 0-1), and poor responders (PR) - 12 patients with RT-resistant tumors (TRG 2-3). Table 1 contains the clinicopathological details and disease status for all included patients. Using post-operative material for research purposes was under local Ethics Committee approval no. KB/430-50/12. All tissue donors signed an informed consent form attesting to their voluntarily and consciously taking part.

2.2 Sample preparation for proteomic studies

The ball mill MM400 (Retsch, Germany) was used to grind the whole frozen tissue samples in liquid nitrogen for 45 seconds at 30 Hz. Tissue was lysed in 100 µL of 1% sodium deoxycholate (SDC) in a buffer containing 50mM NH_4HCO_3. Following homogenization with a Precellys 24 homogenizer (Bertin Technologies, France), samples were sonicated for 10 minutes in a bath on ice. Then, samples were centrifuged for 10 minutes at 11,000 x g at 4°C and the supernatant was moved to fresh tubes. The amount of isolated

TABLE 1 Clinical features of study participants with rectal cancer.

		Total *n* (%)	Good Responders *n* (%)	Poor Responders *n* (%)	Difference *p*-Value (test)
Sex	Females	11 (45.8)	5 (41.7)	6 (50)	1.0 (Chi2)
	Males	13 (54.2)	7 (58.3)	6 (50)	
Age (years)	mean (S.D.) median	66.0 (10.9) 68.5	64 (13.1) 65.0	69 (7.9) 70.5	0.23 (t-test)
BMI	mean (SD)	26.2 (4.2)	25.1 (4.0)	27.3 (4.2)	0.19 (t-test)
Clinical Stage	II	9 (37.5)	4 (33.3)	5 (41.7)	0.50 (Chi2)
	III	14 (58.3)	8 (66.7)	6 (50.0)	
	IV	1 (4.2)	0 (0.0)	1 (8.3)	
RT scheme	39 Gy	11 (45.8)	4 (33.3)	7 (58.3)	0.04 (Chi2)
	42 Gy	8 (33.3)	3 (25.0)	5 (41.7)	
	54 Gy	5 (20.8)	5 (41.7)	0 (13.0)	
RT **RT/CT**		12 (50.0) 12 (50.0)	4 (33.3) 8 (66.7)	8 (66.7) 4 (33.3)	0.22 (Chi2)
Time RT/S (days)	mean (SD) median	57.0 (22.0) 54.5	56.0 (22.2) 55.0	57.0 (22.6) 44.0	0.88 (t-test)
Surgery mode	AR	15 (62.5)	7 (58.3)	8 (66.7)	1.0 (Chi2)
	APR	9 (37.5)	5 (41.7)	4 (33.3)	
ypT	0–2	6 (25.0)	4 (33.3)	2 (16.7)	0.64 (Chi2)
	3	18 (75.0)	8 (66.7)	10 (83.3)	
ypN	negative	16 (66.7)	9 (75)	7 (58.3)	0.67 (Chi2)
	positive	8 (33.3)	3 (25)	5 (41.7)	
LNY	mean (SD)	11.2 (5.1)	10.2 (4.1)	12.0 (4.8)	0.12 (t-test)

BMI, body mass index; RT, neoadjuvant radiotherapy; CT, chemotherapy; Time RT/S, the time from completion of RT to surgery; LNY, node yield; S.D., standard deviation.

protein was measured using Pierce BCA protein assay kit (Thermo Scientific, Rockford, lL, USA) according to the guidelines provided with the product. For in-solution digestion, 10 µl of the sample containing 10 µg of proteins was diluted by adding 15 µl of 50 mM NH_4HCO_3 buffer and then reduced with 5.6 mM DTT at 95°C for 5 min. Then, proteins' thiol groups were alkylated with 5 mM iodoacetamide (IAA) for 20 min at room temperature and in the dark. For digestion, 0.2 µg of sequencing-grade trypsin (Promega) was added to each sample and left overnight at 37°C. Next, 1.5 µg of 10% trifluoroacetic acid (TFA) was added, mixed for 10 minutes, and twice centrifuged for 7 min. at 11,000 x g at 20°C. The purified tryptic peptides were then analyzed by LC–MS/MS.

2.3 Mass spectrometry analysis of proteins

A Dionex UltiMate 3000 RSLC nanoLC system combined with a QExactive Orbitrap mass spectrometer (Thermo Fisher Scientific) was used to conduct the proteome analysis. The peptides were separated on an Acclaim PepMap RSLC nanoViper C18 reverse phase column (75 µm x 25 cm, 2 µm particle size) with temperature kept at 30°C and a flow rate of 300 nl/min. The acetonitrile gradient from 4 to 60% in 0.1% formic acid was used in the 190-minute chromatographic program. Mass spectrometry data were acquired using the top 10 DDA approach, MS scans were registered at the resolution of 70,000 (m/z 200) while MS/MS spectra were registered at 17,500 resolution (also at m/z 200) in a positive mode in mass range of 300-2000 *m/z*. Ten most abundant peaks (2 or more charges) were subjected to fragmentation in HCD collision chamber and the collision energy was set for a constant value of 28%. Protein Discoverer 2.2 software (Thermo Fisher Scientific) was used to process the raw data collected during the study. Using the UniProt human database, proteins were identified with an accuracy of 10 ppm for peptide masses and 0.08 Da for fragment ion masses. Methionine oxidation as a dynamic modification and carbamidomethylation of cysteines as a constant modification were set for all searches, and two missed digestion sites per peptide were allowed. Proteins were considered to be identified if the search engine noticed at least two peptides for each protein and a peptide score reached the significance threshold FDR = 0.01 (as determined by the Percolator algorithm). The total ion current (TIC) was used to normalize the identified proteins' abundance.

2.4 Sample preparation for metabolomic studies

50 mg of pulverized tissue was extracted using 200 ul each of hexane, chloroform, methylene chloride, and methanol. The mixture was sonicated for 10 minutes each time after adding organic solvent, then centrifuged for 10 min at 11,000 x g at 4°C, and dried in a vacuum centrifuge. The dried extract was then subjected to derivatization by adding 40 µl of methoxyamine hydrochloride in pyridine (20 mg/ml) and incubated for 1.5h at 37°C. Next, in the second derivatization step, 90 µl of N-Trimethylsilyl-N-methyl trifluoroacetamide was added, and samples were incubated at 37°C for another 30 min. After derivatization, samples were immediately subjected to a GC/MS analysis.

2.5 Mass spectrometry analysis of metabolites

The GC-MS system (TRACE 1310 GC oven with TSQ8000 triple quad MS from Thermo Scientific, USA) with a DB-5MS column (30 m 0.25 mm 0.25 m) (J & W Scientific, Agilent Technologies, Palo Alto, California, USA) was used to separate and analyze metabolites. The following conditions were maintained for the gradient during chromatographic separation: 2 minutes at 70°C, followed by 10 minutes at 300°C, at 300°C. The source temperature was set to 250°C, the column interface was maintained at 250°C, and the PTV injector was used to inject the sample with a temperature gradient from 40 to 250°C. The electron ionization energy of the ion source, which operated in the range of 50-850 *m/z*, was set at 70 eV. The mixture of retention indexes (RI) containing alkanes was run before relevant analyses. Raw data files were analyzed using MSDial software (v. 4.92). The correction against the alkane series mixture (C-10-36) was implemented directly in MS Dial to generate the RI for each compound. The 28,220 records in the MSP database from the CompMS site were used to identify small molecules. Metabolite was considered as identified if the similarity index (SI) was above 80%. The following analyses did not include the identified artifacts (alkanes, column bleed, plasticizers, MSTFA, and reagents). Results that had been normalized (by applying the TIC approach) were exported and used in statistical analyses.

2.6 Statistical and chemometric analyses

The continuous clinical metadata was compared between GR and PR groups with the T-test, after assessing both groups' normality (with the Shapiro-Wilk test) and homoscedasticity (with the Levene test). The categorical clinical metadata was compared between groups with the chi-square test of independence. Depending on the normality and homoscedasticity of the data (assessed via the Shapiro-Wilk test and Levene test, respectively), differences in the abundances of proteins and metabolites between independent samples were evaluated using the T-test, Welch test, or U-Mann-Whitney test. Identified compounds were considered as differentially accumulated proteins (DAPs) or differentially accumulated metabolites (DAMs) when the p-value was lower than 0.05. For the false discovery rate correction, the Benjamini-Hochberg protocol was applied in each case. The effect size of 0.5 and 0.8 or 0.3 and 0.5 was considered to be medium and high, respectively, in the effect size analysis using the Hedges' g or the rank-biserial coefficient of correlation (an effect size equivalent of the U-Mann-Whitney test) (20). The evaluation of pairwise ratios between the specific compounds in the two groups was conducted using the traditional fold change estimator or the Hedges-Lehmann type fold change estimator. All statistical calculations were performed in Python. Normalized data were log-transformed, scaled with a mean-centered factor, and divided by the standard deviation of each variable for chemometric analyses. To show the general sample distribution, Principal Component Analysis (PCA) and Hierarchical Cluster Analysis (HCA) were used. For each compound, a single-feature logistic regression classifier was created. In addition to computing several quality control metrics, leave-one-out validation was carried out. The accuracy was computed as the mean of the TNR (true negative rate—specificity) and TPR (true positive rate—sensitivity) and to be independent of group size. The univariate ROC curve was generated using all of the feature's data. MetaboAnalyst 5.0 - https://www.metaboanalyst.ca/- was used to carry out the multivariate ROC curve-based exploratory analysis for the prediction of the biomarker panel. ROC curves were created using balanced sub-sampling and Monte Carlo cross-validation (MCCV). The Linear Support Vector Machine (SVM) was used for the analyses, and its built-in algorithm was used to rank the features.

2.7 Functional bioinformatics

String ver. 11.5, available at https://string-db.org, was used to analyze proteomic data (21). Hypergeometric testing with Benjamini-Hochberg multiple corrections was used to search for enriched GO terms and Reactome pathways using a list of genes corresponding to DAPs. For protein class annotation, Panther 17.0 Classification System - http://www.pantherdb.org was used. MetaboAnalyst 5.0, available at https://www.metaboanalyst.ca, was used to analyze metabolomic data. The Quantitative Enrichment Analysis (QEA) algorithm was used to identify the metabolic pathways connected to DAMs. The Joint Pathway Analysis tool in MetaboAnalyst 5.0 and Pathview (https://pathview.uncc.edu/) was used to combine and visualize multi-omic data. Integrated pathway analysis, based on the KEGG database, was implemented to carry out this by uploading a list of genes corresponding to DAPs and a list of DAMs with their fold changes. Additionally, the Pearson coefficients were applied to define the correlations between the differentially expressed variables found at both omic levels; p-values 0.05 were considered significant.

3 Results

3.1 Proteomic and metabolomic profiling of tissue samples

The mass spectrometry-based methods were applied for profiling proteins and metabolites in the tumor tissue of LARC patients who responded differentially to neo-RT. LC-MS/MS label-free approach made it possible to identify 2741 proteins in tissue specimens. The complete list of identified and quantified proteins is presented in Supplementary Table S1A, and the major classes of identified proteins are presented in Supplementary Figure S1A. Among the most numerous classes of proteins in tumor tissue were RNA metabolism proteins, cytoskeletal proteins, protein modifying enzymes, metabolite interconversion enzymes, and translational proteins. An untargeted GC–MS-based profiling allowed the annotation and relative quantification of 119 metabolites, which are listed in Supplementary Table S2A. The most numerous classes of metabolites in tissue samples were amino acids, sugars and derivatives, fatty acids and lipids, carboxylic and hydroxy acids, purines, pyrimidines, and their derivatives (Supplementary Figure S1B). Unsupervised clustering of the samples was carried out using the abundances of all identified proteins and metabolites. PCA and HCA performed based on both proteome and metabolome composition of tumor tissue allowed good separation of two groups of samples representing tumors with good and poor responses to neo-RT (Supplementary Figures S2A–D).

3.2 Proteomic signature of rectal tumor responses to preoperative RT

Among all identified proteins, 1710 showed significantly different (FDR<0.05) abundance between GR and PR, respectively (Supplementary Table S1A). Among the most numerous classes of DAPs were RNA metabolism proteins, cytoskeletal proteins, protein modifying enzymes, metabolite interconversion enzymes, and translational proteins (Supplementary Figure S1C). Identified DAPs were used to perform supervised clustering of samples (Supplementary Figure S2E). Most DAPs were upregulated in the PR group, while only 210 DAPs were upregulated in the GR group. Moreover, 19 DAPs were identified only in the PR group (namely: PROM1, HTATSF1, ND4, IVL, CKMT2, LIG1, BUD31, PTK2, CPSF1, RPS6KA1, ACSM3, ATAD3B, GALNT7, GFM1, COPS8, GTPBP, TRIM2, SPON1, NOX1), while one DAP (INA) was identified only in the GR group.

To further describe the potential of proteins identified in tumor tissues to discriminate patients with different responses to RT, univariate and multivariate classifiers were tested. Based on classical univariate ROC curve analysis, there were 245 proteins (8.9% of all detected proteins) for which a binary classification model (GR vs. PR) was performed with the receiver operating characteristics AUC equal 1 (Supplementary Table S1B). Finally, multivariate ROC curve analysis was performed to obtain a panel of potential proteomic biomarkers of response to neo-RT. Proteomic-based biomarker prediction was performed by multivariate ROC curve-based exploratory analysis. The classification models based on the top 5, 10, 15, 25, 50, and 100 important proteomic features with their corresponding AUC values are presented in Figure 1A. A model built on 50 features reached a predictive accuracy of 100% (Supplementary Figures 3A, B). The predicted class probabilities (average of the cross-validation of 50-mer models) for each sample (GR vs. PR) are presented in Supplementary Figure 3C. The top 20 predicted proteomic biomarkers based on how frequently they were selected during cross-validation are shown in Supplementary Figure 3D, while the complete list of proposed predictors can be found in Supplementary Table S1C. The normalized abundances of the top ten potential proteomic biomarkers with the highest frequency rank and importance based on the 50-mer classification models are presented in Figure 1B.

Furthermore, a functional enrichment analysis of DAPs was carried out, which showed a number of significantly overrepresented GO terms linked to them, including 1070 biological processes, 69 molecular functions, and 304 cellular components. Moreover, the KEGG, Reactome, and WikiPathways databases were used to analyze the functional interactions between DAPs (Supplementary Table S3). The TOP20 enriched processes (WikiPath) and functions (Reactome) associated with DAPs are presented in Figures 1C, D. DAPs' overrepresented functions and processes were generally connected with focal adhesion, VEGFA-VEGFR2 signaling pathway, metabolism of amino acids and proteins, metabolism of RNA, ribosomal proteins, translation factors, cellular responses to stress, proteasome degradation, ketone bodies, peroxisomal beta-oxidation, energy metabolism (glycolysis and TCA cycle), and metabolic reprogramming in colon cancer. Moreover, significantly overrepresented pathways involved in the immune response (T-cell receptor signaling pathway, antigen processing and presentation, leukocyte, and neutrophil-mediated immunity) were connected with DAPs upregulated in the PR group (Supplementary Figure S4). Chosen the most enriched KEGG pathways connected with DAPs, including ribosomal and proteasomal proteins, ECM matrix interaction, proteoglycans in cancer, complement, and coagulation cascades, focal adhesion, and signaling pathways connected with colorectal cancer (VEGF, PI3K-Akt, RAS, WNT, MAPK, NF-KAPPA B) are presented in detail in Supplementary Figure S5.

3.3 Metabolomic signature of rectal tumor responses to preoperative RT

Among 119 metabolites annotated in rectal tumor tissue, there were 28 DAMs, whose abundances were noticeably ($p<0.05$) different in PR and GR, respectively (Supplementary Table S2A); 7 DAMs after the FDR correction remained significant (namely: ribose 5-phosphate, cytosine, L-carnitine, 4-hydroxybutyric acid, phosphoenolpyruvic acid, inosine, and citric acid). The most numerous classes of DAMs were amino acids, sugars, and their derivatives, carboxylic and hydroxy acids, fatty acids and lipids, and purines/pyrimidines and their derivatives (Supplementary Figure S1D). DAMs were used to perform supervised clustering (Supplementary Figure S2F). 15 DAMs were upregulated in the GR group, while 13 DAMs were upregulated in the PR group.

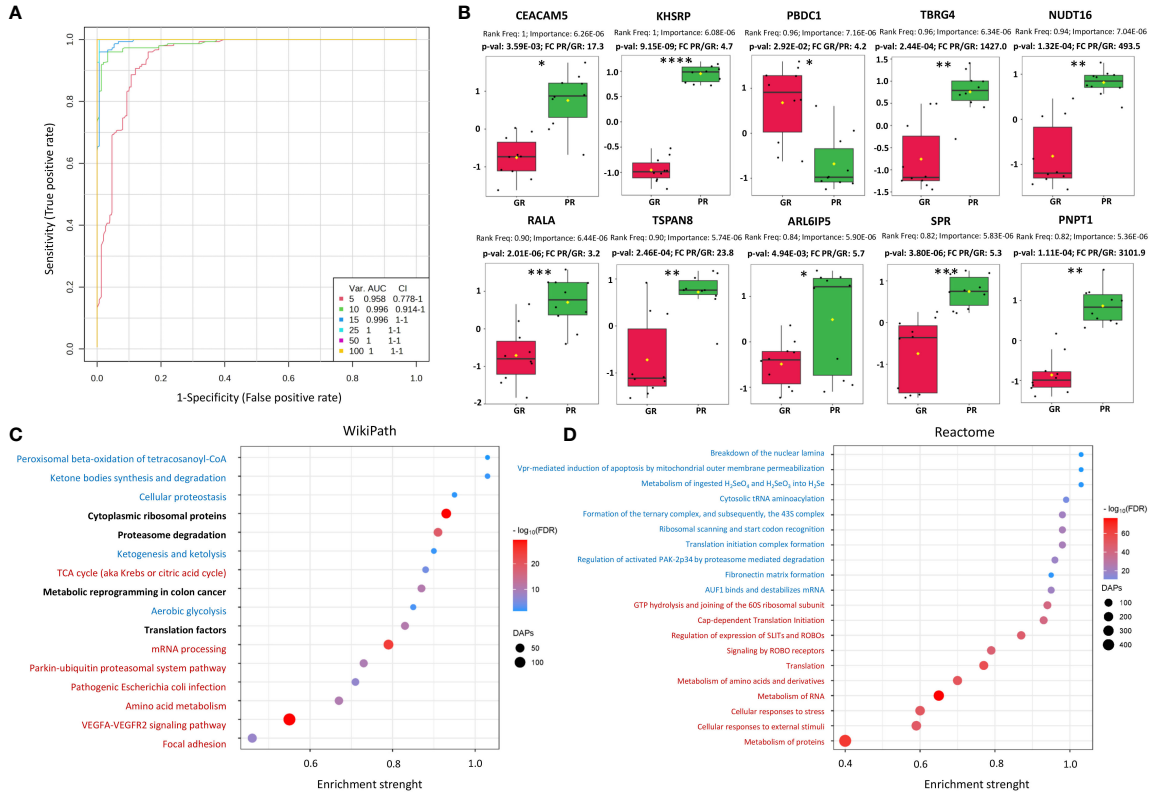

FIGURE 1
Characterization of proteomic signatures of rectal tumors responses to RT. **(A)** Proteomic-based biomarker prediction by multivariate ROC curve analysis: the classification models based on the top 5, 10, 15, 25, 50, and 100 important proteomic features with their corresponding AUC value; **(B)** The normalized abundances of potential proteomic biomarkers with the highest frequency rank and importance based on the selected classification model, p-values and fold change (FC) values are shown, significance after FDR correction are marked with asterisks according p-adjusted values ($p\text{-val}_{adj}$<0.05*, $p\text{-val}_{adj}$<0.005**, $p\text{-val}_{adj}$<0.0005***, $p\text{-val}_{adj}$<0.00005****); **(C, D)** Functional enrichment analysis of DAPs: bubble plots of the TOP20 enriched processes and functions revealed using the Wikipath **(C)** and Reactome **(D)** database, including the top 10 with the largest pathway significance (FDR) (marked in red) and enrichment strength (marked in blue), bolded for both. The highest enriched pathway based on both the significance and pathway impact are bold. The color of the dots represents the p-adjusted values (Benjamini-Hochberg correction), and the size of the dots represents the number of DAPs associated with the GO terms/Reactome pathways.

Univariate classification models tested to classify PR vs. GR samples revealed 24 metabolites with AUC higher or equal to 0.8 (Supplementary Table S2B). Multivariate classification models tested based on the top 5, 10, 15, 25, 50, and 100 metabolites with their corresponding AUC values (0.81-0.91) are presented in Figure 2A. A model built on 50 features showed the highest predictive accuracy (84.8%) and was selected for further testing (Supplementary Figures 6A, B). The class probabilities predicted using this model for each sample are presented in Supplementary Figure S6C. The top 20 predicted biomarkers predicted based on how frequently they were chosen for cross-validation are shown in Supplementary Figure S6D, while the complete list of proposed predictors can be found in Supplementary Table S2C. The normalized abundances of the top 10 potential biomarkers with the highest frequency rank and importance based on the 50-mer classification model are presented in Figure 2B.

The Quantitative Enrichment Analysis (QEA) algorithm and the Small Molecule Pathway Database (SMPDB) were used to analyze the functional enrichment of DAMs. (Supplementary Table S4). Network view of all significantly enriched pathways (FDR < 0.05) associated with DAMs is shown in Supplementary Figure S7, while an overview of the TOP 25 enriched metabolic pathways is presented in Figure 2C. The most significant processes associated with DAMs were connected mainly with energy metabolism (e.g., Warburg effect, gluconeogenesis, transfer of acetyl groups into mitochondria, mitochondrial electron transport chain, citric acid cycle, glycolysis), sphingolipid and glycerolipid metabolism, beta-oxidation of fatty acids, carnitine synthesis, inositol metabolism, and amino acids metabolism.

3.4 Integration of proteomic and metabolomic features that discriminate between good and poor responders to neo-RT

Joint Pathway Analysis in MataboAnalyst 5.0 was used to identify common pathways for DAPs and DAMs found in tumors of patients who responded differently to neo-RT. KEGG pathways with the largest pathway significance ($p < 0.05$) connected with DAPs and DAMs are presented in Figure 3A. Additionally, the top 20 significant enriched KEGG pathways, including the top 10 with

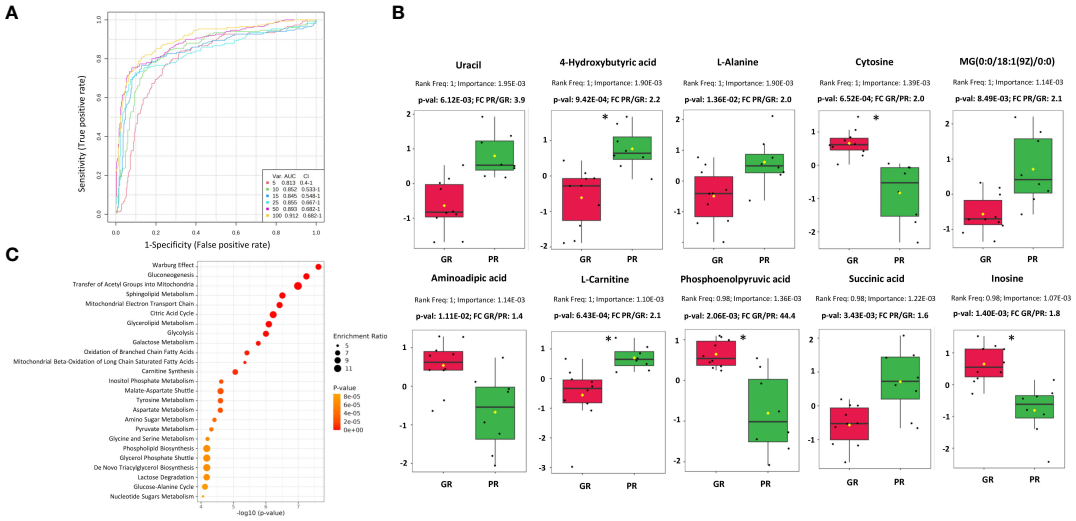

FIGURE 2
Characterization of metabolomic signatures of rectal tumors responses to RT. **(A)** Metabolomic-based biomarker prediction by multivariate ROC curve analysis: the classification models based on the top 5, 10, 15, 25, 50, and 100 important metabolomic features with their corresponding AUC value; **(B)** The normalized abundances of potential metabolomic biomarkers with the highest frequency rank and importance based on the selected classification model, p-values and fold change (FC) values are shown, significance after FDR correction are marked with asterisks according p-adjusted values ($p\text{-val}_{adj}$<0.05) **(C)** Metabolic pathways associated with DAMs based on quantitative enrichment analysis using KEGG database: bubble plot of the TOP 25 enriched metabolite sets.

the largest pathway significance (FDR) (marked in red) and pathway impact (marked in blue) are shown in Figure 3B. The most significant pathways based on FDR (<4.25E-09) were connected with the ribosome, splicesome, proteasome, oxidative phosphorylation, RNA transport, and bacterial infection. The most enriched pathways based on pathway impact (>2) were synthesis and degradation of ketone bodies, purine metabolism, energy metabolism (TCA cycle, glycolysis, gluconeogenesis, PPP, pyruvate metabolism), fatty acid degradation, and metabolism of amino acids (alanine, aspartate, glutamate, valine, leucine, isoleucine). Focal adhesion was the highest enriched pathway based on both the significance and pathway impact (for details see Supplementary Table S5). Components of the most enriched KEGG pathways connected with DAPs and DAMs are presented in detail in Supplementary Figure S8.

Furthermore, Pearson's correlation was used to address any possible relationships between DAPs and DAMs. The investigation turned up several strong correlations (r>0.8) between the variables,

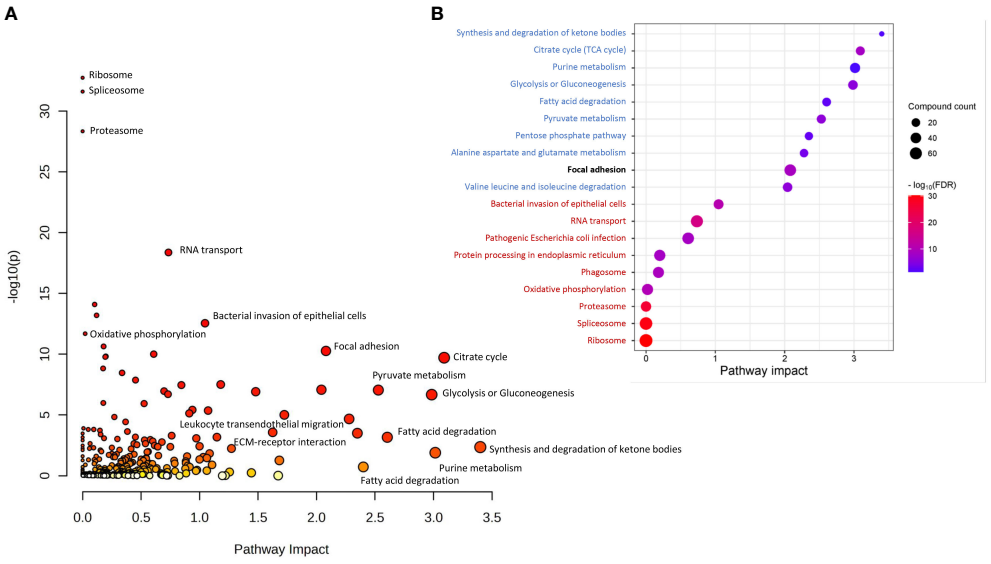

FIGURE 3
KEGG pathways commonly associated with DAPs and DAMs based on Joint Pathway Analysis. **(A)** all significantly overrepresented pathways (p <0.05); **(B)** The top 20 significantly enriched KEGG pathways, including the top 10 with the largest pathway significance (FDR) (marked in red) and pathway impact (marked in blue). The highest enriched pathway based on both the significance and pathway impact is bold.

which are detailed in Supplementary Table S6). For example, CEACAM5 revealed a high positive correlation with a panel of proteins including SLC25A, KHSRP, PNPT1, and MUC 13. On the other hand, there was observed a high negative correlation of CEACAM5 with linoleic acid, oleic acid, phosphoethanolamine, cadaverine, and N-acetyl-aspartic acid. The TOP 25 compounds correlated with CEACAM5 are presented in Supplementary Figure S9. Furthermore, known clinical parameters were subjected to the same correlation analysis, which revealed negative correlations of disease stage with linoleic and arachidonic acids as well as positive correlations of the lymph node yield (LNY) with stearic acid and phosphoethanolamine (Supplementary Table S6). Because the contribution of the applied RT scheme differed between GR and PR groups (Table 1), a putative correlation between the type of RT and the abundance of proteome and metabolome components was also addressed (Supplementary Table S7). When the abundance of the Top-10 DAPs (Figure 1B) and Top-10 DAMs (Figure 2B) in all patients was taken into consideration, components upregulated in the PR group (except alanine) showed a negative correlation while components upregulated in the GR group had a positive correlation with radiation dose, which suggested a potential link between the abundance of differentiating components and response to radiation dose (Supplementary Figure S10). Hence, to verify this possibility, the putative associations between the correlation with radiation dose and components' abundance were analyzed in the PR and GR groups separately to exclude the influence of a hypothetical prognosis factor discriminating between both groups. We found that for the majority of differentiating components, either DAPs or DAMs, the correlations with radiation doses were not statistically significant. Moreover, when significant correlations were found for either PR-upregulated or GR-upregulated components, these correlations observed in each group separately were rather randomly distributed (i.e., either negative or positive) (Supplementary Table S7), which further reduced the prognostic significance of radiation dose.

4 Discussion

Preoperative (neoadjuvant) RT is a valid strategy for the treatment of LARC. However, the major challenge in this therapeutic approach is cancer radioresistance, which may result in recurrence and metastasis. Therefore, there is a lot of interest in understanding the mechanisms of cancer radio-responsiveness and investigating RT-related biomarkers for the improvement of treatment strategies. Here, for the first time, a combined proteomic and metabolomic approach has been used to reveal a set of molecular components associated with different responses of rectal tumors to neo-RT. DAPs and DAMs were linked to metabolic pathways and signaling processes known to be involved in response to radiation. We observed that the proteome components of tumor tissue have a strong capacity to distinguish between patient samples with different neo-RT responses. A few of the Top 10 potential proteomic biomarkers revealed in our study have been previously identified as compounds associated with colorectal cancer's response to RT, including CEACAM5, KHSRP, RALA, and TSPAN8. Proteins that regulate glycolysis (PGK1, PGAM1, ENO1, PKM, TKT), ammonia detoxification (GLUD1), and other metabolic pathways (LDHA, GAPDH, MDH2) were reported to be differentially expressed in mouse xenograft colorectal tumor models with different radio-responsiveness (22). In our study, all these proteins (except PGAM1) were elevated in PR. Other DAPs upregulated in PR (CAD, RALB, FAM120A, PSMC2, LRPPRC, PARP1, PSMB5, ANP32B, IMPDH2, XRCC5, TPD52L2, EIFA5A, DDT, GNB1, HDGF, and MYO1C) were associated with metabolic activity in rectal tumor tissue (18). Similarly, a few DAMs upregulated in PR have been previously presented as small molecules associated with radioresistance, including succinic acid and arachidonic acid (23). Succinic acid is an oncometabolite that alters DNA repair through epigenetic regulation and impacts cancer cells' responses to chemo- and radio-therapy. (24). In our study, we detected significantly elevated levels of both succinic acid and two subunits of succinate dehydrogenase SDHA and SDHB. Furthermore, we observed a significantly elevated accumulation of carnitine (correlated with mitochondrial membrane transporter SLC25A20 - mitochondrial carnitine/acylcarnitine carrier) in PR. Carnitine is essential for shuttling acyl groups through intracellular membranes for fatty acid oxidation (FAO). FAO is essential for the growth and development of many cancers into malignancies. Carnitine is also essential for controlling the acyl-CoA/CoA balance, which controls how carbohydrates and lipids are metabolized. (25). Importantly, we detected a significantly reduced abundance of glutamine in PR and elevated level of proteins connected with glutamine transport and metabolism (SLC1A5 and GLS). In addition to being a crucial component of DNA repair, epigenetic modification, and the reduction of oxidative stress, glutamine metabolism in cancer cells also boosts radioresistance and reduces the effectiveness of radiotherapy and immunotherapy (26). It has been demonstrated that a lack of glutamine increases the epithelial-mesenchymal transition, which in turn promotes the recurrence and metastasis of colorectal cancer (27). Interestingly, different groups of cells present in the tumor may have various nutrient uptake from TME, with glucose being preferentially delivered to immune cells while glutamine and fatty acids are primarily distributed to cancer cells (28). As a result, targeting a single metabolite alone is insufficient to overcome radioresistance because tumor cells and other cells in the TME (including immune system cells) exhibit metabolic heterogeneity (29). Moreover, although the analysis of clinical data revealed statistically significant differences between groups of PR and GR with respect to radiation dose delivered during neo-RT (the contribution of radiation schemes involving higher doses was higher in the GR' group), radiation dose was barely associated with the abundance of differentiating proteins and metabolites (particularly when the correlations with radiation dose were analyzed in each group separately). Therefore, obtained data suggested that molecular profiles characteristic for GR and PR were not associated directly with response to radiation doses.

Obtained proteomic and metabolomic data provided a combination of information on the accumulation of metabolic enzymes and specific metabolites, which enabled to address metabolic reprogramming of rectal cancer. Several identified DAPs and DAMs were functionally linked to alterations in the metabolism of glucose, amino acids, and fatty acids. Tumor cells respond to RT by increasing glucose flux through the upregulation of glycolytic transporters and enzymes, facilitating glucose metabolism including

glycolysis, oxidative phosphorylation, and pentose phosphate pathway (PPP) (28). In PR, we observed significantly elevated levels of glycolytic enzymes GLUT1, HK2, GAPDH, PKM2, and LDHA, combined with decreased levels of glucose and increased levels of lactate, which is considered to contribute to radioresistance (30). Metabolic enzymes involved in oxidative phosphorylation (e.g., MPC elevated in poor responders) and the integrity of mitochondrial function are crucial for cancer radioresistance, while the activity of 6PGD (a component of PPP) enhances the production of NAPDH and nucleotides that promote tumor growth and radioresistance (31). Additionally, tumor cells respond to RT by increasing the metabolism of amino acids like glutamine, serine, and glycine, which provide the biomacromolecules and other materials needed for the production of nucleotides and energy, extending the survival of cancer cells. Glutamine is transported into the cell by SLC1A5 and converted to glutamate by mitochondrial glutaminase (GLS). It has been shown that radiation increases the GLS activity contributing to radioresistance (32). In our study, we detected significantly elevated levels of SLC1A5 and GLS in PR, while the abundance of glutamine was decreased. Moreover, aberrantly activated glycolysis permits tumor cells to indirectly enhance serine/glycine metabolism, increasing one-carbon metabolic flux and facilitating the proliferation of tumor cells and radioresistance (33). Here we detected in PR elevated levels of proteins involved in serine/glycine and one-carbon metabolism (PHGDH, PASAT1, SHMT). Moreover, enhanced accumulation of glycine and serine was also observed. Furthermore, cancer cells may develop radioresistance via reprogramming of lipid metabolism. We detected in PR elevated levels of enzymes (COX-2, ACSS2, FDPS, FASN, ACAT2, ACLY, SLC12A2) and metabolites (arachidonic acid and carnitine) involved in lipid metabolism, which have been linked to radioresistance of cancer cells (29). The major mechanism that enables the development of tumor radioresistance is DNA damage repair, which needs a significant nucleotide accumulation. Hence, activated glucose and amino acid metabolism that provide sufficient substrates and energy for the synthesis of pyrimidines and purines are linked to the survival of irradiated tumor cells. On the other hand, enzymes involved in the *de novo* nucleotide synthesis pathway (e.g. IMPDH) have emerged as targets for radiosensitization (29). Here we detected in PR elevated levels of inosine monophosphate dehydrogenase, while the abundance of inosine was reduced. In general, we concluded that molecular profiles characteristic of PR fit the metabolic reprogramming state that enhances tumor radioresistance, which involves the increased metabolic flux of glucose, fatty acids, lipids, and amino acids (especially glutamine), thus supplying sufficient energy and substrates for DNA damage repair. These metabolic pathways likely involved in the development of tumor radioresistance in the group of PR are illustrated schematically in Figure 4.

In conclusion, here we applied a combined MS-based proteomic and metabolomic approach for the identification in tumor tissue of molecules that discriminate LARCs differentially responded to neo-RT. This revealed molecular pathways and processes associated with DAPs and DAMs, which were linked to favorable and unfavorable responses to the treatment. These included several pathways involved in cellular metabolism and metabolic reprogramming, including energy metabolism, ketone bodies metabolism, fatty acid degradation, metabolism of amino acids and purines, which appeared to play a vital role in the radioresistance of tumors. Hence, our study revealed that multi-component panels of proteins and metabolites may serve as a solid base to develop biomarkers for

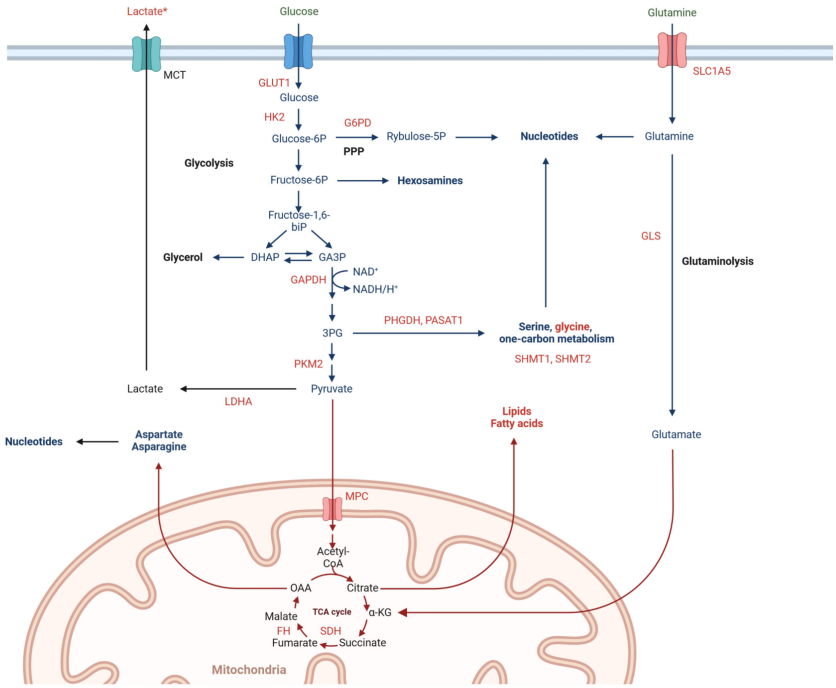

FIGURE 4
Metabolic pathways involved in rectal cancer radioresistance, including significantly upregulated (marked in red) and downregulated (marked in green) abundances of proteins and metabolites in poor responders tumor tissues. *high effect size.

monitoring and predicting the efficacy of preoperative RT in this group of patients as well as serve as therapeutic targets acting in combination with RT. However, our study has some limitations that could be addressed in future research. First, to confirm that the observed signatures were specific for cancer cells not to "normal" cells present in the tumor stroma, additional analyses using isolated cancer cells (e.g., by microdissection) might be instructive. Moreover, to validate the actual predictive potential of proposed signatures, their components should be analyzed in tissue material (e.g., in biopsies) before preoperative RT. Nevertheless, this explorative study provides proof of concept that molecular components of tumors that are associated with differentiated radio-responsiveness of rectal cancer could identified by the metabolomics and proteomics approaches.

Data availability statement

The datasets presented in this study can be found in online repositories. The mass spectrometry proteomics data have been deposited to the ProteomeXchange Consortium via the PRIDE partner repository with the dataset identifier PXD048647 and DOI:10.6019/PXD048647. The mass spectrometry proteomics data are available at the NIH Common Fund's National Metabolomics Data Repository (NMDR) website, the Metabolomics Workbench, https://www.metabolomicsworkbench.org where it has been assigned Study ID ST003045. The data can be accessed directly via its Project DOI: http://dx.doi.org/10.21228/M8S14W. This work is supported by NIH grant U2C-DK119886.

Ethics statement

The studies involving humans were approved by Maria Skłodowska-Curie National Research Institute of Oncology Gliwice Branch Ethics Committee. The studies were conducted in accordance with the local legislation and institutional requirements. The participants provided their written informed consent to participate in this study.

Author contributions

AW: Conceptualization, Data curation, Formal Analysis, Funding acquisition, Investigation, Methodology, Project administration, Supervision, Writing – original draft, Writing – review & editing. LM: Investigation, Methodology, Writing – review & editing. MZ: Resources, Writing – review & editing. MC: Resources, Writing – review & editing. EZ-N: Resources, Writing – review & editing. KP: Formal Analysis, Writing – review & editing. AS: Investigation, Writing – review & editing. PW: Writing – review & editing. MP: Conceptualization, Writing – review & editing.

Funding

The author(s) declare financial support was received for the research, authorship, and/or publication of this article. This study was supported by the National Science Centre, Poland, Grant 2017/26/D/NZ2/00964 (AW, LM, MP).

Acknowledgments

We are grateful to Urszula Strybel for her help in technical assistance.

Conflict of interest

The authors declare that the research was conducted in the absence of any commercial or financial relationships that could be construed as a potential conflict of interest.

Publisher's note

All claims expressed in this article are solely those of the authors and do not necessarily represent those of their affiliated organizations, or those of the publisher, the editors and the reviewers. Any product that may be evaluated in this article, or claim that may be made by its manufacturer, is not guaranteed or endorsed by the publisher.

Supplementary material

The Supplementary Material for this article can be found online at: https://www.frontiersin.org/articles/10.3389/fonc.2024.1323961/full#supplementary-material

SUPPLEMENTARY FIGURE 1
Contribution of identified proteins **(A)**, annotated metabolites **(B)**, DAPs **(C)**, and DAMs **(D)** to different classes.

SUPPLEMENTARY FIGURE 2
Clustering of RC patients based on levels of proteins and metabolites detected in tissue samples. Showed are PCA score plots **(A, B)** and dendrograms resulting from HCA **(C, D)**; a number of samples that were used only for proteomic or metabolomic profiling are marked in asterisk). The colors navy blue and pink, respectively, indicate GR and PR samples. Hierarchical supervised clustering was performed based on levels of DAPs **(E)** and DAMs **(F)**. *sample appearing only in proteomic or metabolomic analysis.

SUPPLEMENTARY FIGURE 3
Biomarker prediction by multivariate ROC curve analysis based on proteomic features. **(A)** - The predictive accuracies of 6 different biomarker models; For the 50-feature panel, the red dot indicates the highest accuracy.; **(B)** - ROC curve for a chosen biomarker model with the highest accuracy; **(C)** -The predicted class probabilities for each sample (GR vs. PR); **(D)** - The top 20 potential proteomic biomarkers predicted based on how frequently they were chosen for cross-validation.

SUPPLEMENTARY FIGURE 4
Overrepresented pathways involved in the immune response connected with DAPs upregulated in PR. **(A)** - bubble plots of the TOP12 enriched immunological processes and functions revealed using the GO terms; **(B)** - chosen significantly overrepresented pathways involved in the immune response.

SUPPLEMENTARY FIGURE 5
Chosen the most enriched KEGG pathways connected with DAPs. **(A)** - Ribosome; **(B)** - Proteasome; **(C)** - ECM-receptor interaction; **(D)** - Proteoglycans in cancer; **(E)** - Focal adhesion; **(F)** - Complement and coagulation cascade; **(G)** - Colorectal cancer; **(H)** - PI3K-AKT signaling pathway; **(I)** - WNT signaling pathway; **(J)** - MAPK signaling pathway; **(K)** - RAS signaling pathway; **(L)** - VEGF signaling pathway; **(M)** - NF-KAPPA B signaling pathway.

SUPPLEMENTARY FIGURE 6
Biomarker prediction by multivariate ROC curve analysis based on metabolomic features. **(A)** - The predictive accuracies of 6 different biomarker models; For the 50-feature panel, the red dot indicates the highest accuracy.; **(B)** - ROC curve for a chosen biomarker model with the highest accuracy; **(C)** - The predicted class probabilities for each sample (GR vs. PR); **(D)** - The top 20 potential proteomic biomarkers predicted based on how frequently they were chosen for cross-validation.

SUPPLEMENTARY FIGURE 7
Network view of significantly enriched metabolic pathways (FDR < 0.05) associated with DAMs based on quantitative enrichment analysis using KEGG database.

SUPPLEMENTARY FIGURE 8
Chosen the most enriched KEGG pathways connected with DAPs and DAMs. **(A)** - Glycolysis/gluconeogenesis; **(B)** - Pyruvate metabolism; **(C)** - Pentose phosphate pathway; **(D)** - Citrate cycle; **(E)** - Purine metabolism; **(F)** - Pyrimidine metabolism; **(G)** - Fatty acid degradation.

SUPPLEMENTARY FIGURE 9
The TOP 25 compounds correlated with CEACAM5 based on Pearson's correlation analysis.

SUPPLEMENTARY FIGURE 10
The results of Pearson's correlation analysis of the Top-10 DAPs and DAMs correlated with radiation dose in all patient groups.

References

1. Zhao F, Wang J, Yu H, Cheng X, Li X, Zhu X, et al. Neoadjuvant radiotherapy improves overall survival for T3/4N+M0 rectal cancer patients: A population-based study of 20300 patients. *Radiat Oncol* (2020) 15(1). doi: 10.1186/s13014-020-01497-4

2. Roeder F, Meldolesi E, Gerum S, Valentini V, Rödel C. Recent advances in (chemo-)radiation therapy for rectal cancer: a comprehensive review. *Radiat Oncol* (2020) 15(1). doi: 10.1186/s13014-020-01695-0

3. Peng YF, Yu WD, Pan HD, Wang L, Li M, Yao YF, et al. Tumor regression grades: Potential outcome predictor of locally advanced rectal adenocarcinoma after preoperative radiotherapy. *World J Gastroenterol* (2015) 21(6):1851–6. doi: 10.3748/wjg.v21.i6.1851

4. Nicholson BD, Shinkins B, Pathiraja I, Roberts NW, James TJ, Mallett S, et al. Blood CEA levels for detecting recurrent colorectal cancer. *Cochrane Database Sys Rev* (2015) 2015(12). doi: 10.1002/14651858.CD011134.pub2

5. Koncina E, Haan S, Rauh S, Letellier E. Prognostic and predictive molecular biomarkers for colorectal cancer: Updates and challenges. *Cancers (Basel)* (2020) 12(2). doi: 10.3390/cancers12020319

6. Mare M, Colarossi L, Veschi V, et al. Cancer stem cell biomarkers predictive of radiotherapy response in rectal cancer: A systematic review. *Genes (Basel)* (2021) 12 (10). doi: 10.3390/genes12101502

7. Lee HH, Chen CH, Huang YH, Chiang CH, Huang MY. Biomarkers of favorable vs. Unfavorable responses in locally advanced rectal cancer patients receiving neoadjuvant concurrent chemoradiotherapy. *Cells* (2022) 11(10). doi: 10.3390/cells11101611

8. Lu M, Zhan X. The crucial role of multiomic approach in cancer research and clinically relevant outcomes. *EPMA J* (2018) 9(1):77–102. doi: 10.1007/s13167-018-0128-8

9. Kwon YW, Jo HS, Bae S, Seo Y, Song P, Yoon SM. Application of proteomics in cancer: recent trends and approaches for biomarkers discovery. *Biomarkers Discovery Front Med* (2021) 8:747333. doi: 10.3389/fmed.2021.747333

10. Kowalczyk T, Ciborowski M, Kisluk J, Kretowski A, Barbas C. Mass spectrometry based proteomics and metabolomics in personalized oncology. *Biochim Biophys Acta Mol Basis Dis* (2020) 1866(5). doi: 10.1016/J.BBADIS.2020.165690

11. Spratlin JL, Serkova NJ, Eckhardt SG. Clinical applications of metabolomics in oncology: a review. *Clin Cancer Res* (2009) 15(2):431–40. doi: 10.1158/1078-0432.CCR-08-1059

12. Chen Y, Yang B, Chen M, Li Z, Liao Z. Biomarkers for predicting the response to radiation-based neoadjuvant therapy in rectal cancer. *Front Biosci (Landmark Ed)* (2022) 27(7). doi: 10.31083/J.FBL2707201

13. Allal AS, Kähne T, Reverdin AK, Lippert H, Schlegel W, Reymond MA. Radioresistance-related proteins in rectal cancer. *Proteomics* (2004) 4(8):2261–9. doi: 10.1002/PMIC.200300854

14. Repetto O, De Re V, De Paoli A, Belluco C, Alessandrini L, Canzonieri V, et al. Identification of protein clusters predictive of tumor response in rectal cancer patients receiving neoadjuvant chemo-radiotherapy. *Oncotarget* (2017) 8(17):28328–41. doi: 10.18632/ONCOTARGET.16053

15. Bowden DL, Sutton PA, Wall MA, Jithesh PV, Jenkins RE, Palmer DH, et al. Proteomic profiling of rectal cancer reveals acid ceramidase is implicated in radiation response. *J Proteomics* (2018) 179:53–60. doi: 10.1016/J.JPROT.2018.02.030

16. Jia H, Shen X, Guan Y, Xu M, Tu J, Mo M, et al. Predicting the pathological response to neoadjuvant chemoradiation using untargeted metabolomics in locally advanced rectal cancer. *Radiother Oncol* (2018) 128(3):548–56. doi: 10.1016/J.RADONC.2018.06.022

17. Rodríguez-Tomàs E, Arenas M, Gómez J, Acosta J, Trilla J, López Y, et al. Identification of potential metabolic biomarkers of rectal cancer and of the effect of neoadjuvant radiochemotherapy. *PloS One* (2021) 16(4):e0250453. doi: 10.1371/JOURNAL.PONE.0250453

18. Babic T, Lygirou V, Rosic J, Miladinov M, Rom AD, Baira E, et al. Pilot proteomic study of locally advanced rectal cancer before and after neoadjuvant chemoradiotherapy indicates high metabolic activity in non-responders' tumor tissue. *Proteomics Clin Appl* (2023) 17(1). doi: 10.1002/PRCA.202100116

19. Strybel U, Marczak L, Zeman M, Polanski K, Mielańczyk Ł, Klymenko O, et al. Molecular composition of serum exosomes could discriminate rectal cancer patients with different responses to neoadjuvant radiotherapy. *Cancers (Basel)* (2022) 14(4). doi: 10.3390/CANCERS14040993

20. Cureton EE. Rank-biserial correlation. *Psychometrika* (1956) 21(3):287–90. doi: 10.1007/BF02289138/METRICS

21. Szklarczyk D, Gable AL, Nastou KC, Lyon D, Kirsch R, Pyysalo S, et al. The STRING database in 2021: customizable protein-protein networks, and functional characterization of user-uploaded gene/measurement sets. *Nucleic Acids Res* (2021) 49 (D1):D605–12. doi: 10.1093/NAR/GKAA1074

22. Islam Khan MZ, Tam SY, Azam Z, Law HKW. Proteomic profiling of metabolic proteins as potential biomarkers of radioresponsiveness for colorectal cancer. *J Proteomics* (2022) 262. doi: 10.1016/J.JPROT.2022.104600

23. Lewis JE, Kemp ML. Integration of machine learning and genome-scale metabolic modeling identifies multi-omics biomarkers for radiation resistance. *Nat Commun* (2021) 12(1). doi: 10.1038/S41467-021-22989-1

24. Xiang K, Jendrossek V, Matschke J. Oncometabolites and the response to radiotherapy. *Radiat Oncol* (2020) 15(1). doi: 10.1186/S13014-020-01638-9

25. Console L, Scalise M, Mazza T, Pochini L, Galluccio M, Giangregorio N, et al. Carnitine traffic in cells. Link with cancer. *Front Cell Dev Biol* (2020) 8:583850. doi: 10.3389/FCELL.2020.583850

26. Alden RS, Kamran MZ, Bashjawish BA, Simone BA. Glutamine metabolism and radiosensitivity: Beyond the Warburg effect. *Front Oncol* (2022) 12:1070514. doi: 10.3389/FONC.2022.1070514

27. Sun H, Zhang C, Zheng Y, Liu C, Wang X, Cong X. Glutamine deficiency promotes recurrence and metastasis in colorectal cancer through enhancing epithelial-mesenchymal transition. *J Transl Med* (2022) 20(1). doi: 10.1186/S12967-022-03523-3

28. Reinfeld BI, Madden MZ, Wolf MM, Chytil A, Bader JE, Patterson AR, et al. Cell-programmed nutrient partitioning in the tumour microenvironment. *Nature* (2021) 593(7858):282–8. doi: 10.1038/S41586-021-03442-1

29. Yu Y, Yu J, Ge S, Su Y, Fan X. Novel insight into metabolic reprogrammming in cancer radioresistance: A promising therapeutic target in radiotherapy. *Int J Biol Sci* (2023) 19(3):811. doi: 10.7150/IJBS.79928

30. Liu KX, Everdell E, Pal S, Haas-Kogan DA, Milligan MG. Harnessing lactate metabolism for radiosensitization. *Front Oncol* (2021) 11:672339. doi: 10.3389/FONC.2021.672339

31. Liu R, Li W, Tao B, Wang X, Yang Z, Zhang Y, et al. Tyrosine phosphorylation activates 6-phosphogluconate dehydrogenase and promotes tumor growth and radiation resistance. *Nat Commun* (2019) 10:1. doi: 10.1038/s41467-019-08921-8

32. Altman BJ, Stine ZE, Dang CV. From Krebs to clinic: glutamine metabolism to cancer therapy. *Nat Rev Cancer* (2016) 16(10):619–34. doi: 10.1038/NRC.2016.71

33. Yang M, Vousden KH. Serine and one-carbon metabolism in cancer. *Nat Rev Cancer* (2016) 16(10):650–62. doi: 10.1038/NRC.2016.81

frontiers | Frontiers in Oncology

TYPE Original Research
PUBLISHED 01 March 2024
DOI 10.3389/fonc.2024.1301059

OPEN ACCESS

EDITED BY
Zsolt Kovács,
George Emil Palade University of Medicine, Pharmacy, Sciences and Technology of Târgu Mureş, Romania

REVIEWED BY
Mario Perez-Medina,
National Polytechnic Institute (IPN), Mexico
Manikandan Murugesan,
University of California, San Diego, United States

*CORRESPONDENCE
Huangxiang Chen
chenxp155691@sina.com

†These authors have contributed equally to this work and share first authorship

RECEIVED 24 September 2023
ACCEPTED 30 January 2024
PUBLISHED 01 March 2024

CITATION
Chen X, Chen Z, Guo J, Xiu Z and Chen H (2024) Preoperative plasma fibrinogen and C-reactive protein/albumin ratio as prognostic biomarkers for pancreatic carcinoma.
Front. Oncol. 14:1301059.
doi: 10.3389/fonc.2024.1301059

Preoperative plasma fibrinogen and C-reactive protein/albumin ratio as prognostic biomarkers for pancreatic carcinoma

Xiaopeng Chen[1†], Zhaohui Chen[2†], Jianyang Guo[1], Zhe Xiu[1] and Huangxiang Chen[1*]

[1]Department of Hepatobiliary Surgery, The Second Hospital of Longyan, Longyan, China, [2]Department of the 9th Affiliated Hospital of Xi'an Jiaotong University, Xian, China

Objective: Pancreatic carcinoma is characterised by high aggressiveness and a bleak prognosis; optimising related treatment decisions depends on the availability of reliable prognostic markers. This study was designed to compare various blood biomarkers, such as neutrophil/lymphocyte ratio (NLR), lymphocyte/monocyte ratio (LMR), platelet/lymphocyte ratio (PLR), C-reactive protein (CRP), albumin (Alb), plasma fibrinogen (PF), and CRP/Alb in patients with pancreatic carcinoma.

Methods: Our study retrospectively reviewed 250 patients with pancreatic carcinoma diagnosed between July 2007 and December 2018. The Cutoff Finder application was used to calculate the optimal values of CRP/Alb and PF. The Chi-square test or Fisher's exact test was used to analyse the correlation of CRP/Alb and PF with other clinicopathological factors. Conducting univariate and multivariate analyses allowed further survival analysis of these prognostic factors.

Results: Multivariate analysis revealed that, in a cohort of 232 patients with pancreatic ductal adenocarcinoma (PDAC), the PF level exhibited statistical significance for overall survival (hazard ratio (HR) = 0.464; $p = 0.023$); however, this correlation was not found in the entire group of 250 patients with pancreatic carcinoma. Contrastingly, the CRP/Alb ratio was demonstrated statistical significance in both the entire pancreatic carcinoma cohort (HR = 0.471; $p = 0.026$) and the PDAC subgroup (HR = 0.484; $p = 0.034$). CRP/Alb and PF demonstrated a positive association (r=0.489, p<0.001) as indicated by Spearman's rank correlation analysis. Additionally, in 232 PDAC patients, the combination of the CRP/Alb ratio and PF had synergistic effects on prognosis when compared with either the CRP/Alb ratio or the PF concentration alone.

Conclusion: PF concentration is a convenient, rapid, and noninvasive biomarker, and its combination with the CRP/Alb ratio could significantly enhance the accuracy of prognosis prediction in pancreatic carcinoma patients, especially those with the most common histological subtype of PDAC.

KEYWORDS

plasma fibrinogen, C-reactive protein/albumin, overall survival, prognosis, pancreatic carcinoma

1 Introduction

Pancreatic carcinoma (PC) is a malignant tumour arising from pancreatic cells. The pancreas is an abdominal glandular organ essential for food digestion and blood sugar level regulation (1, 2). It accounts for 216,000 new cancer cases each year, resulting in more than 200,000 annual deaths worldwide (3, 4). Pancreatic carcinoma is a highly aggressive form of cancer and is typically diagnosed in advanced stages when the tumour has already spread to other organs. Pancreatic ductal adenocarcinoma (PDAC), the most prevalent form of pancreatic carcinoma, constitutes nearly 95% of all pancreatic carcinoma cases (5). Symptoms of pancreatic carcinoma include abdominal pain, unexplained weight loss, appetite loss, nausea, vomiting, jaundice, and alterations in stool colour. Therapeutic approaches for pancreatic carcinoma may include surgical intervention, chemotherapy, radiation therapy, or a combination thereof, with selection dependent on factors such as tumour stage, location, and overall health (6). While these treatments have significantly enhanced the survival prospects for individuals with pancreatic carcinoma over the past few years, the survival status of patients in this situation continues to be grim, with a five-year survival rate typically falling below 10% (7).

The role of several prognostic indicators, such as the C-reactive protein/albumin (CRP/Alb) ratio and neutrophil/lymphocyte ratio (NLR), in the occurrence and development of pancreatic carcinoma has been confirmed (8, 9). Nevertheless, thus far, most of these markers have not been used in the general clinical setting due to a lack of therapeutic effectiveness in pancreatic carcinoma patients. Therefore, identifying novel reliable biomarkers for the application of prognostic factors in pancreatic carcinoma is essential, especially for enhanced risk stratification and more individualised clinical treatment (10).

The potential usefulness of the CRP/Alb as a biomarker has been highlighted in various tumours, such as digestive system tumours and gynaecological carcinomas (11–13). However, the potential of the preoperative CRP/Alb to function as a prognostic indicator in individuals with pancreatic carcinoma and whether its prognostic efficacy surpasses that of other inflammatory prognostic factors are unclear.

Previous studies have suggested that various indicators from the coagulation/fibrinolysis system, especially plasma fibrinogen (PF) and D-dimer levels, are abnormal in cancer patients (14–16). PF is a 340-kDa plasma glycoprotein that is key in the maintenance of haemostasis and participates in both inflammatory mechanisms and tumorigenesis (17). Numerous studies have confirmed that an increase in PF may promote the occurrence and development of various tumours (18–20). However, research examining its prognostic relevance in pancreatic carcinoma is limited.

Hence, our objective was to assess the ability of PF to predict oncological outcomes in pancreatic carcinoma patients in comparison to other inflammation-related metrics (albumin, CRP, and CRP/Alb) as well as cellular indicators (the NLR, lymphocyte/monocyte ratio (LMR), and platelet/lymphocyte ratio (PLR).

2 Methods

2.1 Patients

Between July 1, 2007, and December 1, 2018, 297 patient samples were newly diagnosed as showing pancreatic carcinoma at Longyan Second People's Hospital and the 9th Affiliated Hospital of Xi'an Jiaotong University. The Medical Ethics Committee of the Second People's Hospital of Longyan City has conducted a thorough review of medical records for all patients and approved their usage. The inclusion criteria were summarised as follows: (1) Chinese individuals who underwent radical surgery for primary pancreatic carcinoma and axillary lymph node dissection and (2) who had adequate and useful clinical data in their medical records. Among the exclusion criteria were the following: 1) patients with concurrent liver diseases, autoimmune diseases or coagulopathies requiring anticoagulants (n =15); 2) patients who had distant metastases or other malignancies at the time of diagnosis (n = 9); 3) patients receiving corticosteroids, oral contraceptives or hormone replacement therapy (n = 7); 4) patients who had received neoadjuvant therapy within 3 months (n = 8); and 5) patients with insufficient or invalid medical clinical data (n = 8). Ultimately, following application of the inclusion and exclusion criteria, a retrospective study was conducted involving 250 patients diagnosed with pancreatic carcinoma.

The clinical information gathered from the patient medical records included age, size, histological subtype, grade, lymph node metastasis (LNM) involvement, chemoradiotherapy data, neoadjuvant therapy data, and outcome data. Histopathological examination by two different pathologists confirmed the diagnosis of pancreatic carcinoma in all the samples. The PDAC patients included in the study were all pathologically confirmed and staged according to the 8th edition of the UICC TNM classification.

Pancreatic carcinoma patients underwent regular monitoring through telephone check-ins or postoperative appointments. Overall survival (OS) was characterised as the duration from the surgical procedure to the most recent follow-up visit, which was conducted on December 1, 2023, or deceased due to various reasons. The median duration of follow-up was 38 months, with a range spanning from 2 to 97 months.

2.2 Blood collection and assay methods

The plasma fibrinogen and CRP/Alb concentrations were measured in peripheral venous blood samples collected before breakfast less than 7 days before the start of surgery. Plasma was collected in a 5 ml blood collection tube and processed within 24 hours to measure the plasma coagulation parameters. The plasma fibrinogen levels were measured using the clotting method of Clauss. Using an automatic biochemical analyser (Hitachi 7600, Tokyo, Japan), we measured the CRP and albumin levels. With respect to all pancreatic carcinoma specimens, we used the ACL TOP system (Instrumentation Laboratory, Milan, Italy) to measure

the plasma fibrinogen concentration. Data on white blood cells, neutrophils, lymphocytes, and platelet counts were collected with an automated haematology system (Sysmex XE-5000, Kobe, Japan).

2.3 Optimal prognostic cutoff values for inflammatory parameters

The determination of the optimal cutoff value followed the approach described by Gui et al. in 2021, utilising the minimum p value method (21). According to the prognostic scoring system, the optimal cutoff value for preoperative PF was 3.28 g/L, and for the CRP/Alb ratio, it was 0.18 (Supplementary Figure 1). The corresponding areas under the ROC curve for PF and the CRP/Alb ratio, representing their maximum values, were 0.679 and 0.803, respectively. The samples that were incorporated were split into two categories, where the low-level group comprised values below the optimal cutoff threshold and the high-level group consisted of values surpassing the optimal cutoff threshold.

Out of the 250 patients, the median PF was 3.53 g/L, and the mean PF was 3.31 g/L. These 250 patients were stratified into different groups based on their NLR, LMR, PLR, CRP, and albumin levels utilising the optimised cutoff values obtained from receiver operating characteristic (ROC) curve analysis; these cutoff values were defined as >3.10 mg/L, <3.06 mg/L, >128 mg/L, >5.1 mg/L, and <3.2 g/dL, respectively, to predict OS.

2.4 Statistical analysis

The software used for statistical analysis was SPSS 26.0 (IBM, Armonk, NY, USA). ROC curves were generated to predict 5-year OS and identify the optimal cutoff threshold for coagulation parameters, leading to the use of binary variables as treatment variables. The Chi-square test was applied to analyse the correlations between PF and the CRP/Alb ratio and clinicopathological parameters. The Kaplan–Meier method was used to construct survival curves, and comparisons were conducted using the log-rank test. To evaluate the difference in OS between the high-PF and CRP/Alb groups and between the low-PF and CRP/Alb ratio groups, univariate and multivariate Cox proportional hazards models were employed. Values where $p < 0.05$ were regarded as statistically significant.

3 Results

3.1 Patients' features

From July 2007 to December 2018, 250 patients with pancreatic carcinoma who satisfied all the inclusion criteria were selected (Table 1). The median age at diagnosis was 53.6 years, (ranging, 29-81 years), and consisted of 145 males and 105 females. The 5-year OS rate among the 250 pancreatic carcinoma patients reached 15.8%. Overall, 104 patients exhibited good-to-moderate tumour differentiation, while 146 patients exhibited poor tumour differentiation. According to the 8th edition of the UICC, there were 62 patients with TNM stage T1 tumours and 50 patients with T2 tumours. T3 stage disease exhibited the highest incidence (80 cases), followed by the T4 stage (58 cases). One hundred and four patients (41.6%) had tumours < 2 cm, and 146 (58.4%) patients had tumours ≥ 2 cm. Out of a total of 250 patients, 149 had lymph node metastasis, while 101 did not. Detailed information regarding the treatment attributes, clinical profiles, and histopathological features of these patients is available in Table 1.

3.2 High PF and CRP/Alb and OS in pancreatic carcinoma patients

To assess the prognostic importance of PF and other prognostic parameters, we constructed a Cox proportional hazard regression model for both the pancreatic carcinoma subgroup and the PDAC subgroup. Within the univariate analysis of OS in the 250 patients, differences in several variables, including tumour differentiation (HR = 1.808; p <0.001), LNM (HR = 2.209; $p < 0.001$), clinical T stage (HR = 2.615; $p < 0.001$), PF (HR = 2.384; $p < 0.001$), NLR (HR = 1.384; $p = 0.046$), CRP (HR = 1.385; $p = 0.043$), and CRP/Alb (HR = 2.318; $p < 0.001$), exhibited statistical significance (Table 1). However, in the subgroup consisting of 232 PDAC samples, there was no significant difference in CRP levels ($p = 0.914$) (Table 2).

After adjustments for confounding variables, multivariate analysis revealed that in the entire cohort of 250 patients, CRP/Alb (HR = 0.471; $p = 0.026$), tumour differentiation (HR = 1.745; p <0.001), clinical T stage (HR = 1.513; $p = 0.023$), LNM (HR = 1.459; $p = 0.042$), and the combination of PF + CRP/Alb (HR = 8.034; $p <$ 0.001) were independent factors significantly linked to OS. Moreover, among the subset of 232 PDAC patients, the independent prognostic factors for OS were CRP/Alb (HR = 0.484; $p = 0.034$), PF (HR = 0.464; $p = 0.023$), clinical T stage (HR = 1.510; $p = 0.032$), LNM (HR = 1.483; $p = 0.047$), and the combined variable PF + CRP/Alb (HR = 8.652; $p < 0.001$).

We utilised Kaplan–Meier survival curves based on the PF (Figures 1A, D) and CRP/Alb (Figures 1B, E), and they showed that increased levels of these markers were associated with decreased OS in both the entire group of pancreatic carcinoma patients and specifically in those diagnosed with PDAC. Thus, the patient population was categorised into the following groups: those with elevated and reduced CRP/Alb ratios and those with high and low levels of PF. The five-year OS of patients in the PF level increased group was 12.2%, and that of patients in the PF level decreased group was 17.9%. The five-year OS of patients in the CRP/Alb-increased cohort was 13.6%, and that of patients in the CRP/Alb-decreased cohort was 17.3%.

3.3 Association of CRP/Alb and PF with clinicopathological features of pancreatic carcinoma

The correlation between clinicopathologic factors and CRP/Alb and PF was analysed by the Chi-square test. Among the 250 patients with pancreatic carcinoma, advanced clinical T stage ($p < 0.001$), tumour differentiation ($p = 0.023$), and LNM ($p = 0.005$) exhibited significant correlations with high PF levels (≥ 3.28 g/L); advanced

TABLE 1 Univariate and multivariate analyses of characteristics associated with OS in all 250 pancreatic carcinoma patients.

Characteristics	Univariate			Multivariate		
	Hazard Ratio	95%CI	*P-value*	Hazard Ratio	95%CI	*P-value*
Age, years						
≥50 *vs* <50	1.007	0.733-1.382	0.967	0.924	0.665-1.285	0.638
Gender						
Male *vs* Female	0.863	0.635-1.173	0.347	0.846	0.617-1.158	0.296
Clinical T stage						
>T2 *vs* ≤T2	2.615	1.875-3.647	<0.001	1.513	1.059-2.163	0.023
Tumour differentiation						
Poorly *vs* Well/moderately	1.808	1.307-2.501	<0.001	1.745	1.248-2.440	0.001
Tumour size						
≥2cm *vs* <2cm	1.032	0.755-1.410	0.844	0.992	0.721-1.366	0.962
LNM						
Yes *vs* No	2.209	1.564-3.120	<0.001	1.459	1.014-2.100	0.042
PF						
≥3.28 g/L *vs* <3.28 g/L	2.384	1.655-3.434	<0.001	0.568	0.303-1.064	0.078
NLR						
≥3.10 *vs* <3.10	1.384	1.001-1.915	0.046	1.272	0.906-1.786	0.165
LMR						
<3.06 *vs* ≥3.06	1.072	0.785-1.465	0.661	1.055	0.751-1.483	0.757
PLR						
≥128 *vs* <128	1.022	0.750-1.393	0.892	1.096	0.796-1.507	0.575
CRP						
≥5.1 mg/L *vs* <5.1mg/L	1.385	1.010-1.899	0.043	1.354	0.2326-1.859	0.061
Serum albumin						
<3.2g/dL *vs*≥3.2g/dL	1.245	0.913-1.696	0.166	1.093	0.792-1.508	0.587
CRP/Alb						
> 0.18 *vs* ≤ 0.18	2.318	1.625-3.305	<0.001	0.471	0.243-0.914	0.026
PF+ CRP/Alb						
PF-high+ CRP/Alb-high *vs* PF-high or CRP/Alb-high *vs* PF-low+ CRP/Alb-low	2.662	1.704-4.160	<0.001	8.034	3.410-18.932	<0.001

P-values that achieved statistical significance ($p < 0.05$) are indicated in bold. Alb, albumin; CRP, C-reactive protein; LMR, lymphocyte-monocyte ratio; LNM, lymph node metastasis; NLR, neutrophil-lymphocyte ratio; PF, plasma fibrinogen; PLR, platelet-lymphocyte ratio.

clinical T stage ($p < 0.001$), tumour differentiation ($p = 0.047$), and LNM ($p = 0.002$) exhibited significant correlations with high CRP/Alb levels (≥ 0.18) (Table 3).

Among the 232 patients with PADC, advanced clinical T stage ($p < 0.001$), tumour differentiation ($p = 0.048$), and LNM ($p = 0.033$) exhibited significant correlations with high PF levels (≥ 3.28 g/L). In addition, advanced clinical T stage ($p < 0.001$), tumour differentiation ($p = 0.024$), and LNM ($p < 0.001$) exhibited significant correlations with high CRP/Alb levels (≥ 0.18) (Table 4).

3.4 The prognostic relevance of the CRP/Alb and PF combined indices in 250 patients with pancreatic carcinoma

We further analysed the link between PF and the CRP/Alb ratio utilising Spearman's test (Figure 2). The findings revealed a positive correlation between the CRP/Alb ratio and PF ($r = 0.489$, $p < 0.001$) in all cases of pancreatic carcinoma. Combining the CRP/Alb ratio with the PF could enhance patient stratification by OS (Figures 1C, F).

TABLE 2 Univariate and multivariate analyses of characteristics associated with OS in 232 PDAC patients.

Characteristics	Univariate			Multivariate		
	Hazard Ratio	95%CI	*P*-value	Hazard Ratio	95%CI	*P*-value
Age, years						
≥50 *vs* <50	1.033	0.744-1.436	0.846	0.954	0.674-1.349	0.789
Gender						
Male *vs* Female	0.885	0.644-1.216	0.451	0.877	0.633-1.214	0.429
Clinical T stage						
>T2 *vs* ≤T2	2.664	1.889-3.756	<0.001	1.510	1.036-2.201	0.032
Tumour differentiation						
Poorly *vs* Well/moderately	1.873	1.340-2.619	<0.001	1.796	1.270-2.540	<0.001
Tumour size						
≥2cm *vs* <2cm	1.044	0.755-1.444	0.796	1.078	0.775-1.499	0.655
LNM						
Yes *vs* No	2.417	1.676-3.487	<0.001	1.483	1.005-2.189	0.047
PF						
≥3.28 g/L *vs* <3.28 g/L	2.121	1.462-3.078	<0.001	0.464	0.239-0.899	0.023
NLR						
≥3.10 *vs* <3.10	1.424	1.022-1.2323	0.037	1.388	0.991-1.945	0.057
LMR						
<3.06 *vs* ≥3.06	1.012	0.734-1.396	0.942	0.971	0.683-1.379	0.868
PLR						
≥128 *vs* <128	1.027	0.746-1.414	0.872	1.109	0.799-1.538	0.538
CRP						
≥5.1 mg/L *vs* <5.1 mg/L	1.018	0.737-1.406	0.914	1.093	0.776-1.539	0.613
Serum albumin						
<3.5g/dL *vs* ≥3.5g/dL	1.320	0.956-1.821	0.092	1.137	0.808-1.600	0.462
CRP/Alb						
> 0.18 *vs* ≤ 0.18	2.449	1.694-3.540	<0.001	0.484	0.247-0.946	0.034
PF+ CRP/Alb						
PF-high+ CRP/Alb-high *vs* PF-high or CRP/Alb-high *vs* PF-low+ CRP/Alb-low	2.528	1.599-3.996	<0.001	8.652	3.562-21.015	<0.001

P-values that achieved statistical significance ($p < 0.05$) are indicated in bold. Alb, albumin; CRP, C-reactive protein; LMR, lymphocyte-monocyte ratio; LNM, lymph node metastasis; NLR, neutrophil-lymphocyte ratio; PF, plasma fibrinogen; PLR, platelet-lymphocyte ratio.

Consequently, we categorised patients into three cohorts: (I) those with both low PF and low CRP/Alb, (II) those with either high PF or high CRP/Alb, and (III) those with both high PF and high CRP/Alb. These categories aligned with low, moderate, and high-risk cohorts, respectively. The 5-year OS rates for the 250 patients were 27.8%, 19.5%, and 13.2%, respectively, while for the 232 PDAC patients, the 5-year OS rates were 27.6%, 18.8%, and 12.9%, respectively. Multivariate analysis was also conducted, and as outlined in Table 1, it became evident that patients in both the high-risk and moderate-risk cohorts experienced notably worse prognoses than patients in the low-risk cohorts.

4 Discussion

Pancreatic carcinoma is complex and heterogeneous, leading to varying rates of recurrence and progression (22). With an enhanced comprehension of the molecular biology of pancreatic carcinoma,

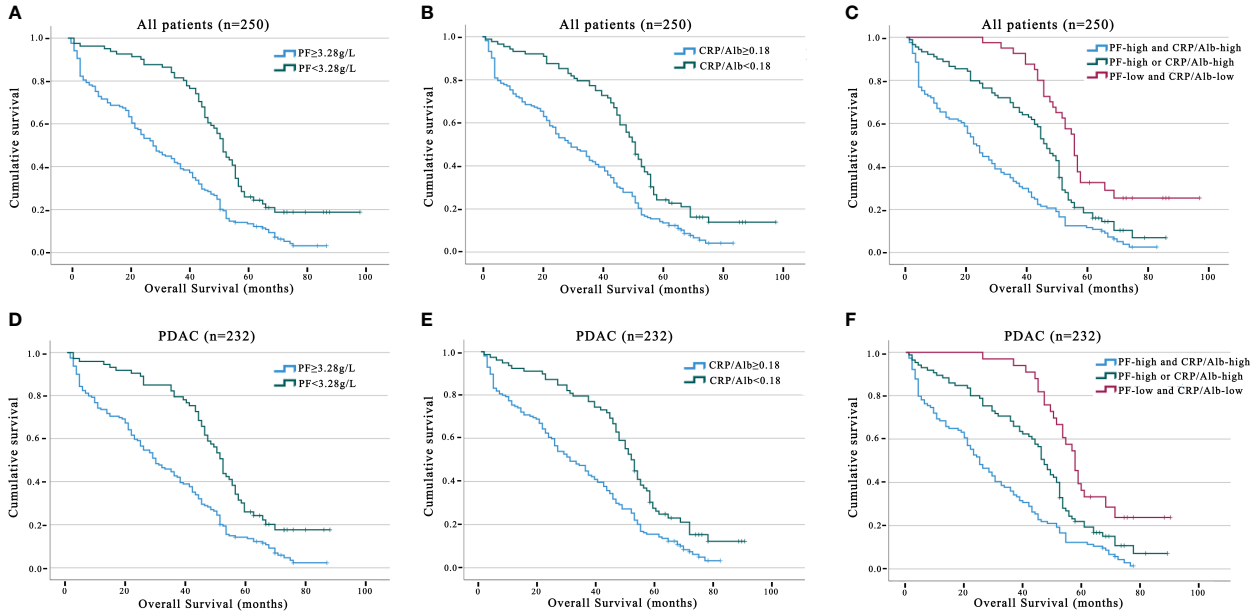

FIGURE 1
Prognosis value of PF, CRP/Alb in all pancreatic carcinoma and PDAC subgroup patients. The five-year OS rate was determined using the Kaplan–Meier method and assessed with the log-rank test. Analysing OS outcomes associated with PF concentration, including all pancreatic carcinoma patients, and the PDAC subgroup **(A, D)**. Analysing OS outcomes associated with PF concentration, including all pancreatic carcinoma patients, and the PDAC subgroup **(B, E)**. OS analysis involving the combined categorisation based on PF and CRP/Alb for all pancreatic carcinoma patients and the PDAC group **(C, F)**.

TABLE 3 Clinicopathological features of 250 pancreatic carcinoma patients stratified by PF and CRP/Alb.

Characteristic	Total n = 250 (%)	PF			CRP/Alb		
		≥3.28g/L	<3.28g/L	*p*-value	≥0.18	<0.18	*P*-value
Age (years, n (%)							
<50	93	65	28	0.551	58	35	0.535
≥50	157	104	53		104	53	
Gender, n (%)							
Male	145	100	45	0.588	99	46	0.176
Female	105	69	36		63	42	
Clinical T stage, n (%)							
≤T2	112	61	51	<0.001	58	54	<0.001
>T2	138	108	30		104	34	
Tumour differentiation, n (%)							
Well/moderately	104	62	42	0.023	60	44	0.047
Poorly	146	107	39		102	44	
Tumour size, n (%)							
<2cm	104	68	36	0.528	66	38	0.708
≥2cm	146	101	45		96	50	
LNM, n (%)							
No	101	58	43	0.005	54	47	0.002
Yes	149	111	38		108	41	

P-values that achieved statistical significance ($p < 0.05$) are indicated in bold. Alb, albumin; CRP, C-reactive protein; LNM, lymph node metastasis; PF, plasma fibrinogen.

TABLE 4 Clinicopathological features of 232 PDAC patients stratified by PF and CRP/Alb.

Characteristic	Total n = 232 (%)	PF			CRP/Alb		
		≥3.28g/L	<3.28g/L	*p*-value	≥0.18	<0.18	*P*-value
Age (years, n (%)							
<50	86	61	25	0.526	54	32	0.671
≥50	146	232	48		96	50	
Gender, n (%)							
Male	135	95	40	0.478	92	43	0.211
Female	97	64	33		58	39	
Clinical T stage, n (%)							
≤T2	106	58	48	<0.001	55	51	<0.001
>T2	126	101	25		95	31	
Tumour differentiation, n (%)							
Well/moderately	96	59	37	0.048	54	42	0.024
Poorly	136	100	36		96	40	
Tumour size, n (%)							
<2cm	94	63	31	0.774	59	35	0.675
≥2cm	138	96	42		91	47	
LNM, n (%)							
No	88	53	35	0.033	44	44	<0.001
Yes	144	106	38		106	38	
CRP/Alb							
≥0.18	150	113	37	0.003			
<0.18	82	46	36				

P-values that achieved statistical significance ($p < 0.05$) are indicated in bold. Alb, albumin; CRP, C-reactive protein; LNM, lymph node metastasis; PF, plasma fibrinogen.

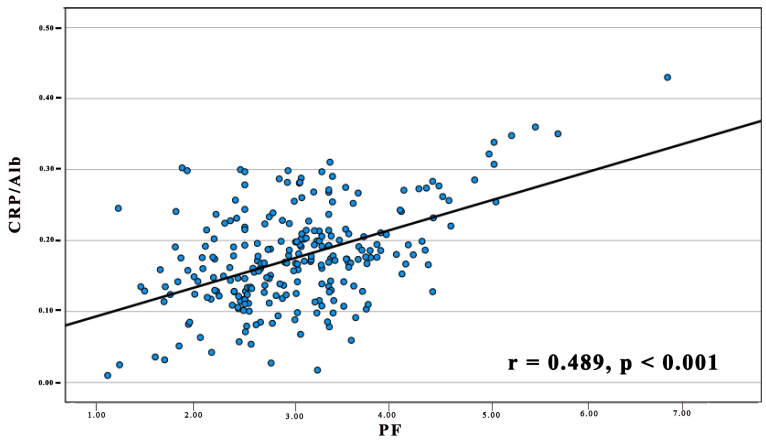

FIGURE 2
The relationship between PF and the CRP/Alb Ratio in 250 Patients diagnosed with pancreatic carcinoma. The preoperative PF displayed a positive association with the CRP/Alb ratio. ($r = 0.489$, $p < 0.001$).

advancements in the diagnosis and treatment of this invasive disease have been achieved. Previous conclusive evidence has shown that the tumour-related inflammatory system is essential for tumour angiogenesis and tumorigenesis and that two parameters (fibrinogen and CRP/Alb) of inflammation-based biomarkers may be associated with the prognosis of pancreatic carcinoma (23–25). PF and CRP/Alb have been correlated with clinical outcomes in many types of tumours (20, 26).

The present study demonstrated the following: (1) pancreatic carcinoma patients with high PF (> 3.28 g/L) and CRP/Alb (> 0.18) levels had lower survival rates; (2) pancreatic carcinoma patients with high PF and CRP/Alb levels had higher tumour grades and clinical stages and were more prone to lymph node metastasis; (3) the levels of PF and CRP/Alb are unrelated to the age, gender, or tumour size of pancreatic cancer patients; (4) A noteworthy association was observed between increased PF levels and higher CRP/Alb values in individuals diagnosed with pancreatic carcinoma; (5) The predictive power of PF for OS was specific to PADC patients and did not extend uniformly to all pancreatic carcinoma cases; and (6) combining PF and CRP/Alb levels has the potential to enhance the accuracy of predicting survival outcomes in pancreatic carcinoma patients. These study results provide unique insights into individual research findings, with a focus on the hypothesis that PF and the CRP/Alb ratio are prognostic factors for pancreatic cancer. We suggest that additional adjuvant therapy may be beneficial for high-risk patients. While these conclusions require further validation, the data offer new insights into the biological invasiveness of pancreatic carcinoma in the Chinese population.

The prognostic importance of the PF level in pancreatic carcinoma can be attributed to its underlying biological mechanisms. As a vital constituent of the coagulation/fibrinolytic system, fibrinogen is a pivotal acute-phase protein, and its plasma levels are significantly influenced by inflammation (27–29). Research has indicated that fibronectin interacts with various growth factors, such as those involved with its role in suppressing cell apoptosis and its interaction with members of the PDGF family. These interactions subsequently lead to tumour cell adhesion, the production of VEGF, metastasis, and the activation of the FGF family (30, 31). In addition, cell line models have demonstrated that fibronectin can induce EMT through the p-AKT/p-mTOR pathway to promote cancer cell motility (32). Within a research investigation involving 211 individuals diagnosed with pancreatic carcinoma, Qi et al. confirmed that the hyperfibrinogen concentration could be a potential factor for evaluating the accuracy of OS prediction (33). In addition, a hyperfibrinogen concentration ≥400 mg/dL was found to be an unfavourable predictor of PFS and OS in patients with pancreatic carcinoma treated with chemoradiotherapy (34). Based on these studies, we suggest that the PF concentration in pancreatic cancer patients can be considered an adverse prognostic marker and tends to indicate a poor prognosis.

In addition, our univariate analysis demonstrated that among 250 pancreatic cancer patients and even within the subset of 232 PDAC patients, an elevated NLR was associated with a shorter OS. This evidence enhances our understanding of the link between chronic inflammation and survival in individuals with pancreatic carcinoma. An elevated NLR predicts a more adverse prognosis for pancreatic carcinoma patients, consistent with the findings of a survey involving 263 pancreatic carcinoma patients (35). The potential biological mechanism of the NLR effect stems from the infiltration of neutrophils and lymphocytes. The chronic inflammatory response induced by tumour cells further enhances the infiltration of neutrophils, further promoting tumour progression through the secretion of interleukin-2 (IL-2), IL-6, IL-10, tumour necrosis factor-alpha (TNF-α), and vascular endothelial growth factor (VEGF) (36, 37). VEGF, known for its role as an oncogene, is acknowledged to enhance cell migration by increasing vascular permeability. Furthermore, elevated levels of TNF-α and IL-10 induce a decrease in the number of lymphocytes and the occurrence of functional impairments (38, 39).

As an acute-phase protein during inflammation, CRP is induced by and synthesised in the liver through proinflammatory cytokines. It is considered a predictive factor for systemic infections (40). Albumin is a circulating protein present in the plasma that is directly involved in the occurrence of inflammation (41). CRP/Alb is a combined index of the serum ALB concentration and total CRP concentration. It was identified as one of the prognostic indicators for sepsis patients and has subsequently been recognised as a prognostic indicator for tumours as well (13, 42). For instance, researchers have shown that, in the assessment of tumour prognosis, The predictive utility of the CRP/Alb ratio is comparable to that of the mGPS. The CRP/Alb ratio may exhibit greater predictive accuracy than the mGPS, possibly due to the theoretical advantage of better utilising the CRP and Alb levels in the CRP/Alb ratio (43). Liu et al. reported that the independent prognostic capability of the CRP/Alb ratio is noteworthy in individuals with stage III and IV pancreatic carcinoma, but evidently not in patients with pancreatic cancer clinically staged as stage I or II (44). The research by Fan et al. substantiated the CRP/albumin ratio's role as a tool for predicting survival rates and gauging the effectiveness of chemotherapy in advanced pancreatic carcinoma (45). Based on the cutoff value (> 0.18) used, our research findings indicate that among 250 pancreatic cancer patients, even within the PADC subgroup, an elevated CRP/Alb ratio signifies a shorter OS. Therefore, the CRP/Alb ratio demonstrates promise as an inflammatory marker, bearing significance for the clinical prognosis of those with pancreatic carcinoma.

Considering both PF levels and CRP/Alb ratios together, we found that patients in the high PF cohort and high CRP/Alb cohort exhibited the lowest survival time. This observation further underscores the connection between high CRP/Alb and PF levels and the inflammatory response in patients with pancreatic carcinoma that ultimately leads to an unfavourable outcome. Both CRP and fibrinogen are critical factors that occur during the acute phase response to inflammation and serve as key acute-phase

proteins (46, 47). Activation of the coagulation system is widely acknowledged to be initiated by inflammation, resulting in an increase in prothrombin and antifibrinolytic factor levels (48, 49). In contrast, elements within the coagulation system, including fibrinogen or fibrin, can independently trigger the onset of the inflammatory process and contribute to the development of subsequent tissue damage downstream (50). Therefore, fibrinogen can be considered an important driving factor in the occurrence of chronic inflammation. Our observation of a robust association between PF and the CRP/Alb ratio highlights the intricate interplay between the coagulation/fibrinolytic system and the inflammatory tumour microenvironment and suggests its potential to impact patient survival (51, 52).

This research is not without limitations, and the primary concern is the retrospective design, which brings the potential for selection bias into consideration. Second, the methods employed to measure PF and the CRP/Alb ratio were not uniform, leading to variations in the optimal cutoff values. Third, potential biases may have arisen from clinical factors, such as ethnicity and age.

In summary, our research suggested that the PF concentration was an accurate, convenient, inexpensive biomarker for pancreatic carcinoma, particularly in the case of PDAC patients. The evaluation of PF and the CRP/Alb ratio may therefore be informative for deciding surgical strategies. Furthermore, the combination of the CRP/Alb ratio and the PF could increase the precision of prognosis prediction in pancreatic carcinoma patients.

Data availability statement

The original contributions presented in the study are included in the article/Supplementary Material. Further inquiries can be directed to the corresponding author.

Ethics statement

The studies involving humans were approved by Medical Ethics Committee of Longyan Second People's Hospital (LYEYEC 2023-025). The studies were conducted in accordance with the local legislation and institutional requirements. The participants provided their written informed consent to participate in this study.

Author contributions

XC: Writing – original draft, Writing – review & editing. ZC: Writing – original draft, Data curation, Formal analysis. JG: Data curation, Writing – original draft. ZX: Data curation, Formal analysis, Writing – review & editing. HC: Writing – original draft.

Funding

The author(s) declare financial support was received for the research, authorship, and/or publication of this article. The author (s) disclosed receipt of the following financial support for the research, authorship, and/or publication of this article: This study was supported by the Longyan Science and Technology Plan Project (2022LYF17045).

Conflict of interest

The authors declare that the research was conducted in the absence of any commercial or financial relationships that could be construed as a potential conflict of interest.

Publisher's note

Supplementary material

The Supplementary Material for this article can be found online at: https://www.frontiersin.org/articles/10.3389/fonc.2024.1301059/full#supplementary-material

SUPPLEMENTARY FIGURE 1
The ROC curves of PF **(A)** and CRP/Alb **(B)** for OS in pancreatic carcinoma patients.

References

1. Collisson EA, Bailey P, Chang DK, Biankin AV. Molecular subtypes of pancreatic cancer. *Nat Rev Gastroenterol Hepatol*. (2019) 16:207–20. doi: 10.1038/s41575-019-0109-y

2. Stoffel EM, Brand RE, Goggins M. Pancreatic cancer: changing epidemiology and new approaches to risk assessment, early detection, and prevention. *Gastroenterology*. (2023) 164:752–65. doi: 10.1053/j.gastro.2023.02.012

3. Siegel RL, Miller KD, Wagle NS, Jemal A. Cancer statistics, 2023. *CA Cancer J Clin*. (2023) 73:17–48. doi: 10.3322/caac.21763

4. Wood LD, Canto MI, Jaffee EM, Simeone DM. Pancreatic cancer: pathogenesis, screening, diagnosis, and treatment. *Gastroenterology*. (2022) 163:386–402 e1. doi: 10.1053/j.gastro.2022.03.056

5. Hu ZI, O'Reilly EM. Therapeutic developments in pancreatic cancer. *Nat Rev Gastroenterol Hepatol*. (2024) 21:7–24. doi: 10.1038/s41575-023-00840-w

6. Halbrook CJ, Lyssiotis CA, Pasca di Magliano M, Maitra A. Pancreatic cancer: Advances and challenges. *Cell*. (2023) 186:1729–54. doi: 10.1016/j.cell.2023.02.014

7. Kolbeinsson HM, Chandana S, Wright GP, Chung M. Pancreatic cancer: A review of current treatment and novel therapies. *J Invest Surg*. (2023) 36:2129884. doi: 10.1080/08941939.2022.2129884

8. Zhou L, Ma S, Balde AI, Han S, Cai Z, Li Z. A retrospective propensity score matched study of the preoperative C-reactive protein to albumin ratio and prognosis in patients with resectable non-metastatic breast cancer. *Med Sci Monit*. (2019) 25:4342–52. doi: 10.12659/MSM.913684

9. Wang Y, Huang G, Li Z. Prognostic significance of inflammatory biomarkers in patients with breast cancer skeletal metastases. *Cancer Manag Res*. (2020) 12:11463–75. doi: 10.2147/CMAR.S277291

10. Cheng Y, Wang K, Geng L, Sun J, Xu W, Liu D, et al. Identification of candidate diagnostic and prognostic biomarkers for pancreatic carcinoma. *EBioMedicine*. (2019) 40:382–93. doi: 10.1016/j.ebiom.2019.01.003

11. Liao CK, Yu YL, Lin YC, Hsu YJ, Chern YJ, Chiang JM, et al. Prognostic value of the C-reactive protein to albumin ratio in colorectal cancer: an updated systematic review and meta-analysis. *World J Surg Oncol*. (2021) 19:139. doi: 10.1186/s12957-021-02253-y

12. Liu Y, Chen S, Zheng C, Ding M, Zhang L, Wang L, et al. The prognostic value of the preoperative c-reactive protein/albumin ratio in ovarian cancer. *BMC Cancer*. (2017) 17:285. doi: 10.1186/s12885-017-3220-x

13. Fang Y, Zheng T, Zhang C. Prognostic role of the C-reactive protein/albumin ratio in patients with gynecological cancers: A meta-analysis. *Front Oncol*. (2021) 11:737155. doi: 10.3389/fonc.2021.737155

14. He X, Huang T, Xue Y, Zhang M, Liu Q, Wang Y, et al. Association of preoperative plasma D-dimmer and fibrinogen and renal cell carcinoma outcome. *J Cancer*. (2019) 10:4096–105. doi: 10.7150/jca.31173

15. Li X, Shu K, Zhou J, Yu Q, Cui S, Liu J, et al. Preoperative plasma fibrinogen and D-dimer as prognostic biomarkers for non-muscle-invasive bladder cancer. *Clin Genitourin Cancer*. (2020) 18:11–19 e1. doi: 10.1016/j.clgc.2019.10.025

16. Ohara S, Suda K, Tomizawa K, Takemoto T, Fujino T, Hamada A, et al. Prognostic value of plasma fibrinogen and D-dimer levels in patients with surgically resected non-small cell lung cancer. *Surg Today*. (2020) 50: 1427–33. doi: 10.1007/s00595-020-02019-1

17. Pieters M, Wolberg AS. Fibrinogen and fibrin: An illustrated review. *Res Pract Thromb Haemost*. (2019) 3:161–72. doi: 10.1002/rth2.12191

18. He SS, Wang Y, Yang L, Chen HY, Liang SB, Lu LX, et al. Plasma fibrinogen correlates with metastasis and is associated with prognosis in human nasopharyngeal carcinoma. *J Cancer*. (2017) 8:403–09. doi: 10.7150/jca.17028

19. Wakatsuki K, Matsumoto S, Migita K, Ito M, Kunishige T, Nakade H, et al. Preoperative plasma fibrinogen is associated with lymph node metastasis and predicts prognosis in resectable esophageal cancer. *World J Surg*. (2017) 41:2068–77. doi: 10.1007/s00268-017-3991-x

20. Perisanidis C, Psyrri A, Cohen EE, Engelmann J, Heinze G, Perisanidis B, et al. Prognostic role of pretreatment plasma fibrinogen in patients with solid tumors: A systematic review and meta-analysis. *Cancer Treat Rev*. (2015) 41:960–70. doi: 10.1016/j.ctrv.2015.10.002

21. Gui H, Song Y, Yin Y, Wang H, Rodriguez R, Wang Z. Prognostic value of preoperative inflammation-based predictors in patients with bladder carcinoma after radical cystectomy. *Open Med (Wars)*. (2021) 16:816–25. doi: 10.1515/med-2021-0277

22. Pandya G, Kirtonia A, Singh A, Goel A, Mohan CD, Rangappa KS, et al. A comprehensive review of the multifaceted role of the microbiota in human pancreatic carcinoma. *Semin Cancer Biol*. (2022) 86:682–92. doi: 10.1016/j.semcancer.2021.05.027

23. Starzer AM, Steindl A, Mair MJ, Deischinger C, Simonovska A, Widhalm G, et al. Systemic inflammation scores correlate with survival prognosis in patients with newly diagnosed brain metastases. *Br J Cancer*. (2021) 124:1294–300. doi: 10.1038/s41416-020-01254-0

24. Stromnes IM. IL18 at the crossroads between chronic inflammation and T-cell exhaustion in pancreatic cancer. *Cancer Immunol Res*. (2023) 11:400. doi: 10.1158/2326-6066.CIR-23-0145

25. Agalianos C, Gouvas N, Manatakis DK, Sideris I, Passas I, Dervenis C. The role of inflammatory markers in predicting resectability of pancreatic ductal adenocarcinoma. *Chirurgia (Bucur)*. (2022) 117:431–36. doi: 10.21614/chirurgia.2603

26. Lin Y, Liu Z, Qiu Y, Zhang J, Wu H, Liang R, et al. Clinical significance of plasma D-dimer and fibrinogen in digestive cancer: A systematic review and meta-analysis. *Eur J Surg Oncol*. (2018) 44:1494–503. doi: 10.1016/j.ejso.2018.07.052

27. Grottke O, Mallaiah S, Karkouti K, Saner F, Haas T. Fibrinogen supplementation and its indications. *Semin Thromb Hemost*. (2020) 46:38–49. doi: 10.1055/s-0039-1696946

28. Qian X, Cai J, Qi Q, Han J, Zhu X, Xia R, et al. Preoperative fibrinogen is associated with the clinical survival of primary liver cancer patients and promotes hepatoma metastasis via the PTEN/AKT/mTOR pathway. *Heliyon*. (2023) 9:e16696. doi: 10.1016/j.heliyon.2023.e16696

29. Preston T, Slater C, McMillan DC, Falconer JS, Shenkin A, Fearon KC. Fibrinogen synthesis is elevated in fasting cancer patients with an acute phase response. *J Nutr*. (1998) 128:1355–60. doi: 10.1093/jn/128.8.1355

30. Qin WZ, Li QL, Chen WF, Xu MD, Zhang YQ, Zhong YS, et al. Overexpression of fibrinogen-like protein 2 induces epithelial-to-mesenchymal transition and promotes tumor progression in colorectal carcinoma. *Med Oncol*. (2014) 31:181. doi: 10.1007/s12032-014-0181-7

31. Martino MM, Briquez PS, Ranga A, Lutolf MP, Hubbell JA. Heparin-binding domain of fibrin(ogen) binds growth factors and promotes tissue repair when incorporated within a synthetic matrix. *Proc Natl Acad Sci USA*. (2013) 110:4563–8. doi: 10.1073/pnas.1221602110

32. Zhang F, Wang Y, Sun P, Wang ZQ, Wang DS, Zhang DS, et al. Fibrinogen promotes Malignant biological tumor behavior involving epithelial-mesenchymal transition via the p-AKT/p-mTOR pathway in esophageal squamous cell carcinoma. *J Cancer Res Clin Oncol*. (2017) 143:2413–24. doi: 10.1007/s00432-017-2493-4

33. Qi Q, Geng Y, Sun M, Chen H, Wang P, Chen Z. Hyperfibrinogen is associated with the systemic inflammatory response and predicts poor prognosis in advanced pancreatic cancer. *Pancreas*. (2015) 44:977–82. doi: 10.1097/MPA.0000000000000353

34. Kurahara H, Maemura K, Mataki Y, Sakoda M, Iino S, Hiwatashi K, et al. Prognostication by inflammation-based score in patients with locally advanced pancreatic cancer treated with chemoradiotherapy. *Pancreatology*. (2015) 15:688–93. doi: 10.1016/j.pan.2015.09.015

35. Ma LX, Wang Y, Espin-Garcia O, Allen MJ, Jang GH, Zhang A, et al. Systemic inflammatory prognostic scores in advanced pancreatic adenocarcinoma. *Br J Cancer*. (2023) 128:1916–21. doi: 10.1038/s41416-023-02214-0

36. Balkwill F, Mantovani A. Inflammation and cancer: back to Virchow? *Lancet*. (2001) 357:539–45. doi: 10.1016/S0140-6736(00)04046-0

37. Kusumanto YH, Dam WA, Hospers GA, Meijer C, Mulder NH. Platelets and granulocytes, in particular the neutrophils, form important compartments for circulating vascular endothelial growth factor. *Angiogenesis*. (2003) 6:283–7. doi: 10.1023/B:AGEN.0000029415.62384.ba

38. Salazar-Onfray F, Lopez MN, Mendoza-Naranjo A. Paradoxical effects of cytokines in tumor immune surveillance and tumor immune escape. *Cytokine Growth Factor Rev*. (2007) 18:171–82. doi: 10.1016/j.cytogfr.2007.01.015

39. Xiang ZJ, Hu T, Wang Y, Wang H, Xu L, Cui N. Neutrophil-lymphocyte ratio (NLR) was associated with prognosis and immunomodulatory in patients with pancreatic ductal adenocarcinoma (PDAC). *Biosci Rep*. (2020) 40:BSR20201190. doi: 10.1042/BSR20201190

40. Suthahar N, Wang D, Aboumsallem JP, Shi C, de Wit S, Liu EE, et al. Association of initial and longitudinal changes in C-reactive protein with the risk of cardiovascular disease, cancer, and mortality. *Mayo Clin Proc*. (2023) 98:549–58. doi: 10.1016/j.mayocp.2022.10.013

41. Zhang CL, Gao MQ, Jiang XC, Pan X, Zhang XY, Li Y, et al. Research progress and value of albumin-related inflammatory markers in the prognosis of non-small cell lung cancer: a review of clinical evidence. *Ann Med*. (2023) 55:1294–307. doi: 10.1080/07853890.2023.2192047

42. Yue L, Lu Y, Li Y, Wang Y. Prognostic value of C-reactive protein to albumin ratio in gastric cancer: A meta-analysis. *Nutr Cancer*. (2021) 73:1864–71. doi: 10.1080/01635581.2020.1817510

43. He X, Li JP, Liu XH, Zhang JP, Zeng QY, Chen H, et al. Prognostic value of C-reactive protein/albumin ratio in predicting overall survival of Chinese cervical cancer patients overall survival: comparison among various inflammation based factors. *J Cancer*. (2018) 9:1877–84. doi: 10.7150/jca.23320

44. Liu Z, Jin K, Guo M, Long J, Liu L, Liu C, et al. Prognostic value of the CRP/alb ratio, a novel inflammation-based score in pancreatic cancer. *Ann Surg Oncol*. (2017) 24:561–68. doi: 10.1245/s10434-016-5579-3

45. Fan Z, Fan K, Gong Y, Huang Q, Yang C, Cheng H, et al. The CRP/albumin ratio predicts survival and monitors chemotherapeutic effectiveness in patients with advanced pancreatic cancer. *Cancer Manag Res*. (2019) 11:8781–88. doi: 10.2147/CMAR.S211363

46. Allin KH, Nordestgaard BG. Elevated C-reactive protein in the diagnosis, prognosis, and cause of cancer. *Crit Rev Clin Lab Sci*. (2011) 48:155–70. doi: 10.3109/10408363.2011.599831

47. Luyendyk JP, Schoenecker JG, Flick MJ. The multifaceted role of fibrinogen in tissue injury and inflammation. *Blood*. (2019) 133:511–20. doi: 10.1182/blood-2018-07-818211

48. Fuellen G, Walter U, Henze L, Bohmert J, Palmer D, Lee S, et al. Protein biomarkers in blood reflect the interrelationships between stroke outcome, inflammation, coagulation, adhesion, senescence and cancer. *Cell Mol Neurobiol*. (2023) 43:1413–24. doi: 10.1007/s10571-022-01260-1

49. Bauer AT, Gorzelanny C, Gebhardt C, Pantel K, Schneider SW. Interplay between coagulation and inflammation in cancer: Limitations and therapeutic opportunities. *Cancer Treat Rev*. (2022) 102:102322. doi: 10.1016/j.ctrv.2021.102322

50. Esmon CT. The interactions between inflammation and coagulation. *Br J Haematol*. (2005) 131:417–30. doi: 10.1111/j.1365-2141.2005.05753.x

51. Heissig B, Salama Y, Takahashi S, Osada T, Hattori K. The multifaceted role of plasminogen in inflammation. *Cell Signal*. (2020) 75:109761. doi: 10.1016/j.cellsig.2020.109761

52. Zabel BA, Allen SJ, Kulig P, Allen JA, Cichy J, Handel TM, et al. Chemerin activation by serine proteases of the coagulation, fibrinolytic, and inflammatory cascades. *J Biol Chem*. (2005) 280:34661–6. doi: 10.1074/jbc.M504868200

frontiers | Frontiers in Oncology

TYPE Original Research
PUBLISHED 05 March 2024
DOI 10.3389/fonc.2024.1344150

OPEN ACCESS

EDITED BY
Zsolt Kovács,
George Emil Palade University of Medicine, Pharmacy, Sciences and Technology of Târgu Mureş, Romania

REVIEWED BY
Roberto Cannella,
University of Palermo, Italy
Stefano Francesco Crinò,
University of Verona, Italy

*CORRESPONDENCE
Yueqin Chen
chenyueqin010@163.com
Sen Mao
xiaomao_s@sina.com

RECEIVED 25 November 2023
ACCEPTED 19 February 2024
PUBLISHED 05 March 2024

CITATION
Zhao L, Cao G, Shi Z, Xu J, Yu H, Weng Z, Mao S and Chen Y (2024) Preoperative differentiation of gastric schwannomas and gastrointestinal stromal tumors based on computed tomography: a retrospective multicenter observational study.
Front. Oncol. 14:1344150.
doi: 10.3389/fonc.2024.1344150

Preoperative differentiation of gastric schwannomas and gastrointestinal stromal tumors based on computed tomography: a retrospective multicenter observational study

Luping Zhao[1], Guanjie Cao[1], Zhitao Shi[1], Jingjing Xu[1], Hao Yu[1], Zecan Weng[2], Sen Mao[3]* and Yueqin Chen[1]*

[1]Department of Medical Imaging, The Affiliated Hospital of Jining Medical University, Jining, Shandong, China, [2]Department of Radiology, Guangdong Provincial People's Hospital, Guangdong Academy of Medical Sciences, Guangzhou, China, [3]Department of Ultrasound, The Affiliated Hospital of Jining Medical University, Jining, Shandong, China

Introduction: Gastric schwannoma is a rare benign tumor accounting for only 1–2% of alimentary tract mesenchymal tumors. Owing to their low incidence rate, most cases are misdiagnosed as gastrointestinal stromal tumors (GISTs), especially tumors with a diameter of less than 5 cm. Therefore, this study aimed to develop and validate a diagnostic nomogram based on computed tomography (CT) imaging features for the preoperative prediction of gastric schwannomas and GISTs (diameters = 2–5 cm).

Methods: Gastric schwannomas in 47 patients and GISTs in 230 patients were confirmed by surgical pathology. Thirty-four patients with gastric schwannomas and 167 with GISTs admitted between June 2009 and August 2022 at Hospital 1 were retrospectively analyzed as the test and training sets, respectively. Seventy-six patients (13 with gastric schwannomas and 63 with GISTs) were included in the external validation set (June 2017 to September 2022 at Hospital 2). The independent factors for differentiating gastric schwannomas from GISTs were obtained by multivariate logistic regression analysis, and a corresponding nomogram model was established. The accuracy of the nomogram was evaluated using receiver operating characteristic and calibration curves.

Results: Logistic regression analysis showed that the growth pattern (odds ratio [OR] 3.626; 95% confidence interval [CI] 1.105–11.900), absence of necrosis (OR 4.752; 95% CI 1.464–15.424), presence of tumor-associated lymph nodes (OR 23.978; 95% CI 6.499–88.466), the difference between CT values during the portal and arterial phases (OR 1.117; 95% CI 1.042–1.198), and the difference between CT values during the delayed and portal phases (OR 1.159; 95% CI 1.080–1.245) were independent factors in differentiating gastric schwannoma from GIST. The resulting individualized prediction nomogram showed good discrimination in the training (area under the curve [AUC], 0.937; 95% CI, 0.900–0.973) and validation (AUC, 0.921; 95% CI, 0.830–1.000) datasets. The calibration curve showed that the probability of gastric schwannomas predicted using the nomogram agreed well with the actual value.

Conclusion: The proposed nomogram model based on CT imaging features can be used to differentiate gastric schwannoma from GIST before surgery.

KEYWORDS

gastric schwannoma, gastrointestinal stromal tumor, computed tomography, diagnosis, nomogram

1 Introduction

Following the broad applicability of esophagogastroduodenoscopy and endoscopic ultrasonography, the detection rate of gastric tumors smaller than 5 cm in diameter increased (1). Therefore, it is important to diagnose accurately and develop therapeutic strategies for small gastric lesions. The major categories of gastric submucosal tumors (SMTs) are stromal, neurogenic, and myogenic tumors (2). Different pathological types of SMTs exhibit different biological behaviors (3). Gastric schwannoma is a rare, slow-growing, benign tumor that mostly arises from Schwann cells in the nerve sheaths of the intermuscular nerve plexus of the stomach and accounts for only 1–2% of alimentary tract mesenchymal tumors. Owing to their low incidence rate, the clinical misdiagnosis rate is as high as 96.7% (4), and most cases are misdiagnosed as gastrointestinal stromal tumors (GISTs). The common computed tomography (CT) imaging features of high-risk GISTs include size ≥5 cm, extraluminal or mixed growth pattern, lobulated contour, heterogeneous enhancement, hypo-enhancement, necrosis, and enlarged feeding vessels (5, 6), making it easier to distinguish from gastric schwannoma. However, for low-risk GIST or atypical imaging features with intermediate- to high-risk GIST with diameters less than 5 cm (7), they usually have CT features similar to gastric schwannoma, and gastric schwannoma is almost always diagnosed as GIST before surgery. Although there are no significant differences or specificities in their clinical characteristics, their treatment methods and prognosis differ (8). Owing to the low malignant potential of gastric schwannoma, endoscopic resection is an effective and safe treatment method, with excellent follow-up results and prognosis (9). However, 10–30% of GISTs are considered potentially malignant tumors exhibiting recurrent and metastatic characteristics. Complete surgical resection is an effective method, but the selection of surgical methods needs to be comprehensively considered. Therefore, the accurate distinction of gastric schwannoma from GIST before surgery is crucial not only in the selection of a clinical plan but also in treatment and prognosis.

Although endoscopic ultrasound examination and endoscopic ultrasound-guided tissue sampling have become important tools for distinguishing solid tumors, including gastrointestinal tumors (10, 11), they are invasive and depend on the skills of the operator and may have limitations in evaluating extraluminal growth tumors, lymph nodes, and the relationship between tumors and adjacent structures. CT is a non-invasive and economical imaging method that can clarify the location, size, growth pattern, adjacent organs, blood supply, and distant metastasis of tumors (12). Recently, most studies have differentiated gastric schwannoma from GIST based on qualitative or quantitative descriptions of CT imaging features or the construction of scoring systems (13–15), but the results vary. A recent study (16) showed that the model based on CT qualitative and quantitative features helps distinguish between gastric schwannoma and GIST using machine learning methods, but the model is difficult to apply in clinical practice. Therefore, we aimed to construct a nomogram prediction model based on CT image features to facilitate the preoperative differential diagnosis of gastric schwannoma and GIST and provide suggestions for clinical decision-making.

Abbreviations: GIST, gastrointestinal stromal tumor; SMT, gastric submucosal tumor; LD, long diameter; SD, short diameter.

2 Materials and methods

2.1 Patients

This retrospective study was approved by the institutional Ethics Review Board of the Affiliated Hospital of Jining Medical University, and the requirement for written informed consent was waived by the Review Board. The study enrolled 277 patients with gastric schwannomas or GISTs from two independent hospitals. From June 2009 to August 2022, a total of 246 patients with gastric schwannoma and GIST (diameter=2-5cm) confirmed by postoperative histopathology and immunohistochemistry were recruited in The Affiliated Hospital of Jining Medical University (Hospital 1). Two gastric schwannoma and Sixteen GIST patients were excluded due to lack of preoperative CT data, five GIST patients were excluded due to the presence of two or more lesions, one gastric schwannoma and seven GIST patients were excluded due to poor image quality, seven GIST patients were excluded due to lack of clinical data, two GIST patients were excluded due to preoperative adjuvant therapy, one gastric schwannoma patient complicated with esophageal cancer, and four GIST patients complicated with gastric, liver, pancreatic cancers and gastric leiomyoma were excluded. Finally, 34 patients with gastric schwannomas and 167 patients with GISTs were consecutively included in the training set to determine the CT image features for differentiating gastric schwannomas from GISTs

and construct a nomogram model. The inclusion criteria were as follows: (1) lesions 2–5 cm in diameter, (2) plain and contrast-enhanced CT examinations within 15 days before surgery, (3) solitary lesions, and (4) complete clinicopathological data and good CT image quality. The exclusion criteria were as follows: (1) having received neoadjuvant therapy before surgery and (2) presence of other tumors (gastric, liver, pancreatic, or esophageal cancer). An external validation set of 13 patients with gastric schwannomas and 63 with GISTs was acquired using the same criteria from June 2017 to September 2022 in Guangdong Provincial People's Hospital (Hospital 2) to validate the performance of the nomogram model. Details of the enrolled patients are shown in Figure 1.

GISTs >5 cm had a higher risk of malignant behavior and were more likely to differentiate from other gastric SMTs. However, gastric schwannomas usually had CT features similar to those of GISTs and were nearly always preoperatively diagnosed as GISTs, especially tumors with diameters less than 5 cm. GISTs had potential risks of metastasis and recurrence. The National Comprehensive Cancer Network guidelines recommend that all GISTs more than 2 cm in diameter must be resected (17). However, there remains some controversy regarding the surgical methods and resection ranges of GIST with a diameter of 2–5 cm (18, 19). Therefore, this study selected tumors with a maximum diameter of 2–5 cm as the research objects.

2.2 CT image acquisition

CT examinations were performed on a multidetector-row CT scanner (Siemens SOMATOM Definition, Siemens Healthcare, City, Germany) in Hospital 1 and on a 256-slice CT scanner (Brilliance iCT, Philips Medical Systems, The Netherlands) and a Lightspeed VCT scanner (GE Healthcare, Chicago, IL) in Hospital 2. The CT parameters were as follows: tube voltage = 120 kV, tube current =150–230 mA, 512 × 512 matrix, tube rotation time = 0.5–0.8 s, field of view of 350 × 350 mm, pitch = 0.6, section thickness = 5 mm, and 1 mm reconstruction interval. Before the CT examination, the patients were required to fast for 6–8 h. Water (500–1000 ml) was orally administered for 5 min before the scan. Subsequently, 80–100 ml non-ionic iodinated contrast medium (350 or 370 mg I/ml) was injected through the median cubital vein using a double-barbed high-pressure syringe at flow rates of 3.0–3.5 ml/s. The arterial, portal, and delayed phases were performed at 25–30, 60–65, and 120–140 s after contrast injection, respectively.

2.3 Imaging analysis

All images were independently and retrospectively reviewed by two abdominal radiologists with 10 and 5 years of experience blinded to the clinical data and pathological information. Any

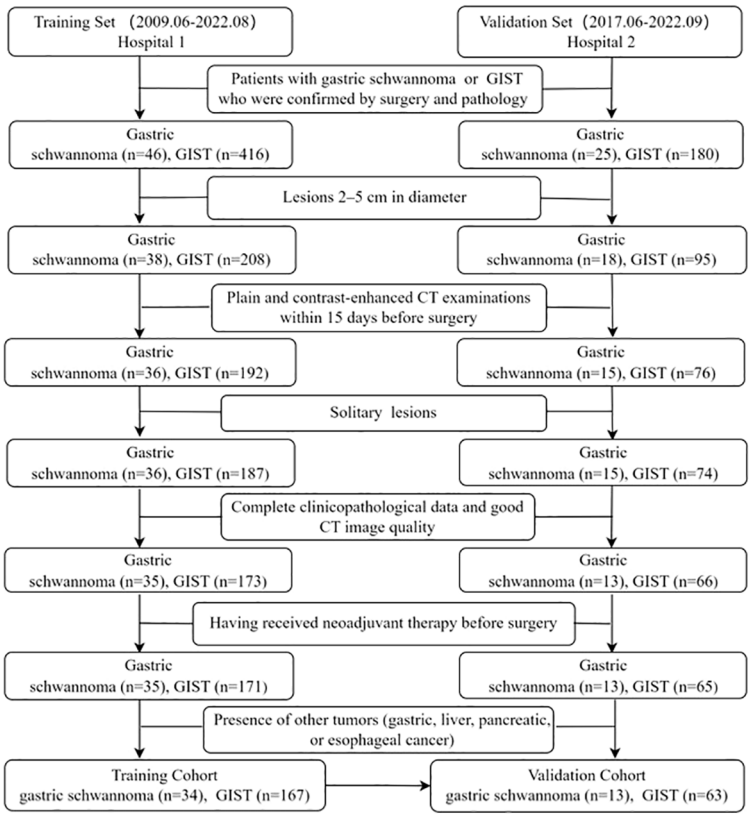

FIGURE 1
Flow chart illustrating the patient selection process.

inconsistency was resolved by consultation with senior supervisors (with 16 years of experience).

All tumors were evaluated for the following CT features: 1) tumor location: the upper, central, and lower parts of the stomach were divided by lines which connected the trisected points on the lesser and greater curvatures (20); 2) contour: regular (round or oval) or irregular; 3) growth pattern: intraluminal, extraluminal, or mixed (21); 4) necrosis, ulceration and calcification: present or absent; 5) tumor vessels: present or absent; 6) tumor-associated lymph nodes: lymph nodes which were enlarged in the fatty space around the tumor (which were confirmed by surgery and pathology) or became small or disappeared after postoperative follow-up, recorded as present or absent; 7) enhancement pattern: homogeneous or heterogeneous (22); 8) enhancement degree: quantitatively evaluated by the difference between the CT values of the enhanced (the larger of either venous phase or delayed phase) and the non-enhanced phases images on the same anatomical slice —a difference <20 Hounsfield units (HUs) was defined as mild enhancement; values of 20–40 HUs were considered as moderate enhancement and >40 HUs as strong enhancement (11); owing to the small number of mild enhancement cases, these were classified as moderate enhancement cases and collectively referred to as mild to moderate enhancement; 9) long diameter (LD)/short diameter (SD) ratio: LD and SD of the central slice of each mass were the maximum and minimum values that were independently measured on CT images in three different orientations (axial, coronal, and sagittal) and LD/SD ratio was calculated (23); and 10) circular regions of interests (ROIs with areas of 16–20 mm^2 and avoiding areas of cystic lesions, calcifications, ulcers, or tumor vessels) were placed at three different homogeneous sites of the lesion and then averaged out, including CT values during non-enhanced (CTV-N), arterial (CTV-A), portal (CTV-P), and delayed phases (CTV-D), were recorded (18).

2.4 Statistical analysis

All statistical analyses were performed using the Statistical Package for Social Sciences software (IBM SPSS Statistics Version 26.0, IBM Corp, Armonk, NY, USA) and R software (version 4.1.3; http://www.R-project.org). The conformity of the variables to the normal distribution was examined using the Shapiro–Wilk test. Normally distributed continuous variables were quantified and reported as the mean ± standard deviation, non-normally distributed variables as median values (Q1, Q3), and categorical data as frequencies (percentages). For quantitative analysis, Student's t-test was used for normally distributed continuous variables, and the Mann–Whitney U test was used for data that were not normally distributed. For qualitative analysis, the Chi-square test or Fisher's exact test was used for categorical variables. The intra-class correlation coefficient (ICC) was calculated for the inter-observer agreement of continuous variables. Good consistency was considered when $0.75 \leq ICC \leq 1$ (24). Each variable that was statistically significant in the univariate analysis ($P<0.05$) was subjected to collinearity assessment and logistic regression analysis with a forward stepwise approach to confirm independent influencing factors in differentiating gastric schwannoma and GIST, which were used to construct a nomogram. Calibration was evaluated using the Hosmer–Lemeshow goodness-of-fit test, receiver operating characteristic analysis was performed using the DeLong method, and the area under the curve (AUC) was used to evaluate the diagnostic efficiency of the model in the training and validation sets. All outcomes were considered statistically significant if $P<0.05$.

3 Results

3.1 Clinicopathological characteristics

The clinicopathological characteristics of patients in the training and validation sets are listed in Table 1. A total of 201 patients, comprising 34 with gastric schwannomas (5 men and 29 women, age 30–80 years, mean 60.38 ± 11.43 years) and 167 with GISTs (66 men and 101 women, age 33–85 years, mean 61.74 ± 11.5 years), were enrolled as the training set. The proportion of female patients in the gastric schwannoma group (29/34, 85.29%) was significantly higher than that in the GIST group (101/167, 60.48%) ($P=0.006$). However, there were no significant differences in age ($P=0.525$) or clinical symptoms ($P=0.405$) between the two groups.

Seventy-six patients were included in the validation set (13 with gastric schwannomas, 6 men and 7 women, age 31–86 years, mean 53.85 ± 14.63 years; 63 with GISTs, 30 men and 33 women, age 40–79 years, mean 62.49 ± 10.33 years). The average age of patients in the gastric schwannoma group was slightly higher than that in the GIST group, and there was a significant difference between the mean ages of the two groups ($P=0.016$). However, there were no significant differences between men and women ($P=0.923$) or in clinical symptoms between groups ($P=0.994$). The clinical symptoms of patients in the training and validation sets were mainly abdominal pain and discomfort, and rare symptoms included melena and hematemesis. Asymptomatic patients were mostly diagnosed during physical examination.

3.2 Inter-observer agreement

The inter-observer agreement in the training and validation cohorts is shown in Table 2. The overall inter-observer agreement for measurements of all continuous variables was excellent in the training and validation sets.

3.3 CT imaging features

A comparison of the CT imaging features in the training and validation sets is shown in Table 3. In the qualitative analysis, tumor location ($P=0.003$), contour ($P=0.003$), growth pattern ($P=0.001$), absence of necrosis ($P=0.001$), presence of tumor-associated lymph nodes ($P<0.001$), enhancement pattern ($P=0.002$), and degree of enhancement ($P=0.006$) were significantly different between the gastric schwannoma and GIST groups in the training set. However,

TABLE 1 Clinical characteristics data of patients in training and validation cohort.

Clinical Characteristics	Training cohort (n=201)			Validation cohort(n=76)		
	Gastric schwannoma (n=34)	GIST (n=167)	*P value*	Gastric schwannoma (n=13)	GIST (n=63)	*P value*
Age (years)	60.38±11.43	61.74±11.35	0.525	53.85±14.63	62.49±10.33	0.016
Sex			0.006[a]			0.923[a]
Male	5(14.71%)	66(39.52%)		6(46.15%)	30(47.62%)	
Female	29(85.29%)	101(60.48%)		7(53.85%)	33(52.38%)	
Clinical Symptoms			0.405[a]			0.994[a]
Present	19(55.88%)	106(63.47%)		7(53.85%)	34(53.97%)	
Absent	15(44.12%)	61(36.53%)		6(46.15%)	29(46.03%)	
Risk category						
Very low /Low risk		118(70.66%)			46(73.02%)	
Intermediate risk		36(21.56%)			15(23.81%)	
High risk		13(7.78%)			2(3.17%)	

Independent samples t tests were applied in continuous variables.
[a]Chi-squared tests were used in categorical variables.

there were no significant differences in tumor vessels (P=0.944), ulceration (P=0.813), or calcification (P=0.900) between the two groups in the training set. In the validation set, there were significant differences in tumor location (P=0.005), absence of necrosis (P=0.015), presence of tumor-associated lymph nodes (P <0.001), and degree of enhancement (P=0.02) between the two groups. However, there were no significant differences in contour (P=1.0), growth pattern (P=0.767), tumor vessels (P=0.379), ulceration (P=1.0), calcification (P=0.582), or enhancement pattern (P=0.692) between the two groups in the validation set.

In the quantitative analysis, the LD/SD ratio values of gastric schwannomas were close to those of GISTs, and there were no significant differences between the two groups in the training (P=0.276) and validation (P=0.600) set cases. The values of CTV-D, CTV-D–CTV-N, CTV-P–CTV-A, and CTV-D–CTV-P in the gastric schwannoma group were significantly higher than those in the GIST group; there were significant differences between the two groups in the training (all P<0.001) and validation (P<0.001, <0.001, <0.001, = 0.012, respectively) sets. The CTV-N value (P=0.034) in the gastric schwannoma group was slightly higher than that in the GIST group in the training set. The values of CTV-P (P = 0.004) and CTV-P–CTV-N (P=0.007) in the gastric schwannoma group were slightly higher than those in the GIST group in the validation set. There were no significant differences in the values of CTV-A (P=0.268), CTV-P (P=0.306), CTV-A–CTV-N (P=0.055), or CTV-P–CTV-N (P=0.297) between the two groups in the training set, and there were no significant differences in the values of CTV-N (P=0.814), CTV-A (P=0.890), or CTV-A–CTV-N (P=0.735) between the two groups in the validation set.

3.4 Establishment of a nomogram model and validation of its predictive accuracy

Each statistically significant variable in the univariate analysis was subjected to collinearity and correlation assessments. Because

TABLE 2 Inter-observer agreement in training and validation cohort.

variables	Training cohort		Validation cohort	
	ICC value	95 %CI	ICC value	95 %CI
LD	0.899	0.860–0.926	0.935	0.878–0.963
SD	0.964	0.952–0.972	0.921	0.839–0.957
CTV-N	0.802	0.669–0.874	0.820	0.730–0.882
CTV-A	0.883	0.795–0.927	0.916	0.870–0.946
CTV-P	0.909	0.882–0.931	0.925	0.885–0.952
CTV-D	0.940	0.922–0.954	0.932	0.894–0.956

LD, SD indicate the tumor of long diameter and short diameter, respectively. CTV-N, CTV-A, CTV-P, and CTV-D CT values during nonenhanced, arterial, portal, and delayed phases, respectively.

10.3389/fonc.2024.1344150

TABLE 3 CT Imaging Features in training and validation cohort.

CT Imaging Features	Training cohort (n=201)			Validation cohort(n=76)		
	Gastric schwannoma (n=34)	GIST (n=167)	*P value*	Gastric schwannoma (n=13)	GIST (n=63)	*P value*
Location			0.003			0.005
Upper Stomach	5(14.71%)	73(43.71%)		2(15.38%)	30(47.62%)	
Central Stomach	21(61.76%)	77(46.11%)		7(53.85%)	30(47.62%)	
Lower Stomach	8(23.53%)	17(10.18%)		4(30.77%)	3(4.76%)	
Contour			0.003			1.0
Regular	29(85.29%)	97(58.08%)		10(76.92%)	46(73.02%)	
Irregular	5(14.71%)	70(41.92%)		3(23.08%)	17(26.98%)	
Growth pattern			<0.001			0.308
Intraluminal Type	7(20.59%)	91(54.49%)		5(38.46%)	34(53.97%)	
Extraluminal or Mixed Type	27(79.41%)	76(45.51%)		8(61.54%)	29(46.03%)	
Necrosis			0.001			0.015[a]
Present	9(26.47%)	97(58.08%)		0(0%)	21(33.33%)	
Absent	25(73.53%)	70(41.92%)		13(100%)	42(66.67%)	
Calcification			0.900			0.582[a]
Present	6(17.65%)	31(18.56%)		0(0%)	6(9.52%)	
Absent	28(82.35%)	136(81.44%)		13(100%)	57(90.48%)	
Ulceration			0.813			1.0
Present	9(26.47%)	41(24.55%)		3(23.08%)	17(26.98%)	
Absent	25(73.53%)	126(75.45%)		10(76.92%)	46(73.02%)	
Tumour-Associated Lymph Node			<0.001			<0.001
Present	18(52.94%)	8(4.79 %)		6(46.15 %)	3(4.76 %)	
Absent	16(47.06%)	159(95.21%)		7(53.85 %)	60(95.24 %)	
Intratumoral enlarged vessels			0.944			0.379
Present	11(32.35%)	53(31.74%)		6(46.15%)	21(33.33%)	
Absent	23(67.65%)	114(68.26%)		7(53.85%)	42(66.67%)	
Enhancement Degree			0.006			0.02
Mild to Moderate enhancement	16(47.06%)	119(71.26%)		6(46.15%)	49(77.78%)	
Strong enhancement	18(52.94%)	48(28.74%)		7(53.85%)	14(22.22%)	
Enhancement pattern			0.002			0.692
Homogeneous	22(64.71%)	65(38.92%)		8(61.54%)	35(55.56%)	
Heterogeneous	12(35.29%)	102(61.08%)		5(38.46%)	28(44.44%)	
LD/SD Ratio	1.27±0.21	1.32±0.23	0.276	1.33±0.28	1.32±0.19	0.600
CTV-N	35.32±4.31	32.92±6.28	0.034	35.15±5.23	36.02±5.79	0.814
CTV-A	49.62±9.17	52.06±12.14	0.268	56.62±13.75	56.30±12.01	0.890

(Continued)

TABLE 3 Continued

CT Imaging Features	Training cohort (n=201)			Validation cohort(n=76)		
	Gastric schwannoma (n=34)	GIST (n=167)	*P value*	Gastric schwannoma (n=13)	GIST (n=63)	*P value*
CTV-P	67.21±10.86	64.08±17.02	0.306	79.62±16.52	67.48±14.04	0.004
CTV-D	77.47±11.81	65.63±13.08	<0.001	88.46±17.80	70.46±12.12	<0.001
(CTV-A)-(CTV-N)	13.5(9,18.5)	17(10,27)	0.055[b]	21(10.5,30.5)	19(9,27)	0.735[b]
(CTV-P)-(CTV-N)	31(24.75,37.25)	29(22,39)	0.297[b]	44(31.5,54.5)	30(22,38)	0.007[b]
(CTV-D)-(CTV-N)	42.15±9.65	32.72±12.60	<0.001	51(38.5,68.5)	33(26,39)	<0.001[b]
(CTV-P)-(CTV-A)	18(11.5,22.25)	10(4,18)	<0.001[b]	23(15,28.5)	9(6,16)	<0.001[b]
(CTV-D)-(CTV-P)	10(6.75,12)	4(-3,7)	<0.001[b]	7(4.5,13)	4(-2,8)	0.012[b]

CTV-N, CTV-A, CTV-P, and CTV-D CT values during nonenhanced, arterial, portal, and delayed phases, respectively.
[a]Fisher's exact tests were applied to categorical variables, and chi-square tests were applied to all other variables.
[b]Mann-Whitney U test was applied to continuous variables, and Student's t-test was applied to all other variables.

of the enhancement pattern and necrosis, the values of CTV-D–CTV-N and CTV-D exhibited multicollinearity and obvious correlation; the enhancement pattern and the value of CTV-D were removed. Logistic regression analysis showed that extraluminal or mixed growth pattern (odds ratio [OR] 3.626; 95% CI 1.105–11.900; P=0.034), absence of necrosis (OR 4.752; 95% CI 1.464–15.424; P=0.009), presence of tumor-associated lymph nodes (OR 23.978; 95% CI 6.499–88.466; P<0.001), and the values of CTV-P–CTV-A (OR 1.117; 95% CI 1.042–1.198; P=0.002) and CTV-D–CTV-P (OR 1.159; 95% CI 1.080–1.245; P<0.001) were independent predictive factors associated with gastric schwannoma (Figures 2, 3 and Table 4). A nomogram model was also established (Figure 4). The final nomogram model yielded AUCs of 0.937 (95% CI 0.900–0.973) and 0.921 (95% CI 0.830–1.000) in the training and validation sets, respectively. The sensitivity, specificity, and accuracy of the nomogram model in the training set were 94.1%, 78.4%, and 81.1%, respectively, whereas those in the validation set were 92.3%, 82.5%, and 84.2%, respectively (Figure 5). The results of the Hosmer-Lemeshow goodness-of-fit test in the training (χ^2 = 3.501; P=0.899) and validation sets (χ^2 = 8.178; P=0.416) indicated that the calibration of the nomogram model was appropriate (Figure 6).

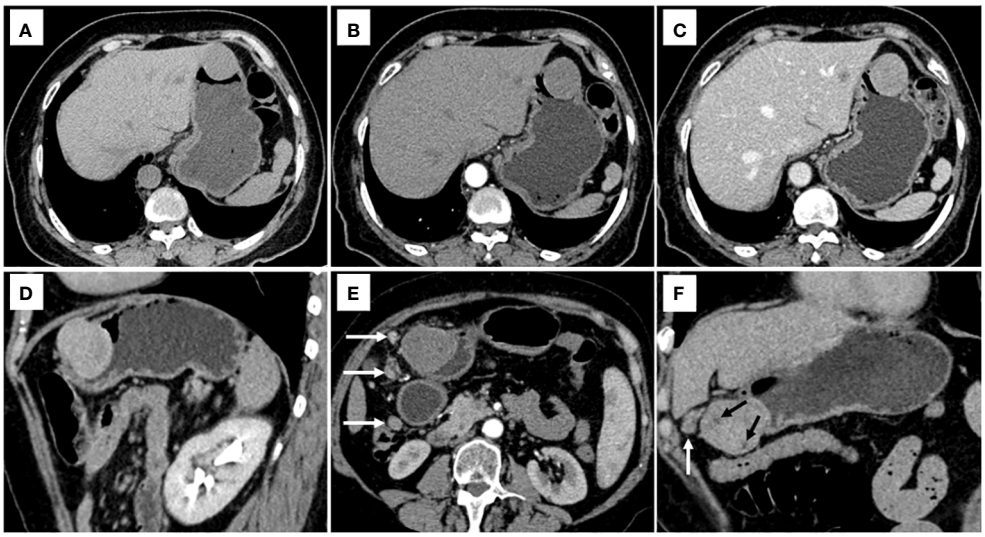

FIGURE 2
CT examination of patient 1, including axial unenhanced **(A)**, arterial phase image **(B)**, and portal phase image **(C)**, and oblique sagittal delayed phases image **(D)**, showed a mixed growth pattern lesion in the central of stomach without peritumoral lymph nodes and necrosis. The value of [(CTV-P) -(CTV-A)] and the value of [(CTV-D) -(CTV-P)] were 30 and 16, respectively. The nomogram accurately diagnosed gastric schwannoma with a predicted probability of 87%. CT examination of patient 2, including axial arterial phase image **(E)**, and coronal delayed phases image **(F)**, showed a mixed growth pattern lesion in the lower of stomach with the peritumoral lymph nodes (white arrow) and necrosis (black arrow). The value of [(CTV-P) -(CTV-A)] and the value of [(CTV-D) -(CTV-P)] were 15 and 16, respectively. The nomogram accurately diagnosed gastric schwannoma with a predicted probability of 92%. Finally, the tumors were confirmed as gastric schwannoma by histopathology.

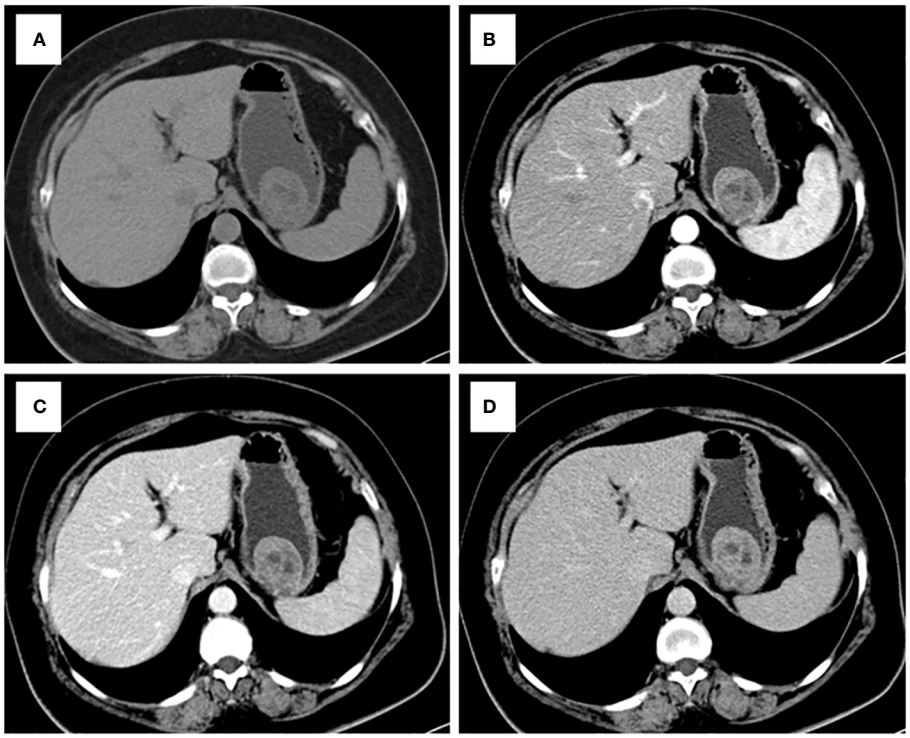

FIGURE 3
CT examination of patient 3, including axial unenhanced **(A)**, arterial phase image **(B)**, and portal phase image **(C)**, and delayed phases image **(D)**, showed an intraluminal growth pattern lesion in in the upper of stomach with necrosis. The value of [(CTV-P) -(CTV-A)] and the value of [(CTV-D) -(CTV-P)] were 9 and 12, respectively. The nomogram accurately diagnosed gastric schwannoma with a predicted probability of 4%. Finally, the tumors were confirmed as GIST by histopathology.

4 Discussion

In the present study, a quantitative description of tumor imaging features was added using five CT imaging features, including extraluminal or mixed growth pattern, absence of necrosis, presence of tumor-associated lymph nodes, and the values of CTV-P–CTV-A and CTV-D–CTV-P, treated as independent predictive factors for the differential diagnosis of gastric schwannoma and GIST (diameters = 2–5 cm) based on logistic regression analysis. The CT-based nomogram derived from these factors had a higher diagnostic efficiency, sensitivity, and specificity in both the training and validation sets. This visualized differential diagnosis nomogram model helps improve the accuracy in predicting tumor properties and provides a favorable basis for clinicians to choose surgical plans.

There were five predictive factors for imaging features that differentiated gastric schwannomas from GISTs in the training set. Compared with previous studies (3, 13), the presence of tumor-associated lymph nodes was also observed in our study, with an OR 23.978, thus indicating that the presence of tumor-associated lymph nodes is the most significant characteristic distinguishing gastric schwannomas from GISTs. Some authors (5, 13, 25, 26) have stated

TABLE 4 Logistic regression analysis of CT features for prediction of Gastric schwannoma.

Constants and Variables	*β value*	Odds Ratio (95 %CI)	*P value*
Growth Pattern(Extraluminal or Mixed Type)	1.288	3.626(1.105~11.900)	0.034
Tumour-associated lymph node (present)	3.177	23.978 (6.499~88.466)	<0.001
Necrosis (absent)	1.558	4.752(1.464~15.424)	0.009
(CTV-P)-(CTV-A)	0.111	1.117(1.042~1.198)	0.002
(CTV-D)-(CTV-P)	0.148	1.159(1.080~1.245)	<0.001
Constant	-6.602		<0.001

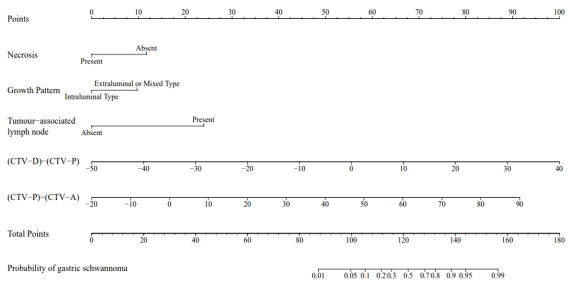

FIGURE 4
A nomogram was developed in the training set incorporating necrosis, growth pattern, tumor-associated lymph node, the value of [(CTV-D)-(CTV-P)], the value of [(CTV-P)-(CTV-A)].

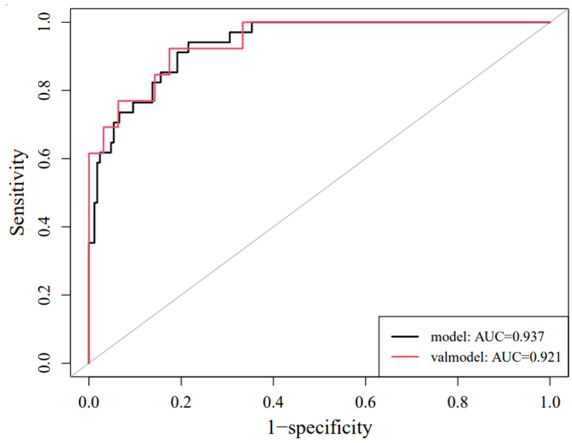

FIGURE 5
ROC curves of the nomogram in the training set and validation set.

that the peritumoral lymph nodes around gastric schwannomas are manifestations of inflammatory reactive hyperplasia, and we agree with this view. In the training set, the extraluminal or mixed growth pattern and absence of necrosis were the other two independent factors (OR=3.626 and 4.752, respectively). In our study, gastric schwannomas mostly occurred in the middle part of the stomach (21/34, 61.76%), typically associated with extraluminal or mixed type (27/34, 79.41%), whereas GIST mainly occurred in the upper and middle parts of the stomach (150/167, 89.82%), with intraluminal growth (91/167, 54.49%), which is consistent with previous reports (13, 16, 27). In this study, gastric schwannomas rarely exhibited intralesional necrosis, and necrosis and calcification were more common in the periphery of the tumor compared with GISTs. Some studies have found that gastric schwannomas grow slowly and that neovascularization provides an adequate blood supply for their growth, thus resulting in rare necrosis; however, GISTs may be potentially malignant, and insufficient internal blood supply can lead to ischemia and necrosis of tumor cells (3, 5), which is consistent with the results of this study.

The results of this study showed statistically significant differences in the values of CTV-D, CTV-P–CTV-A, and CTV-D–CTV-P between gastric schwannomas and GISTs in the training and validation sets. Owing to the different vascularity profiles of gastric schwannoma and GIST, the degree of enhancement of gastric schwannoma was lower than that of GIST in the arterial phase. Previous studies showed that GIST is typically a hypervascular lesion on contrast-enhanced CT (5, 28). It has been suggested that the enhancement of gastric schwannomas occurs over time, with peak enhancement occurring during the delayed phase, which may be related to the slender blood vessels supplying the lesion, thus leading to the slow infiltration of contrast agents from the blood vessels into the surrounding tissue gaps (18, 29). Conversely, as previously mentioned, the value of CTV-D may decline in GIST because of the fast washout of intratumoral contrast agents. These reasons could explain the findings of the current study that showed that the values of CTV-P–CTV-A and CTV-D–CTV-P in gastric schwannomas were significantly higher than those in GISTs.

Wang et al. (16) compared and analyzed several different methods to differentiate gastric schwannomas and GISTs based on machine learning and stated that the logistic regression model could be robust and accurate. In this study, an intuitive visual nomogram model was constructed using five imaging feature predictors screened by logistic regression, which was confirmed to have good consistency with clinical practice in both the training set (AUC = 0.937) and the external validation set (AUC = 0.921). In clinical applications, the selected imaging feature prediction factors are easy to collect and can

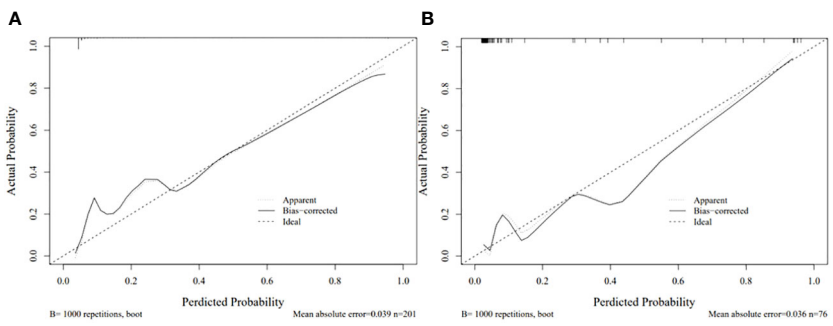

FIGURE 6
Calibration curve for the nomogram in the training set **(A)** and validation set **(B)**. .

conveniently and quickly improve the ability of physicians to distinguish gastric schwannomas from GISTs.

This study has the following limitations. First, in the logistic regression analysis, combined classifications may have influenced the results owing to the small number of tumors with specific sites and growth patterns. Second, this was a retrospective study conducted in two centers only; the sample size was small and inevitably led to certain selection biases. Owing to the small sample size, the results were not sufficiently robust. In future studies, we plan to evaluate the reliability of the current nomogram using data from multiple centers and a prospective design.

In conclusion, this study developed and validated a diagnostic nomogram model based on CT imaging features that allowed the development of an accurate and non-invasive evaluation method for differentiating gastric schwannomas and GISTs. As the basis of the non-invasive semiquantitative examination method, the nomogram model can supplement conventional examination methods and assist clinicians in decision-making.

Data availability statement

The original contributions presented in the study are included in the article/supplementary material. Further inquiries can be directed to the corresponding authors.

Ethics statement

The studies involving humans were approved by Affiliated Hospital of Jining Medical University. The studies were conducted in accordance with the local legislation and institutional requirements. The participants provided their written informed consent to participate in this study.

Author contributions

LZ: Conceptualization, Data curation, Funding acquisition, Writing – original draft, Writing – review and editing. GC: Data curation, Resources, Validation, Writing – original draft. ZS: Data curation, Resources, Validation, Writing – original draft. JX: Data curation, Resources, Validation, Writing – original draft. HY: Writing – original draft, Conceptualization, Formal Analysis, Supervision. ZW: Writing – original draft, Data curation, Resources, Validation. SM: Data curation, Resources, Validation, Writing – original draft. YC: Funding acquisition, Methodology, Resources, Software, Supervision, Writing – review and editing.

Funding

The author(s) declare financial support was received for the research, authorship, and/or publication of this article. This work was supported by the 2022 Jining Key Research and Development Plan Projects (2022YXNS033 and 2022YXNS061) and the Shandong Natural Science Foundation General Project (ZR2021MH109).

Acknowledgments

We would like to thank Editage (www.editage.cn) for English language editing.

Conflict of interest

The authors declare that the research was conducted in the absence of any commercial or financial relationships that could be construed as a potential conflict of interest.

Publisher's note

References

1. Peng H, Han L, Tan Y, Chu Y, Lv L, Liu D, et al. Clinicopathological characteristics of gastrointestinal schwannomas: A retrospective analysis of 78 cases. *Front Oncol.* (2022) 12:1003895. doi: 10.3389/fonc.2022.1003895

2. Kim JY, Lee JM, Kim KW, Park HS, Choi JY, Kim SH, et al. Ectopic pancreas: CT findings with emphasis on differentiation from small gastrointestinal stromal tumor and leiomyoma. *Radiology*. (2009) 252:92–100. doi: 10.1148/radiol.2521081441

3. Choi YR, Kim SH, Kim SA, Shin CI, Kim HJ, Kim SH, et al. Differentiation of large (≥ 5 cm) gastrointestinal stromal tumors from benign subepithelial tumors in the stomach: radiologists' performance using CT. *Eur J Radiol*. (2014) 83:250–60. doi: 10.1016/j.ejrad.2013.10.028

4. Tao K, Chang W, Zhao E, Deng R, Gao J, Cai K, et al. Clinicopathologic features of gastric schwannoma: 8-year experience at a single institution in China. *Med (Baltimore)*. (2015) 94:e1970. doi: 10.1097/MD.0000000000001970

5. Cannella R, Tabone E, Porrello G, Cappello G, Gozzo C, Incorvaia L, et al. Assessment of morphological CT imaging features for the prediction of risk stratification, mutations, and prognosis of gastrointestinal stromal tumors. *Eur Radiol*. (2021) 31:8554–64. doi: 10.1007/s00330-021-07961-3

6. Zhou C, Duan X, Zhang X, Hu H, Wang D, Shen J. Predictive features of CT for risk stratifications in patients with primary gastrointestinal stromal tumour. *Eur Radiol*. (2016) 26:3086–93. doi: 10.1007/s00330-015-4172-7

7. Choi JW, Choi D, Kim KM, Sohn TS, Lee JH, Kim HJ, et al. Small submucosal tumors of the stomach: differentiation of gastric schwannoma from gastrointestinal stromal tumor with CT. *Korean J Radiol*. (2012) 13:425–33. doi: 10.3348/kjr.2012.13.4.425

8. Qi Z, Yang N, Pi M, Yu W. Current status of the diagnosis and treatment of gastrointestinal schwannoma. *Oncol Lett*. (2021) 21:384. doi: 10.3892/ol.2021.12645

9. Hu J, Liu X, Ge N, Wang S, Guo J, Wang G, et al. Role of endoscopic ultrasound and endoscopic resection for the treatment of gastric schwannoma. *Med (Baltimore)*. (2017) 96:e7175. doi: 10.1097/MD.0000000000007175

10. Guo J, Sahai AV, Teoh A, Arcidiacono PG, Larghi A, Saftoiu A, et al. An international, multi-institution survey on performing EUS-FNA and fine needle biopsy. *Endosc Ultrasound*. (2020) 9:319–28. doi: 10.4103/eus.eus_56_20

11. Crinò SF, Bernardoni L, Manfrin E, Parisi A, Gabbrielli A. Endoscopic ultrasound features of pancreatic schwannoma. *Endosc Ultrasound*. (2016) 5:396–8. doi: 10.4103/2303-9027.195873

12. Scola D, Bahoura L, Copelan A, Shirkhoda A, Sokhandon F. Getting the GIST: a pictorial review of the various patterns of presentation of gastrointestinal stromal tumors on imaging. *Abdom Radiol (NY)*. (2017) 42:1350–64. doi: 10.1007/s00261-016-1025-z

13. Xu JX, Yu JN, Wang XJ, Xiong YX, Lu YF, Zhou JP, et al. A radiologic diagnostic scoring model based on CT features for differentiating gastric schwannoma from gastric gastrointestinal stromal tumors. *Am J Cancer Res*. (2022) 12:303–14.

14. Okanoue S, Iwamuro M, Tanaka T, Satomi T, Hamada K, Sakae H, et al. Scoring systems for differentiating gastrointestinal stromal tumors and schwannomas from leiomyomas in the stomach. *Med (Baltimore)*. (2021) 100:e27520. doi: 10.1097/MD.0000000000027520

15. Zhang S, Yang Z, Chen X, Su S, Huang R, Huang L, et al. Development of a CT image analysis-based scoring system to differentiate gastric schwannomas from gastrointestinal stromal tumors. *Front Oncol*. (2023) 13:1057979. doi: 10.3389/fonc.2023.1057979

16. Wang J, Xie Z, Zhu X, Niu Z, Ji H, He L, et al. Differentiation of gastric schwannomas from gastrointestinal stromal tumors by CT using machine learning. *Abdom Radiol (NY)*. (2021) 46:1773–82. doi: 10.1007/s00261-020-02797-9

17. Demetri GD, von Mehren M, Antonescu CR, DeMatteo RP, Ganjoo KN, Maki RG, et al. NCCN Task Force report: update on the management of patients with gastrointestinal stromal tumors. *J Natl Compr Canc Netw*. (2010) 8 Suppl 2:S1–S44. doi: 10.6004/jnccn.2010.0116

18. Chen Z, Yang J, Sun J, Wang P. Gastric gastrointestinal stromal tumours (2-5 cm): Correlation of CT features with Malignancy and differential diagnosis. *Eur J Radiol*. (2020) 123:108783. doi: 10.1016/j.ejrad.2019.108783

19. An W, Sun PB, Gao J, Jiang F, Liu F, Chen J, et al. Endoscopic submucosal dissection for gastric gastrointestinal stromal tumors: a retrospective cohort study. *Surg Endosc*. (2017) 31:4522–31. doi: 10.1007/s00464-017-5511-3

20. Japanese Gastric Cancer Association. Japanese classification of gastric carcinoma: 3rd English edition. *Gastric Cancer*. (2011) 14:101–12. doi: 10.1007/s10120-011-0041-5

21. Kim HC, Lee JM, Kim KW, Park SH, Kim SH, Lee JY, et al. Gastrointestinal stromal tumors of the stomach: CT findings and prediction of Malignancy. *AJR Am J Roentgenol*. (2004) 183:893–8. doi: 10.2214/ajr.183.4.1830893

22. Peng G, Huang B, Yang X, Pang M, Li N. Preoperative CT feature of incomplete overlying enhancing mucosa as a high-risk predictor in gastrointestinal stromal tumors of the stomach. *Eur Radiol*. (2021) 31:3276–85. doi: 10.1007/s00330-020-07377-5

23. Xu JX, Ding QL, Lu YF, Fan SF, Rao QP, Yu RS. A scoring model for radiologic diagnosis of gastric leiomyomas (GLMs) with contrast-enhanced computed tomography (CE-CT): Differential diagnosis from gastrointestinal stromal tumors (GISTs). *Eur J Radiol*. (2021) 134:109395. doi: 10.1016/j.ejrad.2020.109395

24. Koo TK, Li MY. A guideline of selecting and reporting intraclass correlation coefficients for reliability research. *J Chiropr Med*. (2016) 15:155–63. doi: 10.1016/j.jcm.2016.02.012

25. Wang J, Zhang W, Zhou X, Xu J, Hu HJ. Simple analysis of the computed tomography features of gastric schwannoma. *Can Assoc Radiol J*. (2019) 70:246–53. doi: 10.1016/j.carj.2018.09.002

26. Liu M, Liu L, Jin E. Gastric sub-epithelial tumors: identification of gastrointestinal stromal tumors using CT with a practical scoring method. *Gastric Cancer*. (2019) 22:769–77. doi: 10.1007/s10120-018-00908-6

27. Zhang Y, Mao XL, Zhou XB, Yang H, Zhu LH, Chen G, et al. Long-term outcomes of endoscopic resection for small (≤ 4.0 cm) gastric gastrointestinal stromal tumors originating from the muscularis propria layer. *World J Gastroenterol*. (2018) 24:3030–7. doi: 10.3748/wjg.v24.i27.3030

28. Li R, Gan H, Ni S, Fu Y, Zhu H, Peng W. Differentiation of gastric schwannoma from gastric gastrointestinal stromal tumor with dual-phase contrast-enhanced computed tomography. *J Comput Assist Tomogr*. (2019) 43:741–6. doi: 10.1097/RCT.0000000000000902

29. Ji JS, Lu CY, Mao WB, Wang ZF, Xu M. Gastric schwannoma: CT findings and clinicopathologic correlation. *Abdom Imaging*. (2015) 40:1164–9. doi: 10.1007/s00261-014-0260-4

frontiers | Frontiers in Oncology

TYPE Case Report
PUBLISHED 31 May 2024
DOI 10.3389/fonc.2024.1340859

OPEN ACCESS

EDITED BY
Zsolt Kovács,
Sciences and Technology of Târgu Mureş, Romania

REVIEWED BY
Yu-gang Huang,
Hubei University of Medicine, China
Zahra Hosseini-khah,
Mazandaran University of Medical Sciences, Iran

*CORRESPONDENCE
Wenjing Du
chengdu001@sohu.com

†These authors share first authorship

RECEIVED 19 November 2023
ACCEPTED 02 April 2024
PUBLISHED 31 May 2024

CITATION
Liu Y, Mao J, Shen D, Jin B, Wu X, Song C and Du W (2024) Combined treatment for a rare malignant glomus tumor of the esophagus with pulmonary and liver metastases: a case report and review of literature.
Front. Oncol. 14:1340859.
doi: 10.3389/fonc.2024.1340859

Combined treatment for a rare malignant glomus tumor of the esophagus with pulmonary and liver metastases: a case report and review of literature

Yanan Liu[1†], Jingjing Mao[2†], Dongfeng Shen[3], Baoli Jin[1], Xueqin Wu[1], Congcong Song[2] and Wenjing Du[1*]

[1]Shanxi Province Cancer Hospital, Shanxi Hospital Affiliated to Cancer Hospital, Chinese Academy of Medical Sciences/Cancer Hospital Affiliated to Shanxi Medical University, Taiyuan, Shanxi, China, [2]Department of Translational Medicine, Shenzhen Engineering Center for Translational Medicine of Precision Cancer Immunodiagnosis and Therapy, YuceBio Technology Co., Ltd, Shenzhen, China, [3]Department of Tumor Minimally Invasive Therapy, Shanxi Traditional Chinese Medical Hospital, Taiyuan, Shanxi, China

Background: Glomus tumors are typically benign soft tissue tumors that occur at the extremities; malignant and viscerally occurring cases are extremely rare.

Case presentation: We report a 49-year old male patient with a malignant esophageal glomus tumor that was complicated by lung and liver metastases. Genetic test results guided the patient's individualized treatment. Consequently, treatment with Anlotinib combined with Tislelizumab achieved significant clinical benefits.

Conclusion: Our case report demonstrates that immunotherapy combined with anti-angiogenic therapy in patients with malignant esophageal glomus tumors can achieve significant efficacy and suggests the potential value of next-generation sequencing (NGS) detection in guiding personalized treatments in patients with malignant esophageal glomus tumors.

KEYWORDS

malignant glomus tumor, esophageal, anlotinib, immunotherapy, case report

Background

Glomus tumors(GT) are uncommon mesenchymal neoplasms mainly derived from perivascular modified smooth muscle cells, the majority of glomus tumors occurs in the skin and superficial soft tissues of the distal extremities, at a site other than the limbs are extremely uncommon (1–3). Most GTs are benign, malignant glomus tumors are extremely rare accounting for <1% of all glomus tumors. Only a few cases of malignant GTs have been

reported, and most of them were locally aggressive and distally metastatic (3, 4). The diagnosis of malignancy should take into account tumor size, infiltration, mitotic activity, nuclear atypia, and vascular involvement (5). By summarizing the pathological features of 52 cases, Folpe and colleagues proposed a subclassification of atypical and malignant GTs (6). The criteria for the diagnosis of malignancy are as follows: i) deep location of the tumor, ii) size of the tumor>2cm, iii) atypical mitosis or obvious nuclear heterogeneity, iv) mitotic cells accounting for five or more of 50 under high power field (HPF). If a GT is larger than 2cm and deep in location, but without nuclear heterogeneity, it will be classified as an undetermined malignant potential GT (7).

They usually present clinically as a triad of severe subungual pain, tenderness localized over a point, and cold hypersensitivity (8, 9). The optimal treatment of malignant glomus tumors remains unknown, and the current published literature consists of individual case reports or series, local wide excision remains the most viable treatment option.

In this report, our objective was to present a unique case of a malignant esophageal glomus tumor with pulmonary and liver metastases. After treatment, the patient's condition has improved, his quality of life has significantly improved, and their life has also been extended.

Case presentation

A 49-year-old Chinese male initially presented with dysphagia and foreign body sensation without obvious inducement. Later, the patient presented with aggravated dysphagia accompanied by chest and back pain; therefore, he was treated in our hospital. A non-enhanced chest computed tomography (CT) scan showed a large esophageal tumor, and the mass size measurement was around 4.6 × 3.9 × 8.3 cm and located in the middle part of the esophagus. One month later, the patient was admitted to Tianjin Cancer Hospital. CT and endoscopic ultrasound confirmed that the patient had Stage T4 esophageal cancer with multiple mediastinal lymph node enlargements. The patient underwent surgery under general anesthesia with three incisions: radical resection of the lower thoracic segment of the esophagus, partial gastrectomy, tube and gastroplasty, left cervical esophagogastrostomy, thoracic and abdominal lymph node dissection, and jejunostomy. Postoperative pathological and immunohistochemical detection results indicated that the patient had a malignant glomus tumor in the middle section of the esophagus, and no tumor metastasis was observed in the regional lymph nodes. The final diagnosis was confirmed by immunohistochemistry of positive smooth muscle actin (SMA), vimentin, B-cell lymphoma-2 (Bcl-2), and a Ki67 index of 40%. The specimen showed negative staining for CK5/6, CK8/18, P40, S-100, CD34, ERG, EMA, CD31, Desmin, CD117, and LCA. The patient was not treated postoperatively.

The disease progressed by four months after surgery (December 17, 2021). CT examination revealed submediastinoid nodules and multiple nodules in both lungs, and metastasis was considered. January 1, 2022, the patient then underwent chemotherapy with docetaxel and cisplatin for one cycle. Docetaxel 100mg, ivgtt, d1, cisplatin 30mg, ivgtt, d1-3, repeated every 21-28 days. However, cough, hemoptysis, and obvious chest and back pain were observed after one cycle chemotherapy, and symptomatic treatment for medical hemostasis was ineffective.

On February 10, a follow-up examination showed the progression of bilateral lung nodules and liver metastases. At this time, there were nearly 20 bilateral lung metastases, with the largest one having a diameter of 1.2cm. There were multiple liver metastases, with the larger one located in the left lobe of the liver, approximately 3.1 * 2.0cm. Percutaneous selective arteriography was performed under local anesthesia on February 15, 2022. After percutaneous arterial embolization, the hemoptysis was slightly relieved. CT results on March 1 again showed multiple pulmonary nodules that were larger than before, with the diameter of the largest nodule increasing to 1.2 cm. An irregular mass was found near the left side of the chest and stomach, with a size of 4.3 × 2.7 cm, which compressed the left main bronchus, a large amount of fluid in the left thoracic cavity, and abdominal lymph node metastasis, considering the progression of the disease. The patient coughed violently, expelling soft tissue-like masses. These masses were examined pathologically and combined with immunohistochemical results, showed positivity for CD31, SMA, Caldesmon, CD34, and the Ki67 index was 60% (Figure 1). Combined with the history, the presentation was consistent with a malignant glomus tumor.

We combined the results of genetic testing to provide the patient with systemic therapy. NGS test results revealed a mutated gene, KEAP1, associated with immunosuppressive resistance at a high frequency, and the mutation abundance was 29.16%. Therefore, the patient was treated with simultaneous radiochemotherapy: radiotherapy for an irregular mass on the left side of the thoracic stomach, DT: 58 Gy/29 times/43 days, during synchronous paclitaxel (albumin type) (100 mg) weekly treatment four times for a total of 400 mg. CT review 20 days after the final treatment showed that the left lung was re-expanded, and the left pleural effusion was significantly reduced. However, multiple solid nodules in both lung fields were larger than before, and multiple liver metastases were observed on May 10, 2022. The disease progressed rapidly, and Anlotinib targeted therapy was intended, but the patient was unable to tolerate intermittent hemoptysis.

To further control hemoptysis, the patient underwent implantation of 60 I125 radioactive particles into the subcarina mass on June 6, 2022. CT reexamination 20 days after surgery showed that the irregular mass in the left side of the chest and stomach was further reduced. The lesions in both lungs and liver have further progressed, with nearly 30 metastases in both lungs and significantly larger than before, with the largest being approximately 2.1 * 3.6cm. Liver metastasis has also increased compared to before, with the larger one being about 5.9 * 4.3cm. At this time, the patient's general condition is good, and there is no obvious cough, sputum, or hemoptysis. Starting from June 30, 2022, oral administration of anlotinib hydrochloride capsules 12mg, Qd, d1-14, repeated every three weeks. But after 10 days of oral administration, the patient intermittently had blood in the sputum with bright red color, so oral administration of anlotinib hydrochloride capsules was suspended and anti infection and hemostatic treatment was given. On July 15, 2022, a follow-up examination showed that the lung lesion had

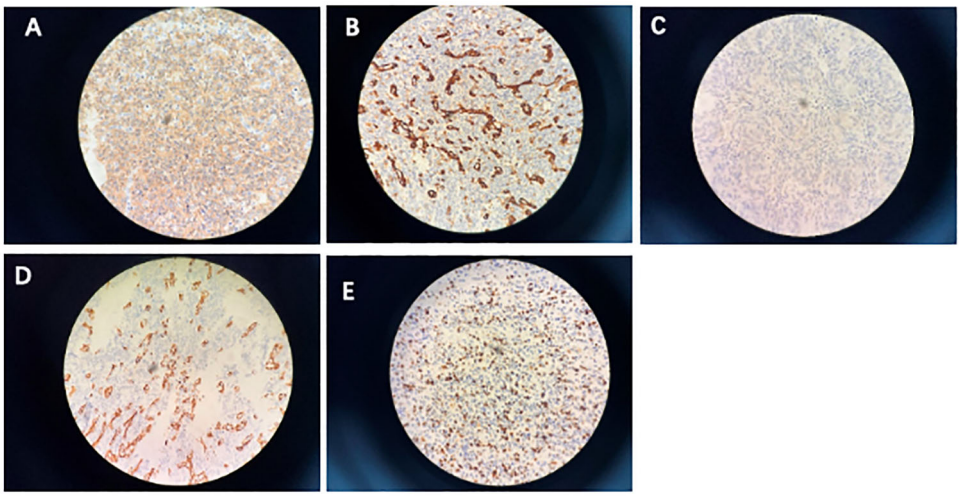

FIGURE 1
Immunohistochemistry. **(A)** Smooth muscle actin; **(B)** CD31; **(C)** caldesmon; **(D)** CD34; **(E)** proliferative index (Ki-67) is approximately 60%.

partially shrunk, with the maximum metastatic lesion shrinking from 2.1 * 3.6cm to 1.8 * 2.8cm, and the maximum liver metastatic lesion shrinking from 5.9 * 4.3cm to 5.3 * 3.5cm. The symptom of blood in sputum disappeared, and the initial treatment was shown to be effective.

Therefore, we once again considered precision treatment for the patient based on the results of genetic testing, which showed that the KEAP1 gene was no longer detected. At this time, the patient's hemoptysis symptoms disappeared. After the patient's cough and hemoptysis symptoms improved, the treatment was restarted on October 17, 2022, with the combination of anlotinib hydrochloride capsules and tislelizumab. The specific dosage was anlotinib 10mg, po, d1-14, tislelizumab injection 200mg, ivgtt, d1, repeated every three weeks. On January 14, 2023, a follow-up examination showed significant reduction in both lung nodules and multiple liver nodules compared to before, once again confirming the good therapeutic effect. According to RECIST 1.1, the efficacy was evaluated as a partial response (PR). After that, the patient continued the intermittent treatment of the scheme for 4 cycles (the treatment was interrupted due to repeated infection of COVID-19 and intermittent hemoptysis), and the last treatment was on June 12, 2023. The latest follow-up and reexamination date is August 25, 2023, indicating that the intrahepatic metastasis has further shrunk, with the largest being about 1.1 * 1.5cm in size, the efficacy was evaluated as PR (Figure 2). No significant changes were observed in the remaining lesions, and no treatment was taken before leaving the hospital. The patient maintained a PR for more than 7 months. Unfortunately, on September 19, 2023, the patient experienced

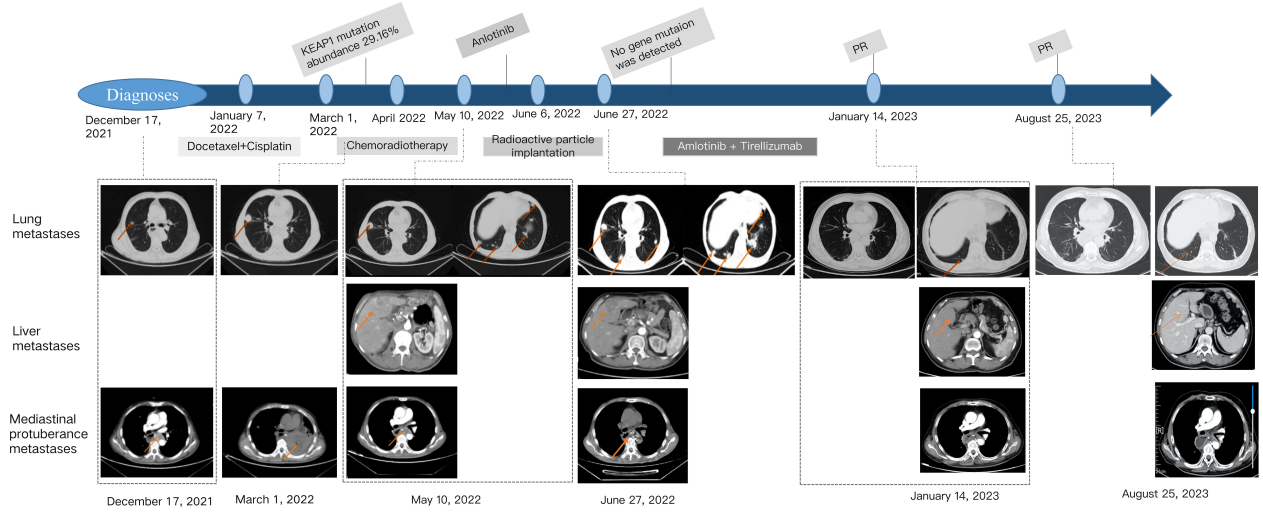

FIGURE 2
Course of the disease with treatment history and images.

vomiting blood and gastroscopy revealed perforation of the residual stomach. Despite receiving active supportive treatment, the patient passed away on October 15, 2023 due to gastrointestinal bleeding.

Discussion

The optimal treatment of malignant glomus tumors remains unknown, especially for patients with metastasis. To date, 16 cases of malignant glomus tumors of esophageal origin have been reported, 7 of these cases exhibited regional or distant metastasis (Table 1) (2, 10–22). Due to the rarity of this disease and scarcity of case reports, we have summarized the three cases of malignant hematoma of the esophagus. Zhang et al. (15) reported the first case of malignant hematoma of the esophagus in a 47-year-old man with local lymph node involvement who underwent surgical resection. At the time of publication, there was no evidence of tumor recurrence 11 months after surgery. Seban et al. (20) reported a second case in a 45-year-old man with fluorodeoxyglucose-avid malignant esophageal hemangioma with multiorgan invasion that spread to the mediastinum, liver, scalp, and pelvis. The patient underwent subcutaneous scalp nodule excision, followed by doxorubicin and pelvic external-beam radiation therapy (EBRT). FDG-positron emission tomography results showed a partial metabolic response in the lung. Pazopanib was later introduced, and a complete metabolic response in the liver and a partial response in the bone and mediastinum were achieved. It was discontinued after three months owing to side effects. Despite stopping treatment, continuous imaging showed progress. Subsequent treatment with Regrafenib, cyclophosphamide, and pelvic EBRT exhibited no response and was poorly tolerated. Xiao et al. (1). reported a third case involving a 57-year-old Hispanic woman with malignant esophageal hematoma and lung metastasis. The patient was treated with palliative radiotherapy while waiting for the patient's NGS to reveal fusion of NOTCH2 (MIR143-NOTCH2). Therefore, a trial of gemcitabine and docetaxel was planned for the patient, but the patient experienced rapid progression and pain after receiving a single dose of gemcitabine, and eventually chose hospice care. Papke et al. (21) reported the fourth case involving a 61-year-old man with malignant esophageal malignant glomus tumor and brain, lung, bones metastasis, but the treatment and prognosis information was not reported. Lastly, Birkness-Gartman et al. (2) reported 3 metastatic esophageal glomus tumor. Patient 1 was a 65-year-old male, he developed metastases to the lung and pericardium 6 years after diagnosis, and was alive at last clinical follow-up (9 years). Patient 2 was a 19-year-old femal developed metastatic disease to the scalp 11 months after resection of her primary tumor, she late developed paraesophageal soft tissue recurrence and metastases to the pleura, pericardium, and diaphragm. She received adjuvant treatment with several

TABLE 1 Review of available case reports of malignant esophageal glomus tumors.

Case No.	Reference (author, year)	Sex	Age	Metastatic site(s)	Intervention	Status at time of publication
1	Rueff, 1967 (10)	Unknown	Unknown	Unknown	Unknown	Unknown
2	Utkin, 1972 (11)	Unknown	Unknown	Unknown	Unknown	Unknown
3	Papla, 2001 (12)	Female	79	Unknown	Unknown	Unknown
4	Altorjay, 2003 (13)	Unknown	Unknown	Unknown	Unknown	Unknown
5	Tomas, 2006 (14)	Female	28	None	Surgery	Alive; NER at 6 months
6	Zhang, 2013 (15)	Male	47	Lymph node	Surgery	Alive; NER at 11 months
7	Bali, 2013 (16)	Female	49	None	Surgery	Alive; NER at time of publication
8	Segura, 2015 (17)	Female	66	None	Surgery	Alive; NER at time of publication
9	Ugras, 2015 (18)	Female	47	None	Surgery	Alive; NER at 10 months
10	Marcella, 2019 (19)	Male	30	None	Surgery	Alive; NER at 1 year
11	Seban, 2020 (20)	Male	45	Liver, lung, mediastinum, bone, skin	Surgery, chemotherapy, EBRT	Unknown; progressive disease
12	Xiao, 2022 (21)	Female	57	Lung, lymph node	Palliative IMRT	Alive; progressive disease on hospice
13	Papke, 2022 (22)	Male	61	Brain, lung, bones	Unknown	Unknown
14	Birkness-Gartman, 2023 (2)	Male	65	Lung, pericardium	Unknown	Alive with disease (9 years)
15		Female	19	Scalp, pleura, pericardium, diaphragm	doxorubicin, ifosfamide, pazopanib, and radiation	Alive with disease (5 years)
16		Female	62	Lymph node	Surgery	Died of disease (4 months)

different regimens (doxorubicin, ifosfamide,pazopanib, and radiation; nirogacestat; axitinib and pembrolizumab) and was alive at last clinical follow-up (5 years). Patient 3 was a 62-year-old femal, she had a large tumor abutting the aorta on imaging. Intraoperatively, the tumor was adherent to the aorta, resulting in a difficult operation. This patient developed an aorto-esophageal fistula 20 days after surgery, resulting in a fatal hemorrhage, total survival time following diagnosis was 4 months. Our case report can enrich the clinical data of malignant esophageal glomus tumors, and this case is the first malignant esophageal glomus tumors case to receive immunotherapy, providing a clinical basis for the treatment of rare malignant glomus tumors.

Our case was diagnosed as malignant hematoma of the esophagus complicated with lung and liver metastases. No significant curative effect was achieved with radiotherapy or chemotherapy, and the disease progressed rapidly. Therefore, we attempted to implement a more precise treatment strategy. The patient underwent NGS using the Yuce biological solid tumor clinical drug 1012+PD-L1 | YuceOne® Pro+. This technology has already been used clinically as an effective tool to create personalized treatment plans. Glomus tumors have been reported to have the highest tumor mutation burden among soft tissue sarcomas, with 16% of participants detecting mutations associated with FDA-approved treatments or drugs in development (22). However, the tumor molecular signatures of our patient did not indicate relevant targets that could be directly affected, but there was a gene that was negatively correlated with immunotherapeutic efficacy – KEAP1 (23). KEAP1 mutations confer worse outcomes to immunotherapy among lung cancer patients with KRAS mutation, and KEAP1 mutations results in distinct immunophenotypes in KRAS mution of lung cancer (24). Among atezolizumab and/or bevacizumab with carboplatin/paclitaxel (CP) chemotherapy clinical trial, KEAP1 mutations were associated with inferior OS and PFS across treatments compared with KEAP1-WT (25). KEAP1 mutation can affect the tumor immune microenvironment and cause immune escape. One lung squamous cell carcinoma study showed that KEAP1 mutation was associated with dramatically lower CD8+ TIL density ($P = 0.005$) (26). KEAP1 mutation in lung adenocarcinoma reduces the dendritic cell and T cell responses that drive immune therapy resistance, leading to immune resistance in lung adenocarcinoma patients (27). This finding suggested against using immunotherapy in this patient. Anlotinib belongs to a class of small-molecule, multi-target anti-angiogenic drugs that have been approved for vesellar soft tissue sarcoma, clear cell sarcoma, and other advanced soft tissue sarcomas that have progressed or recurred (28–30). This drug is contraindicated in patients with a high risk of hemoptysis. Therefore, local radioactive particle implantation was first performed for the patient to relieve the symptoms of hemoptysis, and the subsequent improvement of the patient demonstrated that this step played a key role in the overall treatment of the patient, which also reflected the obvious benefits of multidisciplinary treatment. It has been reported that radiotherapy and chemotherapy can change the immune microenvironment of patients (30–33). Subsequent use of the Yuce biological solid tumor clinical drug 1012+PD-L1 | YuceOne® Pro+, in order to find the targets of effective drugs, showed that no genes negatively related to immune efficacy were detected. Therefore, it can be speculated that the radioactive particle implantation changed the immune microenvironment of the patient. It has been suggested that anti-drugs and PD-1/PD-L1 inhibitors can jointly act on the tumor microenvironment, reshaping the tumor vascular and immune microenvironments, transforming the immunosuppressive state into the immune-promoting state, increasing the invasion of T cells to the tumor, and playing a synergistic anti-tumor effect (1 + 1>2) (34, 35). Anlotinib in combination with immunotherapy has also been reported to significantly improve the prognosis of patients with liver cancer (36). Therefore, we treated the patient with anlotinib combined with Tislelizumab, which showed significant efficacy, significant reduction of intrahepatic lesions, physical improvement, and weight gain of the patient upon follow-up.

The optimal treatment for malignant hematocrystomas of the esophagus remains unclear. A review of published literature shows that extensive local resection remains the most feasible treatment. Mixed success with chemotherapy has also been reported in a small number of cases (15, 37). Our case demonstrates the malignant potential and high aggressiveness of malignant hematoma of the esophagus. Changes in the patient's immune microenvironment were detected by NGS, guiding the targeted therapy of the patient. This suggests that NGS detection can develop an effective personalized treatment plan for this patient group and has great potential for successful treatment of malignant esophageal glomus tumors in the future.

Data availability statement

The original contributions presented in the study are included in the article/supplementary material. Further inquiries can be directed to the corresponding author.

Ethics statement

The studies involving humans were approved by Shanxi Province Cancer Hospital. The studies were conducted in accordance with the local legislation and institutional requirements. The participants provided their written informed consent to participate in this study. Written informed consent was obtained from the individual(s) for the publication of any potentially identifiable images or data included in this article.

Author contributions

WD: Conceptualization, Data curation, Funding acquisition, Writing – review & editing. YL: Conceptualization, Writing – original draft. JM: Writing – original draft. DS: Data curation, Investigation, Writing – review & editing. BJ: Data curation, Formal

analysis, Writing – review & editing. CS: Writing – review & editing, Validation. XW: Data curation, Writing – review & editing.

Funding

The author(s) declare that no financial support was received for the research, authorship, and/or publication of this article.

Conflict of interest

Authors JM and CS were employed by the company YuceBio Technology Co., Ltd.

The remaining authors declare that the research was conducted in the absence of any commercial or financial relationships that could be construed as a potential conflict of interest.

Publisher's note

All claims expressed in this article are solely those of the authors and do not necessarily represent those of their affiliated organizations, or those of the publisher, the editors and the reviewers. Any product that may be evaluated in this article, or claim that may be made by its manufacturer, is not guaranteed or endorsed by the publisher.

References

1. Xiao A, Ahlers M, Dry SM, Weber AT, Chiu VY, Pessegueiro AM. Rare Malignant glomus tumor of the esophagus with pulmonary metastasis: a case report. *AME Case Rep*. (2022) 6:20. doi: 10.21037/acr-21-72

2. Birkness-Gartman JE, Wangsiricharoen S, Lazar AJ, Gross JM. Oesophageal glomus tumours: rare neoplasms with aggressive clinical behaviour. *Histopathology*. (2023) 82:1048–55. doi: 10.1111/his.14888

3. Sun Z, Sun F, Yu C, Xiao H, Xu Q, Gao B, et al. Malignant glomus tumor of prostate: A case report. *Front Oncol*. (2023) 13:1121307. doi: 10.3389/fonc.2023.1121307

4. Lamba G, Rafiyath SM, Kaur H, Khan S, Singh P, Hamilton AM, et al. Malignant glomus tumor of kidney: The first reported case and review of literature. *Hum Pathol*. (2011) 42:1200–3. doi: 10.1016/j.humpath.2010.11.009

5. Gill J, Van Vliet C. Infiltrating glomus tumor of uncertain Malignant potential arising in the kidney. *Hum Pathol*. (2010) 41:145–9. doi: 10.1016/j.humpath.2009.08.003

6. Folpe AL, Fanburg-Smith JC, Miettinen M, Weiss SW. Atypical and Malignant glomus tumors: Analysis of 52 cases, with a proposal for the reclassification of glomus tumors. *Am J Surg Pathol*. (2001) 25:1–12. doi: 10.1097/00000478-200101000-00001

7. Jo VY, Doyle LA. Refinements in sarcoma classification in the current 2013 world health organization classification of tumours of soft tissue and bone. *Surg Oncol Clin N Am*. (2016) 25:621–43. doi: 10.1016/j.soc.2016.05.001

8. Carroll RE, Berman AT. Glomus tumors of the hand: review of the literature and report on twenty-eight cases. *J Bone Joint Surg Am*. (1972) 54:691–703. doi: 10.2106/00004623-197254040-00001

9. Cigna E, Carlesimo B, Bistoni G, Conte F, Palumbo F, Scuderi N. The value of clinical diagnosis of digital glomus tumors. *Acta Chir Plast*. (2008) 50:55–8.

10. Rueff F, Grabiger A. Glomus tumor of the esophagus. *Bruns Beitr Klin Chir*. (1967) 215:106–10.

11. Utkin VV, Berzin SA, Apinis BK. Combination of glomus tumor of the esophagus and diaphragmatic hernia. *Grudn Khir*. (1972) 14:104–5.

12. Papla B, Zieliński M. Glomus tumour of the oesophagus. *Pol J Pathol*. (2001) 52:133–5.

13. Altorjay A, Arató G, Adame M, Szántó I, Garcia J, Forrai G, et al. Synchronous multiple glomus tumors of the esophagus and lung. *Hepatogastroenterology*. (2003) 50:687–90.

14. Tomas D, Tomić K, Bekavac-Beslin M, Jukić Z, Belicza M, Kruslin B. Primary glomangioma of the esophagus mimicking esophageal papilloma. *Dis Esophagus*. (2006) 19:208–11. doi: 10.1111/j.1442-2050.2006.00568.x

15. Zhang Y, Li H, Zhang WQ. Malignant glomus tumor of the esophagus with mediastinal lymph node metastases. *Ann Thorac Surg*. (2013) 96:1464–6. doi: 10.1016/j.athoracsur.2013.01.092

16. Bali GS, Hartman DJ, Haight JB, Gibson MK. A rare case of Malignant glomus tumor of the esophagus. *Case Rep Oncol Med*. (2013) 2013:287078. doi: 10.1155/2013/287078

17. Segura S, Mansoor S, Gorelick AB, Sieber S, El-Fanek H. Glomus tumor of the esophagus: A case report and review of the literature. *Conn Med*. (2015) 79:93–5.

18. Ugras N, Yercİ Ö, Yalçınkaya U, Gülcü B, Öztürk E, Yıldırım Ç, et al. Malignant glomus tumor with oncocytic features: an unusual presentation of dysphagia. *APMIS*. (2015) 123:613–7. doi: 10.1111/apm.12394

19. Marcella C, Shi R, Yu T, Sarwar S, Wang X, Liu Y. Asymptomatic esophageal glomus tumor: case report. *J Gastrointest Oncol*. (2019) 10:1015–20. doi: 10.21037/jgo.2019.05.08

20. Seban RD, Bozec L, Champion L. Clinical implications of 18F-FDG PET/CT in Malignant glomus tumors of the esophagus. *Clin Nucl Med*. (2020) 45:e301–2. doi: 10.1097/RLU.0000000000003029

21. Papke DJ Jr, Sholl LM, Doyle LA, Fletcher CDM, Hornick JL. Gastroesophageal glomus tumors: clinicopathologic and molecular genetic analysis of 26 cases with a proposal for Malignancy criteria. *Am J Surg Pathol*. (2022) 46:1436–46. doi: 10.1097/PAS.0000000000001925

22. Gounder MM, Ali SM, Robinson V, Bailey M, Ferraro R, Patel NM, et al. Impact of next-generation sequencing (NGS) on diagnostic and therapeutic options in soft-tissue and bone sarcoma. *J Clin Oncol*. (2017) 35:11001. doi: 10.1200/JCO.2017.35.15_suppl.11001

23. Marzio A, Kurz E, Sahni JM, Di Feo G, Puccini J, Jiang S, et al. EMSY inhibits homologous recombination repair and the interferon response, promoting lung cancer immune evasion. *Cell*. (2022) 185:169–183.e19. doi: 10.1016/j.cell.2021.12.005

24. Ricciuti B, Arbour KC, Lin JJ, Vajdi A, Vokes N, Hong L, et al. Diminished efficacy of programmed death-(Ligand)1 inhibition in STK11- and KEAP1-mutant lung adenocarcinoma is affected by KRAS mutation status. *J Thorac Oncol*. (2022) 17:399–410. doi: 10.1016/j.jtho.2021.10.013

25. West HJ, McCleland M, Cappuzzo F, Reck M, Mok TS, Jotte RM, et al. Clinical efficacy of atezolizumab plus bevacizumab and chemotherapy in KRAS-mutated non-small cell lung cancer with STK11, KEAP1, or TP53comutations: subgroup results from the phase III IMpower150 trial. *J Immunother Cancer*. (2022) 10:e003027. doi: 10.1136/jitc-2021-003027

26. Jiang T, Shi J, Dong Z, Hou L, Zhao C, Li X, et al. Genomic landscape and its correlations with tumor mutational burden, PD-L1 expression, and immune cells infiltration in Chinese lung squamous cell carcinoma. *J Hematol Oncol*. (2019) 12:75. doi: 10.1186/s13045-019-0762-1

27. Zavitsanou AM, Pillai R, Hao Y, Wu WL, Bartnicki E, Karakousi T, et al. KEAP1 mutation in lung adenocarcinoma promotes immune evasion and immunotherapy resistance. *Cell Rep*. (2023) 42:113295. doi: 10.1016/j.celrep.2023.113295

28. Sternberg CN, Davis ID, Mardiak J, Szczylik C, Lee E, Wagstaff J, et al. Pazopanib in locally advanced or metastatic renal cell carcinoma: results of a randomized Phase III trial. *J Clin Oncol*. (2010) 28:1061–8. doi: 10.1200/JCO.2009.23.9764

29. Motzer RJ, Hutson TE, Tomczak P, Michaelson MD, Bukowski RM, Rixe O, et al. Sunitinib versus interferon alfa in metastatic renal-cell carcinoma. *N Engl J Med*. (2007) 356:115–24. doi: 10.1056/NEJMoa065044

30. Tian Z, Liu H, Zhang F, Li L, Du X, Li C, et al. Retrospective review of the activity and safety of Apatinib and anlotinib in patients with advanced osteosarcoma and soft tissue sarcoma. *Investig New Drugs*. (2020) 38:1559–69. doi: 10.1007/s10637-020-00912-7

31. Che LH, Liu JW, Huo JP, Luo R, Xu RM, He C, et al. A single-cell atlas of liver metastases of colorectal cancer reveals reprogramming of the tumor microenvironment in response to preoperative chemotherapy. *Cell Discovery*. (2021) 7:80. doi: 10.1038/s41421-021-00312-y

32. Wu Y, Yang S, Ma J, Chen Z, Song G, Rao D, et al. Spatiotemporal immune landscape of colorectal cancer liver metastasis at single-cell level. *Cancer Discovery*. (2022) 12:134–53. doi: 10.1158/2159-8290.CD-21-0316

33. Heinhuis KM, Ros W, Kok M, Steeghs N, Beijnen JH, Schellens JHM. Enhancing antitumor response by combining immune checkpoint inhibitors with chemotherapy in solid tumors. *Ann Oncol*. (2019) 30:219–35. doi: 10.1093/annonc/mdy551

34. Fukumura D, Kloepper J, Amoozgar Z, Duda DG, Jain RK. Enhancing cancer immunotherapy using antiangiogenics: opportunities and challenges. *Nat Rev Clin Oncol*. (2018) 15:325–40. doi: 10.1038/nrclinonc.2018.29

35. Pinter M, Jain RK, Duda DG. The current landscape of immune checkpoint blockade in hepatocellular carcinoma: a review. *JAMA Oncol*. (2021) 7:113–23. doi: 10.1001/jamaoncol.2020.3381

36. Han C, Ye S, Hu C, Shen L, Qin Q, Bai Y, et al. Clinical activity and safety of Penpulimab (anti-PD-1) with anlotinib as first-line therapy for unresectable hepatocellular carcinoma: an open-label, multicenter, phase Ib/II trial (AK105-203). *Front Oncol.* (2021) 11:684867. doi: 10.3389/fonc.2021.684867

37. Negahi A, Jahanshahi F, Shahriari-Ahmadi A, Sadeghipour A. Lesser sac glomangiosarcoma with simultaneous liver and lymph nodes metastases mimicking small bowel gastrointestinal stromal tumor; immunohistochemistry and empirical chemotherapy. *Int Med Case Rep J.* (2019) 12:339–44. doi: 10.2147/IMCRJ.S220455

frontiers | Frontiers in Oncology

TYPE Clinical Trial
PUBLISHED 05 July 2024
DOI 10.3389/fonc.2024.1326970

OPEN ACCESS

EDITED BY
Zsolt Kovács,
George Emil Palade University of Medicine, Pharmacy, Sciences and Technology of Târgu Mureş, Romania

REVIEWED BY
Chen Jue,
Yangzhou University, China
Jian Wu,
Affiliated Hospital of Nanjing University of Chinese Medicine, China

*CORRESPONDENCE
Jie Li
qfm2020jieli@yeah.net

†These authors have contributed equally to this work

RECEIVED 24 October 2023
ACCEPTED 17 June 2024
PUBLISHED 05 July 2024

CITATION
Cao L, Zhu G, Wang X, Kuang Z, Song X, Ma X, Zhu X, Gao R and Li J (2024) *Yiqi Wenyang Jiedu* prescription for preventing and treating postoperative recurrence and metastasis of gastric cancer: a randomized controlled trial protocol. *Front. Oncol.* 14:1326970. doi: 10.3389/fonc.2024.1326970

Yiqi Wenyang Jiedu prescription for preventing and treating postoperative recurrence and metastasis of gastric cancer: a randomized controlled trial protocol

Luchang Cao[1†], Guanghui Zhu[1,2†], Xinmiao Wang[1†], Ziyu Kuang[1,2], Xiaotong Song[1], Xinyi Ma[1], Xiaoyu Zhu[1], Ruike Gao[1] and Jie Li[1*]

[1]Department of Oncology, Guang'anmen Hospital, China Academy of Chinese Medical Sciences, Beijing, China, [2]Graduate School, Beijing University of Chinese Medicine, Beijing, China

Introduction: Postoperative recurrence and metastasis of gastric cancer (GC) are primary factors that contribute to poor prognosis. GC recurs at a rate of approximately 70%–80% within 2 years after local treatment and approximately 90% within 5 years. "*Yang-deficient toxic node*" is the core pathogenesis of GC recurrence and metastasis. The *Yiqi Wenyang Jiedu* prescription (YWJP), a form of complementary and alternative medicine in China, is an empirical remedy to prevent postoperative recurrence and metastasis of GC. Taking the main therapeutic principles of "nourishing *Qi* and warming *Yang*, strengthening *Zhengqi*, and detoxifying" can aid in preventing the recurrence and metastasis of GC in patients during the watchful waiting period after surgery and adjuvant chemotherapy. This approach aims to enhance the quality of life of patients. However, high-quality evidence to support this hypothesis is lacking. This study will aim to investigate the efficacy and safety of YWJP to prevent and treat postoperative metastasis and GC recurrence.

Methods: The study will be a multicenter, randomized, double-blind, placebo-parallel-controlled clinical trial. A total of 212 patients who completed adjuvant chemotherapy within 8 months of radical gastrectomy will be enrolled. Patients in the intervention group will receive the YWJP, whereas those in the control group will receive a placebo. The main outcome was the disease-free survival (DFS) rate 2 years after surgery. The secondary outcomes included DFS time, overall survival, annual cumulative recurrence and rate of metastasis after 1–3 years, cumulative annual survival after 1–3 years, fat distribution-related indicators, tumor markers, peripheral blood inflammatory indicators, prognostic nutritional index, symptoms and quality of life evaluation, medication compliance, and adverse reaction rate.

Discussion: There is a lack of effective therapy after the completion of adjuvant therapy during the postoperative period of watchful waiting. This study will be the first randomized clinical trial to evaluate whether complementary and alternative

medical interventions can effectively prevent recurrence and metastasis during the watchful waiting period after GC surgery and to provide evidence for surveillance treatment management after GC surgery.

Clinical trial registration: ClinicalTrials.gov, identifier NCT05229809.

KEYWORDS

randomized controlled trial, recurrence, metastasis, traditional Chinese medicine, gastric cancer

Highlights

- Question
- Can *Yiqi Wenyang Jiedu* prescription reduce the rate of recurrence and metastasis in patients with gastric cancer during the watchful waiting period after surgery?
- Findings
- This randomized clinical trial will involve 212 patients with GC who completed adjuvant chemotherapy after surgery. The primary outcome was disease-free survival at a rate of 2 years after surgery.
- Meaning
- This ongoing clinical trial will supply the treatment management during the watchful waiting period after GC surgery and provide evidence for the effectiveness of complementary and alternative medicine in reducing recurrence and metastasis rates after GC surgery.

1 Introduction

Gastric cancer (GC) is a common malignant tumor of the digestive system, and according to the Global Cancer Statistics 2022, the number of new GC cases worldwide is 968,350, ranking fifth among all malignancies. The number of deaths was 659,853, ranking fifth among all cancer types (1, 2). China has the highest cancer burden worldwide, according to the National Cancer Center of China (3), and they projected that an estimated 4,824,700 new cancer cases and 2,574,200 new cancer deaths will occur in China in 2022. Among these, GC ranked fifth and third among new cases and deaths, respectively. Despite a decline in GC incidence observed in many countries, the total number of GC cases worldwide shows a slow upward trend, particularly in China (4, 5). Even more terrifying is that the global burden caused by the rising trend of GC cases is expected to increase by 62% to 1.77 million cases in 2040 (6). Studies have confirmed that various factors such as *Helicobacter pylori* infection (7), cigarette smoking (8, 9), heavy alcohol consumption (10–12), sex (13), obesity (14, 15), metabolic dysfunction (16, 17), and so on (18–26) are recognized as major risk factors for GC incidence.

Surgery is currently the preferred treatment for GC. The National Comprehensive Cancer Network guidelines (2023. V1) recommend that patients with stage pT3–4 cancer, any N, should undergo post-surgical chemoradiotherapy followed by a period of surveillance and management (27–39). Approximately 70%–80% of patients with GC relapsed within 2 years after local therapy. The median recurrence time for GC is approximately 16.8 months (40–42). Previous studies have shown that *Yang* deficiency is one of the main syndromes of GC (43), *Yang* deficiency and a low metabolic state can stimulate cancer cells to induce metabolic reprogramming and promote postoperative recurrence and metastasis of GC (44–48). Therefore, during the period between postoperative recovery and the onset of GC recurrence and metastasis, identifying effective treatment strategies is crucial and requires urgent attention.

Complementary and alternative medicine is a safe and effective potential choice that can improve the overall survival (OS) of patients with GC (49–51). Previous studies have indicated that patients with GC who experience *Qi* and *Yang* deficiencies after surgery are more susceptible to recurrence and metastasis than those with no *Qi* and *Yang* deficiencies (52, 53). The *Yiqi Wenyang Jiedu* prescription (YWJP) follows the treatment principles of nourishing *Qi* and warming *Yang*, strengthening *Zhengqi*, and detoxifying, and can improve the physical condition and alleviate clinical symptoms in patients with *Yang* deficiency (54, 55). YWJP may improve patients' low metabolic state by regulating the tumor microenvironment and delaying or reversing recurrence and metastasis. Therefore, we plan to conduct a multicenter, randomized, double-blind, placebo-parallel-controlled clinical trial that will apply YWJP, an effective prescription for the prevention and treatment of recurrence and metastasis of postoperative GC at the Guang'anmen Hospital of China Academy of Chinese Medical Sciences, and explore its mechanisms.

2 Materials and methods

2.1 Design

The multicenter, randomized, double-blind, placebo-parallel-controlled clinical study will be conducted at seven hospitals, including Guang'anmen Hospital of the China Academy of Chinese Medical Sciences, Jiangsu Provincial Hospital of Traditional Chinese Medicine (TCM), the First Affiliated Hospital of Guangzhou University of Chinese Medicine, and Yueyang Hospital of Integrated Traditional Chinese and Western Medicine Affiliated to Shanghai University of Chinese Medicine. After signing the informed consent forms, 212 participants will be randomly assigned to the intervention group (YWJP) or the control group (YWJP placebo).

The key herbs of YWJP include *Astragalus membranaceus* (30 *g*), *Codonopsis pilosula* (15 *g*), *Angelica dahurica* (10 *g*), *Curcuma zedoary* (9 *g*), *Rhizoma nardostachyos* (10 *g*), *Polygonum cuspidatum* (10 *g*), *Radix Actinidiae chinensis* (15 *g*), and *Paris polyphylla* (9 *g*) (108 g in total). The control group will receive a YWJP placebo intervention comprising maltodextrin, lactose, bitters, citric acid, and other edible-grade raw materials (108 g in total). All experimental herbs and placebos used in this study will be provided by Jiangyin Tianjiang Pharmaceutical Co., Ltd. All raw materials have undergone safety assessments and quality inspection reports have been issued. YWJP and its placebo have been confirmed to be safe, reliable, controllable in quality, and similar in shape, color, smell, and taste.

The primary and secondary outcomes will be evaluated immediately at the end of the follow-up period. The study process is illustrated in Figure 1. The clinical trial protocol complied with the Clinical Trial Standard Protocol Items: Recommendations for Interventional Trials (56) and Consolidated Standards of Reporting Trials (CONSORT) (57).

2.2 Recruitment

We plan to recruit patients from seven traditional Chinese oncology hospitals nationwide, led by Guang'anmen Hospital, and enroll patients by following up with expert clinics, playing recruitment advertisements on hospital LED screens, and posting recruitment posters. When we encounter potential patients, we will introduce our study protocol, including the objectives, intervention methods, processes, and potential adverse reactions. The research team will conduct repeated screenings of patients on a two-person basis. Patients who meet the inclusion criteria and wish to voluntarily participate in the study will sign an informed consent form.

2.3 Study population

The diagnostic criteria for GC, according to the 2021 Chinese Society of Clinical Oncology (CSCO), will be followed. The diagnosis and treatment of GC follow the clinical guidelines outlined in the 8th edition of the International Union Against Cancer (UICC) classification system (58).

2.4 Inclusion criteria

1. Research cases must be sourced from real-world registration platforms.
2. Stage II–III non-esophageal gastric junction GC that meets the diagnostic criteria and does not indicate tumor recurrence or metastasis by imaging.

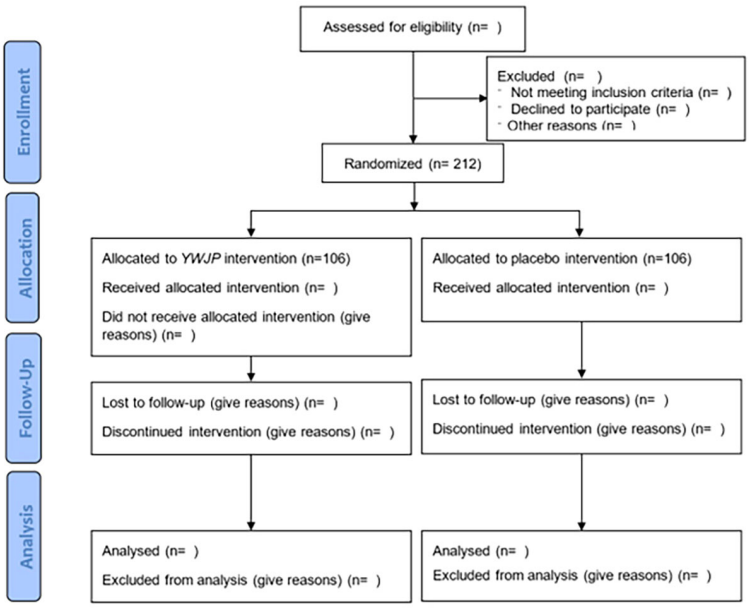

FIGURE 1
CONSORT flow diagram.

3. Patients with GC who underwent radical gastrectomy (R0) within 8 months after surgery and completed at least six cycles of adjuvant chemotherapy with standard regimens (XELOX and SOX).
4. Eastern Cooperative Oncology Group (ECOG) performance status score of 0–2.
5. Patient ages ranging from 18 to 75 years, with no sex limitations.
6. Expected survival time ≥3 months.
7. Patients who voluntarily participated in the study, signed an informed consent form, and participated in the follow-up.

2.5 Exclusion criteria

1. Patients with concomitant primary tumors in other areas.
2. Patients with GC who were pathologically diagnosed with adenosquamous carcinoma, lymphoid interstitial carcinoma (medullary carcinoma), hepatoid adenocarcinoma, squamous cell carcinoma, signet ring cell carcinoma, undifferentiated carcinoma, and other gastric malignancies, such as gastric neuroendocrine tumors, gastric interlobular tumors, and gastric malignant lymphoma.
3. Patients who received neoadjuvant chemotherapy before surgery.
4. Patients who have been and are currently receiving targeted drug therapy.
5. Patients who have undergone or are currently undergoing gastric radiation therapy.
6. Patients who have undergone or are currently undergoing tumor immunotherapy.
7. Patients with mental illness.
8. Patients with severe and uncontrollable organic lesions or infections such as decompensated heart, lung, or kidney failure, who cannot tolerate chemotherapy.
9. Patients who underwent clinical trials of small-molecule drugs within 28 days or large-molecule drugs within 3 months.
10. Patients who are known to be allergic or intolerant to the study drug.

2.6 Criteria for withdrawal and removal

1. Those who experienced unexpected events during the treatment process and were unable to adhere to the protocol.
2. Patients who voluntarily requested withdrawal.
3. The researchers judged patients who exhibited poor compliance and were unable to continue clinical research.
4. Patients experiencing pregnancy, death, or loss of follow-up.

2.7 Randomization and blinding

This study will apply an Interactive Web Response System for central randomization and implement hidden allocation schemes. Patients will be randomly divided into intervention and control groups in a 1:1 ratio based on central randomization. The R software (V3.3.3) will be used to generate random sequences with three rounds of cyclic random statements. The blinding level will be double-blind, in which neither the researcher nor the participant have any idea of the specific details of the study. Anonymizing will be performed by statisticians who did not participate in the clinical trials and divided into two levels. This trial will establish a dedicated "emergency letter" for clinical trials that can only be urgently unblinded when the patient experiences an emergency. Handling this situation requires a clear understanding of the patient's medication information.

2.8 Intervention

The intervention group will receive YWJP, whereas the control group will receive YWJP placebo. Patients will take one pack each time, dilute it with boiling water, and administer it twice daily (in the morning and evening). The course of treatment will be 4 weeks, and six courses are planned.

2.9 Criteria for adherence

After enrollment, patients will take their medication according to the method described in the "intervention" section. During the intervention, symptoms such as nausea, vomiting, liver and kidney dysfunction, diarrhea, and infection will be treated with medication. However, specific symptoms and combined medications must be recorded. Receiving modern antitumor treatment (including chemotherapy, immunotherapy, molecular targeted therapy, and radiotherapy) or taking other Chinese herbal decoctions, Chinese herbal injections, and traditional Chinese patent medicines with antitumor effects during the intervention will be prohibited.

2.10 Criteria for discontinuation

If unexpected adverse events occur, participants should no longer follow the study guidelines for such events. The investigator should comprehensively analyze whether these events are related to the experimental and control drugs used, and should decide whether to discontinue the clinical trial based on the participant's condition. Patients who discontinue trials owing to serious adverse events

should be followed up, and their outcomes should be documented. In addition, participants who could not adhere to the treatment and those who requested active withdrawal, had poor compliance, were pregnant, dead, or lost to follow-up met the criteria for discontinuation.

2.11 Sample size

This was a randomized controlled trial. The primary outcome was the 2-year disease-free survival (DFS) rate of patients with GC after surgery. It was estimated that the DFS rate 2 years after surgery in the control group was 43.9%, whereas the DFS rate in the intervention group was 63.9%. For $\alpha = 0.05$ (bilateral), $\beta = 0.2$. Assuming that the enrollment rate of the study patients remained unchanged, the proportion of the intervention group to the control group was 1:1. The sample size for N1 was 96 cases in the intervention group, and for N2 was 96 cases in the control group, as calculated using the PASS 11 software. However, a detachment rate of 10% must be considered in the research process. Therefore, the intervention and control groups comprised 106 patients each (212 patients total).

2.12 Outcome measurements

The 2-year DFS rate as the primary outcome and DFS, OS, 1- to 3-year cumulative recurrence and metastasis rate, and 1- to 3-year cumulative survival rate as the secondary outcome will be calculated at the end of follow-up. The lymphocyte count-to-monocyte count ratio (LMR) (59), lymphocyte count-to-neutrophil count ratio (LNR) (60), prognostic nutritional index (PNI) (61), Quality of Life Questionnaire of Stomach 22 (QLQ-STO22) (62), M. D. Anderson Symptom Assessment Scale Gastrointestinal Tumor Specific Module (MDASI-GI) (63), Postgastrectomy Syndrome Assessment Scale-45 (PGSAS-45) (64) (diagnosis of the syndrome should refer to the 2014 *Guidelines of Diagnosis and Therapy in Oncology with Traditional Chinese Medicine*), and other secondary outcome indicators will be collected at weeks 0–6, whereas the total fat area (TFA) (65), visceral fat area (VFA) (66), subcutaneous fat area (SFA) (67), visceral adiposity index (VAI) (68), and tumor markers will be collected at weeks 0, 3, and 6. All measurement results will be recorded in the case report form (CRF). The details of outcome measurement projects are shown in Table 1.

2.12.1 Primary outcome

The primary outcome of this study is the 2-year DFS rate after surgery, which refers to the proportion of patients who have not experienced recurrence, metastasis, or (for any reason) death within 2 years after surgery.

2.12.2 Secondary outcome

1. Prognosis related indicators

DFS: Time from randomization to the onset of tumor progression or (for any reason) death in patients.

OS: Time from randomization to death from any cause.

Annual cumulative recurrence and metastasis rate for 1–3 years: The proportion of patients who experience recurrence and metastasis within 1–3 years from the day of surgery to the total number of patients.

Annual cumulative survival rate for 1–3 years: The proportion of patients with a survival period of 1–3 years or more from the day of surgery to the total number of patients.

2. Fat distribution-related indicators

TFA of the abdomen: A CT plain scan will be used to measure the fat area on cross-sectional images, directly reflecting the accumulation of abdominal fat in the human body. It is generally believed that the umbilical plane or L2/L3 gap can better reflect the body's abdominal fat.

VFA: A commonly used indicator in clinical practice to evaluate the level of visceral fat. The precise measurement method is usually based on imaging methods, specifically the area occupied by adipose tissue in a certain section of abdominal CT (flat umbilical section or third lumbar section).

SFA: SFA = TFA − VFA.

VAI: This is another indicator for evaluating visceral adipose tissue accumulation and dysfunction, and is a new visceral fat assessment index calculated based on waist circumference (WC), body mass index (BMI), triglycerides (TG), and high-density lipoprotein (HDL).

TABLE 1 Treatment stage flowchart.

Item	Baseline	Treatment observation				Follow-up
Number of visits	1st time	2nd time	3rd time	4th time	*N*th time	*N* + *X*th time
Observation time	Days −7 to 0	Days 28–35	Days 56–63	Days 84–91	End of *N*th treatment course	Once every 3 months
Inclusion/Exclusion criteria	√					
Sign informed consent form	√					
Collect medical history						
Demographic data	√					
Diagnosis and TNM classification	√					
Past history and comorbidities	√					

(Continued)

TABLE 1 Continued

Item		Baseline	Treatment observation				Follow-up
Clinical observation							
Vital signs		√	√	√	√	√	√
Physical examination		√	√	√	√	√	√
Survival situation		√	√	√	√	√	√
MDASI-GI		√	√	√	√	√	√
Tongue and pulse condition		√	√	√	√	√	√
TCM syndrome		√	√	√	√	√	√
Imaging examination	PET-CT/CT/X-ray	√			√	√	√
	MRI, B-mode ultrasonography	*	*	*	*	*	*
	Bone scanning	*	*	*	*	*	*
	Gastroscope	*	*	*	*	*	*
Tumor marker		√	*	*	√	*	*
Indicators related to fat distribution		√	*	*	√	*	*
QLQ-STO22		√	√	√	√	√	√
PGSAS-45		√	√	√	√	√	√
Safety observation							
Blood routine		√	√	√	√	√	√
Hepatic and renal function		√	√	√	√	√	√
Urine and stool routine		*	*	*	*	*	*
Electrocardiogram		√	√	√	√	√	√
NCI adverse reaction			√	√	√	√	√
Adverse event			√	√	√	√	√
Other work							
Efficacy evaluation			√	√	√	√	√
Drug combination			√	√	√	√	√

*This check is optional.
√ This check is necessary.

Male VAI = [WC/(39.68 + 1.88 × BMI)] × (TG/1.03) × (1.31/HDL);

Female VAI = [WC/(36.58 + 1.89 × BMI)] × (TG/0.81) × (1.52/HDL).

3. Tumor markers: Carcinoembryonic antigen (CEA), carbohydrate antigen 724 (CA724), and carbohydrate antigen 199 (CA199) should be included as tumor markers.

4. Peripheral blood inflammatory indicators:

LMR: Ratio of lymphocyte count to monocyte count

LNR: Ratio of lymphocyte count to neutrophil count

5. Prognostic nutritional index (PNI): Record serum albumin (ALB) and lymphocyte (TLC) counts, with the formula PNI = ALB + 5 × TLC.

6. Symptoms and quality of life evaluation:

The QLQ-STO22 developed by the European Organization for Research and Treatment of Cancer will be used to evaluate the impact of treatment protocols on the quality of life of GC patients.

The impact of treatment regimens on patient symptoms will be evaluated using the MDASI-GI.

The quality of life with GC patients after gastrectomy will be measured using the PGSAS-45, and the intensity of various symptoms of post-gastrectomy syndrome will be understood.

7. Medication compliance: The number and percentage of cases will be calculated based on <80%, 80%–120%, and >120% medication compliance.

Medication compliance = actual dosage/expected dosage × 100% (rounded to two decimal places).

8. Adverse reaction rate: The proportion of adverse reactions caused by drugs in the enrolled population.

2.13 Safety evaluation

Safety evaluations were performed according to the National Cancer Institute's Common Terminology Standard for Adverse Events (CTCAE v.5.0), and patient adverse events were monitored every 3 months from baseline to disease progression, death, or 2 years after surgery. The evaluation methods included routine blood tests, urine tests, biochemical tests, and electrocardiography.

2.14 Data collection and management

Patients will undergo periodic follow-up (once a month during the treatment period and once every 3 months during the follow-up period, including electronic questionnaires or telephone follow-up). After surgery, they will be observed for at least 3 years. Data on vital signs, physical examination, weight, height, body surface area, BMI, ECOG score, KPS score, QLQ-STO22, MDASI-GI, PGSAS-45, peripheral blood inflammatory indicators, blood and urine routine, complete biochemical tests, electrocardiogram, and blood tumor markers will be collected for each treatment cycle and during follow-up visits every 3 months. For participants who did not experience disease progression after completing six courses of treatment, imaging follow-up was conducted every 3 months for 2 years post-surgery and then every 6 months after that until disease recurrence or initiation of alternative therapies. The basic information of the patients and the relevant information required for the study will be recorded in the CRF. Only authorized researchers, representatives of research-undertaking units, ethics committees, and higher-level management departments can access patient records upon reasonable request. No public reports of the results of this study disclose the patient's name or identity. The research team will protect the privacy of the patient's medical data as much as possible within the scope permitted by law.

2.15 Quality control

This study will introduce and promote an ISO quality management system. Personnel at all levels will receive the necessary training in management and quality awareness. A quality control system will be established during project implementation, and relevant quality control measures and evaluation plans will be formulated. The project lead unit will assign special personnel to conduct quality control and supervision of this study, including clinical data collection standards and data verification quality control measures. In addition, the project involves task verification and quality control of participating units to ensure completion. A quality-verification document was created and stored for archival purposes. In addition, Guang'anmen Hospital of the China Academy of Chinese Medical Sciences selected a third party to establish the clinical database of the participants and conducted a statistical analysis of the data.

2.16 Statistical analysis and method

SAS 9.4 statistical software will be used, and full analysis set (FAS) and protocol compliance set (PPS) analyses will be performed on the efficacy indicators. A safety dataset analysis should be conducted for adverse reactions. All statistical tests will be conducted bilaterally, and statistical significance will be set at $p \leq 0.05$. We will analyze whether there are outliers in the data and conduct a professional analysis of outliers to decide whether to accept or reject them. After this, we will analyze the data for missing values and conduct a professional analysis to determine whether the missing values are listed as missing or data transferred. The proportion of shedding cases should not exceed 10%; otherwise, analysis and explanation should be provided. The measurement data were described as mean, standard deviation, median, minimum, and maximum whereas counting data were described as frequency, percentage, etc. Quantitative data analysis will be performed using *t*-tests, rank-sum tests, etc. Counting data analysis will be performed using chi-square tests, ridit analyses, etc. Survival data analysis will be performed using the Kaplan–Meier method, Wilcoxon rank sum test, or log-rank test. A Cox-proportional risk regression model was used for multivariate survival analysis.

3 Discussion

Gastric cancer is an important component of the global cancer burden, and local recurrence or distant metastasis after radical gastrectomy is the primary cause of poor prognosis (26). The guidelines recommend no standard treatment after postoperative adjuvant treatment for GC; watchful waiting is recommended. However, most patients with GC experience recurrence and metastasis within 2–3 years after surgery. Therefore, exploring the efficacy of complementary and alternative medicines during surveillance and watchful waiting periods is necessary to promote adjustment of postoperative monitoring and management programs. Several studies have shown that TCM plays a significant role in preventing and treating GC. TCMs stabilize tumors, reduce recurrence and metastasis rates, alleviate clinical symptoms, improve patient survival and quality of life, and decrease the occurrence of adverse reactions (69, 70). However, the quality of most clinical research on TCM treatment of GC is low. These studies provide a low level of evidence, making it challenging to effectively promote and guide clinical practice. Moreover, no large-sample study has explored the correlation between *Yang* deficiency syndrome and the postoperative recurrence and metastasis of GC. Carrying out well-designed, high-quality clinical research and obtaining robust evidence-based data on TCM treatment for GC are key challenges hindering the widespread adoption of TCM in treating GC. A meta-analysis (71) demonstrated that integrated Chinese and Western medicine treatment could decrease the recurrence rate of GC at 12, 24, and 36 months postoperatively. It was significantly superior to Western medicine treatment alone. *Fuzheng Jiedu* is an effective treatment for postoperative recurrence and metastasis of GC that is used in the Oncology Department of Guang'anmen Hospital of the China Academy of Chinese Medical Sciences. Studies have shown

(52) that the addition of the *Fuzheng Jiedu* prescription (predecessor of the YWJP) for patients with GC can reduce the recurrence and metastasis rates of GC for 2 years after surgery by 18.60%, which is approximately a 25% reduction compared to patients in the same period. Therefore, TCM has therapeutic advantages in reducing the recurrence and metastasis of GC.

The YWJP has the effects of nourishing *Qi* and warming *Yang*, strengthening *Zhengqi*, and detoxifying, which can improve the "*Yang-deficient toxic node*" status of postoperative patients with GC. In this study, we aim to clarify the efficacy and safety of YWJP in preventing and treating postoperative recurrence and metastasis of GC. Furthermore, we aim to explore the correlation between *Yang* deficiency, metabolic abnormalities, gut microbiota, and other factors and their impact on long-term prognosis. Lastly, we seek to identify the mechanisms of postoperative recurrence and metastasis of GC under the guidance of core pathogenesis and possible targets of TCM. The advantages of this study are as follows: (1) it is a high-quality, randomized, double-blind, controlled, multicenter clinical study with a 1:1 random allocation. This design will ensure a better balance between groups and effectively avoid the impact of potentially unknown factors on the test results. Furthermore, simultaneously observing both groups of patients helps to avoid the effect of the trial sequence on the results, thereby enhancing the credibility of the research findings. (2) This research provides a solid clinical foundation for the initial phase. It is centered on the core pathogenesis of the "*Yang-deficient toxic node*" following surgery for GC. The treatment approach of "supplementing *Qi* and warming *Yang* and detoxify" aims to guide personalized treatment strategies aligned with the principles of precision medicine, focused on the effective intervention effect on GC recurrence and metastasis. However, this study has limitations: (1) The experimental design and implementation requirements are demanding. The intervention time is lengthy, the workload is substantial, and the implementation is challenging. (2) The intervention and follow-up periods were lengthy, with a high probability of dropout. (3) Considering the limitations of manpower, economy, and time involved in this clinical study, our follow-up time will be set at 3 years after surgery. However, we will continue to monitor this study to compensate for the restricted follow-up time.

The aims of this study were to evaluate the effectiveness and safety of supplementary and alternative drugs (YWJP) for recurrence and metastasis in patients with GC after surgery and to reveal the influence of *Yang* deficiency syndrome and gut microbiota on recurrence and metastasis. In addition, based on the core pathogenesis of the *Yang-deficient toxic node*, exploring the preventive and therapeutic effects and molecular mechanisms of TCM after GC surgery will establish a foundation for developing a new theoretical framework for preventing and treating GC post-surgery. Ultimately, the results of this study will provide a crucial foundation for patients with GC, clinicians, and policymakers to monitor postoperative treatment management and establish a standardized treatment protocol. In the future, we will promote the clinical transformation of YWJP, develop new Chinese medicines, and conduct high-quality, multicenter, randomized controlled studies internationally to enhance the standardized clinical diagnosis and treatment of GC. In addition, with the advancement of spatial tumor ecology (72, 73), it is crucial to investigate the biological implications of the "disease-symptom-syndrome" of GC and the biological foundation of the population that benefits from TCM prevention and treatment.

Data availability statement

The original contributions presented in the study are included in the article/supplementary material. Further inquiries can be directed to the corresponding author.

Ethics statement

This study has been performed in accordance with the Declaration of Helsinki and has been approved by ethics Committee of Guang 'anmen Hospital, China Academy of Chinese Medical Sciences (Ethics Approval Number: 2021-147-KY). Written informed consent was obtained from the individual(s) for the publication of any potentiallyidentifiable images or data included in this article.

Author contributions

LC: Writing – original draft, Writing – review & editing, Data curation, Methodology. GZ: Methodology, Writing – review & editing. XW: Methodology, Supervision, Writing – review & editing. ZK: Methodology, Writing – review & editing. XS: Supervision, Writing – review & editing. XM: Supervision, Writing – review & editing. XZ: Methodology, Writing – review & editing. RG: Supervision, Writing – review & editing. JL: Supervision, Writing – review & editing.

Funding

The author(s) declare financial support was received for the research, authorship, and/or publication of this article. This work was supported by Science and Technology Innovation Project of China Academy of Chinese Medical Sciences (No. CI2021A01802), National Postdoctoral Research Program (No. GZC20233128), Beijing Major Difficult Diseases Collaborative Research Project of Chinese and Western Medicine (2023BJSZDYNJBXTGG-013), High Level Chinese Medical Hospital Promotion Project (HLCMHPP2023085, HLCMHPP2023001, HLCMHPP2023097).

Acknowledgments

We would like to thank Editage (www.editage.cn) for English language editing.

Conflict of interest

The authors declare that the research was conducted in the absence of any commercial or financial relationships that could be construed as a potential conflict of interest.

Publisher's note

References

1. Bray F, Laversanne M, Sung H, Ferlay J, Siegel RL, Soerjomataram I, et al. Global cancer statistics 2022: GLOBOCAN estimates of incidence and mortality worldwide for 36 cancers in 185 countries. *CA Cancer J Clin*. (2024) 74:229–63. doi: 10.3322/caac.21834

2. Zeng Y, Jin RU. Molecular pathogenesis, targeted therapies, and future perspectives for gastric cancer. *Semin Cancer Biol*. (2022) 86:566–82. doi: 10.1016/j.semcancer.2021.12.004

3. Han B, Zheng R, Zeng H, Wang S, Sun K, Chen R, et al. Cancer incidence and mortality in China, 2022. *J Natl Cancer Center*. (2024) 4(1):47–53. doi: 10.1016/j.jncc.2024.01.006

4. . doi: 10.1016/j.jncc.2022.02.002

5. Wang Z, Han W, Xue F, Zhao Y, Wu P, Chen Y, et al. Nationwide gastric cancer prevention in China, 2021-2035: a decision analysis on effect, affordability and cost-effectiveness optimisation. *Gut*. (2022) 71:2391–400. doi: 10.1136/gutjnl-2021-325948

6. Morgan E, Arnold M, Camargo MC, Gini A, Kunzmann AT, Matsuda T, et al. The current and future incidence and mortality of gastric cancer in 185 countries, 2020-40: A population-based modelling study. *EClinicalMedicine*. (2022) 47:101404. doi: 10.1016/j.eclinm.2022.101404

7. Gonzalez CA, Megraud F, Buissonniere A, Lujan Barroso L, Agudo A, Duell EJ, et al. Helicobacter pylori infection assessed by ELISA and by immunoblot and noncardia gastric cancer risk in a prospective study: the Eurgast-EPIC project. *Ann Oncol*. (2012) 23:1320–4. doi: 10.1093/annonc/mdr384

8. Sadjadi A, Derakhshan MH, Yazdanbod A, Boreiri M, Parsaeian M, Babaei M, et al. Neglected role of hookah and opium in gastric carcinogenesis: a cohort study on risk factors and attributable fractions. *Int J cancer*. (2014) 134:181–8. doi: 10.1002/ijc.28344

9. Steevens J, Schouten LJ, Goldbohm RA, van den Brandt PA. Alcohol consumption, cigarette smoking and risk of subtypes of oesophageal and gastric cancer: a prospective cohort study. *Gut*. (2010) 59:39–48. doi: 10.1136/gut.2009.191080

10. Na HK, Lee JY. Molecular basis of alcohol-related gastric and colon cancer. *Int J Mol Sci*. (2017) 18(6):1116. doi: 10.3390/ijms18061116

11. Tramacere I, Negri E, Pelucchi C, Bagnardi V, Rota M, Scotti L, et al. A meta-analysis on alcohol drinking and gastric cancer risk. *Ann Oncol*. (2012) 23:28–36. doi: 10.1093/annonc/mdr135

12. Moy KA, Fan Y, Wang R, Gao YT, Yu MC, Yuan JM. Alcohol and tobacco use in relation to gastric cancer: a prospective study of men in Shanghai, China. *Cancer Epidemiol Biomarkers Prev*. (2010) 19:2287–97. doi: 10.1158/1055-9965.EPI-10-0362

13. Ferlay J, Shin HR, Bray F, Forman D, Mathers C, Parkin DM. Estimates of worldwide burden of cancer in 2008: GLOBOCAN 2008. *Int J Cancer*. (2010) 127:2893–917. doi: 10.1002/ijc.25516

14. Jang J, Lee S, Ko KP, Abe SK, Rahman MS, Saito E, et al. Association between body mass index and risk of gastric cancer by anatomic and histologic subtypes in over 500,000 east and Southeast Asian cohort participants. *Cancer epidemiology Biomarkers Prev*. (2022) 31:1727–34. doi: 10.1158/1055-9965.EPI-22-0051

15. Yang P, Zhou Y, Chen B, Wan HW, Jia GQ, Bai HL, et al. Overweight, obesity and gastric cancer risk: results from a meta-analysis of cohort studies. *Eur J Cancer (Oxford England: 1990)*. (2009) 45:2867–73. doi: 10.1016/j.ejca.2009.04.019

16. Dabo B, Pelucchi C, Rota M, Jain H, Bertuccio P, Bonzi R, et al. The association between diabetes and gastric cancer: results from the Stomach Cancer Pooling Project Consortium. *Eur J Cancer Prev*. (2022) 31:260–9. doi: 10.1097/CEJ.0000000000000703

17. Dai D, Yang Y, Yu J, Dang T, Qin W, Teng L, et al. Interactions between gastric microbiota and metabolites in gastric cancer. *Cell Death disease*. (2021) 12:1104. doi: 10.1038/s41419-021-04396-y

18. Song P, Wu L, Guan W. Dietary nitrates, nitrites, and nitrosamines intake and the risk of gastric cancer: A meta-analysis. *Nutrients*. (2015) 7:9872–95. doi: 10.3390/nu7125505

19. Tricker AR, Preussmann R. Carcinogenic N-nitrosamines in the diet: occurrence, formation, mechanisms and carcinogenic potential. *Mutat Res*. (1991) 259:277–89. doi: 10.1016/0165-1218(91)90123-4

20. Zhao Z, Yin Z, Zhao Q. Red and processed meat consumption and gastric cancer risk: a systematic review and meta-analysis. *Oncotarget*. (2017) 8:30563–75. doi: 10.18632/oncotarget.v8i18

21. Harrison LE, Zhang ZF, Karpeh MS, Sun M, Kurtz RC. The role of dietary factors in the intestinal and diffuse histologic subtypes of gastric adenocarcinoma: a case-control study in the U.S. *Cancer*. (1997) 80:1021–8. doi: 10.1002/(ISSN)1097-0142

22. Gonzalez CA, Agudo A. Carcinogenesis, prevention and early detection of gastric cancer: where we are and where we should go. *Int J cancer*. (2012) 130:745–53. doi: 10.1002/ijc.26430

23. Choi IJ, Kim CG, Lee JY, Kim YI, Kook MC, Park B, et al. Family history of gastric cancer and helicobacter pylori treatment. *New Engl J Med*. (2020) 382:427–36. doi: 10.1056/NEJMoa1909666

24. Camargo MC, Murphy G, Koriyama C, Pfeiffer RM, Kim WH, Herrera-Goepfert R, et al. Determinants of Epstein-Barr virus-positive gastric cancer: an international pooled analysis. *Br J Cancer*. (2011) 105:38–43. doi: 10.1038/bjc.2011.215

25. Murphy G, Dawsey SM, Engels EA, Ricker W, Parsons R, Etemadi A, et al. Cancer risk after pernicious anemia in the US elderly population. *Clin Gastroenterol Hepatol*. (2015) 13:2282–9.e1-4. doi: 10.1016/j.cgh.2015.05.040

26. Smyth EC, Nilsson M, Grabsch HI, van Grieken NC, Lordick F. Gastric cancer. *Lancet*. (2020) 396:635–48. doi: 10.1016/S0140-6736(20)31288-5

27. Bornschein J, Rugge M. Bright future for endoscopy: the new frontier of gastric cancer secondary prevention. *Gut*. (2020) 69:1723–4. doi: 10.1136/gutjnl-2020-321570

28. Noh SH, Park SR, Yang HK, Chung HC, Chung IJ, Kim SW, et al. Adjuvant capecitabine plus oxaliplatin for gastric cancer after D2 gastrectomy (CLASSIC): 5-year follow-up of an open-label, randomised phase 3 trial. *Lancet Oncol*. (2014) 15:1389–96. doi: 10.1016/S1470-2045(14)70473-5

29. Al-Batran SE, Hartmann JT, Probst S, Schmalenberg H, Hollerbach S, Hofheinz R, et al. Phase III trial in metastatic gastroesophageal adenocarcinoma with fluorouracil, leucovorin plus either oxaliplatin or cisplatin: a study of the Arbeitsgemeinschaft Internistische Onkologie. *J Clin Oncol*. (2008) 26:1435–42. doi: 10.1200/JCO.2007.13.9378

30. Lee JH, Kim HI, Kim MG, Ha TK, Jung MS, Kwon SJ. Recurrence of gastric cancer in patients who are disease-free for more than 5 years after primary resection. *Surgery*. (2016) 159:1090–8. doi: 10.1016/j.surg.2015.11.002

31. Cao L, Selby LV, Hu X, Zhang Y, Janjigian YY, Tang L, et al. Risk factors for recurrence in T1-2N0 gastric cancer in the United States and China. *J Surg Oncol*. (2016) 113:745–9. doi: 10.1002/jso.24228

32. Jin LX, Moses LE, Squires MH 3rd, Poultsides GA, Votanopoulos K, Weber SM, et al. Factors associated with recurrence and survival in lymph node-negative gastric adenocarcinoma: A 7-institution study of the US gastric cancer collaborative. *Ann surg*. (2015) 262:999–1005. doi: 10.1097/SLA.0000000000001084

33. Baiocchi GL, Marrelli D, Verlato G, Morgagni P, Giacopuzzi S, Coniglio A, et al. Follow-up after gastrectomy for cancer: an appraisal of the Italian research group for gastric cancer. *Ann Surg Oncol*. (2014) 21:2005–11. doi: 10.1245/s10434-014-3534-8

34. Fields RC, Strong VE, Gonen M, Goodman KA, Rizk NP, Kelsen DP, et al. Recurrence and survival after pathologic complete response to preoperative therapy followed by surgery for gastric or gastrooesophageal adenocarcinoma. *Br J cancer*. (2011) 104:1840–7. doi: 10.1038/bjc.2011.175

35. Youn HG, An JY, Choi MG, Noh JH, Sohn TS, Kim S. Recurrence after curative resection of early gastric cancer. *Ann Surg Oncol*. (2010) 17:448–54. doi: 10.1245/s10434-009-0772-2

36. Yoo CH, Noh SH, Shin DW, Choi SH, Min JS. Recurrence following curative resection for gastric carcinoma. *Br J surg*. (2000) 87:236–42. doi: 10.1046/j.1365-2168.2000.01360.x

37. D'Angelica M, Gonen M, Brennan MF, Turnbull AD, Bains M, Karpeh MS. Patterns of initial recurrence in completely resected gastric adenocarcinoma. *Ann surg*. (2004) 240:808–16. doi: 10.1097/01.sla.0000143245.28656.15

38. Song J, Lee HJ, Cho GS, Han SU, Kim MC, Ryu SW, et al. Recurrence following laparoscopy-assisted gastrectomy for gastric cancer: a multicenter retrospective analysis of 1,417 patients. *Ann Surg Oncol*. (2010) 17:1777–86. doi: 10.1245/s10434-010-0932-4

39. Honda M, Hiki N, Kinoshita T, Yabusaki H, Abe T, Nunobe S, et al. Long-term outcomes of laparoscopic versus open surgery for clinical stage I gastric cancer: the LOC-1 study. *Ann surg*. (2016) 264:214–22. doi: 10.1097/SLA.0000000000001654

40. Park SH, Lim DH, Sohn TS, Lee J, Zang DY, Kim ST, et al. A randomized phase III trial comparing adjuvant single-agent S1, S-1 with oxaliplatin, and postoperative chemoradiation with S-1 and oxaliplatin in patients with node-positive gastric cancer after D2 resection: the ARTIST 2 trial(☆). *Ann Oncol*. (2021) 32:368–74. doi: 10.1016/j.annonc.2020.11.017

41. Yan X. Investigation of the timing, patterns and prognostic factors of recurrence after curative radical resection for gastric cancer. *Nanjing Med Univ*. (2018) 13–23. doi: 10.27249/d.cnki.gnjyu.2018.000325

42. Turanli S, Atalay C, Berberoglu U, Gulben K. Adjuvant chemoradiation versus chemotherapy for stage III gastric cancer after surgery with curative intent. *J Cancer Res Ther*. (2015) 11:369–74. doi: 10.4103/0973-1482.160050

43. Cao LC. *Investigation of bias constitution and related factors in patients with recurrence and metastasis of gastric cancer and study on the intervention effect of Fuzheng Jiedu prescription*. Beijing: China Academy of Chinese Medical Sciences (2022). doi: 10.27658/d.cnki.gzzyy.2022.000196

44. Zeng H, Liu Z, Wang Z, Zhou Q, Qi Y, Chen Y, et al. Intratumoral IL22-producing cells define immunoevasive subtype muscle-invasive bladder cancer with poor prognosis and superior nivolumab responses. *Int J Cancer*. (2020) 146:542–52. doi: 10.1002/ijc.32715

45. Wang JH. *Study on fecal metabolomics of Yang deficiency and its correlation with intestinal flora structure*. Beijing: Beijing University of Chinese Medicine (2017).

46. Yun MR, Seo JM, Park HY. Visfatin contributes to the differentiation of monocytes into macrophages through the differential regulation of inflammatory cytokines in THP-1 cells. *Cell Signal*. (2014) 26:705–15. doi: 10.1016/j.cellsig.2013.12.010

47. Koundouros N, Poulogiannis G. Reprogramming of fatty acid metabolism in cancer. *Br J Cancer*. (2020) 122:4–22. doi: 10.1038/s41416-019-0650-z

48. Bergers G, Fendt SM. The metabolism of cancer cells during metastasis. *Nat Rev Cancer*. (2021) 21:162–80. doi: 10.1038/s41568-020-00320-2

49. Xie R, Xia Y, Chen Y, Li H, Shang H, Kuang X, et al. The RIGHT extension statement for traditional Chinese medicine: development, recommendations, and explanation. *Pharmacol Res*. (2020) 160:105178. doi: 10.1016/j.phrs.2020.105178

50. Liu Q, Tang J, Chen S, Hu S, Shen C, Xiang J, et al. Berberine for gastric cancer prevention and treatment: Multi-step actions on the Correa's cascade underlie its therapeutic effects. *Pharmacol Res*. (2022) 184:106440. doi: 10.1016/j.phrs.2022.106440

51. Hung KF, Hsu CP, Chiang JH, Lin HJ, Kuo YT, Sun MF, et al. Complementary Chinese herbal medicine therapy improves survival of patients with gastric cancer in Taiwan: A nationwide retrospective matched-cohort study. *J ethnopharmacol*. (2017) 199:168–74. doi: 10.1016/j.jep.2017.02.004

52. Zhang Y. *Study on the correlation between traditional Chinese medicine constitution and postoperative recurrence and metastasis of gastric cancer and quality of life*. Beijing: Beijing University of Chinese Medicine (2019).

53. Cao LC, Wang XM, Zhu GH, Xu BW, Li J. Based on "Yang deficiency and toxin knot" to explore the intervention of five methods of treating yang in gastrointestinal tumors. *J Basic Chin Med*. (2022) 28:1359–62. doi: 10.19945/j.cnki.issn.1006-3250.2022.08.002

54. Yan A. *Study on the intervention of Fuzheng Jiedu prescription on recurrence and metastasis of gastric cancer patients after operation and quality of life*. Beijing: Beijing University of Chinese Medicine (2018).

55. Tan Y. *Correlation analysis of Yang deficiency and biological index after gastric cancer operation and intervention study of Yiqingyang Jiedu prescription*. Beijing: China Academy of Chinese Medical Sciences (2023). doi: 10.27658/d.cnki.gzzyy.2023.000277

56. Chan AW, Tetzlaff JM, Altman DG, Laupacis A, Gotzsche PC, Krleza-Jeric K, et al. SPIRIT 2013 statement: defining standard protocol items for clinical trials. *Ann Internal Med*. (2013) 158:200–7. doi: 10.7326/0003-4819-158-3-201302050-00583

57. Schulz KF, Altman DG, Moher D, Group C. CONSORT 2010 statement: updated guidelines for reporting parallel group randomized trials. *Ann Internal Med*. (2010) 152:726–32. doi: 10.7326/0003-4819-152-11-201006010-00232

58. Amin MB, Edge SB, Greene FL, Brierley JD. AJC. *AJCC cancer staging manual [M]. 8th ed*. New York: Springer (2017).

59. Ma JY, Liu Q. Clinicopathological and prognostic significance of lymphocyte to monocyte ratio in patients with gastric cancer: A meta-analysis. *Int J Surg*. (2018) 50:67–71. doi: 10.1016/j.ijsu.2018.01.002

60. Peng CW, Wang LW, Fang M, Yang GF, Li Y, Pang DW. Combined features based on MT1-MMP expression, CD11b + immunocytes density and LNR predict clinical outcomes of gastric cancer. *J Trans Med*. (2013) 11:153. doi: 10.1186/1479-5876-11-153

61. Nogueiro J, Santos-Sousa H, Pereira A, Devezas V, Fernandes C, Sousa F, et al. The impact of the prognostic nutritional index (PNI) in gastric cancer. *Langenbecks Arch Surg*. (2022) 407:2703–14. doi: 10.1007/s00423-022-02627-0

62. Rausei S, Mangano A, Galli F, Rovera F, Boni L, Dionigi G, et al. Quality of life after gastrectomy for cancer evaluated via the EORTC QLQ-C30 and QLQ-STO22 questionnaires: surgical considerations from the analysis of 103 patients. *Int J Surg*. (2013) 11 Suppl 1:S104–9. doi: 10.1016/S1743-9191(13)60028-X

63. Wang XS, Williams LA, Eng C, Mendoza TR, Shah NA, Kirkendoll KJ, et al. Validation and application of a module of the M. D. Anderson Symptom Inventory for measuring multiple symptoms in patients with gastrointestinal cancer (the MDASI-GI). *Cancer*. (2010) 116:2053–63. doi: 10.1002/cncr.24920

64. Misawa K, Terashima M, Uenosono Y, Ota S, Hata H, Noro H, et al. Evaluation of postgastrectomy symptoms after distal gastrectomy with Billroth-I reconstruction using the Postgastrectomy Syndrome Assessment Scale-45 (PGSAS-45). *Gastric Cancer*. (2015) 18:675–81. doi: 10.1007/s10120-014-0407-6

65. Kurtenkov O, Klaamas K, Miljukhina L. The lower level of natural anti-Thomsen-Friedenreich antigen (TFA) agglutinins in sera of patients with gastric cancer related to ABO (H) blood-group phenotype. *Int J cancer*. (1995) 60:781–5. doi: 10.1002/ijc.2910600609

66. Chen X, Chen W, Huang Y, Xu J, Zeng Y, Shi M, et al. A quantified risk-scoring system including the visceral fat area for peritoneal metastasis of gastric cancer. *Cancer Manage Res*. (2019) 11:2903–13. doi: 10.2147/CMAR

67. Han S, Wang Z, Liu J, Wang HD, Yuan Q. miR-29a-3p-dependent COL3A1 and COL5A1 expression reduction assists sulforaphane to inhibit gastric cancer progression. *Biochem Pharmacol*. (2021) 188:114539. doi: 10.1016/j.bcp.2021.114539

68. Matsui R, Inaki N, Tsuji T, Kokura Y, Momosaki R. Preoperative high visceral fat increases severe complications but improves long-term prognosis after gastrectomy for patients with advanced gastric cancer: a propensity score matching analysis. *Nutrients*. (2022) 14(20):4236. doi: 10.3390/nu14204236

69. Xu B, Wang X, Wang H, Cao L, Ge Y, Yuan B, et al. Efficacy and safety of herbal formulas with the function of gut microbiota regulation for gastric and colorectal cancer: A systematic review and meta-analysis. *Front Cell Infect Microbiol*. (2022) 12:875225. doi: 10.3389/fcimb.2022.875225

70. Yang M, Zhu SJ, Shen C, Zhai R, Li DD, Fang M, et al. Clinical application of Chinese herbal injection for cancer care: evidence-mapping of the systematic reviews, meta-analyses, and randomized controlled trials. *Front Pharmacol*. (2021) 12:666368. doi: 10.3389/fphar.2021.666368

71. Wen YH, Lang J, Deng X, Zhou XX. Meta-analysis of traditional Chinese medicine combined with chemotherapy in preventing postoperative recurrence of gastric cancer. *Hunan J Traditional Chin Med*. (2016) 32:145–7. doi: 10.16808/j.cnki.issn1003-7705.2016.09.073

72. Sammut SJ, Crispin-Ortuzar M, Chin SF, Provenzano E, Bardwell HA, Ma W, et al. Multi-omic machine learning predictor of breast cancer therapy response. *Nature*. (2022) 601:623–9. doi: 10.1038/s41586-021-04278-5

73. Wang FH, Zhang XT, Li YF, Tang L, Qu XJ, Ying JE, et al. The Chinese Society of Clinical Oncology (CSCO): Clinical guidelines for the diagnosis and treatment of gastric cancer, 2021. *Cancer Commun (London England)*. (2021) 41:747–95. doi: 10.1002/cac2.12193

frontiers | Frontiers in Oncology

TYPE Review
PUBLISHED 29 July 2024
DOI 10.3389/fonc.2024.1352845

OPEN ACCESS

EDITED BY
Zsolt Kovács,
George Emil Palade University of Medicine, Pharmacy, Sciences and Technology of Târgu Mureş, Romania

REVIEWED BY
Abhijit Shukla,
Memorial Sloan Kettering Cancer Center, United States
Kunqi Chen,
Fujian Medical University, China

*CORRESPONDENCE
Xiaonan Han
xxh455@case.edu;
xhan1@metrohealth.org

RECEIVED 09 December 2023
ACCEPTED 25 June 2024
PUBLISHED 29 July 2024

CITATION
Esmaeili N, Bakheet A, Tse W, Liu S and Han X (2024) Interaction of the intestinal cytokines-JAKs-STAT3 and 5 axes with RNA N6-methyladenosine to promote chronic inflammation-induced colorectal cancer. *Front. Oncol.* 14:1352845.
doi: 10.3389/fonc.2024.1352845

Interaction of the intestinal cytokines-JAKs-STAT3 and 5 axes with RNA N6-methyladenosine to promote chronic inflammation-induced colorectal cancer

Nardana Esmaeili[1,2], Ahmed Bakheet[1,2], William Tse[1], Shujun Liu[1] and Xiaonan Han[1,2,3]*

[1]Division of Hematology and Oncology, Department of Medicine, MetroHealth Medical Center (MHMC), Case Western Reserve University (CWRU) School of Medicine, Cleveland, OH, United States, [2]Division of Cancer Biology, Department of Medicine, MetroHealth Medical Center (MHMC), Case Western Reserve University (CWRU) School of Medicine, Cleveland, OH, United States, [3]Cancer Genomics and Epigenomics Program, Case Comprehensive Cancer Center, Case Western Reserve University (CWRU), Cleveland, OH, United States

Colorectal cancer (CRC) is one of the most common cancers, with a high mortality rate worldwide. Mounting evidence indicates that mRNA modifications are crucial in RNA metabolism, transcription, processing, splicing, degradation, and translation. Studies show that N6-methyladenosine (m6A) is mammalians' most common epi-transcriptomic modification. It has been demonstrated that m6A is involved in cancer formation, progression, invasion, and metastasis, suggesting it could be a potential biomarker for CRC diagnosis and developing therapeutics. Cytokines, growth factors, and hormones function in JAK/STAT3/5 signaling pathway, and they could regulate the intestinal response to infection, inflammation, and tumorigenesis. Reports show that the JAK/STAT3/5 pathway is involved in CRC development. However, the underlying mechanism is still unclear. Signal Transducer and Activator of Transcription 3/5 (STAT3, STAT5) can act as oncogenes or tumor suppressors in the context of tissue types. Also, epigenetic modifications and mutations could alter the balance between pro-oncogenic and tumor suppressor activities of the STAT3/5 signaling pathway. Thus, exploring the interaction of cytokines-JAKs-STAT3 and/or STAT5 with mRNA m6A is of great interest. This review provides a comprehensive overview of the characteristics and functions of m6A and JAKs-STAT3/5 and their relationship with gastrointestinal (GI) cancers.

KEYWORDS

JAKs, STAT3, STAT5, N6-methylAdenosine (m6A), chronic inflammation, colorectal cancer

Introduction

Colorectal cancer (CRC) ranks as the third most common tumor worldwide, with high incidence and mortality rates annually. CRC is a complex disease caused by various risk factors such as environmental exposure, genetic alterations, and epigenetic modifications (1). Epigenetics is a type of genetic modification that alters gene expression with no change in the nucleotide sequence of genes. Many studies show that RNA modification is an important mechanism of epigenetic regulation, which plays a pivotal role in the occurrence of different diseases (2). RNA modification occurs on all nucleotides: A, U, C, and G (3). However, Adenine is a nucleotide that undergoes a heavy modification in RNA and poses important activities (4). It has been well established that mRNA modification, especially N6-methyladenosine (m6A), mediates various fundamental biological processes (5). The m6A methylation is a reversible process in eukaryotes carried out by methyltransferases and demethylases (6–8). Several studies suggest that m6A methylation is associated with various cancers. Emerging evidence indicates the critical role of the m6A epi-transcriptome in every characteristic of cancer biology. Among all epigenetic modifications, m6A plays a crucial role in the progression and development of CRC (9). In recent years, many studies focused on the significance of m6A in regulating gene expression and disease progression, and several genes have been identified as the new m6A methylation regulation molecules. However, their function and mechanism have not been fully understood.

On the other hand, cell fate, survival, and genome maintenance are regulated via the Janus Kinases/Signal Transducer and Activator of Transcription (JAK/STAT) pathway (10). In general, binding a ligand to a growth factor or cytokine receptor launches the JAK/STAT signaling pathway. The growth factor receptors are auto-phosphorylated in the JAK-independent pathway; however, JAK phosphorylates the tyrosine residues in the JAK-dependent pathway. These phosphorylated sites would later provide docking sites for SH2 domain-containing molecules such as STAT5A/B (11). The crystallization study confirmed the antiparallel dimerization mode of unphosphorylated STATs that switches to parallel dimers upon phosphorylation. This shift between phosphorylation and dephosphorylation modes is the most efficient nucleus translocation form (12). The JAK/STAT pathway also plays a vital role in gene expression in eukaryotic cells. It was shown that STAT3 is highly conserved across different species. For example, STAT3 isolated from the Tasmanian devil facial tumor disease shares more than 99% amino acid sequence homology with human STAT3 orthologue (11). Despite being a transcription factor, STAT5 is essential in gene expression regulation. The complex formation of STAT5 protein requires three different dimer interfaces: (1) the N-domain for oligomerization, (2) the coiled-coil domain for DNA binding, and (3) the SH2 domain, which is required for dimerization via SH2 domain-pY residue. The STAT5A and STAT5B genes are located on chromosome 17q21.2 and show around 92% identity (731 amino acids out of 794). The STAT5A and STAT5B are mainly different at the C-terminal and N-terminal ends. In addition, the DNA binding properties of STAT5A and STAT5B are also different, where STAT5B forms solid bonds with DNA with very different spacing to palindromic invert repeat sequences, which impacts gene regulation. STAT5A and STAT5B show specific functions such as different protein-protein interactions, chromatin assembly, or variation in protein turnover and expression (11). Reports indicate that STAT5B is expressed in natural killer muscle cells, liver hepatocytes, liver endothelium, and cholangiocytes, while STAT5A is mainly expressed in mammary gland epithelial cells (13). The STAT5A and STAT5B proteins are activated by cytokines and hormones such as prolactin and growth hormone (14). STAT5 is also triggered by growth factors such as stem cell factor, FLT3 ligand, epidermal growth factor-, fibroblast growth factor-, platelet-derived growth factor-family members, and other cytokines/growth factors/chemokines (13). Tyrosine phosphorylation, serine/threonine phosphorylation, and other post-translational modifications, such as acetylation/sumoylation, regulate STAT5 activity (11). A large number of studies have reviewed the signaling pathway of STAT3. However, the function of intestinal STAT5 has not been reviewed. In this review, we overview the role and the interplay between mRNA m6A and the JAKs-STAT3 and 5 axes in gastrointestinal (GI) cancer with emphasis on STAT5.

An overview of RNA modification of m6A

It has been well established that methylation of the adenosine base at the nitrogen-6 position is the most abundant internal RNA modification (15). N6-methyladenosine (m6A) is considered one of the most common RNA methylation modifications that function in RNA processing, transport, and other functions (16). In general, m6A methylation modulates target gene expression through changing mRNA stabilization, splicing, degradation, and translation efficiency. The function of m6A has been elaborated in different biological procedures, including stem cell differentiation, embryonic development, DNA damage, and tumor progression (9, 17).

The m6A methylation is determined by a methyltransferase (writers), demethylase (erasers), and binding proteins (readers) (18). The overall picture of m6A methylation is presented in Figure 1. In addition, m6A is abundant in mRNA and non-coding RNA (ncRNA), and its function in ncRNA metabolism is essential (19). To date, 11 readers, seven writers, and two erasers have been identified. In the following sections, we will cover these three components of m6A modification.

m6A writers

Writers carry the beginning process of m6A methylation; different methyltransferases could form a complex to gain more robust catalytic ability. The methyltransferase complex (MTC) contains the m6A/METTL complex (MAC) and the m6A/METTL-associated complex (MACOM) (20). On the other hand,

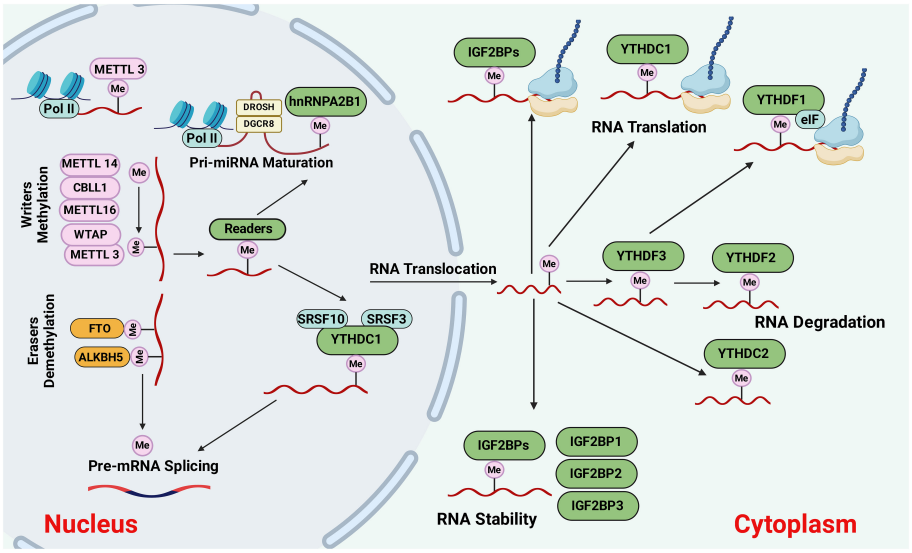

FIGURE 1
The causes and outcomes of m6A methylation. M6A methylation is catalyzed by the writers, including METTL3, METTL14, METTL16, WTAP, or CBLL1. Demethylases such as FTO and ALKBH5 erase the m6A modification through demethylation. The m6A-modified RNAs are recognized by reader proteins, including YTHDC1/2, IGFBP1/2/3, YTHDF1,2,3, and exported to the cytoplasm for degradation, protein translation, and so on. Figure created with BioRender.

MAC has METTL3 and METTL14, which can form a stable heterodimer, which plays a vital role during m6A deposition on nuclear RNAs. METTL14 interacts with METTL3 through their methyltransferase domains (MTD), where METTL3 serves as the methyl catalytic core, while METTL14 stabilizes METTL3 to exert methyltransferase activity and provides an RNA-binding platform (6). However, reports show that METTL3 can function independently from METTL14 and promote the translation of specific mRNAs (21). There is around 22% shared sequence identity between METTL14 and METTL3 (22).

Different types of "writers" (e.g., METTL 3/14/16, WTAP, KIAA 1429, RBM 15/15B, and ZC3H13) are involved in catalyzing the m6A methylation on the mRNA (16). Another type of writer is Wilms' tumor 1-associating protein (WTAP), which forms a complex with METTL3 and METTL14 that regulates m6A. WTAP is universally expressed in the nucleus and acts as a guide to recruit the methyltransferase complex to target transcripts (23). Although the loss of METTL14 promoted tumor proliferation *in vivo*, no impacts on the proliferation of CRC cells *in vitro* were observed. Moreover, the deletion of METTL14 prevents the embryonic stem cell potential for self-renewal and differentiation (24). A recent study by Wang et al. (25) explained the METTL14 role in suppressing CRC metastasis. They also reported that METTL14 is decreased in CRC tissues and correlated with CRC patients' prognosis. In addition, suppression of METTL14 increased the mRNA stability of the arrestin domain containing 4 (ARRDC4), a downstream m6A target of METTL14, via an m6A-YTHDF2-dependent pathway (25).

Studies show that m6A regulates noncoding RNA (ncRNA) expression through a "writer" complex (9, 26). For instance, METTL3 is upregulated in metastasis to promote cell migration and invasion in CRCs by altering miR-1246 expression, while METTL14 suppresses cell proliferation, invasion, and migration in CRCs via miR-375 (27). METTL3 is also involved in tumor progression of other cancers such as leukemia and bladder and gastric cancers via regulation of their downstream genes (17). Studies on methyltransferases in kidney cancer, such as ccRCC, demonstrate that both METTL3 and METTL14 play as tumor suppressors (28–30). METTL3 was shown to be involved in the tumorigenesis and metastasis of colorectal cancer trough YPEL5 expression inhibition in a YTHDF2-dependent manner (31). Most studies on methyltransferases in bladder cancer claim that METTL3 and METLL14 are oncogenes and tumor suppressors, respectively (32).

m6A erasers

Several m6A-specific erasers, AlkB homolog 5 (ALKBH5), and fat mass-and obesity-associated protein (FTO) have been discovered. FTO was first discovered as a gene involved in obesity and energy metabolism and later introduced as the RNA m6A demethylase (33). It is well known that "erasers" such as FTO, ALKBH 3, and ALKBH 5, demethylate m6A, while the functions of "readers" are to identify m6A and selectively bind to target transcripts (34). The discovery of FTO suggested that RNA modification is reversible and dynamic (15). FTO carries out the m6A demethylation process in a Fe(II)- and α-ketoglutarate-dependent enzymatic reaction (35). Functionally, FTO generally acts as an oncogene in different cancers, such as glioblastoma and melanoma, emphasizing the potential of targeting FTO as a therapeutic approach against cancer (36). However, there are several inconsistencies regarding the functions of the FTO in tumor development and prognosis. For example, several reports

indicate that FTO has tumor suppressor activities on CRC invasiveness and metastasis (33), ovarian cancer stem cell self-renewal (37), and papillary thyroid cancer (38). Also, a high relapse rate and poor prognosis in CRC patients were attributed to hypoxia-induced downregulation of FTO protein levels but not RNA. This hypoxia-induced FTO depletion results from ubiquitin-mediated protein proteasome-associated degradation (33).

m6A-readers

m6A readers such as YTHDC1/2, YTHDF1/2/3, insulin-like growth factor 2 mRNA-binding proteins (IGF2BP1/2/3), HNRNP, and eIF3 can recognize the m6A residues. YTH domain family protein 1 (YTHDF1) is an example of an m6A' reader' that enhances the translation efficacy of m6A-modified mRNAs and plays as an oncogene in human cancers. It was shown that high YTHDF1 expression is associated with poor prognosis in hepatocellular carcinoma (HCC) and CRCS. A recent study by Wang et al. (39) found that YTHDF1 is highly upregulated in CRC, supporting the concept that YTHDF1 may convert the deregulated m6A modifications to pro-tumorigenic signals. The expression level of YTHDF1 in human CRC is positively correlated with metastatic progression. Findings from the Ythdf1-knockout mice, CRC cell lines, and primary CRC organoids demonstrated that YTHDF1 executes its pro-tumorigenic impacts by enhancing tumor growth, migration, invasion, and metastasis (39).

In CRC, the epithelial-to-mesenchymal transition (EMT) process, in which cells lose their epithelial traits and acquire mesenchymal features, correlates with a more invasive or metastatic behavior. Throughout the process of EMT, tumor cells experience the breakdown of tight junctions, disturbance in apical-basal polarity, and restructuring of their cytoskeletal framework, facilitating the development of an invasive nature. EMT is irregularly governed by external stimuli originating from the tumor microenvironment within cancer cells, encompassing growth factors and inflammatory cytokines alongside internal physical pressures like hypoxia (40). It was reported that angiogenesis levels are elevated in the early stages of CRC growth. However, this process doesn't show a consistent increase but exhibits an oscillatory pattern (41). EMT regulation demands a robust transcriptional apparatus primarily composed of developmental transcription factors. These factors orchestrate the modulation of epithelial and mesenchymal markers in a synchronized manner. The main groups of EMT-activating transcription factors include the SNAIL family (SNAIL/SLUG), the zinc finger E-box binding homeobox (ZEB) family (ZEB1/ZEB2), and the TWIST family of basic helix-loop-helix (bHLH) transcription factors (TWIST1/TWIST2) (40). Lin et al. (42) presented the importance of m6A modification on EMT regulation in cancer cells and the translation of Snail, an EMT key transcription factor, during this process. They showed that m6A modification levels in mRNA were significantly increased in cancer cells undergoing EMT compared to normal cells. In addition, there is a higher binding affinity between YTHDF1 and CDS of Snail mRNA in cancer cells undergoing EMT. In addition, the deletion of METTL3 and overexpression of ALKBH5 resulted in suppression of the *in vitro* migration, invasion, and EMT of cancer cells. The loss and gain functional studies also demonstrated that YTHDF1 mediates m6A-increased translation of Snail mRNA (42). In addition, the proliferation and growth of HCC cells are inhibited by YTHDF2 through disruption of the stability of epidermal growth factor receptor mRNA. YTHDF3 also negatively modulates the interaction between two long noncoding RNAs, growth arrest-specific 5 (GAS5) and yes-associated protein (YAP), leading to the inhibition of CRC progression (43). It has been well established that IGF2BPs can improve mRNA stability by binding to target transcripts through an m6A motif64 of GG(m6A)C (44). Studies revealed that "readers" such as YTHDF1, IGF2BP1, IGF2BP3, and EIF3B that identify m6A modulation sites are also regulated by ncRNAs (45).

The accumulating evidence revealed that noncoding RNAs (ncRNAs), including microRNA (miRNA), circular RNA (circRNA), and long noncoding RNA (lncRNAs), are involved in the initiation and development of colorectal cancer (1). Circular RNAs are a group of non-coding RNAs without 5′ caps and 3′ polyadenylated tails involved in CRC (46). In addition, the dysregulation of circRNAs leads to the chemoresistance of CRC. Emerging reports suggest that circRNA/microRNA (miRNA)/mRNA regulatory networks play an important role in CRC development and treatment (47). For instance, circ_0007142 increased cell proliferation and metastasis in CRC by regulating the miR-455–5p/SGK1 axis (48). Furthermore, miRNAs and lncRNAs play a pivotal role in diagnosing, prognosis, and treating CRC (49). The miRNAs can function as oncogenes or tumor suppressors, depending on their altered pathways and primary location, such as colon or rectal cancer (50). For instance, miRNA-9 and miRNA-101 act as tumor suppressors in CRC by suppressing colon cancer cell migration (50, 51). On the other hand, miRNA-200, miRNA-17, and miR-141 are three examples of CRC oncogenes that inhibit different tumor suppressor genes and promote cancer cell proliferation (52–54).

It was shown that the higher concentrations of circRNAs positively increase the m6A levels (55). Studies revealed that the sites of circRNAs modified by m6A differ from those of mRNAs modified by m6A, indicating that disruption in the m6A modification of mRNA does not correspond to the m6A circRNAs distraction. Thus, to eliminate m6A modification effects, it is also required to consider the m6A of circRNAs (27). The m6A RNA modifications are dynamic and reversible and regulate RNA metabolism, which can alter the genetic information at the mRNA level. The m6A RNA modifications can also modulate the balanced mRNA expression and facilitate mRNA translation, thereby affecting the levels of the target genes involved in proteins and RNA metabolism. It was shown that RNA metabolism impacts the occurrence and deterioration of diseases, such as cancer and inflammation (56).

In the context of the intestine, m6A is involved in various processes, including intestinal stem cell maintenance and differentiation, intestinal epithelial cells proliferation and regeneration, intestinal epithelial barrier function, and host-microbe interactions. For example, m6A modification of the RNA

molecule has been shown to regulate the expression of critical genes involved in intestinal stem cell maintenance and differentiation, which are crucial for the regeneration and repair of the intestinal epithelium. Also, m6A has been implicated in regulating host-microbe interactions in the gut, which plays a critical role in maintaining gut homeostasis and preventing the development of inflammatory bowel diseases. Overall, m6A modification is a crucial process that plays a key role in various biological processes in the intestine and holds significant promise for developing new therapeutic strategies for treating gut-related diseases.

The function of m6A in colorectal cancer

Around 2 million Europeans and more than 1.5 million North Americans suffer from inflammatory bowel disease (57). Colorectal cancer (CRC) is the second leading cause of cancer-related death worldwide, and metastasis is considered the primary cause of cancer death (58). Many epidemiological data link inflammation to cancer within the digestive system. Inflammation is caused by poor diet, gut microbiota, and widespread infection. For instance, Helicobacter pylori infection causes inflammation in the gut, leading to around 75% of gastric cancers (59). Studies show that the risk of developing colon cancer due to chronic inflammation is very high in autoimmune disorders, ulcerative colitis, and Crohn's disease (60). Data shows that around 50% to 60% of CRC patients ultimately develop metastatic disease, mainly affecting the liver and lungs (39). Despite recent advances in CRC treatments, the survival rate for patients with postoperative and advanced CRC recurrence remains low. Since CRC is mainly diagnosed at an advanced stage of metastasis, the death rate related to CRC metastasis is high (61). Moreover, CRC is highly heterogeneous, making it a very complex disease. Therefore, there is an urgent need to develop sensitive biomarkers capable of accurate prognosis prediction and monitoring therapeutic effects in CRC patients (62). Since epigenetic changes impact tumorigenesis and the progression of CRC, they can be used as potential clinical biomarkers for prognostic and therapeutic uses of CRC (63).

Post-transcriptional modifications of the RNA transcriptome, known as epi-transcriptomics, play critical regulatory roles in gene expression. Recent advances in RNA sequencing technologies discovered various RNA modifications on a transcriptome-wide scale, suggesting that dysregulation of RNA modifications results in tumorigenesis (39). It is well established that CRC occurrence and development are associated with the changes in levels of m6A RNA methylation and m6A RNA methylation regulators (57). Studies show that the amounts of m6A RNA methylation and the expression of its regulatory factors can impact cell proliferation, occurrence, metastasis, stemness-like properties of cancer cells, and invasion in colon cancer (CC) (19, 59). However, the function of m6A RNA modifications in rectal cancer (RC) is not fully understood (59). Recently, methylated RNA immunoprecipitation sequencing (MeRIP-seq) analysis of CRC patients demonstrated that m6A peaks are present in most mRNAs where m6A peaks are differentially methylated (60).

M6A methylation is the most common modification in eukaryote mRNA that functions as both an oncogene and a tumor suppressor in cancer metastasis and the EMT process (64). m6A plays a critical role in various cancers, including leukemia, brain, cervical, endometrial, breast, liver, and lung cancers (32). A regulatory function of m6A has been shown in oncogenesis and development by modifying different target genes (65, 66). Mutation of oncogenes and tumor suppressor genes caused by m6A regulatory factors can affect cancer cell proliferation, metastasis, and infiltration (58). The methylation of m6A regulates miRNA synthesis, processing, and maturation, which are crucial in tumorigenesis and cancer progression (62). The m6A modification also changes the structure of local RNA at the terminal loop region of primary miRNAs (pri-miRNAs), thus stimulating their processing through nuclear transcripts and alternative splicing by modulating RALY binding. A recent study by Wang et al. (63) unraveled an antiviral function for m6A modification in the small intestine during rotavirus infection through ALKBH5. The depletion of Mettl3 in IECs of mice improved their resistance to RV infection and increased the expression of interferons (IFNs) and IFN-stimulated genes (ISGs) (63).

The abnormal methylation of m6A mRNA in CRC could benefit CRC prognosis. Many studies show that RNA m6A regulatory factors, such as METTL3, METTL14, WTAP, FTO, YTHDC1, and YTHDF3, are abnormally expressed in CRC. METTL3 is a 70 kDa protein first identified in Hela cell lysates (67). METTL3 mediates the m6A methylation on mammalian RNAs and is crucial in influencing angiogenesis and promoting tumor progression (68). In CRC tissues, the METTL3 expression is significantly higher than in normal tissues, indicating that METTL3 plays a pivotal role in CRC (57, 69). A recent study (70) revealed that METTL3 upregulation in CRC tissues results in low survival in CRC metastasis. It also improved the stability of PLAU mRNA and promoted CRC cell metastasis through m6A modification. These findings provide novel therapeutic targets for treating CRC metastasis (70).

On the other hand, METTL3 has also been demonstrated as a tumor suppressor in CRC. A recent study (71) claimed that a high content of METTL3 in CRC patients is not beneficial for the cancer cells' growth and division, and it also suppresses CRC cell proliferation, migration, and invasion through p38/ERK pathways, suggesting that METTL3 can be considered that a prognostic factor in CRC patients. In addition, regulators of m6A RNA modification can prevent the occurrence and development of CRC by altering its protein expression level and the protein expression levels of its downstream targets in CRC (57). M6A methylation in lncRNA is also required for cancer cell proliferation, metastasis, and stemness-like properties, including colorectal cancer (CRC) (19). Recently, Zhang et al. (72) also showed that there is a positive correlation between METTL3, LINC00662 (a lncRNA with a length of 2097 nt), and vascular endothelial growth factor A (VEGFA) in CRC tissues. In addition, it was demonstrated that METTL3 dually modulates the stability of the LINC00662 and VEGFA RNAs, thus promoting angiogenesis in CRC. These results together indicate that METTL3 increases CRC progression (72).

The expression level of long intergenic noncoding RNA 460 (LINC00460) was significantly increased in CRC and regulated its growth and metastasis *in vitro* and *in vivo* (73). Also, LINC00460 could promote mRNA stability of HMGA1 via interacting with IGF2BP2 and (DHX9), which leads to a biological response to CRC malignant proliferation and metastasis. Furthermore, m6A modification of HMGA1 mRNA decreased its expression in CRC, and HMGA1 expression regulated by LINC00460 is METTL3-dependant (73).

In tumor tissues, ZEB1-AS1 was significantly overexpressed, which was related to the metastasis of EMT, indicating that ZEB1-AS1 level could be a valuable indicator for predicting the progression and prognosis of CRC (62). METTL3 also enables tumor progression by upregulating lncRNA RP11 and ZEB1 (74) or via the maturation of pre-miR-1246 (75). The METTL3 and METTL14 writers were shown to suppress CRC proliferation and migration via the p38/ERK pathway (71). Methyl CpG binding protein 2 (MeCP2) is a methylated DNA binding protein. Its oncogenic functions in gastric and colorectal cancer and facilitating metastasis of CRC have been documented. In addition, the interaction between MeCP2 and METTL14 was shown to modulate m6A methylation in CRC. In addition, the CRC tumor samples showed a higher expression level of MeCP2, indicating that MeCP2 might act as an oncogene in CRC (6). The m6A methylation regulation function of various studies. However, new reports claim that METTL14 impacts downstream events more than METTL3. Also, the downregulation of METTL14 and YTHDC2 is associated with the poor prognosis of rectal cancer patients (59). METTL14 downregulation in rectal cancer results in reduced immune cell infiltration and poor prognosis indicating that METTL14 expression level could be utilized as an independent prognostic factor in rectal cancer (76).

It was shown that m6A-modified mRNAs are recognized by IGF2BPs, leading to enhanced target mRNA stability, such as MYC, in an m6A-dependent manner (77). IGF2BPs also contain oncogenic roles in cancer cells by stabilizing methylated mRNAs of oncogenic (77). Moreover, Erasers can cause the progression and migration of CRC cells. For example, FTO is involved in the degradation of miR-1266 or reducing expression levels of STAT3, cyclin D, and MMPs to stimulate tumor growth (78). Recently, Bai et al. (79) demonstrated that the CRC cell's tumorigenicity *in vitro* was dramatically suppressed when the expression of YTHDF1 was knocked down. In addition, YTHDF1 silencing inhibited the colonosphere formation ability *in vitro* and Wnt/β-catenin pathway activity in CRC cells. This compelling evidence suggests that YTHDF1 is overexpressed in CRC and functions as an oncogene in CRC (79). According to Zhang et al. (80), the lncRNA NEAT1 is demethylated by ALKBH5, which results in gastric cancer invasion and metastasis through altering the expression of EZH2. On the other hand, ALKBH5 was demonstrated to suppress gastric cancer invasion by downregulating and removing the m6A modifications of PKMYT1 (81). ALKBH5 is an oncogene that accelerates gastric cancer proliferation, metastasis, and invasion (82).

CircRNAs are classified as noncoding RNAs (ncRNAs) and characterized by the covalently closed loop structure without a 3′-poly-A tail or 5′-cap. In general, circRNAs are more stable and resistant to RNA exonuclease degradation. They are valuable prognostic biomarkers and promising targets for treating human cancers (83). YTHDC1 is one of the m6A readers that play critical roles in different cancers, and a high concentration of YTHDC1 was reported in CRC cells and tissues (84). Recently, a direct interaction between YTHDC1 and circFNDC3B in CRC cells was demonstrated. In addition, cytoplasmic export of circFNDC3B in LoVo and HCT116 cells requires YTHDC1, indicating the significance of m6A modification in circ-RNAs (85). A recent study showed that circ_0003215 is downregulated in CRC, and the functional assays demonstrated that the malignancy of CRC was inhibited in both *in vitro* and *in vivo*. Furthermore, circ_0003215 also has m6A methylation, which results in RNA degradation by m6A reader protein YTHDF2 (86). A newly identified circRNA, circ1662, is derived from 3 neighboring exons in the yes-associated protein 1 (YAP1) gene, which seems to play an oncogenic role in CRC, promoting CRC cell invasion and migration. It was reported that circ1662 formation is regulated by METTL3-initiated m6A methylation in CRC cells, and METTL3 apparently can accelerate CRC metastasis using the regulatory mechanism of circ1662. Since circ1662 is positively associated with METTL3 and YAP1 protein expression, it was suggested that circ1662 could be employed as a biomarker to identify cancer metastasis (87). The critical function of m6A-related lncRNAs in the tumor microenvironment (TME) remodeling has been demonstrated (62). Upon cancer development, IL-6 and IL-8 are secreted by tumor-infiltrating immune cells within the tumor microenvironment (TME) (88). A recent study by Liu et al. (89) showed that MIR100HG utilizes a miRNA-independent role in EMT regulation and metastasis in CRC cells by forming a regulatory circuit involving hnRNPA2B1 and TCF7L2. Data collected from 473 CRC specimens and 41 para-cancer tissues established a powerful prognostic model based on 16 genes out of 37 m6A-modified prognostic lncRNAs (90).

The involvement of the epithelial growth factor receptor (EGFR) signaling pathway in CRC progression makes EGFR a valuable therapeutic target in developing tumor-targeted therapeutic drugs. The fragile X mental retardation 1 gene, *FMR1*, is located on human chromosome Xq27.3, which encodes the FMR1 protein, an RNA-binding protein (RBP). It was shown that the FMR1 protein plays a vital role in the growth and progression of various tumors (91). Although the function of FMR1 in regulating CRC tumorigenesis and EGFR signaling pathway is not fully understood, a recent study (92) demonstrated that FMR1 is upregulated in CRC, which is associated with the proliferation and migration of CRC cells. Moreover, FMR1 was shown to recognize the m6A-modification site in EGFR and retained its expression in an m6A-dependent manner. In addition, the FMR1 knockdown effects in CRC cells were eliminated by METTL3, indicating that the METTL3/FMR1/EGFR complex is involved in CRC progression (92).

Mutation in m6A sites of RNA could affect m6A deposition and causes abnormal post-transcriptional regulation, which might result in carcinogenesis (93). The missense rs8100241 variant found in the exon of Ankyrin Repeat and LEM Domain Containing1 (ANKLE1) with a G>A change is linked to reduced CRC risk. Although variant

ANKLE1 [A] is methylated by METTL3, ANKLE [G] could not be methylated. This phenomenon improves the ANKLE1 mRNA stability via m6A, thus decreasing CRC risk (94). Overall, epigenetic changes play a pivotal role in the epithelial-to-mesenchymal transition, a crucial mechanism for metastasis, and mainly include valuable biomarkers in CRCs such as DNA methylation, ncRNA m6A, and mRNA m6A. RNA m6A modification is critical for colorectal organ homeostasis, and its disruption leads to inflammatory disorders and aggressive cancers (19).

m6A modification and its potential in targeted therapy for m6A

Targeted therapy focused on m6A modification has emerged as a prominent area of research for developing new drugs in recent years. It was shown that m6A modifications play an important function in cancer responses to chemotherapy, radiotherapy and immunotherapy, suggesting that m6A regulators could be targeted and used in combination with chemotherapy, radiotherapy, or immunotherapy to treat cancer. The primary targets for m6A modification therapy include FTO inhibitors, METTL3–14 activators/inhibitors that could be used in combination with chemotherapy and immunotherapy (95). The role of METTL3 in CRC cancer has been investigated. Recently, Chen et al. (69) showed that increased expression of METTL3 results in a poor prognosis of CRC while Mettl3 knockout reduces colorectal tumorigenesis. The study also elaborated that the GLUT1-mTORC1 axis is the main METTL3 target in CRC and targeting METTL3 and mTORC1 has a significant potential to inhibit CRC growth, suggesting that METTL3 could be used as a target to treat patients with CRC (69). The association between METTL3 expression and the disease control rate in colorectal cancer (CRC) patients was explored by Li et al. (96). The findings of this study revealed that patients with elevated METTL3 expression had a lower response to chemotherapy leading to poorer treatment outcomes. METTL3 also promotes CRC stemness which consequently contributes to the development of resistance to chemotherapy in CRC patients. However, the knockdown of METTL3 in SW620 and HCT116 cells resulted in higher sensitivity to oxaliplatin-based chemotherapy, compared to the control. In addition, PDX tumor models were injected with METTL3 siRNA to assess the therapeutic effect of METTL3. The IHC results of isolated tumors demonstrated that METTL3 expression significantly reduced in the experimental group treated with METTL3 siRNA. These findings suggest a promising therapeutic scheme for CRC via application of METTL3 inhibitors (96).

The aerobic glycolysis pathway in tumor cells known as the Warburg effect is an abnormal glycolysis that enhances glucose uptake, ATP, and lactate production, promoting tumorigenesis. A recent study by Yang et al. (97) focused on illustrating the role of m6A modification in the Warburg effect in CRC. The study showed that METTL3 knockdown represses Warburg effect in CRC via regulating HIF-1α suggesting that METTL3 is a potential diagnostic marker and therapeutic target (97). Moreover, inhibition of m6A modification due to METTL3 and METTL14 deletion facilitates the IFN-γ-Stat1-Irf1 signal transduction through YTHDF2, resulting in the stabilization of STAT1 and Irf1 mRNA. Consequently, the response to anti-PD-1 therapy is enhanced, highlighting the potential of METTL3 and METTL14 as therapeutic targets for anti-cancer immunotherapy (98).

Recently You et al. (99) constructed small extracellular vesicles (sEVs) that highly express CD47 and increased cyclic arginine–glycine–aspartic modification. This novel strategy was shown to effectively deliver siYTHDF1 to treat gastric cancer with less toxicity via depletion of YTHDF1 leading to suppression of GI cancer progression and metastasis (99). FTO is an essential m6A regulator which its overexpression increases proliferation and migratory potential in MKN28 cells. However, the FTO knockdown suppresses the tumor growth in HGC27 xenograft model. In addition FTO changes the expression pattern of EMT-related genes including E-cadherin and vimentin indicating that FTO possibly functions in the EMT pathway as an oncogene (100). Chemotherapy drug resistance is a major hindrance to achieving treatment in cancers. A potential therapeutic approach to mitigate chemoresistance involves targeting m6A RNA modification. It was shown that YTHDF1 suppression enhances the effectiveness of 5-Fluorouracil and cisplatin chemotherapy drugs in drug-resistant CRC cells (101, 102). Mounting evidence shows that m6A regulation has the potential to be used in targeted therapy for IBD and CRC diseases. There is an urgent need to investigate novel therapeutic strategies targeting m6A for translational clinical applications in IBD and colorectal cancer.

Bioinformatics analysis to study the correlation between m6A RNA methylation and colorectal cancer

In recent years, bioinformatics has emerged as a powerful tool in elucidating the molecular complexities of cancer biology. Combining the capabilities of bioinformatics with experimental evidence enables researchers to explore the interplay between m6A modification and CRC pathogenesis, shedding light on novel biomarkers, therapeutic targets, and potential prognostic indicators.

m6A2Target was the pioneering resource developed in 2020 for targets of m6A writers, erasers, and readers (103). Recently, an updated database called RM2Target has been published (http://rm2target.canceromics.org/). It is more powerful than m6A2Target, encompasses a broader range of RNA modifications, and compiles a significantly larger number of target gene associations (104). The M6ADD database is another platform developed to explore the association between m6A modification and gene disorders and diseases, which consists of 222 m6A-related diseases from both humans and mice. The development of the m6ADD database aims to facilitate researchers in acquiring insights into the functions of particular genes and specific gene-protein interactions (105). The RMDisease, is another example of an RNA modification database developed to address the genetic variants affecting RNA

modifications and their potential association with diseases. This resource integrates data from a large number of RNA modification sites and somatic and germline SNPs, serving as a useful mapping resource for exploring different genetic factors involved in epitranscriptome regulatory pathways and their role in diseases (106). A recently upgraded version of RMDisease database, RMDisease V2.0, has become available by compiling all existing RNA modifications-associated variants and annotating their potential implications in diseases and traits, enabling it to cover a lager range of RNA modification types in different species (107). The m6A-Atlas was released in 2021, offering a more comprehensive perspective of the m6A epitranscriptome. This database resource integrated different m6A sites from seven high-resolution epitranscriptome profiling and diverse post-transcriptional regulatory mechanisms (108). Recently, the m6A-Atlas v2.0 became available to users, enabling them to filter next-generation sequencing results. This database provides a free resource for different m6A enrichment regions for users to screen and filter data.

Furthermore, by integrating annotation data, m6A-Atlas v2.0 facilitates exploring relationships between RNA m6A modification sites and different downstream functional characteristics (109). Human RNA Modifications Disease Database (HRMDD) is another web resource developed recently by collecting 2082 experimentally supported RNA modification-disease associations. The Cancer Genome Atlas (TCGA) analysis was used to evaluate the molecular and clinical aspects of RNA modification regulators in 33 different cancer types, and the roles of RNA modification regulator genes in cancers were visualized and characterized by the development of a regulator-Tool (110). Given that numerous studies evaluating the function of m6A regulators in CRC have been published, further in-depth study into CRC is still required to enhance patient prognosis. Therefore, bioinformatics analysis could be used as an interdisciplinary approach to improve our understanding of CRC at the molecular level by aiding researchers in efficiently and promptly identifying candidate genes. It holds promise for personalized medicine and precision oncology interventions.

An overview of JAKs/STAT signaling pathway

Inflammation is an essential sign of carcinogenesis and tumor progression. It was shown that chronic inflammation is the cause of around 15–25% of cancer cases or deaths worldwide (111). For instance, inflammation resulting from severe *Helicobacter pylori* infection is associated with approximately 75% of gastric cancers. In addition, chronic inflammation resulting from autoimmune disorders, ulcerative colitis, and Crohn's disease enhances the risk of developing colon cancer (112). High levels of cytokines usually characterize inflammation, including interleukin (IL)-6, IL-8, interferon (IFN)γ, tumor growth factor (TGF)-β, tumor necrosis factor-α, vascular–endothelial growth factor and nitric oxide (NO). Reports show that the upregulation of these factors in response to inflammation causes oxidative stress, resulting in DNA damage (111).

The JAK/STAT pathway was first discovered in 1990 when Fu et al. (113) found that the transcriptional activator interferon-stimulated gene factor 3 (ISGF3) responds to IFN-α and is comprised of multiple interacting polypeptide chains (Figure 2). Later on, a proposed model for the signal transduction pathway, which IFN-α induces, demonstrated the signal transduction mode of the JAK/STAT signaling pathway (114). The JAKs/STAT pathway is a pro-tumorigenic signaling pivot that maintains the pro-inflammatory environment. As an evolutionarily conserved pathway, JAK/STAT is essential for proper cellular function. JAKs/STAT was shown to be involved in oncogenesis and progression processes, including cell proliferation, differentiation, invasion, and metastasis. Cancer-related inflammation and mutation of JAKs/STAT components result in various diseases. Many reports emphasized the importance of the JAKs/STAT pathway in malignancies and autoimmune diseases, suggesting that inhibition of the JAKs/STAT pathway could open new promising avenues to treat different diseases (115).

STATs are a family of transcription factors that regulate numerous tumor-associated genes and act as critical cellular mediators in response to various cytokines and growth factors (116). The family of STAT proteins is categorized as conserved transcription factors containing seven members (STAT1, 2, 3, 4, 5a, 5b, and 6). However, the JAK family is comprised of four members: JAK1, JAK2, JAK3, and TYK2 (115). Although differences in the STAT proteins' structure, expression levels, and subcellular localization usually lead to variations in their cellular response, the general knowledge from one member could be applied to others since they share similar structural arrangements of their functional motifs. Since different STATs can interact with the same DNA regulatory element (DRE), the same stimulus can trigger different types of STAT. JAK-STATs pathways are involved in several biological processes. Thus, precise homeostatic mechanisms at various levels must be performed to maintain the signaling pathways.

The alteration in signal transduction functions of different JAK-STATs is carried out through auxiliary STATs recruitment, STAT competition, epigenetic modifications, and recruitment of proteins that inhibit JAK-STAT phosphorylation and DRE binding (117). STAT proteins remain in the cytoplasm when they are inactive. The cytokine receptors are phosphorylated by forming noncovalent binding with JAKs, consequently recruiting STAT proteins. In general, phosphorylation on a C-terminal tyrosine residue activates STAT protein. Thereafter activation, STAT dissociates from JAK and immediately undergoes a stable dimerization upon tyrosine-phosphorylation. They are translocated into the nucleus to modulate the expression of several target genes after binding to specific palindromic DNA elements (e.g., IFNγ-stimulated response element sites) (111, 115). Since STAT1, STAT2, and STAT3 are more stable, it is proposed that the active transcriptional region can regulate the stability of the protein. On the other hand, STAT4, STAT5, and STAT6 can be employed as targets for ubiquitin-dependent destruction (115).

In general, the loss of function or gain of function mutations in JAK-STAT is the leading cause of the initiation and development of tumorigenesis. It was shown that STAT3 and STAT5 are involved in tumor initiation and progression, while STAT1 and

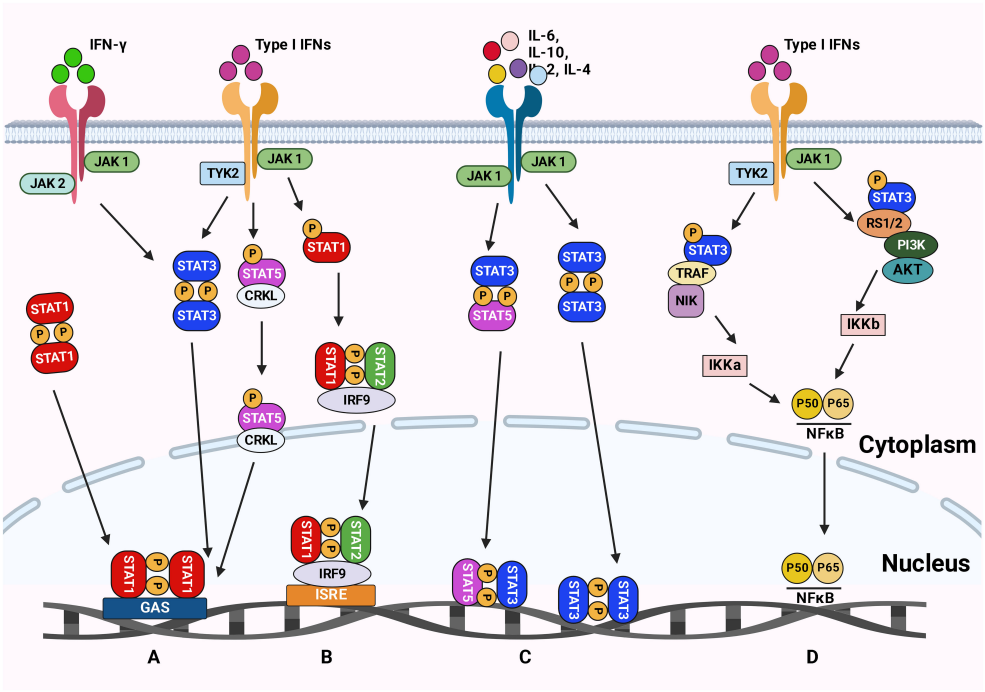

FIGURE 2
The JAK-STAT signaling pathways. **(A)** The type II IFN signaling pathway leads to phosphorylation of STAT1 and induction of inflammatory response. **(B)** The type I IFN signaling pathway results in the phosphorylation of STAT1 and STAT2, which causes an antiviral response. **(C)** Cytokines signal transduction is mediated by JAKs complexes leading to STAT3 and STAT5 phosphorylation. These phosphorylated STATs are then translocated to the nucleus to trigger the transcription of genes involved in inflammation, angiogenesis, and survival. **(D)** The Type I IFN signaling via TYK2 and JAK1 activates the NFκB pathway resulting in a viral response. Figure created with BioRender.

STAT2 play an essential role in anti-tumor defense and long-term immune response (117). For instance, a higher level of nuclear STAT5 is associated with early recurrence and decreased survival rate in prostate cancer, while STAT3 overexpression results in recurrence and poor survival in melanoma, cervical cancer, and colorectal cancer (118). Studies revealed that tumor growth rate and IFN-γ-driven tumor cell killing by NK and T cells were accelerated in STAT1 knockout mice, suggesting that loss of STAT1 negatively affects both innate and adaptive anti-tumor responses (119).

The role of STAT3/5 in GI inflammation and CRC

The transcriptional activators of STAT5 include STAT5A and STAT5B, with 91% similarity at the amino acid level. Although STAT5A has a lower DNA-binding capacity than STAT5B, it can form tetramers and dimers while binding to DNA. However, STAT5B only forms dimer structures (115). According to Lin et al. (2012) normal function of natural killer (NK) cells development and maintenance of $CD8^+$ T cell and $CD4^+CD25^+$ T cell critically depend on STAT5 tetramers (120). Different types of cytokines such as IL-3, prolactin, and the IL-2 cytokine family (e.g., IL-2, IL-4, IL-7, IL-9, and IL-15) can activate STAT5. Also, STAT5 can be activated by EGF, EPO, GM-CSF, TPO, GH, and platelet-derived growth factors (121).

In general, JAK/STAT pathway is a highly conserved signal transduction pathway that regulates different cellular mechanisms related to various diseases, including GI cancer. JAK/STAT5 has been shown to modulate intestinal mucosal immunity (122, 123). The function of intestinal JAK/STAT5 has been documented in different gut cytokines, hormones, and growth factors-mediated mucosal destruction or protection (124). It was reported that JAKs/STAT3 mediates signals from cytokines (e.g., IL-6) or growth factors (e.g., TGF-α) to the nucleus. In addition, regulating intestinal epithelial barrier integrity and transcription induction of antimicrobial peptides by IL-17 would protect the tissue from microbiota translocation and inflammation. However, other cytokines such as IL-4 and IL-13 stimulate the Tuft cell maturation, resulting in the response of parasite antigens (125).

Furthermore, IL-17 regulates intestinal epithelial barrier integrity. The signaling pathway of JAKs/STAT3 is activated upon binding cytokine ligands or growth factors to their receptors on the cell surface, resulting in JAKs activation. The activated JAKs consequently induce the phosphorylation and dimerization of STAT3, stimulating the transcription of several downstream genes (61). Reports show that the overactivation of the JAKs/STAT3 pathway is correlated with CRC-related phenotypes. On the other hand, inhibition of the JAKs/STAT3 signaling pathway induced apoptosis in CRC cells leading to tumor cell invasion and tumor growth restrain (126). The activation of the JAKs/STAT3 signaling pathway results in enhanced expression of malignant phenotypes-associated molecules, such as matrix metalloproteinases, VEGFA,

bFGF, and HGF, consequently developing malignant tumor behaviors, including EMT, migration, invasion, angiogenesis, and metastasis (61). The analysis of target genes and cellular signaling pathways, including JAKs/STAT3 associated with CRC progression and metastasis, can elucidate the underlying mechanism of CRC progression and pharmacotherapy (127).

It was shown that the constitutive activation of STAT3 leads to the development of head and neck tumors, breast cancer, non-small-cell lung cancer, colorectal cancer, and hematological tumors. In addition, high expression of STAT3 and IL-6 can reduce chemotherapy sensitivity in high-grade breast cancer (128). Recently (129) showed that colorectal cancer-associated fibroblasts (CAFs) promote metastasis by upregulating leucine-rich alpha-2-glycoprotein 1 (LRG1). In addition, CAFs-secreted IL-6 (interleukin-6) is responsible for LRG1 up-regulation in CRC, which occurs through direct transactivation by STAT3 following JAK2 activation. Receptor tyrosine kinases such as epidermal growth factor receptors (EGFR) are the upstream activators of the JAKs/STAT3 signaling pathway. Moreover, IL-1 was shown to induce LIF expression and downstream JAK/STAT to generate iCAFs (130). On the other hand, TGF-β antagonizes the generation of iCAF by downregulating IL-1R expression, which promotes shifting to myCAFs. This phenotypic shift of CAFs results in a significant decrease in tumor volume (130). The EGFR is overexpressed in more than 90% of clinical patients. Many studies show that EGFR activates MAPK and JAKs-STAT3 signaling pathways, and STAT3 is involved in the survival of cancer stem cells (CSCs) (131). The JAK/STAT3 signaling pathway is vital in mediating the effects of IL-6 on tumor cell proliferation, survival, invasion, and metastasis. Reports show that selective targeting of STAT3 in cancer could provide multiple benefits, including inhibiting cell-autonomous effects on tumor cell growth and metastasis. Therefore, therapies targeting EGFR and IL-6 pathway components could be used to impair STAT3 activation and signaling (132). Therefore, manipulating the JAKs/STAT3 signaling pathway is a promising approach for metastatic CRC treatment.

Reports show that reduced STAT3 signaling results in the loss of stem cell maintenance, while STAT5 and STAT1 primarily affect cellular survival. Although higher levels of STAT5 were reported in hematological malignancies, recent findings show that STAT5 also mediates solid tumorigenesis (133). STAT5A knockout mice showed defects in progesterone signaling resulting in undeveloped mammary glands and pregnancy difficulties. However, STAT5B knockout mice display dwarfism, lower hepatic RNA biosynthesis capacity, reduced glucose and lipid metabolism, and sexual conversion with marked gender differences (11). It was shown that STAT5A and STAT5B knockout strains are viable. In addition, the Stat5 double knockout embryos are anemic, leukopenic, had smaller spleens and thymi, and disordered thymic architecture, which results in severe combined immunodeficiency phenotype (134).

Evidence indicates that the JAK2/STAT5 pathway is activated in different cancers, suggesting that the AK2/STAT5 signal could be a promising drug target. The biological processes related to JAK2/STAT5 pathway are mainly triggered by transcriptional activation of STAT5 target genes. Recently Wang et al. (135) studied the expression of Matrix Gla protein (MGP) protein in both gastric cancer (GC) and normal tissues. The results show an association between MGP and STAT5 signaling. In addition, the biochemical assays revealed that binding of MGP promotes phosphorylated-STAT5 (p-STAT5), which leads to the suppression of GC cell apoptosis through activating the transcription of downstream genes. In addition, the application of STAT5 inhibitors suppressed the oncogenic effects of MGP, suggesting that GC patients with high levels of MGP expression may show increased sensitivity to STAT5 inhibitor treatment (135). Moreover, there are variations in the association between p-STAT3 and survival in colon cancer, but a high p-STAT3/p-STAT5 ratio indicates a bad prognosis (136). Unphosphorylated STAT5A helps to stabilize the heterochromatin upon binding to heterochromatin protein 1α(HP1α) and acts as a tumor suppressor. The transcriptome profiling study showed that unphosphorylated STAT5A could repress several genes (e.g., *TGFB1* and *FOXQ1*) involved in colon cancer development (137).

The JAK/STAT signaling pathway also makes epigenetic changes that alter gene expression. For instance, histone acetyltransferase p300/CBP can execute acetylation on STAT3, which recruits DNA methyltransferase 1 (DNMT1). STAT3, STAT5A, and STAT5B are highly expressed in most cell types. It was demonstrated that deletion of STAT3 in mice results in embryonic lethality, while deletions of STAT5a and STAT5b lead to developmental and immune defects, respectively (138). Genome-wide analyses by Mandal et al. (139) revealed that STAT5 tetrameric binding motif is associated with transcriptional repression in leukemias. The tetrameric STAT5 is also shown to recruit Ezh2, repressing several genes regulated by STAT5 during B lymphopoiesis (139).

The interaction between m6A and JAKs-STAT3/5 during CRC

Compelling evidence shows that m6A modification governs the expressions and functions of ncRNAs, thus controlling cancer stemness properties. On the other hand, the JAK/STAT3 signaling pathway is important in cancer stemness research as it can link ncRNA and m6A in tumorigenesis and metastasis (64). It was shown that the upregulation of lncRNA ITIH4-AS1 leads to downregulation or depletion of RE1 silencing transcription factor (REST) in CRC, which consequently promotes ITIH4-AS1 expression and induces tumor proliferation and metastasis through JAK/STAT3 pathway (140). Activated JAK1/STAT3 is crucial in gastric cancer proliferation and metastasis (141). Recent findings demonstrated that m6A modification regulates the key molecules in the JAK/STAT3 signaling pathway. The proposed interaction between STAT3 and m6A signaling pathways is presented in Figure 3.

Reports show that the SOCS family modulates several cytokine induced intracellular signal pathways. For instance, SOCS2 regulates different biological processes, such as immune responses (142, 143). SOCS2 is triggered by tyrosine phosphorylation and

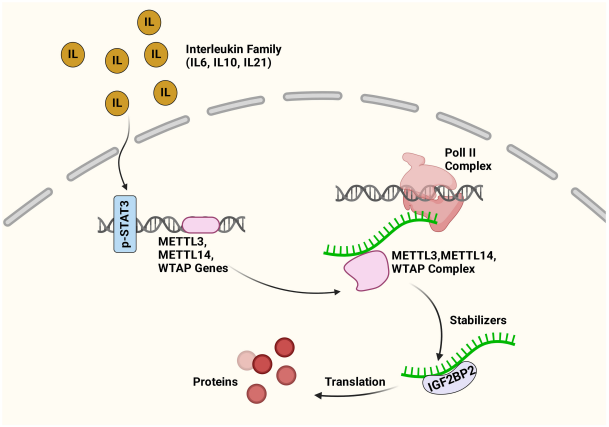

FIGURE 3
Cross-talk between m6A and STAT3 pathways. The inflammatory factors activate the STAT3 pathway. The activated STAT3 increases the expression of METTL3, METTL14, and WTAP genes, consequently enhancing the expression of m6A genes. IGF2BP2 can recognize the methylated mRNA transcripts, and the interaction maintains mRNA stability and expression. Figure created with BioRender.

functions downstream of the JAK/STAT pathway, consequently negatively regulating this signaling pathway (144). It has been shown that the dysregulation of the JAK/STAT signaling pathway is very common in gastric cancer (145). Recently, Jiang et al. (146) used an AGS (human gastric cancer cell line) culture. They showed no difference between STAT1 and STAT3 regarding tyrosine phosphorylation in the MELLT3-KO AGS cells compared to wild-type cells. However, the results of this study demonstrated a negative association between SOCS2 and cell proliferation in gastric cancer cells. In addition, METTL3 knockdown enhanced SOCS2 expression, reducing cell proliferation in AGS cells (146). A study by Wu et al. (147) revealed that expression of JAK2 and SOCS3 due to the loss of METTL3 results in impaired self-renewal capacity and triggers the differentiation of induced pluripotent stem cells.

A study on IL-7/STAT5/SOCS pathways explored the involvement of RNA modifications in T-cell homeostasis (148). Li et al. (148) showed that the mRNAs of the suppressor of cytokine signaling (SOCS) gene family are labeled by m6A enzymes which result in higher mRNA levels in Mettl3-deficient immature T cells. In addition, higher activities of the SOCS gene family could also inhibit the activation of IL-7-mediated STAT5 and T-cell homeostatic proliferation and differentiation (148). Also, m6A modification through METTL3 seems essential for T regulatory cell (Treg)-suppressive functions via IL-2/STAT5 signaling (149), and Treg cells that lack METTL14 cannot inhibit colitis in mice (150). The m6A modification of Jak1 mRNA in tumor-infiltrating myeloid cells (TIM) via METTL3 improves the translation efficiency of JAK1 protein and STAT3 phosphorylation (151). It was shown that low expression of YTHDF2 in multiple myeloma reduces cell proliferation. The RIP sequencing study of m6A revealed STAT5A as a downstream target of YTHDF2, and its binding to the m6A modification site of STAT5A enhances mRNA degradation (152). The role of YTHDF2 in tumor progression has been well-studied. However, the beneficial function of YTHDF2 in the immune response to tumor cells has been recently discovered. YTHDF2 was shown to be upregulated in natural killer cells, a key component of innate immunity, upon activation by cytokines, tumors, and cytomegalovirus infection. YTHDF2 also maintains natural killer cell homeostasis and maturation by establishing a STAT5-YTHDF2 loop (153).

A recent study by Fang et al. (82) emphasized the role of ALKBH5 in gastric cancer. They showed that ALKBH5 is significantly expressed in gastric cancer samples enhancing gastric cell proliferation and metastasis. ALKBH5 also removes the m6A modification of JAK1 mRNA, leading to upregulation of JAK1 expression mediated by LINC00659 in an m6A-YTHDF2-dependent manner, consequently activating the JAK1/STAT3 pathway in gastric cancer. In addition, the ALKBH5 silencing disrupts gastric cancer tumorigenesis via the JAK1 axis (82). A recent study showed that ALKBH5 regulates the activity of STAT3 in osteosarcoma in an m6A-YTHDF2-dependent manner. It was demonstrated that YTHDF2 could read SOCS3, leading to higher levels of m6A-methylated transcript degradation (154). In addition, FTO could negatively regulate STAT3-mediated signaling and induce pro-inflammatory IFN-stimulated genes (ISGs) during the IFN response. Depletion of FTO led to higher phosphorylation and activation of transcription factor STAT3 (155). The upregulation of lncRNA ITIH4-AS1 in colorectal cancer enhances RE1 silencing transcription factor (REST) downregulation or depletion, which consequently upregulates ITIH4-AS1 and promotes tumor proliferation and metastasis through JAK/STAT3 pathway (140).

In general, STAT5 plays a crucial role in the development and differentiation of various cells in the body, including immune cells. In bowel disease, STAT5 is involved in the pathogenesis of IBD and colorectal cancer. STAT5 activation is decreased in patients with IBD, leading to impaired immune function and dysregulation of the intestinal epithelial barrier. This dysregulation of the epithelial barrier can lead to increased intestinal permeability and bacterial translocation, contributing to the pathogenesis of IBD. Additionally, STAT5 plays a role in regulating the differentiation of T cells, which are essential in the immune response in the gut. Dysregulation of STAT5 signaling is associated with an imbalance in T cell populations and the development of IBD.

On the other hand, m6A is a chemical modification of RNA that affects mRNA stability, splicing, and translation efficiency. Growing evidence suggests that there is cross-talk between STAT5 and m6A signaling pathways. For example, STAT5 directly interacts with the m6A methyltransferase METTL3, which adds m6A to mRNA. This interaction leads to increased m6A methylation of STAT5 target genes, resulting in their destabilization and reduced expression. In addition, m6A modification can regulate the activity of STAT5 by affecting the stability and translation efficiency of STAT5 mRNA. Increased expression of METTL3 in colorectal cancer demonstrated dual functionality in gene regulation, encompassing both methyltransferase activity-dependent and -independent functions. METTL3 promotes JAK1 translation by adding m6A modifications to the 3' untranslated region of the JAK1 transcript.

Additionally, redistribution of METTL3 to the STAT3 promoter in collaboration with NF-κB enhances STAT3

transcription, independently of its methyltransferase activity. The concurrent elevation of JAK1 and STAT3 contributed synergistically to activating the p-STAT3 signaling pathway, subsequently increasing cancer cell proliferation and metastasis (156). Figure 4 illustrates the possible interaction between STAT5 and m6A pathways (Figure 4). Overall, it is suggested that a complex interplay between STAT5 and m6A signaling pathways can have important implications for gene regulation and cellular function. Further research is needed to understand better the molecular mechanisms underlying this crosstalk and its relevance to human disease, including gastric cancer.

Conclusion

CRC is a frequent tumor malignancy with high incidence and mortality worldwide. The epidemiological data indicate that the number of CRC patients is increasing annually in developing and developed countries, and the progress of CRC seriously threatens the survival of patients. Also, the advanced stage of CRC patients has poorer outcomes. Due to the lack of diagnostic biomarkers and therapeutic targets, CRC treatment is disappointing. Thus, further exploration of the underlying molecular mechanisms of CRC progression is inevitable (157). The N6-methyladenosine is the most common mRNA modification crucial in tumor metastasis in various cancers. Therefore, exploring how RNA m6A modification is regulated in CRC recurrence and metastasis is of great interest in improving CRC patient prognosis.

The intestinal epithelium undergoes continuous self-renewal to maintain its integrity and functionality. The role of m6A modification in regulating cell differentiation and proliferation in intestinal epithelial cells (IEC) is an important aspect of its function in maintaining gut homeostasis. The m6A modification can regulate the expression of genes that control the commitment of intestinal stem cells to specific lineages, such as absorptive enterocytes, mucus-secreting goblet cells, hormone-producing enteroendocrine cells, and antimicrobial peptide-producing Paneth cells. By affecting the stability and translation of lineage-specific transcripts, m6A modification helps direct stem cells toward different cell fates (158). The JAK/STAT pathway also contributes to the regulation of cell fate decisions in intestinal epithelial stem cells and progenitor cells. Activation of specific STAT proteins can drive gene expression in lineage specification. For instance, STAT3 activation has been linked to the differentiation of intestinal stem cells into absorptive enterocytes, while STAT6 activation may promote the differentiation of goblet cells that secrete mucus. Proper cell turnover in the intestinal epithelium requires balancing cell proliferation and cell death. m6A modification can impact gene expression in cell cycle progression, cell growth, and survival. The JAK/STAT pathway also influences the differentiation and proliferation of IECs. Properly balanced proliferation is essential for maintaining tissue integrity and preventing the accumulation of damaged cells (11). Dysregulation of m6A modification and/or JAK/STAT pathway can disrupt this balance, potentially leading to uncontrolled cell proliferation or impaired differentiation, which is associated with conditions like colorectal cancer (159). Conversely, inadequate activation of the pathway may impair regeneration and healing after injury. The JAK/STAT pathway and m6A modification also contribute to forming and maintaining an epithelial barrier that separates the body's internal environment from the external environment within the gut lumen.

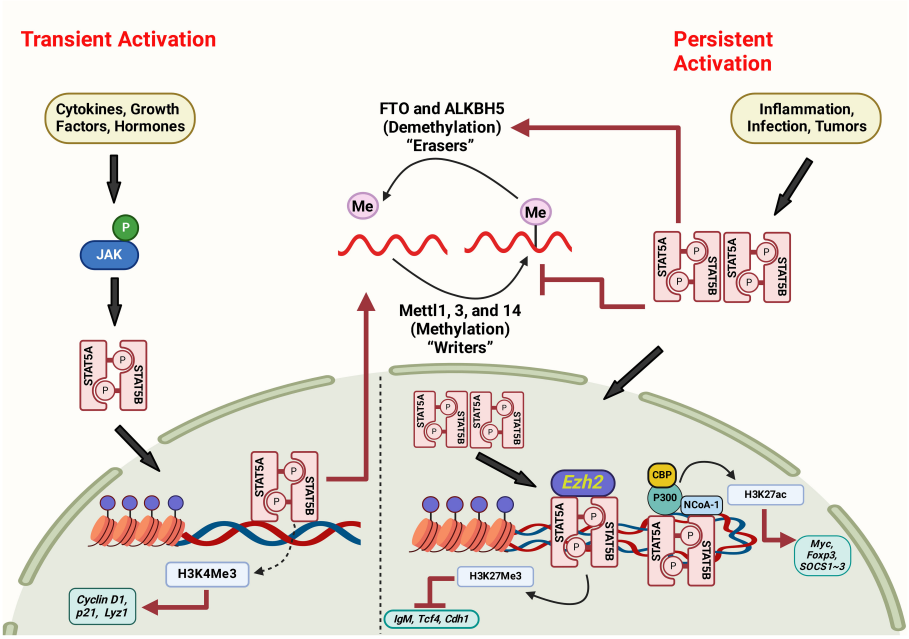

FIGURE 4
The interaction between STAT5 and m6A pathways via persistent and transient activation mechanisms. Figure created with BioRender.

The m6A levels are determined by m6A writers (METTL3/METTL14/WTAP protein complex) m6A erasers (FTO and ALKBH5) and m6A readers (YTHDC1–2, YTHDF1–3, IGF2BP1–3, HNRNPC, and HNRNPA2B1) (1). The collaboration between writers, erasers, and readers of m6A methylation was shown to participate in the progression of various types of tumors. The m6A modification consequently facilitates the recruitment of m6A readers that link m6A-modified RNAs to mRNA processing enzymes, affecting RNA export, splicing, translation, and degradation (39).

The m6A-profiling methods require a large amount of RNA material; thus, m6A distribution profiling in the transcriptome of patient samples, particularly cancer stem cells and the primitive/progenitor cells of normal tissues will be challenging. The emergence of new techniques that utilize a small amount of RNA and provide base-resolution m6A profiles with better quantitative information is desired. Also, CRISPR genome editing and CRISPR-mediated RNA modification approaches would provide informative information about the epistatic relationship between RNA methylation and chromatin dynamics (15). The existence of cancer stem cells (CSCs) in colorectal cancer has been recently indicated. Their role in metastasis, drug resistance, and continual adaptation of cancer cells to the changing tumor microenvironment (TME) has also been discovered. In addition, the accumulation of epigenetic and genetic variability leads to the evolution of the CSC, consequently resulting in tumor growth and maintenance. Thus, exploring key genes involved in transforming tumor CSC and unraveling the underlying mechanisms in colorectal cancer may uncover novel therapeutic targets (160). Although there is mounting evidence of the involvement of m6A in CRC, the expression and functional effects of m6A RNA methylation on CRC are still poorly understood.

The JAK/STAT pathway was shown to be involved in abnormal gene expression related to high cytokine levels. Studies show that JAK/STAT inhibitors could be effectively used to treat multiple diseases, such as rheumatoid arthritis (RA) and systemic lupus erythematosus (SLE), indicating that JAK/STAT serves a vital role in disease development (161, 162). Chronic inflammation was shown to drive tumorigenesis. The JAK/STAT signaling pathway can link inflammation with cancer. JAK/STAT is one of the leading 12 signaling pathways abnormally regulated in cancer. The function of STAT5 in intestinal homeostasis has been proven. It was shown that STAT5 plays an essential role in the interaction regulation of microbiota and IEC, mediating chronic inflammation and promoting mucosal healing. The upregulation of JAK/STAT signaling was shown to be involved in cancer aggressiveness and tumor progression. The increased JAK/STAT signaling in different cancer diseases, including CRC, impairs prognosis and decreases overall survival.

Since JAK/STAT signaling pathway upregulates different aspects of cancer development, including cell growth, differentiation, and survival, its inhibition could be employed as a potential strategy for cancer. Decreased m6A methylation in cells reduces the STAT3 activity, leading to lower cell proliferation, while up-regulation of STAT3 could reverse its effects on cell growth (154). Recently, Fang et al. (82) reported the phosphorylation of STAT3, but not STAT1 or STAT5, by JAK1 in gastric cancer cells. The JAK1 upregulation promoted the STAT3 phosphorylation and activated the JAK1/STAT3 pathway, which accelerated the progression of gastric cancer. M6A is involved in the expression of different transcripts of the STAT3 signaling pathway resulting in activation or inhibition of the STAT3 signaling pathway in various tumors (154). In cholangiocarcinoma tumor cells, the binding of STAT3 to the m6A writer gene results in the upregulation of m6A writers by cytokine IL-6, suggesting that m6A is a potential target in response to inflammation (163). In cancer stemness research, the JAK/STAT3 signaling pathway is pivotal in linking ncRNA and m6A in tumorigenesis and metastasis (64).

In conclusion, the findings emphasize the vital function of m6A RNA methylation and the JAK/STAT signaling pathway in developing various diseases. Thus, deciphering the underlying molecular mechanism and the interplay of these two mechanisms will help us better understand the development of human diseases and provide us with more sophisticated tools to treat diseases in the future. Studies indicate that m6A modification regulates the key molecules in the JAK/STAT3 signaling pathway. Loss of METTL3 affects JAK2 and SOCS3 expression patterns, leading to impaired self-renewal capacity and triggering the differentiation of induced pluripotent stem cells (164). Generally, loss of m6A modification leads to slow mRNA decay while it increases expression of the STAT signaling inhibitory proteins SOCS1, SOCS2, and CISH, consequently inhibiting cytokine-mediated STAT5 activation, T cell proliferation, and T cell differentiation (165).

The perspective of the role of m6A in the JAKs-STAT3/5-induced GI cancer

Studying other m6A-related regulatory factors is necessary, particularly in CRC. It has been proven that the poor prognosis of CRC has been strongly linked to the abnormal expression of m6A regulatory factors. While numerous cellular signaling pathways have been established as contributors to CRC metastasis and their underlying molecular mechanisms have been extensively explored, the complete understanding of their interaction and regulation in CRC progression remains elusive. STAT5 regulates microbiota interaction, and IEC mediates chronic inflammation and promotes mucosal healing. However, the function of STAT5A and B in promoting healing during IBD disease and cancer is not fully understood. Therefore, there is an urgent need to explore the underlying mechanism of the JAK/STAT pathway in intestinal homeostasis to illustrate its involvement in colorectal cancer formation. In addition, more experimental studies are required to attain solid evidence to identify the crosstalk between JAK/STAT and m6A methylation as a possible prognostic biomarker of inflammation and infection and therapeutic developments.

Author contributions

NE: Conceptualization, Validation, Writing – original draft. AB: Writing – original draft. WT: Supervision, Writing – review & editing. SL: Supervision, Writing – review & editing. XH: Conceptualization, Funding acquisition, Supervision, Writing – review & editing, Validation.

Funding

The author(s) declare financial support was received for the research, authorship, and/or publication of this article. This work was supported by NIDDK R01, USA (No. R01DK123299) (XH) and MHMC/CWRU start-up (XH).

Conflict of interest

The authors declare that the research was conducted in the absence of any commercial or financial relationships that could be construed as a potential conflict of interest.

Publisher's note

References

1. Lu S, Ding X, Wang Y, Hu X, Sun T, Wei M, et al. The relationship between the network of non-coding rnas-molecular targets and N6-methyladenosine modification in colorectal cancer. *Front Cell Dev Biol*. (2021), 3393. doi: 10.3389/fcell.2021.772542

2. Chen Z, Qi M, Shen B, Luo G, Wu Y, Li J, et al. Transfer rna demethylase Alkbh3 promotes cancer progression via induction of trna-derived small Rnas. *Nucleic Acids Res*. (2019) 47:2533–45. doi: 10.1093/nar/gky1250

3. Motorin Y, Helm M. Rna nucleotide methylation. *Wiley Interdiscip Reviews: RNA*. (2011) 2:611–31. doi: 10.1002/wrna.79

4. Chen H, Yao J, Bao R, Dong Y, Zhang T, Du Y, et al. Cross-talk of four types of rna modification writers defines tumor microenvironment and pharmacogenomic landscape in colorectal cancer. *Mol Cancer*. (2021) 20:1–21. doi: 10.1186/s12943-021-01322-w

5. Yan H, Zhang L, Cui X, Zheng S, Li R. Roles and mechanisms of the M6a reader Ythdc1 in biological processes and diseases. *Cell Death Discovery*. (2022) 8:237. doi: 10.1038/s41420-022-01040-2

6. Wang S, Gan M, Chen C, Zhang Y, Kong J, Zhang H, et al. Methyl Cpg binding protein 2 promotes colorectal cancer metastasis by regulating N6-methyladenosine methylation through methyltransferase-like 14. *Cancer Sci*. (2021) 112:3243. doi: 10.1111/cas.15011

7. Wei W, Ji X, Guo X, Ji S. Regulatory role of N6-methyladenosine (M6a) methylation in Rna processing and human diseases. *J Cell Biochem*. (2017) 118:2534–43. doi: 10.1002/jcb.v118.9

8. Fang X, Li M, Yu T, Liu G, Wang J. Reversible N6-methyladenosine of Rna: the regulatory mechanisms on gene expression and implications in physiology and pathology. *Genes Dis*. (2020) 7:585–97. doi: 10.1016/j.gendis.2020.06.011

9. Fang Z, Hu Y, Hu J, Huang Y, Zheng S, Guo C. The crucial roles of N6-methyladenosine (M6a) modification in the carcinogenesis and progression of colorectal cancer. *Cell bioscience*. (2021) 11:1–11. doi: 10.1186/s13578-021-00583-8

10. Fultang N, Chakraborty M, Peethambaran B. Regulation of cancer stem cells in triple negative breast cancer. *Cancer Drug Resistance*. (2021) 4:321. doi: 10.20517/cdr

11. Surbek M, Tse W, Moriggl R, Han X. A centric view of Jak/Stat5 in intestinal homeostasis, infection, and inflammation. *Cytokine*. (2021) 139:155392. doi: 10.1016/j.cyto.2020.155392

12. Neculai D, Neculai AM, Verrier S, Straub K, Klumpp K, Pfitzner E, et al. Structure of the unphosphorylated Stat5a dimer. *J Biol Chem*. (2005) 280:40782–7. doi: 10.1074/jbc.M507682200

13. Hennighausen L, Robinson GW. Interpretation of cytokine signaling through the transcription factors Stat5a and Stat5b. *Genes Dev*. (2008) 22:711–21. doi: 10.1101/gad.1643908

14. Han X, Gilbert S, Groschwitz K, Hogan S, Jurickova I, Trapnell B, et al. Loss of Gm-Csf signalling in non-haematopoietic cells increases Nsaid ileal injury. *Gut*. (2010) 59:1066–78. doi: 10.1136/gut.2009.203893

15. Kan RL, Chen J, Sallam T. Crosstalk between epitranscriptomic and epigenetic mechanisms in gene regulation. *Trends Genet*. (2021) 38(2):182–193. doi: 10.1016/j.tig.2021.06.014

16. Sun T, Wu R, Ming L. The role of M6a rna methylation in cancer. *Biomedicine Pharmacotherapy*. (2019) 112:108613. doi: 10.1016/j.biopha.2019.108613

17. Liu X, He H, Zhang F, Hu X, Bi F, Li K, et al. M6a methylated epha2 and vegfa through Igf2bp2/3 regulation promotes vasculogenic mimicry in colorectal cancer via Pi3k/Akt and Erk1/2 signaling. *Cell Death Dis*. (2022) 13:1–12. doi: 10.1038/s41419-022-04950-2

18. Yang Y, Hsu PJ, Chen Y-S, Yang Y-G. Dynamic transcriptomic M6a decoration: writers, erasers, readers and functions in rna metabolism. *Cell Res*. (2018) 28:616–24. doi: 10.1038/s41422-018-0040-8

19. Yang X, Hu X, Liu J, Wang R, Zhang C, Han F, et al. N6-methyladenine modification in noncoding rnas and its function in cancer. *biomark Res*. (2020) 8:1–12. doi: 10.1186/s40364-020-00244-x

20. Li Y, Xiao J, Bai J, Tian Y, Qu Y, Chen X, et al. Molecular characterization and clinical relevance of M6a regulators across 33 cancer types. *Mol Cancer*. (2019) 18:1–6. doi: 10.1186/s12943-019-1066-3

21. Ke S, Pandya-Jones A, Saito Y, Fak JJ, Vågbø CB, Geula S, et al. M6a Mrna modifications are deposited in nascent pre-Mrna and are not required for splicing but do specify cytoplasmic turnover. *Genes Dev*. (2017) 31:990–1006. doi: 10.1101/gad.301036.117

22. Wang X, Huang J, Zou T, Yin P. Human M6a writers: two subunits, 2 roles. *RNA Biol*. (2017) 14:300–4. doi: 10.1080/15476286.2017.1282025

23. Ping X-L, Sun B-F, Wang L, Xiao W, Yang X, Wang W-J, et al. Mammalian wtap is a regulatory subunit of the Rna N6-methyladenosine methyltransferase. *Cell Res*. (2014) 24:177–89. doi: 10.1038/cr.2014.3

24. Geula S, Moshitch-Moshkovitz S, Dominissini D, Mansour AA, Kol N, Salmon-Divon M, et al. M6a Mrna methylation facilitates resolution of naïve pluripotency toward differentiation. *Science*. (2015) 347:1002–6. doi: 10.1126/science.1261417

25. Wang H, Wei W, Zhang Z-Y, Liu Y, Shi B, Zhong W, et al. Tcf4 and hur mediated-mettl14 suppresses dissemination of colorectal cancer via N6-methyladenosine-dependent silencing of arrdc4. *Cell Death Dis*. (2021) 13:3. doi: 10.1038/s41419-021-04459-0

26. Yang X, Liu M, Li M, Zhang S, Hiju H, Sun J, et al. Epigenetic modulations of noncoding Rna: A novel dimension of cancer biology. *Mol Cancer*. (2020) 19:1–12. doi: 10.1186/s12943-020-01159-9

27. Yang M, Sun M, Zhang H. The interaction between epigenetic changes, emt, and exosomes in predicting metastasis of colorectal cancers (Crc). *Front Oncol*. (2022) 12. doi: 10.3389/fonc.2022.879848

28. Gong D, Zhang J, Chen Y, Xu Y, Ma J, Hu G, et al. The M 6 a-Suppressed P2rx6 Activation Promotes Renal Cancer Cells Migration and Invasion through Atp-Induced Ca 2+ Influx Modulating Erk1/2 Phosphorylation and Mmp9 Signaling Pathway. *J Exp Clin Cancer Res*. (2019) 38:1–16. doi: 10.1186/s13046-019-1223-y

29. Wang Q, Zhang H, Chen Q, Wan Z, Gao X, Qian W. Identification of Mettl14 in kidney renal clear cell carcinoma using bioinformatics analysis. *Dis Markers*. (2019) 5648783:11. doi: 10.1155/2019/5648783

30. Zhou J, Wang J, Hong B, Ma K, Xie H, Li L, et al. Gene signatures and prognostic values of M6a regulators in clear cell renal cell carcinoma–a retrospective study using tcga database. *Aging (Albany NY)*. (2019) 11:1633. doi: 10.18632/aging.v11i6

31. Zhou D, Tang W, Xu Y, Xu Y, Xu B, Fu S, et al. Mettl3/Ythdf2 M6a axis accelerates colorectal carcinogenesis through epigenetically suppressing Ypel5. *Mol Oncol*. (2021) 15:2172–84. doi: 10.1002/1878-0261.12898

32. Tao Z, Zhao Y, Chen X. Role of methyltransferase-like enzyme 3 and methyltransferase-like enzyme 14 in urological cancers. *PeerJ*. (2020) 8:e9589. doi: 10.7717/peerj.9589

33. Ruan D-Y, Li T, Wang Y-N, Meng Q, Li Y, Yu K, et al. Fto downregulation mediated by hypoxia facilitates colorectal cancer metastasis. *Oncogene*. (2021) 40:5168–81. doi: 10.1038/s41388-021-01916-0

34. Wang T, Kong S, Tao M, Ju S. The potential role of Rna N6-methyladenosine in cancer progression. *Mol Cancer*. (2020) 19:1–18. doi: 10.1186/s12943-020-01204-7

35. Shi H, Wei J, He C. Where, when, and how: context-dependent functions of Rna methylation writers, readers, and erasers. *Mol Cell*. (2019) 74:640–50. doi: 10.1016/j.molcel.2019.04.025

36. Jeschke J, Collignon E, Al Wardi C, Krayem M, Bizet M, Jia Y, et al. Downregulation of the Fto M6a Rna demethylase promotes emt-mediated progression of epithelial tumors and sensitivity to Wnt inhibitors. *Nat Cancer*. (2021) 2:611–28. doi: 10.1038/s43018-021-00223-7

37. Huang H, Wang Y, Kandpal M, Zhao G, Cardenas H, Ji Y, et al. Fto-dependent N6-methyladenosine modifications inhibit ovarian cancer stem cell self-renewal by blocking camp signalingfto and ovarian cancer. *Cancer Res*. (2020) 80:3200–14. doi: 10.1158/0008-5472.CAN-19-4044

38. Huang J, Sun W, Wang Z, Lv C, Zhang T, Zhang D, et al. Fto suppresses glycolysis and growth of papillary thyroid cancer via decreasing stability of apoe mrna in an N6-methyladenosine-dependent manner. *J Exp Clin Cancer Res*. (2022) 41:1–18. doi: 10.1186/s13046-022-02254-z

39. Wang S, Gao S, Zeng Y, Zhu L, Mo Y, Wong CC, et al. N6-methyladenosine reader Ythdf1 promotes Arhgef2 translation and rhoa signaling in colorectal cancer. *Gastroenterology*. (2022) 162:1183–96. doi: 10.1053/j.gastro.2021.12.269

40. Vu T, Datta PK. Regulation of Emt in colorectal cancer: A culprit in metastasis. *Cancers*. (2017) 9:171. doi: 10.3390/cancers9120171

41. Gurzu S, Jung J, Azamfirei L, Mezei T, Cimpean AM, Szentirmay Z. The angiogenesis in colorectal carcinomas with and without lymph node metastases. *Rom J Morphol Embryol*. (2008) 49:149–52.

42. Lin X, Chai G, Wu Y, Li J, Chen F, Liu J, et al. Rna M6a methylation regulates the epithelial mesenchymal transition of cancer cells and translation of snail. *Nat Commun*. (2019) 10:2065. doi: 10.1038/s41467-019-09865-9

43. Wang X, Lu X, Wang P, Chen Q, Xiong L, Tang M, et al. Srsf9 promotes colorectal cancer progression via stabilizing Dsn1 Mrna in an M6a-related manner. *J Trans Med*. (2022) 20:1–18. doi: 10.1186/s12967-022-03399-3

44. Liu J, Harada BT, He C. Regulation of gene expression by N6-methyladenosine in cancer. *Trends Cell Biol*. (2019) 29:487–99. doi: 10.1016/j.tcb.2019.02.008

45. Kuai D, Zhu S, Shi H, Yang R, Liu T, Liu H, et al. Aberrant expression of M6a mrna methylation regulators in colorectal adenoma and adenocarcinoma. *Life Sci*. (2021) 273:119258. doi: 10.1016/j.lfs.2021.119258

46. Hao S, Cong L, Qu R, Liu R, Zhang G, Li Y. Emerging roles of circular Rnas in colorectal cancer. *OncoTargets Ther*. (2019) 12:4765. doi: 10.2147/OTT

47. Jiang Z, Hou Z, Liu W, Yu Z, Liang Z, Chen S. Circular Rna protein tyrosine kinase 2 (Circptk2) promotes colorectal cancer proliferation, migration, invasion and chemoresistance. *Bioengineered*. (2022) 13:810–23. doi: 10.1080/21655979.2021.2012952

48. Wen T, Wu H, Zhang L, Li K, Xiao X, Zhang L, et al. Circular Rna Circ_0007142 regulates cell proliferation, apoptosis, migration and invasion via Mir-455-5p/Sgk1 axis in colorectal cancer. *Anti-Cancer Drugs*. (2020) 32:22–33. doi: 10.1097/CAD.0000000000000992

49. Huang Z, Yang M. Molecular network of colorectal cancer and current therapeutic options. *Front Oncol*. (2022) 12. doi: 10.3389/fonc.2022.852927

50. Kim H, Kim T, Jaygal G, Woo J, Kim C-J, Baek M-J, et al. Downregulation of mir-9 correlates with poor prognosis in colorectal cancer. *Pathology-Research Pract*. (2020) 216:153044. doi: 10.1016/j.prp.2020.153044

51. Huang Z, Wu X, Li J. Mir-101 suppresses colon cancer cell migration through the regulation of Ezh2. *Rev Esp Enferm Dig*. (2021) 113:255–60. doi: 10.17235/reed.2020.6800/2019

52. Carter JV, O'brien SJ, Burton JF, Oxford BG, Stephen V, Hallion J, et al. The microrna–200 family acts as an oncogene in colorectal cancer by inhibiting the tumor suppressor Rassf2. *Oncol Lett*. (2019) 18:3994–4007. doi: 10.3892/ol

53. Knudsen KN, Nielsen BS, Lindebjerg J, Hansen TF, Holst R, Sørensen FB. Microrna-17 is the most up-regulated member of the Mir-17-92 cluster during early colon cancer evolution. *PloS One*. (2015) 10:e0140503. doi: 10.1371/journal.pone.0140503

54. Ding L, Yu LL, Han N, Zhang BT. Mir-141 promotes colon cancer cell proliferation by inhibiting Map2k4. *Oncol Lett*. (2017) 13:1665–71. doi: 10.3892/ol.2017.5653

55. Zhou C, Molinie B, Daneshvar K, Pondick JV, Wang J, Van Wittenberghe N, et al. Genome-wide maps of M6a circrnas identify widespread and cell-type-specific methylation patterns that are distinct from mrnas. *Cell Rep*. (2017) 20:2262–76. doi: 10.1016/j.celrep.2017.08.027

56. Luo J, Xu T, Sun K. N6-methyladenosine rna modification in inflammation: roles, mechanisms, and applications. *Front Cell Dev Biol*. (2021) 9:670711. doi: 10.3389/fcell.2021.670711

57. Qiao H, Liu L, Chen J, Shang B, Wang L. The functions of N6-methyladenosine (M6a) rna modifications in colorectal cancer. *Med Oncol*. (2022) 39:1–12. doi: 10.1007/s12032-022-01827-4

58. Sung H, Ferlay J, Siegel RL, Laversanne M, Soerjomataram I, Jemal A, et al. Global cancer statistics 2020: globocan estimates of incidence and mortality worldwide for 36 cancers in 185 countries. *CA: Cancer J Clin*. (2021) 71:209–49. doi: 10.3322/caac.21660

59. Chen Y, Wang S, Cho WC, Zhou X, Zhang Z. Prognostic implication of the M6a rna methylation regulators in rectal cancer. *Front Genet*. (2021) 12:604229. doi: 10.3389/fgene.2021.604229

60. Zhang Z, Wang Q, Zhang M, Zhang W, Zhao L, Yang C, et al. Comprehensive analysis of the transcriptome-wide M6a methylome in colorectal cancer by merip sequencing. *Epigenetics*. (2021) 16:425–35. doi: 10.1080/15592294.2020.1805684

61. Liu X, Ji Q, Fan Z, Li Q. Cellular signaling pathways implicated in metastasis of colorectal cancer and the associated targeted agents. *Future Oncol*. (2015) 11:2911–22. doi: 10.2217/fon.15.235

62. Li Z, Liu Y, Yi H, Cai T, Wei Y. Identification of N6-methylandenosine related lncrna signatures for predicting the prognosis and therapy response in colorectal cancer patients. *Front Genet*. (2022) 13. doi: 10.3389/fgene.2022.947747

63. Jung G, Hernández-Illán E, Moreira L, Balaguer F, Goel A. Epigenetics of colorectal cancer: biomarker and therapeutic potential. *Nat Rev Gastroenterol Hepatol*. (2020) 17:111–30. doi: 10.1038/s41575-019-0230-y

64. Qin S, Mao Y, Wang H, Duan Y, Zhao L. The interplay between M6a modification and non-coding rna in cancer stemness modulation: mechanisms, signaling pathways, and clinical implications. *Int J Biol Sci*. (2021) 17:2718. doi: 10.7150/ijbs.60641

65. Deng X, Su R, Weng H, Huang H, Li Z, Chen J. Rna N 6-methyladenosine modification in cancers: current status and perspectives. *Cell Res*. (2018) 28:507–17. doi: 10.1038/s41422-018-0034-6

66. Liu J, Eckert MA, Harada BT, Liu S-M, Lu Z, Yu K, et al. M6a mrna methylation regulates akt activity to promote the proliferation and tumorigenicity of endometrial cancer. *Nat Cell Biol*. (2018) 20:1074–83. doi: 10.1038/s41556-018-0174-4

67. Bokar JA, Shambaugh ME, Polayes D, Matera AG, Rottman FM. Purification and cdna cloning of the adomet-binding subunit of the human Mrna (N6-adenosine)-methyltransferase. *Rna*. (1997) 3:1233–47.

68. Zhao W, Qi X, Liu L, Ma S, Liu J, Wu J. Epigenetic regulation of M6a modifications in human cancer. *Mol Therapy-Nucleic Acids*. (2020) 19:405–12. doi: 10.1016/j.omtn.2019.11.022

69. Chen H, Gao S, Liu W, Wong C-C, Wu J, Wu J, et al. Rna N6-methyladenosine methyltransferase mettl3 facilitates colorectal cancer by activating the M6a-glut1-mtorc1 axis and is a therapeutic target. *Gastroenterology*. (2021) 160:1284–300.e16. doi: 10.1053/j.gastro.2020.11.013

70. Yu T, Liu J, Wang Y, Chen W, Liu Z, Zhu L, et al. Mettl3 promotes colorectal cancer metastasis by stabilizing plau mrna in an M6a-dependent manner. *Biochem Biophys Res Commun*. (2022) 614:9–16. doi: 10.1016/j.bbrc.2022.04.141

71. Deng R, Cheng Y, Ye S, Zhang J, Huang R, Li P, et al. M6a methyltransferase mettl3 suppresses colorectal cancer proliferation and migration through P38/erk pathways. *OncoTargets Ther*. (2019) 12:4391. doi: 10.2147/OTT

72. Zhang G, Wang T, Huang Z, Chen Y, Sun L, Xia X, et al. Mettl3 dual regulation of the stability of linc00662 and vegfa Rnas promotes colorectal cancer angiogenesis. *Discover Oncol*. (2022) 13:1–19. doi: 10.1007/s12672-022-00557-3

73. Hou P, Meng S, Li M, Lin T, Chu S, Li Z, et al. Linc00460/dhx9/Igf2bp2 complex promotes colorectal cancer proliferation and metastasis by mediating Hmga1 Mrna stability depending on M6a modification. *J Exp Clin Cancer Res*. (2021) 40:1–18. doi: 10.1186/s13046-021-01857-2

74. Wu Y, Yang X, Chen Z, Tian L, Jiang G, Chen F, et al. M6a-induced lncrna Rp11 triggers the dissemination of colorectal cancer cells via upregulation of Zeb1. *Mol Cancer*. (2019) 18:1–16. doi: 10.1186/s12943-019-1014-2

75. Peng W, Li J, Chen R, Gu Q, Yang P, Qian W, et al. Upregulated Mettl3 promotes metastasis of colorectal cancer via Mir-1246/Spred2/Mapk signaling pathway. *J Exp Clin Cancer Res*. (2019) 38:1–16. doi: 10.1186/s13046-019-1408-4

76. Cai C, Long J, Huang Q, Han Y, Peng Y, Guo C, et al. M6a "Writer" Gene mettl14: A favorable prognostic biomarker and correlated with immune infiltrates in rectal cancer. *Front Oncol*. (2021) 11:615296. doi: 10.3389/fonc.2021.615296

77. Huang H, Weng H, Sun W, Qin X, Shi H, Wu H, et al. Recognition of Rna N6-methyladenosine by Igf2bp proteins enhances mrna stability and translation. *Nat Cell Biol*. (2018) 20:285–95. doi: 10.1038/s41556-018-0045-z

78. Shen X, Ling X, Lu H, Zhou C, Zhang J, Yu Q. Low expression of microrna-1266 promotes colorectal cancer progression via targeting Fto. *Eur Rev Med Pharmacol Sci*. (2018) 22:8220–6. doi: 10.26355/eurrev_201812_16516

79. Bai Y, Yang C, Wu R, Huang L, Song S, Li W, et al. Ythdf1 regulates tumorigenicity and cancer stem cell-like activity in human colorectal carcinoma. *Front Oncol*. (2019) 9:332. doi: 10.3389/fonc.2019.00332

80. Zhang J, Guo S, H-y P, Wang Y, Wu Y, Meng X-y, et al. Alkbh5 promotes invasion and metastasis of gastric cancer by decreasing methylation of the lncrna neat1. *J Physiol Biochem*. (2019) 75:379–89. doi: 10.1007/s13105-019-00690-8

81. Hu Y, Gong C, Li Z, Liu J, Chen Y, Huang Y, et al. Demethylase Alkbh5 suppresses invasion of gastric cancer via pkmyt1 M6a modification. *Mol Cancer*. (2022) 21:1–15. doi: 10.1186/s12943-022-01522-y

82. Fang Y, Wu X, Gu Y, Shi R, Yu T, Pan Y, et al. Linc00659 cooperated with alkbh5 to accelerate gastric cancer progression by stabilising Jak1 Mrna in an M6a-ythdf2-dependent manner. *Clin Trans Med*. (2023) 13:e1205. doi: 10.1002/ctm2.1205

83. Zhang C, Zhou X, Geng X, Zhang Y, Wang J, Wang Y, et al. Circular Rna Hsa_Circ_0006401 promotes proliferation and metastasis in colorectal carcinoma. *Cell Death Dis*. (2021) 12:1–14. doi: 10.1038/s41419-021-03714-8

84. Tang S, Liu Q, Xu M. Linc00857 promotes cell proliferation and migration in colorectal cancer by interacting with ythdc1 and stabilizing Slc7a5. *Oncol Lett*. (2021) 22:1–10. doi: 10.3892/ol

85. Zeng W, Zhu J-F, Guo J, Huang G-J, Ai L-S, Zeng Y, et al. M6a-modified Circfndc3b inhibits colorectal cancer stemness and metastasis via Rnf41-dependent Asb6 degradation. *Cell Death Dis*. (2022) 13:1–15. doi: 10.1038/s41419-022-05451-y

86. Chen B, Hong Y, Gui R, Zheng H, Tian S, Zhai X, et al. N6-methyladenosine modification of circ_0003215 suppresses the pentose phosphate pathway and Malignancy of colorectal cancer through the mir-663b/dlg4/G6pd axis. *Cell Death Dis*. (2022) 13:1–16. doi: 10.1038/s41419-022-05245-2

87. Chen C, Yuan W, Zhou Q, Shao B, Guo Y, Wang W, et al. N6-methyladenosine-induced circ1662 promotes metastasis of colorectal cancer by accelerating yap1 nuclear localization. *Theranostics*. (2021) 11:4298. doi: 10.7150/thno.51342

88. Kumari N, Dwarakanath B, Das A, Bhatt AN. Role of interleukin-6 in cancer progression and therapeutic resistance. *Tumor Biol*. (2016) 37:11553–72. doi: 10.1007/s13277-016-5098-7

89. Liu H, Li D, Sun L, Qin H, Fan A, Meng L, et al. Interaction of lncrna mir100hg with Hnrnpa2b1 facilitates M6a-dependent stabilization of Tcf7l2 mrna and colorectal cancer progression. *Mol Cancer*. (2022) 21:1–18. doi: 10.1186/s12943-022-01555-3

90. Zeng H, Xu Y, Xu S, Jin L, Shen Y, Rajan K, et al. Construction and analysis of a colorectal cancer prognostic model based on N6-methyladenosine-related lncrnas. *Front Cell Dev Biol*. (2021) 9. doi: 10.3389/fcell.2021.698388

91. Richter JD, Zhao X. The molecular biology of fmrp: new insights into fragile X syndrome. *Nat Rev Neurosci*. (2021) 22:209–22. doi: 10.1038/s41583-021-00432-0

92. Hu Y, Gao Q, Ma S, Yu P, Ding S, Yao X, et al. Fmr1 promotes the progression of colorectal cancer cell by stabilizing egfr Mrna in an M6a-dependent manner. *Cell Death Dis*. (2022) 13:1–14. doi: 10.1038/s41419-022-05391-7

93. Li J, Liang L, Yang Y, Li X, Ma Y. N6-methyladenosine as a biological and clinical determinant in colorectal cancer: progression and future direction. *Theranostics*. (2021) 11:2581. doi: 10.7150/thno.52366

94. Tian J, Ying P, Ke J, Zhu Y, Yang Y, Gong Y, et al. Ankle1 N6-methyladenosine-related variant is associated with colorectal cancer risk by maintaining the genomic stability. *Int J Cancer*. (2020) 146:3281–93. doi: 10.1002/ijc.32677

95. Huang C, Zhang K, Guo Y, Shen C, Liu X, Huang H, et al. The crucial roles of M6a Rna modifications in cutaneous cancers: implications in pathogenesis, metastasis, drug resistance, and targeted therapies. *Genes Dis*. (2023) 10:2320–2330. doi: 10.1016/j.gendis.2022.03.006

96. Li T, Hu P-S, Zuo Z, Lin J-F, Li X, Wu Q-N, et al. Mettl3 facilitates tumor progression via an M6a-Igf2bp2-dependent mechanism in colorectal carcinoma. *Mol Cancer*. (2019) 18:1–15. doi: 10.1186/s12943-019-1038-7

97. Yang Z, Quan Y, Chen Y, Huang Y, Huang R, Yu W, et al. Knockdown of rna N6-methyladenosine methyltransferase mettl3 represses warburg effect in colorectal cancer via regulating hif-1α. *Signal Transduction Targeted Ther*. (2021) 6:89. doi: 10.1038/s41392-021-00473-y

98. Wang L, Hui H, Agrawal K, Kang Y, Li N, Tang R, et al. M6a Rna methyltransferases mettl3/14 regulate immune responses to anti-pd-1 therapy. *EMBO J*. (2020) 39:e104514. doi: 10.15252/embj.2020104514

99. You Q, Wang F, Du R, Pi J, Wang H, Huo Y, et al. M6a reader Ythdf1-targeting engineered small extracellular vesicles for gastric cancer therapy via epigenetic and immune regulation. *Advanced Materials*. (2023) 35:2204910. doi: 10.1002/adma.202204910

100. Shimura T, Kandimalla R, Okugawa Y, Ohi M, Toiyama Y, He C, et al. Novel evidence for M6a methylation regulators as prognostic biomarkers and fto as a potential therapeutic target in gastric cancer. *Br J Cancer*. (2022) 126:228–37. doi: 10.1038/s41416-021-01581-w

101. Nishizawa Y, Konno M, Asai A, Koseki J, Kawamoto K, Miyoshi N, et al. Oncogene C-myc promotes epitranscriptome M6a reader ythdf1 expression in colorectal cancer. *Oncotarget*. (2018) 9:7476. doi: 10.18632/oncotarget.v9i7

102. Chen P, X-q L, Lin X, Gao L-y, Zhang S, Huang X. Targeting Ythdf1 effectively re-sensitizes cisplatin-resistant colon cancer cells by modulating gls-mediated glutamine metabolism. *Mol Therapy-Oncolytics*. (2021) 20:228–39. doi: 10.1016/j.omto.2021.01.001

103. Deng S, Zhang H, Zhu K, Li X, Ye Y, Li R, et al. M6a2target: A comprehensive database for targets of M 6 a writers, erasers and readers. *Briefings Bioinf*. (2021) 22:bbaa055. doi: 10.1093/bib/bbaa055

104. Bao X, Zhang Y, Li H, Teng Y, Ma L, Chen Z, et al. Rm2target: A comprehensive database for targets of writers, erasers and readers of Rna modifications. *Nucleic Acids Res*. (2023) 51:D269–D79. doi: 10.1093/nar/gkac945

105. Zhou D, Wang H, Bi F, Xing J, Gu Y, Wang C, et al. M6add: A comprehensive database of M6a modifications in diseases. *RNA Biol*. (2021) 18:2354–62. doi: 10.1080/15476286.2021.1913302

106. Chen K, Song B, Tang Y, Wei Z, Xu Q, Su J, et al. Rmdisease: A database of genetic variants that affect rna modifications, with implications for epitranscriptome pathogenesis. *Nucleic Acids Res*. (2021) 49:D1396–D404. doi: 10.1093/nar/gkaa790

107. Song B, Wang X, Liang Z, Ma J, Huang D, Wang Y, et al. Rmdisease V2. 0: an updated database of genetic variants that affect rna modifications with disease and trait implication. *Nucleic Acids Res*. (2023) 51:D1388–D96. doi: 10.1093/nar/gkac750

108. Tang Y, Chen K, Song B, Ma J, Wu X, Xu Q, et al. M6a-atlas: A comprehensive knowledgebase for unraveling the N 6-methyladenosine (M6a) epitranscriptome. *Nucleic Acids Res*. (2021) 49:D134–D43. doi: 10.1093/nar/gkaa692

109. Liang Z, Ye H, Ma J, Wei Z, Wang Y, Zhang Y, et al. M6a-atlas V2. 0: updated resources for unraveling the N 6-methyladenosine (M6a) epitranscriptome among multiple species. *Nucleic Acids Res*. (2024) 52:D194–202. doi: 10.1093/nar/gkad691

110. Wang J, Li L, Zhou H, Li S, Tian L, Wang X, et al. Human rna modifications disease database (Hrmdd): A web resource for the molecular and clinical landscape of rna modifications in human diseases. *Genes Dis*. (2023) 10:1157. doi: 10.1016/j.gendis.2022.08.024

111. Sabaawy HE, Ryan BM, Khiabanian H, Pine SR. Jak/Stat of all trades: linking inflammation with cancer development, tumor progression and therapy resistance. *Carcinogenesis*. (2021) 42:1411–9. doi: 10.1093/carcin/bgab075

112. Clarke WT, Feuerstein JD. Colorectal cancer surveillance in inflammatory bowel disease: practice guidelines and recent developments. *World J Gastroenterol*. (2019) 25:4148. doi: 10.3748/wjg.v25.i30.4148

113. Fu X-Y, Kessler DS, Veals SA, Levy DE, Darnell J. Isgf3, the transcriptional activator induced by interferon alpha, consists of multiple interacting polypeptide chains. *Proc Natl Acad Sci*. (1990) 87:8555–9. doi: 10.1073/pnas.87.21.8555

114. Fu XY. A direct signaling pathway through tyrosine kinase activation of sh2 domain-containing transcription factors. *J leukocyte Biol*. (1995) 57:529–35. doi: 10.1002/jlb.57.4.529

115. Hu X, Li J, Fu M, Zhao X, Wang W. The Jak/Stat signaling pathway: from bench to clinic. *Signal transduction targeted Ther*. (2021) 6:402. doi: 10.1038/s41392-021-00791-1

116. Xiong H, Du W, Wang J-L, Wang Y-C, Tang J-T, Hong J, et al. Constitutive activation of Stat3 is predictive of poor prognosis in human gastric cancer. *J Mol Med*. (2012) 90:1037–46. doi: 10.1007/s00109-012-0869-0

117. Owen KL, Brockwell NK, Parker BS. Jak-Stat signaling: A double-edged sword of immune regulation and cancer progression. *Cancers*. (2019) 11:2002. doi: 10.3390/cancers11122002

118. Thomas S, Snowden J, Zeidler M, Danson S. The role of Jak/Stat signalling in the pathogenesis, prognosis and treatment of solid tumours. *Br J Cancer*. (2015) 113:365–71. doi: 10.1038/bjc.2015.233

119. Meissl K, Macho-Maschler S, Müller M, Strobl B. The good and the bad faces of stat1 in solid tumours. *Cytokine*. (2017) 89:12–20. doi: 10.1016/j.cyto.2015.11.011

120. Lin J-X, Li P, Liu D, Jin HT, He J, Rasheed MAU, et al. Critical role of Stat5 transcription factor tetramerization for cytokine responses and normal immune function. *Immunity*. (2012) 36:586–99. doi: 10.1016/j.immuni.2012.02.017

121. Schindler C, Levy DE, Decker T. Jak-stat signaling: from interferons to cytokines. *J Biol Chem*. (2007) 282:20059–63. doi: 10.1074/jbc.R700016200

122. Snow JW, Abraham N, Ma MC, Herndier BG, Pastuszak AW, Goldsmith MA. Loss of tolerance and autoimmunity affecting multiple organs in stat5a/5b-deficient mice. *J Immunol*. (2003) 171:5042–50. doi: 10.4049/jimmunol.171.10.5042

123. Zhao H-M, Wang Y, Huang X-Y, Huang M-F, Xu R, Yue H-Y, et al. Astragalus polysaccharide attenuates rat experimental colitis by inducing regulatory T cells in intestinal peyer's patches. *World J Gastroenterol*. (2016) 22:3175. doi: 10.3748/wjg.v22.i11.3175

124. Salas A, Hernandez-Rocha C, Duijvestein M, Faubion W, McGovern D, Vermeire S, et al. Jak–Stat pathway targeting for the treatment of inflammatory bowel disease. *Nat Rev Gastroenterol Hepatol*. (2020) 17:323–37. doi: 10.1038/s41575-020-0273-0

125. Bar-Ephraim YE, Kretzschmar K, Clevers H. Organoids in immunological research. *Nat Rev Immunol*. (2020) 20:279–93. doi: 10.1038/s41577-019-0248-y

126. Xiong H, Zhang Z-G, Tian X-Q, Sun D-F, Liang Q-C, Zhang Y-J, et al. Inhibition of jak1, 2/stat3 signaling induces apoptosis, cell cycle arrest, and reduces tumor cell invasion in colorectal cancer cells. *Neoplasia*. (2008) 10:287–97. doi: 10.1593/neo.07971

127. Malki A, ElRuz RA, Gupta I, Allouch A, Vranic S, Al Moustafa A-E. Molecular mechanisms of colon cancer progression and metastasis: recent insights and advancements. *Int J Mol Sci*. (2020) 22:130. doi: 10.3390/ijms22010130

128. Shao F, Pang X, Baeg GH. Targeting the jak/stat signaling pathway for breast cancer. *Curr medicinal Chem*. (2021) 28:5137–51. doi: 10.2174/0929867328666201207202012

129. Zhong B, Cheng B, Huang X, Xiao Q, Niu Z, Y-f C, et al. Colorectal Cancer-Associated Fibroblasts Promote Metastasis by up-Regulating Lrg1 through Stromal Il-6/Stat3 Signaling. *Cell Death Dis*. (2021) 13:1–15. doi: 10.1038/s41419-021-04461-6

130. Biffi G, Oni TE, Spielman B, Hao Y, Elyada E, Park Y, et al. Il1-induced jak/stat signaling is antagonized by tgfβ to shape caf heterogeneity in pancreatic ductal adenocarcinomapathway antagonism shapes caf heterogeneity in pdac. *Cancer Discovery*. (2019) 9:282–301. doi: 10.1158/2159-8290.CD-18-0710

131. Lin HC, Ho AS, Huang HH, Yang BL, Shih BB, Lin HC, et al. Stat3-mediated gene expression in colorectal cancer cells-derived cancer stem-like tumorspheres. *Adv Digestive Med*. (2021) 8:224–33. doi: 10.1002/aid2.13223

132. Johnson DE, O'Keefe RA, Grandis JR. Targeting the Il-6/Jak/Stat3 signalling axis in cancer. *Nat Rev Clin Oncol*. (2018) 15:234–48. doi: 10.1038/nrclinonc.2018.8

133. Park SD, Saunders AS, Reidy MA, Bender DE, Clifton S, Morris KT. A review of granulocyte colony-stimulating factor receptor signaling and regulation with implications for cancer. *Front Oncol.* (2022) 12. doi: 10.3389/fonc.2022.932608

134. Yao Z, Cui Y, Watford WT, Bream JH, Yamaoka K, Hissong BD, et al. Stat5a/B are essential for normal lymphoid development and differentiation. *Proc Natl Acad Sci.* (2006) 103:1000–5. doi: 10.1073/pnas.0507350103

135. Wang M, Chen L, Chen Y, Wei R, Guo Q, Zhu S, et al. Intracellular matrix gla protein promotes tumor progression by activating Jak2/Stat5 signaling in gastric cancer. *Mol Oncol.* (2020) 14:1045–58. doi: 10.1002/1878-0261.12652

136. Klupp F, Diers J, Kahlert C, Neumann L, Halama N, Franz C, et al. Expressional Stat3/Stat5 ratio is an independent prognostic marker in colon carcinoma. *Ann Surg Oncol.* (2015) 22:1548–55. doi: 10.1245/s10434-015-4485-4

137. Hu X, Dutta P, Tsurumi A, Li J, Wang J, Land H, et al. Unphosphorylated stat5a stabilizes heterochromatin and suppresses tumor growth. *Proc Natl Acad Sci.* (2013) 110:10213–8. doi: 10.1073/pnas.1221243110

138. Kiu H, Nicholson SE. Biology and significance of the jak/stat signalling pathways. *Growth factors.* (2012) 30:88–106. doi: 10.3109/08977194.2012.660936

139. Mandal M, Powers SE, Maienschein-Cline M, Bartom ET, Hamel KM, Kee BL, et al. Epigenetic repression of the igk locus by Stat5-mediated recruitment of the histone methyltransferase Ezh2. *Nat Immunol.* (2011) 12:1212–20. doi: 10.1038/ni.2136

140. Liang C, Zhao T, Li H, He F, Zhao X, Zhang Y, et al. Long non-coding rna itih4-as1 accelerates the proliferation and metastasis of colorectal cancer by activating Jak/Stat3 signaling. *Mol Therapy-Nucleic Acids.* (2019) 18:183–93. doi: 10.1016/j.omtn.2019.08.009

141. Su C, Wang W, Wang C. Igf-1-induced mmp-11 expression promotes the proliferation and invasion of gastric cancer cells through the Jak1/Stat3 signaling pathway. *Oncol Lett.* (2018) 15:7000–6. doi: 10.3892/ol

142. Dimitriou ID, Clemenza L, Scotter AJ, Chen G, Guerra FM, Rottapel R. Putting out the Fire: Coordinated Suppression of the Innate and Adaptive Immune Systems by Socs1 and Socs3 Proteins. *Immunological reviews.* (2008) 224(1):265–83.

143. Palmer DC, Restifo NP. Suppressors of cytokine signaling (Socs) in T cell differentiation, maturation, and function. *Trends Immunol.* (2009) 30:592–602. doi: 10.1016/j.it.2009.09.009

144. Letellier E, Haan S. Socs2: physiological and pathological functions. *Front Bioscience-Elite.* (2016) 8:189–204. doi: 10.2741/E760

145. Khanna P, Chua PJ, Wong BSE, Yin C, Thike AA, Wan WK, et al. Gram domain-containing protein 1b (Gramd1b), a novel component of the Jak/Stat signaling pathway, functions in gastric carcinogenesis. *Oncotarget.* (2017) 8:115370. doi: 10.18632/oncotarget.v8i70

146. Jiang L, Chen T, Xiong L, Xu JH, Gong AY, Dai B, et al. Knockdown of M6a methyltransferase mettl3 in gastric cancer cells results in suppression of cell proliferation. *Oncol Lett.* (2020) 20:2191–8. doi: 10.3892/ol

147. Wu R, Liu Y, Zhao Y, Bi Z, Yao Y, Liu Q, et al. M6a methylation controls pluripotency of porcine induced pluripotent stem cells by targeting Socs3/Jak2/Stat3 pathway in a Ythdf1/Ythdf2-orchestrated manner. *Cell Death Dis.* (2019) 10:1–15. doi: 10.1038/s41419-019-1417-4

148. Li H-B, Tong J, Zhu S, Batista PJ, Duffy EE, Zhao J, et al. M6a mrna methylation controls T cell homeostasis by targeting the Il-7/Stat5/Socs pathways. *Nature.* (2017) 548:338–42. doi: 10.1038/nature23450

149. Tong J, Cao G, Zhang T, Sefik E, Amezcua Vesely MC, Broughton JP, et al. M6a Mrna methylation sustains treg suppressive functions. *Cell Res.* (2018) 28:253–6. doi: 10.1038/cr.2018.7

150. Lu TX, Zheng Z, Zhang L, Sun H-L, Bissonnette M, Huang H, et al. A new model of spontaneous colitis in mice induced by deletion of an rna M6a methyltransferase component mettl14 in T cells. *Cell Mol Gastroenterol Hepatol.* (2020) 10:747–61. doi: 10.1016/j.jcmgh.2020.07.001

151. Xiong J, He J, Zhu J, Pan J, Liao W, Ye H, et al. Lactylation-driven mettl3-mediated rna M6a modification promotes immunosuppression of tumor-infiltrating myeloid cells. *Mol Cell.* (2022) 82:1660–77.e10. doi: 10.1016/j.molcel.2022.02.033

152. Hua Z, Wei R, Guo M, Lin Z, Yu X, Li X, et al. Ythdf2 promotes multiple myeloma cell proliferation via stat5a/map2k2/P-erk axis. *Oncogene.* (2022) 41:1482–91. doi: 10.1038/s41388-022-02191-3

153. Ma S, Yan J, Barr T, Zhang J, Chen Z, Wang L-S, et al. The rna M6a reader ythdf2 controls nk cell antitumor and antiviral immunity. *J Exp Med.* (2021) 218: e20210279. doi: 10.1084/jem.20210279

154. Yang Z, Cai Z, Yang C, Luo Z, Bao X. Alkbh5 regulates stat3 activity to affect the proliferation and tumorigenicity of osteosarcoma via an M6a-ythdf2-dependent manner. *EBioMedicine.* (2022) 80:104019. doi: 10.1016/j.ebiom.2022.104019

155. McFadden MJ, Sacco MT, Murphy KA, Park M, Gokhale NS, Somfleth KY, et al. Fto suppresses stat3 activation and modulates proinflammatory interferon-stimulated gene expression. *J Mol Biol.* (2022) 434:167247. doi: 10.1016/j.jmb.2021.167247

156. Sun Y, Gong W, Zhang S. Mettl3 promotes colorectal cancer progression through activating jak1/stat3 signaling pathway. *Cell Death Dis.* (2023) 14:765. doi: 10.1038/s41419-023-06287-w

157. Guo Y, Guo Y, Chen C, Fan D, Wu X, Zhao L, et al. Circ3823 contributes to growth, metastasis and angiogenesis of colorectal cancer: involvement of mir-30c-5p/tcf7 axis. *Mol Cancer.* (2021) 20:1–21. doi: 10.1186/s12943-021-01372-0

158. Liu Z-X, Li L-M, Sun H-L, Liu S-M. Link between M6a modification and cancers. *Front bioengineering Biotechnol.* (2018) 6:89. doi: 10.3389/fbioe.2018.00089

159. Delaunay S, Frye M. Rna modifications regulating cell fate in cancer. *Nat Cell Biol.* (2019) 21:552–9. doi: 10.1038/s41556-019-0319-0

160. Wei R, Quan J, Li S, Liu H, Guan X, Jiang Z, et al. Integrative analysis of biomarkers through machine learning identifies stemness features in colorectal cancer. *Front Cell Dev Biol.* (2021) 9:2428. doi: 10.3389/fcell.2021.724860

161. Thomas S, Fisher K, Snowden J, Danson S, Brown S, Zeidler M. Effect of methotrexate on jak/stat pathway activation in myeloproliferative neoplasms. *Lancet.* (2015) 385:S98. doi: 10.1016/S0140-6736(15)60413-5

162. Clark JD, Flanagan ME, Telliez J-B. Discovery and development of janus kinase (Jak) inhibitors for inflammatory diseases: miniperspective. *J medicinal Chem.* (2014) 57:5023–38. doi: 10.1021/jm401490p

163. Ye H, Chen T, Zeng Z, He B, Yang Q, Pan Q, et al. The M6a writers regulated by the Il-6/Stat3 inflammatory pathway facilitate cancer cell stemness in cholangiocarcinoma. *Cancer Biol Med.* (2022) 19:343. doi: 10.20892/j.issn.2095-3941.2020.0661

164. Wu R, Liu Y, Zhao Y, Bi Z, Yao Y, Liu Q, et al. M6a methylation controls pluripotency of porcine induced pluripotent stem cells by targeting Socs3/Jak2/Stat3 pathway in a ythdf1/ythdf2-orchestrated manner. *Cell Death Dis.* (2019) 10:171. doi: 10.1038/s41419-019-1417-4

165. Cao L, Morgun E, Genardi S, Visvabharathy L, Cui Y, Huang H, et al. Mettl14-dependent M6a modification controls inkt cell development and function. *Cell Rep.* (2022) 40:111156. doi: 10.1016/j.celrep.2022.111156

Frontiers in Oncology

Advances knowledge of carcinogenesis and tumor progression for better treatment and management

The third most-cited oncology journal, which highlights research in carcinogenesis and tumor progression, bridging the gap between basic research and applications to imrpove diagnosis, therapeutics and management strategies.

Discover the latest Research Topics

See more →

Frontiers

Avenue du Tribunal-Fédéral 34
1005 Lausanne, Switzerland
frontiersin.org

Contact us

+41 (0)21 510 17 00
frontiersin.org/about/contact